

UNIVERSITY OF STRATHCLYDE

STRATHCLYDE INSTITUTE OF PHARMACY AND BIOMEDICAL SCIENCES

**Informing the Next Generation of Auditory Midbrain
Implants: Neuronal Population Dynamics in the
Auditory Cortex and Midbrain, and the Potentials of
Optogenetic Stimulation**

Aimee Bias



A thesis submitted in partial fulfilment of the requirements for the
degree of Doctor of Philosophy

March 2020

Candidate's Declaration

I, Aimee Bias, certify that this thesis is the result of my original research, and has been composed by me. This work of approximately 80000 words has not been previously submitted for examination which has led to the award of a degree.

The copyright of this thesis belongs to the author under the terms of the United Kingdom Copyright Acts as qualified by University of Strathclyde Regulation 3.50. Due acknowledgement must always be made of the use of any material contained in, or derived from, this thesis.

Signed: 

Date: 02/03/2020

Acknowledgments

I would first like to extend my sincere thanks to Dr Shuzo Sakata for his wisdom and expertise throughout this project. His continuous availability and patience for questions (of which there were many!) was very much appreciated. Thank you also to my secondary supervisor Prof. Keith Mathieson for his advice and assistance with posters and reports, and to Ruaridh Winstanley who maintained the μ LED probes and with whom I collaborated on to create the μ LED control system.

I would also like to thank Action on Hearing Loss for their financial support of my PhD project and for the opportunity to share my work and meet other auditory PhD students at their annual PhD Student Day.

I would also like thank Dr Daniel Lyngholm for all of his help, and his extreme patience when teaching me experimental techniques and data analysis. An extra special thank you goes to Amisha Patel for her constant support since day 1 – we made it! Thank you also to the other members of Sakata Lab throughout the years, in particular Mirna Merkler – your support was truly invaluable.

Many thanks also to the staff of the BPU unit – Linda, Carol, Lee, Kevin, Pete and Brian – for taking such excellent care of my animals. Thanks go also to my colleagues on level 4 for all the coffee, cake and chat, and to all the good dogs I saw while walking to and from the office.

Final thanks to my family and in particular to Jonathan Failes for his love and support throughout.

Abstract

The performance of current generation central auditory neuroprosthetics lags behind the cochlear implant. As these new devices utilise speech processing algorithms based on the cochlea, more information may be required regarding the neuronal population activity of potential prosthetic sites, in order to optimise stimulation to mimic the area's natural inputs and achieve useful sound perception. Additionally, electrode-based devices afford poor spatial resolution, which optogenetics may solve.

Simultaneous silicon probe recordings were performed in the inferior colliculus (IC) and auditory cortex (AC) of awake, head-fixed mice, and repetitions of natural sound stimuli played. The two areas are different in their general cell population metrics, levels of inter-trial LFP coherence, and neuronal entrainment, with the AC favouring entrainment frequencies below 30Hz and the IC apparently entraining over a wider range of 2-200Hz. The proportion of putative AC narrow-spiking interneurons is higher during natural sounds as opposed to spontaneous activity alone.

Using linear classification analysis, a spike rate code was generally found to be sufficient for distinguishing between natural sound stimuli, in both the AC and IC. However, the IC achieved comparable performance to the AC using fewer single or multi units. This could be due to the lower trial-trial variability (Fano factor) of the IC cell population. Dimensionality reduction revealed, qualitatively, the presence of distinct cell populations in both brain areas, responding to different aspects of the natural sound

A viral injection protocol for expression of the Chronos opsin through the depth of the mouse ICC was optimised, and light activation confirmed. A control system for a μ LED device was created and used in a pilot experiment, which served to highlight the importance of artefact-reducing device design.

The findings indicate that IC neurons tend to fire in the same way (i.e. more reliably) to successive repetitions of natural sound when compared to the auditory cortex, and that AC narrow-spiking interneurons may have different functions between spontaneous and evoked activity. Optogenetics is a promising approach to improving auditory implant resolution, given well designed light delivery devices and accompanying software.

Contents

Candidate's Declaration	i
Acknowledgments	ii
Abstract	iii
List of Figures	vi
List of Tables	xii
List of Equations	xiii
Nomenclature and Abbreviations	xiv
Chapter 1 Introduction	1
1.1 Project Motivations	1
1.2 Scope of the Review	2
1.3 Auditory System Overview	3
1.4 Principles of Neuronal Coding	31
1.5 Spectral Processing in the Auditory Pathway	39
1.6 Temporal Coding in the Auditory Pathway.....	45
1.7 Additional Sound Coding Principles.....	51
1.8 Mathematical Modelling of Neuronal Activity	55
1.9 Electrophysiology	60
1.10 The Curse of Dimensionality.....	68
1.11 Pathologies of the Auditory System	69
1.12 Auditory Neuroprosthetics	70
1.13 Optogenetics	77
1.14 Project Aims and General Hypotheses	91
Chapter 2 Materials and Methods	97
2.2 Animal Maintenance	98
2.3 Headcap Manufacture	99
2.4 Surgical Techniques.....	100
2.4 Recording Procedures.....	106
2.5 Post Recording Procedure	117
2.6 Data Analysis	119
Chapter 3 Characterisation of Single Neuron and Population Activity During Natural Sound, in the AC and IC	140
3.1 Introduction	141
3.2 Basic Properties of Recorded Data	145

3.3 General Appearance and Variability of Neuronal Spiking During Natural Sound	153
3.4 Inter-Trial Coherence of LFP During Natural Sound	163
3.5 Entrainment of Neurons to LFP during Spontaneous Activity and Natural Sound	169
3.6 Discussion.....	176
Chapter 4 Linear Classification of Natural Sounds using Spike Rate in the AC and IC 185	
4.1 Introduction	186
4.2 Success of Linear Classification using Spike Rate	191
4.3 Discussion and Conclusions.....	229
Chapter 5 Non-Negative Matrix Factorisation for Characterisation of Neuronal Populations During Natural Sound	237
5.1 Introduction	238
5.2 Qualitative Analysis of Spatiotemporal Modules	242
5.3 Identification of State Through Spatiotemporal Modules.....	248
5.4 Discussion.....	258
Chapter 6 Optogenetics for Auditory Implants.....	262
6.1 Introduction	263
6.2 Expressing the Chronos Virus in the Mouse Inferior Colliculus	267
6.3 μ LED Experiments	275
6.4 Discussion.....	286
Chapter 7 General Discussion	293
7.1 Brief Summary of Key Results and Relation to Hypotheses	293
7.2 Implications and Relevance of the Project.....	295
7.3 Current Limitations and Potential Improvements	299
7.4 Future of the Work.....	302
7.5 Final Thoughts	304
References	305

List of Figures

- 1.1 Schematic of the central auditory pathway
- 1.2 Sound waves
- 1.3 Peripheral auditory system
- 1.4 Anatomy of the cochlea and basilar membrane
- 1.5 Mouse inferior colliculus (coronal view)
- 1.6 Classes of spiking behaviour after a depolarising current
- 1.7 Two principal inferior colliculus cell morphologies
- 1.8 Cortical layers
- 1.9 Maps of primary and core auditory cortical areas.
- 1.10 Mechanisms of neural coding
- 1.11 Cortical states
- 1.12 Simplistic representations of tonotopic maps in the primary auditory cortex and central nucleus of the inferior colliculus
- 1.13 Simplistic FRA examples
- 1.14 Temporal components of a sound wave
- 1.15 Entrainment
- 1.16 Dynamic range of an auditory neuron
- 1.17 Common terminology in mathematical modelling
- 1.18 Classification vs Regression models
- 1.19 Simple linear non-linear Poisson model (schematic)
- 1.20 Microelectrodes
- 1.21 Cochlear implant (electrodes)
- 1.22 21 electrode surface auditory brainstem implant

- 1.23 Penetrating single shank auditory midbrain implant
- 1.24 Electrical vs optogenetic stimulation
- 1.25 The three main families of microbial opsin
- 1.26 Waveguide device
- 1.27 μ LED probe

- 2.1 Flow diagram of auditory experiments
- 2.2 Flow diagram of optical experiments
- 2.3 Headcap components
- 2.4 Location of anchor and recording screws for headcap surgeries
- 2.5 Viral injection surgery
- 2.6 Craniotomy locations for auditory experiments
- 2.7 Silicon probes (no shanks)
- 2.8 Auditory recording schematic and protocol
- 2.9 Neural data recording and stimulation equipment
- 2.10 Optogenetic recording schematic and protocol
- 2.11 Representative relationship of voltage vs intensity at tip of the optic fibre
- 2.12 μ LED experiment probe configurations
- 2.13 Event detection schematic
- 2.14 Principals of spike sorting
- 2.15 Cell waveform metrics
- 2.16 Current Source Density example
- 2.17 Entrainment
- 2.18 Prediction of natural sound stimuli through linear classification
- 2.19 Cell pairing nomenclature for pairwise correlations

- 2.20 Input and output matrices in spectral and spectrotemporal decomposition
- 3.1 Summary of animals used for simultaneous recordings
- 3.2 Flow chart of surgeries and experiments
- 3.3 Summary of probe position (histology)
- 3.4 Cell metric summary
- 3.5 Appearance of natural sound stimuli in time and frequency domains
- 3.6 General MUA changes during natural sound stimuli
- 3.7 Type and number of SUA/MUA and Fano factor comparisons
- 3.8 Strength of negative correlations between PSTH and Fano factor, with increasing time window
- 3.9 Mean Fano factors of single and multi units during natural sound, with increasing time window
- 3.10 Median Fano factor and proportion of time spent below the baseline for single and multi units, with increasing time window
- 3.11 Example plot of LFP phase across time (two frequency bands)
- 3.12 ITC of auditory cortex and inferior colliculus during natural sound stimuli
- 3.13 ITC in the auditory cortex over depths relative to cortical sink layer/channel
- 3.14 Entrainment (illustrative examples)
- 3.15 Proportions of cell populations displaying significant neuronal entrainment
- 3.16 Rates of entrainment during spontaneous activity and natural sound stimuli, in the auditory cortex and inferior colliculus
- 3.17 Levels of entrainment across narrow and broad spiking cell groups in the auditory cortex
- 4.1 Schematic of sound segments selected for classification analysis
- 4.2 Summary of classification results from Run 1

- 4.3 Explained variance in first 5 Principal Components
- 4.4 Negative controls summary
- 4.5 Number of stimuli indistinguishable from chance, against classification error of the dataset, for three selected stimuli lengths
- 4.6 Number of predictors vs performance for example 4 time bins, for single/multi units in the auditory cortex and inferior colliculus
- 4.7 Relationship between frequency range and number of predictors
- 4.8 Frequency range and prediction error of all datasets
- 4.9 Summary of Fano factor in single and multi units in the auditory cortex and inferior colliculus, for increasing time window
- 4.10 Relationship of Fano factor and prediction error
- 4.11 Fano factor differences between narrow and broad spiking cells in the auditory cortex
- 4.12 Relationship between spike rate and prediction error
- 4.13 Summary of pairwise noise correlations across increasing time windows, for single and multi units in the auditory cortex and inferior colliculus
- 4.14 Relationship of pairwise noise correlations and prediction error
- 4.15 Effect of cortical depth on pairwise noise correlations
- 4.16 Relationship between Distance between IC cells and correlation strength for a single time bin
- 4.17 Pairwise noise correlation strengths for cortical cell types
- 4.18 Summary of pairwise signal correlations across increasing time windows, for single and multi units in the auditory cortex and inferior colliculus
- 4.19 Relationship of pairwise signal correlations and prediction error
- 4.20 Signal correlations with cell pairs grouped by depth and relative distance, for one example stimuli (1000ms).
- 4.21 Relationship between Distance between IC cells and signal correlation strength for a single stimuli length (1000ms)

- 4.22 Signal correlations in type specific cell pairs, for example 1000ms stimuli length

- 5.1 Example matrix decompositions for auditory cortex and inferior colliculus single unit populations
- 5.2 Example matrix decompositions for auditory cortex and inferior colliculus single unit populations
- 5.3 Number of resulting modules from spatial decomposition
- 5.4 Identification of changes in cortical state from spatial module strength in the auditory cortex
- 5.5 Classification of natural sound trials into putative synchronised and desynchronised states
- 5.6 Classification error for states 1 and 2 in auditory cortex (three stimuli lengths)
- 5.7 Fano factor and spikes per bin in each state (three stimuli lengths)
- 5.8 Pairwise noise and signal correlations in each state (three stimuli lengths)
- 5.9 Classification of inferior colliculus natural sound trials into putative synchronised and desynchronised states, using auditory cortex results
- 5.10 Classification error for states 1 and 2 in inferior colliculus (3 stimuli lengths)
- 5.11 Fano factor and spikes per bin in each state (three stimuli lengths)
- 5.12 Pairwise noise and signal correlations in IC multi units (three stimuli lengths)

- 6.1 Goals of the proposed optogenetic experiments
- 6.2 Optimisation of Chronos expression in the mouse inferior colliculus central nucleus
- 6.3 Full histological summary of Chronos expression in a single animal
- 6.4 Viral expression in chronic recording experiments
- 6.5 Optical activation using Chronos and optic fibre at 0-1V

- 6.6 Schematic of 96 channel μ LED probe
- 6.7 Schematic of control software for μ LED probe
- 6.8 Screenshot of protocol creation GUI
- 6.9 Placement of μ LED and recording probes in the mouse cortex
- 6.10 Neurotrace screenshots of recording trace during light stimulation
- 6.11 Positive saturation of amplifier and recording during LED stimulation
- 6.12 Negative saturation of amplifier and recording during LED stimulation
- 6.13 Effect of pulse shaping on generated current

List of Tables

- 1.1 Biophysical cell classifications in the inferior colliculus
- 1.2 Layers of the auditory cortex
- 1.3 Range of common opsins
- 2.1 Optimisation of viral injection coordinates and locations
- 2.2 Craniotomy locations
- 2.3 Silicon probe information
- 2.4 Typical auditory stimulation protocol
- 2.5 Typical optogenetic stimulation protocol
- 2.6 μ LED experimental protocols
- 2.7 Microscope filter and excitation wavelength combinations
- 2.8 Key data files
- 2.9 Binning of LFP Phases
- 2.10 Definition of cell pair groupings
- 3.1 Breakdown of frequency bands showing significant differences between conditions
- 4.1 Negative control summary
- 4.2 Correlations between pairwise noise correlations and prediction performance
- 4.3 Correlations between pairwise signal correlations and prediction performance
- 6.1 Summary of initial 8 animals used in optimisation of Chronos expression
- 6.2 Optimisation of μ LED experimental equipment – Problems and Solutions

List of Equations

- 2.1 z-score of neuronal firing rate in response to puretone stimuli
- 2.2 Octave range of a dataset
- 2.3 Current Source Density
- 2.4 Fano factor
- 2.5 Bin Average (ITC)
- 2.6 ITC (of a bin)
- 6.1 Capacitive Current
- 6.2 Inductive Voltage

Nomenclature and Abbreviations

Brain Areas and Biological Terminology

A1	Primary Auditory Cortex
AC	Auditory Cortex
BOLD fMRI	Blood Oxygen Level Dependant functional Magnetic Resonance Imaging
CN	Cochlear Nucleus
DCIC	Dorsal Cortex of the Inferior Colliculus
DCN	Dorsal Cochlear Nucleus
dMGB	Dorsal division of the Medical Geniculate Body (thalamus)
ECoG	Electrocorticography
EEG	Electroencephalography
EMG	Electromyography
IC	Inferior Colliculus
ICC/CNIC	Central Nucleus of the Inferior Colliculus
LCIC	Lateral Cortex of the Inferior Colliculus
LLN	Lateral Lemiscal Nuclei
LFP	Local Field Potential
LSO	Lateral Superior Olive
LdT	Laterodorsal Tegmentum
L1, 2 etc	Layer (typically cortical)
MEG	Magnetoencephalography
MGB	Medical Geniculate Body (thalamus)
mMGB	Medial division of the Medical Geniculate Body (thalamus)
MNTB	Nucleus of the Trapezoid Body (SOC)
MSO	Medial Superior Olive

NF2	Neurofibromatosis Type II/2
NREM	Non Rapid Eye Movement (sleep)
PPT	Pedunculopontine Tegmentum
REM	Rapid Eye Movement (sleep)
SOC	Superior Olivary Complex
SGN	Spiral Ganglion Neurons
vMGB	Ventral division of the Medial Geniculate Body (thalamus)
VCN	Ventral Cochlear Nucleus

Data Analysis

CSD	Current Source Density
ITC	Inter-Trial Coherence
FF	Fano Factor
FIR	Finite Impulse Response (filter)
GLM	Generalised Linear Models
IIR	Infinite Impulse Response (filter)
ks-test	Kolmogorov-Smirnov statistical test
LNP	Linear nonlinear Poisson model
MUA	Multi Unit Activity
NMF/NNMF	Non-Negative Matrix Factorisation
P2T	Peak-To-Trough amplitude
PSTH	Peri-Stimulus Time Histogram
PCA	Principal Component Analysis
SUA	Single Unit Activity

Terminology in Auditory Research and Devices

ABI	Auditory Brainstem Implant
ACE	Advanced Combination Encoders
AM	Amplitude Modulation
AMI	Auditory Midbrain Implant
BF	Best Frequency
BMF	Best Modulation Frequency
CF	Characteristic Frequency
CI	Cochlear Implant
CIS	Continuous Interleaved Sampling
FM	Frequency Modulation
FRA	Frequency Response Area
pps	Pulses Per Second
Q10dB	Quality factor at 10dB (tuning sharpness metric)
Q20dB	Quality factor at 20dB (tuning sharpness metric)
STRF	Spectro-Temporal Receptive Field
SPEAK	Spectral Peak Coding

Equation Terms and Measures

σ^2	Variance (sigma squared)
σ	Standard Deviation (sigma)
C	Capacitance (farads)
d	change in a quantity
dB	Decibels

kHz/Hz	Kilohertz/hertz (frequency metric)
I	Current (Amps)
L	Inductance (Henrys)
u	Mean
V	Voltage (Voltage)

Chemicals

AAV	Adeno-Associated Virus
ChR2	Channelrhodopsin 2 (opsin)
DAPI	4',6-diamidino-2-phenylindole
GABA	Gamma Aminobutyric Acid
GaN	Gallium Nitride
GFP	Green Fluorescent Protein
H ₂ O ₂	Hydrogen Peroxide
O ₂	Oxygen (gas)
PBS	Phosphate Buffered Saline
PFA	Paraformaldehyde
PBST	Phosphate Buffered Saline (with Triton-X)
YFP	Yellow Fluorescent Protein

Hardware and Software

CMOS	Complimentary Metal-Oxide-Semiconductor
DAQ	Data Acquisition Board (National Instruments)
GUI	Graphical User Interface
labVIEW	laboratory Virtual Instrument Engineering Workbench

LED	Light Emitting Diode
MATLAB	MATrix LABoratory – data analysis software
NA	Numerical Aperture
PCB	Printed Circuit Board
μ LED	Micro Light Emitting Diode
μ TP	Micro Transfer Printing
VI	Virtual Instrument (a LabVIEW program)

General

BPU	Biological Procedures Unit (University of Strathclyde)
PPL	Project License (Animal Experimentation)

Chapter 1 Introduction

1.1 Project Motivations

Hearing loss is unfortunately both an increasingly common and potentially debilitating health condition. Effectively communicating with family, friends and society in general is incredibly important for a person's health and wellbeing, and disruption to this has huge potential to impact on a person's quality of life. Its effects are particularly applicable to the aging population, with hearing loss recently linked to an increased risk of Alzheimer's (Livingston et al., 2017).

While a large variety of devices and treatments exist, these are not always suitable for the individual's situation. Devices which activate auditory neurons and replace the function of auditory areas of our brain are a relatively new technology, and as such are not fully optimised. Several avenues of research are seeking to improve upon these issues for the next generation of implants. These include improving the performance of the devices by developing more efficient or more selective technologies to stimulate cells – for example, improving the spatial resolution of devices has the potential to increase frequency resolution. Additionally, work is ongoing to better understand how auditory information is being transferred and processed in the brain, so that speech translation algorithms can be better designed.

This project was born of an attempt to address both areas of concern – better understanding of auditory coding on the neuronal level and improving the spatial resolution of auditory midbrain-based stimulation devices. The work presented compares and contrasts neuronal activity recording simultaneously from in the inferior colliculus and the auditory cortex during natural sound stimuli, and explores an alternate stimulation method with the potential to improve device resolution.

The first three results chapters focus on the first of these challenges, presenting analysis of neuronal spiking data recorded simultaneously from the auditory cortex (AC) and inferior colliculus (IC) of mice, during presentation of natural sound stimuli. Chapter 3 seeks to confirm and identify general differences in neuronal properties during both spontaneous neuronal activity, and during natural sound. Continuing directly from Chapter 3, Chapter 4 looks specifically at decoding of natural sound stimuli, using basic mathematical prediction models. In Chapter 5, the dimensionality of the neuronal data is examined, with the aim of identifying distinct but dynamic neuronal populations and linking these to function during presentation of sound.

To address the issue of frequency resolution, Chapter 6 looks to the field of optogenetics, and the use of μ LED (micro-LED) technology as a viable, high spatial resolution alternative to electrical stimulation.

1.2 Scope of the Review

This literature review will cover a wide variety of topics in order to provide context to the remainder of the thesis. The review will begin with an overview of the auditory system (with a primary focus on the central pathway), with details on connections, anatomy, cell morphology and function. The auditory cortex and inferior colliculus will be given particular focus, in order to highlight differences in anatomy and cell morphology.

Following on from this, the general principals of neural coding will be explained, including the most common strategies employed by neurons, and the potential effects of global brain state. The focus will then shift to specifically the auditory system, with dedicated sections on spatial and temporal coding of sound - both general principals and specifically in the auditory cortex and inferior colliculus. An understanding of the underlying coding mechanisms of the auditory system will prove imperative to identifying potential functional differences between the AC and IC and forming hypothesis, and inform the choice of analysis as used in results Chapters 3, 4 and 5.

With the principals of neuronal activity laid down, the use of silicon probes will be justified through a thorough examination project requirements and a breakdown of the features of both silicon probes and other available measurement technology and techniques. An understanding of electrophysiology techniques will provide context to Materials and Methods.

Moving from the neuron scale, pathology in the auditory system is briefly summarised (with a focus on Neurofibromatosis II) – serving to outline the original motivation for the thesis project. With the issues clearly established, the currently available devices for sensorineural hearing loss are reviewed – namely, the cochlear, brainstem and midbrain neuroprosthetics, including their history and current drawbacks. This will also include a brief summary of speech processing algorithms, for better identification of where improvements might be made in future iterations.

The remainder of the review deals with optogenetics and its potential in auditory implants. Beginning with a history and definition of optogenetics, the review will discuss important variables to consider when choosing an opsin and an expression

method. It will conclude with details on the current situation regarding optogenetics in the auditory system, discuss the likely future of the technology, and review currently available optogenetic tools and justify the choice of tools for the project. The relevant results chapter here will be Chapter 6.

1.3 Auditory System Overview

1.3.1 Auditory System Basics

The Pathway

To put the presented work into context, an understanding of the general structure and complexity of the auditory system is imperative. The auditory pathway (Figure 1.1) is, at its most simplistic, a means of transferring of acoustic information from the outside world to higher order brain structures, where the sound is perceived. While ascending through the many “stops” or “stations” in the auditory pathway, information is transformed, integrated and split in a multitude of ways along this and many other ascending, descending and commissural pathways, as well as reflexive pathways to the spinal nerves and spinal cord.

The first distinction to make is a split into the peripheral and central pathway. The peripheral pathway consists of the outer, middle and inner ear, whose principal role is to transform sound vibrations into electrical signals in neurons. From here, electrical impulses generated by the hair cells of the cochlear are passed via the auditory nerve to the cochlear nucleus of the brainstem, where they ascend through each stage of the pathway (Figure 1.1).

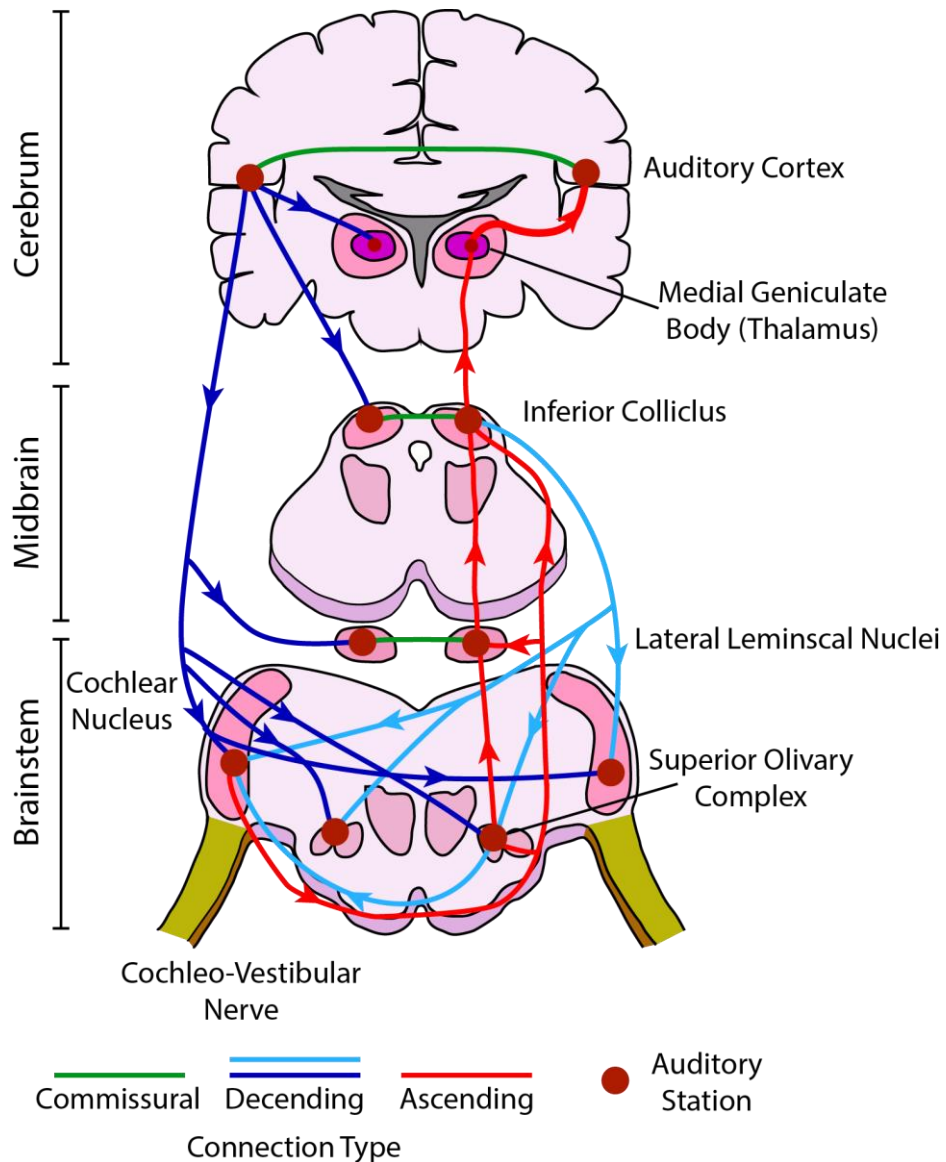


Figure 1.1. Schematic of the central auditory pathway including major ascending and descending connections. Some connections are omitted to maintain clarity Adapted from (Pujol, 2016, Saldaña, 2015, Winer and Schreiner, 2005)

Sound Vibrations

The phenomenon of “sound” is caused by vibrations of the air, and sound vibrations are themselves caused by vibration of the source object. Sound waves are longitudinal, consisting of areas of high and low pressure. Various properties of the wave determine how it is perceived – because the speed of the sound is constant, perceived frequency is a function of wavelength. A shorter wavelength (distance between peaks/troughs of pressure) results in a higher pitched sound, with longer wavelengths perceived as lower in pitch (Figure 1.2). Higher amplitude vibrations are perceived as louder. In addition, sound waves are usually complex (such as speech,

music etc) and consist of many overlapping/nested components. The overarching outline, or *envelope* of the sound, determines its temporal structure, while the fine detail is important for pitch..

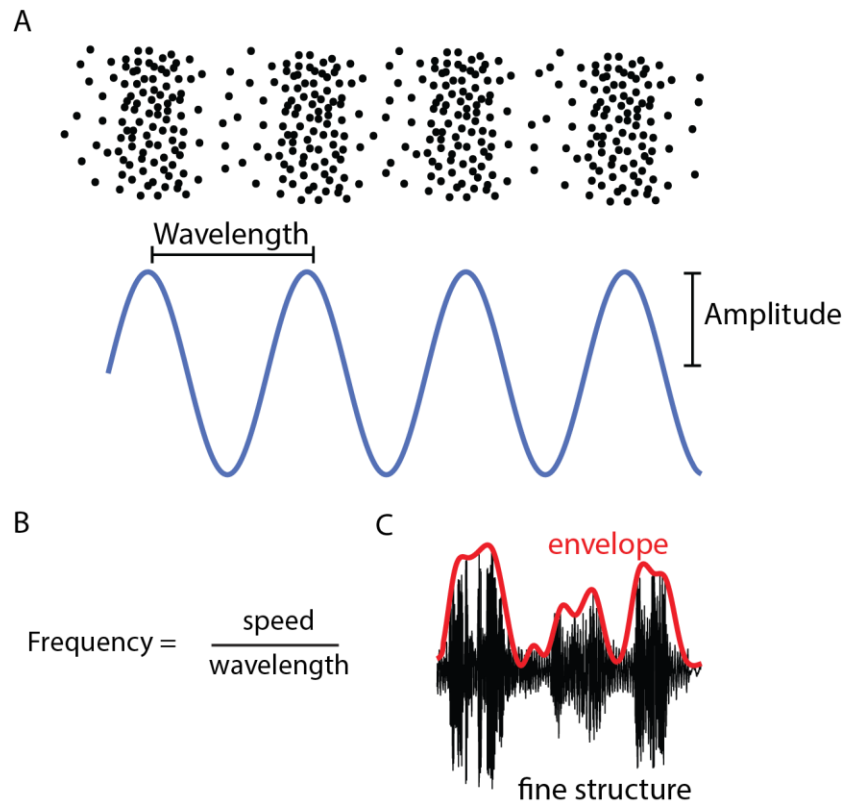


Figure 1.2: Sound waves. (A) Top: Example distribution of air particles creating a “sound wave”, showing areas of rarefaction and compression. Bottom: Sinusoidal wave representing the distribution of particles, with important measurements highlighted. (B) Relationship of speed and wavelength that generates the frequency of the sound wave. Note, speed of sound is constant (in a given medium) and thus changes in the wavelength affect frequency. (C) Example complex sound wave showing important components. Red: sound envelope, or periodicity of the sound. Black: fine temporal structure that conveys the frequency/pitch heard

The human auditory system is capable of perceiving sounds between 20-20 kHz, though the upper limits of this decrease quickly with age and chronic exposure to loud sounds, such as concerts and factory workplaces.

A highly important feature that the auditory system uses to transfer sound information is tonotopy. Throughout stages in the system, neurons are often arranged into what is termed a tonotopic gradient, where the preferred frequency of that neuron (i.e., the frequency to which it responds most strongly to) changes through the structure. In the principal branch of the central auditory pathway, tonotopy is conserved from the cochlea, all the way to the cortex, though exact representations/patterns vary to some degree.

A Note on Natural Sound

The term “natural sound” or “naturalistic sound” will be mentioned throughout this review and thesis – referring to sound that is natural in origin, such as vocalisations and environmental noises (running water, rustling leaves). In comparison, artificially generated sounds such as pure frequency tones, and trains of clicks at a specific temporal frequency, do not hold both the spectral and temporal complexity as well as the behavioural relevance that natural sound usually has.

In this literature review, the general principals by which the brain codes both spectral and temporal information of sounds will be discussed. However, as accurate perception of, and reaction to, these sounds is often critical for the animal (and may be dependent on other sensory systems), the brain’s encoding of natural sounds is understood to contain additional layers of complexity, particularly in the higher processing centre of the auditory cortex. These mechanisms will be explored in the relevant review sections, and in Results Chapters 3 and 4.

1.3.2 The Peripheral Auditory Pathway

Purpose of the Peripheral Pathway

The auditory system begins with the peripheral auditory pathway. The principal role of this pathway is to collect sound waves from the environment and transform them into a pattern of electrical impulses, which the brain can then perceive as sound. Figure 1.3 outlines the key components

External Ear Canal and Middle Ear

Environmental sound waves are first funnelled into the external ear canal by the outer pinna. The waves then vibrate the tense tympanic membrane. The tympanic membrane is connected to the oval window of the cochlea through a series of minuscule bones (ossicles), the malleus, incus and stapes, which further amplify the vibrations. Due to their arrangement, the movement of the bones amplifies the vibrations and passes them into the fluid of the cochlea (the ‘footplate’ of the stapes rests against the oval window of the cochlea).

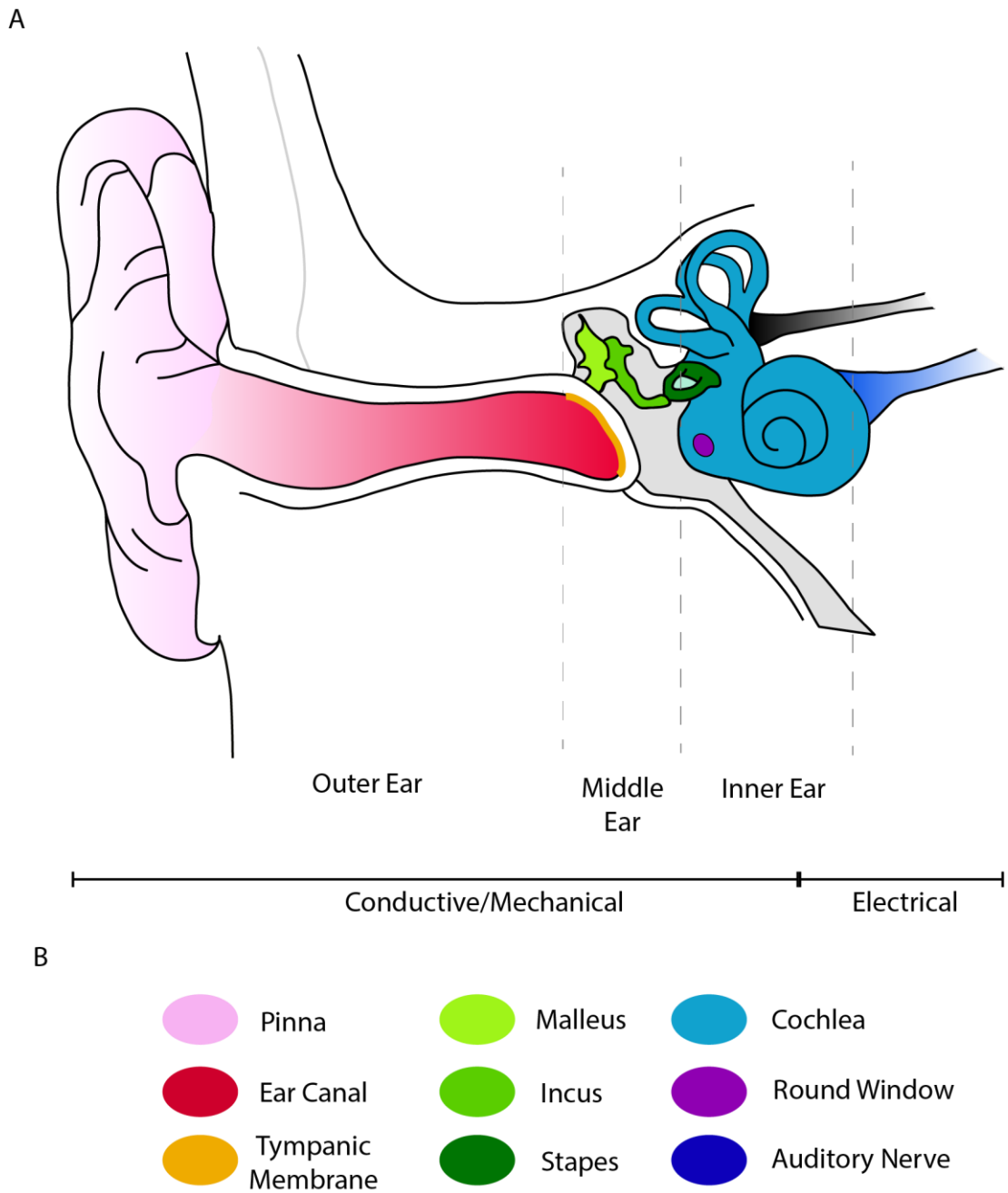


Figure 1.3: Peripheral auditory system, showing the outer, middle and inner ear. (A) Colour-coded diagram (see Key, (B) of main components and configurations of the outer, middle and inner ear. Also indicated is the sound representation at each point – from mechanical pressure changes to electrical impulses. Image adapted from (HearingSolutions, 2020)

Cochlea (Inner Ear)

The cochlea is a coiled, fluid filled tube, containing many structures crucial for translation of sound waves into electrical signals (Figure 1.4). Several membranes partition this tube lengthways into separate fluid filled chambers. The *scala media* is the middle cochlear chamber, filled with endolymph fluid. It also contains the Organ of Corti, which in turn lies upon the basilar membrane. It is using the basilar membrane that the auditory system is first able to distinguish different frequencies of sound. As detailed in Figure 1.4, the membrane (in blue) is narrower and stiffer at its base at the oval window, but wider and less stiff (by around 100x) at the apex. Incoming sound waves produce vibrational peaks in the membrane (by movement of the endolymph) determined by their wavelength. Shorter wavelength, high frequency sounds do not travel far up the membrane before their energy is expended, whereas lower wavelengths travel in the direction of the apex. In this way, the anatomy is designed to distinguish between sound frequencies, and the first instance of tonotopy is created.

The Organ of Corti also contains the hair cells (inner and outer), and tectorial membrane, surrounded by endolymph fluid, which has a unique ionic composition, with high potassium levels inferring a highly positive potential. Hair cells are attached at their base to the basilar membrane, while the tectorial membrane lies along their top side, across their many stereocilia (similar to the microvilli of the digestive system, but for the purposes of mechanosensing). Movement of the basilar membrane causes lateral movement (and a resulting shearing force), bending the stereocilia of the inner hair cells. In response to this mechanical bending, potassium channels are opened, resulting in depolarisation as potassium floods in (endolymph is particularly rich in potassium ions). This in turn results in neurotransmitter release from the base of the cell, innervating the dendrites of spiral ganglion neurons.

Bundles of spiral ganglion axons make up the auditory nerve (a portion of cranial nerve VIII, vestibulocochlear). Different inner hair cells positioned along the basilar membrane are thus activated by different incoming frequencies, meaning the auditory nerve branches they supply maintain tonotopy. As we will see, many of the higher auditory structures also show and continue this tonotopy to some degree (though it becomes far more spatially complex than the linear basilar membrane).

The outer hair cells provide mechanical amplification of sound, in a mechanism known as the “cochlear amplifier”. In response to electrical stimulation, the hair cells rapidly

change their length and stiffness, referred to as “electromotility”. This alters the sensitivity of the cochlea and produces amplification and sharpening frequency tuning (Ryan and Dallos 1975, Dallos and Harris, 1978). Movement of the OHC has to be incredibly fast in order to match the animal’s frequency hearing limits – this rapid motility is achieved by the protein prestin (Ashmore, 2008, Zheng et al., 2000). The OHC are innervated by neurons from of the olivocochlear system, originating in the superior olivary complex of the in the brainstem and whose nerves form part of cranial nerve VIII (Spöndlin, 1969).

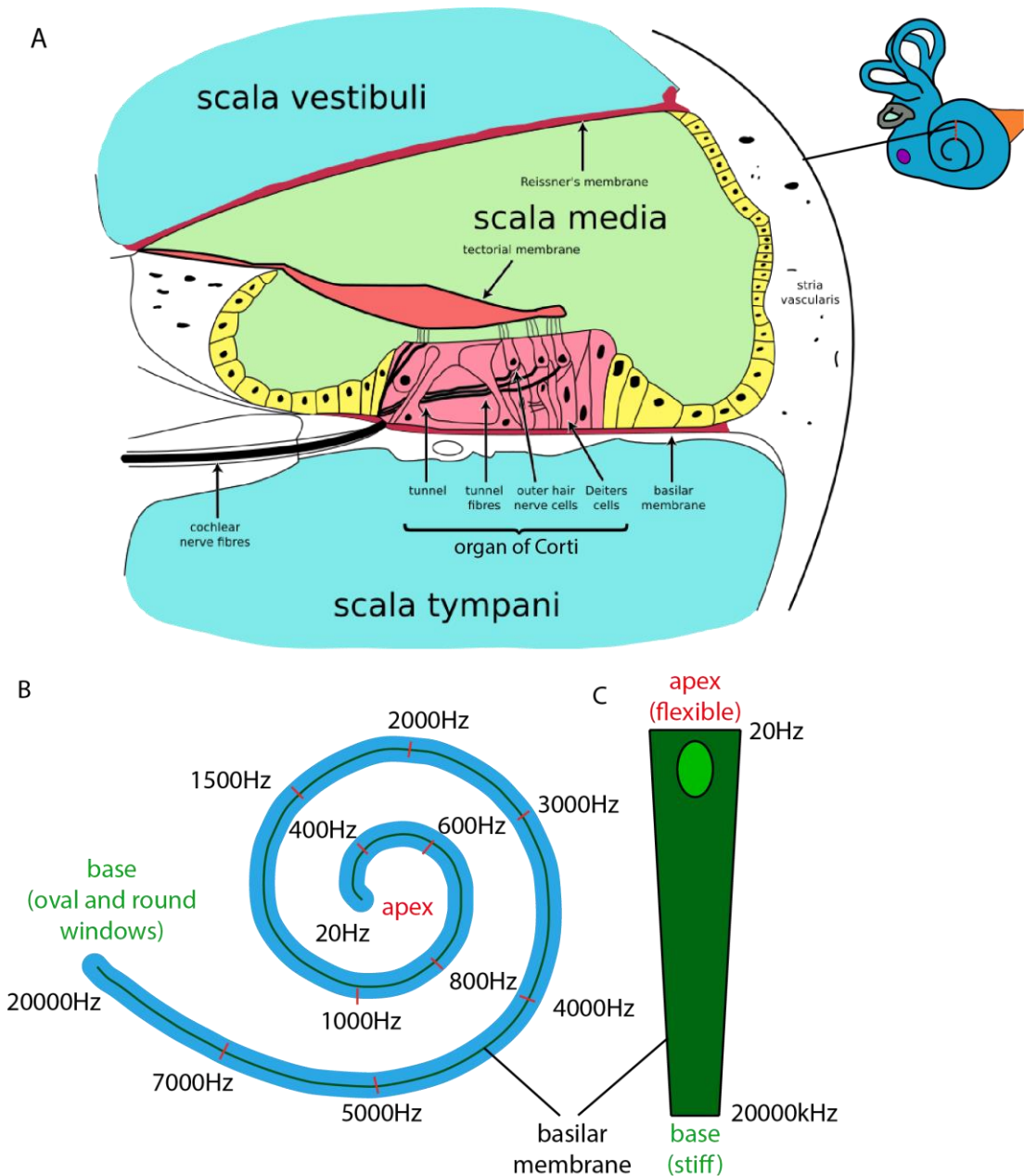


Figure 1.4: Anatomy of the cochlea and basilar membrane. (A) Cross section through the cochlea tube, showing the relative positions of internal structures. Adapted from: (Wikipedia, 2010) (B) Simplistic view of cochlea tube and basilar membrane, indicating the changing tonotopy of the membrane. (C) Top down view of uncoiled basilar membrane, showing wide and floppy apex (low frequencies) and thin, stiff based (high frequencies)

1.3.3 The Central Auditory Pathway

What is termed the central auditory pathway is split into two – the lemniscal and non-lemniscal/lemniscal adjunct. These pathways are essentially parallel but visit different regions of each brain area as they ascend. The lemniscal pathway, ending in the primary auditory cortex, is the primary pathway for transmission of sound information. In general, neurons along the lemniscal pathway tend to be sharply tuned, and maintain a tonotopic connection from area to area. In the non-lemniscal pathway, exact functions tend to be less well understood, but are likely complimentary in nature to the lemniscal conveyance of accurate auditory information.

A common neuron arrangement in the auditory system is the frequency band lamina/sheet (occasionally referred to – albeit overly simplistically - as an isofrequency sheet). Such a “sheet” consists of several 1000s flattened neurons, with each sheet responding to a narrow frequency range. The sheets are then arranged into a tonotopic gradient. (Fekete et al., 1984). Very often, this representation is not exactly linear, and will differ between species, with preference assigned to biologically useful frequency ranges (vocalisation, for example) (Suga and Jen, 1976, Winer and Schreiner, 2005, Garcia-Lazaro et al., 2015).

Auditory Nerve

The auditory nerve (part of the vestibulocochlear cochlear nerve/cranial nerve VIII) carries the electrical impulses from the cochlear spiral ganglion neurons (SNG) and the hair cells to the cochlear nucleus (CN) of the brainstem. The fibres of the nerve are arranged tonotopically, making isofrequency connections between the cochlea and the CN, and are short and well myelinated - information transfer is far quicker.

Cochlear Nucleus

The Cochlear Nucleus (CN) is the first stage of the central auditory pathway and one of the first areas of the auditory system to develop.

The two constituent nuclei (dorsal CN and ventral CN) are tonotopic, but process sound in different ways due to a difference in their prominent cell type (Brawer et al., 1974, Cant and Morest, 1979). The DCN contains mainly fusiform cells with a wide, branching dendritic tree. Inputs must then be summed for the response to be significant, resulting in the integration of incoming signals. The VCN meanwhile, is the opposite, consisting of mainly bushy cells where the auditory nerve synapses directly onto the soma of the cell. This means that inputs from the nerve are largely preserved from the original signal, allowing for easier binaural comparisons when the signal reaches the SOC. (Rhode and Greenberg, 1992).

As well as the lemniscal connection to the SOC, there exist direct projections of the cochlear nucleus to both the contralateral IC and MGB, non-lemniscal pathways which may represent some form of non-auditory processing, given that the two target areas have multimodal inputs (Malmierca et al., 2002, Schofield et al., 2014).

The primary auditory cortex feeds back, bilaterally, to the CN (Feliciano et al., 1995). Cholinergic cells of the SOC also project back to the CN, likely providing feedback in sound processing (Mellott et al., 2011). Interestingly, cholinergic projections to the CN were also seen from the pedunculo-pontine tegmental nucleus (PPT) and laterodorsal tegmental nucleus (LDT) (Mellott et al., 2011). Given the role of these areas in sleep and arousal, it is likely these connections represent a system to modulate sound processing during different states of the brain.

The CN is also the first instance of a the frequency band lamina cell arrangement, further arranged as a tonotopic gradient as can be seen throughout the lemniscal auditory pathway.

Complex signal processing takes place in the cochlear nucleus, with local CN circuitry filtering and lowering signal noise through inhibition, amplifying weak signals, and disinhibiting certain inputs, which sharpen/broaden cell responses as required by the environmental context (Berrebi and Mugnaini, 1991, Winer and Schreiner, 2005). By the time the signals leave the CN, they have been decomposed into several temporal, spectral and spatial streams, each to be processed by specific higher order areas.

Superior Olivary Complex

The next stage in the pathway is the Superior Olivary Complex (SOC). The number and size of sub-nuclei in the complex is dependent on species (4-9) (Moore and Moore, 1971), as is their relative representations, due to the different sound

processing requirements of different species. Like the CN and other stages, the whole complex can be generally subdivided further – in this case into the Medial Nucleus of the Trapezoid Body (MNTB), a Lateral SO, and a Medial SO, all of which are tonotopic (Winer and Schreiner, 2005). As a whole, the SOC is responsible for processing incoming sound from both areas to provide localisation cues, with evidence to suggest that high and low frequency sounds are localised by different mechanisms - differences in sound amplitude and by relative timings, respectively (Tollin, 2003).

The MSO is responsible for processing interaural time differences (ITD) to localise sound (Yin and Chan, 1990), It does this by integrating excitatory inputs from the ventral cochlear nucleus and more local inhibitory inputs from the MNTB, with relative timings providing information as to the sound source's location in space (Brand et al., 2002, Couchman et al., 2010). The LSO is also involved in sound localisation, but uses differences in sound amplitudes, or interaural level differences, to help localise the sound (Tollin, 2003).

The SOC, though also having ascending outputs to the LLN and IC (Cant and Benson, 2006, Schofield, 2005), also projects backwards to the cochlea and cochlear nucleus to control the properties of hair cells and neurons and thus modulate incoming signals as required, through negative feedback (Spangler et al., 1987, Warr, 1992).

Lateral Lemniscal Nuclei

The Lateral Lemniscal Nuclei (LLN) are the next stage in the central auditory pathway, located in the pons (Winer and Schreiner, 2005). Like the SOC, there are wide species differences. There are 3 nuclei, the dorsal, intermediate and ventral, which all contain neurons of specific neurotransmitters – while the dorsal nuclei has >85% GABAergic neurons, this percentage is only around 18% in the intermediate nucleus (Saint Marie et al., 1997). In the ventral nucleus, most neurons (around 65-90%) are inhibitory, with a histological study indicating extensive co-localisation of both GABA and glycine (Riquelme et al., 2001, Saint Marie et al., 1997). . Each nucleus may have a slightly different function and set of connections, but all project up to the inferior colliculus with predominantly inhibitory action (Shneiderman et al., 1988, Zhang et al., 1998).

The Ventral LLN (VNLL) represents an important source of inhibition to the inferior colliculus with the ipsilateral VNLL being an important source GABAergic inputs to the central nucleus. (Zhang et al., 1998, González-Hernández et al., 1996). The VLNN is known to receive significant input from octopus cells of the cochlear nucleus, cells

which respond excellently to the onset of sound; this pathway in turn controls the inhibitory action of the VNLL (Schofield and Cant, 1997, Nayagam et al., 2005). Together, the evidence suggests the VNLL is responsible for encoding the precise onset of sound, and thus controlling spike timing in higher auditory centres (Covey and Casseday, 1991).

The dorsal LLN (DNLL) is slightly different from the ventral and intermediate nuclei, in that it primarily receives inputs from the SOC rather than the cochlear nucleus (as well as commissural connections - likely inhibitory- from the contralateral DNLL), suggesting an involvement in the further processing and conveyance of binaural/sound localisation information (Shneiderman et al., 1988, Oliver and Shneiderman, 1989, Huffman and Covey, 1995).

The intermediate LLN is also an important source of inhibition to the IC, itself receiving and integrating excitatory inputs (cochlear nucleus) and inhibitory inputs (including the ipsilateral MGTB) (Huffman and Covey, 1995). Studies on the function of this area are not extensive, but due to the area's prominence in the echolocating bat, it may be involved in the types of sound processing associated with echolocation (Covey and Casseday, 1991).

Inferior Colliculus

General Properties of the Inferior colliculus

The inferior colliculus (IC) in the midbrain (Figure 1.5) is one of the largest auditory nuclei, and is considered a "hub" or main integration station in the auditory pathway. Inputs and outputs are numerous and multi-directional, – taking inputs from the CN, SOC, LLN and from all over the auditory cortex, as well as local and commissural connections (Oliver, 1987, Glendenning et al., 1992, Saint Marie et al., 1997, Winer et al., 1998). In its role as an auditory hub, the inferior colliculus takes in and integrates input from all these sources, then processes and passes the information on to the appropriate stations – either further up the primary pathway or feeding back to modulate the activity of previous nuclei. Glutamate and GABA are the principal neurotransmitter types for excitatory and inhibitory cells, respectively (Oliver et al., 1994, Merchán et al., 2005). Both excitatory and inhibitory neurons project to the contralateral IC (Chen et al., 2018). The commissural connections to the contralateral IC are important to the processing of sound; there is evidence for their involvement in modulating neuronal response gain, interaural level differences and the frequency

receptive fields of neurons (Malmierca et al., 2005a, Orton and Rees, 2014, Ono and Oliver, 2014).

A very recent publication has revealed that cortical input to the IC is not limited to the auditory system, with retrograde tracing in rats revealing some degree of connections from the visual, somatosensory, motor, and prefrontal cortexes (Olthof et al., 2019). These connections appear to target both excitatory and inhibitory neurons in the IC, and speak to the apparent variability of cortical feedback origin, even before the thalamic nuclei. Most likely, their purpose is to inform the IC of visual information, self-generated sounds, and modulate the IC's responses during certain tasks/behaviours. In a continuing trend, the IC can be further split into 3 main functional/anatomical zones – the central nucleus ICC/CNIC, lateral nucleus (LNIC,

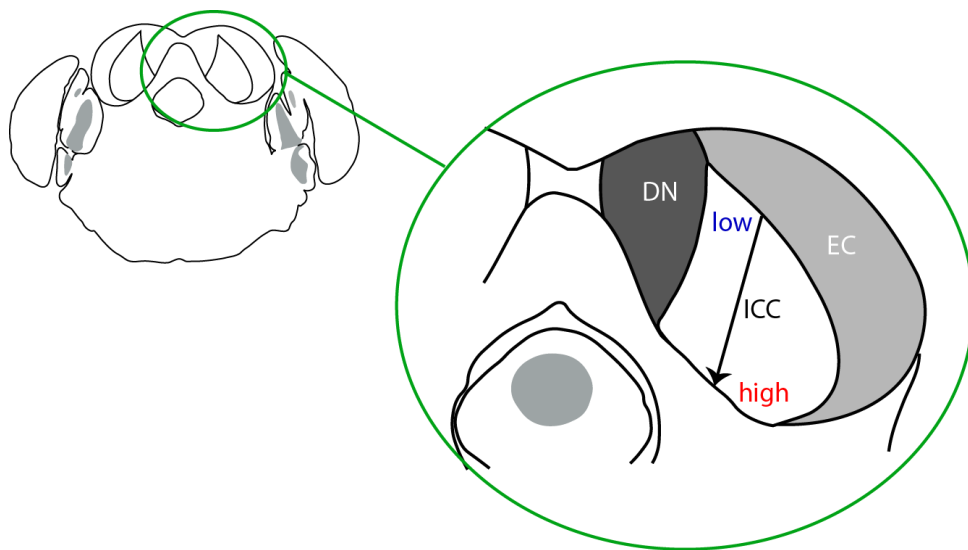


Figure 1.5: Mouse inferior colliculus (coronal view). 5.07cm anterior to bregma reference point. The direction of the tonotopic gradient of the ICC (Stiebler and Ehret, 1985). DN: dorsal nucleus. EC: external cortex (lateral nucleus)

sometimes called the external cortex) and Dorsal Cortex (DCIC) – see Figure 1.5 for a coronal slice through the mouse IC. Both areas predominantly receive ascending inputs (Chen et al., 2018).

A goal of neuroscience research is to classify neuronal types throughout the brain; doing so can shed light on mechanisms and circuitry underlying brain functionality and connectivity. Cell properties such as morphology, neurotransmitter expression, biochemical properties, and synaptic organisation are commonly used to define cell classes. With this information, we can start to determine the underlying circuitry and functional roles of the IC.

Cell Types of the Inferior Colliculus: Biophysical Properties

Neurons can be categorised by their electrical response properties, in turn determined by the nature of their ion channels. The firing properties of these neurons will determine their ability to respond to, pass on, and integrate incoming excitatory or inhibitory information.

Sivaramakrishnan and Oliver in the early 2000s did extensive work on the rat IC, and separated IC neuronal types in 6 distinct patterns based on their firing appearance and ion channel diversity on injection of a depolarising/hyperpolarising current (mimicking excitatory/inhibitory input respectively) (Sivaramakrishnan and Oliver, 2001). The study does not distinguish between IC areas. The vast majority of work in this area has been done in the rat (Li et al., 1999, Peruzzi et al., 2000), with some confirmation of similar patterns in the mouse (Reetz and Ehret, 1999, Basta and Vater, 2003). The properties of each neuronal type are summarised in the Table 1.1 table and Figure 1.6. A rebound spike is a phenomenon whereby a cell fires an action potential following termination of a hyperpolarising current.

Table 1.1 and Figure 1.6 are adapted from the aforementioned work by Sivaramakrishnan et al in 2001, based on 104 neurons in the rat, and is a good point of reference. While cells do appear nicely categorised, these exact cell types have not been confirmed in every species, nor their properties fully linked to morphology or other cell metrics. These studies do however serve to highlight the heterogeneity of IC biophysics. It may be that to some degree, the biophysical properties of auditory neurons are linked to dendritic complexity - it was observed that buildup-pauser neurons had relatively simple dendritic branching compared to other types, leading to an interesting avenue of research into causality (Peruzzi et al., 2000).

Table 1.1: Biophysical cell classifications in the inferior colliculus. Table adapted from Sivaramakrishnan and Oliver 2001.

Behaviour	Prevalence	Spike train appearance	Response to hyperpolarisation	Morphological links (relative to other cells)
Sustained-regular (S-R)	19.2%	Sustained response, regular ISI	Rebound spike	
Rebound regular (R-R)	10.6%	Regular ISI	Rebound spike and rebound	Somatic area > BP
Rebound adapting (R-A)	25%	Non-uniform ISI (increasing)	Rebound spike and rebound	Somatic area > BP
Rebound transient (R-T)	21.1%	Transient response	Rebound spike and rebound	Somatic area > BP
Buildup-pauser (B-P)	15.4	Pause before spike train, or after initial spike	Slower build-up to resting potential, no rebound spike	Somatic area <R, simplicity of dendritic branches <O, R
Onset (O)	8.6	Single spike	Rebound spike	

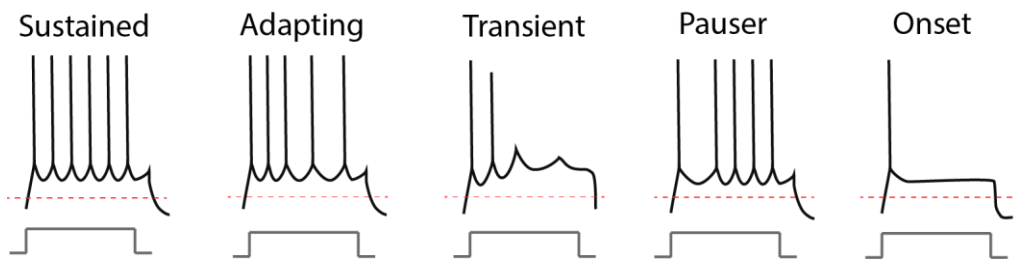


Figure 1.6: Classes of spiking behaviour after a depolarising current. Black: neuronal spike Grey: Injected depolarising current. Red: resting membrane potentials. Adapted from Sivaramakrishnan 2001, showing effects of depolarising current only (Sivaramakrishnan and Oliver, 2001)

In 2005, the biophysical properties of specifically GABAergic (inhibitory) IC neurons were investigated, with two principal types emerging (each with two subtypes)(Ono et al., 2005). “Tonic type” neurons displayed repetitive firing activity on depolarisation (similar to the “sustained” category from Sivaramakrishan et al). One subtype shows this behaviour with a slight adaptation, while the other displays the repetitive firing, but only after a prolonged delay. The other subtype (“transient”), match the transient class described previously – firing 2-3 spikes after the start of the depolarisation and then ceasing activity. Transient neurons either showed a depolarising afterpotential (hump) immediately after spiking, or hyperpolarised after the spike. While not matching exactly to the previous 6 classes system, there are similarities between the systems. As GABAergic neurons are decidedly less numerous than their glutamatergic counterparts, previous non-specific studies may have missed some smaller subclasses. An extensive study across multiple animals, using tagging techniques to determine cell type, may reveal a potential classification system based on biophysical properties alongside neurotransmitter type. This information would be highly useful in determining the mechanisms behind the functionality of each cell type.

Cell Types of the Inferior Colliculus: Morphology

In terms of cell morphology, there are generally two clearly identifiable types – though these can differ a little in exact definition between species. The first of these is the disc-shaped cell (Oliver and Morest, 1984). As the name suggests, their dendritic fields spread out into only 2 of 3 dimensions (see Figure 1.7A, left), so that sheets of these cells form the characteristic layers of the ICC (Figure 1.7B). These cells have been observed in most species studied, such as the mouse (Meininger et al., 1986), the rat (Faye-Lund and Osen, 1985) and the cat (Oliver et al., 1991).

The remaining percentage of cells are generally termed “stellate cells”, having a more spherical, rounded dendritic field (Figure 1.7B, right) that spans multiple layers of disc-shaped cells and are thus likely involved in interlayer communication and integration (Oliver and Morest, 1984, Meininger et al., 1986, Oliver et al., 1991).

Despite the (relatively) clear morphological distinction, this property does not correspond to a particular neurotransmitter profile, nor with their biophysical responses.(Peruzzi et al., 2000).

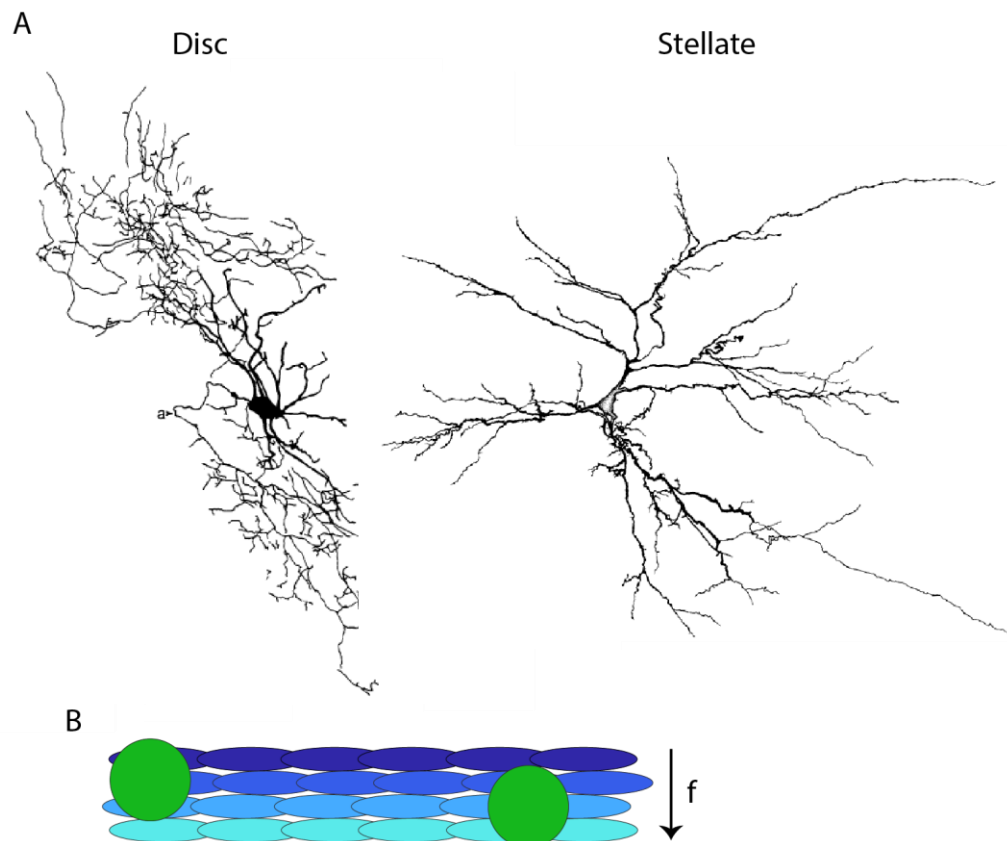


Figure 1.7: Two principal inferior colliculus cell morphologies. (A) Shape of dendritic fields in a disc shaped (left) and stellate cell (right), images from (Oliver et al., 1991) (B) Arrangement of disc shaped (blue) and stellate (green) cells that create frequency band lamina in the ICC. Frequency tuning changes with successive layers (f, downward arrow).

Cell Types of the Inferior Colliculus: Neurochemical expression

IC neurons can also be categorised based on their neurotransmitter synthesis. Approximately 20-25% of IC neurons are GABAergic and thus have an inhibitory action (Oliver et al., 1994, Merchán et al., 2005). These are of particular interest and are the focus of most research in this area, as inhibition will prove to be an important element of sound tuning. The remaining 75% are excitatory, glutamatergic neurons, expressing VGLUT2 (Ito et al., 2011). GABAergic and glutamatergic populations display similarly heterogeneous responses to pure tone sound, but may differ in their responses to amplitude modulated sounds; GABAergic cells also display higher spontaneous firing rates (Ono et al., 2017).

Of the GABAergic neurons, there is evidence to suggest 2-4 distinct classes (Ono et al., 2005, Ito et al., 2009, Geis and Borst, 2013, Beebe et al., 2016). One of the most commonly recognised distinctions is between the Large (LG) and small (SG) neurons. LG cells (diameter $>16.5\mu\text{m}$) were found to contain VGLUT2 axosomatic endings (Ito et al., 2009). Their smaller counterpart (diameter $<10.7\mu\text{m}$) lack the VGLUT2 endings

(Ito et al., 2009). These types exist in different proportions in each area of the IC, and dendritic morphology (stellate or disc) does not predict which type a cell will be (Oliver et al., 1994).

Studies have shown that the majority of GABAergic neuron projecting forward to the medial geniculate body are of the LG type, suggesting they play an important role conveying sound information along primary auditory pathway. The evidence suggests an integrating function; the cells are large, have a relatively low input resistance, receive short-latency excitatory inputs, and have short first spike latencies (Geis and Borst, 2013). The feedforward inhibition they generate (potentially reaching before any excitatory signals) could be a potential mechanism of filtering and shaping sound signals as required.

A recent study sought to further classify GABAergic neurons, and found 4 classes based on the presence of VGLUT2 and perineural nets (PN) [Beebe, 2016]. VGLUT2+, PN+ neurons are thought to correspond with the LG neuron class, with perineural nets exerting a neuroprotective effect and restricting plasticity, essentially “locking in” these cells to the circuit, which speaks to an essential and consistent role in conveying sound signals. Additional classes were VGLUT2+/PN-, VGLUT2-/PN+ and GABA only – it is speculated that these are the “true interneurons” of the IC, having only local connections (Beebe, 2016).

In short, cells in the IC can be categorised based on a number of properties, which also speak to different aspects of their functionality. However, as of yet there is no single, unified classification system that incorporates all variations and categorises all cells into distinct types with distinct functions. Such research would require a great amount of multi-dimensional data, and if properties continue to exist on a spectrum (size etc), the task also requires agreement on thresholding

Central Nucleus

The central nucleus of the inferior colliculus (ICC) is by far the most studied sub-nucleus of the inferior colliculus. Being a key component of the central auditory pathway, it is highly tonotopic (Figure 1.5), with frequency band lamina the most striking cellular feature (Schreiner and Langner, 1997). It primarily receives ascending input from the brainstem auditory nuclei, – the dorsal and ventral cochlear nuclei and the lateral lemnisci nucleus (monoaural information) and the SOC (binaural information) (Brunso-Bechtold et al., 1981, Malmierca et al., 2005b, Loftus et al., 2010). These inputs are not distributed evenly however, and appear to be dependent

on the frequency of the sound (Aitkin et al., 1985, Maffi and Aitkin, 1987). The wealth of connections from sub-collicular auditory nuclei (each with demonstrated information specialities), supports the role of the ICC as an integrator, processing multiple dimensions of auditory information and feeding this forward to the thalamus. LG neurons are more numerous here than in other IC parts, further supporting the importance and relevance of their tectothalamic connections to the ICC's functionality. These cells are randomly distributed throughout the structure (Ito and Oliver, 2012).

The ICC is comprised of frequency band lamina, composed of disc-shaped cells. Stellate cells, with their wider profile, cover multiple layers with their dendritic field and provide a means of communication between layers.

In terms of frequency tuning, the majority of ICC neurons are frequency tuned, being part of a frequency band lamina – but the exact characteristics or “sharpness” of this tuning is variable. A gradient of tuning sharpness exists across frequency band lamina – sharper tuned neurons are found in the centre, with neurons responding to a wider range of frequencies as we move outwards (Ehret et al., 2003). Gradients are also seen in onset latency (time to respond to the sound), threshold needed for a neuron to respond, and periodicity (preferred sound modulation frequency) (Langner et al., 1987, Schreiner and Langner, 1988).

Current literature on the central nucleus and its responses to sound is extensive, methodical and has been instrumental to our understanding of the auditory system as a whole – spectral and temporal processing will be covered in a later section. However, the role of the lateral and dorsal nuclei has been somewhat neglected, and as such a lot of the subtleties of the area's function in auditory coding may not be well understood.

Lateral Nucleus/External Cortex

The lateral nucleus (or external cortex) is distinguished from the central nucleus by the lack of an isofrequency layered cellular structure, and overall lower cell density. It does not contain disc shaped cells, and instead has two to three layers – a fibrous outer layer, and at least one inner layer of small cells (Faye-Lund and Osen, 1985, Oliver, 2005). The lateral nucleus receives input primarily from the medullary dorsal column nuclei, and the trigeminal system of the pons, as well as the LLN and descending projections from the auditory cortex. (Aitkin et al., 1981, Winer et al., 1998, Bajo et al., 2007). Unlike the ICC, the area is not strictly tonotopic, and neurons have long latencies and broad spectral tuning (Aitkin et al., 1975, Aitkin et al., 1981).

Evidence from the guinea pig and the owl suggests the area is involved in localising sound with respect to our body (Binns et al., 1992, Singheiser et al., 2012). Future literature may shed further light on the role of the lateral cortex within the IC and the auditory system as a whole.

Dorsal Cortex

The DCIC comprises of a layered structure similar to the lateral cortex (Morest and Oliver, 1984), though recent literature in the mouse suggests the DCIC is far smaller and that the IC extends further than previously believed (Barnstedt et al., 2015) This is not yet observed in other species. Layer V of the auditory cortex has significant projections to the DCIC - thought to modulate learning-induced auditory plasticity (Bajo et al., 2007, Bajo et al., 2010) - as well as a number of commissural and local connections (Saldana and Merchan, 2005). The dorsal cortex appears to be involved in speech/vocalisation, with its broadly tuned neurons very receptive to vocal stimuli over other noises (Aitkin et al., 1975, Aitkin et al., 1994). Frequency gradients have also been observed to some degree, and the area is likely to have a modulatory effect, due to auditory cortical feedback (Barnstedt et al., 2015) Similar to the lateral cortex however, the frequency range covered by the DCIC is incomplete, lacking higher frequency representations (Romand and Ehret, 1990). Literature has also demonstrated that the area suppresses responses to frequently heard sounds while enhancing novel stimuli, suggesting a role of the DCIC in aiding the detection of novel environmental sounds (Lumani and Zhang, 2010, Patel et al., 2012). Though the picture is incomplete, the DCIC would appear to play a supporting, modulatory role in the auditory pathway.

Notes on The Non-Lemniscal Components of the IC

In general, the lateral and dorsal cortexes are less well understood in terms of their spectral and temporal coding. There are several potential reasons for the lack of literature on these structures as compared to the ICC. Firstly, they are not part of the central pathway, which tends to be the focus of most research. Secondly, the non-lemniscal components do not follow the clear tonotopic gradient as seen in the ICC, , and at least in the dorsal cortex, may actually bleed into the ICC's gradient – so identification of patterns may be inconsistent between studies. Thus, the area does not present a particularly attractive or easy area of study.

Medial Geniculate Body

After the inferior colliculus, auditory signals travel to the thalamus. The mammalian thalamus contains many different nuclei, each dealing with a specific area of neural processing (sensory, motor, association or interlaminar). The Medial Geniculate Body (MGB, the last “stop” before the AC) deals with audition, with its counterpart the Lateral Geniculate Nucleus dealing with vision. Its inputs are primarily from the inferior colliculus, thalamic reticular nucleus, and the auditory cortex, though as we will see, the exact nature of these inputs is dependent on the MGB subdivision (Calford and Aitkin, 1983, Crabtree, 1998, Winer et al., 2001). In humans, the MGB’s primary function is to modulate sound encoding to aid speech recognition, based on external inputs from cortical and limbic systems (Winer et al., 2001, von Kriegstein et al., 2008). Similarly to the CN, evidence has been found for PPT/LDT connections to the MGB, and so across species the area likely modulates perception of sound during various brain states (Motts and Schofield, 2010).

The proportion of GABAergic neurons varies between subdivision. In the cat, the proportion of GABAergic neurons is 33% in the ventral division, 26% in the dorsal, and 18% in the medial, suggesting differences in sound processing and the role of thalamic inhibition in their respective targets (Huang et al., 1999, Huang and Winer, 2000). Cortical input is much stronger here than in the inferior colliculus (Winer and Schreiner, 2005). The dominant cell type is variable between subdivisions, of which there are three. Differing from the inferior colliculus, the MGB has fewer descending inputs, having mainly ascending and ipsilateral projections, and also has a variety of cell types/morphologies (Winer, 1992). Once again, there is a high degree of species variability in size, with the MGB being largest in carnivores, and the exact internal circuitry also varies (Winer and Schreiner, 2005).

The Ventral MGB is the primary nucleus and part of the lemniscal pathway, containing a tonotopic gradient as is typical of other nuclei on the primary pathway (Imig and Morel, 1985). As the next stage in the lemniscal auditory pathway, it receives tonotopic input from the ICC, and is fact somewhat similar to the IC aside from an increased cortical input and more varied local response (Andersen et al., 1980, Winer and Schreiner, 2005, Hackett, 2011). The bushy tufted neuron is the prominent neuronal type in this division, whose dendritic fields are aligned to create a laminar structure similar to the layers of the ICC (Clerici and Coleman, 1990, Clerici et al.,

1990). Smaller stellate cells have been observed in varying proportions between species (Morest, 1971, Winer et al., 1999, Clerici et al., 1990).

The vMGB projects primarily to layer IV and lower layer III of the primary auditory cortex and other tonotopically organised areas of the AC, continuing the lemniscal pathway (Lee et al., 2004, de la Mothe et al., 2006, Smith et al., 2012). Research in the mouse vMGB has revealed the presence of two sub compartments of the vMGB, finding that axons from the medial vMGB (tonotopically organised along the medio lateral axis) project to the anterior auditory field (AAF), while those in the lateral part (tonotopic along the dorso-ventral axis) projected to the A1 (Horie et al., 2013). These results strongly suggest parallel thalamic inputs of sound information to A1 and AAF (at least in the mouse), and a distinct functional role for these cortical areas and the thalamic areas these connections arise from.

There is evidence of gradients for synchronisation to repetitive stimuli, responses to broad band stimuli and general temporal response properties (Rodrigues-Dagaeff et al., 1989).

The dorsal MGB's primary inputs are the dorsal cortex of the IC, and the lateral tegmental area (Calford and Aitkin, 1983). The dMGB is essentially the parallel to the dorsal IC – having long latencies and broad tuning curves (Winer and Schreiner, 2005). The dMGB has more diverse functional and spatial cortical targets, projecting to cortical layers III and IV like the ventral division, but instead to secondary auditory areas, a connection potentially involved in auditory spatial processing (Kimura et al., 2003, Kimura et al., 2004, Smith et al., 2012). It may also be involved in attention and more general, global thalamic control of cortical excitability (Winer et al., 2005). This division also contains bushy cells like the ventral division, but these are not arranged in layers, and medium stellate cells are numerous (Clerici et al., 1990, Winer et al., 1999).

The medial division of the MGB appears unique amongst auditory nuclei. It has only a very coarse tonotopic gradient, and receives input from a variety of non-auditory areas, plus the lateral IC (Rouiller et al., 1989). It has a diverse range of neurons morphologies, including magnocellular neurons (small soma, few thick dendrites in a stellate-type arrangement), medium stellate cells, and bushy cells (Clerici et al., 1990, Winer et al., 1999). They also have a wider size range than other divisions and vary in their dendritic branching and physiological properties (Smith et al., 2006). The MGB also has the largest diversity of projections in the MGB – connecting a broad range

of tonotopic and non-tonotopic cortical areas, and interestingly terminating in layer I (and layer VI), unlike the classical thalamic target of layer IV observed in other divisions (Rouiller et al., 1989, Huang and Winer, 2000, Jones, 2003, Lee and Winer, 2008a, Lee, 2015). Via a further connection to the amygdala, the mMGB becomes involved in autonomic learning related to auditory cues (Iwata et al., 1986, LeDoux et al., 1991). There is good evidence for a direct, high speed, non-lemniscal inputs from the CN, thought to be involved in priming the auditory cortex for rapid decision making, given this area's connections to various non-auditory areas (Anderson et al., 2006, Schofield et al., 2014). Given the high heterogeneity of the mMGB's cell types and connections, further research into its functionality would be an interesting point of research for expanding our knowledge of the non-lemniscal auditory system.

As a whole, the MGB appears to be more related/involved in higher level processes associated with sound (learning, speech processing etc) (Edeline, 2003, von Kriegstein et al., 2008). This is logical, given its proximity and multitude of connections to the final stage in the pathway, the auditory cortex. The mMGB and dMGB appear to augment the function of the auditory thalamus beyond the traditional thalamocortical relay of sound information (i.e. the vMGB). With the wealth of experimental techniques now available, their exact functions can be explored further to enhance our understanding of the subtleties of the auditory pathway and its position and role within the brain as a whole.

Auditory Cortex

The auditory cortex (AC) is a cortical structure comprised of many subdivisions, and the highest level of the auditory pathway. With its position as the highest point in the auditory pathway, and in its multiple connections with non-auditory areas, the auditory cortex appears responsible for the processing and perception of sounds, decoding the information within and contextualising within the animal's environment. The wealth of descending connections to sub-cortical auditory areas represent ongoing feedback mechanisms, modulating how incoming sound is received based on the current environment.

As with other cortical structures, the auditory cortex is arranged in 6 layers (though in the mouse, layers II and III are indistinguishable, and are referred to as layer II/III). Each layer is distinct in its neuronal and neurotransmitter type, and inputs/outputs (thalamic, commissural, cortical, corticofugal projections). Descriptions of each layer

can be derived from Figure 1.8 and summarised in Table 1.2 (with A1 specific connections noted in bold).

The two main cell classes in the cortex are the excitatory pyramidal/principal neurons (around 85%) and interneurons (generally inhibitory, around 15%). (DeFelipe and Fariñas, 1992, Kanari et al., 2019).

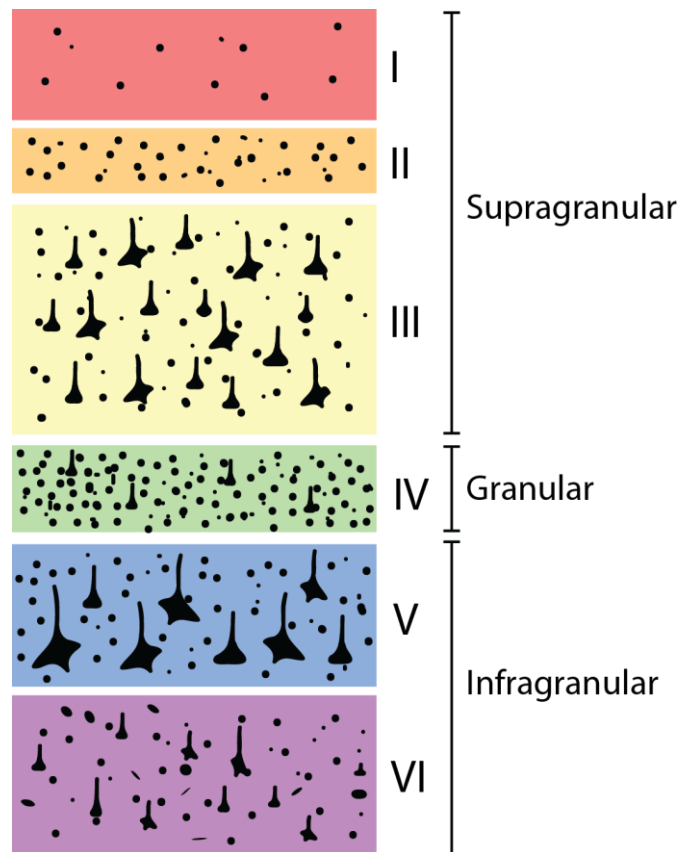


Figure 1.8: Cortical layers. Relative size, shape and distribution of cells (black) are indicative of cellular makeup of layers. Smaller, round cells: granule cells. Larger/shaped cells: pyramidal

Table 1.2: Layers of the auditory cortex. Primary AC specific inputs and outputs are noted in **bold**. References: (Kelly and Wong, 1981, Huang and Winer, 2000, Smith and Populin, 2001, Read et al., 2002, Winer, 2006, Lee and Winer, 2008c, Wallace and He, 2010).

Layer	Cell types	Cell density	Inputs	Outputs
I	GABA	Very sparse	mMGB, AC	L II
II	Pyramidal (s), GABA	Sparse		L II/III/IV, cortex
III	Pyramidal (m), GABA	Dense	vMGB , cortex	Commissural
IV	Pyramidal (L), GABA	Dense	vMGB	Commissural
V	Pyramidal (L), GABA	Medium density	L I/III/IV	MGB, IC, Pons
VI	Pyramidal (several types), GABA (several types)	Low-medium density	LI, mMGB	MGB
Layer	Cell types	Cell density	Inputs	Outputs
I	GABA	Very sparse	mMGB, AC	L II
II	Pyramidal (s), GABA	Sparse		L II/III/IV, cortex
III	Pyramidal (m), GABA	Dense	vMGB , cortex	Commissural
IV	Pyramidal (L), GABA	Dense	vMGB	Commissural
V	Pyramidal (L), GABA	Medium density	L I/III/IV	MGB, IC, Pons
VI	Pyramidal (several types), GABA (several types)	Low-medium density	LI, mMGB	MGB

The diversity of auditory cortical neurons is vast. In a recent study of the mouse visual cortex, single cell transcriptomics revealed 42 different types of neuronal cells (23 GABAergic and 19 glutamatergic) - and this is a single species (Tasic et al., 2016).

Studies are still ongoing in an attempt split these groups neurons and gain more knowledge of cellular circuit and information processing. A recent study identified 17 different kind of pyramidal cells in the rat somatosensory cortex, based significantly on their dendritic arborisation (Kanari et al., 2019). Neuron classes may also be layer-specific - in just layer V of the visual cortex, a recent study revealed 3 types of pyramidal neuron, receiving different inputs, and having different functions (Kim et al., 2015).

Interneurons are a diverse class of cell with many sub-types, though the vast majority are inhibitory in nature, using the neurotransmitter GABA (Markram et al., 2004). Spiny stellate cells are a known class of excitatory (glutamatergic) interneuron that are seemingly specialised to process thalamic input. They are found only in layer IV and relay thalamic input to layers II/III (Feldmeyer et al., 2002). Based solely on morphology, there are many identified types of interneurons, including basket (large, small and nest), chandelier, Martinotti, bipolar, double bouquet, bitufted, and neurogliaform cells (Markram et al., 2004). Further classifications are possible based on electrical, ion-channel, molecular, and synaptic properties, with such a diverse range of neurons speaking to a dynamic and variable role of inhibition within different cortical circuits (Markram et al., 2004).

Inhibitory interneurons can be classified based on their expression of certain proteins, here, three well known and non-overlapping classes are Parvalbumin (PV), Somatostatin (SOM) and Vasointestinal Peptide (VIP), accounting for the majority of inhibitory interneurons (Xu et al., 2010, Rudy et al., 2011). PV+ neurons comprise around 40% of the GABAergic neuron population (Xu et al., 2010, Rudy et al., 2011). These are generally of the basket and chandelier morphology and make powerful inhibitory synapses with pyramidal and other PV+ cells – in the context of sensory systems, they are thought to provide gain control by pooling their local input and feeding it back. (Xu et al., 2010, Kubota et al., 2016, Moore and Wehr, 2013). SOM neurons make up around 30% of the GABAergic population and are usually of the Martinotti cell type (Lee et al., 2010). They have high levels of spontaneous activity, and being wired to both receive and provide strong inhibition, they are thought to modulate fine scale up and down regulation of overall inhibition levels in the cortex (Fanselow et al., 2008, Urban-Ciecko and Barth, 2016). VIP+ cells are the least numerous type, but appear to inhibit both PV+ neurons (weakly) and SOM+ neurons (strongly) – this disinhibition would appear to be important in specific behavioural conditions (Pi et al., 2013, Lee et al., 2013, Fu et al., 2014, Karnani et al., 2016)

As a general rule, pyramidal and interneurons may be classified in neural recordings based on the shape of their waveform and their temporal firing properties. This has led to pyramidal cells being referred to as “broad/regular spiking” cells, with interneurons, having a narrower waveform and faster spiking often known as “narrow/fast spiking” (McCormick et al., 1985, Connors and Gutnick, 1990, Frank et al., 2001). This classification will be used in the upcoming results chapters of the

thesis. The interaction of pyramidal cells and interneurons creates the complex circuits throughout the cortex and its layers. Together, they maintain a balance of excitability and inhibition within the cortex and shape neuronal responses (such as dynamic frequency tuning).

The auditory cortex is not a single homogenous area – it can be split into areas based on structure and function. Areas can be grouped into central (or core) regions and secondary (often termed belt, or parabelt) regions, generally grouped around the core (Hackett, 2011). The number of sub-areas identified, as well as their core/belt classification, can vary between species, though the primary auditory cortex A1 is always present in some form as a core area Figure 1.10 (Hackett, 2011).

Defining a core auditory region is dependent on a number of features (outside of spatial arrangements) such as: good, low latency responses to pure tones, narrowly tuned, with a “best” frequency; dense thalamic inputs from the vMGB, and dMGB (i.e. the lemniscal pathway), architecture matching other sensory cortexes (such as well-developed layer 4), and characteristic chemical expression (i.e. cytochrome oxidase, acetylcholinesterase, and parvalbumin) (Kaas and Hackett, 2000). They are also tonotopically organised, though this is not a feature restricted to core areas.

The core areas appear to function in parallel, receiving parallel inputs from the thalamus, however, they are all densely interconnected, and can be serially connected with belt regions (input tends to flow outwards from the core) (Kaas and Hackett, 1998).

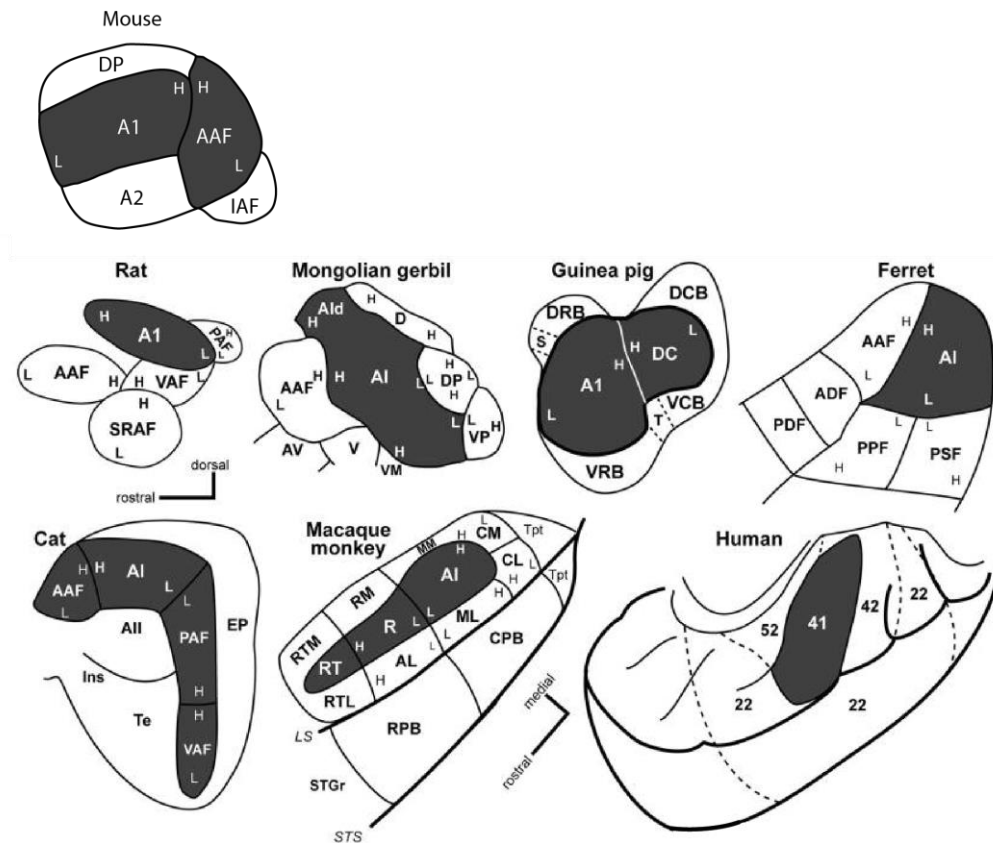


Figure 1.9: Maps of primary and core auditory cortical areas. Primary areas are grey shaded. “H” and “L” indicate high and low frequency ends of a tonotopic gradient, respectively. A1, primary auditory cortex; A2, secondary auditory cortex; IAF, insular auditory field; DP, dorsal posterior field; AAF, anterior auditory field; VAF, ventral auditory field; PAF, posterior auditory field; SRAF, suprarhinal auditory field; D, dorsal (field); VP, ventroposterior (field); V, ventral (field); AV, anteroventral (field); DC, dorsocaudal (area); DCB, dorsocaudal (belt area); VCB, ventrocaudal (belt area); DRB, dorsorostral (belt area); VRB, ventrorostral (belt area); ADF, anterior dorsal field; PDF, posterior dorsal field; PPF, posterior pseudosylvian field; PSF, posterior suprasylvian field; EP, posterior ecosystem gyrus; Te, temporal cortex; RM, rostromedial area; RTM, rostrotemporal medial area; RTL, rostrotemporal lateral area, RPB, rostral parabelt area; CL, caudolateral (belt area); CM, caudomedial (belt area); MM, middle medial (belt area); AL, anterolateral area; CPB, caudal parabelt area; Tpt, temporal parietotemporal area; STG, superior temporal gyrus. Mouse map adapted from (Guo, 2012), remaining Image from (Hackett, 2011)

While the majority of inputs to the AC come from the MGB, not all areas of the MGB connect to all areas of the AC, and as a general rule, the vMGB projects predominantly to tonotopically organised core zones such as the A1, the dMGB to secondary areas, and the mMGB to all (Huang and Winer, 2000, Hackett, 2011, Smith et al., 2012).

The AC also contains many commissural and local connections – a study in the cat found that each of 13 primary and secondary auditory areas studied received varied input from 3-6 contralateral AC areas and 5-8 ipsilateral areas. (Lee and Winer, 2008c, Lee and Winer, 2008b). Such commissural connections are important for creating a unified perception of the auditory space.

The AC has a great many descending connections to various subcortical auditory nuclei. This feedback is responsible for modulation of neuronal properties in order to augment sound perception dynamically.

The corticothalamic tract originates from layer VI, and connects back to the MGB in a matter similar to the ascending systems – A1 connects tonotopically to the vMGB, while secondary fields such as the AAF project to both the vMGB and d/mMGB (Budinger et al., 2000). Recent evidence suggests the A1-vMGB connection connected to accurate detection of harmonics, and important feature for perception of sounds from distinct sources within a complex auditory scene (Homma et al., 2017).

Most corticocollicular connections arise from the A1 (layer V), with a form of tonotopy – projections from high frequency A1 areas connect onto the ventromedial IC, while those from low frequency connect to dorsolateral areas, both contra and ipsilateral (ipsilateral more numerous). (Winer and Prieto, 2001, Bajo et al., 2007). Connections from secondary/belt auditory areas also exist, though are less strong and more variable than those from the A1 (Herbert et al., 1991). The existence of direct cortical connections to the ICC is still debated, with some studies showing no connections, but others indicating the opposite (Herbert et al., 1991, Saldana et al., 1996, Bajo et al., 2007). It is possible the differences are due to the exact definition of each IC subdivision – inputs may be arriving at the IC area borders.

It would appear that the corticocollicular connections function to modulate responses, either directly in the IC, or by contacting cells in the IC which further project up and down to other auditory areas such as the superior olive (Groff and Liberman, 2003). Experimentally, it has been found that activation of these A1 projections sharpens/amplifies responses to that A1s area frequency (Zhang and Suga, 1997, Gao and Suga, 1998). There is also evidence for the connections being involved in sound localisation (Nakamoto et al., 2008). This is a useful feature of the auditory system, allowing the animal to focus in on contextually/behaviourally relevant sounds – for example, speech, or predictor calls. One of the auditory cortex's roles thus appears to be the provision of feedback appropriate to the current context, into order to increase the effectiveness of sound perception for any given situation. As such, there is recent evidence demonstrating the corticofugal connection mediates a sound-induced, instinctive "flight" behaviour in mice (Xiong et al., 2015)

There evidence that the auditory cortex also connects via layer V bilaterally with the SOC, specifically to the ventral nucleus of the trapezoid body and the LSO, the former

of which is clearly tonotopic, speaking to a potential feedback function in the control of incoming binaural information (Feliciano et al., 1995, Budinger et al., 2000). As the SOC also innervates the cochlea outer hair cells, the auditory cortex may have an indirect effect on cochlea amplification (Spoendlin, 1969).

Again from layer V, the auditory cortex (primarily A1), has connections with the cochlear nucleus – to the dorsal region and extensively to the granule layer domain surrounding the ventral area (Feliciano et al., 1995, Schofield and Coomes, 2005, Meltzer and Ryugo, 2006). A1 connections to the brainstem can modulate the incoming information close to the source, aiding in the perception of behaviourally relevant sounds. Evidence from mice has shown that A1 modulation of the DCN results in changes to the best frequencies of its neurons, a possible mechanism for enhancing perception of certain sounds (such as predatory calls or important species-specific vocalisations) (Kong et al., 2014)

The auditory cortex also projects to a number of non-auditory areas, such as the amygdala (LeDoux et al., 1991), superior colliculus (Paula-Barbosa and Sousa-Pinto, 1972, Druga and Syka, 1984) and basal ganglia (Reale and T.J, 1983) implying a role in autonomic, animal behaviour and other systemic effects. Crucially, the AC is plastic, and can learn and be modified, with this plus extensive interconnectivity making it difficult to truly define distinct, strict and unmoving zones.

1.4 Principles of Neuronal Coding

1.4.1 Neuronal Coding Mechanisms

Decoding and Encoding of Stimuli

If organisms perceive and respond to various external stimuli in distinct ways, it stands to reason that each stimulus was represented differently in the brain. Evidently, the information will be represented by neuronal activity (i.e. action potentials and resultant “spiking” of electrical activity), and exactly when, where, how, and with “who” a neuron responds makes up the study of neural coding.

Decoding describes how researchers (in the form of an artificial computer-based decoder), or a part of the living brain, can determine the nature of a presented stimuli or resultant behaviour, when provided with a set of neuronal responses. The response of a neuron can be highly complex and multi-dimensional, but it may be that some variables (e.g. the average firing rate) are more important for determining the stimuli. Knowing which parameters of a neuron/neuronal population response are important

for decoding a sound stimulus will be crucial information for creating a midbrain implant – where neurons should be stimulated to replicate the same pattern.

Encoding refers to the opposite concept - how the neurons generate their responses to stimuli. A population of neurons activating together, as opposed to a single neuron, is likely to contain more information about a stimulus, or can encode a range of stimuli, due to the inherent higher dimensionality in their potential responses.

Basic Coding Mechanisms

There are several basic methods whereby a neuron can change its output to represent a stimulus. The explanations below are adapted from the 2015 review by Panzeri et al, (Panzeri et al., 2015), with Figure 1.10 providing graphical representations of the concepts described. Note that the concepts described below are merely building blocks in generating the incredible complexity involved in the translation and coding of stimuli by neuronal populations, throughout the brain's pathways.

A *firing rate code* means that the information is conveyed in the average firing rate of a neuron, and does not depend on the exact pattern of the spikes (Shadlen and Newsome, 1998). The window for this averaging may also be important. A *temporal spike code*, on the other hand, conveys information in the exact timing pattern of the spikes (Ince et al., 2013). Somewhat related to this, information can be conveyed by the delay between the stimuli and the neuron response, known as a *latency code* – this is used in the auditory system in the context of intensity and stimuli localisation (Eggermont, 1998, Panzeri et al., 2001).

All these concepts are combined, and expanded, within a neural population. The heterogeneity of coding of the constituent single units lends itself well to expanding the range of information that can be conveyed. As well as utilising the concepts described above, the pattern and timing in which neurons in a population fire may be important to convey stimulus information (Havenith et al., 2011) (Figure 1.10A), and gaps in firing (silent periods) may indicate the absence of that neuron's preferred stimuli (Schneidman et al., 2011).

Neuronal coding is also influenced by global oscillations in the LFP (Local Field Potentials - lower frequency electrical activity of the brain), which can modulate the neurons' excitability, or susceptibility to firing, adding further layers of complexity (Figure 1.10E). This is a highly important and influential mechanism in the auditory cortex, and will be expanded upon in a later section.

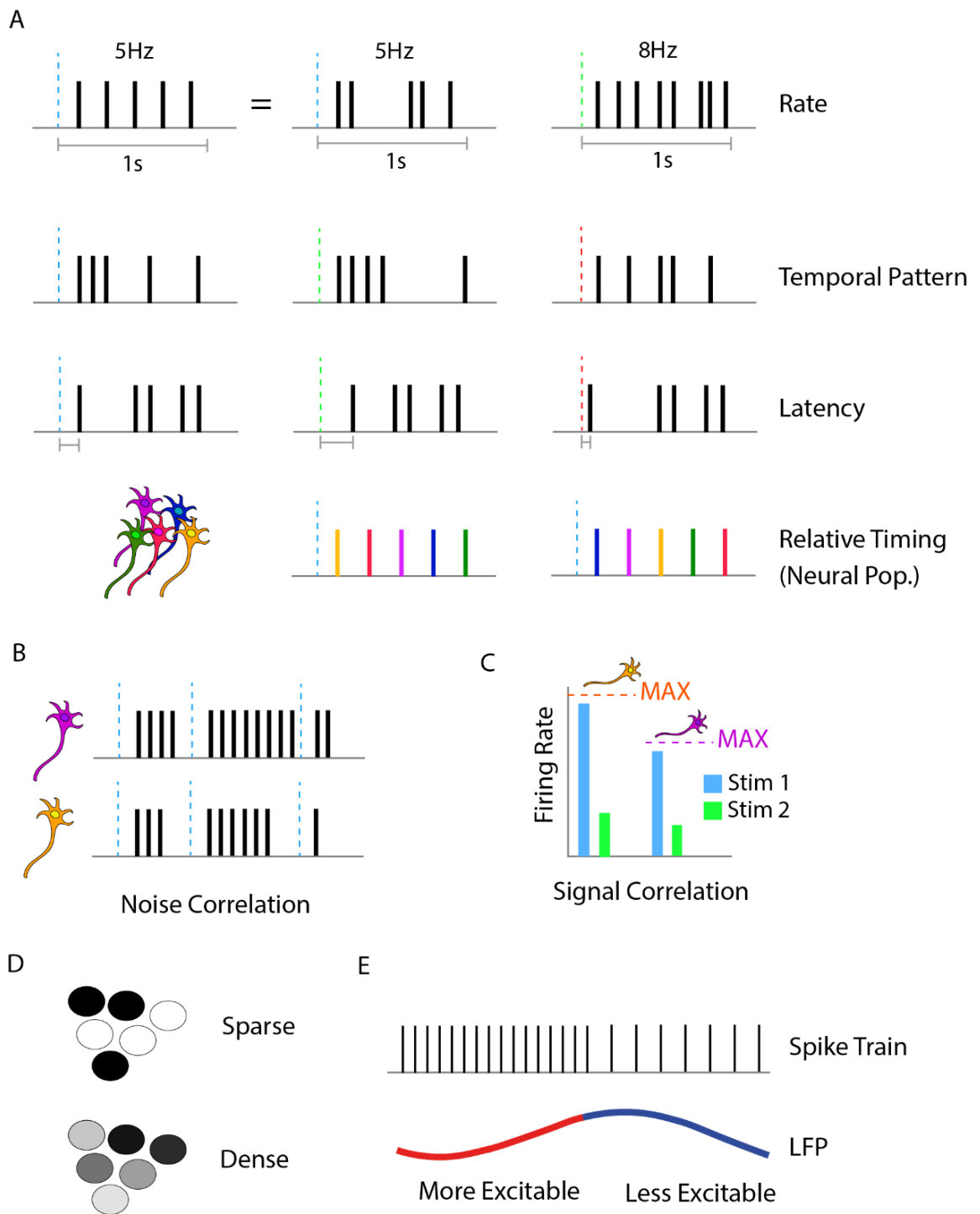


Figure 1.10: Mechanisms of neural coding. Vertical black lines indicate a hypothetical spike (A) From top to bottom: Rate coding, temporal pattern, Latency, Relative timings. (B) Pairwise Noise correlation. (C) Pairwise signal correlation. (D) Sparse and dense spatial coding. (E) Modulation of excitability by LFP phase

The concept of a spectrum of dense to sparse neural coding strategies (Barlow, 1972, Olshausen and Field, 2004) is also of interest, see Figure 1.10D. Dense coding means that a range of information is encoded by the varying firing of an entire population of neurons. It is thus highly efficient in terms of space, and while a lot of the capacity is

redundant, this makes this strategy better at dealing with faults or noise within the population. In a sparse coding strategy, an item of information is encoded by a specific set of highly tuned neurons. It is thus energy efficient, easier to decode, and stimuli are represented distinctly and without overlap. Indeed, current literature suggests it to be the predominant strategy in a number of sensory modalities (Vinje and Gallant, 2000, Hromadka et al., 2008, Dodds and DeWeese, 2019). However, space can become an issue as more neurons are required to convey the same amount of information as a corresponding dense coding population.

Neuronal Correlations

Within a neural population, noise and of signal correlation are also important to consider (Figure 1.10B and C). The following description of these concepts is largely derived from the 2011 Nature Neuroscience review by Cohen and Kohn (Cohen and Kohn, 2011). Correlation in this context refers to a measure of how similar two or more neurons are, in terms of their firing responses. The *noise correlation* of a pair of neurons refers to the level of firing correlation that is unrelated to the stimuli, implying there is a shared input to some degree. As an example, if a neuron fires differently during 3 identical stimuli presentation (say 10, 2 then 6 spikes), a neuron with which it has high noise correlation will also display a similar, stimuli independent fluctuation (say, 12, 3 and 7 spikes). The exact temporal properties of these fluctuations are variable—modulating spike rate on potentially longer timescales of seconds (Smith and Kohn, 2008, Ecker et al., 2014), but generally on shorter timescales of milliseconds to 100s of milliseconds (Bair et al., 2001, Mitchell et al., 2009). Research into correlations is generally conducted on the scale of behavioural trials (100s of milliseconds).

Some facts about noise correlations are generally agreed upon. At least in the cortex, they tend to be small, and overall positive (Kohn and Smith, 2005), with neuronal pairs closer together being more strongly correlated (Constantinidis and Goldman-Rakic, 2002, Smith and Kohn, 2008). Values of between 0.1-0.2 are most common – while clearly small, these can still have substantial effects on neuronal coding.

However, as with most measures of neuronal activity, there are several factors that will influence the strength, patterns and overall contribution of correlations to information encoding. For example, different cortical areas, and different layers of the cortex, have been shown to have different levels of correlation (Cohen and Kohn,

2011). Motor cortex correlations are also consistently less strong than sensory areas (Maynard et al., 1999).

Signal correlations are another type of correlation, these refer to how well correlated the neurons responses are, when responding to a specific stimulus (essentially how similarly “tuned” are they). As an example, a neuron may respond at 90% of its maximum firing rate for a 1 kHz stimuli, but only 10% for a 3 kHz stimuli – a neuron with high signal correlation with the first would respond similarly to these same stimuli. These are generally less well studied than noise correlations.

The methodology behind the calculation of correlations is in itself a potentially contentious issue and may explain some of the variability observed across studies. Again, the Cohen and Kohn 2011 review provides an excellent overview of the subject, with the main points summarised below. Aside from the biological influence on the correlations which are the subject of the analysis, the experimenter may introduce artificial biases or influencing factors into the calculations. Exactly how spike trains are derived can be influential, as there is a tendency for higher correlations with higher spike rates (de la Rocha et al., 2007). Higher spike rates should be purely biological, but could also be the result of low data quality, inaccurate spike sorting, or the exact threshold used to define a spike.

Following on from this, the window used to define correlations is also influential – as stated previously, the timescales over which correlations exist is likely to be variable, and stimuli/state dependant. The brain is coding and integrating information over different time scales, and so the window size, and the definition of a window’s start point will clearly influence what is seen. For example, windows can be locked to the stimulus presentation (most common) or to the underlying brain oscillations, and each gives slightly different results (Kayser et al., 2012). Smaller window sizes also generally result in smaller values of correlation (Cohen and Kohn, 2011).

Other potential influences on correlation strengths could include cell type (Constantinidis and Goldman-Rakic, 2002), population sizes, or the exact environment or task being run.

Exactly how noise and signal correlations influence stimuli coding is a highly interesting topic of discussion. The general question seems to be if correlations enhance, inhibit, or give additional information about the coding of information. Currently, there is some evidence and theory for all. One perspective is if a neuronal

population is less heterogenous (i.e., responses are similar due to noise or signal correlations), it will be unable to represent as many dimensions of data as one without this property, given a maximum firing rate. Considering the trial-trial variability in neurons, this variability can be worked around by averaging a population response (a task the brain can perform). However, given a high level of positive correlations (i.e. a low signal-to-noise ratio), after a certain number of neurons in the population, this averaging won't help as the response saturates. In this way, noise correlations can be limiting to the information transferred by a population of neurons. An interesting paper in 2014 proposed an additional layer of complexity – it is in fact the pattern of correlations that is the deciding factor, and depending on the situation, correlations can indicate, more, less or no change in the information being coded (Moreno-Bote et al., 2014).

Another school of thought suggests that noise correlations themselves are coding mechanisms – on top of the general mechanism of spike rate. A 1999 study by Panzeri et al suggested that noise correlations are actually a separate mechanism of coding information (outside of simple firing rate), if they are modulated by the stimulus itself (Panzeri et al., 1999). Another interesting proposition is that levels of neuronal noise correlation represent the level of uncertainty surrounding a stimulus – if the neurons are all “in agreement” they will be positively correlated – “disagreements” would be represented by a negative correlation (Fiser et al., 2010). Noise correlations are also thought to in some way reflect or influence the outcome of an animal's perceptual choice. It is frequently observed that fluctuations in individual neurons are predictive of a perceptual decision, and that this is easily observable suggests many neurons are fluctuating so (and thus have higher noise correlations) (Nienborg and Cumming, 2010).

Clearly, the importance of correlations to the encoding of information in the brain cannot be understated, however, the exact appearance and underlying mechanisms of these patterns would appear to be highly situationally dependant. For any given experiment, the potential influences are likely to be different, and should be explored on a case-by-case basis in order to get the fullest picture of neuronal coding. Correlations have also been studied primarily in cortical area, with their influence in other regions still being a largely open question.

Understanding the influence and extent of correlations and each of the preceding coding strategies is imperative to understanding the dynamic relationships between

this study's target brain areas, and to formulate stimulation/encoding strategies for the hypothetical midbrain implant. Thus, the influence of correlations on sound encoding in both the cortex and the colliculus is examined within this thesis.

1.4.2 Global Brain State and its Influence on Sensory Processing

Clearly, raw sensory input is the primary modulation of cortical and subcortical activity, but there is another more subtle and dynamic influence on neuronal activity – brain state. Brain state can be recognised by changes in EEG, with these changes then influencing neuronal population activity (Harris and Thiele, 2011). Unlike action potentials, brain state is generally observed to change on the scale of seconds-minutes, not milliseconds. Traditionally, the definition of brain state is tied to our definitions of sleep. Non-REM (NREM) sleep, also known as “slow-wave sleep” is characterised by slow, synchronised activity of neurons (strong fluctuations) and increases in low frequency EEG activity (Davis et al., 1937), while waking, and/or REM sleep sees more desynchronised activity and a shift from low to high frequency in the LFP, and smaller overall fluctuations (Aserinsky and Kleitman, 1953, Jouvet, 1962). A graphical representation of this is shown in Figure 1.11.

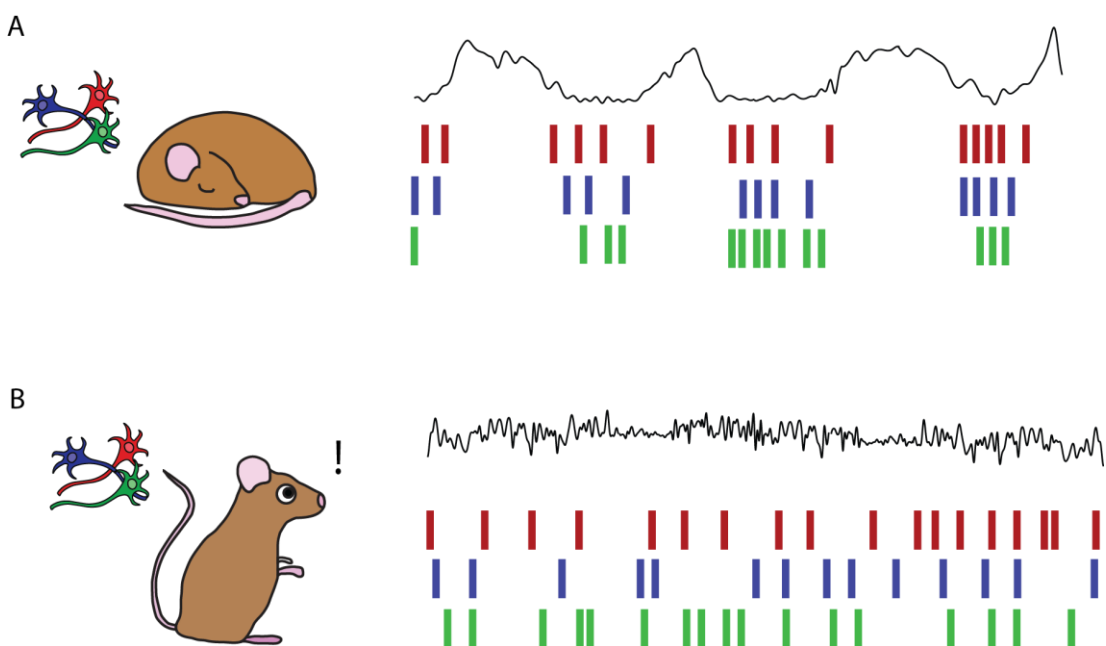


Figure 1.11: Cortical states. (A) Synchronised state, with neurons firing together, generating slow frequency waves in the LFP. (B) Desynchronised state, with neurons less synchronised and LFP having more high frequency activity. Image adapted from (Harris and Thiele, 2011)

In actuality, cortical state is a continuum, with “desynchronization” and “synchronisation” being opposite ends. Desynchronization is associated with

alertness (except in REM sleep) state, generally associated with decreases in low frequency power (delta, theta) and increases in higher (alpha, beta, gamma) (Steriade et al., 1996) . In the synchronised state, low frequency (delta/theta) power is high, and neuronal population firing rate is strongly and slowly modulated on these scales (see Figure 1.10 and 1.11) (Steriade et al., 1993). Pupil diameter is a known correlate of brain state, with small diameter indicated more synchronised state/sleep, and dilation corresponding to synchronous states/attention (Reimer et al., 2014, Reimer et al., 2016).

Common ways to assess cortical state include examination of the relevant frequency spectrum, and more specifically the “delta ratio” – the ratio between delta wave power and power over the rest of the spectrum (exact ways of calculation vary between researcher, but the principle of assessing low frequency power fluctuations is the same). If possible, the researcher should measure pupil diameter – as previously stated, this correlates with state. EMG can also help too, to identify periods where the animal is active. Between these metrics, reasonably accurate estimations can be made of the ongoing brain state, which can be used to add depth to analysis of stimuli responses or behavioural experiments.

Global modulation is known to influence co-fluctuations and pairwise correlations between neurons, with the synchronised state eliciting higher correlations (Cohen and Kohn, 2011, Ecker et al., 2014, Noda and Takahashi, 2015). This in turn can result in an increased trial-trial variability in responses, with neuronal firing fluctuating with little relation to the stimuli itself.

The exact origin of the global fluctuations is currently under debate. Investigation of sleep states has led to identification of certain brainstem nuclei as origin points. Nuclei such as the pedunculo pontine tegmentum (PPT) and laterodorsal tegmentum (LdT), exhibit clear changes in cholinergic neuron activity during, and in the transitions between, different attentional/sleep stages (Datta and Siwek, 1997, Sakai, 2012, Boucetta et al., 2014, Van Dort et al., 2015). It is thus reasonable to assume their influence on brain states, although the true mechanism is likely to be much more complex. Though the areas are not directly connected to the cortex, they may influence brain state by way of thalamic nuclei (such as the reticular nucleus) (Fuentelba and Steriade, 2005).

The exact effect of brain state on the encoding and processing of sensory stimuli is dependent on the sensory modality. In a later section of the thesis, the potential effects of brain state on auditory coding are very briefly examined.

1.5 Spectral Processing in the Auditory Pathway

1.5.1 Overview and Basic Principles

Incoming sound is composed of both spectral and temporal information. In the review of auditory pathway anatomy and physiology, one of the principal methods of encoding sound frequency is observed. This is a spatial code, in the form of a tonotopic gradient of neurons that is maintained throughout the stages of the primary pathway. However, even within these gradients there exists additional complexity to the spectral coding of sounds.

Conveyance of spectral information begins in the cochlea, which can be thought of as a filter bank. Incoming sound waves are “filtered” into bands due to varying vibrational qualities of the basilar membrane and transmission of signals to distinct groups of hair cells. The cells, through patterned spiking, then convey the timing and amplitude information about that frequency, which is passed on up the auditory pathway.

The ability to distinguish between frequencies is determined by critical bands in hearing, which are defined in the cochlea. Critical bands are essentially the filters of the cochlea; incoming frequencies lying within the same band are integrated, and can't be distinguished in the other's presence. Critical bands thus are an important consideration in the design and functioning of cochlear implants (as well as central auditory implants).

Particularly in the central pathway, neurons are arranged in such a way as to have a spatial pattern for spectral information (the tonotopic gradient). Figure 1.12 provides a simplistic representation of tonotopic gradient appearance in two example brain areas - the AC and IC.

That neurons simply have a “preferred frequency” is a fairly simplistic explanation of spectral coding – the response of a neuron to a given frequency can vary with the intensity of the sound, and also with environmental context or the type of sound, and it may also show preferences along these gradients.

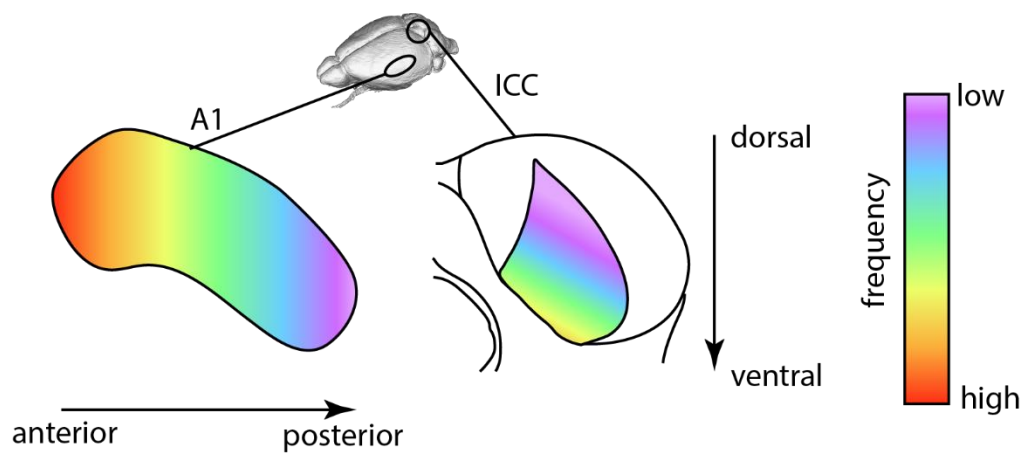


Figure 1.12: Simplistic representations of tonotopic maps in the primary AC and central IC nucleus. These are merely examples to show how gradients can be in different structures, and are not to-scale representations and do not incorporate non-linearities

The subtleties of neuron's response to the spectrum of sound frequencies can be defined using a number of parameters. The Best Frequency (BF) of a neuron is the frequency which elicits the largest response, regardless of the intensity. Similar to this is the Characteristic Frequency (CF), the frequency that the neuron responds to at the lowest sound intensity – this can differ from the BF. This lowest sound intensity is known as the minimum threshold. A response bandwidth refers to the range of frequencies over which the neuron will respond. To further assess tuning, the quality factor is the relative sharpness of tuning, at a given intensity/dB level (i.e. Q10dB, Q20dB), while the slope can be calculated in dB/octave.

To derive these properties, the Frequency Response Area (FRA) of a given auditory neuron can be calculated. (Figure 1.13). The FRA indicates how strongly a neuron responds to the range of available frequency, across a range of intensities. FRAs can be assessed by presenting a range of pure tones, and can be single (i.e. V-shaped) or multi-peaked, if the neuron has multiple BFs – as well as a few other shapes. (Sutter and Schreiner, 1991, Recanzone et al., 2000), see Figure 1.13.

In practice, a V-shaped FRA indicates there is a reaction to a broad range of frequencies at a high intensity, narrowing to the best/preferred frequency. Alternatively, there may be no response at all, as some neurons don't show responses to pure tones and are instead responsive to complex sound features. Using FRAs, we can build a map of neuronal responses in an area.

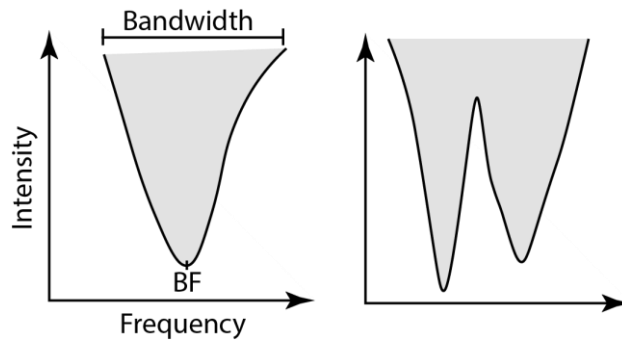


Figure 1.13: Simplistic FRA examples. To illustrate intensity /frequency relationships. Left: V-shaped, Right: Multi-peaked

It is worth noting that in terms of spectral processing, the FRA is still fairly simplistic, and can mask intricacies in the time course of a neuron's response. Neurons are capable of showing a varied timescale of responses to a tone, which can in itself contain information. For example, the latency between the tone and the response can vary for different intensities of sound, or can indicate how close a frequency is to that cell's BF. To capture these responses, a Spectro-Temporal Receptive Field (STRF) can be derived, using more complex time-and-frequency varying stimuli, as opposed to the pure tone. Briefly, this looks at the time course of the stimuli before each spike of a cell, and averages this to display the neuron's response in two dimensions of frequency and time. The STRF can be used as the input to a number of mathematical models of spike train prediction, though there are questions as to its relevance to all kinds of input as the stimuli (for example, pure tones vs naturalistic sound) used to generate the STRF can actually have an effect on the final map—(Eggermont, 2011). For example, it has been found that STRF derived from artificial stimuli often differed from those derived using natural stimuli in terms of their latency, bandwidth and best frequency (Laudanski et al., 2012). Thus, the stimuli used to generate the STRF, plus the context in which it will be applied, must be carefully considered when making conclusions.

Spectral processing is also heavily modulated by intrinsic and extrinsic inputs to an area (such as feedback mechanisms), balancing excitation and inhibition by interneurons as needed contextually, to sharpen or broaden tuning (Zhang et al., 1997, Wenstrup and Leroy, 2001, Wu et al., 2008). The effect of inhibition on frequency tuning is apparent when applying the two-tone paradigm. In these experiments, a secondary, variable tone is presented just before or after the pure tone of interest (Egorova et al., 2001). This secondary tone can cause an enhanced response to the tone, can suppress it, or can have no effect at all. These effects are crucial for shaping tuning curves, particularly in the IC.

When discussing spectral tuning properties in the IC and AC in this Review, explanations will be limited to generalisations and common observations. There are extensive interspecies and sub-area differences, occasionally with weak/conflicting/missing evidence, and so the information provided will be enough to give a general overview of each area and to link to function and the potential influences on sound coding – though more details and background may be found in the relevant results chapters. It will also serve to identify gaps in knowledge that the thesis will attempt to address. In the vast majority of cases, experiments in the AC and IC are performed separately – thus the approach of simultaneous recordings presented in this thesis may offer additional insight these studies do not. The approach has the potential to provide more direct comparisons of neuronal behaviours – data is obtained under very similar (if not the same) experimental conditions.

1.5.2 Spectral Processing in the IC

Central Nucleus

Almost all ICC neurons are tuned to some degree (Ehret and Schreiner, 2005). The ICC has a very prominent tonotopic gradient, with cells in a single frequency band lamina responding to very similar frequencies. (Poon et al., 1990, Romand and Ehret, 1990, Schreiner and Langner, 1997). One layer roughly corresponds to one critical band (Schreiner and Langner, 1997). The exact mapping of frequencies depends on the animal, with frequencies involved in species-specific vocalisations (i.e. natural sounds) more strongly represented in the IC (Suta et al., 2003, Malmierca et al., 2008, Portfors et al., 2009). There is also evidence for a secondary, shallow frequency gradient from dorsomedial (low CF) to lateral/ventrolateral (high CF) within a single frequency band lamina (Schreiner and Langner, 1997). GABAergic and glutamate cells have demonstrated similar responses to pure tones in terms of thresholds, response latencies and frequency tuning (Ono et al., 2017).

The range of quality factors across the IC (i.e. the sharpness of tuning and overall frequency resolution) is invariably large, with some interspecies differences, inferring a behavioural role (Kelly et al., 1991, Syka et al., 2000, Egorova et al., 2001). In addition, neurons can have inhibitory response (i.e. the two tone-paradigm), further shaping the neuron's response – a given frequency may excite or inhibit the cell. There are different ways of classifying each cell based on its frequency response profile. Egorova et al in 2001 provide an excellent breakdown of putative ICC cell

classes, which is summarised below. They classify 4 cell types, based on their patterns of excitation and inhibition frequency responses (Egorova et al., 2001). Class I neurons are generally excitatory, with steep high frequency slopes and shallow low frequency sloping. Inhibition either side of the CF is asymmetrical (higher thresholds below the CF). Class II neurons are largely shaped by inhibition. Inhibitory side bands are near symmetrical, and result in very steep, sharply tuned slopes in the excitatory response. Class III neurons show weak, symmetrical inhibition, resulting in shallow, broad excitatory responses. Class IV are complex, and usually have multiple CFs and inhibitory areas. There is evidence to suggest that these cells types are arranged in a gradient of tuning width within single isofrequency layers. Class II neurons with high resolutions and sharp tuning are found in the centre of the sheet, with the overall proportion of broadly tuned class III neurons increasing as we move outwards (Ehret et al., 2003)

A secondary classification defines cells on the relative shapes of the response. Thus, a type "I" is narrowly tuned, with inhibitory side bands, a type "V" is broadly tuned, and a type "O" is generally inhibitory, save a small area of excitatory responses around the CF (Ramachandran et al., 1999).

As both of these studies have overlapped to some degree, and thus regardless of the exact classification, there is strong evidence for the existence of cells with differing frequency responses within the IC, resulting in a heterogenous population capable of coding and encoding the vast range of sound in our environments.

Tuning curves are also dynamically shaped by external input, particularly corticofugal, and in a manner specific to the previously described class of ICC neuron (Jen and Zhang, 1999, Yan et al., 2005).

Dorsal and Lateral Cortex

Current literature does not extensively cover tonotopic arrangements in the dorsal and lateral/external cortex. Overall, they do not seem to cover the entire tonotopic range seen in the ICC (Stiebler and Ehret, 1985) and neurons in general are more broadly tuned than their ICC counterparts (Aitkin et al., 1975, Syka et al., 2000).

The nature of the tonotopic gradient in the dorsal cortex is currently under debate. While a few studies suggest an arrangement distinct from the ICC, most seem to support the continuation of the ICCs gradient into the dorsal cortex (Serviere et al., 1984, Stiebler and Ehret, 1985, Schreiner and Langner, 1988). It is possible that a

true functional distinction of the DC and ICC in smaller species is harder, despite anatomical borders.

In the lateral/external nuclei, tonotopy appears more distinct from the ICC, though the exact directional layout varies between species (Aitkin et al., 1978, Roth et al., 1978, Stiebler and Ehret, 1985).

1.5.3 Spectral Processing in the AC

Being the highest auditory area, spectral processing in the AC is complex. Primary/core areas of the AC tend to have simple V-shaped FRAs, and can contain the full range of cochlea frequencies (albeit with biased representations) (Sally and Kelly, 1988). The core areas tend to have both local tonotopy (neighbouring neurons have similar CF) and a global/area wide gradient (Merzenich et al., 1975), with primary areas having the smoothest gradient. Frequency-responsive neurons also change the temporal profile of their responses depending on the stimuli and its context – the “preferred” stimuli will elicit a sustained response throughout the stimuli whereas other stimuli will elicit an onset response followed by a transient response (Bar-Yosef et al., 2002, Wang et al., 2005).

There is also evidence of tuning bandwidth gradients interleaved within the tonotopic map, resulting in a wide, complex map of spectral tuning and integration (Schreiner et al., 2010). At least in core areas, evidence suggests that best/characteristic frequency tuning is largely conserved across cortical layers, though deeper layers exhibit broader tuning (Phillips and Irvine, 1981, Shen et al., 1999, Wallace and Palmer, 2008). The range of quality factors, or tuning sharpness, is highly variable as in the ICC, resulting in a wide range of bandwidths for frequency integration (Recanzone et al., 1999, Schreiner et al., 2000, Imaizumi and Schreiner, 2007). Though only a tendency, sharpness of tuning in primary areas seems to increase with increasing frequency, and overall the tuning selectivity is more narrow in primary areas (Phillips and Irvine, 1981, Cheung et al., 2001). There is also some evidence to suggest that pyramidal cells in primary auditory areas have a narrower bandwidth than interneurons within the same cortical layer (Atencio and Schreiner, 2008).

Outside of primary areas, there is a the tendency for tonotopic gradients to be weaker (no local clustering of CFs, but evidence of a global gradient), or there to be no tonotopy at all (Schreiner and Cynader, 1984, Redies et al., 1989, Loftus and Sutter, 2001). There may also be under or over representations of some frequency ranges,

potentially a behavioural adaptation as similarly to the inferior colliculus, the effect is species dependant (Redies et al., 1989, Thomas et al., 1993, Bizley et al., 2005, Schreiner and Winer, 2007).

1.6 Temporal Coding in the Auditory Pathway

1.6.1 Overview and Basic Principles

As well as the spectral information, sound also has a complex temporal structure. This is generally broken down into two streams of information – the fine detail or texture, and the outer contour or envelope (Figure 1.14), or the periodicity of the sound – how it changes in time. Correct representation of this periodicity is essential in particular to the perception of naturalistic sound, such as speech, animal vocalisations and sounds produced by the environment.

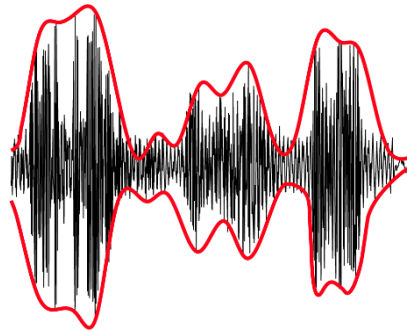


Figure 1.14: Temporal components of a sound wave. Fine (black) and outer contour (red) of a segment of natural sound comprised of animal calls and water sounds (around 2s)

Any given sound envelope is essentially composed of many underlying sinusoidal varying signals. Fluctuations in the envelope are often referred to as Amplitude Modulation, or the periodicity of the sound.

The auditory system directly encodes this information with two main strategies: synchronisation/phase locking, and mean firing rate. Synchronisation refers to the phenomena of neurons firing precisely at the frequencies of a stimulus envelope, the upper frequency of which decreases as we move up the auditory system (Joris et al., 2004, Panzeri et al., 2010). In the cochlea, the exact upper limit is widely debated, with upper limits of at least 10000Hz seemingly possible (Verschooten et al., 2019). By the primary auditory cortex, this upper limit has fallen to around 30Hz, indicating a gradual change in temporal coding strategy through the central auditory pathway (Liang et al., 2002, Zeng, 2002). For frequency information above this, information is instead encoded as a function of the average firing rate of the neuron.

Neurons often display preferential tuning to a particular modulation rate, with their degree of phase locking decreasing to either side of this (Langner, 2004), or are simply most sensitive to slow modulation rates, and will decrease their degree of phase locking as frequency increases. As with spectral tuning, these response profiles can take many shapes, including multi-peaked.

Though it was not analysed to the fullest potential in the thesis, the simultaneously recorded data obtained from large populations of IC and AC neurons has the potential to provide an excellent opportunity to examine the representations of temporal sound components between the IC and AC, and in the future may provide information on relative timings of the two areas under different sound stimuli.

1.6.2 Temporal Coding in the IC

The inferior colliculus employs both synchronisation and rate codes for encoding temporal information of sound. IC neurons are known to have a variety of biophysical properties and temporal responses to stimuli, as we have seen, and so temporal encoding is brought about through variations in these responses. Most work on periodicity does not currently differentiate between IC subdivisions and so properties are generic unless specified. GABAergic and glutamatergic neurons differ in their responses to amplitude modulation, with more glutamatergic neurons showing synchronisation to the sound as the temporal frequency increases – suggesting this cell type might better follow fast temporal changes in the sound envelope (Ono et al., 2017).

Similar to spectral tuning, the neurons often show preferred amplitude modulation frequencies, creating periotopic gradients. A logarithmic gradient of periotopy existing orthogonal to the frequency band laminae of the central nucleus (Schreiner and Langner, 1988), but the exact spatial arrangement and starting point of the gradient varies across species (Schreiner and Langner, 1988, Pinheiro et al., 1991). Interestingly, in the ICC there would appear to be a trade-off between amplitude modulation and spectral modulation, that shifts with the tonotopic gradient. For example, neurons with a low spectral BF were sensitive to fast changes in amplitude, and slow changes in frequency. Moving through the tonotopic gradient, this relationship flips over (Rodriguez et al., 2010). The authors speculate that this may be highly significant to the IC's efficient coding of natural sound, which itself often shows the same trade-off in properties (frequency modulation is slow when temporal modulation is high, and vice versa) (Singh and Theunissen, 2003).

In terms of phase locking, IC neurons generally synchronise to envelope frequencies ~100-200Hz (Schuller, 1979, Rose and Capranica, 1985, Rees and Moller, 1987, Muller-Preuss et al., 1994, Zheng and Escabi, 2013) , though significantly higher numbers (600Hz+) have been observed in some neurons (Langner et al., 2002). If not employing a synchronisation code, IC neurons will represent frequencies with rate modulation as previously described.

Given that the IC displays both coding mechanisms varying degree, it is speculated that the IC, as a hub of auditory processing, may be the switching point for all but the lowest temporal frequencies high frequencies – from a synchronisation based code prominent in lower auditory areas, to the rate based code favoured by the auditory cortex. The increased reliance of the IC on a rate-based code rather than synchronisation (which is the preference earlier in the pathway), may be a potential influence on the success of auditory midbrain implants, whose algorithms have been designed for stimulation of the auditory nerve. As such, additional layers of complexity may be required to ensure the most accurate representation of sounds, particularly those with complex temporal components such as natural sounds.

Thus far, research into the IC's responses to sounds with complex periodicity (i.e. naturalistic sounds such as speech) is generally carried out using artificially generated Amplitude Modulation stimuli, specific animal vocalisations, or is focused on the of mapping gradients and thresholds. As such, research into the more generalised behaviour of neurons of the ICC during natural sound is not as extensive, but may be important when designing robust stimulation strategies for the auditory midbrain implant – naturally and as a whole, what are the characteristics of IC neural responses to natural sound (including successive repetitions of the same stimuli)? This is something this thesis attempts to answer, with direct comparisons to cortical responses providing additional context. More details on the current literature will be provided in results Chapters 3 and 4.

1.6.3 Temporal Coding in the AC

General Mechanisms

Dual coding strategies for temporal information within the sound have been touched upon previously – namely, rate and phase locking. Progressing through the system, the balance of which frequencies are represented by each strategy changes/swaps. While phase locking is employed for the majority of frequencies in the auditory nerve, in the auditory cortex, a rate code is favoured to represent modulation frequencies

above approximately 50Hz (Joris et al., 2004) with phase-locking used only for relatively slow frequencies below this. This is speculated to be due to the increasing complexity of the time-varying signal as we progress through the auditory system, and by the time we reach the final station, phase-locking alone is not sufficient to represent the potential range and depth of temporal information (Wang, 2007). As in the colliculus, this limit can be exceeded in rare cases – synchronisation was seen up to 250Hz in the monkey (Steinschneider et al., 1980).

Like spectral coding, neurons can be arranged periodotopically – having a preferred temporal frequency (referred to as the Best Modulation Frequency, BMF) to which they respond most strongly and sustainably to (Wang et al., 2003, Wang et al., 2005). In fact, neurons in both the primary and secondary/belt auditory cortex show their strongest responses when stimulated by their preferred frequency being modulated in time, as opposed to a simple pure tone (Liang et al., 2002), perhaps indicative of an increased relevance of amplitude modulated sounds as opposed to (usually unnatural) pure tone stimuli.

Despite the lowered reliance on phase-locking to convey temporal information, the auditory cortex displays an interesting, similar behaviour termed “entrainment”, where responses are locked instead to the underlying cortical LFP, which in turn is modulated to match important temporal features of the sound.

Entrainment

In cortical areas, entrainment appears to be a key mechanism in the coding of natural sounds with complex/semi-periodic sound envelopes. Slow oscillations (for example, in the delta/theta range), are a common observation in cortical LFP. Somewhat similarly to the brain states described previously, it is believed that these oscillations also change the excitability of neurons, but on the time scale of 100s of milliseconds, rather than seconds. Looking closely at the synchronisation coding of the auditory cortex, what is observed is that neuronal spiking is synchronised specifically to these underlying oscillations in LFP, which in turn reflect slow temporal aspects of the sound being presented. This phenomenon, known as entrainment (Figure 1.15), would appear to be a way by which the brain creates an ongoing frame of reference for neuronal firing to follow, and create a stronger temporal code as opposed to synchronisation to sound alone. It adds robustness and enhanced perception of relevant sound features on important time scales (Kayser et al., 2015, O'Connell et al., 2015). Entrainment is not an auditory-specific mechanism. Entrainment to periodic

visual stimuli has been well documented (Williams et al., 2004, Schroeder et al., 2008).

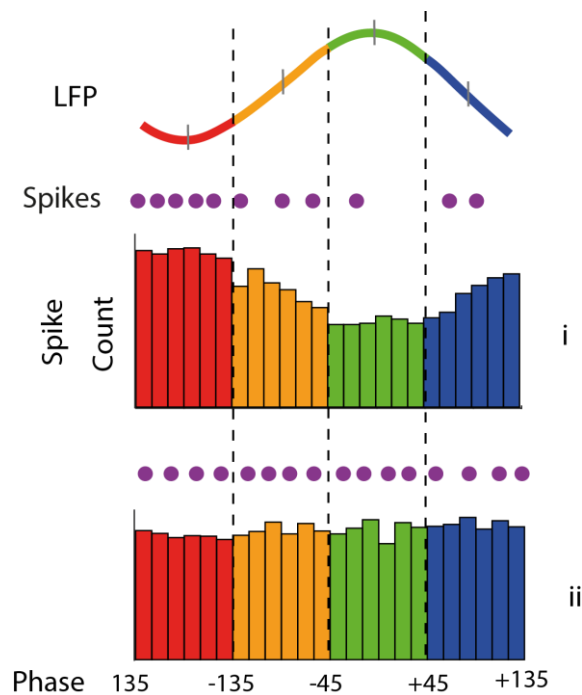


Figure 1.15: Entrainment. From top to bottom: Representative LFP trace with phase bins marked. Purple “spikes” underneath indicate a preference for firing in phase 1 (red), this is further represented by a histogram of spike phases (i). In ii) Spikes are evenly distributed across LFP phases, and thus entrainment is not present. Phase is given in degrees

Entrainment is particularly associated with enhancement of naturalistic or behaviourally relevant sound features (such as speech and calls) (Giraud and Poeppel, 2012). More generic periodic stimuli (such as click trains with no associated behavioural task) are more likely to use the simple synchronisation code. Because of this relationship with higher order sound stimuli, it is generally assumed that entrainment occurs principally in the cortex – though in this thesis, the same analysis is applied to the IC data, resulting in some interesting observations.

A lot of recent literature focuses on the specific functions and mechanisms of entrainment in the animal kingdom. In the monkey, oscillations aligned with the temporal structure of the task and stimuli, so that periods of high neuronal excitability began to accompany behaviourally relevant sound features - resulting in response enhancement (O’Connell et al., 2015).

A previous 2009 study by Kayser et al. (again in monkeys), found that by including the current LFP phase of each neuronal spike, the amount of information regarding the stimuli was significantly enhanced over spike rate alone, seeming to confirm that

entrainment to LFP enhances the coding of complex sound stimuli (Kayser et al., 2009). This effect was limited to slower timescales (<30Hz LFP). A 2005 study in the macaque provided evidence for nested entrainment – theta modulating delta, and gamma modulating theta – promoting the idea of a hierarchical, nested modulation system (Lakatos et al., 2005).

Though the majority of animal work in this area is done in monkeys, a recent study in rats incorporated phase information into mathematical models of neuronal activity, finding that models built with this information better replicated the recorded neuronal responses (in silence and during natural sound stimuli). For sound stimuli, this effect was most prominently seen at low LFP frequencies (2-12Hz) (Kayser et al., 2015). Additionally, there may be a cell type specific behaviour during entrainment – narrow spiking cortical interneurons were found to favour entrainment to higher LFP frequencies (Yague et al., 2017). This additional dimension to the phenomenon has yet to be fully explored, and investigation is likely to yield interesting conclusions regarding cortical circuits and dynamic functionality of cell types.

Entrainment is also able to be observed to some degree in humans, and due to its apparent importance in speech perception, it is a common avenue of investigation. Due to technological limitations in resolution (deriving from a difficulty in recording directly from brain tissue), studies in humans are usually not accompanied by neuronal spiking activities, instead they look closely at the first stage of LFP/sound stimulus coupling. Speech is constructed from building blocks of different time scales – syllables make up words, which in turn make up sentences. Comprehension of syllables (4-8Hz range) is essential for accurate speech perception, and thus generally the range of interest in human studies (Elliott and Theunissen, 2009). For example, human cortical entrainment during stimuli was shown to be enhanced at the 4-7Hz – the range at which the envelope of the stimuli (intelligible sentences) had highest spectral power (Peelle et al., 2013). LFP/sound coupling at this frequency range (and the importance of this range to speech intelligibility) is confirmed by many studies, with some showing that disruption of speech at this scale had the effect of decreasing intelligibility and levels of cortical entrainment at the theta scale (Luo and Poeppel, 2007, Ding et al., 2014, Doelling et al., 2014). It has also been implicated in dyslexia (Leong and Goswami, 2014).

The focus here and in literature is generally at the theta timescale, however, with observations of theta-nested delta and gamma-nested theta LFP, perception of

speech components are enhanced in a time-hierarchical manner (Lakatos et al., 2005, Canolty et al., 2006, Panzeri et al., 2010, Di Liberto et al., 2015).

Further evidence of this phenomenon in animals was observed in a 2012 study where time bins were carefully selected (both in their duration and to be either phase or stimuli locked) and linear classification analysis revealed a theta timescale reference frame to be most successful in decoding analysis (Kayser et al., 2012).

However, the fact that speech is more quasi-periodic than a true periodic signal may complicate the reality. The slew of evidence does at least suggest a strong role for entrainment in successful speech comprehension, but may not be the only mechanism (Alexandrou et al., 2018). Literature is also lacking as to the origin of the entraining LFP, be it cortical, thalamic or otherwise. Thus, the exact mechanisms and origins of entrainment and speech perception in general should be topics of future research.

It is also not known if entrainment of this kind occurs to any degree in subcortical structures. Understanding the mechanisms of entrainment has implications in the improvement of speech processing algorithms for auditory implants and is thus a topic of analysis in this thesis.

1.7 Additional Sound Coding Principles

1.7.1 Intensity Coding in the Auditory Pathway

After the pitch and temporal structure, another main property of sound to be coded is intensity – i.e. how loud a sound is perceived. This thesis does not look extensively at the topic of intensity coding, and so all that will be covered is one of the more important mechanisms that is also highly relevant to auditory implants – dynamic range (Figure 1.16).

In the context of neuronal activity, the dynamic range is the intensity range over which a neuron can represent the intensity with a linear increase in its firing rate. Above and below this, the response saturates. Within this dynamic range small changes in intensity are able to be distinguished more clearly. After saturation, this becomes near impossible. As with most other sound features, neurons can also prefer a selected intensity. A low dynamic range is a crucial drawback of a lot of auditory implants. The elicited response from neurons quickly saturates within a very small range of electrical current, meaning a full representation of intensities with good resolution is often impossible.

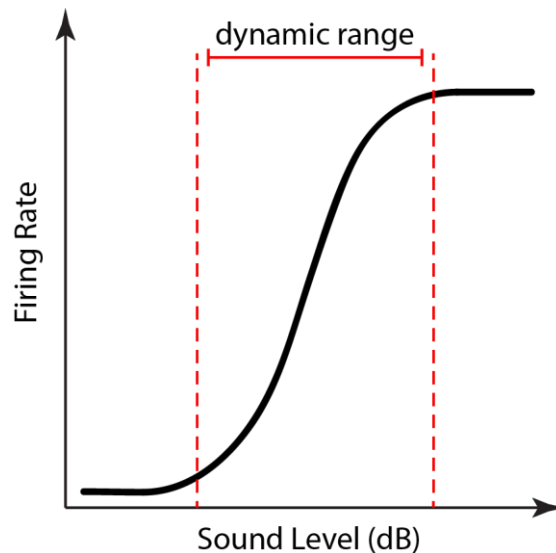


Figure 1.16: Dynamic range of an auditory neuron. Segment enclosed by red dotted lines is the “dynamic range”, during which the neuron’s response is not saturated

1.7.2 Frequency Modulation

Another way sound can vary and can be coded is in frequency modulation – i.e. how fast does the sound change pitch? In auditory research, this is usually explored by playing frequency sweeps, where the pitch of sound moves from one to another. Neuronal responses to frequency sweeps (and their functional significance) have been extensively investigated in the echolocating bat, whose calls are comprised of them (Bodenhamer and Pollak, 1981, Ferragamo et al., 1998, Sanderson and Simmons, 2000). In one study, some neurons appear tuned to frequency sweeps that are involved distinguishing between calls from other bats (Andoni and Pollak, 2011), suggesting a role of these selective neurons in animal communication. The direction, velocity and context of the sweep are all important variables to consider. As in amplitude modulation, neurons can also have a preferred FM frequency, with neurons often having higher responses to modulated versus unmodulated sounds, or even exclusively responding to the modulated sounds (Liang et al., 2002).

1.7.3 Binaural Coding

Most species of animal have two ears, one on either side of the head. In this way, animals are able to pinpoint the location of sound, by using the inter-aural time difference, or the time between the onset of sound in one ear, and then the other. Extensive study of binaural coding does not fall within the project’s remit, particularly as much of this processing is done in the SOC (Schwartz, 1992), and the protocol

used in the presented research does not incorporate any interaural differences – in fact, the speaker is placed directly in front of the animal.

1.7.4 Effect of Global Brain State on Sound Coding

Brain states are well known to affect the encoding of sensory stimuli, including auditory. In the auditory cortex, a state of alertness results in more broad frequency tuning (Lin et al., 2019), and by actively listening during a variety of auditory attention tasks, responses to relevant stimuli (i.e. specific tones) are stronger (Fritz et al., 2005).

On the opposite end of the spectrum, anaesthesia has been observed to cause significant changes in the auditory response of the auditory cortex compared to the awake state, meaning that older studies that commonly utilised anaesthetised presentations should be interpreted carefully. It is a common observation that the number of responding single units is decreased when compared to the awake state, and although the characteristic frequency remains similar, the bandwidth/tuning has been observed to narrow in a number of studies. (Gaese and Ostwald, 2001, Noda and Takahashi, 2015). Overall, the strength and duration of neuronal responses, particularly to brief stimuli, is reduced under anaesthesia compared to the awake condition (Wang, 2007).

Changes in properties between wakefulness and anaesthesia should be compared to that during sleep as far as possible, being a more natural change in brain state. During NREM sleep, some responses similar to the anaesthetised condition are observed, although the changes do not appear in all cells, suggesting that to some degree, the normal auditory response may be preserved during natural sleep –the exact effects of sleep on auditory processing are likely to be complex and dynamic.

In a 1998 study, approximately half of neurons displayed a decrease in evoked and spontaneous firing rates that was linked to brain state (i.e. sleep) (Pena et al., 1999). A later study observed a sharpening in the receptive field during slow wave sleep in guinea pigs, but only in cells that displayed a decreased activity overall during the sleep state (again, close to half the population at 48%) - plus, their response latency was increased (Edeline et al., 2001). Other cells in the population had either increased responses, or were seemingly uninfluenced.

Overall, slow wave sleep is linked to a suppression of quiet sounds but a maintenance of response to louder sounds (Issa and Wang, 2011). There is more evidence that particularly loud, unexpected stimuli are processed the same regardless of cortical

state, whereas lower level, repetitive stimuli are adapted to faster in the desynchronised state as compared to synchronised (Castro-Alamancos, 2004, Otazu et al., 2009). This likely has an evolutionary basis – unexpected sounds are probably something important (predator, alarm etc), but we can “zone out” background noise when sleeping in the manner of a filter (Harris and Thiele, 2011).

There is also evidence for a decrease in trial-trial variability between the synchronised and desynchronised state (Curto et al., 2009, Marguet and Harris, 2011, Pachitariu et al., 2015). A 2011 study by Marguet and Harris used urethane anaesthesia to examine sound representation during both synchronised and desynchronised states (Marguet and Harris, 2011). Though anaesthesia generally causes synchronisation, urethane is a common and desirable anaesthetic agent as it is possible to observe both synchronised and desynchronised states. They identified clear differences in reliability of neuronal responses to repeated stimuli – in the desynchronised state, responses were more predictable trial-trial - with the opposite found in the synchronised state. In the synchronised state, spiking responses were also predictable from the LFP itself (a measure of global activity), but not from the stimulus amplitude, suggesting the synchronised state neurons are acting in response to modulation outwith purely the stimuli. Another study based in the AC and MGB (Sakata, 2016) saw similar results. They found an increased reliability of firing in both the AC and MGB during the desynchronised state. Interestingly, they also observed some cell type and layer-specific responses during each state, also recorded in a cortex only study in 2012 (Sakata and Harris, 2012) .

How brain state affects non-cortical structures is an interesting subject, but not one that has been explored completely. Focusing on the auditory midbrain, it has been established in a few studies that in the central nucleus, frequency tuning was unchanged between awake and anesthetized animals (Langner et al., 2002, Portfors and Felix, 2005).

However, a recent paper focusing on the non-lemniscal pathway components of the IC (specifically the shell L1) found evidence of state-dependant effects on tuning. (Chen and Song, 2019). Tuning selectivity under isoflurane anaesthesia was found to be broader/less specific than tuning of the same cells during the awake behaving state. Locomotion is also known to modulate brain activity – in the auditory cortex, gains are decreased, while they are increased in the visual cortex, with the exact mechanisms and functions still being relatively unclear. In this work, they interestingly

found that inhibitory neuron activity was correlated with locomotion, and moreover, tuning sensitivity of excitatory neurons was also increased during movement, compared to when the animal was stationary, meaning that the locomotion “state” was also able to affect this non-lemniscal pathway. There is far less research done into the non-lemniscal pathway, and is thus a very interesting avenue to explore in relation to brain state.

In relation to the current project, the effect of brain state is not a specific focus (except as a small analysis in results Chapter 5), but is instead a potential explanation for trial-trial variability – as examined in results Chapters 3 and 4. Anything affecting basic frequency tuning will in turn affect coding of natural sounds too – thus the influence of global brain state is an important factor to consider in the analysis of data. Additionally, the relevance of the sound to the animal may have a subsequent effect on its overall arousal/attentional state.

1.8 Mathematical Modelling of Neuronal Activity

1.8.1 Basic Principles

The growing trend for mathematical models of biological systems is highly relevant in a neuroscience context. By building various classes of model, neuronal systems can be systematically examined and perturbed in an attempt to unravel fundamental mechanisms of the brain. Results can then be validated (or not) *in vivo*. This project will touch on various kinds of models, generally most simplistic ones, and this section will highlight briefly the principles of some major kinds, and the relevance of each (particularly to auditory coding and auditory neuroprosthetics).

Firstly, what is a model? Fundamentally, a model is a function describing a relationship between an output variable(s) and an input or range of inputs. If the model accurately reflects the real system on some level, given a new set of inputs, it will be able to generate the output expected from the real system. By manipulating inputs and model architectures, questions can be asked far more easily and quickly than doing a set of *in vivo* experiments. Of course, the model is highly unlikely to truly mimic the intricacies of the animal brain, and so the outputs must be carefully interpreted. The practical uses of models are easily apparent – for example, in neuroprosthetics. The choice of inputs and outputs to models is highly dependent on the question being asked, and on the data available. Spike rate of single neurons, and LFP power, are common examples.

Looking specifically at the field of neuroscience, broadly, there are two forms of modelling. Decoding models take existing neural activity, and try to work out what stimulus elicited the reaction, essentially decoding the information held within the neural activity. For example, in Chapter 4 neurons are presented with natural sound stimuli, a model built using some of the recorded data, then remaining data inputted to assess if the model can successfully decode or predict which stimuli was applied.

Encoding models operate in the opposite way – taking an input stimulus and predicting the neurons' response. These are typically more complex. To construct them, extensive knowledge of neuronal activity over the range of stimuli is required. Additional complexity/realism can be added by integrating potential sources of noise, and the statistics of a typical spike train. This is essentially how auditory implants operate – the responses to stimulation at each electrode is mapped, then used to generate the appropriate stimulation pattern given a novel sound stimulus.

This thesis will focus almost exclusively on decoding models, though the potential benefits of using encoding models (particularly in the context of auditory implants) will be discussed. Decoding models are simpler to implement and can still provide a wealth of information about neuronal activity depending on our input parameters and careful interpretation.

1.8.2 Decoding Models

When making decoding models, there are two potential pitfalls – over and underfitting (Figure 1.17). In overfitting, the model becomes too specialised to the data used to train it, and may begin to also predict the noise of a training dataset. Thus, when data of a similar format (perhaps recorded on a separate day) is input, the model performs poorly, as it is not truly describing the underlying, fundamental relationship of two or more variables. Accuracy on an individual dataset may have to be sacrificed for overall robustness of results on other data. Underfitting is a similar issue, where the model is too simplistic to fully represent the variable. This could be due to a low range or amount of input data, or a solving method involving too few iterations.

To evaluate models, a subset of the data is used to train the model, then the remaining data used to test the model's accuracy – this is known as cross validation. This can be applied with different numbers of "folds". For example, in 10-fold cross validation, 90% of the data to trains the model, and the remaining 10% to test. This is then repeated for an additional 9 subsections of data, and the average error taken. A fairly

typical metric for model performance is the “mean squared error”, but others exist depending on the researcher’s needs.

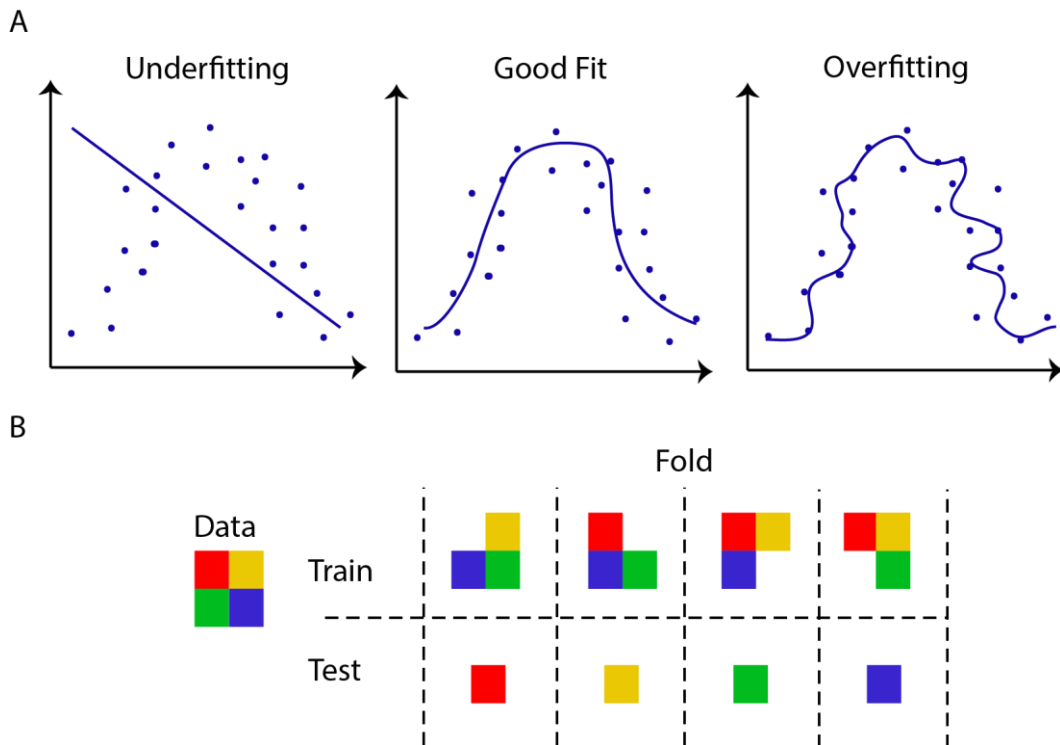


Figure 1.17: Common terminology in mathematical modelling. (A) Graphical representation of the concepts of under, good and overfitting data. Single dots are hypothetical datapoints, solid line represents the line described by the equations of the model. (B) Basic diagram illustrating cross validation. At each “fold” a portion of the data is used for training, and another for testing – this is repeated with different segments. The example shows 4-fold – 75% data used to train, remaining 25% to test.

Classification Models

In a classification model (Figure 1.18), the general principle is to determine to which discrete group, or class, some data belongs. The model itself is trained using existing data from each class, to give the spread of typical responses for that class. The model is created by solving a series of equations to arrive at the unifying relationship between the input and output – and there are a vast number of ways to do this, depending on the input data, computational power available, etc. Within neuroscience, a typical use for classification models is with behavioural responses – for a very simple example, determining if the neuronal activity of a particular group of cells can predict if the animal performed the task correctly, or incorrectly. Another example might be (taking EMG and EEG as inputs) is the animal in REM, NREM or awake state?

Regression Models

Another type of model is the regression model (Figure 1.18). They differ from classification models in that they describe a continuous variable (for example, sound amplitude). As with classification, these models can have multiple inputs and multiple outputs, resulting in a regression equation describing the relationship between the inputs and outputs, with each input typically being given a “weighting” depending on its contribution to the output. A simple example of this in neuroscience (and indeed in this project) would be trying to predict the amplitude of a sound wave, based on the ongoing spike rate of a neuronal population.

The “goodness of fit” or accuracy of a regression model may be assessed by using the R^2 metric.

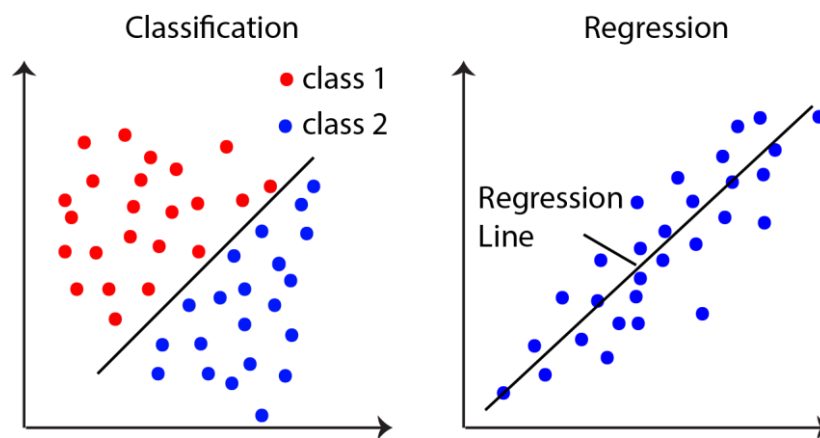


Figure 1.18: Classification vs Regression models. Dots indicate hypothetical datapoints. Axis are generic

1.8.3 Encoding Models and Adding Additional Complexity

Given appropriate time, computational power, and researcher experience, it is easy to expand the scope and of mathematical models to describe and predict highly complex data in an accurate and/or robust manner. Non-linearities can be incorporated into the equations, which is often beneficial in models of neuronal responses, (usually non-linear to some degree) and thus may help to better capture the intricacies of the data. Generalised Linear Models (GLM), a common model type, are flexible models that can describe non-linear aspects of data in a linear fashion, by deriving *linking functions*. This is but one type of model – the list is extensive. In recent years, machine learning is emerging as an excellent tool to efficiently create robust models describing highly complex data.

Though encoding models are somewhat beyond the scope of this review and the thesis, it is worth describing one typical example/building block – the linear-nonlinear Poisson model (LNP) (Figure 1.19).

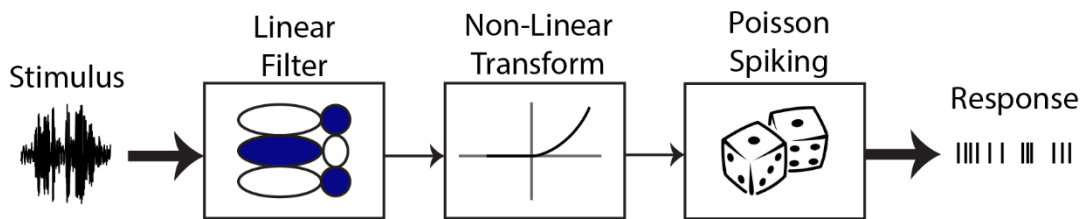


Figure 1.19: Simple linear non-linear Poisson model (schematic). An example stimulus is a burst of sound, the resulting response is a spike train

As the name suggests, these models consist of a linear filter (such as the STRF of a neuron) to filter the incoming stimuli. A non-linearity is then incorporated to better mimic neuronal responses and ensure non-negativity, and finally, a spike train is generated, based on known spike train statistics (i.e. Poisson process). The complexity of such models can be very easily increased by the addition of more neurons (with their own linear filters), which in turn can feedback and influence responses of other neurons in the model. Spiking history, additional noise, or state information (to name a few typical examples) can be slotted into the model to affect spike patterns and probability, adding additional layers of complexity mimicking real neuronal networks. Tweaking these factors systematically can then help glean additional information about influences and balances within populations. Two excellent reviews (Paninski et al., 2007, Aljadeff et al., 2016) provide clear explanations of the building blocks and concepts behind encoding models. It is important to consider that as the model increases in complexity, so too does the computational power required. Though, with the recent advent of machine learning, it is becoming easier to efficiently solve highly complex neuronal network models.

The field of mathematical models of neurons and neuronal populations is a complex, interesting, and rapidly expanding field. Open-source software and online tools (such as 2019's Open Source Brain (Gleeson et al., 2019)) are opening up the field to neuroscientists with minimal mathematical or computing experience and even providing access to supercomputers to solve particularly complex models. This is sure to result in the emergence of exciting neuroscientific theories across a spectrum of topics.

1.9 Electrophysiology

1.9.1 History of Electrophysiology

Electrophysiology is, at its most basic, the capture of electrical signals from the body, such as the heart, muscle, and - the focus of this thesis - neurons. As charged ions pass in and out of neurons, there is a difference in electrical potential (voltage) between the inside and outside of the membrane. This results in the generation of electrical fields, the measurement of which is the focus of electrophysiological techniques. Depending on the technique used, this electrical activity can be observed across a range of timescales and spatial resolutions. The electric field recorded will be the superposition of field changes in all areas of a neuron - and of the surrounding neurons, depending on the resolution of the technique employed. In the majority of techniques, the activity is recorded from outside neurons, termed an *extracellular* recording.

The origin of electrophysiology can be traced back to the 1700's and the work of Luigi Galvani on the concept of "Animal Electricity" (Piccolino, 1998). The field then progressed through the development of new devices and techniques, such as the extensive work of Edgar Adrian, who (among a great many other things) developed a way to amplify the neural signal – a crucial step to truly examine the data (Adrian, 1926). In the 1950's Hodgkin and Huxley proposed their mathematical principles and recording methods for the generation and propagation of action potentials in neurons – the theory of which is still very pertinent today (Hodgkin and Huxley, 1952, Hodgkin et al., 1952).

The late 1950s through to the 70s saw the development of tungsten microelectrodes (Hubel, 1957, Baldwin et al., 1965), patch clamping (Neher and Sakmann, 1976, Sigworth and Neher, 1980), , and the basic concept of electrode microarrays. After this point, due to discoveries in microfabrication, the potential for smaller and smaller, and better, recording devices became a reality, leading to the miniaturisation of devices and manufacture from flexible, biocompatible materials. In this project, electrophysiology refers almost exclusively to the activity of neurons in the mouse brain.

The major goal of this project is to record the activity of neurons in two brain areas simultaneously. There exists a wide variety of recording techniques for neural activity – however, there are some specific requirements related to the desired outcomes that will guide the current choice.

1.9.2 Project Requirements for Electrophysiology Method

The current project requires a high temporal resolution to probe neuronal firing activity in the form of individual spiking events (the high resolution voltage deflections resulting from action potentials). This means the recording device should have a sampling frequency reaching or exceeding 10 kHz. LFP (low frequency activity) is also of interest, so the method used must have a way of sampling this.

For the project, there is a requirement to record many neurons throughout the area of interest, in order to sample enough cell types and examine population activity. This means the method should have the capacity to both record many neurons, but also have spatial coverage appropriate to the area of interest. The ICC for example, is approximately 2 mm deep in mice and this should be covered as much as possible, and the A1 stretches around 1 mm anterior-posterior (Paxinos and Franklin, 2012). Ideally, to make layer/depth specific analysis easier, the device would be linear. The spacing of recording sites needs to be appropriate to the area, and allow easy effective spike sorting of single units (it should not have spacing that will potentially miss neurons). However, the electrodes should also not be spread out over too much of a depth, as it needs to fit within the brain area of interest.

The recordings will be acute, with the animal head-fixed, and recordings will be done over two separate days to gather as many neurons as possible. Any device must thus be suitable for an *in vivo* environment and be able to be inserted multiple times with minimal damage to tissue and/or risk of breakage. Similarly, multiple areas will be probed simultaneously, meaning the device needs to be easy to use and its associated hardware reasonably compact.

The search is further narrowed by defining what is not required. Chemical or in-depth membrane properties of neurons and their synapses are not required, similarly, extracellular recordings are more than adequate for the project's needs. Cell type specificity (such as through genetically coded indicators) is not required. The method does not need to be wireless, as recordings can be completed in head-fixed animals due to the passive, acute nature of the recordings. Additionally, wireless solutions typically have limitations on data transfer, and the channel count and sampling rate should be as high as possible. Incorporating wireless power can also result in a significant weight increase (batteries, coils etc). Similarly, the device does not need to be implanted chronically. With acute recordings, multiple neuronal populations can be sampled, and chronic tissue responses to the device are not applicable.

1.9.3 Non-Electrophysiological Methods

There are other methods to examine neuronal activity, aside from the direct measurement of electrical activity (electrophysiology). Such methods measure quantities related to electrical activity of neurons, such as blood flow (BOLD fMRI - (Ogawa and Lee, 1990, Ogawa et al., 1990)), magnetic fields (MEG - (Cohen, 1968, Cohen, 1972)), and calcium transients (genetically encoded calcium indicators i.e. GCaMP6 - (Chen et al., 2013)). These methods can be non-invasive, but on the whole are lacking in both spatial and/or temporal resolution and may require prohibitively expensive equipment. As such, only electrophysiology methods are considered.

1.9.4 Potential Electrophysiology Options

EEG

EEG involves recording electrical signals from the surface of the scalp, and is thus non-invasive. It is commonly used for application such as human BCI and non-verbal communication machines. The signal being recorded is the summation of neuronal activity over a relatively large area, at frequencies up to ~1000Hz. Depending on the questions being asked, the activity and power of specific frequency bands can be examined. These have been associated with attentional levels, memory (for example) (Klimesch et al., 1998, Klimesch, 1999, Jasper and Andrews, 2010), and abnormalities are associated with neuropathologies such as epilepsy (Noachtar and Remi, 2009). For this project however, it is not suitable by itself. It is non-invasive and painless, but these are not important features for this experiment. The crucial issues are that of spatial resolution and strengths of signals, both of which are reduced due to signals needing to pass through the scalp, skull and brain membranes (Nunez et al., 1994). Higher frequencies in particular are attenuated by the skull (Jackson and Bolger, 2014). While lower frequency (<1000Hz) neuronal signals will be examined, these can be obtained more directly from the brain using other methods.

ECoG

Electrocorticography is very similar in principle to EEG but recorded from the surface of the brain. Signals are thus of better quality but are not recording the specific signals desired – namely, individual spiking of neurons at depths, simultaneously but distinctly. ECoG of some degree is incorporated into the headcap design. By recording with a simple screw on the surface of the brain, brain states are potentially monitored.

Patch Clamping

With patch clamping, a tight, high impedance seal is created around a small portion of the cell membrane, to accurately measure membrane properties including current flow/action potentials (Neher and Sakmann, 1976). While capable of giving excellent information about that neuron and its connections, it is difficult to do *in vivo* and once again does not fit the remit of recording at depths simultaneously.

Microelectrodes (single)

Microelectrodes are immediately a more attractive option for recording, as they are sized on a similar scale to neurons and can directly record extracellular activity from individual neurons.

Single microelectrodes are generally made from insulated metal wires (i.e. tungsten) or glass micropipettes filled with high molar potassium chloride (Ling and Gerard, 1949, Hubel, 1957), though more exotic materials such as carbon fibre can also be incorporated (Armstrong-James and Millar, 1979). A sharp tip is imperative to minimise tissue damage and increase resolution. Single wires are common, as is a configuration known as the tetrode, consisting of 4 tightly wound fibres resulting in 4 recording sites in close spatial proximity at the tip of the device (McNaughton et al., 1983). The main issue with these types is again depth coverage and the number of neurons able to be recorded simultaneously (realistically, only a handful). They are well suited for functional mapping studies, as wires/pipettes can be steadily advanced through a structure to record from multiple neurons, and this has been well employed in inferior colliculus studies (Schreiner and Langner, 1988, Langner et al., 2002).

Microelectrode Arrays

With the advent of microfabrication and silicon wafers came the creation of microelectrode arrays. Arrays of microscopic electrodes and their associated wires can be patterned onto 3D silicon substrates with high accuracy and in a variety of configurations (Bai and Wise, 2001, Csicsvari et al., 2003, Blanche et al., 2005), or shaped into arrays of fine tips through microfabrication processes (Campbell et al., 1991). Microelectrode arrays can and have taken a variety of forms in recent years, with commercial companies such as NeuroNexus, Cambridge Neurotech, and Blackrock Microsystems providing a vast array of different configurations (NeuroNexus, 2019, NeuroTech, 2019, Microsystems, 2018), some of which are displayed in Figure 1.20. Due to their high temporal and spatial resolution and capacity for highly simultaneous recording of neurons throughout a structure's depth,

they are an excellent choice for the current application. Microarrays are generally either 2D or 3D, with each having applications to which they are best suited.

2D Silicon Microelectrodes

2D microarrays (Figure 1.20B) generally take the form of a thin silicon-based shank, containing microelectrodes in various configurations, coated with a biocompatible material for stability. Design features to consider include number of electrodes, electrode spacing, electrode configuration (linear etc), length and number of shanks – and often there are trade-offs between these. There is the potential for excellent depth coverage, and anterior-posterior coverage with multi-shank configurations. Typically, a single shank can contain between 4 and 32 channels. Devices are suitable for acute recordings, provided the researcher takes care with insertion and cleaning of the probe after use. Chronic-specific devices are also available.

One of their current issues with silicon microelectrode arrays include their inflexibility. Silicon is able to bend, but the discrepancy between the Young's Modulus of tissue and probe is large (10^5 - 10^7 Pa (Polanco et al., 2016)) and still causes tissue damage over time. Great care must thus be taken when inserting. Effects may be mitigated by habituating animals well, and by using sturdy equipment unsusceptible to movement. Silicon probes are also not inexpensive (\$400-\$1000 depending on the configuration) and so require very careful handling and cleaning to get the most use.

High Density Microarrays

Very recently, the Neuropixel probe has arrived on the market (Figure 1.20C). Compared to traditional silicon probes, these have an incredibly high number and density of channels over a long shank, resulting in incredible potential for simultaneous recording of 100s of single units from many brain areas. This is possible through the use of CMOS technology, allowing for incredible fast switching of the active channel far higher than the sampling frequency, so that data is still read in simultaneously from all channels at a rate of 20 kHz. Amplification and filtering is done at the probe base, resulting in very clean data transmission (Jun et al., 2017).

This project does not utilise them for the following reasons. Firstly, they were only released towards the end of the project. Secondly, they cannot record the full AC and IC depths simultaneously, and so for this particular study, they are not suited. Potentially, two probes could be used (and record simultaneously from the auditory thalamus), but this adds needless complexity and cost. However, the potential of these devices for exploring the brain (including chronically) has already proved exceptional. A recent study utilised Neuropixel probes to record, overall, 24 000 neurons in 34 brain regions (not simultaneously) during behavioural tasks, identifying new connections and regions involved which had not been considered (Allen et al., 2019).

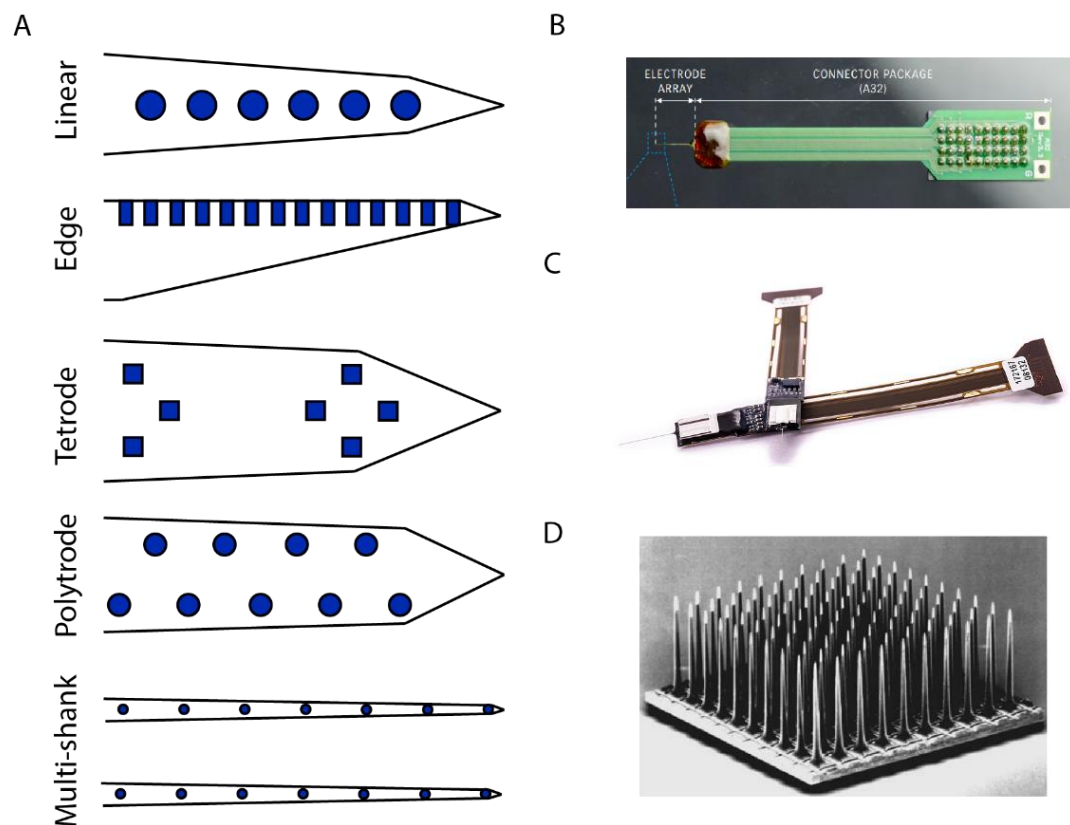


Figure 1.20: Microelectrodes. (A) Electrode configurations for NeuroNexus silicon probes (adapted from design catalogue, (NeuroNexus, 2019)) (B) NeuroNexus silicon probe. (C) Neuropixels high density probe (IMEC, 2020) (D) Utah 3D array (electron micrograph, from (Kim et al., 2006))

3D Microelectrode Arrays

Traditional 3D Arrays

3D microarrays were created to provide good surface spatial coverage, particularly for larger animals (including humans). They consist of a bed of multiple penetrating shanks arranged in a grid, with a single recording site at the end of each tip. The most ubiquitous of these is the Utah array as seen in Figure 1.20D (Campbell et al., 1991),

which sees most use in the field of human and monkey neuroprosthetics (Schultz and Kuiken, 2011). These forms of microarray are excellent in their chosen application, but for acute recordings they would be inconvenient in terms of size, lack of simultaneous depth recording and high acute tissue damage. One potential (but somewhat time consuming) solution to these issues was demonstrated by Ogawa et al in 2011, where they manually created a 2x4 (i.e. 8 shank) array by gluing together two Neuronexus probes (4x8 electrodes) (Ogawa et al., 2011). This created a 3D array with depth recording for investigating sound coding across a large area of the primary auditory cortex in rats – something which Utah arrays cannot provide.

Super-Flexible Arrays

At the cutting edge of 3D microarrays (in a sense) are electrode nets and meshes. These are very likely to be the future of chronic recordings in humans, and usually consist of thin, highly flexible (comparable to tissue) ribbons arranged as meshes/grids, containing electrodes of the same scale as neurons (Yang et al., 2019). These are injected into the relevant brain area and cover a wide range of depths. They are inherently suitable for chronic recordings as, while the initial surgery is complex, due to their high flexibility and biocompatibility/biomimicry they can remain within the brain for long periods of time without causing damage (Fu et al., 2017). Their complexity means they are not a viable solution for the current application, but they may be a potential technology when creating new generations of auditory implants.

1.9.5 Choice of Device and Strategy

Considering the options above, in this instance, 2D silicon microarrays are an excellent choice, offering high temporal resolution for spiking and LFP activity, depth of recording, appropriate electrode spacing and overall electrode count, and ease of use for acute recordings. In the future, should the species or functionality required change, other forms of electrophysiology recording may be considered. The 2D microarray also allows relatively easy simultaneous recording from two brain areas, which is a crucial feature that will add weight and context to observations. Simultaneous recording from many brain regions at once is fast becoming the standard for electrophysiological research, particularly since the advent of the high density Neuropixel probe, thus it is important to take this approach to ensure relevance in the systems neuroscience sphere.

1.9.6 The Mouse as a Model for Hearing Research

Because of the high resolution activity to be examined, recording electrical activity from humans is not feasible (this is to say nothing of the ethical, time and monetary considerations) – thus, as is common in scientific research, animal models are used. This project is based in the mouse, and the next section will discuss the rationale for this choice.

In general, mice are excellent animal models. They (and their brains) are relatively small, meaning pathways have been well mapped and the main circuitry is well understood. Genetic modifications can be easily introduced, and the animals breed quickly, meaning less reliance on viral injections and thus a simplification of experiments. From a neuroscience standpoint, mice are easy to headfix due to their small size, and thus neural recording probes can be easily inserted during acute recordings. They also share most of the same basic neuronal types (pyramidal, interneurons etc) as humans as well as displaying the stereotypical layered cortex - with slight differences in separability of the layers.

Specifically, why should mice be used for hearing studies (pioneering work has been done generally in the cat and guinea-pig) - and what are the potential limitations? Usefully, the common c57 mouse line displays progressive hearing loss, starting around the age of 6 months, making it a model for sensorineural age related hearing loss (Henry and Chole, 1980). The structure of their cochlea and middle ear is the same as humans, plus tonotopy is conserved throughout the central auditory pathway, paralleling our assumptions on the human pathway. The pathway itself is largely the same, though there are some interspecies differences in, for example, the relative size of certain nuclei.

One of the main differences between human and murine hearing is the difference in range of hearing. For humans, this is 20 Hz-20 kHz, whereas mice start and end higher (3 kHz- around 100 kHz). They also have a smooth brain, though for our purposes of passive listening experiments, extensive cognition potential is not required. As mentioned, there are also differences in relative sizes and shapes of the auditory nuclei, though the fundamental pathway and basic functions remain the same.

1.10 The Curse of Dimensionality

In recent years, the focus of neuroscience research is shifting from analysis of single units and correlated pairs, to the dynamic activity of neuronal ensembles and their function, particularly in the sensory cortexes. Data is encoded not just in the spiking of individual units, but in the ways they interact together as a population (Panzeri et al., 2015).

Advancements in silicon probe technology (such as Neuropixels (Jun et al., 2017)) and chronic preparations), fluorescent imaging techniques, and the optogenetic toolbox have provided unprecedented opportunities observe and manipulate large numbers of neurons simultaneously, on a variety of timescales and during a vast array of multi-modal stimuli and behavioural paradigms. After appropriate analytical techniques have been applied, the dynamics of neuronal population activity can be observed, with hypotheses then formed on their function and potential influences.

A potential bottleneck in analysis of these large datasets is the so-called “curse of dimensionality”. A recording from a single Neuropixel probe contains both the high and low frequency activity of hundreds of neurons (of multiple cell types), across several brain areas. Depending on the configurations, hundreds of trials of multiple stimuli types may be applied, over several hours, days or even weeks – plus there is an ongoing influence of attentional state. As such, robust hypotheses and efficient analytical pipelines are required in order to make relevant and useful conclusions from the data.

To help with this, dimensionality reduction may be employed. With these techniques, the number of dimensions required to explain the variance in the data is reduced, by condensing a high number of dimensions into a smaller number of new, relevant dimensions (comprised of co-variations of the original dimensions). Dimensions are unlikely to be combined in a purely linear manner – instead, each component of the new dimension will be weighted according to its contribution. Consider a hypothetical situation involving 10 neurons. After applying dimensionality reduction, it may be that neurons 1, 2, 3 and 4 are not contributing at all to the variance seen in the output data – they may be untuned to the current stimuli, for example, and output only spontaneous activity. As such, these “dimensions” can be given minimal attention. Conversely, 70% of the variance may be explained by the activity of neurons 5, 7 and 9, with the remaining 30% explained by 6, 8, and 10. As such, 10 dimensions has been reduced (essentially) to only 2.

In conjunction with its obvious application in reducing complexity of calculations, the ways in which researchers apply and interpret the raw results of the dimensionality reduction can themselves be highly informative as to the structure of neuronal population activity. Hypothetical neurons 5, 7 and 9 may turn out to be excitatory, and spaced closely together, while 6, 8 and 10 may be interneurons having a secondary, supporting role. Through inspired interpretation of dimensionality reduction outputs, it may be possible to gain insight into the character and dynamics of neuronal populations. An excellent review by Cunningham and Yu in 2014 talks extensively about the principles, motivations and applications of dimensionality reduction to neural data, and should be referred to as expansion of this short review (Cunningham and Yu, 2014). The applicability of dimensionality reduction, and the available techniques, will be expanded upon in the Chapter 5.

1.11 Pathologies of the Auditory System

1.11.1 Types of Hearing Loss

As should be apparent from the review so far, the auditory system is incredibly complex. Unfortunately, this often means there are more places to go wrong - pathologies are common throughout the hearing pathway, resulting in varying degrees of hearing loss. Hearing loss can be broadly split into two categories – conductive and sensorineural. Conductive hearing loss derives from issues with the conductive portion of the pathway (tympanic membrane, ossicles etc), and generally results in sounds being muffled and speech hard to follow. This could arise through infection, damage (e.g. perforated ear-drum), fluid/wax build up, or abnormal growth of middle ear bones (Bansal, 2013a).

Sensorineural hearing loss involves the neuronal/cellular portion of the pathway, and tends to present in a more complex manner (difficulties understanding speech, disruption to hearing certain frequencies, issues with sound localisation, as well as muffled sounds and/or tinnitus). Common causes include trauma of the cochlea and/or auditory nerve (e.g. a car accident), as well as various infections and congenital abnormalities in the cochlea and/or auditory nerve (Bansal, 2013b). The causes of these conditions are generally more difficult to treat than conductive loss.

1.11.2 Neurofibromatosis Type II

One specific cause of sensorineural hearing loss is Neurofibromatosis Type II (NF2). NF2 is a severe, but rare (1 in 25000 (NINDS, 2019)) genetic disorder, typically

characterised by the presence of benign tumours around the patient's nerves and brain, particularly bilateral tumours on either side of the brainstem and vestibulocochlear nerve (known as acoustic neuromas) (Evans, 2015). Though benign, the placement of these tumours and the resulting pressures on key nerves causes a variety of neurological symptoms, such as balance issues, tinnitus, headaches, gradual hearing loss and limb weakness. Current surgical interventions unfortunately require the transection of the vestibulocochlear nerve - usually resulting in permanent and irreversible hearing loss, and no benefit to be gained from a cochlear implant (CI) (Evans, 2009).

1.12 Auditory Neuroprosthetics

1.12.1 Principles of Neuroprosthetics

Neuroprosthetics are devices made to augment, repair or replace lost nervous function in the body. In the context of auditory pathologies, this refers to devices involving a set of electrodes that are inserted into the cochlea or appropriate area of the brain. Environmental sound is picked up by an external microphone, and a sound processing algorithm transforms this into spectral and temporal patterns of electrical stimulation. Applied to the area, this would then ideally restore some level of sound perception.

1.12.2 Cochlear Implants

If the pathology lies in the cochlea itself, but the auditory nerve/spiral ganglion cells are still intact, restoration of some degree of hearing may be possible with a cochlear implant (CI) - arguably the most successful neuroprosthetic to date. CIs work on the principle of activating the remaining nerves with electrical pulses to induce hearing sensation – placing electrodes to replicate/replace hair cells' input along the tonotopic gradient of the cochlea. Incoming sound is digitised by a unit on the outside of the skull, then transmitted to an internal processor for translation into electrical stimulation patterns (Rubinstein and Miller, 1999). These patterns are then relayed to the electrode, which is implanted into the cochlea (Figure 1.21).



Figure 1.21: Cochlear implant (electrodes). Modern implants can cover the full range of the cochlea.
Source: (MED-EL, 2017a)

The CI has been implanted in over 300 000 patients (NIDCD, 2015) since 1957, and its current, multi-channel form means good to excellent restoration of speech recognition is very much a reality. However, noisy rooms often cause problems with speech recognition – despite increasingly complex speech transformation algorithms (Moser, 2015) . Additionally, while modern devices by companies such as MED-EL have up to 24 individually addressable electrodes (MED-EL, 2017b), the reality is that far fewer distinct spatial locations are individually addressable. The cochlea is bathed in electrolytic fluid, and so electricity spreads outwards from the intended site of stimulation, overlapping with the fields of neighbouring electrodes (Weiss et al., 2016). In addition, with the increased field of activation, it becomes more likely that axons (and so upstream neurons) are inadvertently activated.

The CI is also not a solution for all hearing pathologies. Even if the cochlea and hair cells are functioning as normal, or their function can be replaced by the CI, a damaged or lost auditory nerve means the signals cannot be transferred to the brain, and sound is not perceived. This can arise from many things, such as congenital aplasia of the cochlea or auditory nerve, or ossification following meningitis (Sennaroglu and Ziyal, 2012). It is also a side effect of the tumour removal surgery in NF2 (Evans, 2009).

1.12.3 Auditory Brainstem Implants

With NF2 in mind, the first Auditory Brainstem Implants (ABI) were designed (Edgerton et al., 1982). Taking its cue from the CI, the ABI has many of the same parts, but the electrodes are instead laid over the surface of the cochlear nucleus to cover the tonotopic gradient (see Figure 1.22 for a modern example) (Wong et al., 2019) .They can be implanted at the same time as the tumour removal surgery, eliminating the need for additional, risky surgeries.



Figure 1.22: 21 electrode surface auditory brainstem implant. Source: (McCreery and Otto, 2011, Berndt and Deisseroth, 2015)

The first multi-channel ABIs were implanted in the early 90s (Laszig et al., 1991, Nevison et al., 2002). Since then, there have been additional cohorts and follow up studies in patients of all ages and conditions – with mixed results (Schwartz et al., 2008, Goffi-Gomez et al., 2012, Colletti et al., 2014). Potential reasons for disappointing results include the difficulty of surgery and tumour removal (and the long-term mechanical pressure exerted by tumours themselves), and the resulting damage to the surrounding structures (McCreery, 2008, Matthies et al., 2014). Colletti and colleagues, after their study of both NF2 and non-tumour patients, speculate that the surgical area may contain other important auditory structures or essential pathways, which are then damaged during surgery (Colletti et al., 2009). Even in those patients where the device is “successful”, performance still lags behind that of the CI, which was unexpected.

Many of the reasons put forward are common to both NF2 and non-tumour patients, mainly the surgical difficulty, and electrode misalignment or migration (Behr et al., 2014). CI based processing and stimulation strategies continue to be used, despite the increased coding complexity higher in the auditory pathway (Lenarz et al., 2006). Current spread (an inadvertent activation of more neurons) remains an issue. An alternative, penetrating ABI provided better selectivity, but produced no significant differences in speech understanding when compared to the traditional surface electrode (McCreery, 2008, Otto et al., 2008).

1.12.4 Auditory Midbrain Implants

The ABI, in its current and future iterations, would appear to be a potential solution for some sensorineural hearing loss pathologies, but looks less promising for NF2, the condition it was originally created to treat. Auditory researchers revisited the central auditory pathway, and identified a potential new site for an auditory implant: the inferior colliculus. Several criteria were outlined (Lim et al., 2007, Lim et al., 2009, Lim and Lenarz, 2015), which the inferior colliculus was identified as meeting:

- Surgical accessibility (a more surface structure)
- A defined neurological organisation - i.e. tonotopy
- A reasonably low level of auditory coding complexity

Higher structures, such as the medial geniculate nucleus and auditory cortex, were discounted due to their less consistent tonotopy, increased coding complexity, and potential for plasticity (Lim et al., 2011). A penetrating Auditory Midbrain Implant (AMI) was designed in the early-mid 2000's by Thomas and Minoo Lenarz (and colleagues), Figure 1.23. The device is similar in principle, and in several components, to existing CI and ABIs – but instead of the surface array, the electrode array is arranged on a single penetrating shank, to be implanted into the tonotopic gradient of the ICC (Lenarz et al., 2006).

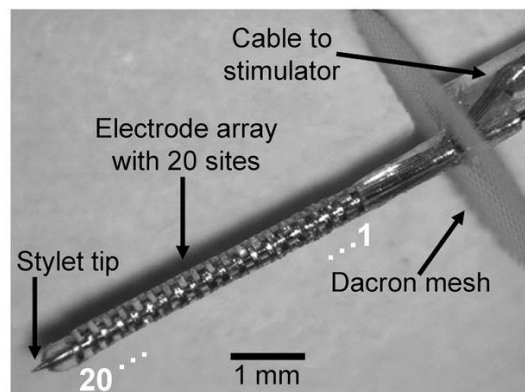


Figure 1.23: Penetrating single shank auditory midbrain implant. Source: Lenarz et al, 2006

The results from the first human clinical trials (of 5 patients) were first reported in 2007, and reviewed in 2009 (Samii et al., 2007, Lim et al., 2007, Lim et al., 2009). The authors note the difficulty (and importance) of correct electrode placement. The device was implanted fully into the central nucleus in only 1 of 3 cases, and predictably, this patient showed the most favourable results (Lim et al., 2009). The authors attribute the misplacement to a number of things, principally the fact that the surgery was developed and tested in fresh cadavers, whose tissue did not shift and settle in the same way as live tissue, leading to misplacement of the electrode enough to miss the central nucleus (Lim et al., 2009).

All three patients saw some improvement. Mis-implanted patients saw least benefit, with improvements limited to lip reading boosts and environmental awareness (Lim et al., 2009). In a follow-up paper in 2015, the first patients are discussed further, noting the device's long term (6 year) safety record, and the continued benefits of environmental sound awareness, and basic speech perception, which are

comparable to NF2 ABI patients (Lim and Lenarz, 2015). The second, ongoing clinical trial uses a two shank AMI, as it was discovered that this has the potential to vastly improve the device's potential for speech replication (Lim and Lenarz, 2015). This trial has 5 participants, and is expected to release first results in early 2021 (Hannover Medical School - NCT02984202, 2016).

However, as discussed, the continued use of CI based stimulation strategies could be limiting the abilities of central auditory devices. Ideally there should be new strategies developed around the coding of the inferior colliculus.

1.12.5 Speech Processing Algorithms

Each of the implants described above relies on a sound processing algorithm. This part of the device is responsible for translating the sound in the environment into a spatiotemporal pattern of electrical impulses. The majority of the work presented here is on the cochlea implant – but as ABIs and AMI employ the same processing strategies, the review below is still highly applicable (Lim et al., 2009). Keeping these processing strategies in mind when interpreting data may offer up areas for their improvements/fine-tuning.

The basic principle of these devices is the idea of a “filter bank”. The device filters the incoming broadband sound into a series of narrow band signals. The envelope of these signals is then extracted and rectified, non-linearly mapped, and used to modulate a pulse train. The signal is mapped to the dynamic range of that electrode site (Loizou, 2006, Wouters et al., 2015). In this context, the dynamic range is the range between the stimulation amplitude that elicits a threshold response (edge of hearing) and that which results in uncomfortable/painfully loud sound. This mapping between dB level and stimulation level is generally non-linear, and specific for each electrode and each patient. Thus, the incoming sound is translated into a spatial-temporal-amplitude pattern electrical stimulation. This is somewhat similar to the principle of the cochlea – the basilar membrane and its locational frequency specificity basically acts as filter bank, with spiral ganglion neurons then generating the “pulse train”.

The rate of stimulation is also important – in theory, the higher the pulse rate, the more distinctive that sound component will be, and the better speech recognition the patient will show. The issue of stimulation rate did, until recently, restrict the use of optogenetic stimulation, in auditory implants for a long time. It is obviously important

to obtain a good temporal resolution – otherwise, intricacies in speech may not be properly conveyed, resulting in poor recognition. A typical range for modern CIs is ~800-2500 pulses per second (Loizou, 2006, Arora, 2012), with similar strategies used in ABI and AMIs. While in general, it appears that high stimulation rates increase performance, this is not a hard and fast rule, and the actual effect would seem to be dependent on a number of variables such as the encoding strategy and the patients themselves (Loizou et al., 2000, Kim et al., 2000, Plant et al., 2007, Weber et al., 2007, Shannon et al., 2011). Additionally, increasing the pulse rate comes at a drawback of increasing channel cross talk (Middlebrooks, 2004).

There are several different strategies for stimulating the electrode channels/frequency band in an auditory prosthetic device. Electrodes can be stimulated entirely independently, in small groups (pairs, quartets), or simultaneous activation of all electrodes (plus hybrid approaches of these). The two main strategies are highlighted below, though it should be noted that optimisations and hybrids of these (often proprietary) are common in order to get the best speech reproduction possible, and are still a subject of research and a distinguishing features between manufacturers. As well as utilising the on-device electrodes, it is also possible to employ current steering to generate additional, “virtual channels” between each regular channel, in order to increase resolution (Koch et al., 2007, Choi and Hsu, 2009).

Continuous interleaved sampling (CIS) is a strategy which stimulates all electrodes in sequence, in a non-overlapping (interleaved) pattern, so as to avoid electrode interactions (Wilson et al., 1991). Stimulation rate employed is variable (250pps to several thousand) (Loizou, 2006).

The “n-of-m” strategy is another type – originally known as SPEAK (spectral peak coding) (McDermott et al., 1992) and now existing in a more advanced form as ACE - Advanced Combination Encoders - (Vandali et al., 2000), incorporating higher stimulation rates than SPEAK (e.g. 250pps vs 900 pps) (Psarros et al., 2002). The principle of this strategy is that it continually monitors the filter output and selects the highest of these for stimulation, rather than stimulating all electrodes as in CIS, with the range and the exact electrodes changing dynamically as the sound input spectrum changes.

As with stimulation rate, preferences vary but in general, the ACE strategy is preferred, and gives better results in speech recognition tests than CIS or the similar SPEAK (Kiefer et al., 2001, Psarros et al., 2002, Skinner et al., 2002). This may be due to its

selectivity and the theoretical benefits of higher stimulation rate – as it is only trying to replicate the louder (and presumably more important) sounds, there may be less confusion with background noise.

Given that these algorithms will naturally work better when given both more channels (either physically, or by increasing the resolution of existing ones), there exists an opening for a new method of stimulation that meets this requirement. Having stimulation that is more delicate or sensitive may also increase the dynamic range at each site, meaning each frequency can be better represented. It is worth noting that a stimulation rate of at least 250Hz is needed to match SPEAK, and ideally even higher, given the success of ACE and CIS. This has for a long time been a “sticking point” in the search for new stimulation methods.

It may also be that these strategies, though employed successfully in the CI, may need refinement or adaptation to the different architecture and environment of the brainstem and midbrain. Additionally, electrical stimulation, either by its nature or the slight mis-positioning of the original implant, can spread into neighbouring, non-auditory areas when used in the brain – for example, the superior colliculus in the midbrain. This has resulted in a number of non-auditory side effects, including vertigo, nausea, and visual disturbances, and often leads to patients stopping the use of devices – making the fitting of the device a waste of time, money, and a highly disappointing experience for the patient. By recognising the requirements for new devices or stimulation strategies (i.e. stimulation rate), other stimulation methodologies can be examined, such as optogenetics.

1.12.6 Optogenetics for Auditory Neuroprosthetics

Planned improvements to the AMI do not solve one of the original issues with electrically-based stimulation devices – the number of independently activatable channels is still limited by current spread, which in turn limits the frequency resolution. No matter the speech processing algorithm used, this is a fundamental problem. Optogenetics may now offer a potential solution (Figure 1.24). By inducing neurons in a particular area, or of a particular type, to express light activated proteins, they can instead be activated by light. Only cells containing the necessary protein (opsins) will be activated – and coupled with the overall lower spread of light in tissues, this is theoretically translated into an improved spatial (and thus spectral) resolution – a long term goal of auditory implant development (Deisseroth, 2011, Moser, 2015). It may also help reduce side effects caused by current spread into neighbouring brain areas,

such as facial tingling, headaches and vertigo (Moser, 2015, Lundin, 2016). The next section of this literature will be dedicated to setting down the principles of optogenetics and choice of opsins, the viability of optogenetics as an electrode alternative.

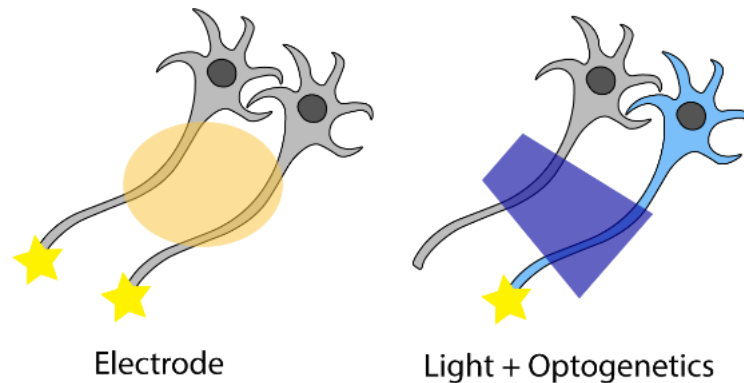


Figure 1.24: Electrical vs optogenetic stimulation. Only the neuron containing opsins (blue) can be activated by light. Adapted from (Deisseroth, 2011)

1.13 Optogenetics

1.13.1 History and General Principles

Optogenetics has been defined as: “the combination of genetic and optical methods to achieve gain or loss of function of well-defined events in specific cells of living tissue” (Deisseroth, 2011). Since 2005, the depth and breadth of its use has undergone a veritable explosion, with the technique being instrumental in a vast number of discoveries about neurological circuits and their functions. By inducing the expression of light sensitive proteins using a variety of techniques, the cells can thus be activated/deactivated with light as desired, allowing us to probe neural circuits.

In the majority of cases, the light sensitive protein will be one of the “microbial opsins”. Of the entire family of microbial opsins, three of these make up the majority of available optogenetic tools: bacteriorhodopsins, halorhodopsins, and the most ubiquitous, channelrhodopsins. Their basic mechanisms are detailed in Figure 1.25. All work on the principle of exciting or suppressing cell membranes through transportation of charged particles.

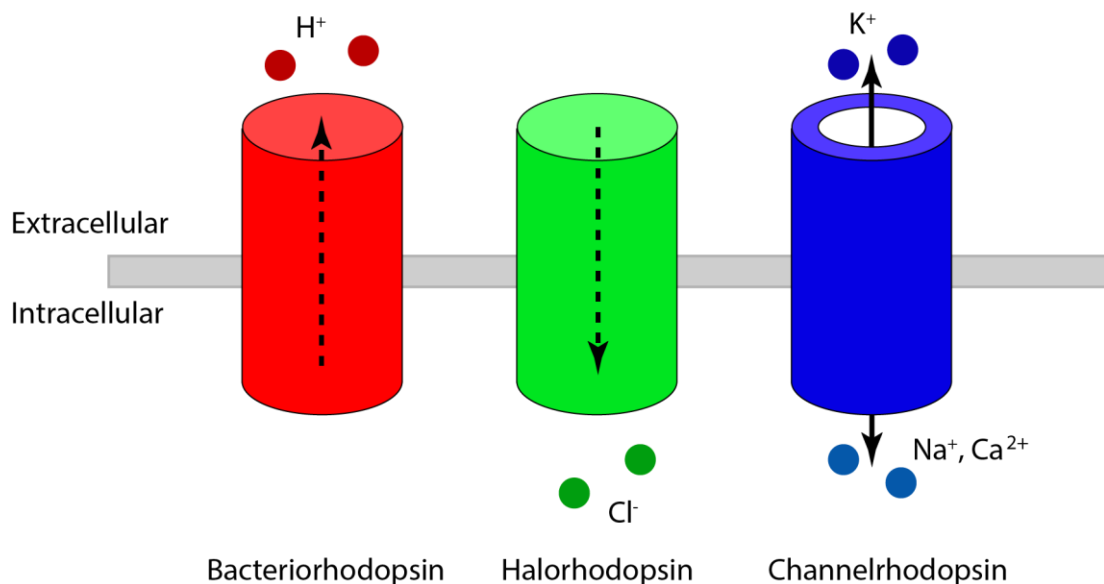


Figure 1.25: The three main families of microbial opsin. Bacteriorhodopsins pump protons out of the cell, while halorhodopsins pump chloride ions in – having an inhibitory effect on the cell. Channelrhodopsin (ChR) is principally an excitatory opsin and light gated ion channel, allowing flow of ions through the membrane, causing depolarisation. Inhibitory ChRs, allowing inward flow of chloride ions, have also been engineered and later discovered in nature. (Berndt et al., 2014, Berndt and Deisseroth, 2015, Deisseroth, 2015)

Since the original descriptions of channelrhodopsin (ChR) 1 and 2 in 2002 and 2003 respectively (Nagel et al., 2002, Nagel et al., 2003), and bacterorhodopsins (BR) and halorhodopsins (HR) some 30 years prior (Oesterhelt and Stoeckenius, 1971, Matsuno-Yagi and Mukohata, 1977), new microbial opsins have been discovered and engineered, continually expanding the range of temporal kinetics (i.e. latency and refractory periods), excitation wavelengths, and light sensitivity. Table 1.3 below contains some examples of commonly used opsins. This is NOT an exhaustive list – many of the opsins in the table are variations on a base molecule (such as NpHR, or Chrimson) that improve upon important variables as stated above, or trafficking to membrane (generally denoted by an “e” at the start of the name). Additionally, values stated as usually best estimates, as different groups can report slight changes in values, based on differing experimental setups. Generally, there are trade-offs between variables (i.e. red shifted opsins will be slower) – but this is becoming less of a reality through targeted engineering. Additionally, while a peak wavelength is stated, the actual bandwidth that can elicit a response is usually wider. In Table 1.3, a number of well known (but potentially) older opsins are presented, in order to illustrate the breadth of properties available. As previously mentioned, work is constantly ongoing to engineer and discover new and improved opsin types – there are a great many of these, offering improvements to the base opsin in terms of basic

qualities such as of sensitivity, kinetics and membrane expression levels. For example, ChETA opsins were mutated from ChR2, but provide much faster, cleaner kinetics at the expense of lowered maximum photocurrents (Gunaydin et al., 2010). ChR2, as essentially the first opsin to be used in neuroscience extensively, is usually cited as a benchmark/comparison for describing new opsin variations.

Table 1.3: Range of common opsins. ChR: Channelrhodopsin, BR: Bacteriorhodopsin, HRL Halorhodopsin. Table partially adapted from (Yizhar et al., 2011)

Opsin Name	Class	Effect	Wavelength (peak, nm)	Sensitivity (mW/mm²)	Off Kinetics (ms)	Ref.
ChR2	ChR	Excitatory	470	0.1-1	11	(Nagel et al., 2003, Boyden et al., 2005)
eNpHR3.0	HR	Inhibitory	570	5.42	4.2	(Gradinaru et al., 2008, Gradinaru et al., 2010)
Chronos	ChR	Excitatory	470	0.05	3.6	(Klapoetke et al., 2014)
ChrimsonR	ChR	Excitatory	590	0.02	15.5	(Klapoetke et al., 2014, Hight et al., 2015)
VChR1	CHR	Excitatory	535		133	(Zhang et al., 2008)
ArchT3.0	BR	Inhibitory	540	~1	5	(Chow et al., 2010, Han et al., 2011, Mattis et al., 2011)

1.13.2 Opsin Selection

There is a huge breadth of opsins available beyond Table 1.3, and so for any given application, researchers should select the most suitable tool. Important features and points of consideration are discussed below.

The choice of light wavelength is highly dependent on the experimental protocol. Blue/Green light, while the most common activating wavelengths for opsins are more damaging to cells, and do not travel as far through tissue (Mager et al., 2018b, Yizhar et al., 2011). This has driven the search for more “red-shifted” opsins – not only can they reach further into the tissue, but it also opens up the possibility of dual colour excitation/inhibition of different cell classes in the same area, with a smaller risk of cell damage in chronic experiments (Klapoetke et al., 2014, Moser, 2015). Using highly sensitive opsins can be useful – by reducing the level of light required to activate the opsins, the power requirement of devices is reduced, a crucial step for the eventual creation of optogenetic based implants (Moser, 2015). Additionally, lower light intensity could help prevent any effects of long-term stimulation.

Off-kinetics, and kinetics in general, are often a crucial variable. After a certain threshold of pulse frequency, cells will not be able to maintain time-locking to the stimuli. Having a fast recovery time has been one of the major hurdles for optogenetics’ use in auditory applications - the SPEAK algorithms requires a stimulation rate of at least 250Hz (McDermott et al., 1992, Moser, 2015, Jeschke and Moser, 2015).

Opsins are also available as both excitatory and inhibitory (Deisseroth, 2015). Depending on the questions being asked, the researcher may wish to either excite or inhibit a cell group or type, to examine its influence in a circuit or behaviour.

1.13.3 Inducing Opsin Expression

There exist a number of methods to express opsins in cells, of varying degrees of difficulty and suitability to a given experiment.

The easiest way to do this is through (principally murine) transgenic lines, where opsin is expressed in all cells, or specific brain areas or cell types (Fenno et al., 2011, Zhang et al., 2010). While these are easy to work with, this approach is not particularly feasible in animal models beyond mice and rats. Additionally, as neuroscience begins to probe highlight specific brain areas, pathways, and cell types, there is a requirement for greater freedom in choosing the specifics of opsin expression.

A common approach to introduce expression of opsins in a species is through targeted viral injections. The simplest way of doing this is packaging the desired opsin with a virus, usually an adeno-associated virus (AAV)(Monahan and Samulski, 2000). A fluorescent marker (such as GFP, YFP or mCherry) can be combined with the opsin for later histological evaluation of targeting success (Guo et al., 2015, Hight et al., 2015). By optimising the viral injection location, volume and characteristics, the cells in a given brain area can be targeted (Yizhar et al., 2011). A useful tool in some circuitry investigation are retroviruses (e.g. rabies) – their use can induce opsin expression in targets downstream from the injected area (Callaway, 2008). To obtain cell-type specificity, the virus can be altered to contain a promoter specific to the cell type of interest (e.g. cholinergic cells) – this would work in a wild type animal (Yizhar et al., 2011). Alternatively, recombinases can be used (e.g. Cre recombinase) to allow opsin expression only when both parts of a structure are present (Gong, 2007, Yizhar et al., 2011). Commonly, a Cre recombinase coupled virus is injected into a transgenic animal containing the recombinase driver in only the target cells, leading to cell-specific opsin expression (Tsai, 2009, Zhang et al., 2010, Yizhar et al., 2011). A dual viral injection of a Cre recombinase coupled virus with the opsin, and a cell-targeted recombinase driver, may also be the best approach depending on the desired outcome (Yizhar et al., 2011). Any method involving viral injections, though it can offer excellent specificity for probing highly specific mechanisms in the brain, comes with a number of caveats. These include mistargeting during surgery (missing the desired area and hitting an unwanted one), tissue damage to overlying structures, and overall added costs (viral purchase and animal costs during incubation period). Oftentimes, the researcher will not know exactly where the virus has expressed, and will need to confirm correct (or incorrect) targeting with histology after the conclusion of the experiments.

The current project uses a stereotaxically targeted viral injection approach in wild-type animals, as we are aiming not for cell type specificity, but coverage of a relatively large brain area in the mouse – to which this technique is suited.

1.13.4 Chronos

There is a constant search for opsin with better qualities (faster, more sensitive etc), either through genetic engineering, or through extensive genetic sequencing of natural species. One such search was very fruitful - Chrimson was discovered in 2014,

when researchers *de novo* sequenced 127 algal species (Klapoetke et al., 2014). Discovered along with Chrimson was a blue activated opsin known as Chronos.

Compared to other well-known opsins (see Table 1.3), Chronos is currently one of the best choices for central auditory applications. It has very fast kinetics, can be stimulated with high fidelity up to 200-250Hz, which is the minimum required for the SPEAK algorithm (Hight et al., 2015). This property of Chronos to produce spikes with high temporal fidelity has been extensively explored. A pair of papers were released from collaborations in Massachusetts, looking at the temporal properties of Chronos in the cochlear nucleus, and in the inferior colliculus.

Comparing the responses of both ChR2 and Chronos in the cochlear nucleus, the neuronal firing induced by Chronos was found to synchronise significantly more than ChR2 to light pulse trains of 56, 168 and 224 pulses/s (Hight et al., 2015). Additionally, in the mouse inferior colliculus, Chronos was found to produce robust, consistent spike trains in response to high frequency pulses, which could be used in linear classifier models to correctly determine the parent pulse rate that produced a given spike train (Guo et al., 2015). This accuracy extended to higher frequency pulse trains than ChR2, indicating Chronos's potential for use in auditory implants. Interestingly, this robust coding was not translated into the auditory cortex, appearing to have been reformatted along the way, so as to be indistinguishable from trains produced by ChR2 at the same light frequency (Guo et al., 2015). This poses some interesting questions about exactly how auditory information is transformed through the auditory pathway – specifically between the IC and AC. How are simple sounds (such as trains of pure tones) encoded by neuronal populations, as compared to more complex, naturalistic sounds – can optogenetics be used to replicate the IC neuronal activation patterns? Answering these is crucial for proving the viability of any optogenetic based auditory implants.

The requirement for blue light is, for the immediate future, acceptable, as a good spatial resolution is desired over a large depth of tissue – though potential effects of phototoxicity should be considered and appropriately mitigated. This is explored in later sections. The high sensitivity is also good, meaning Chronos can be activated with low power (good for miniaturisation of medical devices), with less chance to damage cells. In 2018, an updated version of Chronos (Chronos ET/TS) with improved membrane trafficking was published, after researchers encountered issues with low levels of membrane expression (Keppeler et al., 2018).

Chronos, at the time of writing, is now available in a genetic mouse line (Daigle et al., 2018) – when this project was begun, it was not. As this project does not require particular cell type specificity, only to cover as much of the IC as possible (avoiding other areas), a simple targeted viral injection (AAV5) into the inferior colliculus of wild type mice is sufficient for the project.

1.13.5 Optogenetics in Humans

The advent of Chronos has made the use of optogenetics in auditory implants a real possibility. However, while faster, Chronos cannot match the temporal precision of electrical stimulation, and we have the additional hurdle of expressing opsins in humans.

Retrosense Therapeutics were the first organisation to run clinical trials (currently Stage I/II for safety and tolerability studies) for optogenetic gene therapy in the human retina, with an optogenetic promotor termed RST-001 (Allergan - NCT02556736, 2015). Companies such as GenSight Biologics have then, alongside new gene therapies, developed custom goggles for use with ChR2 transfected tissue – they filter the incoming light so that it is at ChR2's activation wavelength, allowing more extensive activation of the transfected retina (GenSight-Biologics, 2018). However, as the technologies are still emerging, the safety and ethics of viral expression in humans should continue to be closely monitored.

1.13.6 Light Delivery Systems for High Spatial Resolution Optogenetics

In order to obtain the spectral resolution benefits offered by optogenetics, the light supply itself is of critical importance. Optical fibres are often used to deliver light to surface structures, or implanted chronically to hit deeper ones, but the resolution of these is not sufficient for auditory implant purposes. Tissue damage is common when implanting larger fibres (200-400µm diameter) or when trying to reach deeper structures from the surface, requiring high light intensities that can excessively heat the tissue.

Thus, a light delivery system for a chronically implanted auditory implant has several requirements. In defence of neural cells, the device must have a thin profile, and not heat excessively. Conversely, the light must be bright enough able to provide light of sufficient brightness for the chosen opsin. In order to fully utilise the tonotopic gradient and achieve the best spectral resolution, the light emitting points should be as small and focused as possible (ideally close to a cellular scale), and the amount of these

should be scalable to target as much of the structure as possible. A less important issue in early development (but nonetheless important) is that of manufacture – the implant should be manufacturable on a large scale and for an acceptable price. If not, the implant may never be a viable choice. Current light delivery technologies can be loosely split into two main categories.

External Light Sources

Considerations for External Light Sources

The defining feature of the first category of devices is that they have the light source away from the stimulated area (i.e. further up the probe), and light is delivered down to emission points on the probe. They include waveguides (where light is coupled into a device and “guided” to emission points, see Figure 1.26), and multi-point emitting optical fibres, where the fibres have been shaped and modified to have multiple points of emission (though the light source remains external) (Wu et al., 2013, Pisanello et al., 2014). These devices have good tissue compatibility, and less potential for light-based recording artefacts, as well as reduced heating. However, increasing the number of individually addressable channels exponentially increases the complexity of device manufacture.

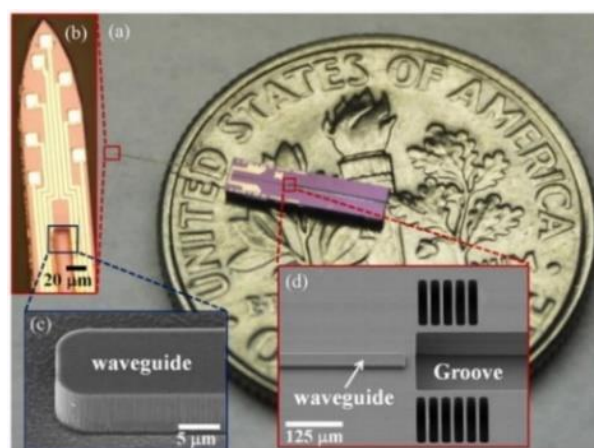


Figure 1.26: Waveguide device. Optical fibre sits in the groove and light transmitted down the waveguide. Source: Wu et al, 2013

To provide the light, both lasers and LEDs may be considered. These sources, particularly lasers, may also be bulky, limiting freely moving experiments (Moser, 2015). Looking forward to the future of human prosthesis, the device must be wireless and not bulky, meaning laser based methods are basically off the table – though LED based devices are still an option. For example, researchers have recently combined μ LEDs onto the top of glass Utah arrays for high resolution in a planar space (Scharf et al., 2018). These are unsuitable for midbrain and cochlear auditory prosthetics but

this technology may yet prove fruitful for brainstem implants, whose tonotopic gradient lies parallel to the surface of the structure. It may be that external light devices are excellent in a purely research environment (where bulky light sources and lower channel count can be worked around), but for the future of neuroprosthetics, a more adaptable approach may be required. They present a better option for integrated recording/stimulation devices as wiring and light source is held away from recording wires.

Examples of External Light Devices

A recently presented device offered 6 stimulation sites and 40 recording sites, and was validated in the awake mouse cortex (Li et al., 2018). Dual-colour devices (Kampasi et al., 2018), that may be interesting from an excitation/inhibition shaping frequency tuning angle, might also be a good avenue for research.

From a research perspective, it is worth noting that other laser-based techniques can be utilised, such as two-photon optogenetics (based on two-photon microscopy), where cells are stimulated in highly specific patterns and with excellent spatial and temporal resolution (Szabo et al., 2014). Simultaneous imaging and activation is also possible (Packer et al., 2015), and with holography techniques (Hernandez et al., 2016) becoming the new standard, these patterns can be 3D. While unsuitable for auditory implants, these techniques are nevertheless excellent for probing the function and mechanisms of specific brain circuits. Submillisecond control *in vivo* is possible through the use of Chronos (Ronzitti et al., 2017), and the technique has proven excellent for probing and imaging zebrafish motor circuits and identifying individual neurons involved in behaviours (Dal Maschio et al., 2017).

Internal Light Sources

Considerations for Internal Light Sources

The other approach is to have the light sources directly beside the cells to be stimulated. This increases the complexity of manufacture as the lighting sources and their circuits must be incorporated onto a thin device. There is also the potential for adverse heating effects as the lights will emit heat, and the base shank must be as low-profile as possible to make it suitable for insertion. The thermal conductivity properties and overall engineering of such devices are thus extremely important. Adding recording electrodes further increases this complexity, and as such, few dual devices exist and will have a low channel count. Not only is the complexity increased, but having electronics/metal in dense arrangements, and fast delivery of pulses,

results in large artefacts in the recording, when the lights are turned on – the source of these will be discussed in Chapter 6. Coupling losses found in external devices are largely eliminated however, potentially reducing the overall power requirements.

μLED Devices

Micro-LED (μLED) devices are currently considered one of the best options for use in optogenetic-based neuroprosthetics (Moser, 2015). These devices incorporate μLEDs onto traditional electrode materials/configurations, generally as penetrating shanks (e.g. silicon probes). The development of micro transfer printing (μTP), has significantly aided this endeavour (Meitl et al., 2005). μLEDs cannot be manufactured directly on all materials, and their “on-board” creation also adds significant complexity to design and manufacturing approaches. By creating components (μLEDs) and shanks separately, then placing the components later through μTP, there is greater freedom in material choice (i.e. for improved thermal properties or flexibility), and increased flexibility in circuitry design. The process is also more efficient and cost effective, as many LEDs can be manufactured at once.

Though previously sapphire was used for the ease by which LEDs can be directly manufactured onto it, this material is not ideal for *in vivo* recordings as it is brittle and difficult to thin down to a suitable thickness (Moser, 2015). Devices are now generally manufactured from silicon wafer (Wu et al., 2015). μLED devices are reasonably scalable, sufficiently bright, and eliminate potentially bulky external lights, making them more suitable for implantation. However, these benefits come at the expense of potential for tissue heating, and complexity when trying to combine them with recording electrodes. Most currently existing devices incorporate Gallium Nitride (GaN) based μLEDs onto silicon substrates, with an excellent channel counts available. When choosing a light delivery device for auditory implants, a key goal is to stimulate at a high frequency resolution - thus channel count is a very important consideration. With internal light devices being more reliant on active electronics, it is very feasible to be able to illuminate the LEDs in rich spatiotemporal patterns. As most are based on existing silicon probe designs, devices have the potential for easy incorporation into existing hardware setups (e.g. wireless/freely moving experiments).

A typical example of a μLED probe was presented by Scharf et al in 2016 (Figure 1.27), following promising intensity and temperature characterisation of a proof-of-concept/prototype GaN μLED sapphire-based device (5 LED sites), and a full sapphire device validated *in vivo* (McAlinden et al., 2013, McAlinden et al., 2015,

Scharf et al., 2016). By incorporating LEDs onto a more traditional silicon probe substrate, more desirable dimensions to be reached – the shanks could be manufactured to 100 μm wide (tapering to 1 μm) and only 40 μm thick, down from 150 μm x 100 μm in sapphire. μLEDs are 25 μm wide, with 50 μm spacing, bringing them to a cellular level and offering potential for excellent spatial resolution. The device is inherently scalable, with a 96 channel, 6 shank version to be used in this project, with each LED individually addressable.

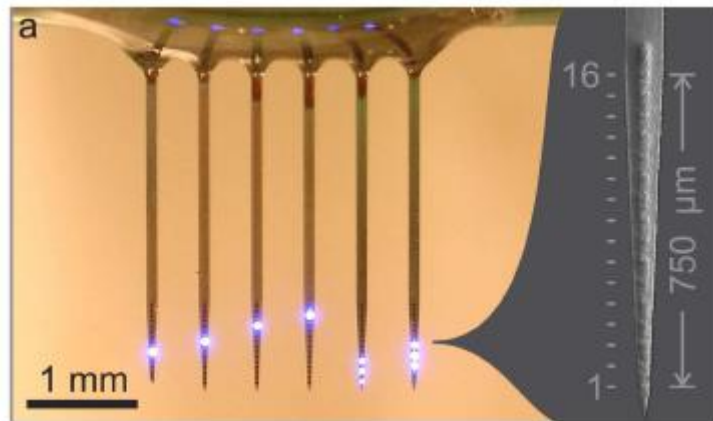


Figure 1.27: μLED probe. 6 Shank prototype, showing illuminated LEDs on each shank. Source: Scharf et al., 2016

Brightness is unlikely to be an issue, with intensity at a single LED able to be 150 mW/mm^2 at its surface, which is more than sufficient for all opsins. However, as temperature increases are a common concern for internal light systems, temperature modelling was employed to determine a viable range of operation. Using a protocol of 2.8 Hz, 50 ms pulses up to the full 150 mW/mm^2 irradiance, the average temperature at cells immediately adjacent to the LED was $\sim 0.5^\circ\text{C}$, which is within safety parameters. It should be noted however that short periods of rising to 2-4 $^\circ\text{C}$ were experienced at these parameters, and so careful consideration should be taken in designing chronic stimulation patterns (150 mW/mm^2 is in fact a very high irradiance for most opsins).

The probe was validated *in vivo* through depth specific activation of the neocortex of the mouse – successive LEDs were illuminated alongside an inserted recording probe, where separate LEDs elicited depth specific CSD and spiking in GABAergic cells expressing ChR2. However, at present, the device does use blue light, which is falling out of favour among auditory prosthetic researchers in favour of red shifted wavelengths, which should be considered in future iterations. It is also not currently

wireless, but as with red-shifting, this is becoming a focus of research now the feasibility of the devices in generally has been demonstrated.

Since 2016, many labs are seeking to design new and improved μ LED devices, since their potential usefulness as both a research and a medical device is clearly apparent. In Section 1.13.7, the focus will be on μ LED based devices designed with medical (i.e. auditory implant) applications in mind. Oftentimes, improvements are engineered to some properties, while neglecting others that would make the device viable (i.e. exceptionally high channel counts but excessively thick shanks) – but the technology is now at the stage where engineering and medical/biological sciences are truly beginning to converge to create useful devices for medical applications.

1.13.7 Progress Towards an Optogenetic Auditory Implant

Improvements to μ LED Devices

The μ LED device described above marked a turning point in this technology due to the manufacturing method on silicon wafers, and crucially contains significantly more LEDs than previous device iterations (such as the 2015 device from Wu et al, which had 3 sites per shank (Wu et al., 2015)). μ LEDs appear well placed to become the integral stimulation device for future optogenetic auditory implants. However, to be fully realised as a stimulation device for humans, there are a number of hurdles still to be jumped, and research is ongoing simultaneously on a number of fronts.

The current focus is on μ LED devices for auditory implants, but we must often look to innovations in other applications with different priorities, to find technological advancements to incorporate into auditory specialised devices. Wireless technology is currently the focus for stimulation of the peripheral nervous system, such as in humans for medical interventions (e.g. sacral nerve control for overactive bladders), or pure research purposes (e.g. to probe the spinal cord and associated circuitry) (Samineni et al., 2017, Mickle et al., 2019, Sivaji et al., 2019). Battery size and capacity are crucial considerations for a viable device, and so it is hoped that progression in these fields will spill over into μ LED probe technology. Incorporation of recording technology adds an additional need for fast, wireless, data transfer.

In order to increase intensity and spatial reach of the light within tissues, a recent device has incorporated micro-reflectors into a 32 channel μ LED device, with the aim of achieving intensity and thus enhancement of depth stimulation capacity of devices. With a reported 65% intensity increase over an unmodified LED, and an acceptable

temperature increase, this may be a promising approach for applications where stimulation at depth is required, or exceptionally low power is needed. It has, however, not been validated *in vivo* (Wasif et al., 2019). Similarly, by moulding PDMS micro-lenses (potentially down to 10s of μm in diameter) and attaching them over the μLEDs , Klein et al were able to increase peak light intensity in water by 95% over an unmodified μLED (Klein et al., 2019). Stimulating more of a given isofrequency layer in the ICC, for example, may turn out to be advantageous for obtaining a robust response.

A crucial hurdle of these devices before they can be used in humans (or indeed chronically in animals) is flexibility. Silicon is an improvement over the early use of sapphire, but is still not the ideal material as its flexibility does not match that of brain tissue, by several orders of magnitude (Polanco et al., 2016). As such, flexible devices that can maintain dense channel count are attractive for minimising tissue damage and making chronic implantation in humans fully viable. The state of the art in this area use cochlear implants as a motivation, and take similar approaches, placing μLEDs on thinned, flexible polymer substrates such as Paralyne C or polyimide, while still maintaining high (32 and 144) μLED count (Klein et al., 2018, Reddy et al., 2019). Modelling of thermomechanical properties indicates the devices to be suitable for their intended purpose, but with only the 2019 device being tested in living tissue (brain slices) it remains to be seen what issues may arise from their use. Given sufficient advances in microfabrication technology, it is possible that devices intended for the brain may take their cues from the state-of-the-art in flexible/mesh recording probes, switching out electrodes for cellular scale μLEDs .

There may be occasions, particularly for research purposes or seizure detection, where combining stimulation with recording electrodes would be beneficial. This is one of the major variables where μLED devices suffer compared to waveguide-based devices. Having both the LEDs and the wiring for LEDs in close proximity to the recording wires can cause complex electromagnetic/photoelectric effects, the outcome of which is large artefacts in recorded data as LEDs are switched on and off. These issues will be explored in more depth in Chapter 6, but have the real potential to constrict device use and operating limits. Mitigating these artefacts is thus a major focus. Though yet to be published and fully peer-reviewed, a recent in-progress publication sets out to minimise these artefacts, through multi-layer metal shielding, doping of silicon substrates and careful shaping of the input signals (Kim et al., 2019).

A single shank of this optoelectrode has 8 recording electrodes and 3 stimulation μ LEDs, and was validated *in vivo* in the mouse hippocampus and found to greatly reduce the various forms of artefact.

As it stands so far, μ LEDs offer an excellent option for optogenetic stimulation of auditory neurons. Compared to external light-based devices, they currently have increased channel counts, brightness, multiple site configurations and spacing, and better options for wireless communication. Incorporation of recording electrodes poses an issue, but may be overcome with considered probe design. As the focus of the field shifts to red shifted opsins for cochlea implants, there is expected to be a surge in publications for devices offering high resolution, flexible, red-shifted μ LED probes. This technology is highly applicable to the brainstem and the midbrain implant also.

Development of Viable Opsin Approaches

Now that temporal properties have been, to a degree, solved, concern in the optogenetic implant community has shifted to other concerns. It would be first advantageous to prove the hypothetical increased frequency resolution of optogenetic devices. One of the first studies to examine this came from Dieter et al, 2019. By stimulating the cochlea optogenetically and recording within the ICC, they found optogenetic stimulation often produced comparable spectral selectivity excitation to auditory pure tones, especially when compared to electrical stimulation (Dieter et al., 2019). However, it may be a concern that the stimulation strategies taken were not directly comparable (different number of electrodes, different distances along the cochlea length) and so while this study provides an excellent starting point, more work should be done to validate the results (across multiple auditory centres, if possible).

Another major concern for a chronic optogenetic devices is the use of blue light and its phototoxicity in cells. The lab of Tobias Moser has recently engineered super-fast variants of the Chrimson opsin. They are comparable, and perhaps faster, than Chronos, whose properties have been described previously– at temperatures of 34 degrees celcius, the lab quotes a time off of 1.6ms for the vf (very fast) variant, which is excellent for use in auditory implants (Mager et al., 2018a). Presented alongside the engineering of the Chrimson variants was its validation *in vivo* – specifically in the mouse cochlea. SGN were transfected via AAV, and cells could then be stimulated with an optical fibre, producing high fidelity spikes up to 200Hz stimulation rate, which is very promising. (Mager et al., 2018b). As it has only become a priority recently, as

of yet there are no μ LED devices incorporating yellow/red μ LEDs, though the use of micro-transfer printing will facilitate their incorporation onto a variety of substrates. This is likely to be the focus over the next few years, especially for cochlear implants, but will require additional material considerations and optimisation.

1.14 Project Aims and General Hypotheses

1.14.1 Identified Aims

In this introductory chapter, the current state of auditory system research has been reviewed, with a focus on auditory implants for hearing loss. There have been several areas in which knowledge has been identified as lacking or would benefit from variations in the experimental/analytical approaches.

Firstly, though research is extensive in both the AC and the IC individually, examining both areas simultaneously, during complex stimuli and under the same experimental conditions, has the potential to increase our understanding of sensory processing as a whole, even outwith the context of auditory implants. By continually making direct comparisons under similar experimental conditions, results can be viewed more in the context of an interconnected system, rather than individual/distinct stages in a sensory pathway.

Comparing the relative response of IC and AC neurons, across multiple trials, time bins, and during non-specific natural stimuli, key differences are more starkly highlighted, and in turn can either solidify or expand existing knowledge of these areas' coding strategies. The performance of IC implants currently lags behind that of cochlear implants, and so any new insights into sound processing in the IC may augment speech processing algorithms and stimulation techniques, while also supporting or discrediting the use of the AC as a future implant site.

In particular, the research should focus on natural sound. This has been explored in terms of synthetic AM/FM modulated sounds, vocalisations, and entrainment (in the cortex at least), but the field may benefit from a general overview and direct comparison of each area's responses on a dynamic, trial-trial basis, using real natural sounds comprising of multiple sources (animals, environmental noise etc). Natural and multi-layered sound stimuli are the most relevant sound for auditory implants. It would also be interesting to compare the behaviour of different cortical cell types during the stimuli, to gain more knowledge of their dynamic functions.

For improving the spatial resolution of devices, μ LEDs have been identified as the most promising new technology, with super-fast opsins such as Chronos being attractive options. However, their implementation *in vivo* on such a large scale (i.e. 96 channel probes), or their use in the auditory midbrain, has not yet been established.

Thus, the thesis aims to take a two-pronged approach to solve the existing issues with auditory midbrain implants, while simultaneously expanding on knowledge of auditory and sensory neuroscience. Specifically, the two overarching aims are to:

- Investigate and directly compare relevant properties of the auditory cortex and inferior colliculus during natural sound stimuli, using simultaneous silicon probe recordings of neuronal spiking and Local Field Potentials
- Investigate the viability of an optogenetic approach to auditory midbrain implants, through the use of the fast Chronos opsin and a state of the art μ LED device

1.14.2 General Hypotheses

Given existing knowledge of the auditory system's anatomy and physiology, general hypotheses resulting from the thesis aims can be established.

- AC and IC neurons and neuronal populations will have fundamentally different properties. This is well established so many results may be replications
- The AC and IC will vary in their approaches to encoding natural sound

Validation of the above hypotheses will be attempted using a variety of analytical techniques. The most basic of these includes waveform analysis and Fano factor (Chapter 3), but in Chapter 4 will extend to linear classification analysis using spike rate and subsequent analysis of these inputs (Fano factor, firing rate, frequency tuning etc). In Chapter 5, dimensionality reduction is used in the form of Non-Negative Matrix Factorisation to qualitatively compare dynamic population activity in both areas.

Brain rhythms on the delta and theta scale have been proven to strongly influence sound coding in the auditory cortex, particularly for contextually relevant, natural sounds. In this thesis, analytical methods are employed to examine the relative strengths of LFP in the AC and IC during natural sound, and to look for evidence of entrainment at a wide variety of timescales. Global brain state also has a role, at longer timescales, and while this is by no means a focus of thesis, some small

observations regarding its influence are made. Knowing the influence of brain rhythms will also help to new approaches to accurate sound replication by auditory implants.

From this knowledge, it is hypothesised that:

- Entrainment to LFP is an important cortical mechanism and will be confirmed in the auditory cortex during natural sound. Entrainment in the IC is not well supported at present, and given that it is a non-cortical area, observation of the phenomenon entrainment is not expected to any significant degree
- The timescale on which auditory coding takes place is highly important

These hypotheses are tested by calculating the inter-trial coherence across successive trials of the same stimulus in both brain areas (Chapter 3). Entrainment of neuronal spiking to LFP is then examined (frequencies 2-200Hz) during both silence (spontaneous) and natural sound stimuli in both brain areas (Chapter 3). Briefly, in Chapter 5, the potential influence of global brain state is examined.

In Fano factor analysis (Chapter 3) and linear classification (Chapter 4), trial-trial variability and decoding success are examined using a spike rate code over a variety of timescales from 10-1000ms, with expected peak performance around 200ms (theta range).

Through employing optogenetics and μ LED probes, the project aims provide evidence for the viability of an optogenetic approach in fixing the issue of low frequency resolution in electrode-based devices. As will become evident, experiments in this area did not progress as far as desired, but results can still be explored in the context of the original hypotheses:

- μ LED probes, combined with a fast-responding opsins such as Chronos, can improve spatial (and thus spectral) resolution of auditory implants. The focus will be on the auditory midbrain implant, which is promising but currently limited by this and other factors.
- μ LEDs can be employed successfully in the research laboratory, combining with existing electrophysiology equipment and utilising easy to use hardware, software and providing recognisable outputs to be easily incorporated into existing analysis pipelines.

Chapter 6 is dedicated to exploring these hypotheses and goals. Viral injections are optimised to obtain expression of the Chronos opsin throughout the depth of the

mouse ICC, in preparation for future μ LED experiments. Optical activation is confirmed via a surface optical fibre. A pilot study with μ LED probes then, while unsuccessful in terms of obtaining data, was nevertheless imperative in establishing the system in the lab, with many improvements in hardware, software and analysis highlighted for the future.

1.14.3 Summary of Results

The main results of each chapter are summarised and linked to the above hypotheses.

Chapter 3 examines both the basic properties of AC and IC neurons, and the phenomenon of entrainment. AC and IC neurons are confirmed to be fundamentally different in terms of their waveform metrics, spontaneous firing rates and (though the evidence was less strong in this chapter) trial-trial variability. AC neurons are clearly split into two putative populations, as previously described in literature – broad spiking, pyramidal neurons and narrow spiking interneurons. IC neurons are almost all “narrow spiking” and cannot be split further. The IC also has a higher spontaneous firing rate overall. Cortical narrow and broad spiking cells often differ in their properties, which will be discussed in more detail in the relevant chapters. There is a tendency for IC neurons to have a lower trial-trial variability during natural sound when compared to the AC, though this effect was most strongly seen using channel MUA. The Fano factor is generally fairly variable, overall, and also increases with increasing time bin.

Both the AC and IC displayed evidence of inter-trial coherence, though like the Fano factor, this was fairly variable across recording channels. Interestingly, the IC displays stronger ITC, and for longer, than the AC – possible interpretations of this are described in Chapter 3. ITC in the cortex is limited to frequencies less than 20-30Hz (as expected), but ITC in the colliculus appears to extend to at least 100Hz. There is also a slight influence of channel depth on cortical ITC, with channels closer to the putative sink/input layers displaying stronger values.

Entrainment appears to be present in both the AC and IC, conflicting with the original hypothesis. The AC follows expected trends, showing entrainment predominantly at frequencies >20 Hz (and peaking at 8-10Hz), while like ITC, the IC shows evidence up to 200Hz. This is an unusual result, and will be explored in detail in Chapter 3.

Entrainment is also lower in strength than expected and seen in less of the neuronal population than previous literature has suggested.

In Chapter 4, linear classification is used as a method of comparing coding strategies in the AC and IC, on a range of timescales. Despite a lower number of inputs overall, the IC is capable of achieving comparable classification success to the AC. In subsequent analysis, this does not appear to be due to the frequency range covered by the population, but potentially by the lower trial-trial variability of IC neurons as compared to AC. High noise correlations were indicative of exceptionally poorly performing sets, which is logical given the type of analysis. Despite previous evidence in the literature, there was no significantly higher classification performance using delta/theta time bins, though there was a slight trend.

Chapter 5 is a largely exploratory chapter, utilising dimensionality reduction in the form of Non-Negative Matrix factorisation to identify dynamic populations of neurons within the dataset, and to see how, when and how reliably each responds to natural sound stimuli. Datasets were reliably split into a small number of distinct populations, responding to different segments of the sound. IC populations appears to be tonotopically organised, but other than this, there were no real quantitative differences between the areas. Using a single dataset, there was slight evidence for state transitions to be visible in the power of some populations, and it was found that the putative desynchronised state resulted in better cortical classification performance (using linear classification as before). This was not evident in the IC, though state determination here was overall less distinct.

Chapter 6 focused on optogenetics and μ LED probes. Coordinates and viral injection number/volumes were optimised to express the Chronos opsin throughout the depth of the mouse ICC. Optical responses could be elicited with a surface optical fibre, with the strength of response decreasing with depth. A μ LED control system was developed in conjunction with a collaborator at the Institute of Photonics, allowing for a range of customised protocols to be run on a 96 channel μ LED device (as described in the literature review). After designing protocols, a pilot experiment using a ChR2 mouse and μ LEDs in the cortex was run. The experiment was a success in terms of the surgery and animal remaining viable, and for the running of the software, but due to large electromagnetic/photoelectric artefacts, the data could not be analysed. Improvements for protocol and hardware as identified by this pilot experiment are

discussed in detail, including the addition of extra shielding, pulse shaping, and minimising use of high currents and voltages.

Chapter 2 Materials and Methods

2.1 Breakdown of Auditory Experiments

This section will detail the materials and methods used within this project. As there were both auditory and optical experiments, plus data analysis, the techniques will be grouped generally (i.e. “surgical procedures”, “data analysis” etc). Please refer to Figure 2.1 and 2.2 that detail which sections of this chapter are relevant for other chapters. Auditory experiments were always chronic, typically involve a recovery surgery to place a headpost, followed by habituation, craniotomy and awake recordings.

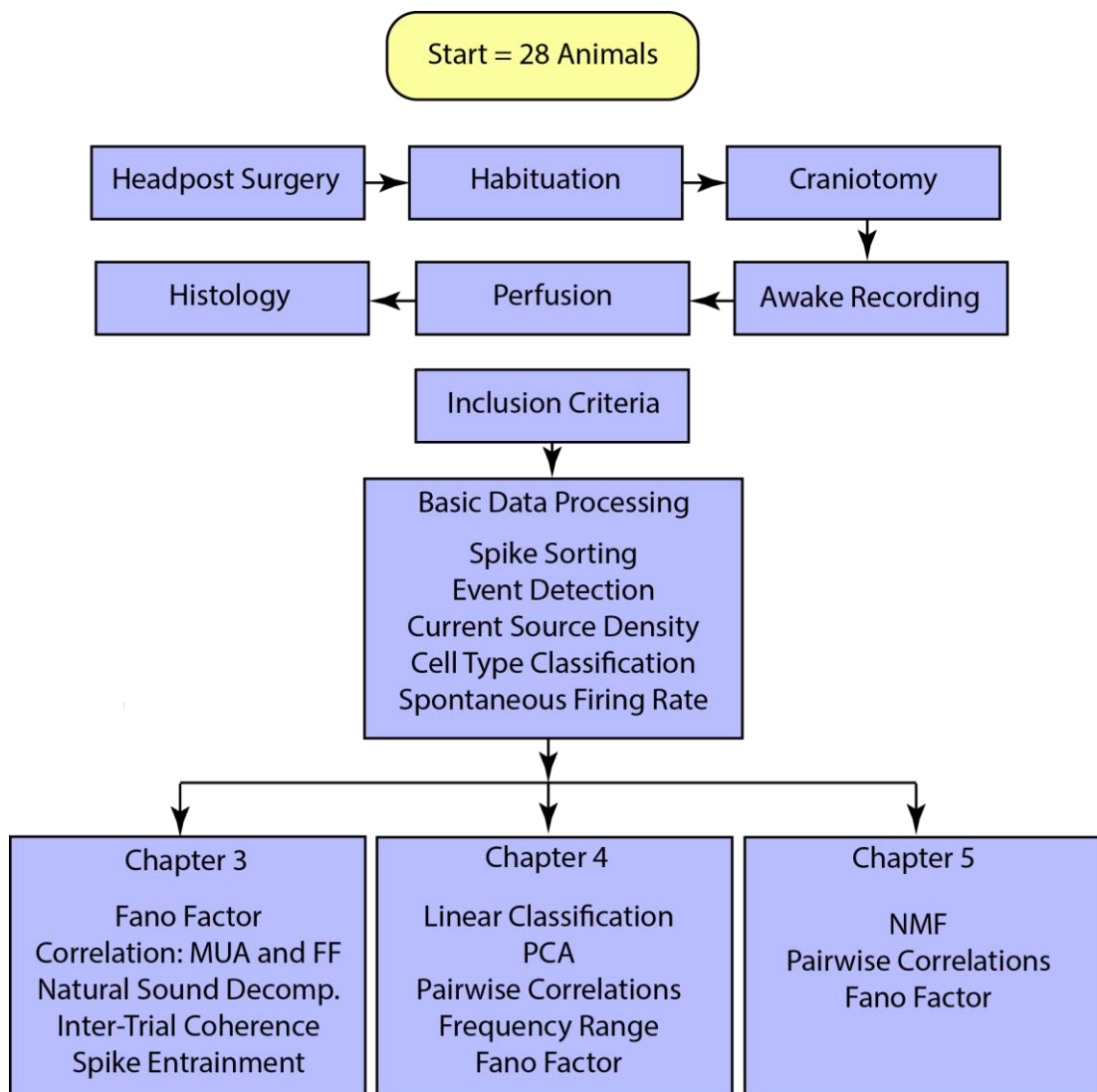


Figure 2.1: Flow diagram of auditory experiments. Analysis relevant to each chapter is listed within the bottom boxes

2.1 Breakdown of Optical Experiments

Chronos optogenetic experiments could be acute (recording is done anaesthetised) or chronic (recording is done awake). These involve viral injection surgery (with or without headpost) followed by habituation (if appropriate) and optical recording experiments.

μ LED experiments were performed on only 1 mouse (plus one for optimisation of equipment). Both surgery and recording were performed under urethane anaesthesia.

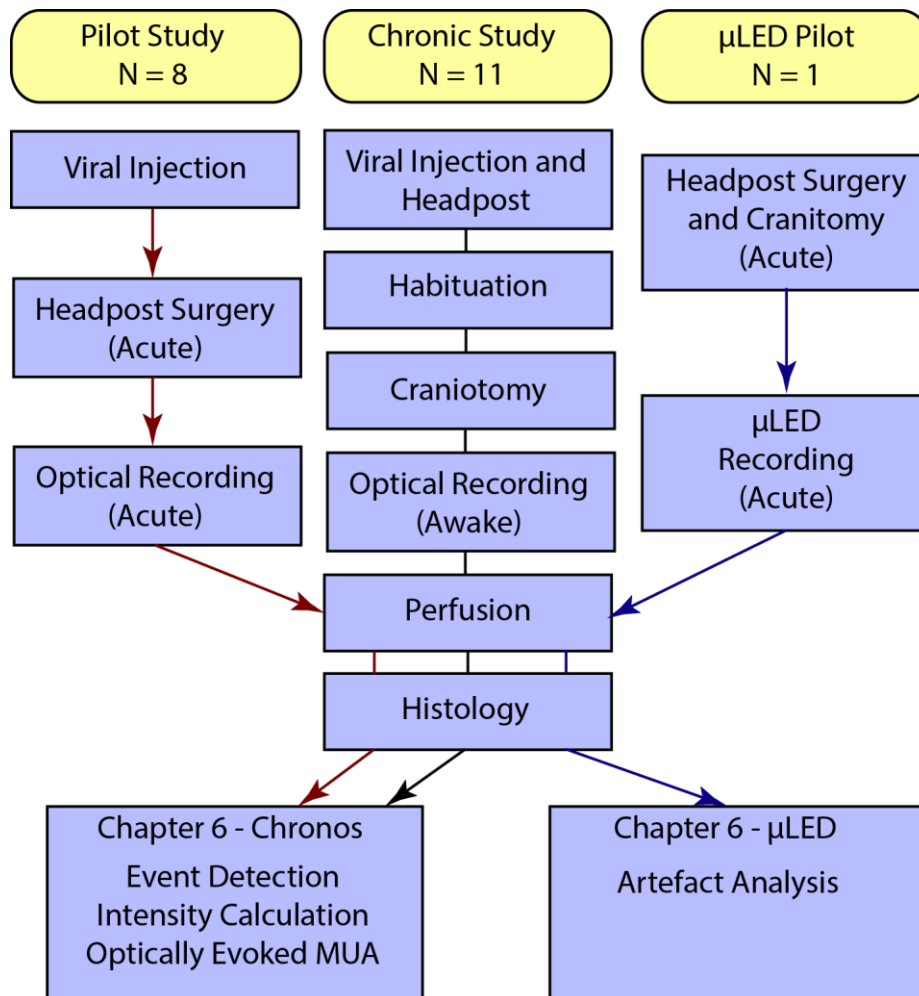


Figure 2.2 Flow diagram of optical experiments

2.2 Animal Maintenance

2.2.1 Ethical Approval

All animal experiments were performed in accordance with the UK Animals (Scientific Procedures) Act of 1986 Home Office regulations and approved by the Home Office

and University's Ethical Committee. Specifically, the project was performed under Project License PPL70/883, Protocol 2.

2.2.2 Animal Details

For simultaneous recording, mice between the ages of 21-55 weeks and of both sexes, with a CBA/Ca or a C57BL/6 background. A total of 26 mice were prepared for chronic recordings (see Chapter 3 for a breakdown of fates)

For viral injections, the animals were aged between 8-10 weeks at the time of injection, and were of a wild type c57/BL6 background. The mice were majority male (3:1) due to the limited availability of mice at specific ages. 8 animals were used to characterise the viral expression, with a further 9 used for general optogenetic experiments.

Two mice were used for μ LED experiments (one wild type C57BL/6 for optimisation, one PV-ChR2, CBA).

2.2.3 Animal Housing

Animals were held in cage racks in the University of Strathclyde Biomedical Procedures Unit (BPU), in a room with a 12hr/12hr light/dark cycle.

Animals were housed cages with high cage tops. Food and water were provided *ad libetum*. Animals were group housed as same sex littermates (pairs or triplets) as animal availability permitted, with surgeries for all animal in a cage performed on the same day if possible. All experiments were performed in the light period.

2.3 Headcap Manufacture

Headcap components for later head-fixation of the mouse, and recording of EEG, EMG (plus a ground wire) were created manually before surgeries. These were sterilised along with surgical equipment.

The connections between the brain and the ground, EEG and EMG wires of the recording rig were realised using a handmade electrical connector/headcap piece. Three pins of a black connector strip were cut, and the long pins cut using wire cutters. Two pieces of thin single core wires were cut to size (EEG – 1.2cm, Ground – 1.0cm) and the insulation stripped from the last 0.5cm and 0.1mm from the opposite end. For the EMG recording, a thicker, multicore wire was cut to size (1.0cm), and half of the insulation stripped to leave the cores free (plus a small area was exposed on the opposite end). For the EEG and Ground wires, the uninsulated 0.5cm was coiled

around a small stainless steel skull screw, loose enough so the screw could still rotate. Flux was applied to the cut pin side of the connector to aid soldering, and the wires soldered onto their individual connection (for arrangement, see Figure 2.3). The structure was then covered with dental cement for robustness. The headcap was sterilised along with surgical equipment.

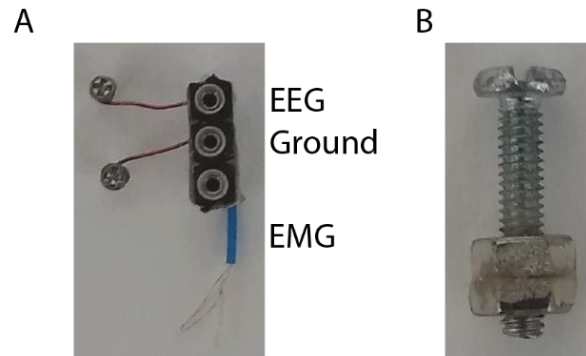


Figure 2.3: Headcap components. (A) Headcap connector piece. Recording wires are later inserted into the metal lined holes on top of the connector. The top screw is EEG, middle is ground and final connector is the EMG wire. Exposed metal fibres are fanned out and inserted into the neck muscle. (B) Headcap nut – consists of two nuts held together by dental cement (ivory). Screw is used for initial manufacture and during the cementation process to the animal's skull, after which it is removed

The headpost itself was created by threading two M2.5 nuts onto a screw, and gluing together with dental cement, ensuring the resultant two nuts could be removed fully from the screw later. The screw aided with positioning and holding during cementing procedure, and was then removed at the end of the surgery once cement had fully set.

2.4 Surgical Techniques

2.4.1 Headpost Surgery

Chronic Condition

Animals were anaesthetised with isoflurane (1.5%, 0.5-1% maintenance O₂ between 0.8-1l/min), then their head/ear area shaved with an electric razor. The animals were then transferred to in a stereotaxic apparatus (SR-5M-HT, Narishige) with mandibular or ear bars and breathing apparatus. Breathing and pinch reflexes were monitored throughout the surgery and levels of anaesthetic were adjusted accordingly. Body temperature was maintained at 37°C by a heat mat and sensor (40–90–8C, 392 FHC). Local and long-term analgesia was administered subcutaneously before beginning aseptic surgery (Lidocaine 0.05 mL, 2%, on skull surface and Rimadyl, 0.05 mL of 5%, on the animal's back). 0.5 mL of warm saline was also administered subcutaneously. Eyes were kept moist by administering ointment (Lacri-Lube, Allergan). The remainder of the surgery was completed under aseptic conditions

(autoclaved gown, drapes and surgical tools, plus sterile gloves), and with a microscope (SZ51, Olympus). Before placing drapes, work areas (including microscope) were sterilised with successive applications of antibacterial spray (Trigene), and ethanol (70%). The shaved area was cleaned briefly with ethanol, and antibacterial liquid (Betazyme). The skull was exposed with a vertical scalpel incision and cleaned with successive applications of ethanol (70%) and H₂O₂ (3%, to dissolve periosteum membrane).

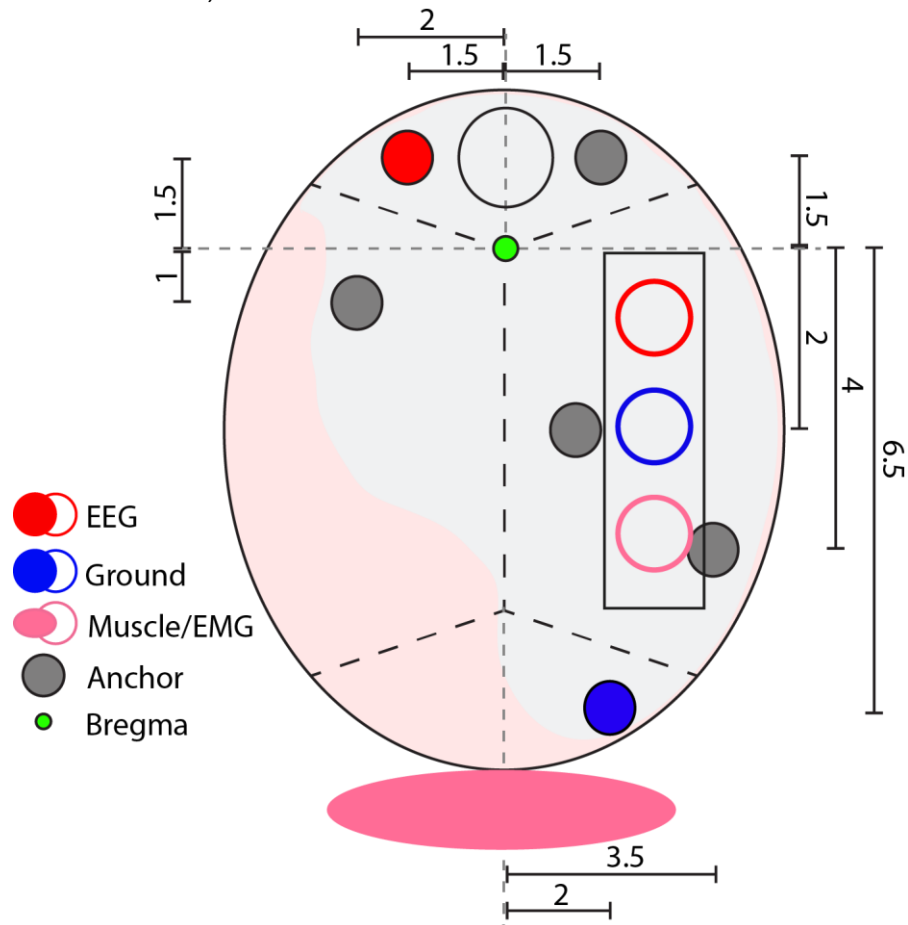


Figure 2.4: Location of anchor and recording screws for headpost surgery. Small green circle marks reference point bregma, dotted black lines indicate skull suture lines. Grey circles indicate position of anchor screws. Red circle indicates EEG recording screw, blue circle indicates ground screw. Rectangle containing three circles of colours shows the position of the headcap connector, with colours indicating to which screw it is connected. The pink connector is connected to the muscle (pink oval) at the back of the neck. The large unfilled circle at the front indicates the position of the headpost nut. Grey colouring on the skull indicates the rough extent of dental cement coverage. All measurements of screw locations are shown relative to bregma and in mm

Positions for anchor, cerebellar ground and frontal EEG screws were marked using callipers and pencil, relative to bregma reference point, then holes drilled with a small dental drill, and stainless steel skull screws inserted (see Figure 2.4) and fixed in place with dental cement (Simplex Rapid Powder + Liquid, Kemdent), along with a set of nuts for later head fixation. The EMG wire was inserted into upper trapezius muscle.

Exposed skull was covered in Kwik-Sil polymer (World Precision Instruments), and animal was allowed to recover for at least 5 days before habitation.

Acute Surgeries

Headpost surgeries could also be performed acutely, under terminal anesthesia (such as for the Chronos pilot study). These were identical to the chronic condition, apart from the anesthesia protocol. Please see section 2.3.4 at the end of this surgical techniques section for details on urethane anesthesia.

2.4.2 Viral Injection Surgeries

Preparation

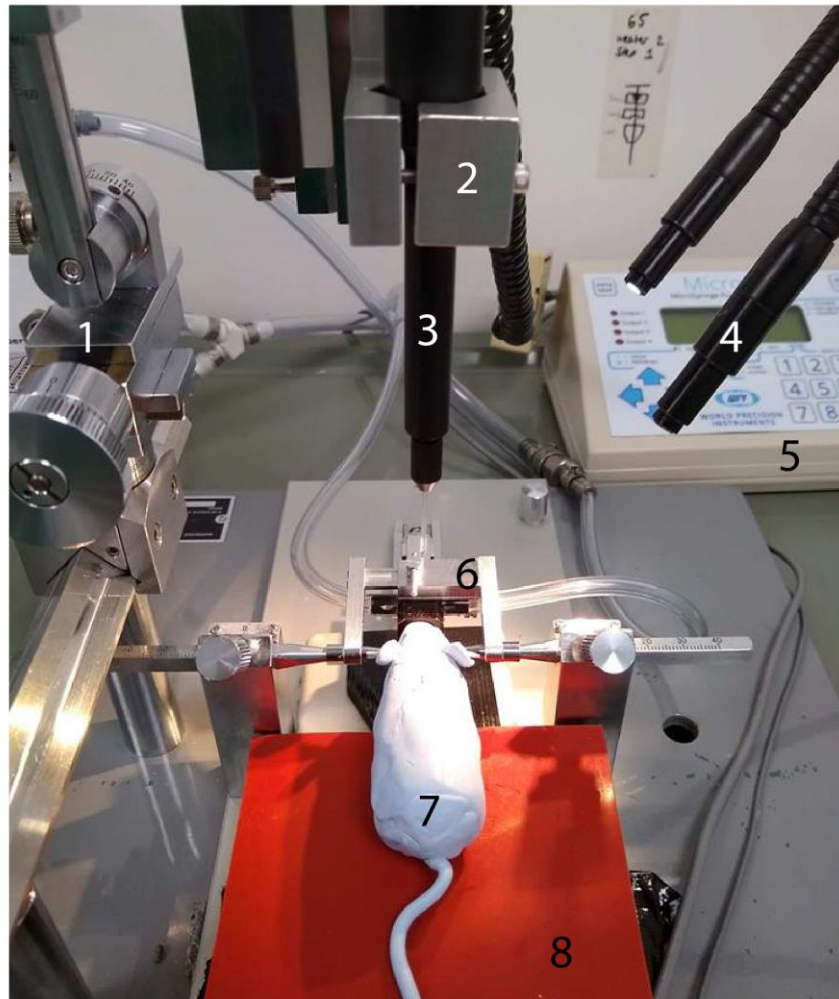
Before surgery, glass micropipettes were formed by pulling glass tubes (World Precision Instruments) to the correct width with a heating device (Narishige, PC-10) and were then filled with mineral oil. Before beginning surgery, the pipette was fitted into the microinjector and attached pump (World Precision Instruments, Sys-Micro4), held by a motorised stereotaxic manipulator (Narishige, SR-5M-HT). Aliquots of rAAV8-syn-Chronos-GFP virus (titre 5.8×10^{12} vg/mL, dot blot, Gene Therapy Center Vector Core, University of North Carolina) were mixed with fast green dye for visualisation during surgery.

Recovery Surgery

The animal and skull surface were prepared as described previously for headpost fixation, and equipment is set up as in Figure 2.5. Viral injections were performed before drilling any holes for headpost fixation. Under sterile surgical condition, measurements were made using the stereotaxic manipulator. A small craniotomy was made at -5.1mm anterior, -0.9mm lateral from bregma, over the inferior colliculus. Sufficient virus for the injection(s) was withdrawn into the micropipette during sterile surgery. After confirmation of injection coordinates, the micropipette was lowered over to touch the surface of the brain. The equipment was then normalised to 0 μ m depth. The micropipette was then advanced slowly to the deepest injection site and left for 5-10 minutes at its final depth. The virus was injected at a rate of 30 nL/min, with the pipette left in place for 10 minutes after virus had been injected to minimise leakage. The pipette was then slowly removed/moved to second injection site and the second injection (if being performed) was done in the same way as the first. After both injections, the pipette was removed fully, and either the incision stitched up (pilot

study, for later acute surgery and recording) or headpost implanted (chronic recording).

A



B

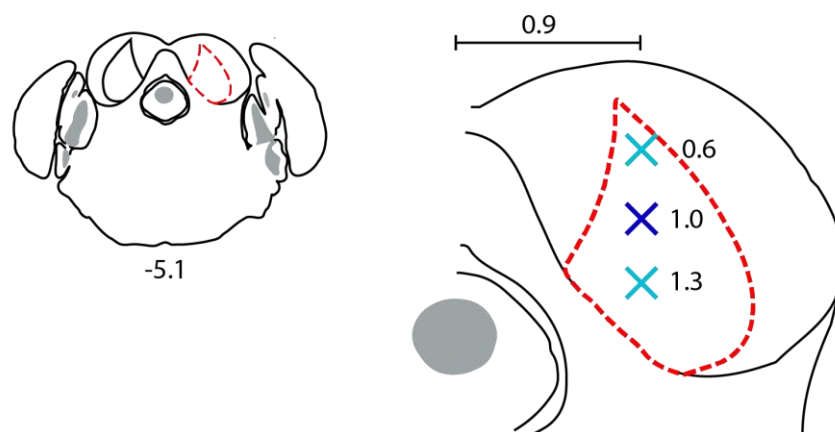


Figure 2.5 Viral injection surgery. (A) Schematic of surgery setup. 1 – Motorised manipulator base, distances can be manipulated from here. 2 – injector holder. 3 – micro-injector (connected to 5), connected to glass pipette. 4 – Light. 5 - micro-injector control unit. 6 – earbars for holding mouse in place. 7 – Mouse. 8 – heat mat (controlled by a central unit, not shown). (B) Viral injection locations, inferior colliculus. Measurements are given relative to midline. Light blue shows locations of dual injections, dark blue is single injection.

Conditions for Pilot/Optimisation Study

Table 2.1 details the 4 injection conditions that were investigated. Animals were left to incubate for at least 4 weeks.

Table 2.1: Optimisation of viral injection coordinates and locations. Table details number of animals, injections, volumes and locations. Locations are given in millimetres relative to bregma or midline (anterior-posterior/depth/medial-lateral)

Condition	# Animals	# Injections	Injection Volumes (µl)	Injection Location(s)
1	2	1	0.5	-5.1/0.9/-1.0
2	2	1	0.3	-5.1/0.9/-1.0
3	2	2	0.4	-5.1/0.9/-1.3 + - 5.1/0.9/-0.6
4	2	2	0.2	-5.1/0.9/-1.3 + - 5.1/0.9/-0.6

2.3.3 Craniotomy for Recording

Either a day before recording (chronic condition) or during/following non-recovery headpost surgery (acute condition), craniotomies were performed to give access to the brain surface.

Chronic Condition

A day before recording, mice were anaesthetised as before and given local and long-term anaesthesia, and 0.5 mL warm saline subcutaneously as before. Full sterile environment was not required as animal would be perfused within 2-3 days of the surgery, however, surfaces and equipment were cleaned thoroughly with ethanol.

Acute Condition

After headpost surgery was complete, animals were fixed in place using said headpost and equipment turned to allow better access to the appropriate side of the skull.

General Procedure

After removing the Kwik-Sil layer, the skull was cleaned with saline and ethanol. For access to the auditory cortex, a flap of skin and muscle was retracted on the left hand side. The desired edges of the craniotomies were pencilled onto the skull (see Figure 2.5 and Table 2.2).

Table 2.2: Craniotomy Locations. All distances are given in millimeters. Ant-Pos: anterior-posterior axis, coordinates are relative to bregma. Med-Lat: Medial-Lateral position. Except in μ LED, craniotomies were performed over the left hemisphere

Location	Top Medial Corner Ant-Pos/Med-Lat (mm)	Width - Med-Lat (mm)	Length - Ant-Post (mm)
Auditory Cortex	-2 / 4	2	2
Inferior Colliculus	-5 / 0	2	1-2
Cortex (μ LED)	0 / 0	2	5

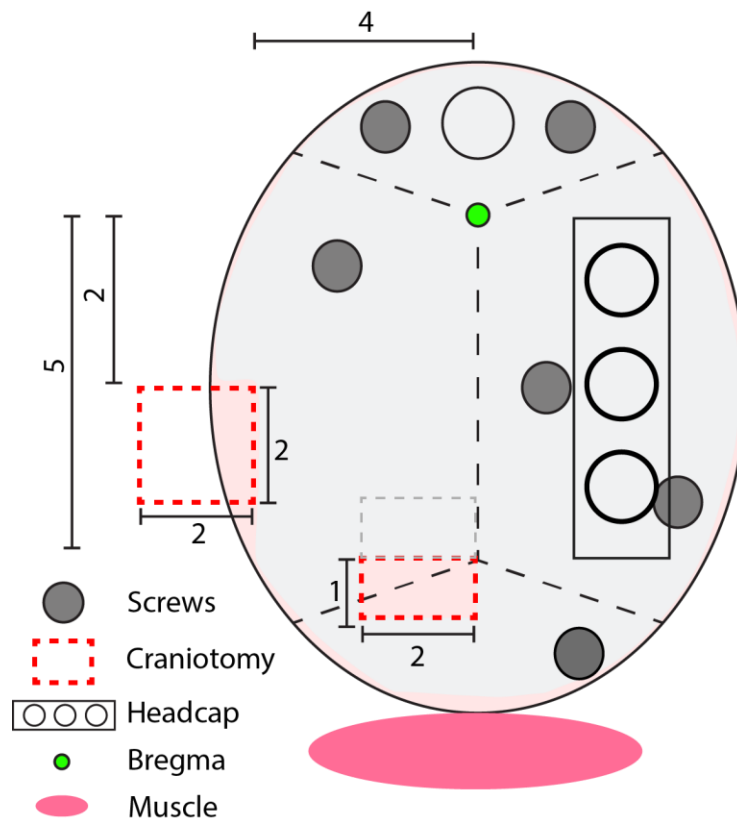


Figure 2.6: Craniotomy locations for auditory experiments. Grey circles indicate positions of existing screws (anchor and otherwise). Black rectangle indicates headcap connector, frontal circular outline is position of headcap nut. Grey indicates both new and additional dental cement coverage after this secondary surgery. Red dotted rectangles show locations and sizes of craniotomy windows. Measurements are given in mm relative to bregma (green circle). Grey dotted outline on posterior craniotomy site indicates the size of the window in later surgeries.

Using a small drill bit, the pencilled edge was slowly worn away, then the flap of bone removed with fine craniotomy tweezers. Note, in later surgeries, the inferior colliculus craniotomy was extended forwards across the back suture (see diagram in Figure 2.6, grey dotted outline) so that the front edge of the craniotomy was not located along a large sinus. This was found to reduce the occurrence of excessive bleeding during and after surgery, with the drawback of exposing more of the brain than is strictly

necessary. Exposed skull and brain were re-covered with Kwik-Sil, 0.5 mL warm saline delivered subcutaneously, and the animal removed from anaesthesia and allowed to recover (chronic) or moved to a heated cage for transport to recording rig (acute).

2.3.4 Acute Anesthesia

In the first 8 animals for viral injection (pilot study) and for μ LED experiments, headpost surgery was performed under terminal anaesthesia (urethane). Craniotomies were also performed at this time.

Animals were terminally anesthetised with urethane (20% in PBS, 1.5g/kg) in a series of 3 intraperitoneal injections, spaced 20 minutes apart. After injections, animals were prepared for headpost surgery and craniotomy as described previously. Isoflurane was usually administered alongside urethane, but at a lower rate (0-0.5l%) and breathing rate very closely monitored.

2.3.5 Post Surgical Care

After a recovery surgery ended, animals were administered an additional 0.5 mL of warm saline (subcutaneous), weighed, and allowed to recover in their home cages, with a heat mat heating one half of the cage. Animals were monitored closely during and just after recovery from anaesthesia, to ensure there were no signs of excessive pain or stress, unexpected mobility issues, and that the animal was able to eat and drink. Soft food (baby food) was provided alongside normal pellets in a plastic dish in easy reach of the animal.

Following headpost/viral injection surgery, animals were inspected and weighed at least once per day until weight had stabilised (3 days minimum). Close monitoring for signs of post-surgical infection continued until the recording stages.

Following craniotomy, there was an increased risk of bleeding due to the location of the IC craniotomy, thus, animals were closely monitored for a few hours post-surgery. Animals were recorded from the following day and monitored for signs of pain throughout recording.

2.4 Recording Procedures

2.4.1 Habituation

Habituation to head fixation and sound presentation took place for a minimum of 5 days, in increasing time increments (from 5 minutes up to 1 hour). Mice were head-

fixed using the previously implanted nuts and placed in a solid plastic tube (eyes and ears free) within a soundproof box, with auditory stimuli played by a speaker directly in front of the animal, 10cm away. The habituation/recording setup is detailed in Figures 2.8 and 2.9.

2.4.2 Probe Layout

For simultaneous recordings, two silicon probes were used (Neuronexus Technologies). Details can be found in Table 2.3 and Figure 2.7. The initial 2 animals (3 recordings) were completed with 25 μ m spacing IC probes. In μ LED experiments, the 16x4 linear probe was used. Details of the silicon μ LED probe will be provided in a later section.

Table 2.3: Silicon probe information. "Area to be recorded" indicates the usual area

Area to be recorded	Arrangement	Name	Shank Spacing	Shanks	Electrodes per shank	Electrode spacing
Auditory Cortex	Linear	A4x16-6mm-50-200-177-A64	200 μ m	4	16 (64)	50 μ m
Inferior Colliculus	Linear	A1x32-10mm-50-177-A32	N/A	1	32 (32)	50 μ m

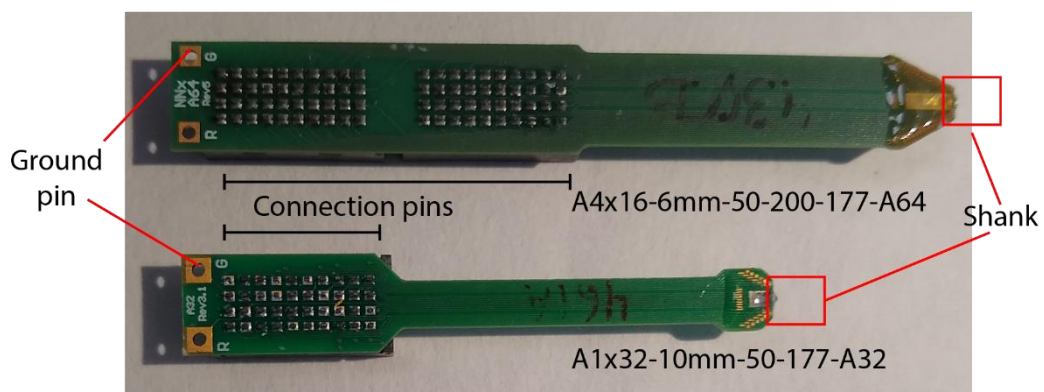
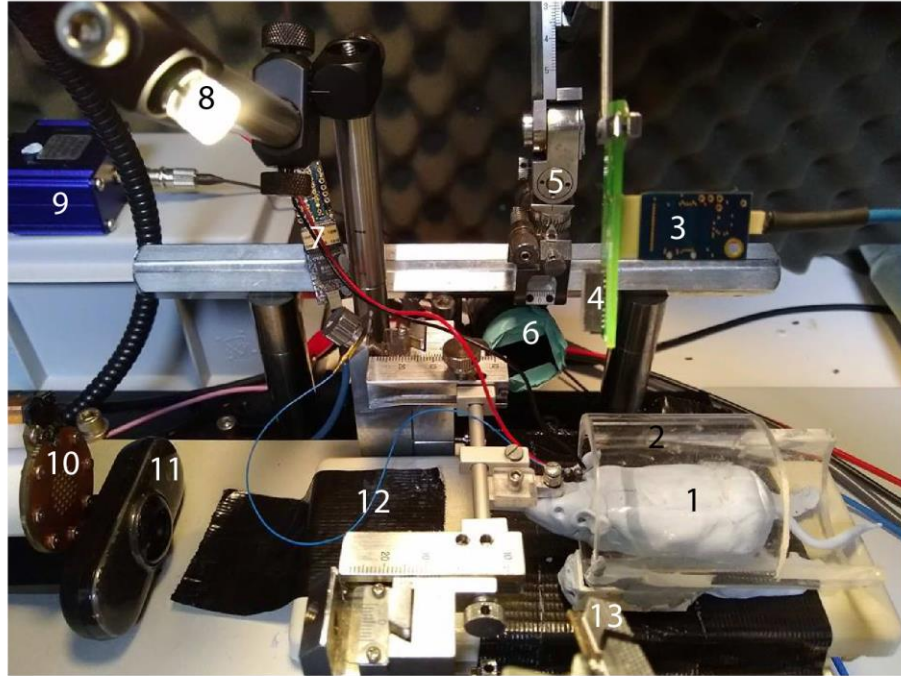


Figure 2.7: Silicon probes (with no shank). Connection pins are located on the reverse side of the probe, and plug into amplifier cards. 6 mm and 10 mm refers to the length of the shank

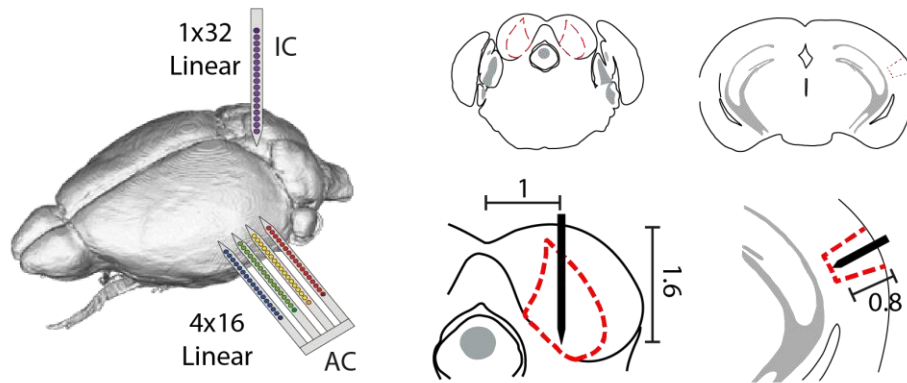
2.4.3 Simultaneous Silicon Probe Recordings from Auditory Cortex and Inferior Colliculus

Position of Equipment for Habituation and Recording during Auditory Stimuli Sound Calibration

A



B



C

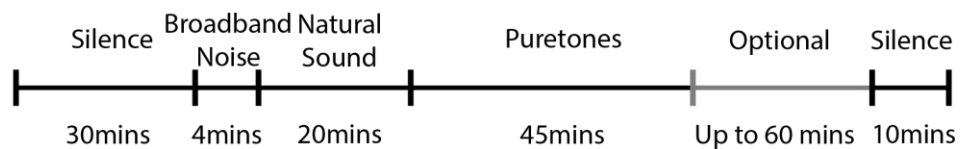


Figure 2.8: Auditory recording schematics and protocol. (A) Layout of recording equipment. 1 – Mouse. 2 – Plastic tube. 3 – Amplifier card for probe. 4 – Connector site for 1x32 linear probe. 5 – Manipulator for 1x32 probe. 6 – Infrared camera. 7 – EEG/EMG and ground connectors. 8 – Light. 9 – LED driver. 10 – Speaker. 11 – Camera. 12 – grounding wire to equipment. 13 – Connection site for 4x16 linear probe. (B) Schematic of probe insertion locations. Left – IC, Right – AC. Black = probe. (C) Typical timeline of auditory stimulation

Calibration files were generated before each recording using a custom program. A microphone was placed in the same position as the mouse, and a series of broad band noise and puretones of varying intensities played to generate the calibration file. This file was then used by the LabVIEW auditory stimuli programs to provide the appropriate voltages to the TDT box (Figure 2.9).

Probe Insertion

Mice were head-fixed as in habituation (Figure 2.8), and the Kwik-Sil removed. Exposed brain surface was kept moist using saline. Neuronal activity in the auditory cortex and inferior colliculus was recorded simultaneously with a 64 channel or 32 channel silicon probe (NeuroNexus Technologies), described above. Probes were inserted manually using a micromanipulator (Narishge) under microscope (SZ51, Olympus), at a rate of approximately 10 μ m/s until all electrodes were within the brain. Details of equipment location can be seen in Figure 2.8. Probes were then left for 30 minutes before beginning recording, to allow tissue to settle and spikes to stabilise. Mice were monitored with webcams (Baslar/Logitech) transmitting to an external computer, and pupil recordings taken if possible.

Finding Auditory Responses

As the probe was being inserted, auditory responses were checked to verify the probe was recording from the correct area. In brief, after the probe was partially inserted, loud broad band noises were played and the output traces examined. Auditory responses were characterised by a consistent, strong downward deflection in the LFP immediately after stimuli was played. Ideally, this would be seen across all shanks (cortex) and along the full depth of the probe (colliculus).

Data Acquisition

Broadband signals from the probes were amplified (RHD2132 Amplifier board and RHD2000 System, Intan Technologies, LLC) relative to the cerebellar ground skull screw, and digitized at 20 kHz (RHD2000, Intan Technologies, LLC). Sync channels were output by a DAQ Board (NI USB 6211, National Instruments) into the digitisation board. Recordings were supervised by a custom Labview VI (National Instruments). For histological verification of probe position, both probes were dipped in Dil (Invitrogen, D-282, ~10% in ethanol) before insertion. In total, recordings consisted of

98-100 channels (1-2, optical and auditory sync, 3:98 probes, 99-100 EEG screw and EMG wire).

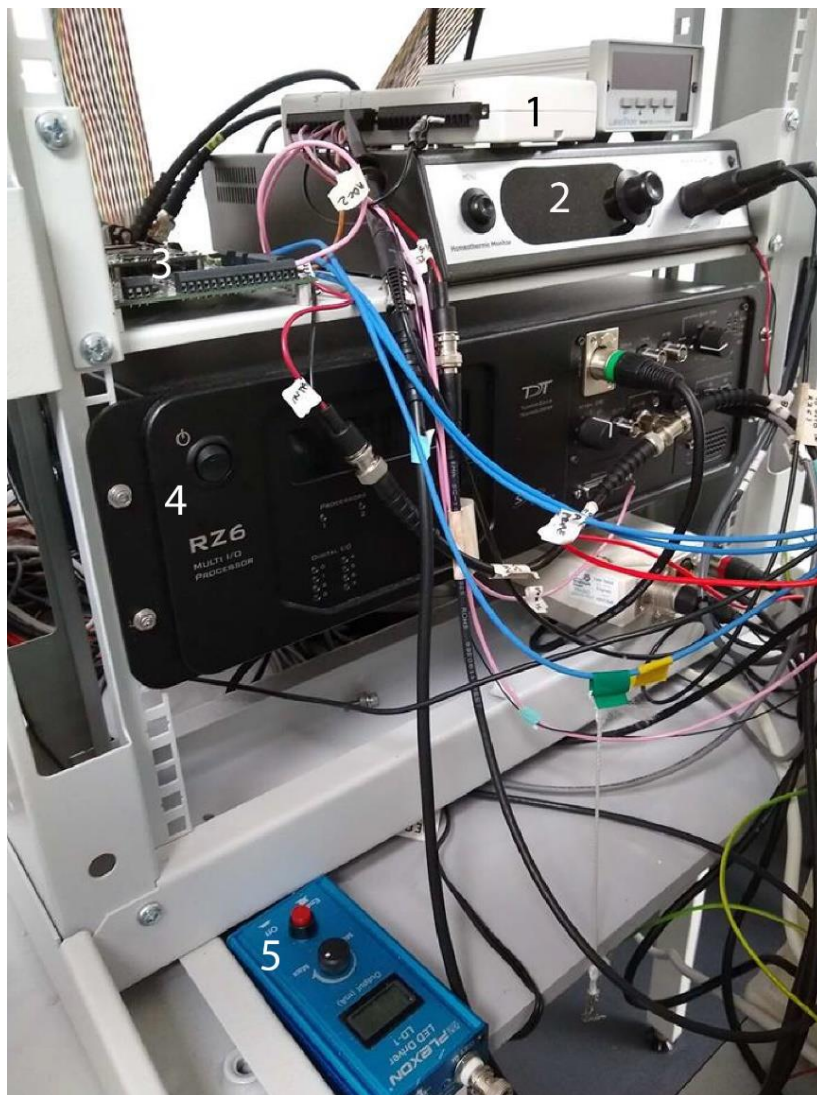


Figure 2.9: Neural data recording and stimulation equipment. 1- NI DAQ box. 2 – Heat mat controller for anaesthetised recordings, 3. Intan Amplifier Board. 4 – RZ6 Sound Generator box. 5 – LED driver

Presentation of Acoustic Stimuli

After a 20-30 minute period of silence and darkness (for spontaneous activity), acoustic stimuli were presented. Acoustic stimuli were generated digitally (sampling rate 97.7 kHz, RZ6 Multi I/O Processor, Tucker-Davis Technologies) and delivered in free-field through a calibrated electrostatic loudspeaker (ES1, Tucker-Davis Technologies) located 10 cm in front of the animal, in a single-walled soundproof box (Industrial Acoustics Company) with the interior covered by 2 inches of acoustic absorption foam. A typical stimulation protocol is summarised in Table 2.4.

Table 2.4: Typical auditory stimulation protocol

Stimulation	Sound ON time	Intensity	Frequency	Reps	Duration	Description
Spontaneous	N/A	N/A	N/A	N/A	20-30 mins	No stimulation – dark. For assessing spontaneous activity of cells
Broad band noise	100 ms	0-80 dB	Broad band white noise 0-48 kHz	50	5 mins	Bursts of “white noise” containing all frequencies. Determining hearing threshold
Pure tones	100 ms	30-70 dB	3-48 kHz, 1/8 octave steps	50	40 mins	Tones of a single pitch. Assessing frequency response of cells
Natural Sound	10 s	65 dB	3-48 kHz, varying	100	20 mins	Natural sound (animal calls, water, leaves...). More natural responses to sound
Click Trains	5 ms, 10 s train 2,4,8,16,32 2,64 Hz	65 dB	Broad band white noise 0-48 kHz	30	20 mins	Fast clicks of broad band noise. For temporal properties

Typically, 2 recordings were performed per animal, over 2 consecutive days. The craniotomy site was covered with fresh Kwik-Sil between recording sessions.

A single, 10 second segment of natural sound was used. The stimulus sounded like an “auditory snapshot” of a noisy jungle – consisting of overlapping sounds from nature (such as rushing water and animal calls). It was not spectrally homogenous or periodic, as the sound components could be heard distinctly, were usually transient, and were of different intensities (e.g. sudden loud animal call or slow increase in leaves rustling). The sound envelope and scalogram of the sound can be found in Chapter 3.

Though several different sound stimuli are applied, not all were used for analysis due to time constraints and a strong focus on natural sounds. However, this data (broad band noise, click trains) represents a potential source of information for future studies.

2.4.4 Optogenetic Stimulation of Virally Injected Animals (Inferior Colliculus)

Optic Fibre Positioning

A modification to the auditory only protocol was made by introducing an optical fibre (200 µm core, 0.39 NA, Thorlabs) coupled to a blue LED (465 nm, Plexon). The fibre was positioned to be almost parallel with the 32 channel silicon probe, around 100 µm above the recording electrodes, so as to illuminate the area of the brain from which the probe would be recording from. It was secured to the probe with blutack.

Probe Insertion

As described in section 2.4.3, the probe was inserted slowly, and left for 30 minutes to settle. Position of the optic fibre was monitored under the microscope – if the fibre shifted away from the centre of the probe, the probe was removed and the fibre repositioned. Probe was dipped in DIl to facilitate histological evaluation.

Finding Optical Responses

Similar to searching for an auditory response, before recording, an optical response was searched for. The exposed inferior colliculus surface was systematically probed with the silicon probe/optic fibre. The probe was inserted slowly as described, to bring the fibre close to the brain surface. The LED was then flashed at a high intensity (3-5 V power, for the experiment presented in Chapter 6, approximately 50 mW/mm² at 5V, with exact intensity dependant on optical fibre at time of recording), and the recorded responses checked by eye for a true optical response (i.e. not an artefact),

generally seen as an increase in the firing rate (the trace gets “noisier”) that decreased with depth. Light artefacts presented as an upward shift in the LFP for the duration of the light. If and when a true optical response was reliably observed, the auditory/optical stimulation protocol began.

Optical Stimulation Protocol

A protocol similar to the auditory only stimulation previously described was presented, with the addition of blue light pulses separately and/or simultaneously with auditory stimulation (Figure 2.10). Light stimulation is controlled by an LED Driver (LD-1, Plexon), driving the 465 nm LED module outputting to a 200 μm patch cable coupled to the optical fibre described previously. The exact protocol is outlined in Table 2.5 below, with pulse widths being given first for optical stimulation, then auditory. LED steps is used to determine a voltage that causes a strong response without excessive light artefacts, this shall be termed *best V*. Stimulations that include auditory and optical contain both an auditory only set, then an auditory + optical set, to assess the effect of light stimulation on the normal response.

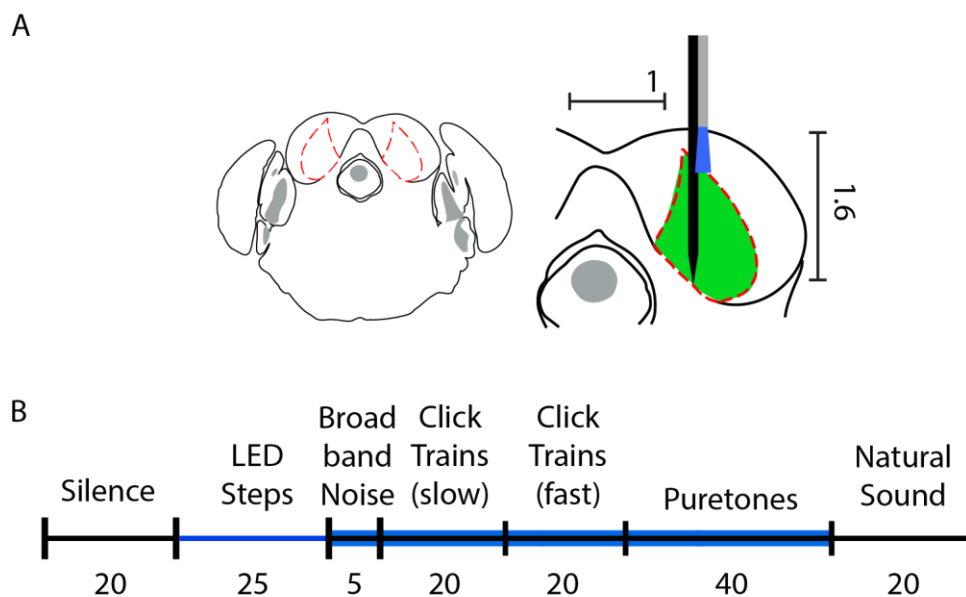


Figure 2.10: Optogenetic recording schematic and protocol. (A) Position of recording probe (black) and optic fibre (grey, blue light path). Green indicates ideal viral coverage of the ICC. Distances are given in mm. (B) Typical stimulation protocol. Single black line = auditory only, blue – optical only, blue on black – auditory stimulation is accompanied by simultaneous optical stimulation (see Table 2.5).

LED steps presented random combinations of duration (10,25,50,100 ms) and voltage (steps of 0.2 from 0.2-1 V, then steps of 0.5 from 1-5 V). Light intensity at the fibre tip is calculated in mW/mm^2 , by taking the surface area of the optical fibre and the power emitted at the tip, measured for each voltage by an optical power meter (PM100A, ThorLabs). In the analysis presented in Chapter 6, only the range of 0-1 V is

examined. This gave reasonably responses and sufficient intensity to give some depth expression, but with minimal optical artefacts in the recorded data. How this intensity increases with voltage in the presented experiment is seen in Figure 2.11.

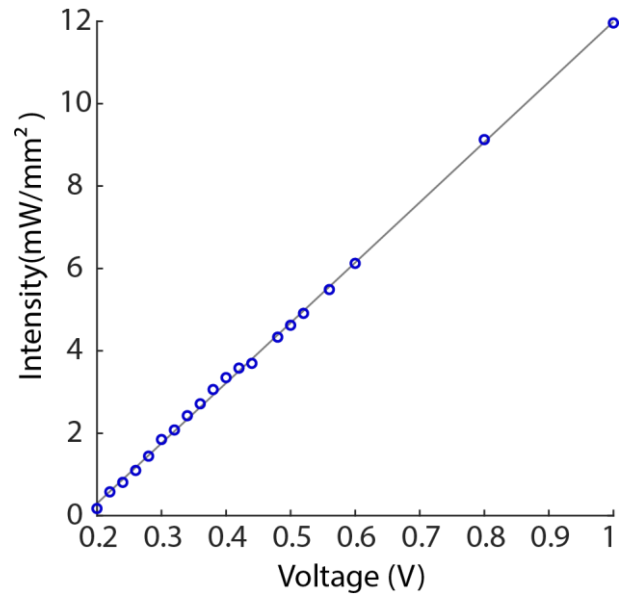
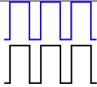
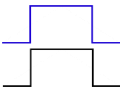
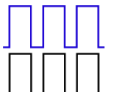
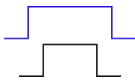


Figure 2.11: Representative relationship of voltage vs intensity at tip of the optic fibre. 0.2-1 V only are displayed (each step – small circle), as values above this were generally not used in analysis due to artefacts. Relationship is approximately linear, shown by a best fit line

Table 2.5: Typical optogenetic stimulation protocol. In trace insets, black – sound, blue – LED illumination

Stimulation	Pulse Width	Intensity	Frequency	Reps	Time	Description
LED	100 ms	Best V	N/A	100	1 min	For tagging optically activated cells
Spontaneous	N/A	N/A	N/A	N/A	20-30 min	No stimulation – dark, silence. For assessing the spontaneous activity of the cells
LED Steps	10-100 ms	0-5 V	N/A	50	25 min	Varying light intensities – checking activation intensity 
Broad band noise/LED	100 ms	0-80dB/best V	Broad band 0-48 kHz	50	5 min	Bursts of “white noise” containing all frequencies, with simultaneous LED. Determining hearing threshold 
Click/Light Pulse Trains (Slow)	5 ms (1 s train) 2,4,8,16,32,64 Hz	65 dB	Broad band 0-48 kHz	30	20 min	Short bursts of broad band noise, LED light or both simultaneously 
Click/Light Pulse Trains (Fast)	1 ms (1s train) 2,50,100,150,200,250,300 Hz	65 dB	Broad band 0-48 kHz	30	20 min	Short bursts of broad band noise, LED light or both simultaneously. Assessing Chronos properties
Pure tones/ LED	100 ms/ 200 ms	30-70 dB/0.6	3-48 kHz, 1/8 octave steps	50	40 min	Tones of a single pitch. Frequency response of cells 
Natural Sound	10 s	65 dB	3-48 kHz, varying	100	20 min	Natural sound clips (animal calls, water, leaves...). More natural responses to sound

2.4.5 μ LED Pilot Experiment in the ChR2 Mouse Cortex

External Hardware and Software Configurations

As the development of external hardware and software to operate the probe was part of the project itself, details of it and its optimisation can be found in Chapter 6.

μ LED Probe Insertion

The μ LED experiment was performed under urethane anaesthesia (20% in PBS, 1.5g/kg, see Section 2.3.4). Both probes were dipped in Dil. The animal (PV-ChR2, CBA) was secured with mandibular bars in the recording rig, as both earbars and a normal headcap would have not allowed for μ LED insertion, due to the wide probe PCB.

A 64 channel silicon probe (as used previously for the auditory cortex) was inserted vertically, on the far left edge of the craniotomy. The μ LED probe was inserted at a 20 degree angle, 400 μ m lateral to the recording probe insertion. The final configuration can be seen in Figure 2.12. Both probes were left for 30 mins to settle. Surface was kept moist with saline. Details of insertion positioned can also be see in Figure 2.12.

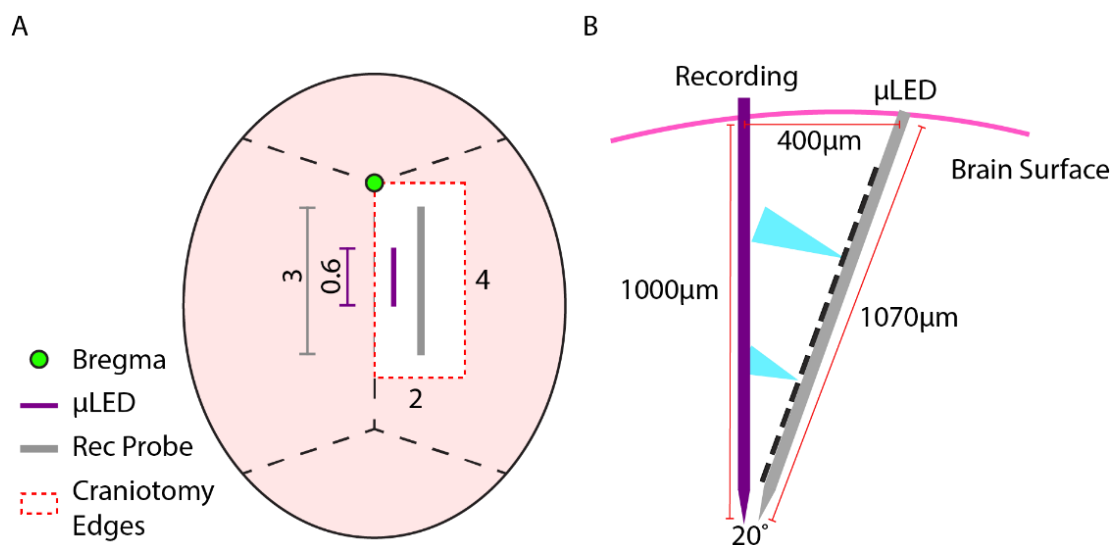


Figure 2.12: μ LED experiment probe configurations. (A) Location of 4x16 channel linear recording probe (purple) and 6 shank μ LED probe (grey). Distances are given in mm. (B) Side view of planned probe insertion distances, colours corresponding to (A).

Optical Stimulation

Two protocols were run using μ LED probes, as detailed in Table 2.6. A repetition includes all available μ LEDs. Each intensity (with n repetitions) was run separately from high to low intensities. Within each intensity, the order of μ LED illumination was pseudorandomised at each repetition.

Table 2.6: μ LED experimental protocols

Type of stimulation	Intensities	Time ON (ms)	Time OFF (ms)	Repetitions (each intensity)	Approx. Time
Spontaneous Activity (10 mins)					
Checkerboard	0, 15, 25, 50, 100	5	5	500	~30 mins
Spontaneous Activity (5 mins)					
Intensity	125, 100, 75, 50, 30	50	150	100	~1hr
Spontaneous Activity (10 mins)					

2.5 Post Recording Procedure

2.5.1 Transcardial Perfusion

After all recordings of any kind, animals were deeply anesthetised with a 50:50 mix of lidocaine and pentobarbital, 150 μ l, injected intraperitoneally. Once reflexes had disappeared, animals were perfused transcardially first with room temperature PBS, followed by ice cold PFA (4% in PBS).

Brains were removed and fixed in PFA (4% in PBS) overnight, then transferred to a 30% sucrose solution for cryoprotection.

2.5.2 Brain Preparation and Staining

Brains were sectioned to 80 μ m thickness coronal sections using a microtome (SM2010R, Leica), after fixing to the stage by covering with embedding matrix (OCT, CellPath) and freezing with dry ice (CO₂) in the surrounding tray). Sections were transferred to 0.1 M PBS, then washed in PBST (1x, 0.1% Triton X, 10 minutes) and PBS (x2, 0.1 M, 5 minutes). For both probe track verification, and Chronos expression, sections were stained with DAPI (1/5000, Invitrogen) and washed with PBS once more. For assessing viral injection spread, anti-GFP staining to enhance the signal was not required as the expression was (usually) strong enough to be seen by eye. Sections were mounted on glass microscope slides in 1% gelatine and dried overnight.

Coverslips were covered in Fluoromount (Invitrogen) and placed over the slices, left to dry and then sealed with nail polish.

2.5.3 Epifluorescence Microscopy

Slices were viewed with an epifluorescent microscope (Eclipse E600, Nikon) using x4, x10 and x20 objective lenses, and pictures taken with WinFluor (University of Strathclyde) and various filters for different colours for each stain (see Table 2.7). Images were pseudo-coloured and stacked in ImageJ.

Summary figures (single slice) of viral expression were obtained by overlaying the viral expression pattern at the target coordinate (-5.07 mm from bregma) from each animal onto an image of the coronal slice at that coordinate. Multi-slice summary figures (showing expression anterior and posterior to the target) were created in a similar manner, but for each animal individually, and using only a rough outline of the viral expression.

Table 2.7: Microscope filter and excitation wavelength combinations

Filter	Filter Wavelength (nm)	Excitation Wavelength (nm)	Colour	Measured Properties
TRITC	605-655	530-635	Red	Dil
FITC	515-555	470	Green	GFP-Chronos
DAPI	435-485	364	Blue	DAPI

2.5.4 Data Inclusion Criteria - Histological

After histological analysis, an animal's datasets could be excluded from data analysis if the probe(s) were clearly not in the target brain area(s) – and so the data was not recorded from the correct area. Criteria for dataset inclusion at this stage was that the majority of the Dil (i.e. putative probe position) was in the relevant brain area, with the area of highest intensity (i.e. the most likely probe location) well within the boundaries. For the auditory cortex, the boundaries were the anterior-lateral boundaries of the primary auditory cortex (-2.15 mm to 3.63 mm from bregma). The probe also had to be inserted at a suitable angle to hit the full depth of A1, this was judged largely by eye by comparing slice features and the atlas. For the inferior colliculus, the dye had to be present within the anterior-lateral boundaries of the central nucleus (-4.95 mm to 5.31 mm), ideally centred at 5.07 as the ICC fades out quickly on either side. For the ICC, the probe also had to be located within the medial-lateral spread

(approximately 0.5-1.5 mm). Some deviation from the vertical was allowed, as long as the majority of the probe remained within the central nucleus. These coordinates were found using a mouse brain atlas (Paxinos and Franklin, 2012) and examining the stained brain slices for prominent features in order to find the correct location. Medial-lateral measurements for the ICC were completed after taking the image, in ImageJ.

Chapter 3, Figure 3.3 summarises the histology results. One AC dataset was removed as the probe was far outwith boundaries, and an IC set was removed as the probe was placed too medial. In general, IC anterior-posterior location was good, and centred around 5.07 mm as expected. Overall, some leeway was given to positioning, as Dil spread is not always consistent/linear (particularly if there were multiple insertions) and position was occasionally hard to identify as slices did not fully resemble atlas pages (due to unaligned brain cutting, damage during brain removal, etc).

2.6 Data Analysis

2.6.1 Basic Data Preparation

Analysis Code

Unless otherwise stated, the MATLAB scripts used to analyse the neural data were developed or used historically within the Sakata Lab. Bespoke scripts to apply core functions to the current data were largely written by the researcher. Code can be provided upon request. Any relevant native MATLAB functions are provided in *italics*. Raw neurological data was viewed in the Neurotrace program, where all channels could be viewed simultaneously.

Data Inclusion Criteria

After recording and histology, some datasets were excluded as their quality was too low. A low quality recording was one in which there was very little/low amplitude/no spiking activity, situations easily identified after spike sorting due to the lack of identified units. This was generally accompanied by “flat” LFP. Recordings with excessive muscle noise were also excluded, depending on their severity and success of filtering to remove. In general, only datasets containing simultaneous data were included, though one high quality AC only, and one high quality IC only, were also included. Please see Chapter 3, Figure 3.1 for a breakdown of animals.

Required Files

All data analysis was performed offline. In MATLAB (Mathworks) sync channels (generated during the neural recording in order to record the exact time stimuli were presented, relative to the neural activity) were extracted, downsampled to 5 kHz from 20 kHz, and event files for each stimulus type derived, which contained the exact timing information of each stimuli (termed an “event”), relative to the probe data. LFP signals were extracted from the probe data with a low pass filter (800Hz) and downsampled to 1 kHz.

Data Structure

All files relating to each recording were stored in a separate folder. Details of these can be found in Table 2.8. Timings (on and off) of each kind of event were extracted from the data using the appropriate (auditory or optical) syncchannel , and the order and label files (see Figure 2.13).

Table 2.8: Key data files

Data File	Contents
Main Folder	
Meta file	Animal (weight, sex, age etc) and recording details (time of recording, probe information, stimuli information)
dat file	Main data file containing entire recording, all channels, all frequencies, 20 kHz sampling rate
EEG file	Downsampled Data file (1 kHz)
spikeStruct	Contains cluster information, particularly single units
muaStruct	Contains spiking information for each recording channel of the probe
Event subfolder	
BBN/Natural Sound/Puretones – event file	Timings of each stimulus (ms). Created by using label, order and sync pulses.
BBN/Natural Sound/Puretones – label file	Details of each stimulus (frequency, dB, time on etc)

BBN/Natural Sound/Puretones – order file	Order in which the stimuli were presented
Sync file	Corresponds to .dat file, square pulses indicate timing of stimuli

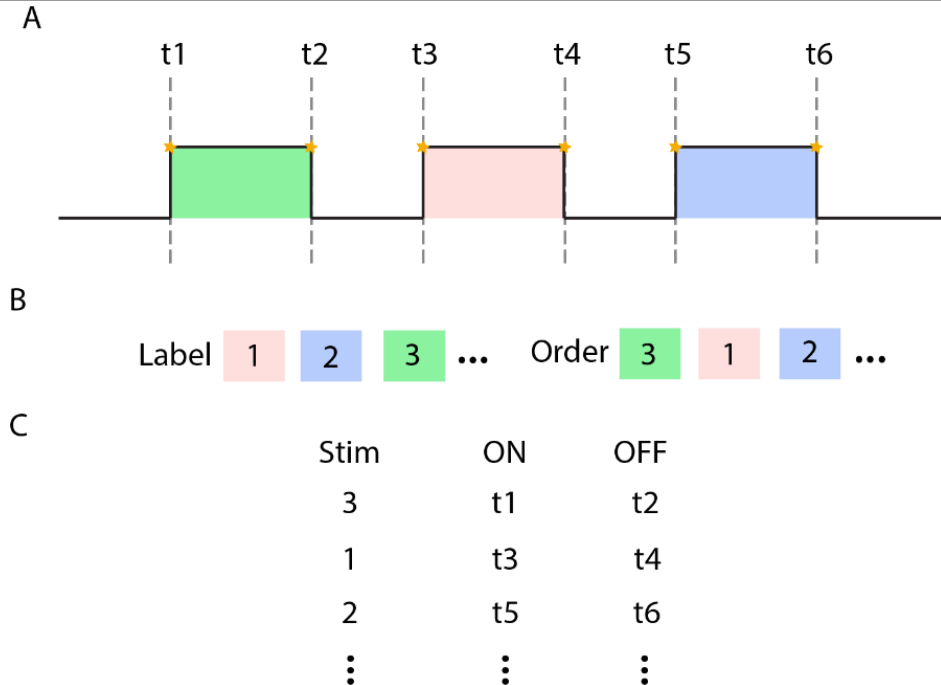


Figure 2.13: Event detection schematic. (A) Applied stimuli with detected on/off times (yellow stars, denoted t1 etc). (B) Label and order examples. The label file describes each type of unique stimulus, then the order files says which stimulus was applied in what order. (C) Applying the known order of stimuli to “name” each stimulus that was applied. The created event file has the order of the stimuli applied, label number, and on/off time in ms (relative to the start of the data file).

2.6.2 General Neuronal Data Analysis

Spike Sorting

Spike detection and sorting was performed offline using Kilosort (Pachitariu et al., 2016) with manual curation performed using the Phy template GUI (Rossant et al., 2017). The Kilosort program generates groups (“clusters”) of spikes that it has identified as being related to each other. either The user is then required to manually classify these clusters as either Single Units (i.e. all spikes are assumed to come from the same cell), Multi Units (spikes come from multiple cells) or Noise (“spikes” are not from neurons, are instead artefacts). Within the phy template GUI, the user can sort through the identified clusters, with the GUI displaying the autocorrelograms, a selection of the spikes in context on the recording channels, and the Principal

Components of that cluster, among other useful metrics. Graphical representations of these views can be found in Figure 2.14.

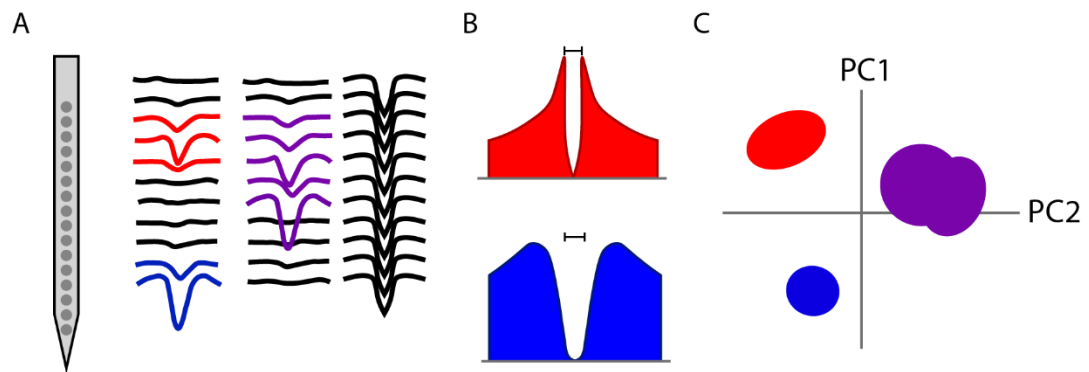


Figure 2.14: Principles of spike sorting. (A) Blue and red show single units (well separated spatially). Purple shows a cluster composed of at least two units. Black (third column) is noise – present in all channels, symmetrical. (B) autocorrelogram of red/blue cells. Note the clear refractory period. (C) Coloured cells represented in Principal Component space (red and blue, well separated). Purple is clearly composed of two clusters.

Single units were defined as displaying a clear, high amplitude waveform predominantly on a single channel (spreading to 1-2 channels/50-100 μm on either side), having a clear refractory period in the autocorrelogram, and being densely clustered and well separated from other units in principal component space (representing each spike in terms of its fundamental variables) – see Figure 2.14, red and blue. If this was not the case, but activity was clearly not noise (for example, low or multiple amplitudes, unclear refractory period, or evidence of >1 cluster in PC space), it was sorted as a multi unit (see Figure 2.14, purple). Partial clusters (e.g. single units with abrupt reductions in spiking due to animal movement) were left “unsorted” but included in channel MUA, see later.

Clusters often require merging or splitting due to under or over clustering. The user’s classification of each cluster (including any merging or splitting they have done), are saved alongside the spike information generated by Kilosort, and can be read, converted to MATLAB format, analysed, and further visualised with a combination of custom MATLAB code and open source functions, and saved in an appropriate and easily accessible format (CortexLab, 2019). Spike waveforms could be extracted and averaged from the raw data using recorded spike times for each cluster, and various metrics computed and added to the other spike information.

Single units identified by manual spike sorting were then further judged automatically on a variety of cell quality metrics, via a dedicated MATLAB script. The principal metric was mahalanobis distance/isolation distance (Schmitzer-Torbert et al., 2005) which is

a measure of how close together spikes in a cluster are – how close spikes are to the cluster mean. This was calculated using freely available MATLAB code from the Cortex Lab's GitHub (CortexLab, 2019). An additional measure to find very high quality clusters was the contamination rate. This is an estimate of proportion of spikes inside the cluster boundary that are not from the cluster (false positive rate).

Definition and Inclusion Criteria of Single and Multi Units

For the purposes of this analysis, single units are defined as well clustered units with all spikes putatively originating from a single neuron. Single units whose activity did not continue for the entire recording (i.e. partial units) were excluded from the single unit grouping. To be included in analysis, single units required a mahalanobis distance of ≥ 20 and have a spontaneous firing rate of > 0.1 Hz.

Following the spike sorting definition, a multi unit in this analysis within this thesis consists of all the multi units (identified by manual sorting), single units (with no quality threshold) and partial units on a single channel, essentially defining a small population around each channel. Except in a very small minority of cases, multi units as identified by manual sorting were localised to a single channel. They were only included in the channel that recorded their highest amplitude, which could be extracted from the data generated by Kilosort so the spikes were not included on multiple channel MUA. Thus, for a 16 channel recording, approximately 16 (channel) multi units were expected. This definition of multi units was created in order to have more units in the inferior colliculus – all the units around each channel would be being stimulated in auditory implants and so it was a logical way of defining population activity. Multi units were defined in the same way as the cortex, as it proved to be a good and logical way to define a population (in the context of implants and layers) and to utilise as many as the recorded spikes as possible. Units created in this way would also be more consistent and easier to analyse than regularly defined multi units, which were often of low quality.

Spike Waveform Quantification

To compute the properties of each putative cell, up to 200 waveforms were extracted at random from the raw data. These were averaged into a single waveform, from which various metrics were assessed with a custom MATLAB script. Figure 2.15 shows the metrics computed.

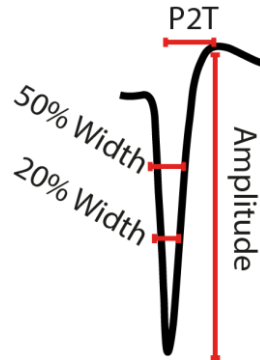


Figure 2.15: Cell Waveform metrics. Figure shows a typical waveform and what measurements are taken to describe it (red lines). P2T is the Peak to Trough time. Metrics are generally reported in mV and ms

Cell Type Classification

To decide on thresholds for classification into with narrow or broad spiking cells, histograms of the following waveform measurements were plotted as histograms to look for biomodalities; Peak to Trough Amplitude, 20% width, 50% width, amplitude, spontaneous firing rate. Biomodalities were exhibited in Peak to Trough, 20% and 50% width (as predicted by literature). Examples will be shown in Chapter 3. Scatter plots of P2T vs 20% width, and P2T vs 50% width, were plotted, and basic, two group k-means clustering (MATLAB *kmeans*) was applied to help separate groups. Though two clusters were observed for both comparisons, it was slightly clearer in the P2T/20% width, and so thresholds for each (0.4, 0.35) were determined and used to categorise cells.

Spontaneous Firing Rate

The general spontaneous firing rate (i.e. in the absence of auditory and visual stimuli) was derived from a 20 minute segment before or after the sound stimuli presentations, depending on the dataset (some recordings had less spontaneous activity at the beginning). The number of spikes belonging to each neuron/multi unit was divided by the time in order to give a spike rate in Hertz. In other instances such as z-scoring, spontaneous activity was chosen to be the period of time directly before the stimulus was applied, of a length ideally matching that of the stimulus in assessment. Rate was calculated by dividing by this time period, as before.

Assessment of Firing Rate Over Time (PSTH)

Spikes across all trials of a stimulus (including a period of time before and after, relative to the stimulus) were sorted into 5 ms bins to create a Peri-Stimulus Time Histogram (PSTH) of activity over the time course of the stimulus. Spike counts were then smoothed with a Gaussian kernel ($\sigma = 5$) to obtain a smooth trace of firing over time for visualization.

“Barcodes” of groups of cells/MUA, showing time points of common activity during the natural sound stimulus, were also generated. A z-score was obtained for each time point, using a baseline firing rate from a period of time preceding each repeat of the stimulus.

If it was >2 (a standard threshold), the value at this time point was incremented by 1. After all datasets were included, this resulted in an array where the number at each time point indicated how many clusters had an evoked response at that point. This was converted into a % of total clusters and displayed.

2.6.3 Assessment of Best Frequency and Frequency Range

Due to the limited range of stimuli applied, the characteristic frequency of a neuron could not be reliably determined. Thus, best frequency was used in assessing tuning characteristics. This was calculated by determining a z-score for each combination of frequency and intensity (dB). The z-score represents how far away from the baseline firing rate the measurement is, in terms of standard deviations from the baseline.

$$zscore = \frac{(x - mean)}{\sigma} \quad (2.1)$$

Where x = the mean firing rate of the neuron during the presented stimulus/stimulus segment, $mean$ is the mean spontaneous firing rate preceding the stimulus (determined by averaging the firing rate across each segment of silence preceding each repetition of the stimulus) and σ is the standard deviation of the baseline.

The baseline used was the 100 ms immediately preceding each stimulus. To get a better assessment of evoked responses, particularly with brief responses, the spiking activity 10 ms-50 ms after the stimulus was taken. Spontaneous and evoked activity was translated into spikes/s for comparison despite differences in the lengths of time being analysed, and the z-score calculated from this.

Generally, a z-score threshold of 2 is used to define a neuron as responsive to a stimuli (i.e. the neuron’s activity during a stimulus is increased over its spontaneous

activity by at least 2 standard deviations of said spontaneous activity). In the case of this analysis, a cell was only assigned a best frequency if at least one stimulus gave a z-score of 1.5. This is slightly lower than the standard threshold of 2 but the threshold was revised downward after frequent observations of clear (but very brief, around 5 ms) evoked responses. When averaging this 5 ms response across 40 ms, the average spike rate became low and based on z-scoring, the neuron would appear to have had no significant response. The lowered threshold allowed for more neurons responding this way to be “caught” and included in frequency analysis. Without including a response threshold, including untuned neurons where the “best frequency” may be fairly random is risky. The best frequency was then defined as the frequency at which the strongest (i.e. highest z-score) was observed.

Frequency Range

With the best frequency of each unit calculated, the frequency range of a dataset was calculated by looking at the range of frequencies covered by the component cells. It was computed in octaves by taking the minimum and maximum best frequency (f_{\max} and f_{\min}) found in a dataset’s units, and using the equation:

$$octave\ range = \log_2 \frac{f_{\max}}{f_{\min}} \quad (2.2)$$

2.6.4 Current Source Density

Current source density analysis identifies both current sinks (incoming neuronal connections) and current sources (neuronal output) (Freeman and Nicholson, 1975, Nicholson and Freeman, 1975). After identifying sinks and sources, and applying knowledge of the cortex’s functional arrangement, true depth estimations can be made for silicon probe channels.

EEG data was lowpass filtered at 300 Hz. The following equation was then applied to each channel:

$$CSD = \frac{(V_a + V_b) - 2V_o}{d^2} \quad (2.3)$$

Where V_b and V_o are one and two channels away from V_a , respectively, and d is the spacing between channels. The resultant data had 2 less channels, and no spatial filtering was applied beforehand.

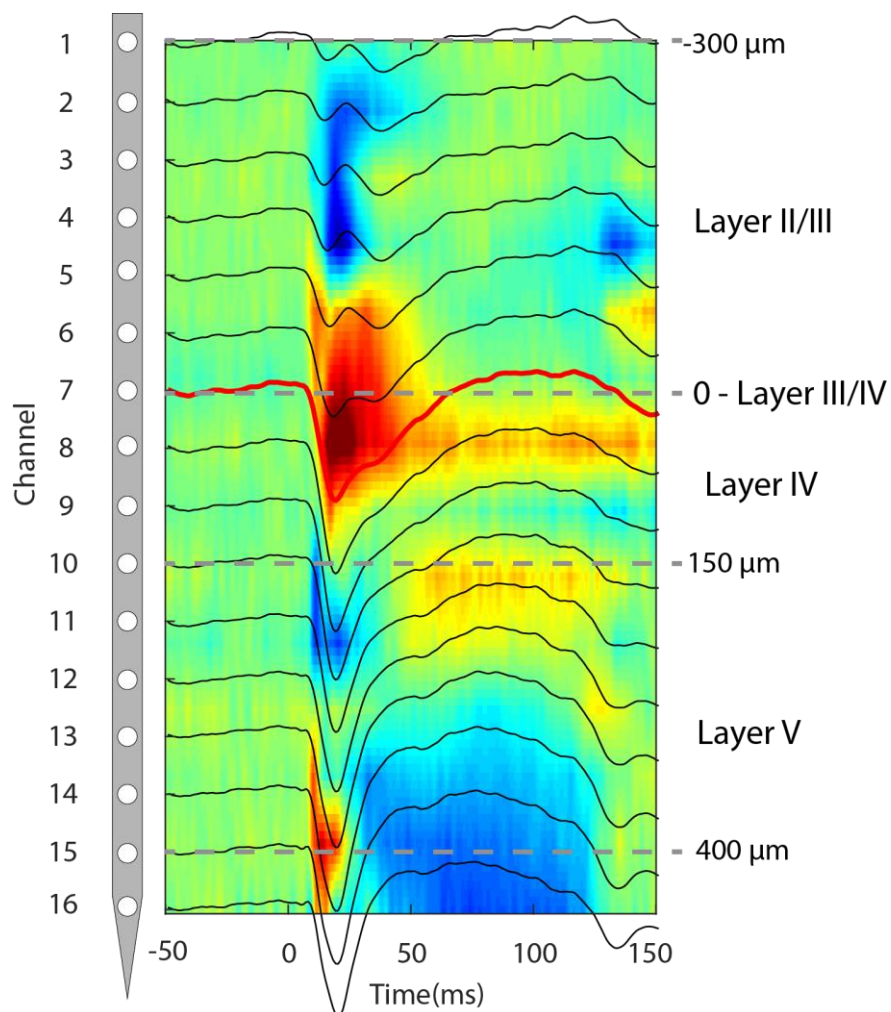


Figure 2.16: Current Source Density example. Figure shows a colour scaled CSD over 16 channels, -50 ms before and 150 ms after an applied stimulus. Red Areas indicate current sink, while blue are current sources. ERP traces are overlaid onto the coloured image, with a simple probe schematic indicating the probe layout. Putative cortical layers and depths are indicated.

Of particular interest was the main sink channel, cortical layer III/IV (thalamorecipient layers, lemniscal central pathway). The strongest sink channel was identified by finding the channel with the largest value in the first 50 ms following presentation of a stimulus. By setting this channel as depth 0, other channels can be assigned relative depths. Following on from this, knowing the strongest channel of each single and multi unit, a depth relative to layer III/IV can be assigned.

2.6.5 Fano Factor

Calculation of Fano Factor

The Fano factor is a measure of spike count reliability across trials and was calculated thus.

$$Fano\ Factor = \frac{\sigma^2}{u} \quad (2.4)$$

Where σ^2 is the variance (standard deviation²) of spike rate across trials, and u is the mean across trials. The time bin used for the analysis varied – it will be stated in any results regarding the Fano factor.

Correlations between MUA and Fano Factor

PSTH was calculated across trials (generally, 100), using a range of bin widths. To accompany the binned spike rate, the Fano factor was computed for each time bin. This resulted in two arrays: MUA over time course of the stimulus (spikes/s), and Fano factor over the time course of the stimulus. The Pearson's correlation coefficient between the arrays was then calculated (MATLAB *corr*). Smoothing generally resulted in stronger correlations. A p-value indicating the significance of the correlation was calculated simultaneously and used to exclude some values ($p < 0.01$).

2.6.6 Natural Sound Decomposition

The sound envelope was derived using the MATLAB *envelope* function (Hilbert filter length of 500 samples/5 ms). This was then downsampled to 1000 Hz, from 96.4 kHz. For visualisation purposes only, the signal was further smoothed with a moving average filter (MATLAB, *smooth*).

Time/frequency variation of both the sound and sound envelope (scalogram) were derived using MATLAB's *cwt* function – a wavelet transformation. Frequency components were derived using the Chronux toolbox (Mitra and Bokil, 2008, <http://chronux.org>, 2018).

2.6.7 Inter-Trial Coherence

Calculation

Inter-trial coherence (ITC) was measured as a way of assessing the degree of LFP synchrony across successive sound trials. For each LFP channel, data was decomposed into frequency components using a wavelet transformation with the resulting complex data containing both amplitude and phase information. Wavelet data could then be further split into frequency bands as required. To compute the ITC,

a bin of 5 ms with a 2 ms overlap was used. For each time bin, data was averaged across the bin (1 kHz sampling rate). The complex/phase information was then divided by the absolute value of the data, and then summed across trials. This absolute value of this summation was divided by the number of trials, resulting in a value between 0 and 1 for ITC. If the accompanying phase was not uniformly distributed across trials (assessed using Rayleigh's test), the ITC was said to be significant for that time bin.

$$bin\ average = \frac{\sum_{i=1}^s LFP_i}{s} \quad (2.5)$$

Where LFP at each sample in the bin (current sample = i) is summed and divided by the total number of samples (s).

$$ITC_b = \frac{\sum_{t=1}^T \frac{complex(bin\ average)_t}{abs(bin\ average)_t}}{T} \quad (2.6)$$

Where T is the number of trials (current trial = t), and ITC is the inter trial coherence at that given time bin. This is repeated for all time bins to make a single array, and repeated for each LFP frequency band to give the value of ITC over the period of sound presentation, for each given LFP frequency band. Code for calculating ITC was adapted from EEGLAB (Delorme and Makeig, 2004).

ITC Depth Distribution

For the purposes of this analysis, "sink" channels were at -50 μ m, 0 μ m and 50 μ m depths relative to the CSD derived sink channel. This is to account for small discrepancies in calculated sink channel.

ITC Metrics

Two main features of ITC were examined – the mean ITC over sound presentation, and the % time spent significant. Note that calculations for the mean ITC did not include time points where the coherence was non-significant (Rayleigh's criterion). The metric is thus a measure of the typical strength of the ITC, not its pattern/appearance in time. Data is displayed as medians +/- median absolute deviation

2.6.8 Spike Entrainment

Base Calculation

Neurons are known to entrain to LFP oscillations, particularly in the cortex. This means that they fire at particular phases of a specific frequency/small range of

frequencies (see Figure 2.17). This can be assessed by examining the entrainment of isolated single units or our self-defined multi units (i.e. the single units) to a channel of LFP at various frequencies.

Entrainment is assessed for both spontaneous activity (20 minutes at the start or end of the recording) and during natural sound stimulation (around 20 minutes with the 1 second inter-trial intervals removed to make a continuous signal). Entrainment is not examined at specific time points of the stimulus presentation, instead, the continuous signal is treated as “evoked” data.

For each unit, the comparison LFP channel is chosen to be +/-8 channels away (i.e. 400µm) to avoid any interference from spiking on that channel. This LFP is filtered into 17 narrow bands of frequencies between 2 and 200 Hz, with the width of these bands gradually increasing with increasing frequency (i.e. first band is 2-3 Hz, last band is 180-200 Hz). In analysis, bands are defined by their starting frequency. Filters are designed using MATLAB’s *designfilt* function, specifying “bandpassFIR”, defining pass and stop band frequencies using predefined band widths, a stopband attenuation of 50 dB, Passband Ripple of 0.01 Hz and a Kaiser Windowing design method.

The phase at each point in the filtered LFP is derived using a Hilbert Transform (MATLAB *hilbert*), and separated into real (amplitude) and complex (angle) components. The angle component is converted to degrees.

The phase in degrees of each spike in a unit is derived using knowledge of spike timings relative to the extracted LFP. Spikes are then assigned into 1 of 4 phase bins, as detailed in Figure 2.17 and Table 2.9. If the distribution of spikes in each bin is not uniform (i.e. most spikes fall into one bin, see Figure 2.17 i), it is deemed a significant modulation, as assessed by using Rayleigh’s circular stats criterion.

As well as by the percentage of a unit’s total spikes in each phase, entrainment was quantified as “rate difference”. Spikes have been previously sorted into their firing phase, and if there is no entrainment/phase preference, 25% of the spikes will fall in each phase (see Figure 2.17). The rate difference is then the difference between the phase with the highest firing minus the phase 180° away. Thus, if one phase has 40% of all spikes, and the opposite bin has 10%, there is a 30% rate difference.

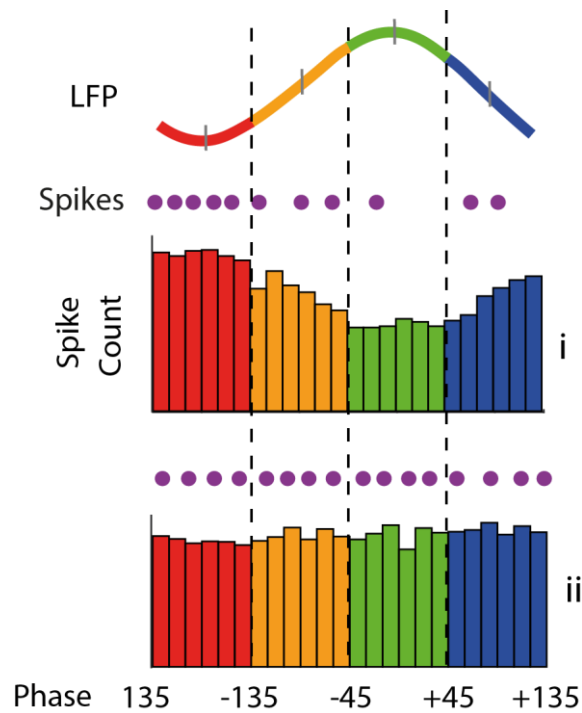


Figure 2.17: Entrainment. Top, LFP trace, dotted lines and coloration indicates “bin”. (i) Schematic of entrained cell. Purple dots denote hypothetical spikes, underlying histogram indicates the relative spike count (fewer spikes shown for clarity). (ii) Schematic of un-entrained cell. Spikes are distributed evenly in all 4 bins, as indicated by flat underlying histogram.

Table 2.9: Binning of LFP Phases

Bin	Colour	Start (deg)	End (deg)
1	Red	135	-135
2	Yellow	-135	-45
3	Green	-45	45
4	Blue	45	135

2.6.9 Decoding Analysis

Linear Classification

Linear classification can calculate how well groups of predictors (such as the firing patterns of several neurons) can predict which of a range of stimuli was presented. Natural sound was used as the stimulus, and was treated in a manner similar to Kayser et al, 2012, where a longer natural sound stimulus was cut into 10 random sections, of length based on the timescales of various cortical oscillations (Kayser et al., 2012). The goal was to compare prediction performance between the AC and IC. The general procedure is outlined in Figure 2.18.

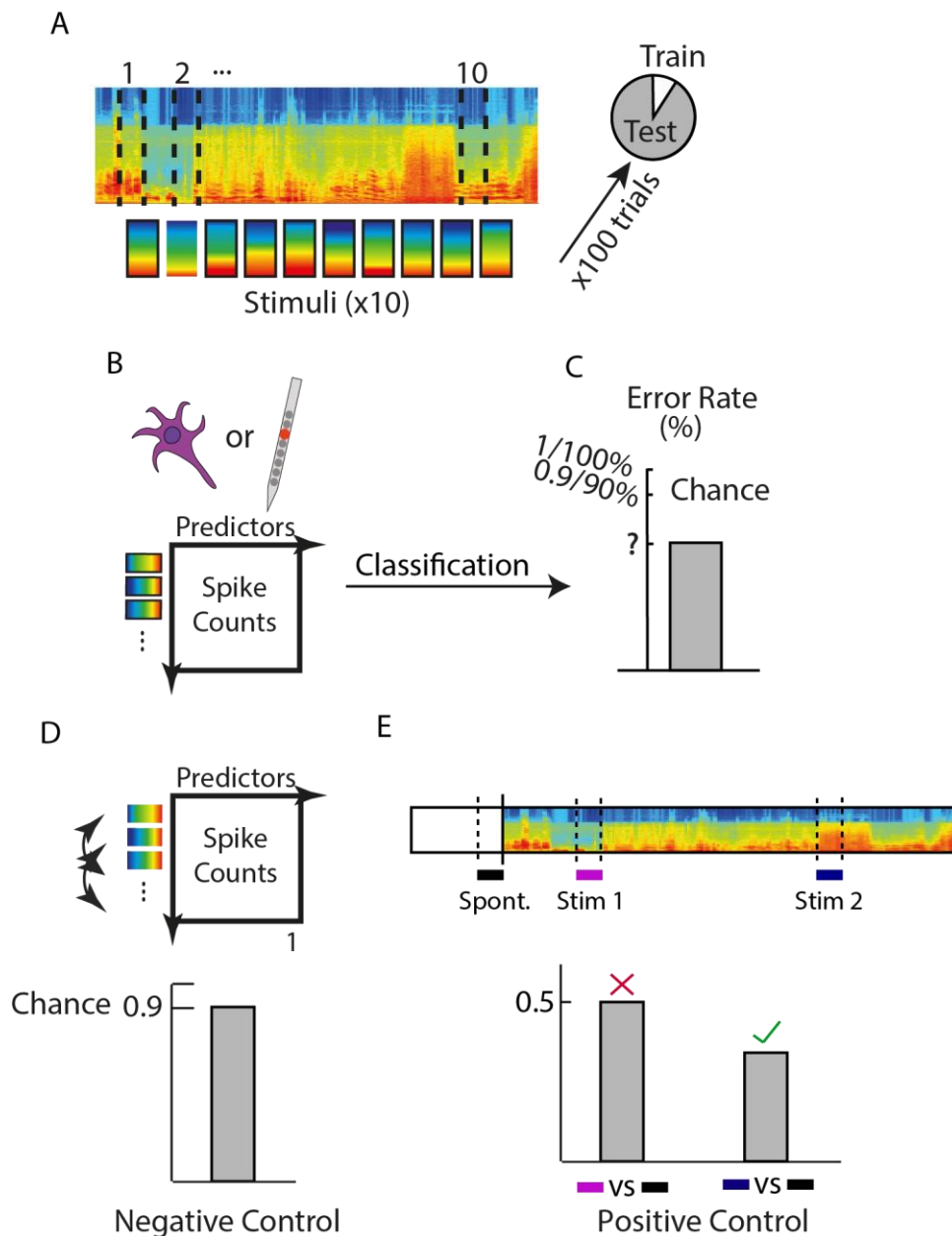


Figure 2.18: Prediction of natural sound stimuli through linear classification. (A) Chunking of each 10s segment into 10 "stimuli", 10% used to train and 90% to test. (B) Using the single unit or channel spikes counts, a matrix is formed and used to train and test the classifier. (C) Chance level is given as 0.9 – 10% of the time, the classifier is right (i.e. by random chance). (D) Errors over repetitions show a normal distribution. Negative controls are formed by shuffling rows, and give chance level error. (E) Positive controls created from a "spontaneous" and an "evoked" stimuli. Bars indicate that the classifier could not distinguish between spontaneous (black) and stim 1 (purple), with a 50% error, but that it could tell the difference between stim 2 and spontaneous, and was able to predict the correct "stimuli" more than 50% of the time

Firstly, the start and end times of 10 sub-stimuli were selected pseudo-randomly from the 10 second presentation of natural sound; these timings were relative to time 0 and could occur between 0 and 10. Rarely, there was slight overlap in segments, particularly for longer stimuli lengths. As there were usually 100 repetitions of natural sound, the selected timings were normalised to the start of each 10 second sound

stimulus repetition, to in term generate repetitions of the sub-stimuli. These relative timings could then be used to extract the neural data for analysis. The following was then done separately on each recorded brain area, and for each set of 10 stimuli in turn.

The number of spikes occurring in each of the 10 stimuli, for each repetition, was extracted for each of the single units in the area, or the MUA activity on each channel.x A “prediction matrix” of (nTrials*nStimuli) x nClusters was thus derived for each dataset.

Linear classification with 10-fold cross validation (MATLAB *cp*) was then performed on the created prediction matrixes (see Figure 2.18). With this approach, 90% of the data (i.e. 90 of 100 trials) is used to “train” the classifier, with the remaining 10% used to test how well it performs. This gives the decoding performance of the classifier – i.e., using the data provided in training, how well can the classifier correctly classify the test data? This performance is measured as a Prediction Error. An error of 0 means the classifier predicted each stimulus perfectly (best performance), while 1 (100% error), meant it was never correct (worse possible performance). A value of 90% error (0.9) is chance level – with 10 stimuli, the classifier will choose the correct stimulus 10% of the time by chance.

The process was repeated 150 times with negative/positive controls, and with different “stimulus” lengths.

Negative Controls

The relationship between predictor and stimulus was disrupted by random stimulus and trial shuffling (Fig 2.18D) – i.e. the rows of the prediction matrix were shuffled. The expectation was that prediction error would rise to chance level in these controls.

Positive Controls

Positive controls were used to ascertain whether or not spontaneous (silent period) and evoked data (natural sound) was distinguishable, see Figure 2.18E. Each of the 10 stimuli of each of the 10 lengths was compared, in binary classification, to an equal length of spontaneous activity before the stimulus began. An error of 50%/0.5 indicates that particular stimulus is indistinguishable from spontaneous activity. Positive controls were further quantified for each dataset by examining how many of the 10 stimuli were indistinguishable from spontaneous activity

Dimensionality Reduction - PCA

To better compare the two brain areas (each of which had varying numbers of cells), Principal Component Analysis was performed to reduce the dimensions of the input data. The input data is highly multi-dimensional (a dataset with 20 units has 20 dimensions over which the data is varying), but it is likely that the variability seen in the data can be explained by a few of these.

In principal component analysis, the original data is transformed into a new set of dimensions that are independent from each other, with each dimension (or Principal Component) explaining a portion of the variability within the original data. PCs are returned in order of their explained variance. Data is also normalised before this process so as to be on the same scale – otherwise there is likely to be skewing. In this case of neuronal spiking, variation in the spike trains is explained using weighted combinations of the recorded units, essentially defining a population.

As a conceptual example, 70% of the spike train variation seen in a dataset of 20 units may be caused/explained by a combination of units 3, 10 and 16, with 20% explained by a combination of units 4 and 12. PCA always returns the same number of PCs as original dimensions, but the general approach is to use the PCs needed to explain $\geq 80\%$ of the variance. While a small amount of information is lost, the benefit gained from having fewer dimensions in computations is desirable. One drawback with the basic PCA approach is that it can return negative values, and these are difficult to interpret in the context of spike trains and neurons.

PCA was performed using the MATLAB function *pca*, using the default “Singular Value Decomposition” algorithm. Alongside values for each identified Principal Component, there is an accompanying value of explained variance - i.e. how much of the variability in the data can be explained by the PC. This variability data is also saved, and principal components are sorted in order of high to low explained variance. For the purposes of the analysis, both 3 and 5 PCs are used as predictors for classification analysis as described above (i.e. the PCs that should explain most of the data variance), for direct comparison with the use of *all* predictors vs the dimensionally reduced dataset.

2.6.10 Pairwise Neuronal Correlations in Natural Sound

Signal and noise correlations were computed in a pairwise fashion, between all possible pairs of units in a dataset. Correlation was computed using the MATLAB *corr*

function, to derive Pearson's Correlation Coefficient. The correlation for each cell pair was then pooled across datasets for each kind of data (i.e. AC SUA, AC MUA, IC SUA, IC MUA).

Signal Correlations

Signal correlation was calculated by averaging the unit's response to each stimulus across trials, creating an array of 1 x nStimuli to be correlated against that of other units.

Noise Correlations

Noise correlations during the natural sound stimulus were generally calculated using the input matrix to the classification analysis, with each column being one cell and each row being the spike rate during one trial of one stimulus (of 10 total). For each of the 10 stimuli, the mean spike rate across trials was removed from all trials of this stimulus, leaving an estimation of the non-evoked "noise". This was repeated for all 10 stimuli, and then the results concatenated together to form a single array for each cell/multi-unit, which could be correlated against another unit.

Pair Characterisation

Neuronal pairs and their correlations were also split into subgroups for some analysis – both location based and cell type based. These are outlined in Table 2.10 and Figure 2.19.

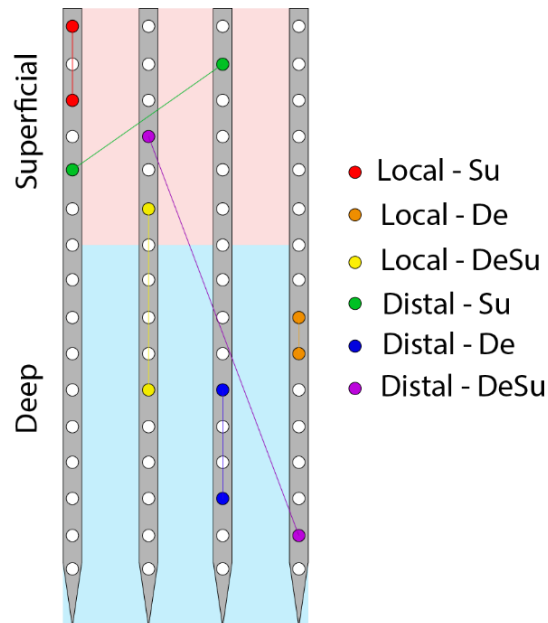


Figure 2.19: Cell pairing nomenclature for pairwise correlations. Image shows 4 shank probe schematic. Coloured channel pairings and key indicate the naming of cell pairs of which there is a cell on each indicated channel. Upper pink background channels are superficial (above and including sink channel) and lower blue background channels are deep (below 0) – note the exact sink channel, and thus these definitions, will changed based on the dataset

Some analysis also involved simple distance measurements – these were calculated using relative depth and shank spacing (hypotenuse of the triangle).

Table 2.10: Definition of cell pair groupings. Relative depth refers to the sink channel identified by CSD.

Group name	Description
Locational	
Superficial-Local	Both cells >0 relative depth, same shank
Superficial-Distal	Both cells >0 relative depth, different shank
Deep-Local	Both cells <=0 relative depth, same shank
Deep-Distal	Both cells <=0 relative depth, different shank
Superficial-Deep-Local	One cell >0, other <=0 relative depth, same shank
Superficial-Deep-Distal	One cell >0, other <=0 relative depth, different shank
Local	Any depth, same shank
Distal	Any depth, different shank
Cell Type	
Broad-Broad-Local	Both broad spiking, same shank
Narrow-Narrow-Local	Both narrow spiking, same shank
Broad-Narrow-Local	One broad, one narrow – same shank
Broad-Broad-Distal	Both broad spiking, different shanks
Narrow-Narrow-Distal	Both narrow spiking, different shanks
Broad-Narrow-Distal	One broad, one narrow – different shanks
Broad-Broad	Both broad spiking
Narrow-Narrow	Both narrow spiking
Broad-Narrow	One broad, one narrow

2.6.11 Delta Ratio

The delta ratio is a metric used to quantify the power of the delta LFP band compared to the rest of the LFP spectrum, which in turn is an indication of global brain state (higher delta power ratio – synchronised state). The exact definitions of these bands can change, but in this case the ratio between the 0.1-3 Hz band and the 0.1-40 Hz band was calculated. The ratio was calculated on a single probe channel. The power at each frequency for a given time bin was derived using the Chronux toolbox function *mtspectrum* (Mitra and Bokil, 2008, <http://chronux.org>, 2018), and divided to calculate the ratio.

2.6.12 Non-Negative Matrix Factorisation

Pre-Processing of Data

The base code for the decomposition was very kindly provided by Dr Arno Onken (University of Edinburgh). In order to apply the code to the project's data, additional code was written to arrange the data in the required format, with minor adaptations made to the base code to facilitate this. With NMF (Lee and Seung, 1999, Onken et al., 2016), the aim is to decompose neuronal population activation into "modules" and the activation strengths of said modules in time (i.e. time bins during natural sound) and space (i.e. individual single/multi units). Spiking timings were discretized into 100 ms bins, and sorted into trials, so that each trial had 1000 equally spaced bins locked to the start of the stimulus. This information could then be shaped into various matrices, in order to obtain the desired outcomes. This is another form of dimensionality reduction, but unlike PCA, outputs cannot be negative and so it is easier to interpret from a neuronal population standpoint.

Spatial Decomposition

The aim with spatial decomposition was to gauge the influence of each cell on a module, and how that modules changes in time. A matrix of spike counts was created, of the size $N \times T$, where N = number of units (variable), and T is the time point (trials*number of time bins in a trial, data was concatenated). This then resulted in two matrices of $N \times M$, where N = cell and M = modules, and $M \times T$, where the T dimension was split back up into trials* time points in a trial to clearly show the activation of each module at each point in time, across multiple trials. A graphical representation of this is displayed in Figure 2.20A.

Spatiotemporal Decomposition

The desired output in this case was to see specifically how each cell contributed at any given time point, in more detail than simple spatial patterns. Input was a $(N \times T_p) \times T_r$ matrix, where N = units, T_p = time points in a trial and T_r = trials. This decomposed into a $M \times T_r$ matrix and a $(N \times T_p) \times M$ matrix, which was further split into $M \times N \times T_p$ matrixes to show the general activation strength of any given cell during each time point and in each module, which the $M \times T$ shows the variation of this across trials. A graphical representation of this is displayed in Figure 2.20B.

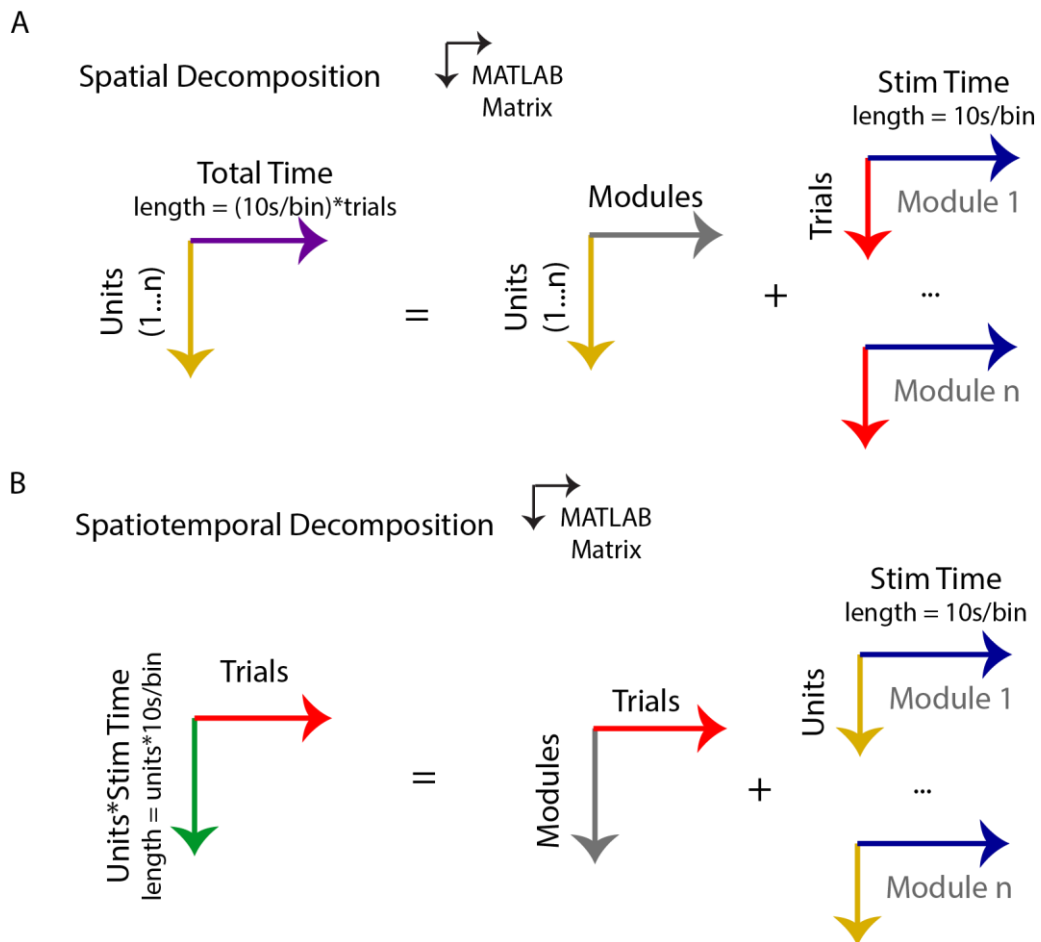


Figure 2.20: Input and output matrices in spectral and spatiotemporal decomposition. Arrows indicate dimensions of a 2D MATLAB matrix, lengths are provided. Colours denote different quantities, secondary colours indicate a combined length of two sub-quantities (i.e. a dimension containing trials (red) and stim time (blue) in a single dimension is denoted purple). (A) Spatial decomposition. (B) Spatiotemporal decomposition

2.6.13 Optically Evoked MUA Activity

To obtain a measure of optogenetic activation, raw probe data was filtered with a high frequency band pass filter (750-5000 Hz) to exclude low frequency oscillation/some light artefacts and keep high frequency spiking activity. This data was then half-wave rectified (to make all values positive). To obtain a single value for MUA activity during stimulation, the baseline activity (average activity 50 ms before stimulation) was subtracted from the average activity (μV) in the middle of the stimulation (exact time dependant on stimulus length). The middle was taken as the start still shows some influence of the light artefact. To create the graphs of intensity versus MUA activity for each channel, a 3rd order polynomial (*polyfit*) was fitted to the data and plotted on a log x scale.

2.6.14 Statistical Analysis

Data was, in general, non-normal. Data was tested for normality by using a one-sample Kolmogorov-Smirnov test (*kstest*, $p < 0.05$). As such, non-parametric tests were usually used, unless otherwise stated. All statistical analysis was performed in MATLAB with existing statistical functions (these are listed in *italics* after their associated test).

For comparisons of two variables of non-normal, unpaired data, a Wilcoxon rank-sum test (*ranksum*) was used. For paired data, the Wilcoxon rank-sign test was used (*signrank*). For between group comparisons (i.e. comparison of time bins within AC), a Kruskal Wallis test was used (*kruskalwallis*). Multiple comparison post-hoc statistics were derived using Bonferroni method (*multcompare*). P values of < 0.05 were taken to be significant, unless otherwise stated in the results.

For comparisons of two variables of normal, unpaired data, a two sample t-test was used (*ttest2*). For paired data, the paired t-test was used (*ttest*). Threshold was set at $p < 0.05$.

To compare distributions of data, a two sample Kolmogorov-Smirnov test was employed (*kstest2*), with p values of < 0.05 being significant unless otherwise stated.

In instances where 2-way comparisons were desired, the data was not normal. The 2-way ANOVA equivalent, the Friedman test, could be employed, but does not offer information on interaction effects. It is therefore not strictly possible to make conclusions regarding interaction effects when examining 2-way data. As an alternative, analysis will employ multiple statistical tests with limitations made on conclusions. In an example from Chapter 4, Kruskal-Wallis was used to examine the effect of time bin *within* each individual brain area (AC or IC), with individual Wilcoxon rank-sum or Wilcoxon rank-sign tests performed for each time bin individually to observe the effect of brain area *for that time bin only*. Conclusions must be carefully worded.

For phase/entrainment analysis information, Rayleigh's test for circular uniformity was employed. A p value of < 0.01 indicated that the phase distribution was not uniform – i.e. was biased/skewed, and some level of phase entrainment or phase synchrony exists.

The employed test and p value thresholds will be stated alongside each set of results, for confirmation.

Chapter 3 Characterisation of Single Neuron and Population Activity During Natural Sound, in the AC and IC

Chapter 3 discusses the results of initial analysis of the auditory cortex and inferior colliculus during spontaneous activity and natural sound. Section 3.1 provides an introduction to the chapter aims, existing literature, and hypothesis. Section 3.2 provides an overview of data recorded, including surgical success, histology and waveform metrics. Section 3.3 looks at the basic appearance of neuronal activity during natural sound, including example MUA, a spectral breakdown of the natural sound stimulus, and a short study of trial-trial variability during natural sound. Section 3.4 looks at the inter-trial coherence of LFP during natural sound, comparing between areas and cortical depths. Section 3.5 examines evidence of entrainment to LFP during spontaneous activity and natural sound . It compares activity between the auditory cortex and inferior colliculus, and across several frequency bands, plus cell type specific effects. In the final section 3.6, results are briefly outlined and then then discussed in the context of existing literature and potential novelty. Finally, limitations in the current approach are identified, and future work discussed.

3.1 Introduction

3.1.1 Aims of the Chapter

This chapter aims primarily to compare and contrast properties of the auditory cortex and inferior colliculus (specifically A1 and ICC) during their responses to natural sound, in order to inform future analysis and identify functional differences. The focus is on lemniscal areas as this is where auditory implants will be inserted. Properties relating to natural cell behaviours, particularly during natural sound coding and processing, are important for designing and troubleshooting future auditory implants.

The analysis presented here will primarily focus on comparing general properties such as cell metrics, trial-trial variability and levels of entrainment, with comparisons strengthened by the simultaneous nature of the recordings. Results from this chapter have guided later hypotheses and analysis direction, while also confirming the general hypotheses and providing an introduction to the datasets. The paragraphs below will set out the rationale behind each analysis, and the resulting hypothesis. It should be noted that, at least in the first half, the chapter is meant to serve as an introduction to the data, so the questions asked are fairly generalised. The aims of this chapter are as follows:

- To adequately summarise the multi-dimensional data, along with highlighting common problems with experiments of this type.
- To compare the basic properties of neurons in both areas (including spike rates and waveform features)
- Investigate metrics of trial-trial variability in the data, in two brain areas. In particular, if the trial-trial variability in the IC is relatively high, this would have implications in auditory implant research – implants are unlikely to be able to replicate this variability in real time, resulting in potentially less naturalistic sound encoding.
- As a highly important feature of natural sound coding in the auditory cortex, entrainment in the AC and IC is investigated during both natural sound and spontaneous activity, with the aim to identifying differences

3.1.2 Relation to Previous Literature

Trial-Trial Variability

The variability of brain responses from trial to trial was selected as a subject for analysis. A low trial-trial variability indicates a reliability in neuronal responses of that

area across successive trials of the same stimulus, while a high variability may indicate the presence of external factors or additional, ongoing features on different timescales that are being coded simultaneously. The analysis in this Chapter will be limited to merely describing any immediate differences between the AC and the IC, but Chapter 4 will begin to dissect the underlying mechanisms and functionality.

Fano factor is a well-established method for examining the trial-trial variability in neuronal spike rates, though it is difficult to find literature describing it fully in the current context. It has been well investigated with regards to attentional state, with synchronisation increasing variability and thus Fano factor (Sakata, 2016, Lombardo et al., 2018). In the presented work, Fano factor is calculated throughout the 10 seconds of the natural sound stimulus, using a range of time bins, given the multi-timescales of the natural sound stimulus and the effect of time bin selection on coding (Panzeri et al., 2010, Kayser et al., 2012). If natural sound is being coded on particular timescales, trial-trial variability is expected to be reduced over these scales.

Inter-trial coherence quantifies the extent of LFP coherence at different frequency bands, between successive trials of a stimulus (Tallon-Baudry et al., 1996, Makeig et al., 2004). It is a common marker for auditory neuropathology – as sensorineural hearing loss progresses, cortical phase synchrony (as quantified by the ITC) decreases (Nash-Kille and Sharma, 2014). Given the involvement of LFP in the phenomena of entrainment, monitoring consistency of LFP is across trials seems logical and will offer further insight into coding mechanisms on additional timescales.

Entrainment

Entrainment is an important feature of the cortex's response to naturalistic stimuli, enhancing perception of periodic features. Evidence of this is searched for in both the AC and IC, and during natural sound and spontaneous activity. In the AC, current literature suggests that entrainment occurs predominantly at frequencies less than 30Hz, (Kayser et al., 2015), which is logical given the AC's limit for a phase locking temporal code (Zeng, 2002). Given the general acceptance of entrainment as a cortical feature, entrainment has yet to be observed in the IC.

As entrainment is a mechanism of enhancement of sound perception, it is expected for it to be prominent at relevant frequencies – this is well established using created stimuli/tasks and in human speech (Lakatos et al., 2008, Peelle et al., 2013). In this case, the interest is in prominent frequencies of the sound envelope (<30 Hz). Currently, most evidence suggests a conservation of levels of entrainment between

spontaneous and evoked conditions, at least up to ~20-30 Hz (Szymanski et al., 2011, Kayser et al., 2015) . In this analysis however, frequency bands are extended up to 200 Hz, which may identify differences.

By splitting up the cortical cell population into narrow and broad spiking cells, differences in levels of entrainment are expected, as putative inhibitory neurons are important for contextual adjustment of frequency selectivity (Li et al., 2014, Kato et al., 2017).

Inferior Colliculus Responses to Natural Sound

The inferior colliculus is well mapped in terms of tonotopic gradient, frequency tuning, AM and FM modulation, and periodicity (Schreiner and Langner, 1988, Krishna and Semple, 2000, Egorova et al., 2001, Hage and Ehret, 2003, Morrison et al., 2018). Natural sound coding in the IC is generally investigated in the context of vocalisations. Species-specific vocalisations are strongly represented by specially tuned cells or by non-linearities in the tonotopic gradient in several species (Suta et al., 2003, Portfors et al., 2009), however, general information about the area's responses during naturalistic stimuli is lacking. A 2017 study examined temporal jitter across trials of speech sounds and speech-in-noise in the guinea pig ICC, and found that timing differences in the ICC were very low during clear speech, but substantially more variable trial-trial when noise was included (White-Schwoch et al., 2017). Unlike in the auditory cortex, the effect of brain state on sound coding of the IC is not fully understood; while spectral and temporal tuning in the central nucleus is seemingly the same in awake animals as it is in the anaesthetised condition (Alkhatib et al., 2006, Langner et al., 2002), there is recent evidence to suggest modulation of neuronal activity in the non-lemniscal areas of the IC, with spectral tuning selectivity of excitatory neurons being decreased under isoflurane anaesthesia (Chen and Song, 2019). With these studies however, it must be noted that properties are compared between the awake state and anaesthesia, which may not be representative of activity during more natural synchronised states (i.e. sleep). As such, the question of IC modulation by global brain state remains a largely open question, especially given the multitude of non-lemniscal, modulatory connections to the IC from other auditory areas such as the MGB and CN that have connections to brain nuclei assisted with state changes (Motts and Schofield, 2010, Mellott et al., 2011).

With the present study, basic properties of the area are examined, such as trial-trial variability (in spike rate and in LFP), and any evidence of entrainment.

Auditory Cortex Responses to Natural Sound

The auditory cortex, as a higher processing centre, is more explored in terms of its responses to natural sound, with entrainment and phase information proving important to encoding of naturalistic sound stimuli as discussed in the literature review. One aspect in which this work adds novelty is in the different conditions it compares. Previous work compares spontaneous and natural sound (Kayser et al., 2015) and cell types (Sakata and Harris, 2012, Sakata, 2016), but in the current study, all these conditions are investigated simultaneously, with the additional comparison of single unit vs population/channel MUA activity and direct comparisons to the IC. Interneurons of the AC are responsible for shaping frequency tuning as required, and so cells of the AC will often be split into putative excitatory and inhibitory populations for further analysis. (Wang et al., 2000, Wu et al., 2008).

3.1.3 Hypotheses

The auditory cortex and inferior colliculus are fundamentally different structures, both in terms of their anatomy, their connections, and their known functionality regarding sound processing. These differences should infer variations in the basic properties of recorded neurons, and in their properties regarding mechanisms known to be important to naturalistic sound processing. This chapter attempts to demonstrate this by applying a range of analytical techniques to data recorded simultaneously from both areas, and comparing this between brain areas and with results from previous literature. The focus is on neuronal behaviour during natural sound, as accurate conveyance of this type of sound is crucial for the long-term success and widespread adoption of any auditory implant. It is hoped that the properties of IC neurons observed here will support the ICC as a promising implant site.

- AC and IC neuronal population will differ in their basic metrics, including spontaneous spike rate, and ability to distinguish distinct cell types
- Given the clear influence of attentional states on AC excitability and sound processing, and existing evidence suggesting that tuning in the ICC is unaffected, it is hypothesised that the inferior colliculus neurons will demonstrate lower trial-trial variability than the auditory cortex. However, it must be acknowledged that IC activity during the spectrum of natural global brain states is not yet fully characterised

- Literature supports LFP entrainment for frequencies <30Hz, the data is expected to confirm that AC entrainment occurs mainly at frequencies less than 30 Hz. Observing and confirming true entrainment in the IC will be difficult given a lack of previous literature, and would be unexpected, given the areas subcortical position

3.1.4 Main Findings

- IC neurons have a significantly higher spontaneous firing rate compared to AC neurons. A bimodality (indicating both broad and narrow spiking sub populations) was present only in the cortex
- Fano factor and continuous firing rate during natural sound are negatively correlated. This correlation increases in strength with time bin, but the overall number of units showing the correlation decreases
- IC Fano factor has a tendency (particularly with MUA units) to be lower than comparable AC units
- ITC is present in both brain areas, being less consistent and weaker in the AC and predominantly at frequencies less than 30 Hz. IC ITC appears to be present up to 200 Hz
- Entrainment appears to be visible in both brain areas during both natural sound and spontaneous activity. There are no clear or significant differences between strength or dominant frequency bands between spontaneous and natural sound
- AC displays entrainment predominantly at frequencies less than 30 Hz. This would appear to reach 200 Hz in the IC
- Narrow spiking cells show a tendency to entrain LFP to natural sound, as opposed to during spontaneous activity

3.2 Basic Properties of Recorded Data

The data recorded is highly dimensional, comprising of multiple separate recordings during which a variety of auditory stimuli were presented. Each recording then contains nearly 100 channels of neural data from two brain areas, comprised of the activity of hundreds of neurons (each with varying properties) The first step to successful in-depth analysis is to first examine the appearance and scope of the data, through quantification of basic parameters. More specifically, this serves the purpose of introducing the researcher and reader to the range of data obtained.

3.2.1 Dataset and Recording Summaries

The data was first summarised in terms of its very basic properties, surgical success, animals, and single units obtained. Understanding the basics of the data may prove important later for explaining the analysis techniques chosen (and their relative successes). These are presented in Figures 3.1 and 3.2.

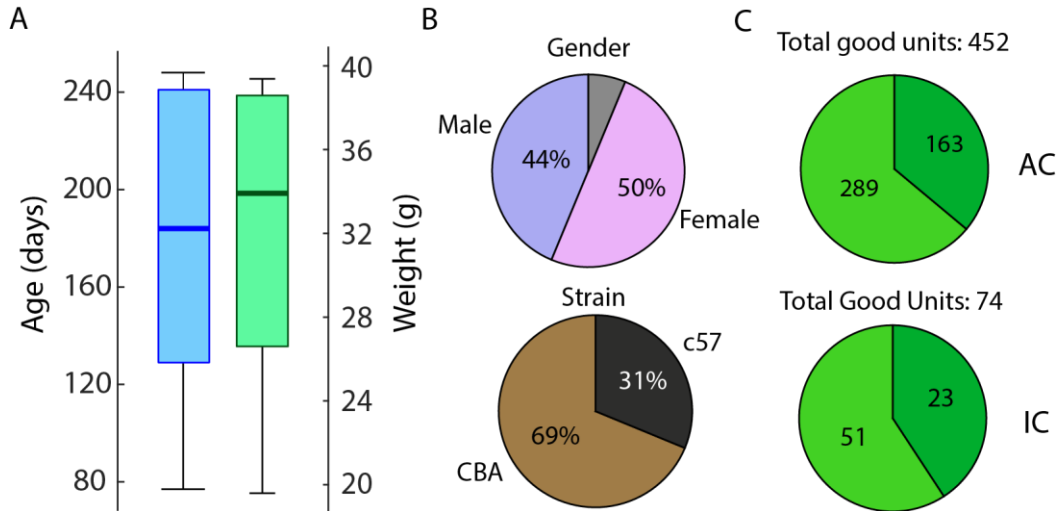


Figure 3.1: Summary of animals used for simultaneous recordings (A) Age (left, blue) and weight (right, green) of all animals whose recordings are used in the present study ($N = 15$). (B) Pie charts showing balance of gender (top) and strain (bottom). Note the grey section indicates a mouse for whom data could not be found. (C) Total number of single units isolated from each brain area over 23 recordings. A “good unit” (dark green) is defined as having an isolation distance of ≥ 20 , while a “very good unit” (light green) also has a contamination rate of < 0.2

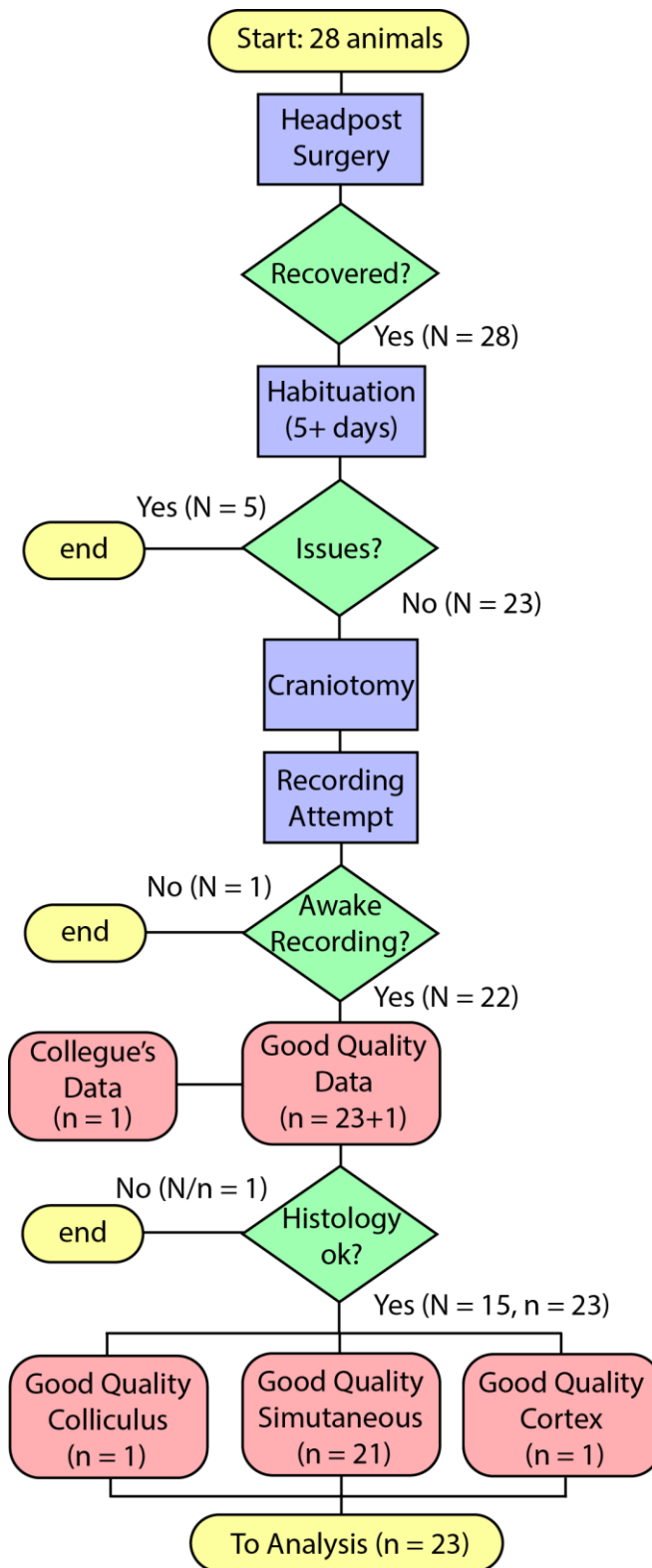


Figure 3.2: Flow chart of surgeries and experiments. The chart indicates the process of taking each animal from initial surgery till analysis of data. Yellow ovals = start or end point, Blue squares indicate a procedure, Green diamonds indicate a threshold/decision, pink rectangles indicate data. N = number of animals passing each threshold, n = number of datasets

A reasonable range of weights is observed across the animals in the study. Higher weights are attributable to older CBA animals. It should be noted that older (6 months +) c57 mice could not be used, due to the onset of age-related hearing loss – this is not present in CBA animals (which were favoured because of this). There is approximately a 50:50 gender balance in animals. A total of 451 good units were isolated for the AC (an average of 20 per recording), an acceptable number. Far fewer units were isolated from the colliculus, despite the channel count being only half that of the AC probe. Potential reasons for this will be noted in the discussion section.

Initial headpost surgery was 100% successful, in that all 28 animals recovered from surgery and had no serious post-surgical complications or infection that would require culling of the animal (Figure 3.2). The most common cause of no recordings (N = 5) was headcap failure, which generally occurred within the first few habituation sessions. Failure was usually linked to either screws being inserted to an insufficient depth, or dental cement not adhering well (generally due to insufficient cleaning of the skull). It should be noted that headcap surgery protocol was altered after approximately a third of the recordings were taken, to include an extra anchor screw on the far right – this appeared to greatly increase stability and removed headcap failure entirely. Another animal loss was due to the animal becoming completely deaf following incorrect ear-barring and failed healing of the ear drum.

More recordings were taken than ultimately used, with some being discarded before post recording analysis – sometimes, neither recording from an animal was suitable for analysis. The reasons for this were primarily instability, particularly of the colliculus recording site. The underlying reasons for this, and measures taken to mitigate, will be outlined in the discussion. Low quality datasets were characterised by low numbers of single units/spiking activity. Some recordings were also removed from further analysis due to persistent high muscle noise, presenting as strong high frequency noise that disrupted both spiking and LFP. Analysing these recordings would prove difficult due to their inconsistency and would introduce non-biological trial-trial variabilities. In total, 23 recordings were obtained, originating from 15 animals (including 1 set from a colleague).

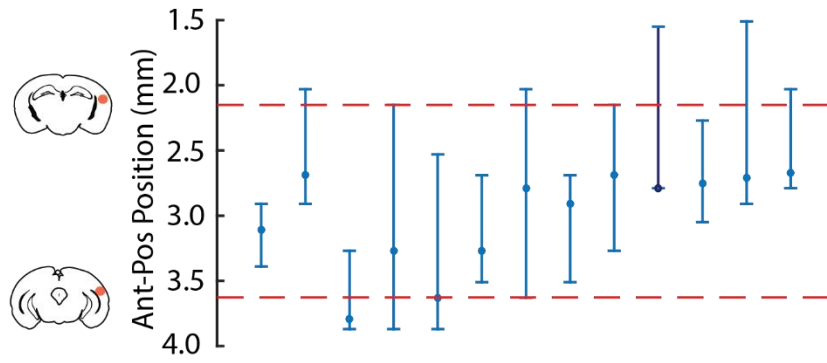
3.2.2 Histological Evaluation

For the purposes of hypothesis validation and project aims, data was only included if a reasonable assumption could be made that it came from the target areas of the brain – the primary AC and IC central nucleus.

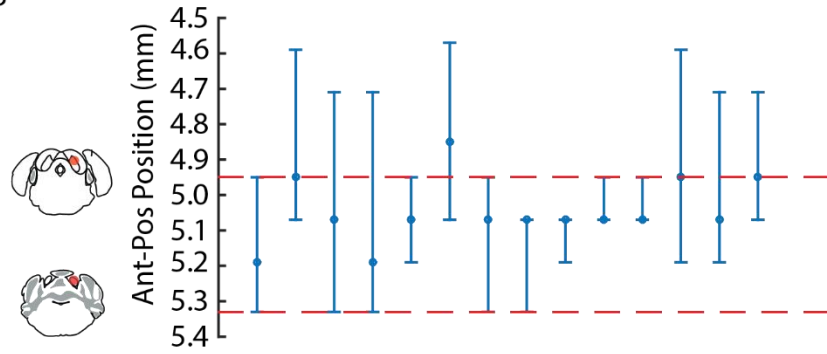
for traces of Dil which was used to coat the probe. Figure 3.3 displays the estimated position and spread of Dil (and so, the probe) in all datasets, with a representative image shown for each brain area.

Due to the spread of Dil, the exact anterior-posterior position could not be determined exactly, so was assumed to be roughly in the middle of the spread/where the Dil was strongest. The spatial limits of each target area (A1 and ICC) were determined from a mouse brain atlas, with probe position measured relative to the midline of the slice (Paxinos and Franklin, 2012). Anterior-posterior position was determined by matching the slice containing the strongest Dil signal to positions in the atlas, based on visible anatomical features (Paxinos and Franklin, 2012). Cortex datasets were included if the Dil spread fell well within the limits of the primary auditory cortex – only one dataset was removed due to being very anterior (IC recording quality was also poor and so the whole simultaneous set was discarded). A colliculus recording was discarded due to the probe being too medial and entirely missing the central nucleus. In general, IC datasets were included if the majority of the probe appeared to be in the central nucleus. Some leniency was granted due to Dil spread and imprecise brain slicing, leading to slight discrepancies in feature identification and measurement (this explains some included datasets being slightly anterior, Figure 3.3B and C).

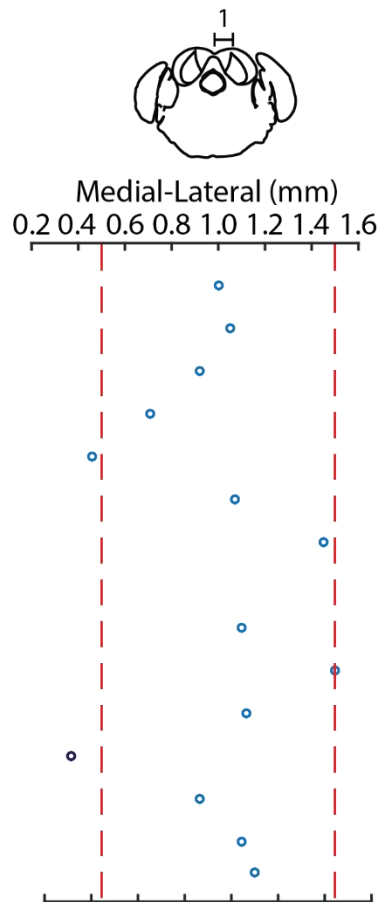
A



B



C



D

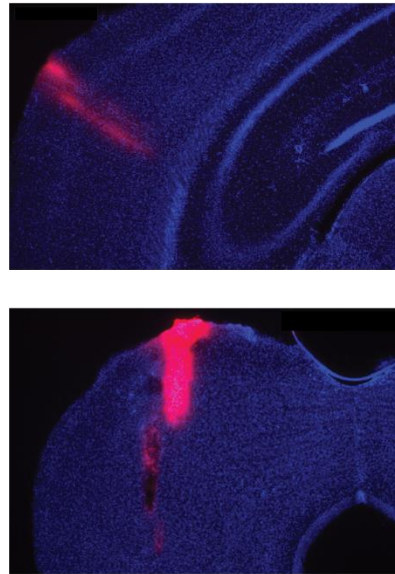


Figure 3.3: Summary of probe position (histology). (A) - Anterior-posterior spread of Dil in AC datasets passing data quality threshold. Dark blue indicates a dataset that was removed after this evaluation. "Error bars" indicate the approximate anterior-posterior spread of Dil. (B) As (A) but for the inferior colliculus (C) Medial-Lateral coordinates of Dil appearance in the inferior colliculus. Dark blue indicates a dataset that was removed from further analysis (D) Two typical histological images within the given coordinates, left: AC, right: IC. Blue: DAPI, red: Dil (probe). Scale bars = 500 μ m

3.2.3 Comparison of Cell Metrics in the AC and IC

Particularly in the AC, in which pyramidal cells and interneurons are differentiable by their waveform shapes, a summary of single unit properties is the next logical step in summarising the recorded data. By measuring properties of the average waveform for each single unit (see Materials and Methods), single units in the cortex were split into broad and narrow spiking cell types. This classification is utilised in later analysis. Spontaneous firing rate is also briefly examined.

A clear visual bimodality in cortical cells is observed in three of the displayed metrics – peak-to-trough (P2T), 20% and 50% width (Figure 3.4A), and non-normality of the data was determined using the one-sample Kolmogorov-Smirnov test. Due to the clearer distinction, and past literature, peak-to-trough and 20% width were chosen as thresholding metrics (Sakata and Harris, 2012, Yague et al., 2017). After observation, 2 group k-means clustering, and a review of the literature, thresholds of 0.4 (P2T) and 0.35 (20%) were chosen to separate narrow and broad spiking cells. This resulted in a general proportion of 72:28 broad:narrow. This is slightly different from literature, which generally reports around 10-15% narrow spiking cells (Sakata and Harris, 2009, Yague et al., 2017). In Figure 3.4C, high values of peak-to-trough are due to a bug within the MATLAB code that meant peak-to-trough amplitude could very occasionally not be calculated correctly – despite considerable time put into investigating the cause, the issue could not be adequately resolved.

The spontaneous firing rates of narrow spiking (NS) cells trend/skew towards higher values (Figure 3.4D), and are significantly different from broad spiking cells ($p = 0.0096$, Wilcoxon rank-sum test, Median and interquartile ranges: BS – 7.57/3.41/1.14, NS – 15.39/4.92/1.10).

The inferior colliculus cell population did not display any bimodalities, instead heavily trending towards very narrow waveforms. In terms of spontaneous firing rate, the IC cell population has a higher spontaneous firing rate (though the AC has lots of outliers) – this is seen in Figure 3.4B (median of 3.86 vs 8.42, $p = 1.36e-4$, Wilcoxon rank-sum test).

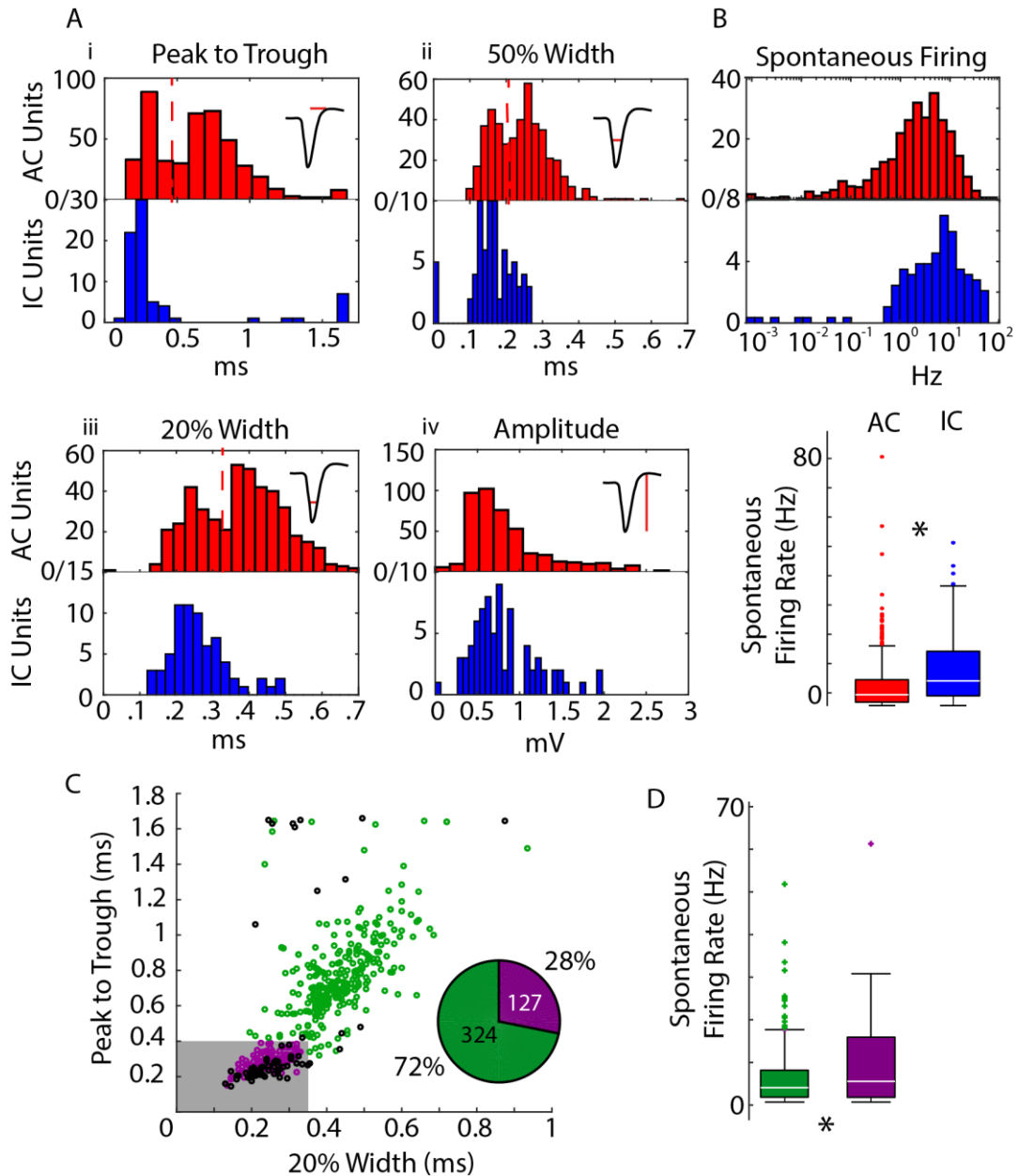


Figure 3.4: Cell metrics summary. (A) Distributions of various waveform metrics for cortex cells (top, $n = 451$) and colliculus cells (bottom, $n = 71$). Dotted lines indicate presence of bimodalities (narrow/broad split). Insets indicate the measurement on a typical waveform (B) Boxplots of spontaneous firing rate for AC vs IC, difference is significant, $p = 1.36e-4$, Wilcoxon rank-sum test. (C) Scatter plot of cortex and colliculus cells showing the presence of two groups. Grey box indicates decided thresholds for narrow ($n = 127$) and broad spiking cells ($n = 324$). Purple – narrow cortex cells, green = broad cortex cells, black – colliculus cells. Inset: pie chart showing proportions of broad/narrow spiking cells in the general cortex population. (D) Spontaneous firing rate distribution for broad and narrow spiking cells, star indicates a significant difference ($p = 0.0096$, Wilcoxon rank-sum test).

3.3 General Appearance and Variability of Neuronal Spiking During Natural Sound

After summarising the very basic properties of the data, attention is turned to how neurons generally behave during naturalistic sound stimuli – as this will be the focus of most analysis. After presenting an overview of data appearances, important properties are recognised that may explain later results. First, the raw data (MUA traces over time) is examined, followed by the trial-trial variability in neuronal responses. MUA is chosen as the focus for the majority of this analysis for several reasons. There are far more MUA units, capturing more of each areas response than individual single units can alone (while still including their contribution). Practically, use of MUA means more units in the IC, making analysis of this area a lot easier. More generally, it is channel MUA activity that will be elicited using auditory implants, and so it has a direct relevance in this regard. The aim of giving an overview of activity is better met with the more data is included.

3.3.1 Natural Sound is Composed of Many Simultaneous Frequency Components

Sound (particularly complex sounds such as environmental noise, wildlife calls and human speech), contain variations in both time and frequency domains. Taking a typical sound trace, it can be split into the fine detail and the “envelope” of the sound (periodicity). Each can then be split further into constituent frequency components, changing over time. The brain is known to encode information regarding both components of sound, and so a good initial step is to examine the appearance of the naturalistic sound stimulus used, so that key time periods or increases in frequency band strength can be identified for comparison with later results.

Figure 3.5 presents scalograms of the sound fine detail and envelope of the 10 second natural sound stimuli presented in experiments (previously described in Materials and Methods). There are few low frequency components in the fine detail of the natural sound. Some transient increases are observed around 64 and 125 Hz, as well as patterns in frequencies above this. These increases match nicely with the increasing amplitude of the sound envelope (black), as expected. The sound envelope (Figure 3.5C and D, black outline) contains many low frequency components, again varying in strength with the sound envelope. There is almost constant 0-8 Hz activity, with some distinct increases in higher frequencies at specific time points (e.g. 4-5

seconds). This is likely then to be an interesting timescale to examine in our future analysis.

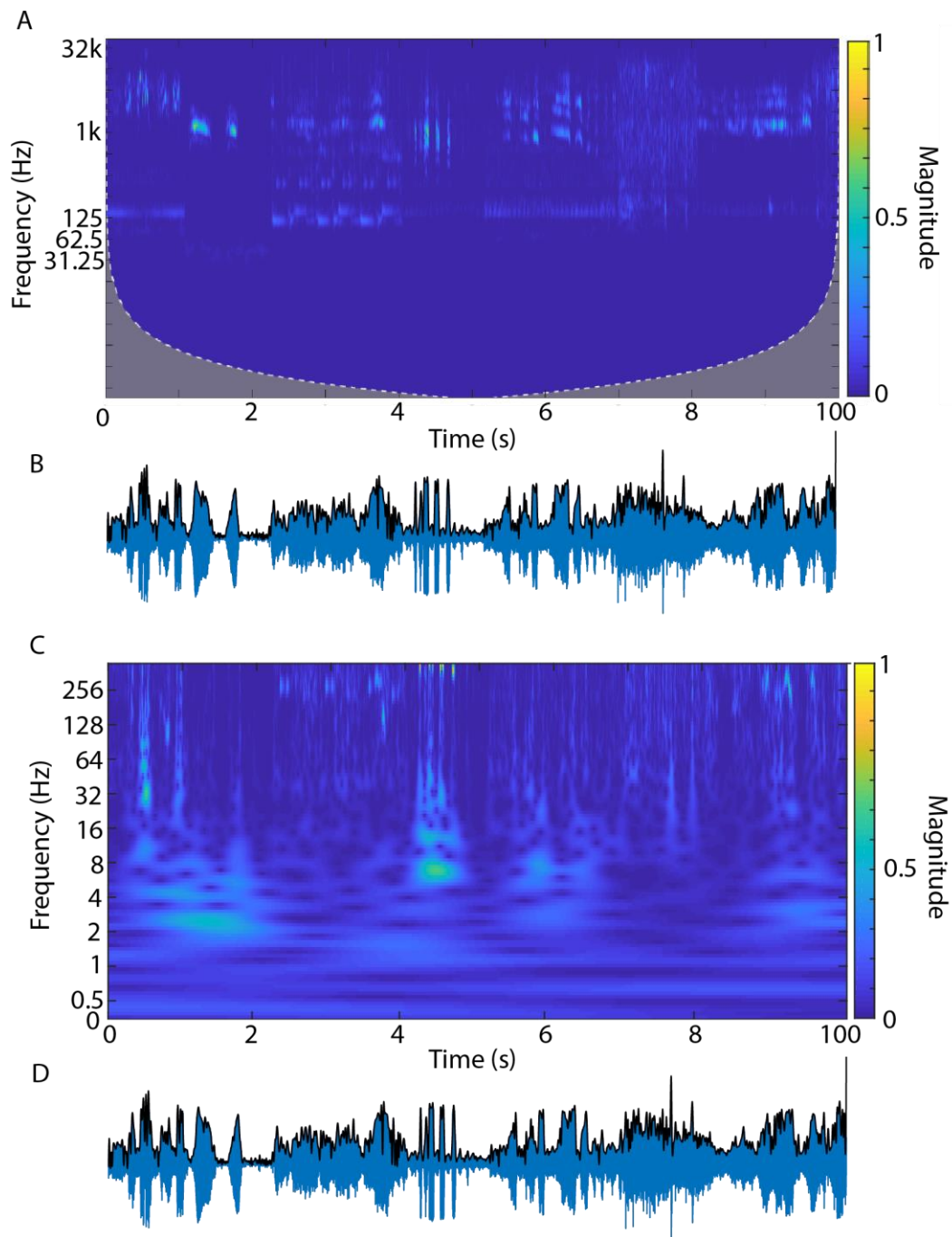


Figure 3.5: Appearance of natural sound stimuli in time and frequency domains (A) Scalogram of sound fine detail, up to 32 kHz. Grey shading within the scalogram indicate sections of the data that may be affected by edge artefacts introduced during frequency calculations – data within should be treated as suspect (B/D) Sound stimuli trace. Fine detail (blue) and smoothed envelope (black), over the 10 second stimuli. (C) Scalogram of low frequency sound envelope (sampling rate 1 kHz), up to 500 Hz

3.3.2 Qualitative Correlations of Multi Unit Activity and Sound Envelope

In an initial analysis of the neural data, the general appearance of high frequency (spiking) activity, over the time course of the natural sound stimulus, is displayed. As there are peaks and troughs in the sound envelope/amplitude, similar time locked increases/decreases in spiking activity are expected. To examine this, a barcode is created (see Materials and Methods and Figure 3.6A) of the evoked activity of all multi units recorded in each brain area, to highlight any areas of the sound to which the majority of neurons are responsive. Alongside this, a small snapshot of individual MUA is presented (Figure 3.6C) to highlight similarities and variability.

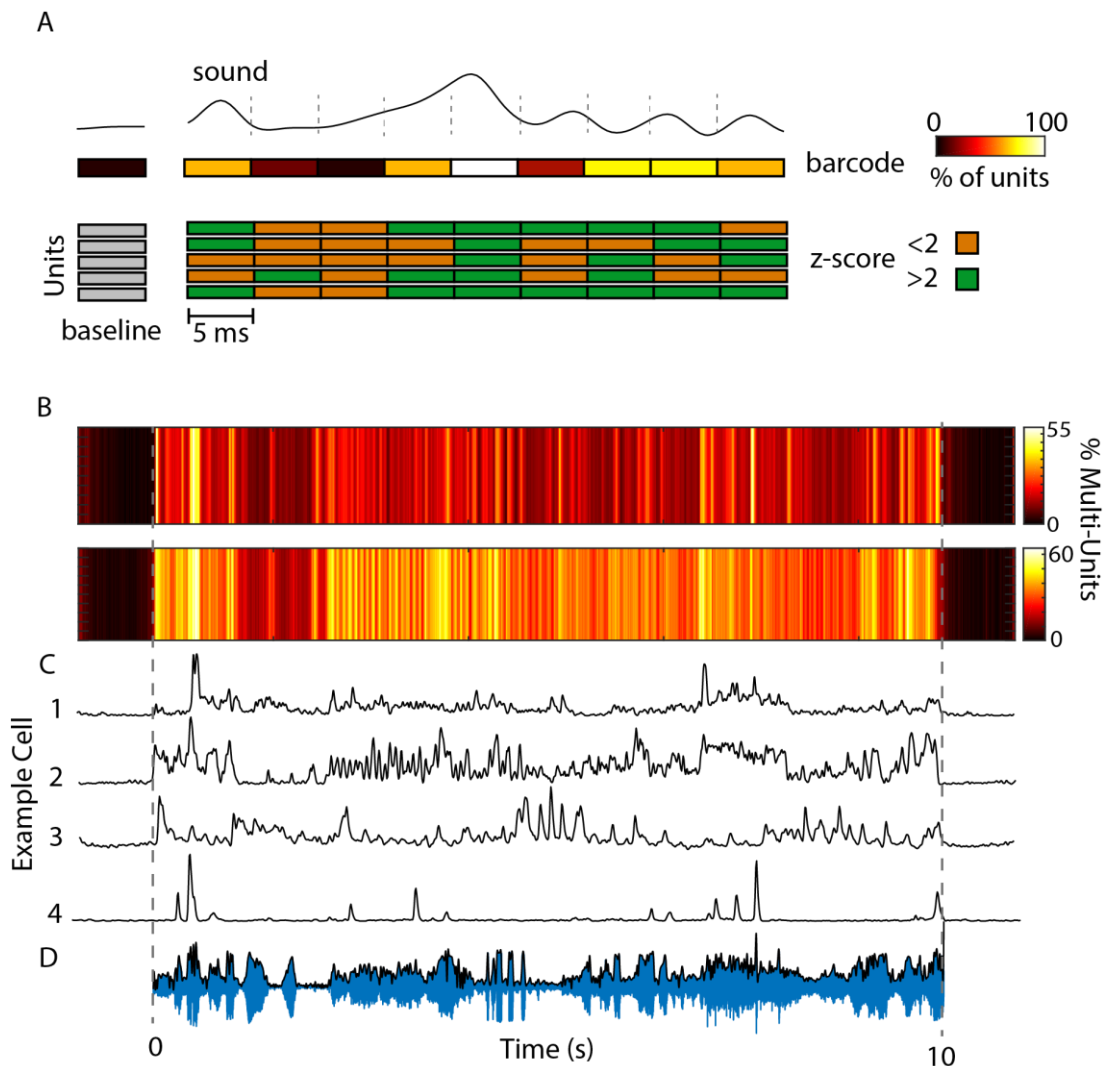


Figure 3.6: General MUA changes during natural sound stimuli. (A) Brief graphical explanation on how barcode was derived from the activity of all units in a population – see also Materials and Methods (B) “Barcode” of MUA activity (see Methods) giving an indication of what time points neurons are responsive to. Bin size was 5 ms. Colour strength – percentage of all MUA units responding. Top – AC, Bottom – IC. (C) Example MUA PSTH over 100 trials, presented as single trace, for 4 example AC neurons (1-4) (D) Natural sound fine detail (blue) and envelope (black).

From the barcode summary, there are clearly identifiable time periods of neuronal activation – as expected, they line up with increases in sound amplitude. Interestingly, examining the individual population traces (Figure 3.6B), each responds slightly differently. For example, example 2 has a strong (visual) correlation with the envelope, whereas example 4 appears to be responding only to specific features of the sound (perhaps sharp amplitude increases). Barcodes of single unit activity show similar patterns. This analysis serves to identify the differences in neuronal responses with regards to natural sound and is indicative of the presence of dedicated neuronal populations.

3.3.3 The Trial-Trial Variability of Neurons During Natural Sound

The above analysis provides (essentially) an average response of all the neuronal units. However, as the hypothesis is that each brain area is differently affected by external factors, it is also beneficial to look at the underlying trial-trial variability to tell us more of the story. This is examined over various time bins and includes single units as a direct comparison.

Fano Factor and Trial Averaged Spike Rate are Often Negatively Correlated

First, it is beneficial to confirm a known phenomenon that in general, as spike rate increases, the Fano factor or variability decreases (Mitchell et al., 2007, Qi and Constantinidis, 2012). The windowed Fano factor (at 7 bins of increasing size) is correlated with the similarly windowed spike rate (PSTH) across the 10 seconds of natural sound (Figure 3.7A). A negative correlation is expected, that as the spike rate increases, Fano factor decreases.

It is found that units generally had either no significant correlation, or a negative correlation – positive correlations were rare (red bars). The strength of correlations is examined further in Figure 3.8, but there are no significant differences in the overall distributions shown in Figure 3.7 for no or negative correlations between AC and IC ($p = 0.8827, 0.1287$, Kolmogorov–Smirnov 2-sample), but there was for positive ($p = 0.0275$, Kolmogorov–Smirnov 2-sample test), although the overall number was very low and likely due to inhibition of a small number of cells. Essentially, AC and IC show the same pattern of cells having each type of correlation, over increasing time bins. Generally, as the time bin increases, so too does the number of negative correlations. At larger time bins in particular, the colliculus sees more negative correlations than

the cortex. There are no differences in distribution between MUA or SUA ($p > 0.05$, Kolmogorov–Smirnov 2-sample test).

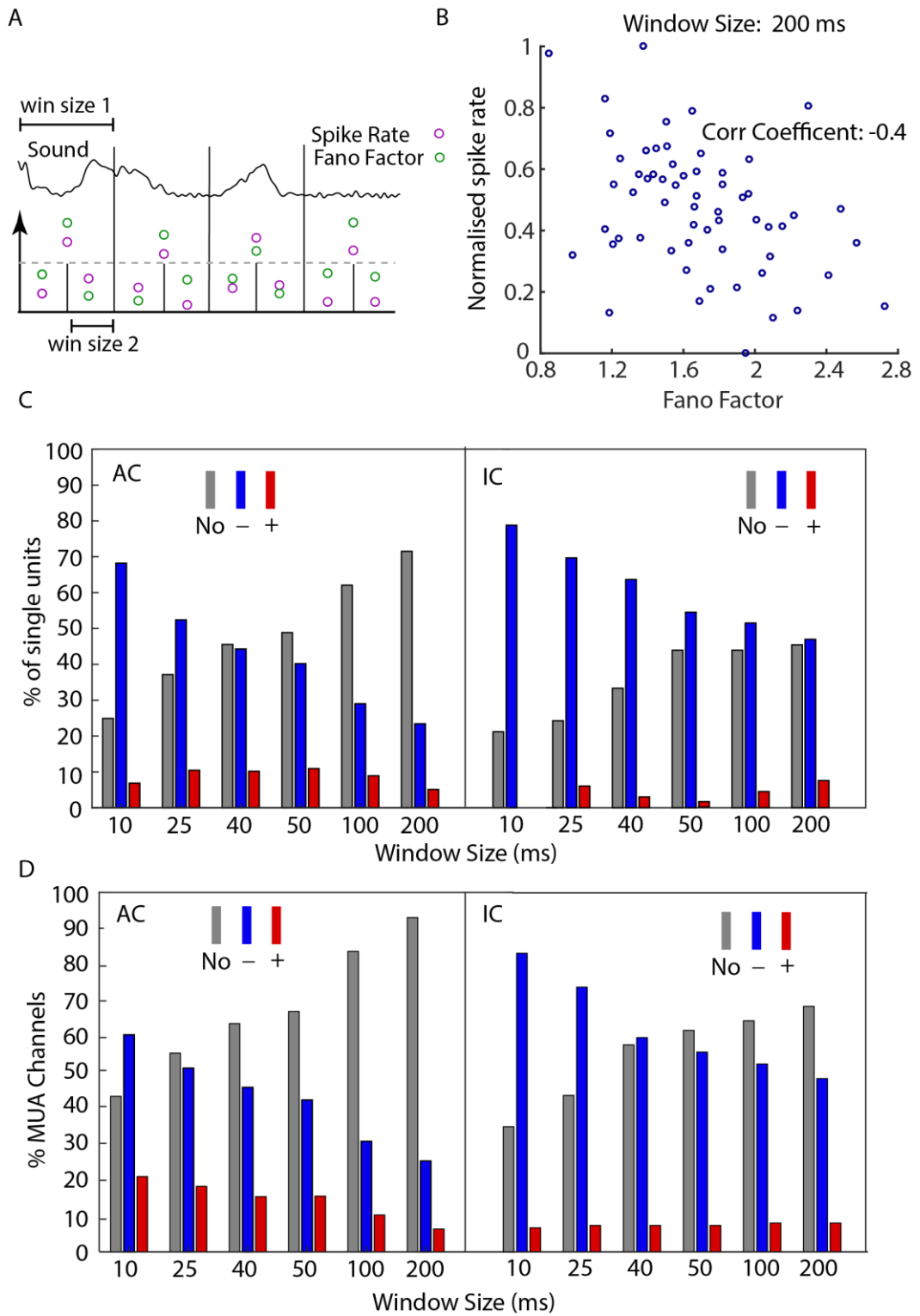


Figure 3.7: Type and number of SUA/MUA and Fano factor correlations. (A) Graphic of how windowed activity and Fano factor are obtained (B) Example scatter plot of binned Fano factor against binned spike rate (normalised) from a typical cortical multi unit, 200ms bin. Pearson correlation coefficients (shown) for each unit are used to derive panel C,D and Figure 3.8 (C) Percentage of AC/IC SUA channels ($n = 955/177$) showing either no (grey), negative (blue) or positive (red) correlations, with non-overlapping time bins for MUA and Fano factor calculations. Left – cortex, right – colliculus. (D) As above, but for multi units AC/IC ($n = 385/66$).

Strength of Negative Fano Factor/Spike Rate Correlations is Variable, but Stronger at Longer Time Bins

Next, overall strength of the significant negative correlations is examined ($p < 0.05$, Pearson's correlation coefficient), over 6 time bins (Figure 3.8).

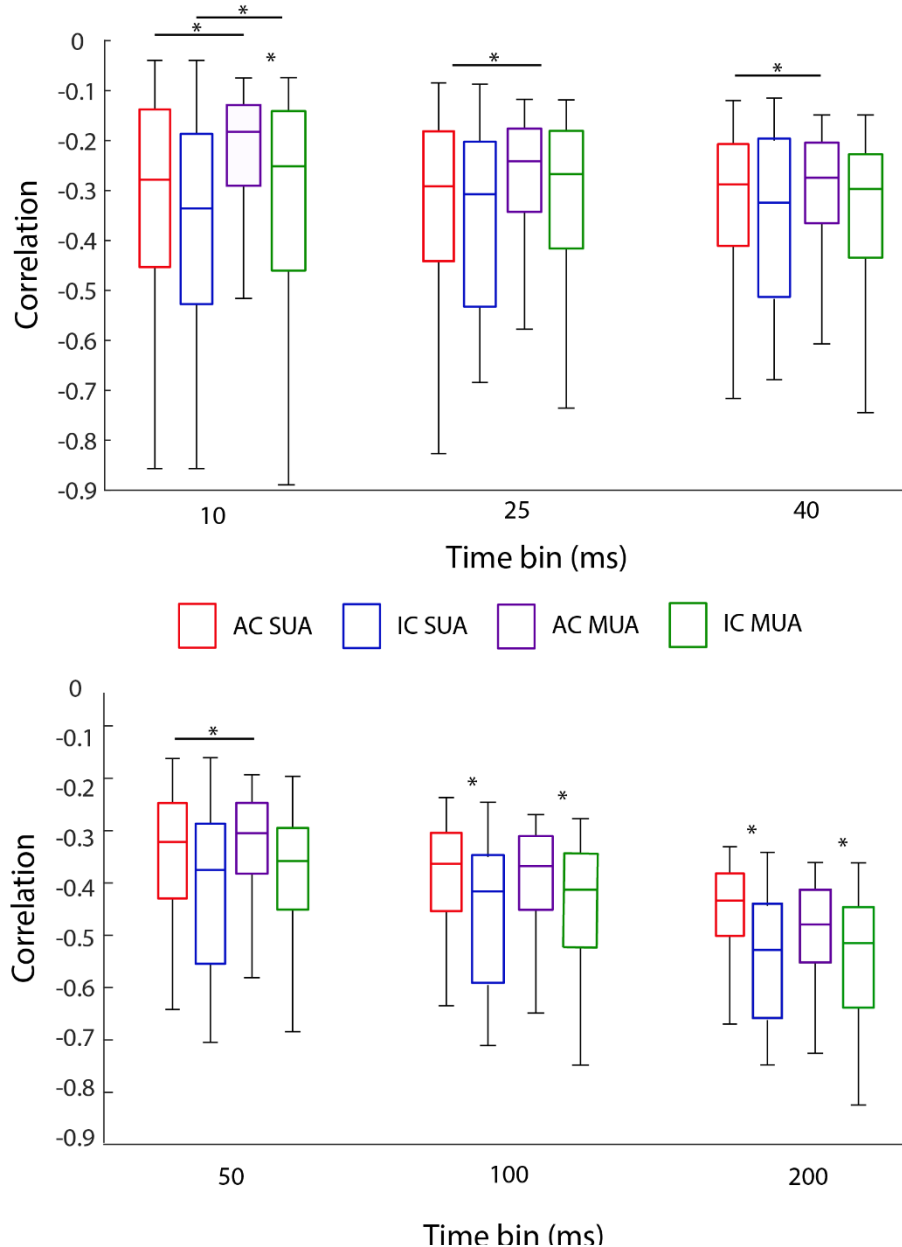


Figure 3.8: Strength of negative correlations between PSTH and Fano factor, with increasing time window. Top graph, time bins 10, 25, 40, bottom graph time bins 50 100, 200. Significance stars indicate significant difference between values ($p < 0.025$, Bonferroni after Kruskal Wallis. Effects between area and unit (i.e. AC SUA vs IC MUA, are not shown).

Correlation strength is quite variable, particularly in small time bins, but this variability decreases as bin increases. There is a significant effect of time bin at all input conditions ($p < 4.51e-24$, Kruskal-Wallis). The general trend is that as time bin increases, correlation strength increases (with some differences in number of overlapping groups depending on the input condition). This is interestingly accompanied by an overall decrease in the number of correlations (Figure 3.7).

There is no significant effect of brain area until later time bins (100 ms+), after which the colliculus consistency has a higher correlation, with both single and multi units ($p < 0.025$, Bonferroni after Kruskal-Wallis). Regarding single and multi units, the effect of these only seems to exist for the cortex, and then only at shorter time windows ≤ 50 ms ($p < 0.025$, Bonferroni after Kruskal-Wallis).

Overall, negative correlations are dominant over positive ones. Correlations are variable in strength, but this variability decreases with increasing time window. The median correlation strength increases with increasing time bin, but at the same time, the overall number of correlations decreases. At longer time bins, the colliculus has significantly higher correlation strengths than the cortex, while at shorter bins, cortical multi units have a slightly lower correlation than corresponding single units.

This evidence suggests an increase in spike rate is associated, at least with natural sound stimulation, with a decrease in overall variability. In particular, it seems that the inferior colliculus has a stronger relationship in this regard, indicating a propensity for more consistent responses between trials.

Mean Fano Factor During Natural Sound is Skewed to Values <1

Next, the Fano factor values themselves are investigated, along with their relationship to the sound. Values of <1 might be expected during natural sound indicating a spiking distribution less variable than a Poisson process, as neurons as a general rule increase their firing above spontaneous activity (often assumed to be a Poisson process) in predictable ways during repeated presentations of the same stimulus. This is not a hard and fast rule however, and values should be compared relative to each other when calculated in the same way.

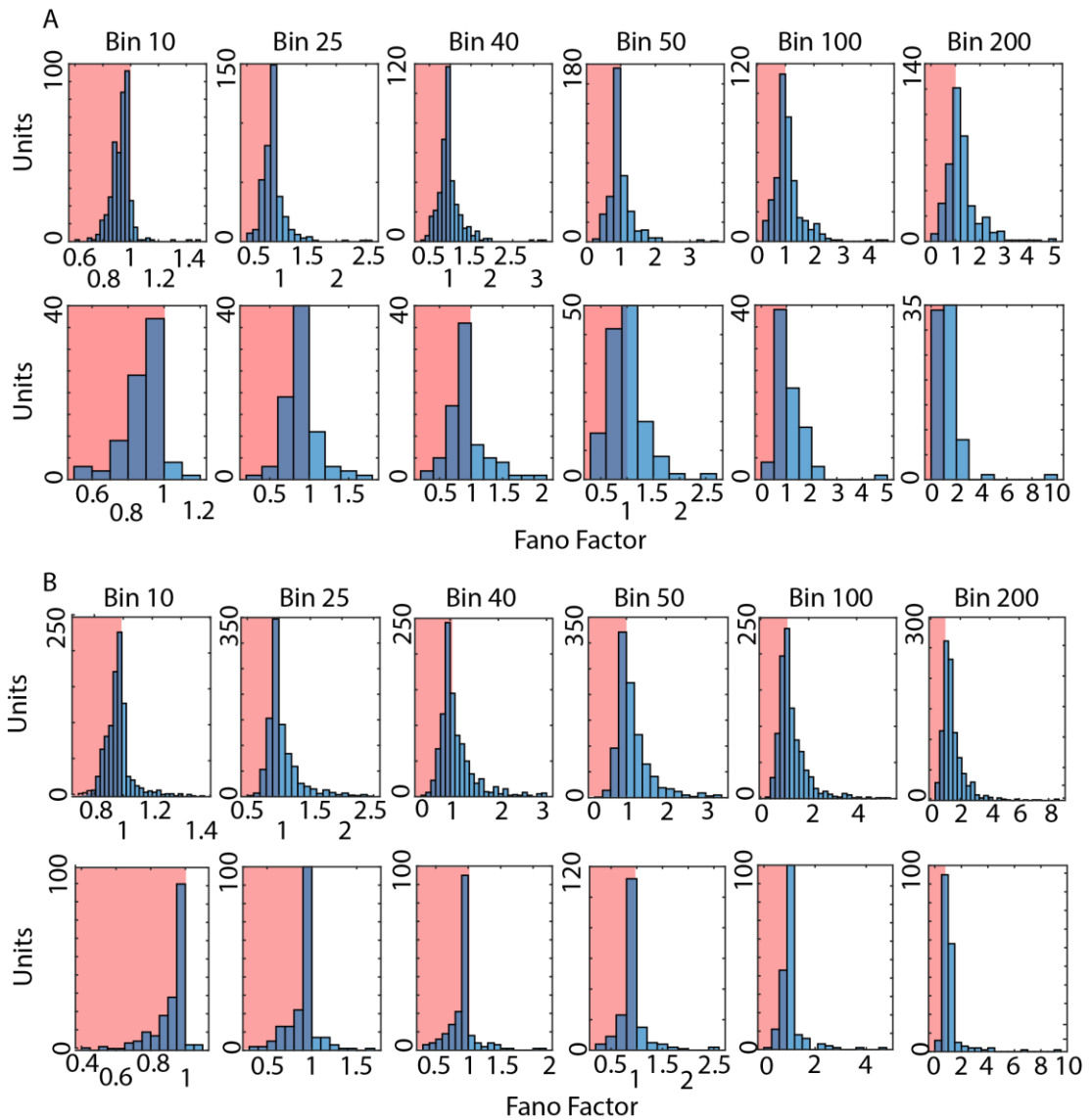


Figure 3.9: Mean Fano factors of single and multi units during natural sound, with increasing time window (A) Histograms of mean Fano factor calculated for each single unit in Top-AC $n = 385$, Bottom-IC $n = 66$. Pink shaded area indicates Fano factors below 1. (B), as A, but for MUA (cortex $n = 955$, IC $n = 177$).

The mean Fano factor was calculated across the whole 10 seconds for all units in each condition, in order to show a skewing towards/around 1 and lower, as expected (Figure 3.9). The majority of units lie around or below 1, indicating the decrease in variability during the 10 seconds. Some units show outliers, likely due to a low firing rate, overall low evoked response rate, or noisy trials. The proportion above this (those with high variability) tends to increase with the size of the time bin as might be expected, indicating variability of response is smaller at smaller time bins, but increases as bin increases. Thus, overall, Fano factors reduce below 1, indicating a decrease in variability associated with the sound stimulus. In addition, as neuronal

spike rate approaches the refractory period and reaches a saturation point, a decrease in variability is expected.

The range and median of Fano factor are visualised with boxplots in Figure 3.10, as well as the proportion of the 10 seconds where the Fano factor was below the baseline (usually very close to 1, calculated during spontaneous activity).

Comparison of Fano Factors between AC and IC Reveal Significant Differences in Strength and Time Spent Below Baseline Variability

Figure 3.10 examines both the raw value of the Fano factors, and the overall time spent below baseline (as previously mentioned, this was close to 1). The focus here is on the differences between cortex and colliculus, so multi and single units are split up and are not directly compared at the present time.

In Figure 3.10, it is seen that, in general, and particularly for small time bins, single units and for the inferior colliculus, median Fano factors sit below 1. There is a trend of decreasing variability across the population with time bin size. For MUA, the AC is quite commonly at and around 1 rather than below (indeed, much higher at larger time bins). This might be due to the higher Fano factors from very few units skewing the data, or perhaps a constituent single unit was lost part way through the recording. Other potential explanations will be mentioned in the discussion.

IC Multi Units have Significantly Lower Fano factors than AC Multi Units

For single units, there is only a single bin where the median value of the Fano factor is significantly different higher in the IC compared to the AC (10 ms, $p = 0.0297$, Wilcoxon rank-sum test). From this point, it is hard to identify a clear trend, but it may be that the IC Fano factor is generally slightly higher than AC data.

However, for MUA, IC Fano factor is always lower, and clearly less variable than in the auditory cortex ($p < 0.0003$, Wilcoxon rank-sum test). It can thus be said that the evidence for IC activity to be less variable is stronger than the alternative.

IC Fano Factors Remain Below Baseline Levels for Significantly Longer Periods than in the AC

The time spend below baseline sits around 50-60% for both single and multi units, with a reasonably high variability. In single units, all but the first time bin (10 ms) show that the Fano factor remains below the baseline for slightly longer than the AC (p value < 0.011212 , Wilcoxon rank-sum test). In multi units, this relationship is seen for *all* time bins ($p < 4.32e-7$, Wilcoxon rank-sum test). However, due to the high

variability, it may not be appropriate to make strong conclusions about differences between AC and IC % time.

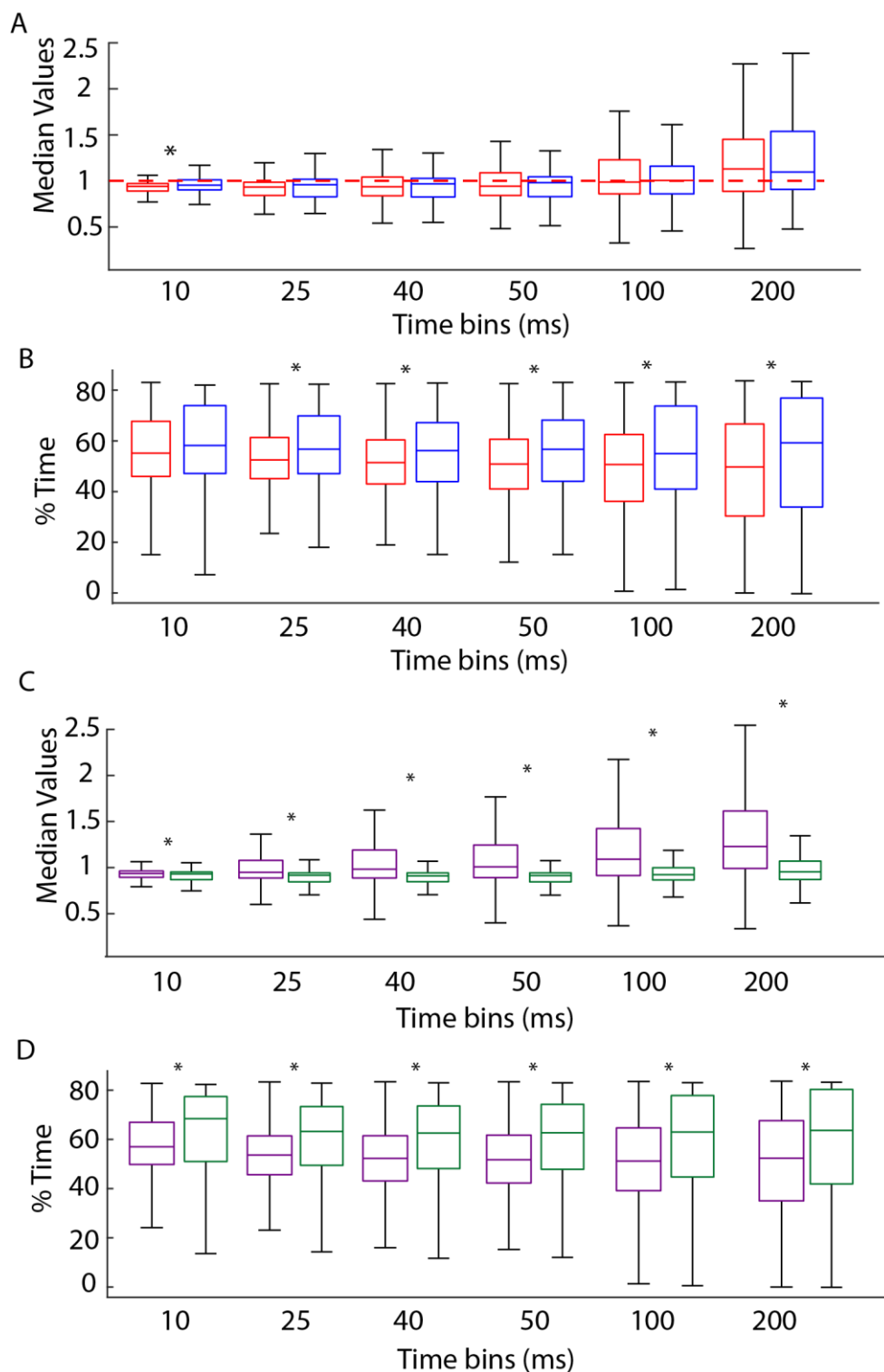


Figure 3.10: Median Fano factor and proportion of time spent below the baseline for single and multi units, with increasing time window. (A) Single unit median values in the cortex (red) vs the colliculus (blue). (B) Percentage of time spent below Fano factor baseline. (C) As (A), but for MUA cortex (purple), and colliculus (green) (D) As (B), but for multi units. Significance stars indicate significant differences between AC and IC ($p < 0.01$, Wilcoxon rank-sum test).

3.3.4 Summary of Observations of Neuronal Activity During Natural Sound

The results reported in Section 3.3 are briefly summarised. Firstly, natural sound is clearly composed of multiple frequencies, over a wide range. Most neurons displayed a sound evoked response to varying degrees, though slight differences in “preferred” sections of the sound by individual units may indicate the presence of tuned units or populations.

PSTH traces are often negatively correlated with trial-trial variability (Fano factor), with the number of units being correlated decreasing with time bin even as negative correlation strength increases. A higher percentage of IC units showed this negative correlation, as opposed to the AC. Trial-trial variability during natural sound stimuli decreases to varying degrees across single, multi and AC/IC units, with the average value across the 10 seconds skewing towards <1 (a Poisson process). It is observed that that, at least in multi units, IC units have both a smaller, and a less variable, Fano factor than AC units, indicating a trend towards IC neuronal responses being more reliable, matching previous observations of negative PSTH/Fano factor correlations .

3.4 Inter-Trial Coherence of LFP During Natural Sound

3.4.1 Introduction

It has just been observed that neurons change their response patterns throughout a given natural sound stimulus, and there is generally an accompanying reduction in variability. As discussed briefly in the introduction to this chapter, and more extensively in the introductory literature review chapter, underlying brain rhythms as observed in LFP can, by entraining themselves to sound shape, act as a frame of reference for neurons to phase lock their responses to, improve sound encoding and thus being a crucial factor in the perception of natural sounds. As conductors of the neural responses, these rhythms are likely to be having direct effects on the variability of the neuronal response. To our knowledge, entrainment to LFP is not something which has been documented in the inferior colliculus to the same degree as the cortex, and so observations will have to be carefully considered.

Firstly, the inter-trial coherence of channels will be investigated, describing phase synchronisation in time across successive trials of the stimulus – does the LFP response in a predictable way? The immediate question is of volume conductance

skewing the results, and so although data is presented using channel LFP, it was repeated for CSD, with only minor differences (to be discussed).

ITC in the cortex is also investigated at depths, where, working on the current assumption that the entraining LFP is not itself generated in the cortex and instead comes from external areas, it is expected that this effect to be seen most strongly at sink/cortical input channels. For this analysis, CSD was principally used (the effect seen was still present using LFP, but weaker).

3.4.2 ITC can be Observed in Raw LFP Phase Plots

By plotting raw LFP phase (Figure 3.11), the across trial phase synchrony can be observed (to then be quantified by ITC). These can be seen by “stripes” of a single phase across all (or most) channels. Breaks are likely due to movement or potentially brain state changes (see Discussion). ITC appears sharper in IC, this is a trend observed in most datasets showing ITC. AC has a tendency to “break up” and be patchy over the trials, despite a general trend for coherence. There is also a time dependency, with the synchrony appearing to correspond to the sound amplitude/areas of activity, and particularly at the initial sound presentation. This higher variability in response in the AC has parallels in previous Fano factor results.

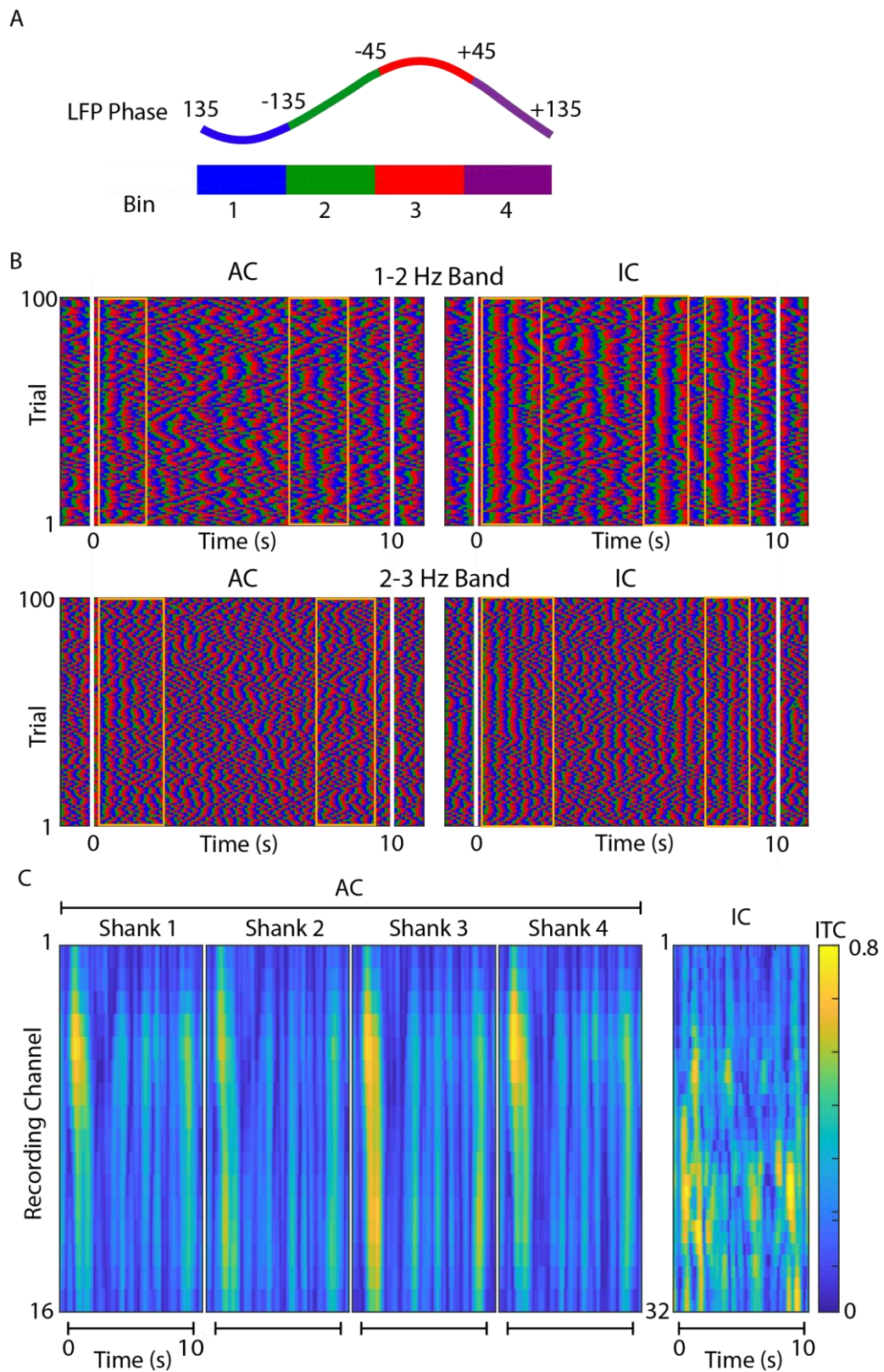


Figure 3.11: Example plot of phase across time (two frequency bands). (A) Representation of how LFP phase is sorted into 4 bins. (B) Examples of phase coherence at two frequency bands. Top 1-2 Hz frequency band, bottom 2-3 Hz band. Left column - cortex, right - column colliculus. White lines indicate start and end of sound stimuli. Orange boxes indicate some sections where LFP trial-trial coherence is particularly visible Y axis – trials (1-100). (C) Strength of ITC over time in each shank of an example dataset. Shank 1-4 AC, 5 IC

3.4.3 ITC is Observed at Different Frequencies and for Varying Periods of the Stimulus between AC and IC

Observation of the raw data would suggest differences between the AC and IC, and so next, where the ITC becomes significant is quantified. This includes for how long it is significant, and what values it takes during this time (Figure 3.12).

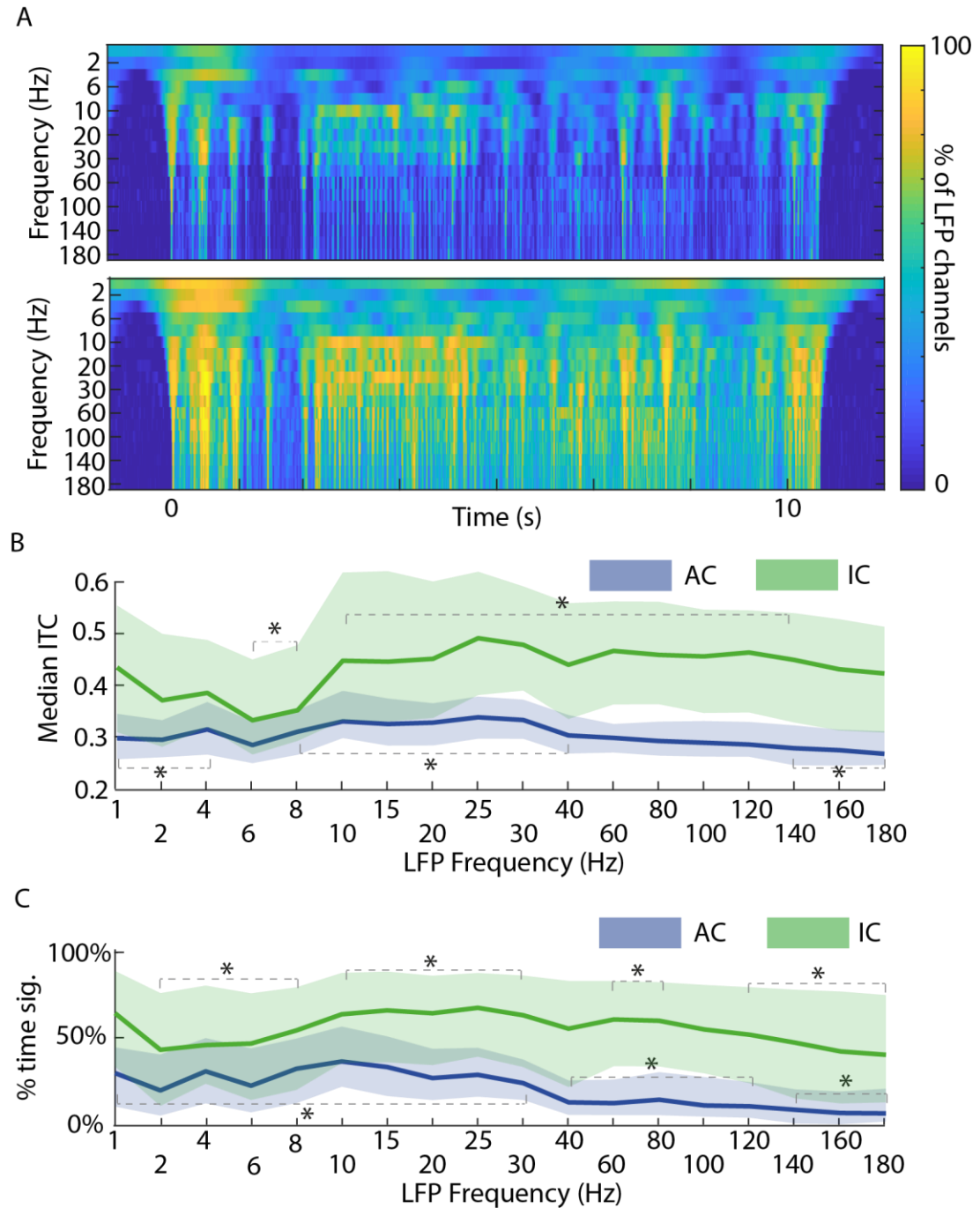


Figure 3.12: ITC in the auditory cortex and inferior colliculus during natural sound (A) “Barcode” of % of LFP channels at those time points showing significant ITC of any strength ($p \leq 0.01$, Rayleigh’s test for circular uniformity). (B) Top – median ITC over 10 seconds of natural sound, for all LFP channels. Blue – AC, Green – IC. Bounded lines are shown median \pm interquartile ranges. Significance stars indicate significant trends across stimuli length (some omitted for clarity). Points grouped together by grey lines and a significance star are significantly different from all other points, but not from each other – Bonferroni after Kruskal-Wallis for each brain area. There is always a significant difference between AC and IC for all stimuli lengths (not shown, $p < 1.79e-32$, Wilcoxon rank-sum tests) and are calculated for each time bin individually. (C) As above, but detailing the % of time spent significant ITC ($p < 4.57e-30$, Wilcoxon rank-sum test). AC $n = 1408$, IC $n = 672$.

The barcodes summarise what has been seen previously, that activity clearly lines up with particular segments of the sound. Lower frequency ITC seems less precise, and more spread out in time, than those at higher frequencies, which may be responding to specific features of the sound (i.e. the three pronged shaped at the start). The ITC shown before and after the sound at low frequencies is likely a combination of phase resetting effects, and a slight filtering artefact. Figure 3.12B displays the median ITC of the LFP from all probe channels, after filtering into a series of frequency bands – though these are discrete data points they have been connected together as the frequency bands directly neighbour each other. The shaded area indicates the interquartile range of the ITC at each given frequency band. The median ITC is significantly higher in the inferior colliculus for all time bins, though does show more variability ($p < 1.79e-32$, Wilcoxon rank-sum test). This difference is especially apparent at frequencies above ~20 Hz, where it appears stronger than at lower frequencies. A similar effect is seen for time spent significant, shown in Figure 3.12C. The percentage of the 10 seconds of stimulus time that the calculated ITC is significant ($p < 0.05$) is calculated for each LFP channel (and each filtered frequency band), and the median plotted with the interquartile ranges as the shaded area. The figure shows that colliculus phases are coherent for a larger percentage of the time (though the high variability across channels, in actual strength should be noted). Though not shown, similar effects are visible if CSD is used as an input, again showing a significant difference between areas, but having overall lower strengths and larger p values.

Quantifying the strength of ITC, increased and maintained values are seen in the IC over the AC, though it is fairly variable. This will be addressed in the discussion, but the exact mechanism/reason behind this is not yet clear.

3.4.4 Cortical ITC Displays a Tendency for a Depth Dependency

When looking at the example data in Figure 3.11, there is a depth dependence on the ITC in the cortex, with an apparent focal point roughly corresponding to the sink channel. Using CSD as an input, LFP channels are separated into superficial (above sink), sink and deep (below sink) as detailed in Materials and Methods. Sink channels are assumed to include those directly above and below the CSD derived sink (i.e. +/- 50 μm). Other distances have also been tested (i.e. 100 μm either side) but gave very similar results. Results are displayed in Figure 3.13.

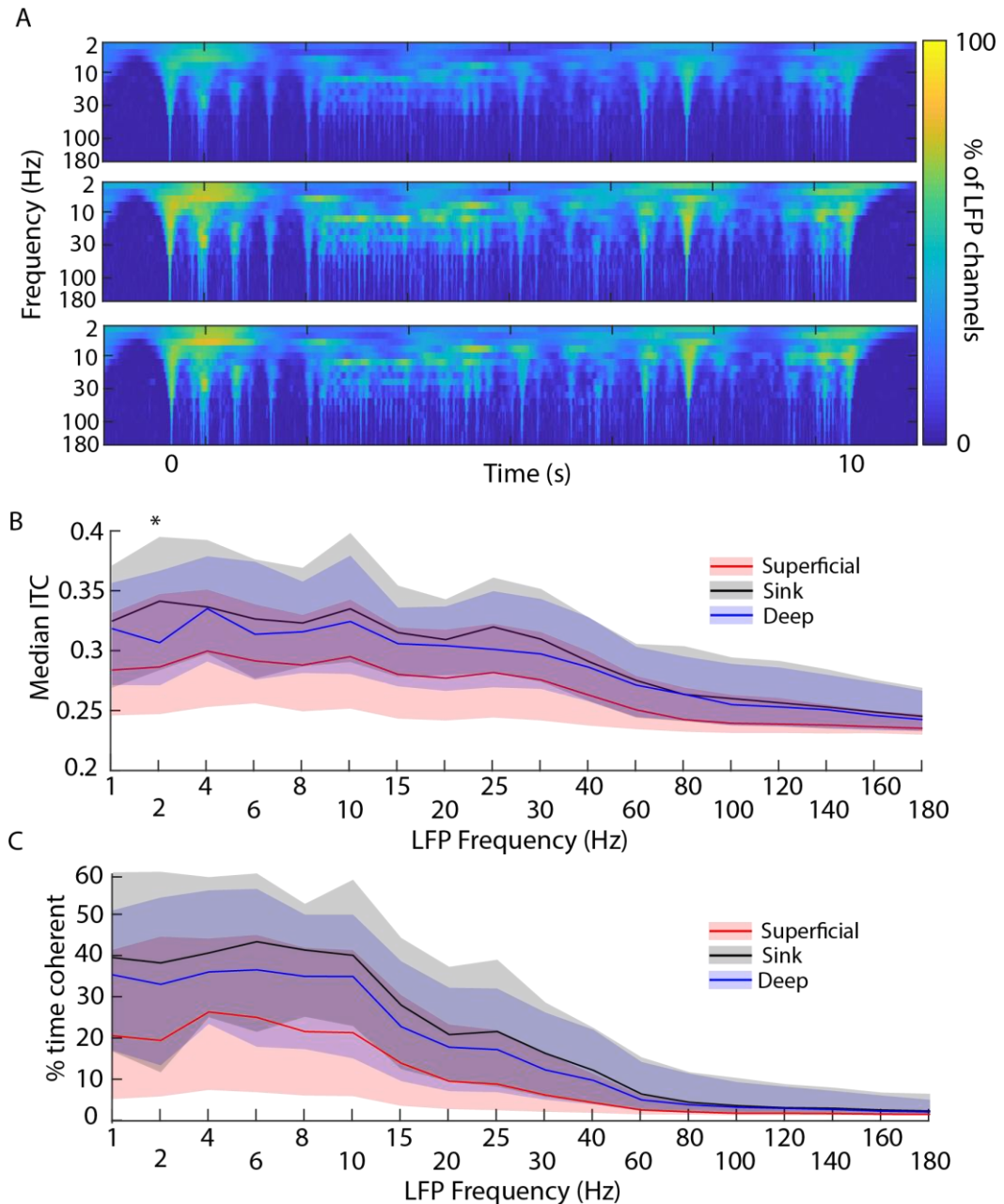


Figure 3.13: ITC in the auditory cortex over depths relative to cortical sink layer/channel (A) Barcodes of ITC for superficial (top), sink (middle), and deep (bottom) channels. (B) Median ITC over sound stimulus. Banded lines show median +/- interquartile range. The superficial channels are always significantly different from the deeper ($p < 1.12e-6$) and from sink ($p < 7.71e-6$). Significant star at 2Hz indicates where sink and deep channels are different ($p = 0.0016$). All stats are Bonferroni after Kruskal Wallis. (C) As B, but for time spent coherent. Deep and sink are never significantly different. The superficial channels are always significantly different from deeper ($p < 3.25e-10$) and from sink ($p < 4.82e-8$). Number of channels are unbalanced: Superficial – 501, Deep – 565, Sink - 182

Again, the ITC (and the proportion of the stimuli for which this is significant) is calculated for each channel (and each frequency band) and the median taken of each group of channels (classified based on their estimated depth).

Though interquartile ranges are large, there is a significant effect of channel depth at all stimuli lengths ($p < 0.05$, Kruskal-Wallis). After multiple comparisons, this difference is primarily between sink and superficial channels and deep and superficial channels (all stimuli significant, $p < 1.12e-6$, Bonferroni after Kruskal-Wallis). Superficial channels have lower ITC. There is only one case where sink and deep channels are significantly different ($p = 0.0016$, otherwise $p > 0.1631$).

There is also an effect ($p < 0.01$, Kruskal-Wallis) for the time spent significant, with post hoc comparisons noting that both deep and sink channels are significantly stronger than superficial channels ($p < 4.83e-8$, Bonferroni after Kruskal-Wallis), but indistinguishable from each other ($p > 0.092$) Similarly to the above, ITC occurs less often in superficial channels. There is also a trend shown with multiple comparisons tests that levels of ITC drop with increasing frequency, something observed in AC data previously.

3.5 Entrainment of Neurons to LFP during Spontaneous Activity and Natural Sound

3.5.1 Introduction

As discussed in the introduction, LFP is reflective of local network activity, and in a phenomena known as entrainment, neuronal spiking is often seen to be oscillatory or phase locked to this activity (i.e. the spikes occur predominantly in one LFP phase, of a given frequency). This phenomenon is thought to enhance perception of temporal features of the sound – the “up” phase of the LFP reflects an increase in excitability of the cells, and these short state changes are lined up with temporal features of the sound.

In this section, levels of cellular entrainment to various frequency bands of LFP are assessed, in both the AC and the IC, and during both spontaneous activity and natural sound. As in previously described literature, it is expected to see entrainment occurring preferentially to frequencies relevant to the temporal properties of the stimulus (the sound envelope, < 30 Hz) (Szymanski et al., 2011, Kayser et al., 2015).

Expectations for inferior colliculus data were unclear. What will be presented may be the result of strong phase locking (rather than specifically entrainment in the LFP sense) in the IC, given than it will be observed up to higher frequencies than entrainment has been seen at. This will be discussed further later.

3.5.2 Illustrative Examples of Entrainment

The example in Figure 3.14 shows two typical cells - from the AC (top) and another from the IC (bottom). Entrainment has been calculated and visualised from data taken during the presentation of the natural sound stimuli used in previous analysis – the silence between each 10 second stimuli is removed to give continuous data for analysis. In both the raw phase distribution plots (grey, left) and the rate difference

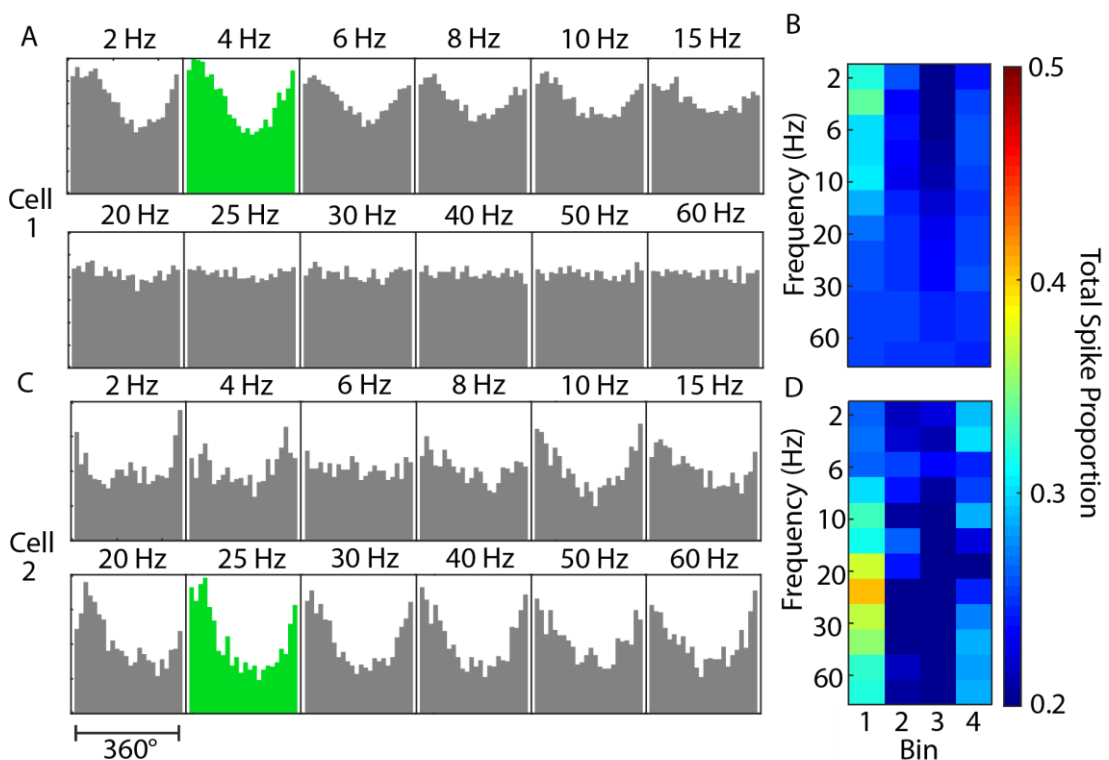


Figure 3.14: Entrainment (illustrative examples). (A) Distribution of spikes with continuous LFP phase (Grey histograms), across frequencies 1-80Hz. Green highlights the frequency with highest entrainment – i.e. the highest preference for a particular phase. (B) Rate differences at each frequency between high and low phases for the example cell in (A). Colour bar indicates proportion of spikes in each phase. (C) As (A), but for a colliculus cell showing more entrainment and to higher frequencies. (D) As (B), but for the colliculus cell shown in (C).

plots (right), there is a clear effect of frequency band on the preferred phase. It is the rate difference (the differences between % spikes at strongest phase and 180 degrees opposite) that is quantified and compared in the coming analysis.

3.5.3 Summary of Entrainment in the Auditory Cortex and Inferior Colliculus

First, the overall strengths of entrainment are summarised, in order to highlight fundamental properties of the data. These are displayed in Figure 3.15.

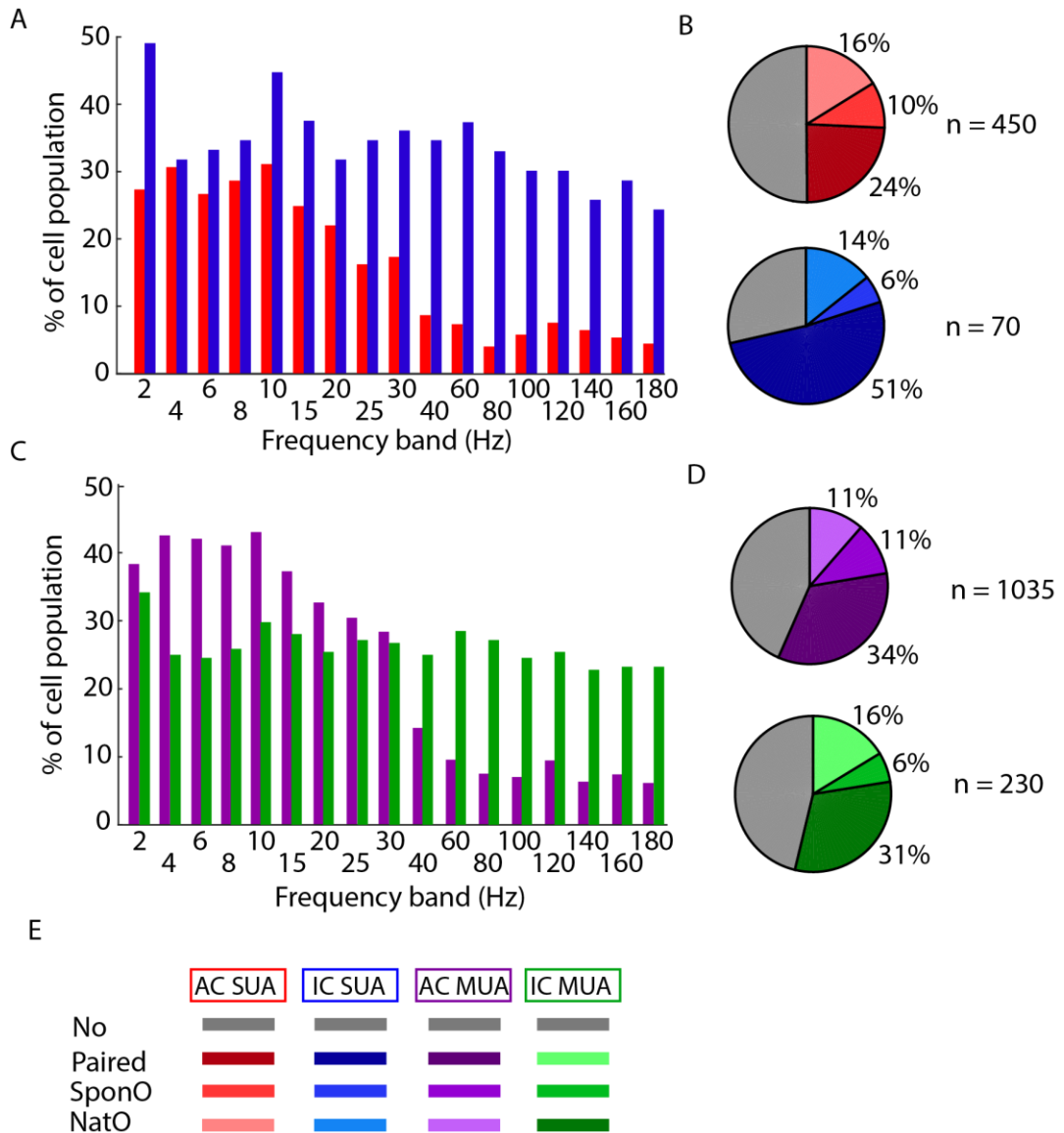


Figure 3.15: Proportions of cell populations displaying significant neuronal entrainment ($p < 0.01$, Rayleigh's test for circular uniformity). (A) Proportion of single unit population (cortex – red, colliculus – blue) displaying significant entrainment to during either spontaneous activity or natural sound, at specified frequency bands. (B) Breakdown of population showing any entrainment to both spontaneous and natural sound (darker colour), spontaneous only (middle colour) and natural sound only (lightest colour), for cortex (top, red shades) and colliculus (bottom, blue shades). (C) as (A), but for multi units (cortex – purple, colliculus, green). (D) as (B), but for multi units (cortex, top, purple shades, colliculus, bottom, green shades). (E) Colour key

AC cells appear to entrain more often to lower frequencies (< 30Hz), while a similar proportion of colliculus cells is entrained at all frequencies. This is consistent with the observed limits of synchronisation coding in the AC. Patterns are similar in single and multi unit graphs, save that cortical multi units show a higher proportion of population entrainment when compared to colliculus at the same frequencies.

Looking at entrainment to specific categories of LFP, around half (50% SUA, 56% MUA) of units recorded show a significant entrainment to at least one form of LFP. These proportions are changed in the colliculus, with 71% of IC single units displaying entrainment. Overall, slightly more cells are entrained solely to natural sound vs entrained solely to spontaneous activity.

3.5.4 Summarising Entrainment Strength Reveals Differences in Data Groups

Levels and strengths of entrainment are now examined in more detail, quantified as rate differences. There is also an interest in the differences between the cortex and the colliculus (Figure 3.16). Only the significant modulations ($p < 0.05$, Rayleigh's test for circular uniformity) are included.

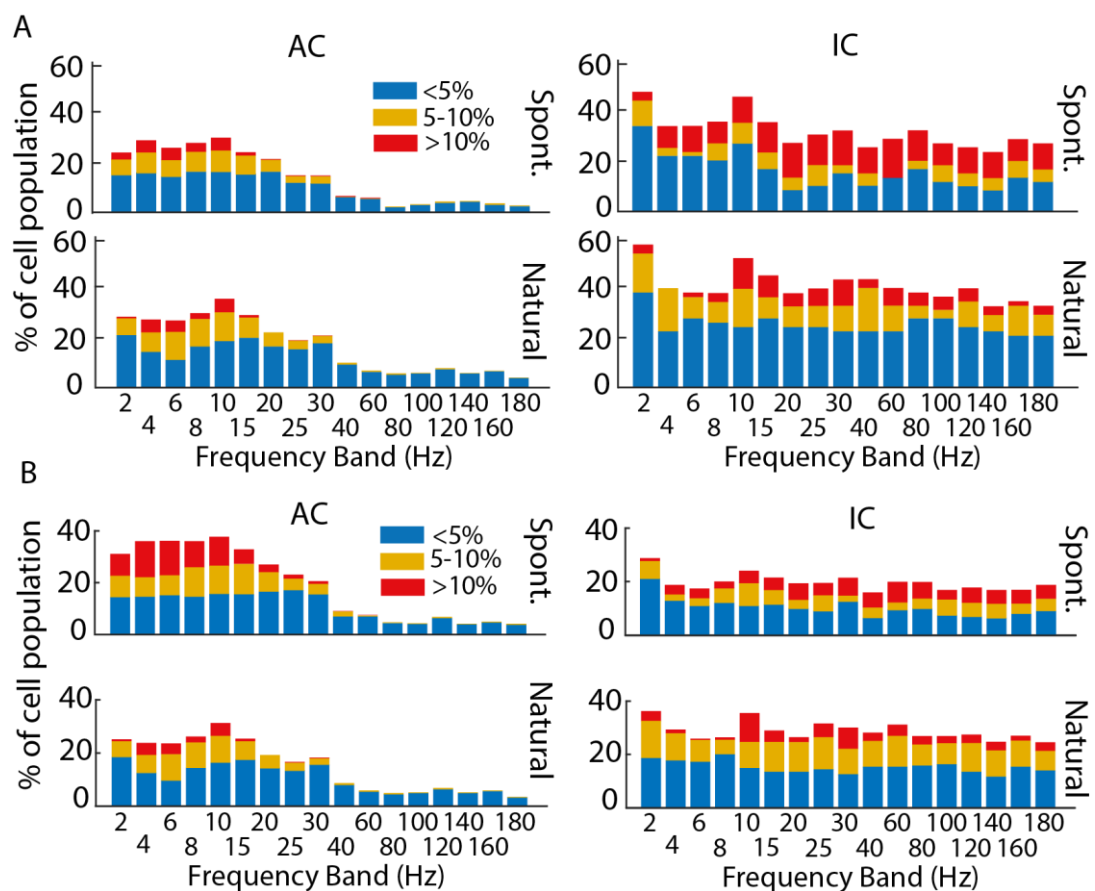


Figure 3.16: Rates of entrainment during spontaneous activity and natural sound stimuli, in the auditory cortex and inferior colliculus (A) Single unit cortex (left, n = 225), colliculus (right, n = 50) rates of entrainment, during spontaneous activity (top) and natural sound (bottom). Bars show levels of entrainment in % of total cell population, for each frequency band. Blue - <5% rate difference, Yellow 5-10%, Red 10%+. (B) as A), but for multi units in cortex (n = 580) and colliculus (n = 122)

Entrainment is Not Present in All Cells, and is Usually Low Strength

Overall, less than 40-50% of a population will show any entrainment to a given frequency band. Most entrainment appears to be low level (<5%), though at some frequencies in the AC (2-10 Hz), this can approach 40%. Entrainment appears overall higher in the colliculus, and up to higher frequencies.

AC Entrainment is Most Dominant at Frequencies <30Hz, While IC Remains Consistent Across All Bands

One distinct trend in the data is for AC entrainment to peak at around theta frequencies (~8 Hz), then fall to almost 0 after about 30 Hz. The colliculus, however, is reasonably stable across all frequencies. Comparing the distributions, a 2-sample Kolmogorov–Smirnov test reveals a significant difference in AC and IC entrainment distribution in both single units and multi units ($p < 0.035$). At higher frequency bands (25 Hz+), entrainment strength matches the distribution and is significantly stronger in the IC (see Table 3.1 for exact bands).

There are No Observable Differences in Entrainment Between Natural Sound and Spontaneous Activity

Between natural sound and spontaneous activity, there are no significant differences in distribution. There is little evidence of a consistent pattern differences at specific frequencies or frequency ranges.

Multi Units have Stronger Entrainment in the Cortex, but not the Colliculus

Comparing single and multi units, in the cortex, multi units typically have a higher rate of entrainment at the cortex relevant frequencies (i.e. < 30 Hz). In the colliculus, there were no observable differences between single and multi unit analysis ($p > 0.115$, Wilcoxon rank-sum test).

Statistical Summary of Differences and Brief Summary

Table 3.1 states in which frequencies the various conditions displayed significant differences, using the appropriate statistical test for the given comparison. All bands are included together.

Table 3.1: Breakdown of frequency bands showing significant differences between conditions

Comparison	Fs significant differences (Hz)	p-values (significant)
Nat vs Spon		
AC SUA	N/A	All >0.15
IC SUA	30,120,140	0.0203, 0.0251,0.0170
AC MUA	2	4.45e-5
IC MUA	2,160	0.0039,0.0395
AC vs IC		
SUA Nat	6, 30-180	0.002 – 0.0459
SUA Spon	25-40,100-180	7e-5 – 0.0361
MUA Nat	All except 2, 10, 15	1e-11 – 0.018
MUA Spon	All except 10-20	2e-8 – 0.011
SUA vs MUA		
AC Nat	4-20	2e-6 – 0.0029
AC Spon	2-20	0.0001 – 0.0231
IC Nat	N/A	All >0.115
IC Spon	N/A	All >0.138

In summary, entrainment generally occurs in ~40-50% of a given cell population, is low level, and see the cortex favouring lower frequencies unlike the colliculus. There are no apparent differences in strength between entrainment at spontaneous or during natural sound, at any frequency band. Multi units in the cortex have stronger entrainment than single units – this is not observed in the colliculus. Table 3.1 reveals no particular pattern to differences between conditions (except some general trends that were previously described), and so conclusions regarding specific frequency dependant effects are difficult.

3.5.5 Entrainment Properties in Two Cortical Cell Types

Narrow Spiking Cells are More Likely to be Entrained, but Strength of Entrainment is Generally Equal between Cell Types

As cortical cells can be sorted into one of two types (broad spiking, putative pyramidal, versus narrow spiking, putative PV-positive fast spiking interneurons), and that these

types have different firing properties and functions, the following analysis examines cell type specific differences in entrainment (Figure 3.17).

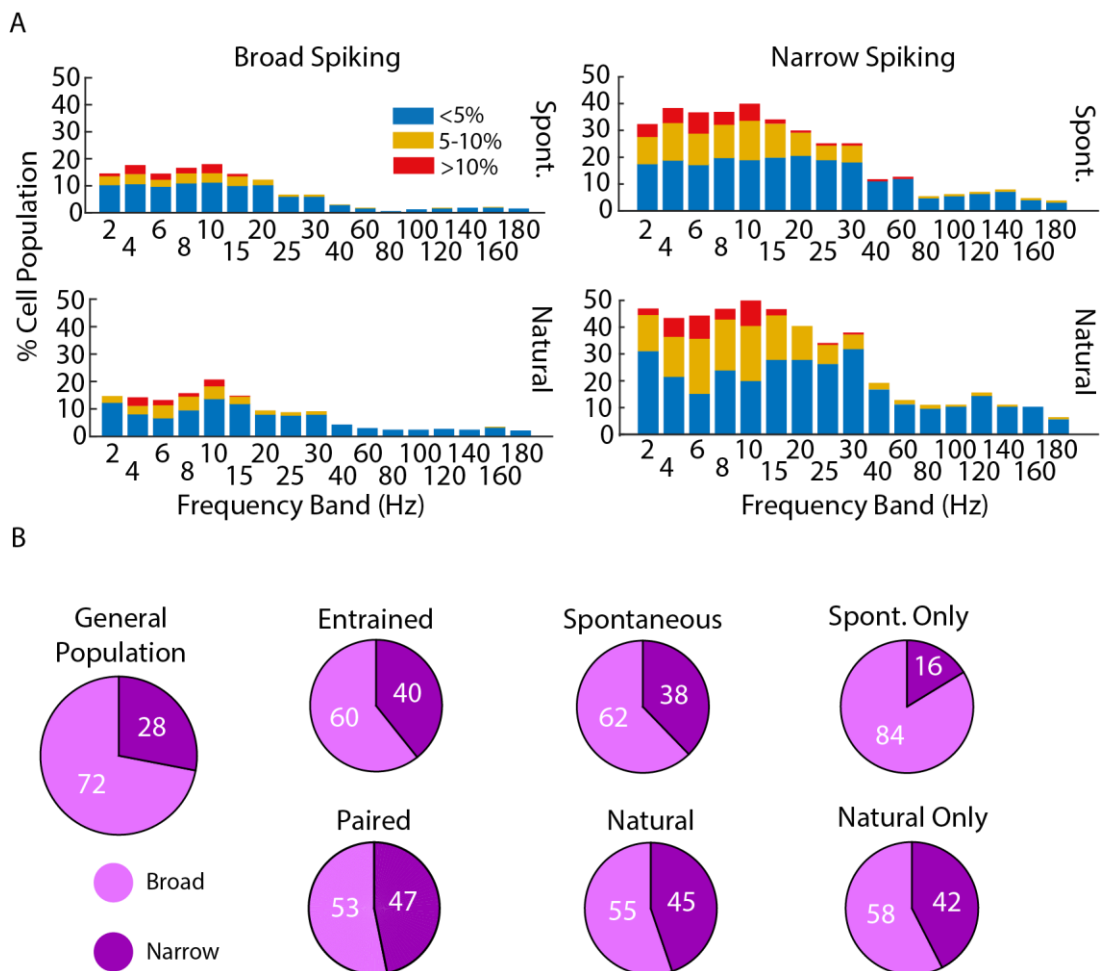


Figure 3.17: Levels of entrainment across narrow and broad spiking cell groups in the auditory cortex. (A) Rate difference bar graphs for each frequency band, for cortex (left) and colliculus (right) during spontaneous (top) and natural sound (bottom). Blue - <5%, Yellow - 5-10%, Red - 10+% rate difference. (B) Pie charts showing proportions of entrainment property groups comprising of broad and narrow spiking cells. Broad - light purple, Narrow - dark purple

Something which is immediately apparent from Figure 3.17 is that, as a population, narrow spiking cells are more likely to show entrainment to natural sound or to natural sound and during spontaneous activity. In Figure 3.17A, the frequency distribution patterns of broad and narrow spiking cells were common only for spontaneous activity, and not for natural sound ($p = 0.0305$, 2-sample Kolmogorov–Smirnov test). Despite this, there were no significant differences in entrainment strength for any frequency bands, for any condition, between broad and narrow spiking cells ($p > 0.05$, Wilcoxon rank-sum test).

Narrow Spiking Cells are Unlikely to Entrain to Spontaneous Activity Alone

The importance of entrainment in narrow spiking cells is further emphasised in Figure 3.17B. The general population of cells has a 72:28 balance of broad to narrow spiking. However, for the entrained populations, this balance is shifted. For populations showing any entrainment, paired entrainment (natural sound *and* spontaneous) and to natural sound only, narrow spiking cells make up a larger proportion. However, looking only at cells entrained to spontaneous activity, the proportion of narrow spiking shrinks dramatically, especially when compared to natural only (15% vs 40%) This would tend to suggest that any given narrow spiking cells is more likely to be entrained than a broad spiking counterpart, and that they will favour entrainment to natural sound over spontaneous activity.

3.6 Discussion

3.6.1 Summary of Results

In this chapter, the basic properties of the recorded neuronal data were examined, followed by comparing and contrasting properties important to natural sound encoding. In this way, fundamental differences between the AC and IC have been highlighted.

The initial hypothesis that the AC and IC will differ in the distribution of their basic cell metrics was confirmed – though this was entirely expected. There is also some evidence of the IC having lower trial-trial variability during natural sound, than the AC – and on both and spiking and an LFP timescale.

In terms of frequency patterns, entrainment in the AC matches literature as expected by not being present to any great degree at frequencies greater than 30Hz, but differs to a significant degree in terms of overall numbers and strength (Kayser et al., 2015). Narrow spiking cells displayed a preference for entrainment to natural sound over spontaneous activity alone, not reflected by broad spiking cells. Multi units tended to show stronger entrainment than single units, perhaps due to higher and/or more consistent spiking. Entrainment in the IC is different, as hypothesised, however, results should be interpreted carefully. Single and multi units here were indistinguishable.

3.6.2 Comparisons to Previous Literature

Cell Type Proportions

The bimodality in cell waveform metrics that observed in the auditory cortex data mirrors a number of past publications, though the percentage of narrow spiking cells (putative narrow-spiking interneurons) observed is almost double that observed in studies using similar classification strategies (28% vs 14% (Sakata, 2016) , 15% (Yague et al., 2017) , 10% (Sakata and Harris, 2012) and 8.2% (Sakata and Harris, 2009)). The same metrics were used to classify (20% width and peak to trough), though thresholds for 20% width were slightly different, and so this may account for some of the differences. Some of the cells in the other studies were also recorded during anaesthesia, which may have affected results. Additionally, one study used an isolation distance of 50, rather than 20 as used here, so units were of far higher quality.

One difference in this study has compared to previous is in the spike sorting software used. This chapter uses the newer Kilosort, compared to the older Klusta or KlustaKwik. Potentially, this newer software is better at isolating fast spiking neurons. Aside from this, there may be additional, unknown biases in the recording or analysis procedure which has resulted in the higher proportion, such as consistent over or under clustering affecting proportions of certain cell types/appearances. A significantly higher spontaneous firing rate is observed in the putative interneuron population, suggesting that the classification is to some degree correct.

As expected, there was no bimodality in ICC cells based on their width – the cell types in the ICC are fundamentally different to the AC, and are difficult to differentiate without in depth frequency response mapping, or morphological staining.

Trial-Trial Variability

Generally, the auditory cortex has a higher trial-trial variability than the inferior colliculus, at least for multi units. The recordings were ~20 minutes long, which is long enough to observe changes in attentional state, known to affect the trial-trial variability in the auditory cortex (Marguet and Harris, 2011). Thus, the relatively higher values observed, plus their variability, may be explained by this phenomenon. To the best of our knowledge, there are no existing literature on IC single and multi unit trial-trial variability during presentation of natural sound, and no studies directly compare them to the auditory cortex during the same stimulus. This is further explored in Chapter 4, where this is related to spike rate coding.

Inter-Trial Coherence

Inter-trial coherence has proved, at least in humans, to be an important variable in encoding natural sound – thus it is logical that we have observed it in this context, and that it is strongest during periods of sound. The cortical ITC is seen predominantly at lower frequencies, fitting with what was expected from the literature on LFP entrainment and phase locking limits (Zeng, 2002, Kayser et al., 2015). As the ITC at the sink channel and below was significantly stronger than in superficial channels, this would weakly suggest that the LFP originates from the cortical sink channel and/or the layers below this (IV-VI)(with a possible origin thus being the thalamus, given that it inputs to layer IV and VI. Again, this researcher could not identify any literature discussing ITC in the IC. Care must be taken when interpreting the strong results observed in the IC – that coherence is strong in every frequency band up to the 180-200 Hz band does not have a good explanation. Interestingly, there is slight trend for the strength of coherence in lower frequency bands (containing <10 Hz) to be lower than that of higher bands. Also, both the strength and time spent coherence is highly variable across IC channels. In any case, IC ITC is stronger and clearer than that in the cortex, indicating more consistency in the LFP across successive trials and further supporting the argument of lower variability during natural sound for the inferior colliculus.

Entrainment

The results of entrainment in the cortex follow the literature – to a degree. The frequencies at which it is strongest, and the overall limit, roughly match what is seen in Kayser et al 2015, however, the overall strength of entrainment is far lower (results were usually very small, 0-10%, whereas rates of 30% to 60% were commonly observed Kayser et al's study) (Kayser et al., 2015). Additionally, in the auditory cortex only 50% (SUA) or 56% (MUA) of units showed entrainment – in a 2017 study, this number in single units was 87% (Yague et al., 2017). There is also no appearance of a narrow spiking cell preference for higher frequencies as was observed in the same study (Yague et al., 2017) – however, it is observed that far more of the narrow spiking cell population is entrained, when compared to the broad spiking, and also that they are more likely to be active with natural sound alone, or to both natural and spontaneous, rather than be spontaneous specific. This is a novel and logical observation, and also can be said to extend upon the 2017 observations.

Exactly what causes the observed discrepancies is not fully understood. As the filtering protocol was identical to the 2015 paper, it may be simply that either the LFP or spiking data (or both) is not of consistent quality, resulting in observations being harder to make. To determine a significant entrainment, a more conservative p value threshold of 0.01 is used, however, 0.05 was also tried and did not add many more units.

Similarly to the ITC, entrainment results in the IC should be interpreted carefully. The raw data does appear to be clearly entrained, and an examination of filtered data reveals filtering to be working correctly, at least to some degree. A discussion of what could be done to improve the reliability of results is found in Section 3.6.3.

3.6.3 Limitations and Considerations

Lack of IC Single Units

One of the main limitations in this analysis, and one that continues in the remaining chapters, is the lack of single units recorded from the inferior colliculus – this prompted the use of multi units. This has meant that comparison, particularly directly between simultaneously recorded neurons, is difficult. The lack of units is thought to be a combination of both experimental and analytical factors. From a brief review of the IC literature, single channel microelectrodes would even now seem to be the method of choice to record single units (Grana et al., 2017, Herrmann et al., 2017), and from IC studies using silicon probes, it is found that multi unit analysis is favoured over single units (Miyakawa et al., 2013, Schnupp et al., 2015). A few quotes from the literature suggest strongly that the isolation of single units in IC recordings is a common issue, or at least inconsistent - though no paper offers an explanation.

“At most recording sites, multiunit activity was observed, but less frequently the responses of well isolated single neurons could be studied” (Malmierca et al., 2008)

“During most recordings, only 2-4 channels contained single-units. The majority of channels contained 0 or 1 well-isolated single units, but some channels contained up to 2 single units.” (Shaheen and Liberman, 2018)

From observation of the current data, a few explanations can be offered. The ICC usually has a very strong and sharp evoked response in the LFP, accompanied by lots of spiking activity (more so than the AC). It is possible that isolation of single units from within this burst of activity is very difficult. There may also be a lot of high frequency multi unit noise caused by the background activity, that low pass filtering

would not remove – again making isolation of clean single units difficult. During manual spike sorting, it was observed that IC clusters were very often strongly contaminated in their refractory period.

Another issue may be more experimental. The IC is located at the back of the skull, and was sometimes found to be unstable due to the lack of cement coverage (due to muscle directly behind) and nearby anchor screws, plus proximity to the neck muscles and shoulders. This could easily result in probe movement, damaging IC tissue and cells. An additional anchor screw was added to the contralateral side in later experiments, but very medial (~3-4 mm) and also close to the Lamba landmark so as to add general stability to the area. This improved stability and eliminated head cap failure, but issues with IC data were still somewhat present.

Fano Factor Discrepancies

A Fano factor of 1 indicates a Poisson process, or a generally accepted model of spontaneous neuronal firing. It was observed that the Fano factor recorded is not always around or below 1, and can in fact reach much higher values. As comparisons are generally relative, rather than focusing on comparison to specific literature values, this is somewhat acceptable for the current chapter, though care must take care when comparing results to previous literature. It is most likely due to some single or multi units being of lesser quality (missing spikes, for example), or animal movement during the period of natural sound. This would lead to some trials having vastly different (i.e. lower) spike rates than most, skewing and increasing the variability of the Fano factor. It would also have been beneficial to have a reliable way of determining brain state, but as pupil monitoring was not done, this additional layer cannot be added.

ITC in the Inferior Colliculus

As previously mentioned, caution must be taken in the interpretation of results in the ICC. One explanation for the spread of ITC across many frequencies, and its strength, may simply be the low quality (or generally less oscillatory nature) of LFP in the ICC. As phase analysis will assign phases regardless of relative amplitude of that frequency band, it may be that the actual LFP bands are nearly flat, but coincidentally their phases line up. The high variability of the ITC in the IC is likely due to firstly, some low quality datasets and secondly, some channels not being fully in the ICC so having slightly different evoked responses.

Entrainment

As covered, the observations of entrainment differ from recent literature in overall number and strength, particularly in the auditory cortex. A small part of this may be attributable to a more conservative threshold for significant rate modulation (0.01), but this does not explain it all. Other factors may include animal movement during some trials, and a low quality LFP in some datasets. The analysis would have perhaps benefited from examining each dataset individually, to determine if some were skewing results. A threshold for removing “noisy” or bad trials, perhaps determined by a relatively lowered spike rate or high power in low LFP may also have cleaned results.

Similarly to the ITC, interpretation of entrainment results in the ICC should be made cautiously. While more neurons are entrained, this entrainment is of a similar strength and proportion across all frequency bands observed, with any one neuron often “entrained” to the majority of bands – this last point in particular may not make sense alongside known properties of the ICC, as its neurons appear to have preferred amplitude modulation frequencies (a somewhat related property) (Schreiner and Langner, 1988) Admittedly, entrainment in the ICC has not been investigated and so neurons may behave differently in this regard. There are several methods of increasing the reliability of results in the future. Firstly, cross validation should be introduced to some degree. Secondly, optimisation of filtering so that frequency bands are clearly distinguished – currently, there is a very slight overlap in the bands, which, while not a strong issue in the cortex, may mean that exceptionally strong ICC evoked responses are persisting across many frequency bands as they aren’t being fully removed. Thirdly, the number of phase bins could be increased to 8, prioritising stronger phase locked responses.

The entrainment analysis does not look at relationships (i.e. correlations or coherence) between LFP and ongoing sound envelope. MUA, spiking variability and ITC react during particular periods of the sound stimulus, but the exact nature and strength of the relationship has not really been explored. Such analysis would have helped to strengthen the claims of entrainment being present (or not), particularly in the inferior colliculus. Without fully breaking down the temporal aspects of the sound, it may be difficult to distinguish between true entrainment and phase locking. While selecting an LFP channel far away from the cell may mitigate this, in the inferior colliculus the LFP can be strong in all channels.

3.6.4 Functional Implications

Much of the work in this chapter was confirmatory, thus there are few new implications on area functionality to identify. Additionally, due to the lack of data from the inferior colliculus, and the unexpected nature of the results, there should be hesitation in making strong conclusions or implications at this stage.

However, there are multiple pieces of evidence that point to the inferior colliculus having a lower trial-trial variability during the presentation of natural sound, when compared to the auditory cortex (a conclusion further supported by Chapter 4). This supports the evidence presented in the introduction to this chapter and in the literature review that the ICC is less influenced by brain state, and maintains reliable spike rates despite these shifts in global brain state. Favouring a reliable coding mechanism at this crucial auditory processing stage is highly logical – neurons should represent the raw sound as faithfully as possible for as long as possible, so that the auditory cortex and higher processing centres can together process the data largely unbiased. This has implications for the success of IC implants – if sound information is conveyed in a predictable way each time, the stimulation pattern of the implant has no need to change dynamically.

Interestingly, the IC has slightly weaker ITC at the lower frequencies that the AC favours. Precisely what this means is difficult to assess without further investigation, but perhaps the IC has a focus on these higher frequencies for some as yet unknown reason.

Entrainment in the AC was observed, but not to the same degree as previous literature (Kayser et al., 2015, O'Connell et al., 2015). That results are not as strong as in previous papers may be due to the choice of stimulus and the contextual environment for the mouse. Not being required to attend to the stimulus for the purposes of a behavioural task, and the sounds not being from mice or specific predators, may have reduced the need for entrainment for perception enhancement, particularly as the stimulus is repeated for 20 minutes. This supports the idea that the function of entrainment is to enhance perception of behaviourally/contextually relevant sounds over background noise. In noisy environments (e.g. the “cocktail party”) entrainment in the auditory cortex focuses on the most relevant and important stimuli of the current context (Zion Golumbic et al., 2013).

One of the more interesting observations was the propensity for the narrow spiking interneuron population to be entrained to specifically natural sound, or at least not to spontaneous activity alone. This speaks to the presence of an interesting dynamism in the activity and function of interneuron populations during different levels of sensory input, and solidifies their importance for encoding natural sound stimuli. The influence of inhibition is apparent during both spontaneous activity (to balance increased excitability (Haider et al., 2006)) and auditory evoked activity (i.e. frequency tuning (Wu et al., 2008)), but given results observed here, their mechanism of action and interaction with other features (i.e. LFP) may differ between conditions.

3.6.5 Further Work

Improvements to the Current Research

Gathering more single and multi units from the inferior colliculus, through further improvements to surgery procedure, recording protocols, and spike sorting, would be highly beneficial for all aspects of current and future analysis. It would allow more robust and statistically significant conclusions to be made.

The existing analysis may benefit from optimisation, to reduce the effect of artefacts and spike identification inconsistencies on the variability of results. This maybe be done by designing thresholding systems or ways to identify noisy trials or inconsistent single units caused by external processes. More filters may also be incorporated along with additional methods to ensure robustness of results, such as cross-validation.

Expansions on the Current Research

One interesting avenue of research is the influence of brain state on the properties examined in this chapter. With a reliable method of determining state (i.e. pupil monitoring), the effect of state on ITC and entrainment may be investigated. Learning more of the effects of brain state on sensory perception would have widespread functional implications both for the auditory system and systems neuroscience in general. Of particular interest would be the effect of state on broad and narrow spiking population activity.

The trial-trial variability (Fano factor and ITC) may be further characterised by altering the definitions of the time bins used. In the presented research, these were locked definitively to the stimulus and to each other, but as will be discussed in the Chapter 4 introduction, it may be that time bins should be dynamic and locked to different

aspects of the envelope, or the underlying entraining LFP. An improved performance of mathematical models incorporating these dynamic time bins would imply functional importance of the phenomenon, and results from such analysis may shed further light on the underlying rhythms on which stimuli are encoded.

The entrainment results presented were generalised to simply “evoked activity”. By calculating entrainment at - for example - specific segments of sound, during different attentional states, and for new and behaviourally relevant sound stimuli, a clearer picture of entrainment’s dynamic role in sound processing may be obtained.

Chapter 4 Linear Classification of Natural Sounds using Spike Rate in the AC and IC

In Chapter 4, the analysis of Chapter 3 is expanded, using linear classification to decode stimuli from neuron responses in the auditory cortex and inferior colliculus. Section 4.1 introduces aims, relevant literature and hypothesis for the chapter. Section 4.2 explores the results of linear classification. An overview is first given, including an analysis of positive and negative controls, followed by the relationship between success and number of input predictors, and how this differs between the brain areas. Further analysis in the form of frequency ranges, Fano factor and pairwise correlations are also presented in an attempt to explain the classification results seen. Finally, in section 4.3, results are related to hypotheses and previous literature, current limitations are noted, functional implications are speculated upon and suggestions are made for further investigations.

4.1 Introduction

4.1.1 Aims of the Chapter

In the previous chapter, a broad number of neuronal properties have been examined, characterising and contrasting each brain area and linking results to previous literature and in the context of auditory implants. While clear differences are noted, particularly in ITC and entrainment, their function in neuronal coding is only speculated. In this chapter, there are two main aims:

- Investigate the effectiveness of a simple spike rate code at differentiating between natural sound stimuli, in both the AC (A1) and IC (ICC). This will be done with simple linear classification, with relative successes being indicative of variations in sound encoding strategies and general properties between the brain areas, as per the initial hypothesis.
- Investigate and identify potential mechanisms for any observed differences and similarities in model performance, through analysis of model input data

Knowing this information is important both in the context of auditory implants and systems neuroscience in general. If success rates are low using a simple rate code and stimulus-locked time bins, it may be that to be most effective, devices in the IC will need to diversify or dynamically adapt methods of stimulation, or ideally record and incorporate additional information from the brain (i.e. LFP) in order to guide stimulation patterns to effectively replicate naturalistic sound in a way that is accurately interpreted by higher processing centres. In general, knowing more regarding each area's responses during typical sound stimuli will be beneficial for designing the most effective and natural stimulation protocols.

4.1.2 Relation to Previous Literature and Results

LFP Influences on Sound Coding

The evidence is clear that the brain encodes sound using patterns of neuronal activity on a range of time scales, each conveying some layer of the information (Panzeri et al., 2010). Precisely what governs the neurons on this time scale is still somewhat under debate, but as detailed in the literature review and entrainment analysis in Chapter 3, underlying LFP rhythms during naturalistic sound (or indeed other forms of stimuli) “conduct” the neuronal excitability to enhance encoding. In any case, timescales are important.

A highly interesting paper on the topic was published by Kayser et al in 2012. In this paper, they performed decoding (namely, classification analysis) on a series of 10 randomly selected epochs of a spike train generated during a 52 second naturalistic sound stimulus. The information in these epochs was either left as a simple spike rate, or partitioned – either into equal time bins locked to the epoch, or by the underlying phase of LFP at various frequencies. Incorporating this extra information (particularly phase) resulted in better classification performance, adding weight to the hypothesis that LFP is imperative for guiding neuronal spiking. A theta reference frame proved most effective. In this chapter, a similar (albeit simpler) approach is taken to examine IC responses alongside AC and perform additional analysis on inputs to explain results.

It is also known from the literature review that the brain has a range of encoding mechanisms for frequency and periodicity information outside of entrainment, including phase locking, rate codes, and tonotopy/periodotopy, spike latencies, and population patterns/interactions. Without recording electrodes and feedback loops within stimulation devices, this cannot be replicated at present.

In auditory implants, the aim is to convey as much of the sound information with as little latency and as much accuracy as possible. At the very least, for devices to be functional, contextually relevant stimuli should be clearly differentiable. In this Chapter, another aim is to ask how effective a simple spike rate code is at differentiating between naturalistic stimuli. Instead of time or phase partitioning the data, the simple spike rate of units is used, during the 10 randomly selected epochs from the 10 seconds of sound. Only basic linear classification is used, as a baseline for future analysis, and to avoid the excessive computation time other methods may require. A range of stimuli lengths is examined, between 25 ms and 1000 ms, given the apparent importance of certain frequencies.

Where the study matches and expands upon previous analysis is in the comparison of results across time bins, input data types (i.e. SUA and MUA) and brain areas, and in the subsequent analysis of the input data in an attempt to highlight the various mechanisms and approaches at play. Focusing on the auditory cortex, there is the opportunity to split data in broad and narrow spiking cells and compare their results.

Classification Analysis

Classification (linear or otherwise) is a commonly used decoding technique to identify distinct neuronal responses are between discrete stimuli, and by changing input types

and timescales, different aspects of coding can be examined. In auditory research, it has proven to be a good tool for examining the brain's response to different natural sounds, such as auditory scene analysis (Staeren et al., 2009), speech phonemes (Mesgarani et al., 2008), speech/music versus other natural sounds (Zuk et al., 2019), letters (Wang et al., 2018), sound envelope shapes (Osman et al., 2018), and in segmenting a single segment of natural sound, as has been discussed (Kayser et al., 2012). These studies can utilise both high (spiking) and low (LFP/EEG/MEG) frequency activity. More generally, classification-based methods have been used to look at memory (Dong et al., 2016), distinguish responses using μ LED probes (Scharf et al., 2016), and in automated “scoring” of the current sleep state (Rytönen et al., 2011) – to name but a few examples. Thus, given the extensive history of classification methods for this kind of data and questions being asked, it seems a highly appropriate analysis for this chapter.

Influences of Trial-Trial Variability

Given what was observed in Chapter 3, and in the literature review, trial-trial variability in the cortex appears to be larger than subcortical areas (e.g. IC), and is known to be modulated by brain state (Marguet and Harris, 2011, Sakata, 2016). The effect of brain state on IC activity is less clear, as described in the introduction of Chapter 3 – briefly, while ICC frequency tuning is seemingly unaffected by state, this is not the case in the non-lemniscal areas (Chen and Song, 2019, Alkhatib et al., 2006, Langner et al., 2002). In addition, current literature is based on awake versus anaesthesia and not more natural brain states, and the IC is connected to other auditory nuclei with the potential for brain-state dependant modulation. In the current task of passive listening to natural sounds, it is expected that brain state will change over the time of presentation, influencing cortical trial-trial variability. In Chapter 3, a trend for the IC to have lower variability than the cortex is seen and is thus something expected here. Logically, it is also expected that a higher trial-trial variability will negatively influence classification analysis, and so this may be a potential explanation for any results observed. As such, trial-trial variability is a key analysis of this Chapter.

Influence of Correlations on Sound Coding

As previously mentioned in the literature review, pair-wise neuronal correlations are thought to influence neuronal coding in a variety of ways, potentially decreasing or themselves carrying additional information about a given stimulus (Panzeri et al., 1999, Fiser et al., 2010, Moreno-Bote et al., 2014). In the context of the current

analysis, the investigation into correlations is not extensive. Logically, given the type of model being used, higher signal correlations are expected to result in poorer performance, as they eliminate difference between stimuli that model success is dependent on. Noise correlations in this context are likely to influence the trial-trial variability of the neurons, potentially negatively affecting the overall success of the analysis. Correlations between pairs of narrow spiking cells have been observed to be higher than equivalent broad spiking pairs in the in prefrontal cortex of the monkey, and so this is another expected observation in the data (Constantinidis and Goldman-Rakic, 2002).

4.1.3 Hypotheses

There is extensive evidence that cortical neuronal activity is modulated by ongoing brain state - in turn, this could influence the trial-trial variability of the cortical responses to repeated stimuli (Lin et al., 2019, Fritz et al., 2005, Curto et al., 2009, Noda and Takahashi, 2015) . Indeed, there is evidence that trial-trial variability of cortical neurons increases in the desynchronised state (Marguet and Harris, 2011, Sakata, 2016). The central nucleus of the inferior colliculus, a subcortical auditory processing “hub”, thus far shows little evidence of being as affected by global state modulations - though non-lemniscal portions do exhibit effects (Chen and Song, 2019, Alkhatib et al., 2006). In its role as a integration site and key thalamic relay, the IC may benefit from an increase reliability of response to ensure accurate encoding of sound information – this was observed to some degree in Chapter 3 with IC MUA in particular having a lower trial-trial variability during natural sound. Decoding stimuli from a simple (spike rate) code is likely to have varying levels of success in each area, which will be observable using simple classification analysis. Success of a simple rate code in decoding natural sounds in the IC bodes well for the future of auditory implants, for which the creation of precisely timed spike patterns may prove a challenge. That natural sound is clearly coded on specific timescales (i.e. theta) suggests that the integration window will further affect classification results. The specific hypotheses of this chapter are thus that:

- The inferior colliculus will perform better or comparably to the auditory cortex overall when using simple spike rates as an input, due in part to the expectation of a lower trial-trial variability. This will be especially apparent when using MUA given results from Chapter 3, and that there is more data overall to work with in these sets

- Stimulus length will influence results, given the varying timescales of neuronal encoding. Lengths around 150-300 ms, corresponding with theta frequencies, are expected to be best
- Any observed differences in performance between AC and IC will be accompanied by differences in trial-trial variability and/or correlations of contributing neurons
- Neuronal correlations have the potential to affect classification performance, by flattening activity across all examined stimuli and limiting the stimulus-specific variability. As such, these will be investigated alongside the primary results, and it is hypothesized that high noise and signal correlations will be indicative of a poorly performing dataset, as stimuli are distinguished less clearly

4.1.4 Main Findings

- The inferior colliculus performed comparably (overall, with all data combined) to the auditory cortex – but with fewer input neurons. This was the same for both SUA and MUA
- Stimulus length did not have a strong effect on performance
- If the neurons of a dataset covered a wider frequency range this generally indicated classification better performance. IC frequency ranges were significantly smaller than AC, not explaining the previous results
- Overall, IC neurons trial-trial variability was both significantly smaller, and less variable, than the AC. This was the case for 17 stimuli lengths between 25 and 1000 ms (overall variability increased with increasing length)
- Positive and negative controls explained exceptionally poor performing datasets, as stimuli were indistinguishable from spontaneous activity
- High signal and noise pairwise correlations indicated exceptionally poorly performing datasets

The linear classification approach used here, while informative as a starting point, is limited. With the approaches taken here, it is difficult to say exactly what neuronal pattern results from what aspect of the sound – as the dimensionality of the stimulus has been considerably reduced. Options for examining this properly will be explored in the discussion.

This chapter also provides an excellent stepping-stone into discussions on further types of analysis that would utilise the simultaneous aspect of the data – such as predicting AC activity from IC.

4.2 Success of Linear Classification using Spike Rate

Linear classification was performed as detailed in Materials and Methods and the above introduction.

4.2.1 Methodology

As detailed in Materials and Methods, 10 random stimuli are selected from the natural sound segment. 10 stimuli are derived for each time bin, resulting in 17 stimuli sets total. An example of how these are derived is displayed in Figure 4.1; briefly, segments of the 10 s natural sound stimulus are randomly selected, 10 of equal length for each stimulus length examined. Additionally, 4 “runs” of these configurations are run, with different stimulus locations.

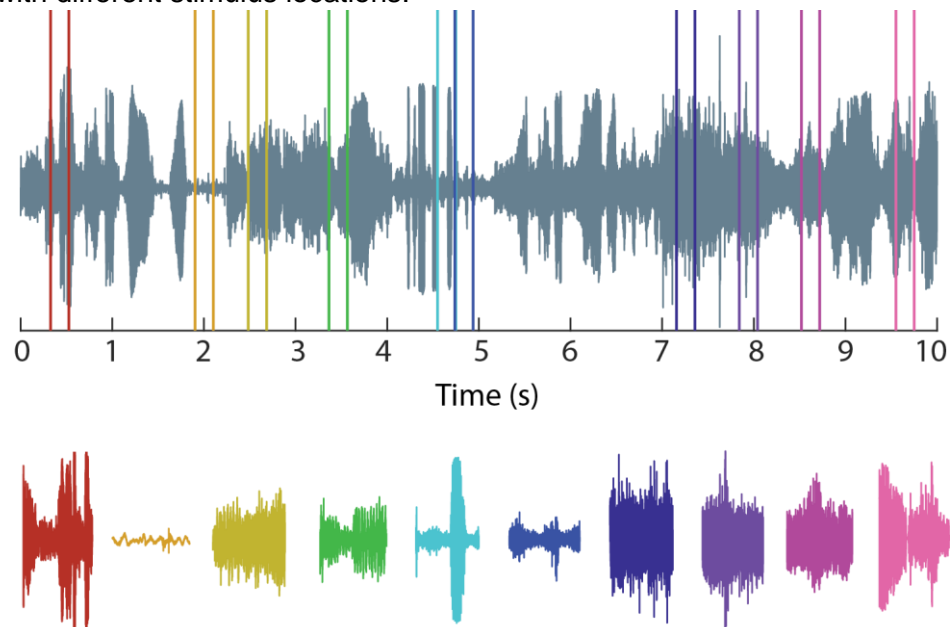


Figure 4.1: Schematic of sound segments selected for classification analysis. Top – 10 second natural sound trace. Coloured vertical lines indicate the start and end of each of the 10 segments (for run 2). Bottom row displays the colour coded segments.

4.2.2 Overall Success of Linear Classification

The analysis is run comparing the 17 stimuli sets, and 4 “runs”. Classification error is derived from the average of 100 repetitions of the analysis. In each repetition, 10-fold cross validation, where 90% of the data is used to train a model and the remaining 10% used to test – repeated a total of 10 times with different segments of the data (see Materials and Methods 2.6.9).

Linear Classification Success does not Vary between Stimulus Sets

There are no differences observed between “runs”, for any type of input or at any stimulus length ($p \gg 0.05$, Kruskal-Wallis), except in a single stimulus for AC MUA ($p = 0.0194$, Bonferroni after Kruskal-Wallis). However, as this is a very isolated occurrence, it is assumed that there are no significant differences between the runs and so run 1 is used for the remainder of our analysis unless otherwise stated. Chance level (i.e. the classification success level that would be obtained from random guessing by the model) is 0.9, or 90% error.

Summary of Linear Classification Outcomes

First, classification results from a single run are summarised, during all lengths of stimulus/frequency bands (Figure 4.2). Results of using AC and IC data, single and multi units are examined. The spike rate data is also run through Principal Component Analysis (see Materials and Methods), and both 3 and 5 PCs are used in addition to “all” raw units.

Dimensionality Reduction Does Not Adequately Capture Variability of Datasets

The Friedman’s test compares conditions to identify between group values, as data is technically paired across three groups. Results from using all predictors, 3PCs and 5PCs are compared. If success is comparable between groups, these PCs may have adequately captured the variability of the data. The following examines the success of using PCs for each type of dataset.

AC SUA – At all stimulus lengths, there is a significant effect of predictor (Friedman’s test, $p < 4.34e-4$). After post hoc analysis (Bonferroni), using All predictors, versus 3 PCs, always gives a significantly better response ($p < 0.0004$). Between All and 5PCs, 10 of the 17 stimulus lengths show significant differences, with All predictors performing better/having a lower error (significant p values < 0.0378). Occasionally, differences are observed between 3 and 5 PCs, with 5PCs performing better (6 of 17, significant $p < 0.0345$).

IC SUA – there is no effect of predictor type on this data, except for two stimulus lengths ($p = 0.011$ and $p = 0.030$, Friedman’s test). After applying Bonferroni correction however, there are no between group differences identified.

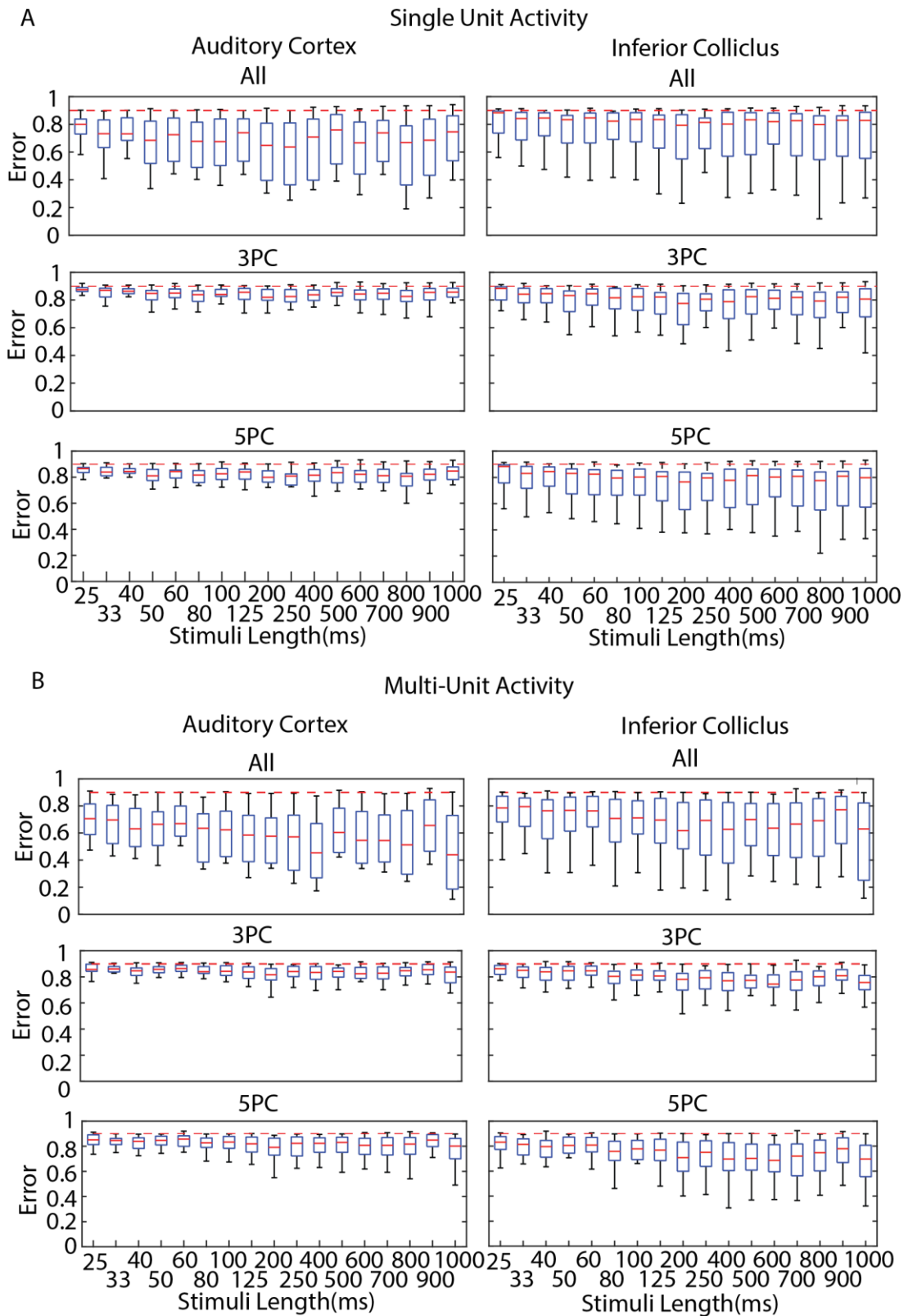


Figure 4.2: Summary of classification results from Run 1. (A) Boxplots showing the range of performances across 21-23 datasets (each dataset calculated from the mean of 100 repetitions of the same stimuli set). Top Row – Using all available predictors, AC (left) IC (right), Second row, 3 principal components only, Third row, 5 principal components only. Dotted red line indicates 0.9 or 90% error (i.e. chance level). (B) As in A but using multi units as inputs.

AC MUA – These follow similar pattern as for AC single units ($p < 1.26e-5$, Friedman's test). At all stimulus lengths there is a difference between All and 3 ($p < 1.26e-5$, Bonferroni correction), and for all stimulus lengths between All and 5 ($p < 0.0164$). No between group differences are apparent for 3PCs vs 5PCs in this case.

IC MUA – there are between group differences visible for 15 of 17 stimulus lengths (significant p values < 0.0085). After post hoc analysis, between All and 3PCs, the median error of the All condition is significantly lower than 3PCs in 15 of the 17 lengths (significant p values < 0.0107). Between All and 5PCs is significant in only 2 lengths ($p = 0.018$ and $p = 0.049$).

In summary, there is a tendency in the AC for significantly better performance using All predictors, as opposed to only 3PCs. This would suggest that 3PCs are not sufficient to fully encapsulate the data. 5PCs is likely also not sufficient in the majority of cases, though the evidence is slightly less strong. In the inferior colliculus, there are no apparent differences between using any of the three inputs. This may be due to the overall lack of units (i.e. around 3-5), and the removal of datasets with fewer units than these for this comparative analysis, resulting in a low number of datasets for comparison (i.e. 16 out of 23 for single units). The overall low success of 3 or 5 PCs is indicative of the neural datasets being highly dimensional – 3-5 dimensions is not sufficient to fully encapsulate and describe the activity of the neuronal populations recorded.

Classification Success is Comparable Between AC and IC, but IC Achieves this with Fewer Inputs

For each individual stimulus length, and for single and multi units, the effect of brain area is examined. Given the relatively low performance of 3 and 5 PCs, these are not included in this analysis.

For every length, using single units, there are no significant differences when using "all" predictors ($p \gg 0.065$, Wilcoxon rank-sum test). This is the same for multi units ($p > 0.0783$, Wilcoxon rank-sum test). Examining the raw data, the IC has a higher range across all stimulus lengths, possibly due to some datasets having very poor performances (this will be discussed later). In summary, there appears to be no difference in performance between brain areas, despite datasets having varying numbers of input predictors. Ideally here, a paired test would be performed, but as simultaneous AC/IC data was not available for every set and every stimulus length, this reduced the numbers of sets available to be paired and so an unpaired test might

give a more trustworthy result at the expense of additional considerations during interpretation. Excluding all non-paired sets gave 16 datasets overall, and a Wilcoxon rank-sign test on these revealed no significant inter-area differences ($p > 0.958$). There were no differences for MUA either (20 datasets, $p > 0.179$).

There is No Strong Effect of Stimulus Length on the Success of Linear Classification

For all types of input (AC/IC single and multi units), there was an attempt to identify a trend of performance across time bins, since this was observed in previous literature. Even before multiple comparisons, there is no significant effect of time bin except for AC MUA (p values AC SUA: 0.4149, IC SUA: 0.9936, AC MUA: 0.0045, IC MUA: 0.2076, Kruskal-Wallis). After multiple comparisons (Bonferroni), this effect is not seen in any case. There is perhaps a slight tendency for middle lengths (around 250ms) to have a slightly lower median classification error (but also a wider range) – but this is purely observational.

Use of Multi Units Results in Higher Classification Success

For AC and IC, the difference between using single units or multi units as inputs is examined, for All predictors only. In the auditory cortex, using multi units results in lower performance error (significant $p < 0.0236$, Wilcoxon sign-rank test) for 14 of 17 stimulus lengths. In the colliculus, this difference is significant for all lengths ($p < 0.04$). A conclusion may be that the use of multi units results in better classification, most likely a result of an increase in the number of predictors.

Summary of Observed Results

In this section, median performance levels of all datasets are examined, looking for variables that have affected the classification result.

Using different sections of sound (i.e. different runs/stimulus sets) has resulted in no statistical differences, indicating that the effects are purely due to the number/type of inputs, or length of time examined.

As expected, using all of the available data results in the best performance, though in some cases, 5PCs can be sufficient to match this performance. 3PCs is likely not enough to fully encapsulate the variability of auditory cortex data – as explained later, this “explained variability” is in itself quite variable. There appears to be no differences between using AC or IC data, despite AC having in general, far more input predictors. This is something that will be examined later. Using multi units also improves

performance in both areas, again possibly because of the increased number of inputs. Evidence is lacking, but there is a slight trend for middle stimulus lengths (around 250ms) to perform better, albeit with higher ranges. There would appear to be a large variability in classification success across datasets, which is examined in the following analysis.

4.2.3 Explained Variance using Principal Components

As data is high dimensional, it would be beneficial if the activity/variability could be reduced down to a few components. This can give information about the underlying data, in terms of population structure and overall complexity. This also means models are easier to implement computationally (though results and correlates to brain functionality must be carefully considered). It has been previously seen that 3 PCs was not sufficient to represent the data – 5 was sometimes acceptable. Thus, the “explained” variance of each PC is plotted in Figure 4.3 below, for 4 example stimulus lengths. Note, this analysis did exclude some IC datasets that did not include 5 PCs (SUA 7, MUA 17).

The explained variance in the auditory cortex, especially for the first component, is highly variable, in all shown stimulus lengths. This variability decreases with successive principal components. In the IC, there is slightly less variance, and overall higher explained variance in the first component (not significant for single units, $p > 0.0846$, but is significant for multi units, $p < 0.0096$, Wilcoxon rank-sum test). Given the high variability, it is possible that in some datasets, 5PCs is not sufficient to explain more than 80% of the variance, which is the threshold aimed for with this kind of dimensionality reduction.

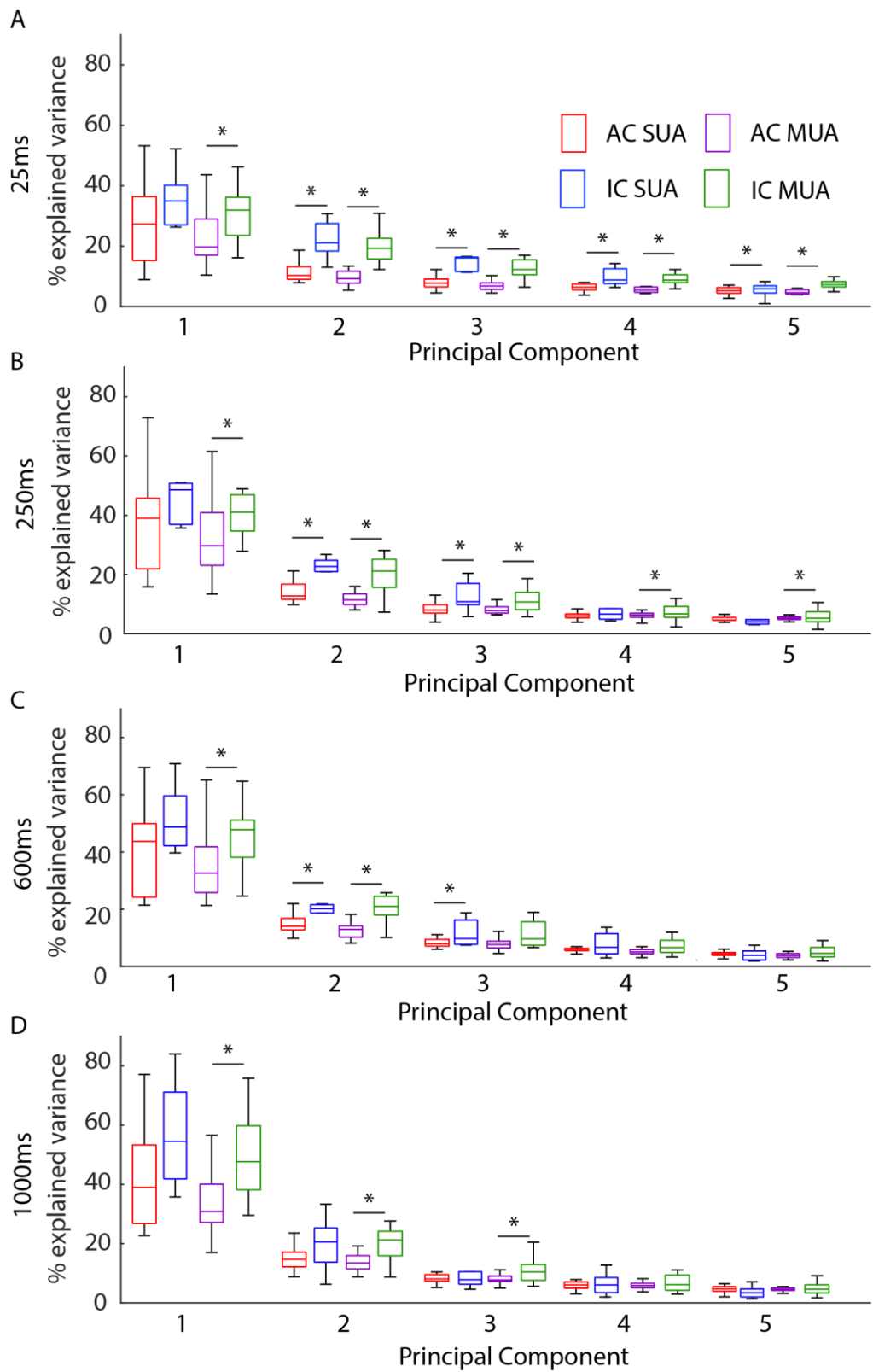


Figure 4.3: Explained variance in first 5 Principal Components. (A) Explained variance for each principal component, 25 ms stimuli length. (B) as (A), but 250 ms. (C) As previous, but 600 ms. (D) As previous, 1000 ms. Significance stars indicate a significant difference in the explained variance between the AC and IC in either SUA or MUA condition. Significant p values < 0.04 , Wilcoxon rank-sum test. Data is unbalanced, particularly for IC SUA. n : SUA 18 vs 7, MUA 17 vs 17

4.2.4 Positive and Negative Controls Reveal Reasons for Poor Performances

Poorly Performing Datasets

Summary analysis revealed that while good performance was possible, a lot of datasets were very close to chance level. One potential reason is that the data was indistinguishable from baseline (i.e. spontaneous firing) – this could happen if there were not many cells, or there were not many spikes. The spike rate during a given stimulus would then appear very low, potentially similar in appearance to the associated spontaneous activity. Therefore, the differences between each condition would be small, and accurate classification made difficult. Alongside the main analysis, negative and positive controls were also run.

Negative Controls Reveal Some Datasets are Indistinguishable from Chance Level

As outlined in methods, for negative controls, data is row shuffled, maintaining the overall spike rate but destroying the relationship between spiking and specific stimuli instances. Classification success is then expected to be ~ 0.9 , or chance level, and this is indeed the case for all data. This is summarised for run 1 in Figure 4.4, and in Table 4.1, where cells indicate for each dataset how many classification sets (of 17 stimulus lengths) were indistinguishable from row shuffled data.

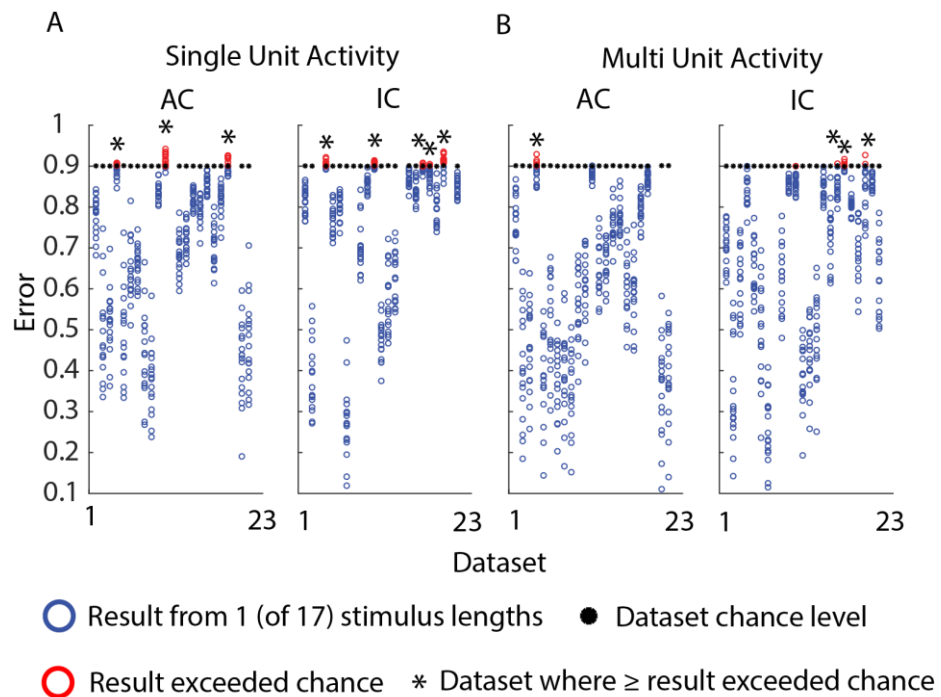


Figure 4.4: Negative control summary. Each column contains all stimuli of a single dataset, and plots their prediction performance. (A) Single units (B) multi units

Table 4.1: Negative control summary. Numbers indicate the number of stimulus lengths (max 17) that are indistinguishable from the associated chance level, for that dataset. Light grey shading indicates all stimuli were distinguishable (error < 0.9). Dark grey shading – no data for this set. The final column summarises the number of datasets where 1 or more time bins shows poorer performance than chance level, for each of 4 runs and 4 conditions.

Run	AC SUA																							
	1	2	3	4	5	6	7	8	9	10	11	12	13	14	15	16	17	18	19	20	21	22	23	Total
1				7							15													2
2				6							14													2
3				4							14													2
4				7							16													2
	IC SUA																							
1				11							9							6	2		12			5
2				13							8							9			13			4
3				7							7							5	3		9			5
4				12							11							7	2		13		1	5

Table 4.1 Continued

Run	AC MUA																							Total
	1	2	3	4	5	6	7	8	9	10	11	12	13	14	15	16	17	18	19	20	21	22	23	
1				4																				1
2				7																				1
3				6								1												2
4				3								1												2
	IC MUA																							
1											1						1	8			2			4
2																		7			2			2
3															1			6			5			3
4											1							9			4			3

This summary plot has helped identify a potential issue. Comparing normal results to negative controls, in certain datasets (x-axis), most stimulus lengths (each blue circle) are greater than or equal to that dataset's negative control (black). This is also seen in Table 4.1 – across all the runs, it is generally the same datasets whose runs are equal or worse than shuffled controls. Thus, the reason these datasets perform badly in classification is that a significant portion of stimulus length sets are indistinguishable from each other, resulting in poor classification. MUA generally sees less of these situations.

Positive Controls Indicate Some Stimuli May be Indistinguishable from Spontaneous Activity

This issue is examined further using positive controls. In these, for each *individual* stimulus in a set (i.e. 10 total), a binary classification analysis is run, to see if the stimulus is distinguishable from a period of spontaneous activity (of equal length) directly before the sound starts. In this case, chance level will be 50%

Due to the high number of repetitions, even if numbers were very close together, the stats indicated significant differences. Thus, for clarity, positive control results are quantified by how many of the binary classifications (out of 10) gave an error of < 0.5 , in Figure 4.5.

In some cases, results were returned as NaN – this was because the classification in some repetitions could not be performed due to very few/no spikes and thus trials being indistinguishable from each other. As this could be partially due to low spontaneous activities, these sets were not strictly considered as being “indistinguishable from spontaneous” – while indeed they might be, a more conservative estimate is taken. If NaNs are included, the overall conclusion from positive controls does not change, it simply increases the number of indistinguishable sets.

Looking at the three example time bins in Figure 4.5, there is a clear trend between number of indistinguishable stimuli, and error – if more stimuli are indistinguishable, the error tends to increase. It is most obvious at the lowest performances – before ~ 0.8 , there is not much of a relationship. Thus, this may be one of the factors having an effect for particularly poorly performing datasets.

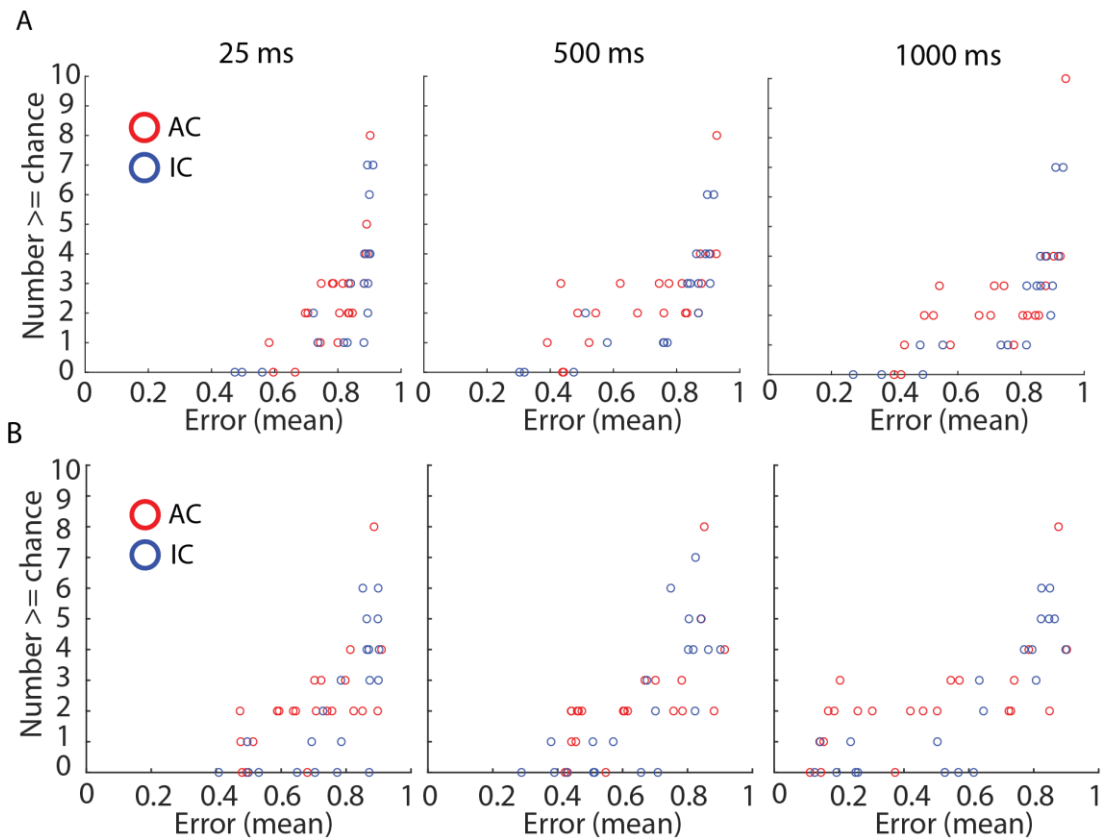


Figure 4.5: Number of stimuli indistinguishable from chance, against classification error of the dataset, for three selected stimuli lengths. (A) SUA (B) MUA. Red – AC, Blue – IC.

4.2.5 Number of Predictors has Effects on Classification Performance

Brief Summary

The above can partly explain low performances, but sheds no light on the underlying mechanistic reason behind classification performances. It has been observed that using multi units, and more predictors (All vs PCs) tends to result in higher performance levels. This is logical as there is more data to cover the variability. In this next section of analysis, the relationship between number of predictors and prediction performance is summarised. Figure 4.6, contains scatter plots of the number of predictors in a dataset versus its classification outcome, and overlays simple linear regression lines.

What is apparent from the example lengths in Figure 4.6, from boxplots summarising the lines of best fit, and previous summary comparisons in Section 4.4.2 is that the IC is able to reach comparable performance levels to the AC, but with fewer predictors. It should be noted that this relationship is not necessarily seen within a single dataset, and is more of a generally trend or potential, though what little paired data (i.e. an animal having a both a high quality AC and IC dataset, with a high number of single

units for direct comparisons) exists at least suggests this relationship exists within simultaneous datasets.

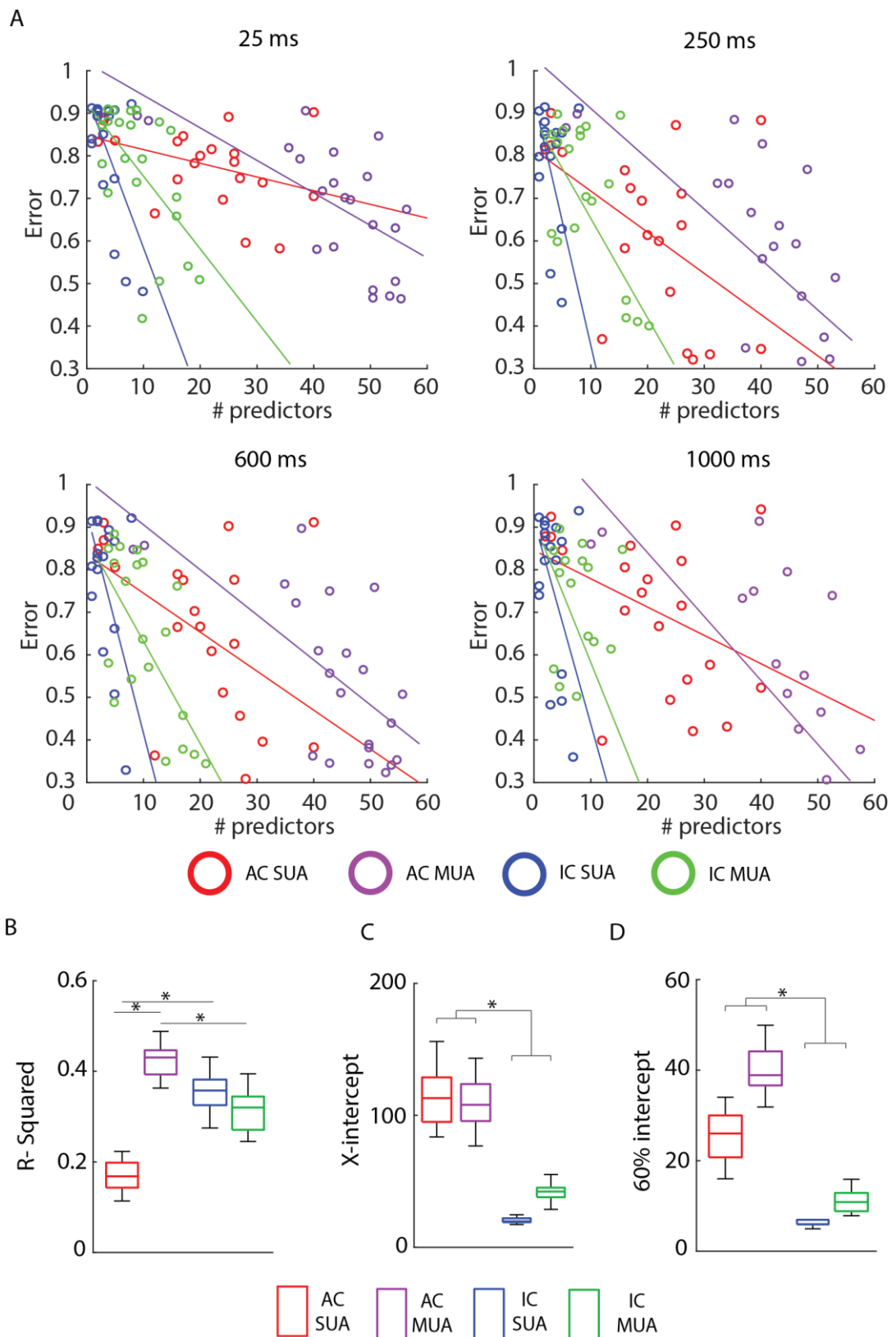


Figure 4.6: Number of predictors vs performance for example 4 time bins, for single/multi units in the auditory cortex and inferior colliculus. (A) Clockwise from top left: 25 ms, 250 ms, 1000 ms, 600 ms. Straight lines indicate line of best fit (MATLAB fitlm), circles are individual data points (datasets). (B) Boxplots of values derived from best fit lines. Significance stars indicate a p value < 0.0028, Bonferroni after Kruskal-Wallis).

Number of Predictors and Classification Success are Linearly Correlated (R^2)

Examining the adjusted R squared values across all stimulus lengths (Figure 4.6), the strength of the linear relationship between performance and number of predictors is described. There are differences between all groups except IC SUA and MUA ($p = 1$) and IC SUA and AC MUA ($p = 0.0847$). Otherwise, p values are all < $8.1332e-4$ (Bonferroni after Kruskal-Wallis).

Overall, the AC multi units have the strongest relationship ($R^2 = 0.433$), closely followed by IC SUA (0.3582) and IC MUA (0.3215). In AC single units, there is a trend, but the relationship is not very strong ($R^2 = 0.1681$). In general, there appears to be a strong relationship between the number of predictors and the performance level.

IC Can Achieve Comparable Results to AC but with Fewer Inputs (x -Intercept)

To quantify how many predictors are needed to attain good performance, the x -intercepts of the data are examined, including all stimulus lengths (Figure 4.6B). Differences between single and multi units cannot be distinguished in either the AC ($p = 1$), or the IC ($p = 0.0732$, Kruskal-Wallis), despite the visual differences in best fit lines in Figure 4.6 In AC vs IC comparisons, AC x -intercepts were significantly larger (AC SUA vs IC SUA $p = 4.1587e-10$, AC MUA vs IC SUA $p = 1.11e-8$, AC SUA vs IC MUA $p = 3.5573e-4$, AC MUA vs IC MUA $p = 0.0028$, Bonferroni correction after Kruskal-Wallis).

These comparisons reveal clear differences between AC and IC intercepts. As the x -axis displays the number of predictors, this indicates that theoretically, the IC would be able to achieve “perfect” performance using fewer inputs than the AC. This means that there is something fundamental about the IC data that makes it more successful/more efficient at representing sound when partitioning it in this way.

Assuming no plateau within the data, and that the overall potential of each area has not been reached, it can be stated that there is a clear difference between areas – while performance levels are comparable/indistinguishable between areas, these levels are able to be reached with differing numbers of predictors. The issue of plateauing will be discussed later.

IC Can Achieve Comparable Results to AC but with Fewer Inputs (0.6 Intercept)

As further quantification, the intercept of the best fit line with a performance level of 0.6 is plotted in Figure 4.6B.

AC single units were not different from AC multi units ($p = 0.3260$), but both had significantly higher intercepts than IC single and multi units (*AC SUA vs IC SUA* $p = 7.6755e-7$, *AC MUA vs IC SUA* $p = 3.4752e-12$, *AC SUA vs IC MUA* $p = 0.0281$, *AC MUA vs IC MUA* $p = 1.2092e-5$, Bonferroni after Kruskal-Wallis). IC SUA and MUA can also not be distinguished ($p = 0.0847$). Thus, the same differences between AC and IC seen using the x-intercept measurement are confirmed.

Summary of Predictor Number Results

This analysis leads to potentially interesting avenues to explore – what is it about IC data that makes it better for classifying natural sound segments? In the next analysis, data is not partitioned into individual datasets and is collated as all cells/multi units together, to focus on fundamental neuronal population differences.

The preceding section is summarised by saying that there is a clear (but not strict) relationship in each set of data between number of predictors and overall classification performance – this is expected, by simple virtue of having more information to work from. By examining details of this relationship however, it is also seen that statistically, the inferior colliculus may be able to reach comparable classification performance to the cortex (using both paired and unpaired data), despite having a fewer number of predictors. These apparent differences provide motivation for examining the input to the classification further. The following section looks for potential differences and variables that may be causing the previous observations, and speculate as to what results mean for neuronal population coding overall.

4.2.6 Dataset Frequency Range May Affect Classification Performance

Rationale

Natural sound is composed of many frequencies. Naturally then, if the neurons recorded cover more of the tonotopic gradient, a hypothesis is that distinct responses for different stimuli are more likely. This is quantified by calculating the frequency range for each dataset. As outlined in Materials and Methods, this involves finding the best frequency of all tuned units (to prevent false data skewing range), then taking the maximum and minimum frequency to find the range. This is expressed in octaves.

Frequency Range Increases with Number of Predictors

First, how the frequency range changes with varying numbers of predictors is considered. Here, the frequency range is defined as the number of octaves between each dataset's highest frequency tuned cell and its lowest. It is viable to suggest that sets with low numbers of units may not cover the full range (particularly in the ICC which is strongly tonotopic across the depth of recording). This potential relationship is quantified frequency range against the number of predictors is plotted in Figure 4.7, with lines of best fit plotted across data points to visualise the strength of any linear relationships.

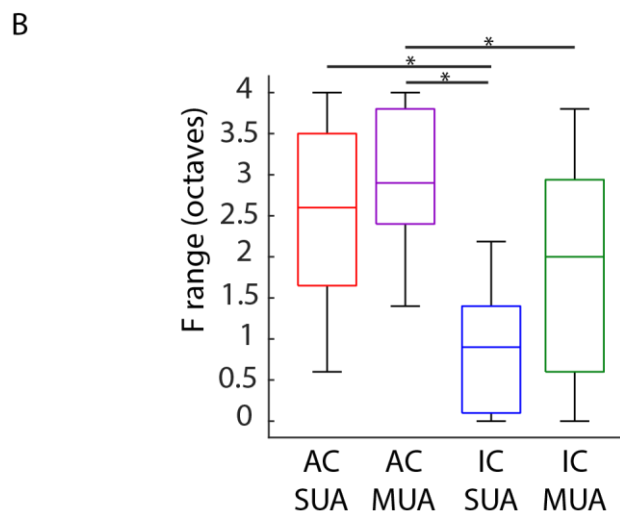
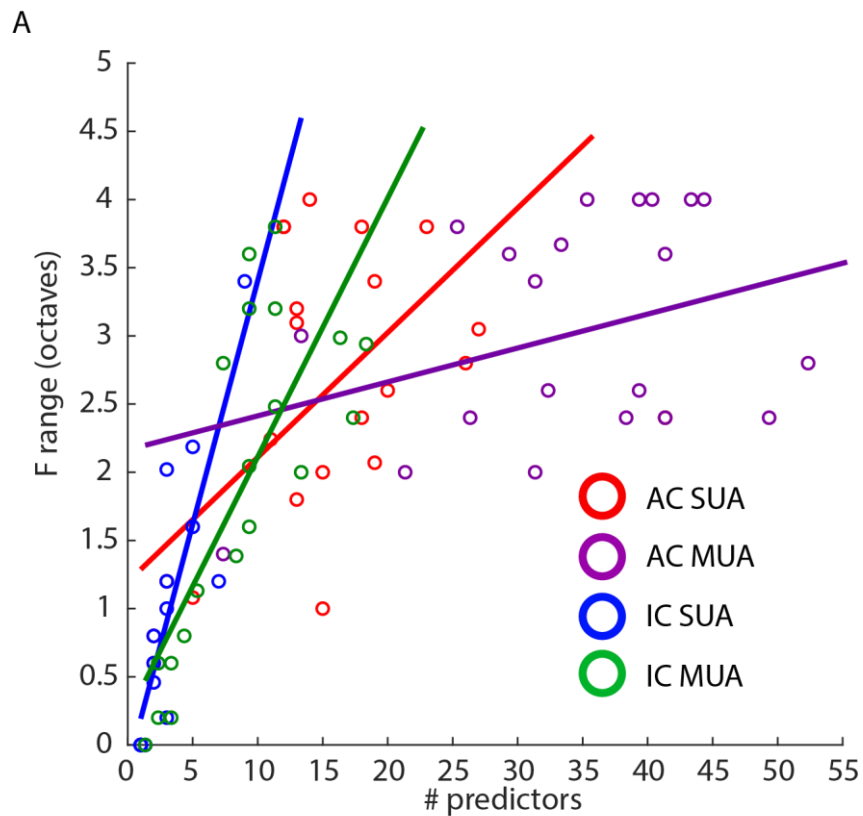


Figure 4.7: Relationship between frequency range and number of predictors. (A) Scatter plots and best fit lines indicate the relationships between frequency range and number of predictors for each type of data input. (B) Frequency ranges as boxplots for all conditions, significance stars indicate $p < 0.0089$, Bonferroni after Kruskal-Wallis).

Particularly for the IC, as expected, there is a strong relationship between the number of predictors and the resultant frequency range, for both single and multi units ($R^2 = 0.7038, 0.5965$). AC single units show the same trend (0.3129), but multi units do not (0.0693). The lack of a relationship for multi units is logical – within a single shank, cortical layers do not have a laminar tonotopy so adding more cells doesn't necessarily increase the tonotopic range. In the ICC, more electrodes indicate that more of the tonotopic range is covered, resulting in a stronger relationship. Also of note from this summary and in particular Figure 4.7B is that the IC ranges are not larger than the AC ones.

Frequency Range May be Linearly Correlated with Classification Success

Next, frequency range against performance is plotted to see if the range has a direct influence on the dataset performance. This is seen in Figure 4.8, for 4 example stimulus lengths (all are included in Figure 4.8B).

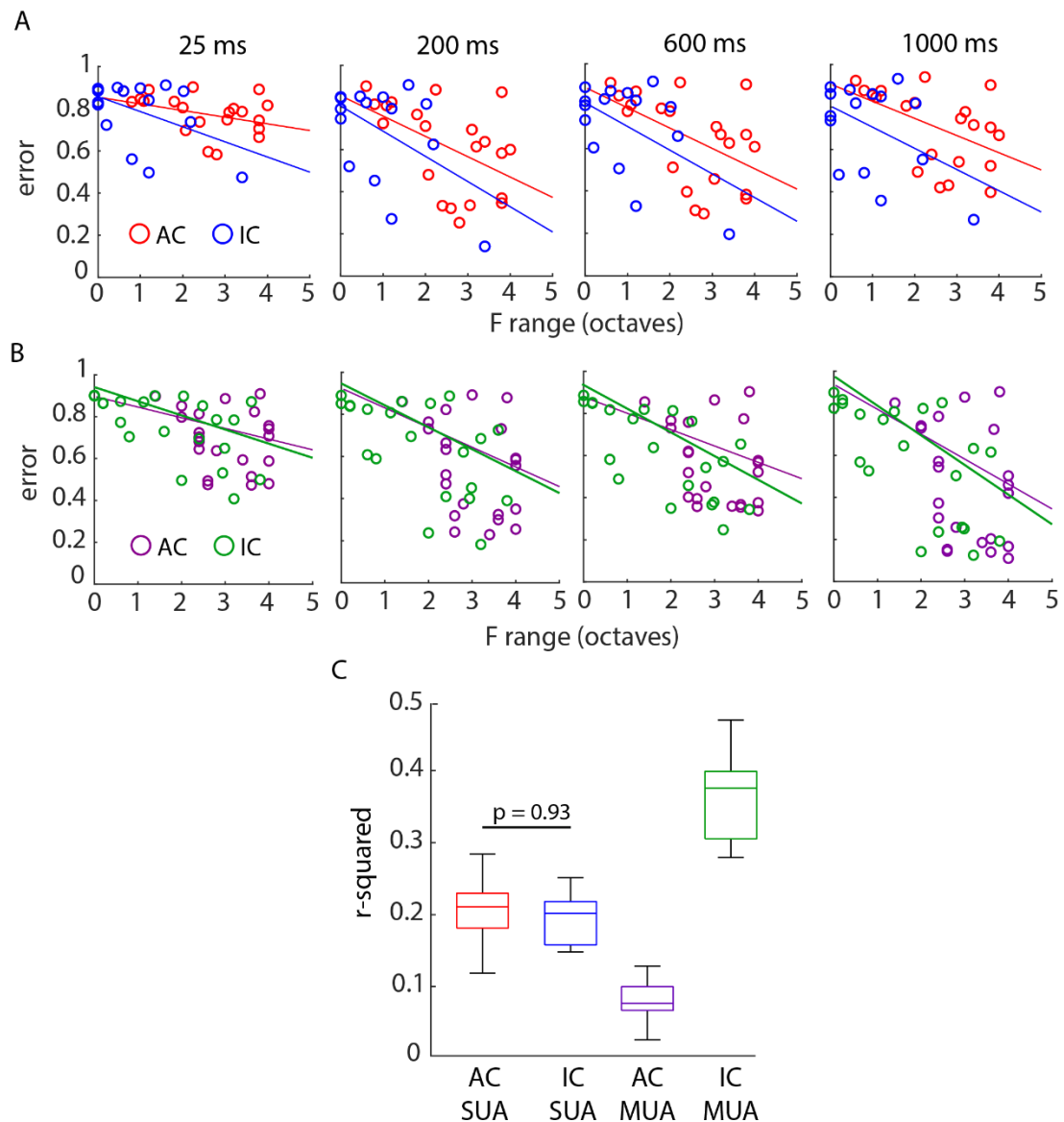


Figure 4.8: Frequency range and prediction error of all datasets. (A) Frequency range against error for single units, 4 example stimuli lengths. Red = AC, Blue = IC (B) As (A), but for multi units (purple = AC, green = IC) (C) Boxplots of r-squared values summarising all stimuli lengths. All groups are significantly different ($p < 0.0027$) except AC SUA vs AC MUA ($p = 0.9286$, Bonferroni after Kruskal-Wallis).

In the example figures, there are rough trends of performance increasing as frequency range increases, with no clear differences between AC and IC. The median R^2 are not particularly high, but support the visual trend.

Looking to Figure 4.8, there is evidence of some linear relationship between frequency range and performance, except in IC SUA ($R^2 = 0.211, 0.202, 0.076, 0.375$

respectively). It is particularly strong for inferior colliculus multi units at 0.375. The relationship strengths are all significantly different ($p < 0.0027$, Bonferroni after Kruskal-Wallis), except between AC SUA and MUA.

With this evidence, it can be said that having a high range of frequencies covered (and in turn, a generally higher number of predictors) results in better performance, and that the IC often has comparable frequency ranges to the AC, indicating it may be a slight influence for IC datasets performing better, with fewer inputs.

4.2.7 Trial-by-Trial Spike Count Variability (Fano Factor)

Use of Fano factor

In this analysis, the neural data provided (i.e. multiple trials of the same stimuli) is used to create a model that best represents this data overall. If any one trial is a good representation of all trials (i.e., if there is a low trial-trial variability), the classification is expected to perform better. Thus, in the next series of analysis, trial-trial variability of units is quantified using the Fano factor metric (see Materials and Methods). The Fano factor is calculated for each of the 10 stimuli, then a median taken to represent that cell. The data displayed and the stats use the median, as the data was skewed. It should also be noted that outliers are omitted in the figures for clarity but are included in the calculation of medians and in statistical tests.

Summary of Fano Factors Reveals Differences between Brain Areas

In Figure 4.9, boxplots of Fano factors in each brain area and across stimulus lengths are displayed.

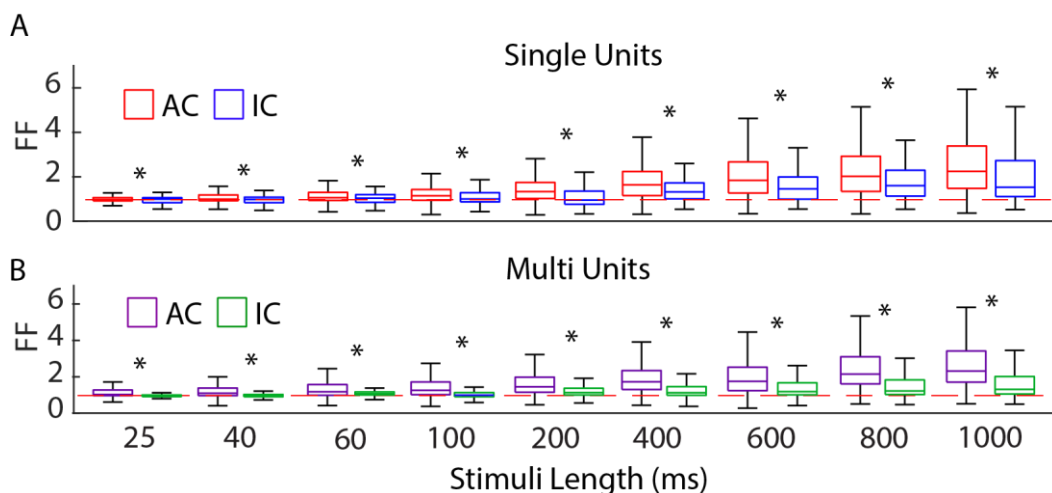


Figure 4.9: Summary of Fano factor in single and multi units in the auditory cortex and inferior colliculus, for increasing time window. Not all stimuli lengths are shown, for clarity. (A) Fano factor comparisons between AC and IC for single units ($n = 436$ and $n = 67$). Significance stars indicate p values < 0.01 , Wilcoxon rank-sum tests for each stimuli length. (B) as A, but for multi units ($n = 973$, $n = 201$). Red dotted line indicates a Fano factor of 1 for comparison purposes

Fano Factors are Smaller and Less Variable in the IC Compared to AC

Comparing the Fano factors between AC and IC single units, separately for each stimulus length, the IC is significantly lower, for all stimulus lengths ($p < 0.0067$, Wilcoxon rank-sum test). This is also seen in MUA data ($n = 973$ vs $n = 201$, $p < 3.97e-18$). Despite the very unbalanced data, it appears that overall, IC Fano factors are smaller during all the natural sound sub-stimuli presented.

Cortical Multi Units Display Significantly Smaller Fano factors

For each stimulus time individually, and for each brain area, the Fano factor differences between the single unit and multi unit populations is examined. For the auditory cortex, there is a significant difference, with multi units having lower variability ($p < 0.02$, Wilcoxon rank-sum test). This is not seen in the inferior colliculus (only in the first stimulus, $p = 0.033$), otherwise, $p > 0.098$. A reason for this may be the overall low numbers of IC units – potentially, a given IC multi unit may be made of only one or two single units, so will be more directly comparable.

There is a Trend of Increasing Fano factor with Increasing Stimulus Length

There is a general trend of Fano factor increasing with stimulus length, with there being a significant effect of stimulus length for all situations examined ($p \ll 0.01$, Kruskal-Wallis). Post hoc comparisons confirm this trend. Summarising briefly, in the AC single units, each stimulus is indistinguishable from 2-3 stimuli on either side but is significantly different from all others ($p < 0.01$, Bonferroni after Kruskal-Wallis). For multi units, this group overlap is smaller (0-2 stimuli). The IC shows the same general trend, but with far higher overlaps (4-6 stimuli at least, on either side).

Fano Factor is Linearly Correlated with Classification Success in Most Cases

These results are promising – there is a clear inter-area difference that can account for the better performance we see. If each individual cell is less variable, there is less variability to negatively affect classification performance, meaning a stimulus can be represented by a smaller number of reliable units. Now, the effect of Fano factor is performance can be directly assessed and represented in Figure 4.10.

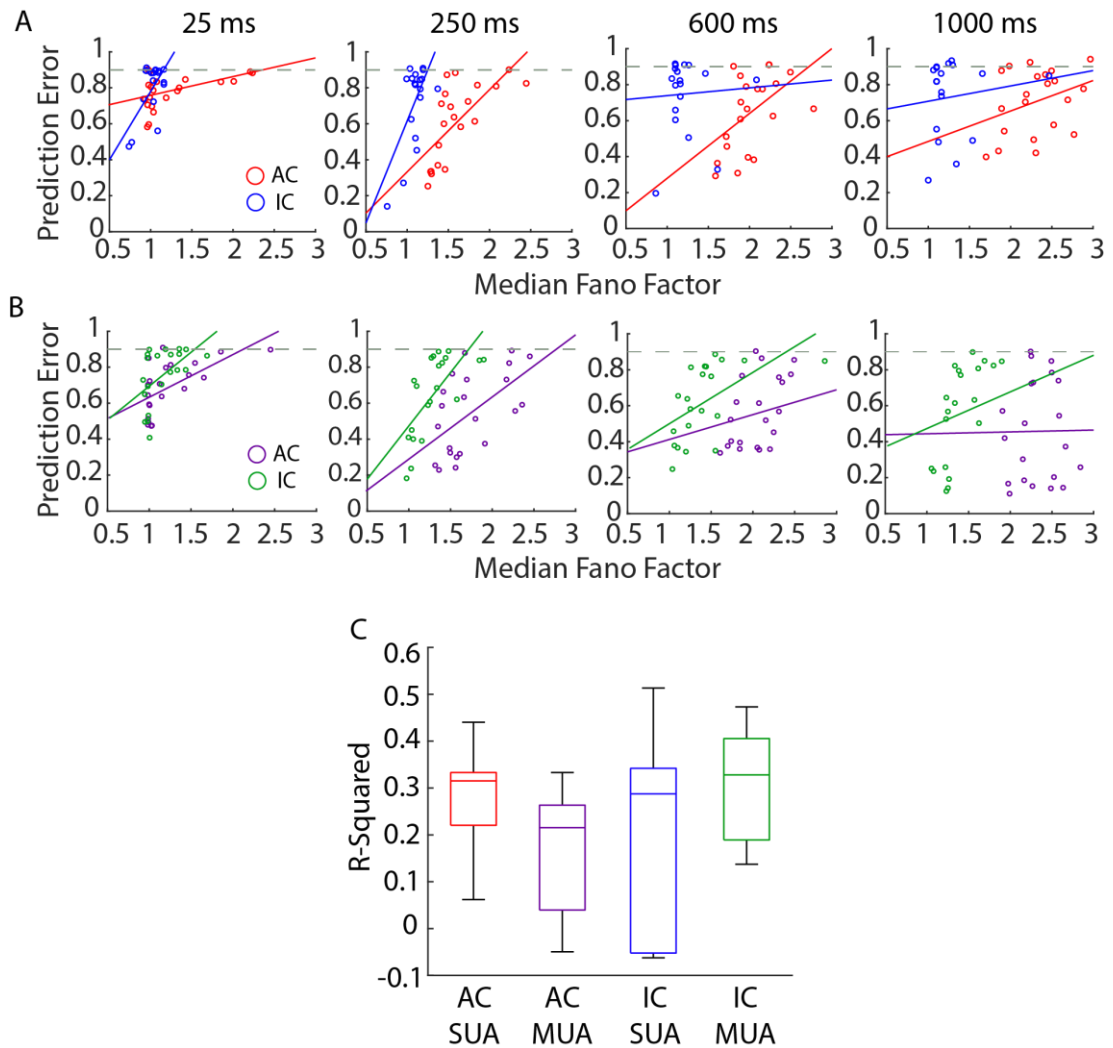


Figure 4.10: Relationship of Fano factor and prediction error. Each point represents a single dataset, median Fano factor of the unit in that dataset (A) Scatter plots and best fit lines for 4 example stimuli lengths. Red – AC, Blue – IC. (B) As in A, but for multi units. Purple – AC, Green – IC. (C) Adjusted R squared values of best fit lines across all stimuli lengths. All relationships are significantly different except AC SUA vs IC SUA, other p value range: $3.77e-13$ - 0.0027 , Bonferroni after Kruskal-Wallis)

The median Fano factor is taken for the units in each dataset, and used to assess the strength of a linear relationship.

In Figure 4.10, 4 example stimuli are displayed, in which the influence of Fano factor is visible in most cases. In general, there is evidence of a linear relationship (R^2 : 0.351,

0.287, 0.215, 0.3279 for AC SUA, AC MUA, IC SUA and IC MUA respectively). The R^2 values are summarised in Figure 4.10C, with medians reasonably similar, but some stimulus lengths appearing to have a bad relationship, especially in the IC single units. Middle stimulus lengths appear to have the best relationships.

In summary, Fano factor is an influencing factor on the performance – and with the Fano factor of the IC cell population being significantly smaller than the AC, it can be surmised that this is a further contributing mechanism to the ICs comparable performances.

Narrow Spiking Cells Display Higher Trial-Trial Variability

Given a previous observation of cell type specific differences, Fano factor between cell types in the AC is also explored. The cortex appears more variable - it may be that one cell type is particularly influential.

A tentative hypothesis is that narrow spiking cells, being heavily involved in tuning, and having a tendency to be faster spiking, will be less variable. As shown in Figure 4.11, this was not the case.

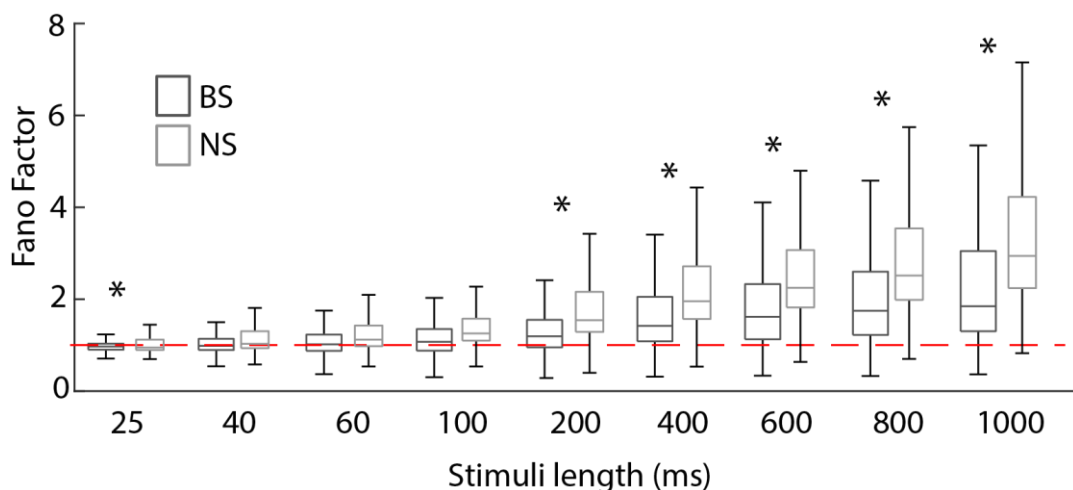


Figure 4.11: Fano factor differences between narrow and broad spiking cells in the auditory cortex. Selection of stimuli shown for clarity. Broad, dark grey, $n = 297$, Narrow, light grey, $n = 297$. Significance stars note a p value of < 0.031 , Individual Wilcoxon rank-sum for each stimulus length. Red line indicates a Fano factor of 1

For the majority of stimulus lengths, narrow spiking cells have a significantly higher Fano factor ($p < 0.031$, Wilcoxon rank-sum tests) than broad spiking, though the data is variable. This is interesting, as the opposite was expected given narrow spiking are also generally fast spiking. It is a possibility that, due to the long recording time, the

cortex experiences state changes, which in turn affects frequency tuning - in which narrow spiking cells are important.

As with the general data, there is a trend for higher stimulus lengths to be significantly more variable trial-trial. With broad spiking cells, using Bonferroni comparisons, there are 3-4 groups overlapping on either side of each stimulus. This is the same for narrow spiking cells (but with slightly less of an overlap)

4.2.8 Relationship of Spike Rate versus Classification Performance

A potential influencing factor may also be spike rate – lower spike rates, either biologically or due to spike sorting errors, may adversely affect the prediction performance by having less information to work with. The spike rate for each single or multi unit was derived as a single average over the ~20 minutes of natural sound.

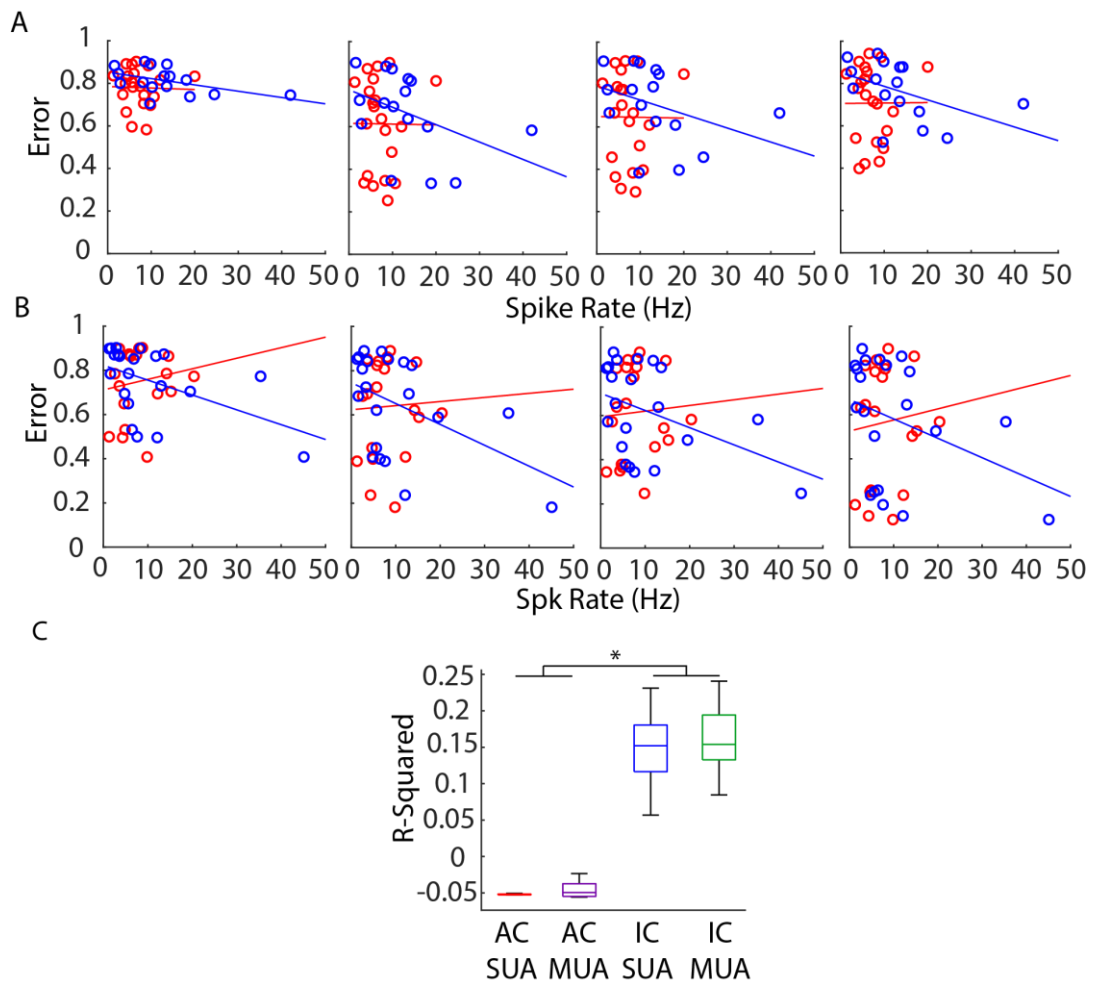


Figure 4.12: Relationship between spike rate and prediction error. (A) example 4 stimulus lengths with scatter plots and best fit lines, illustrating the relationship for single units. Red – AC, Blue – IC. (B) as A, but for multi units. (C) Boxplots summarising R-squared values of the best fit line for each stimulus. Significance stars indicate p values < 0.045 after Kruskal-Wallis, Bonferroni corrections.

There is no clear relationship for the auditory cortex (median R^2 , -0.05237, -0.04949). For IC, the relationship is slightly stronger and is more visible in Figure 4.12A. ($R^2 = 0.15207, 0.15394$). It may be the low numbers of predictors is influencing the results – as more predictors are added, there is a natural chance of increasing the range of spike rates. Thus, it can be said that in the IC, spike rate may be influencing performance, but not to a high degree.

The relationship of median spike rate against number of predictors is also briefly examined (not displayed graphically). There was only a relationship for IC single units and AC multi units ($R^2 = 0.4321, 0.2972$, vs -0.0320, 0.015 for AC single and IC multi units).

4.2.9 Noise Correlations and Classification Success

Noise correlations are known to effect or be a part of neural coding, and so may be contributing to the performance. If a pair of neurons are noise correlated, this means their firing shows a high level of correlation that is unrelated to any ongoing stimuli – implying a potential shared input. If noise correlation is high among neuron pairs, it may be likely that the actual signal evoked changes are “getting lost” among high noise, and responses to individual stimuli are very similar. Characterisation of these fluctuations is desirable, to then look at their potential contribution to performance.

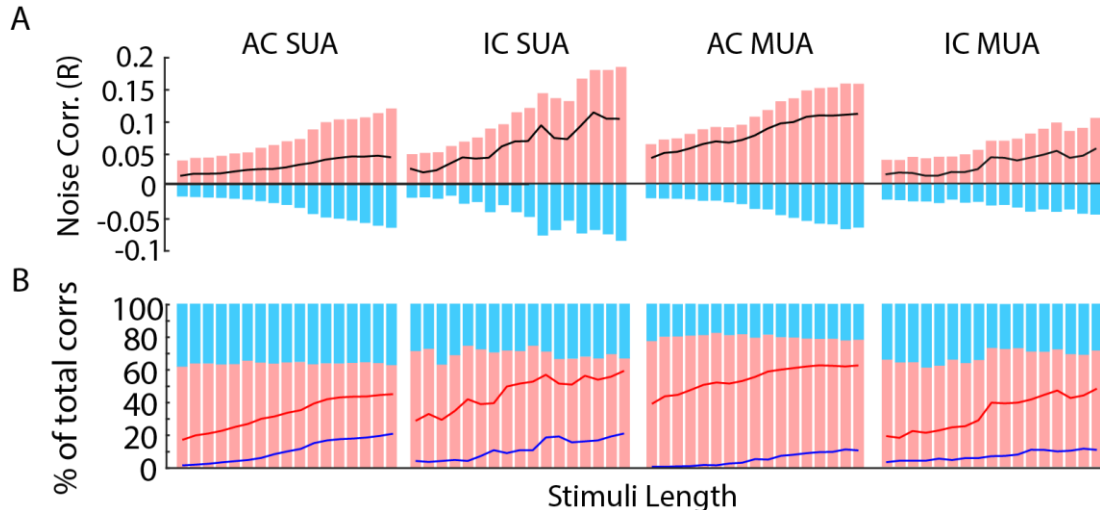


Figure 4.13: Summary of pairwise noise correlations across increasing time windows, for single and multi units in the auditory cortex and inferior colliculus. (A) Mean signal correlations at each stimulus length (25-1000 as previous) – blue = negative, pink = positive. Black line indicates the median. (B) Proportion of each type of noise correlation. Pink/red – positive, Light blue/blue – negative. Lines indicate the proportion of significant correlations at each stimulus length $p < 0.05$. Stimulus lengths not shown, go from 25-1000 ms

First, pairwise noise correlations are plotted to simply observe any potential differences, in Figure 4.13.

Average Pairwise Noise Correlations are Small and Positive, Positive Correlations Dominate, Correlations Increase with Stimulus Length

Taking the median correlation at each stimulus length (black line, Figure 4.13) overall, correlations are positive. This is confirmed by observing that positive correlations (pink) are generally higher than negative (blue). Considering proportions, overall, in the auditory cortex, ~60% of the calculated correlations are positive, while 40% are negative. This value includes all correlations, not only significant ones ($p < 0.05$). Looking purely at significant correlations, in the AC, the proportion of both positive and negative correlations increases steadily from ~0 for 25ms length, up to ~50%/30% by 1 second (red and blue lines, Figure 4.13B). In the inferior colliculus, more of the correlations are positive (~70%), with slightly more being significant compared to AC. The relationships are very similar in multi units, except that they reach overall higher correlations.

It is also seen that the strength of correlations increases with time bin, both positive and negative, and for both areas. Overall, taking the median (black), there is a small, increasing positive correlation. In general, positive correlations have a higher amplitude than negative. Again, this is the same in multi units, but with the larger amplitudes overall when compared to single units.

The above relationships are similar in multi units, except that the proportion of positive correlations has increased, as has the proportion of significant correlations. Inferior colliculus multi units seem to have both smaller and less noise correlations than the corresponding cortex.

IC Pair-Wise Noise Correlations are Higher than AC

For single units, there is a significant effect of area on all correlations, with the IC having higher correlations at 16 of 17 stimulus lengths ($p < 0.0286$, Wilcoxon rank-sum test). For positive only, this is the same ($p < 0.0012$), but there are only two lengths that show differences when looking solely at negative correlations ($p = 0.0422$, $p = 0.0014$, Wilcoxon rank-sum test).

For multi units, the AC now has higher noise correlations than the IC, at all stimulus lengths, for all correlations, ($p < 4.03e-29$) and positive only ($p < 7.66e-24$), but for 12 of 17 for negative ($p < 0.046$).

AC Multi Units have Higher Noise Correlations than Single Units, with the Opposite True in the IC

In the AC, multi units consistently have a higher correlation than corresponding single units, when all correlations are considered at all stimulus lengths ($p < 2.17e-161$), and also for positive only ($p < 2.08e-50$) and negative ($p < 0.0181$, Wilcoxon rank-sum tests).

In the IC, single units are higher using all correlations for 12 of 17 lengths ($p < 0.047$), 16 lengths of positive ($p < 0.044$) and 10 for negative ($p < 0.0166$, Wilcoxon rank-sum tests).

Summary of Pairwise Noise Correlation Strengths

In summary, there is a clear effect of area on correlation strengths (particularly if all or only positive correlations are included), but this effect reverses if using single or multi units. This reversal is also observed between AC and IC - with the AC, multi units have higher correlations, with the opposite in the IC. This may be due to fundamental differences between cortical and colliculus multi units/populations, but due to the very unbalanced nature of the comparisons in a lot of cases, this conclusion should be taken with caution. There is no particular pattern to which stimuli show significant differences (or do not).

Exceptionally Poor Classification Performance is Accompanied by High Noise Correlation

Now that correlations are observed to be present in the data, a potential relationship between these correlations and the performance of our datasets is explored. Scatter plots (Figure 4.14) of a run's average correlation are created (median of all constituent pairs) versus the dataset's performance, for a selection of 4 stimulus lengths.

Through the examples in Figure 4.14, generally, there is no linear relationship between median correlation strength and performance, as most correlations are small, the line is nearly vertical. In some instances, there is a slight suggestion of a relationship, due to one or two datasets low performing datasets having particularly high median correlations. Given the remainder of the data however, it cannot be said there is a particularly *linear* relationship here, and particularly high correlations may just be a potential indicator for especially bad performance. It would be expected that high noise correlations would cause this by blurring the lines between stimuli and making them indistinguishable from one another. Table 4.2 shows the relationships

for each condition and each type of correlation – displayed as a table for clarity due to low values.

In the case of AC MUA (bold, Table 4.2), all and positive correlations, there is slight evidence of a relationship, but this is not seen across all bins (see the high standard deviation).

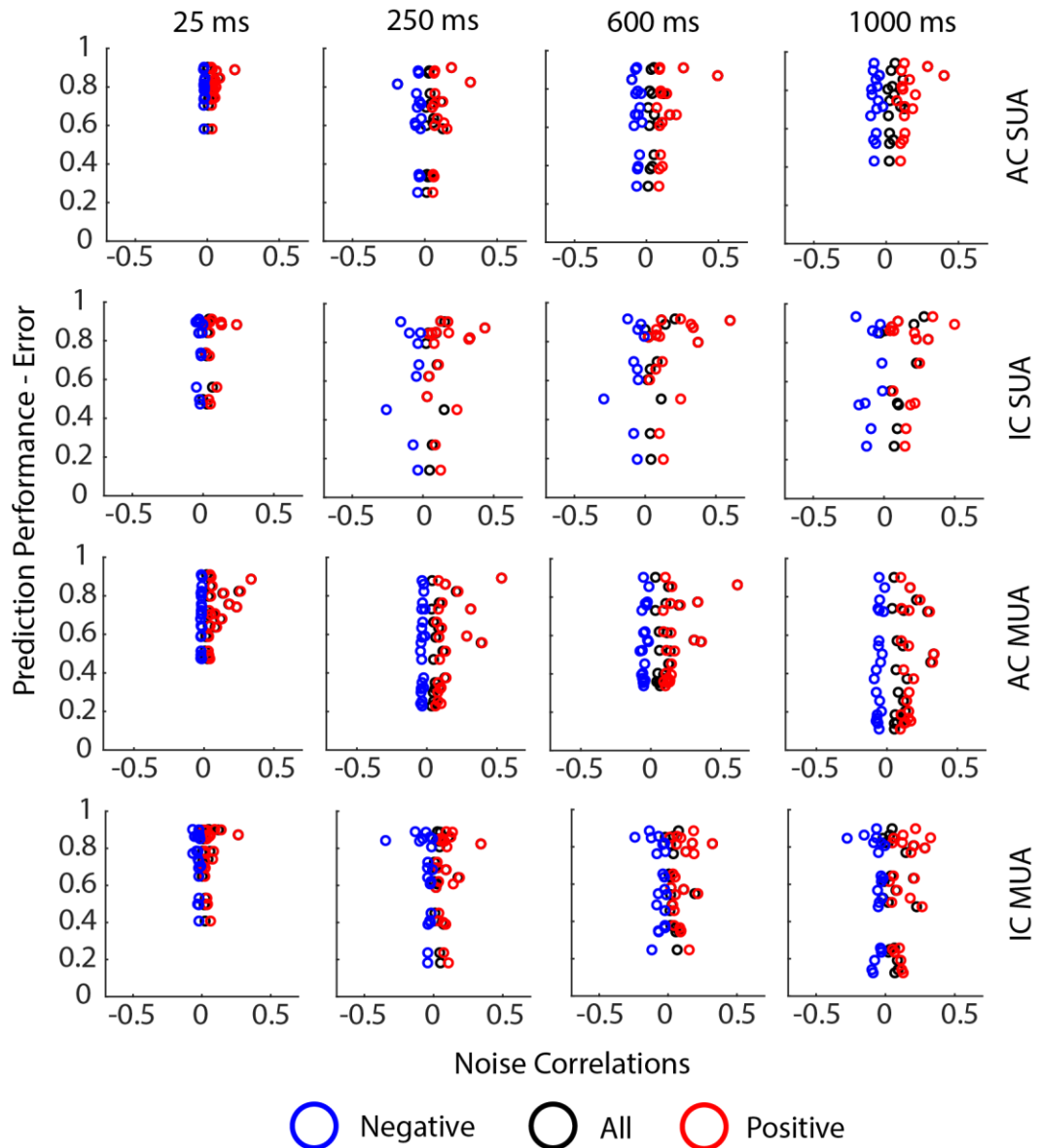


Figure 4.14: Relationship of pairwise noise correlations and prediction error. Rows, top to bottom show different input types, columns are 4 example stimulus lengths. R-squared values are summarised in Table 4.2

Table 4.2: Relationships (*R squared*) between pairwise noise correlations and prediction performance.

Bold numbers indicate some evidence of a relationship

Condition (mean (STD))	All Correlations	Positive Only	Negative Only
AC SUA	0.056 (0.061)	0.085 (0.059)	-0.045 (0.040)
IC SUA	0.005 (0.052)	-0.004 (0.045)	-0.036 (0.080)
AC MUA	0.133 (0.042)	0.127 (0.042)	0.069 (0.079)
IC MUA	-0.020 (0.022)	0.048 (0.034)	0.025 (0.057)

In summary, it can be said that for either brain area, noise correlations do not have a linear relationship with prediction performance, but that particularly high correlations may be indicative of a poorly performance (i.e. near chance level) dataset. Because of this poor relationship, and reasonably similar strengths between AC and IC it is probably not worth directly comparing the two brain areas directly, and instead the focus is put on analysing the differences within each area

Proximity of Neurons in a Pair may have an Effect on Levels of Noise Correlation

Because some area differences are observed, and at least an observational relationship, it would be interesting to confirm a mechanism for the correlations seen. It is known that correlations are higher the closer neuronal pairs are together, but a simple distance calculation between pairs did not reveal such a relationship. Literature also suggests that the layer location, as well as the true physical distance, has an effect on the strength of correlations. Thus, in the cortex, cell pairings were split into 6 groups, as seen in Figure 4.15 – see also Materials and Methods for a graphical explanation of pairing naming conventions. Briefly, local (L) in the first half of the pairing name means both cells of the pair are on the same shank, distal (D) means they are on different shanks. Superficial (Su) indicates both cells are on or above the sink channel, deep (De) are below this, and pairing may also contain a superficial and a deep cell (SD). Firstly, the correlation strengths for each of these groups is plotted, as all correlations, then positive and negative only. Only the highest time bin (1000ms) is selected, though relationships for other stimulus lengths are summarised and confirmed in Figure 4.15C and E.

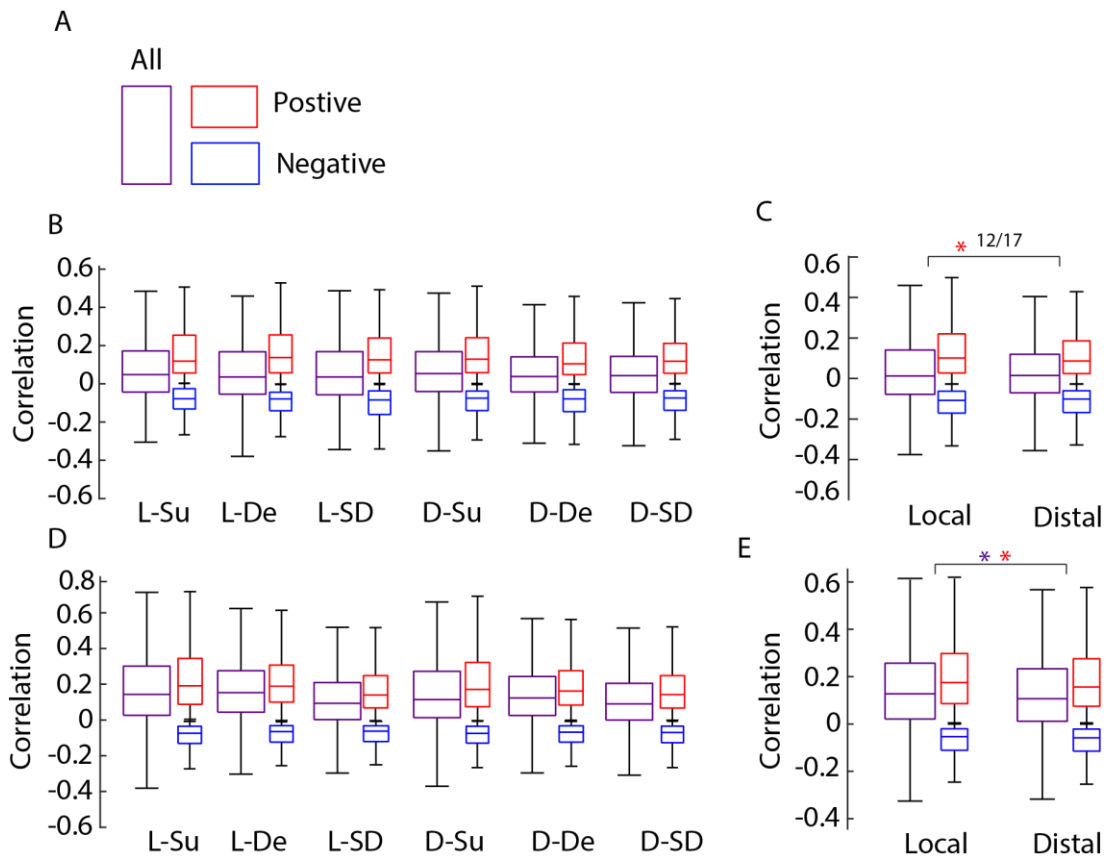


Figure 4.15: Effect of cortical depth on pairwise noise correlations . Key – L = local/both cells on the same shank, D = deep/each different shanks, Su = both Superficial, De = both deep, SD one superficial, one deep. (A) Key (B) All (purple), Position (red) and negative (correlations) for different kinds of cell pairs. See text for stats breakdown. (C) As (B), but split only into local and distal pairings. Coloured significance stars indicate a significance for all stimulus lengths at that type of correlations, $p < 0.05$, unless otherwise stated, for Wilcoxon rank-sum tests (D) as (B), but multi units. (E) as (C), but for multi units. $p < 0.01$.

In the left-hand side of Figure 4.15, the longest stimulus is presented (as the strongest correlations were seen here). For single units, there is no significant effect of pair grouping in All/negative correlations ($p = 0.31/0.6712$, Kruskal-Wallis). However, there was a significant effect of grouping for positive correlations ($p = 0.013$, Kruskal-Wallis). This was not present after post hoc analysis (Bonferroni). Looking at other stimulus lengths, some smaller stimuli had evidence of group differences for all correlations, but again these disappeared after Bonferroni correction. As a summary, most stimuli had significant effects of grouping ($p \ll 0.04$, except time bin 13, $p = 0.095$, Kruskal-Wallis), but was not evident after correction.

For multi units (Figure 4.15) there were significant effects in the All, and positive groups ($p = 6.51e-60/1.8e-47$), but not for negative ($p = 0.194$). This persisted across all stimulus lengths. Examining multiple comparison outputs, there was a clear

condensing of six groups into three, based mainly on shank position of each cell in the pairing: (L-Su, L-De; D-Su, D-De; L-SD, D SD, $p < 0.01$ Bonferroni after Kruskal-Wallis). It may be that this type of analysis has struggled to identify subtle differences related to relative depths of cell pairings.

Thus, given the multi unit evidence for depth dependence, the single and multi units data is further condensed into local and distal pairing, leaving two groups, and in here, more differences are observed.

For single units, there is no significant difference between local and distal pairings if comparing all or negative correlations ($p \gg 0.05$ at all stimulus lengths), but again, there is an effect for positive correlations ($p < 0.042$ for 12 of 17 stimuli), with local pairings having higher correlations. For multi units, all and positive correlations are significantly higher in local pairs at all lengths, while negative correlations show no differences (all $p < 6.26e-14$, positive $p < 13-1.03e-6$, negative $p > 0.08$, Wilcoxon rank-sum tests).

Distance Between IC Cell Pairs may not be Indicative of Noise Correlation Strength

The influence of distance between IC cell pairs and the strength of correlations is briefly examined in Figure 4.16.

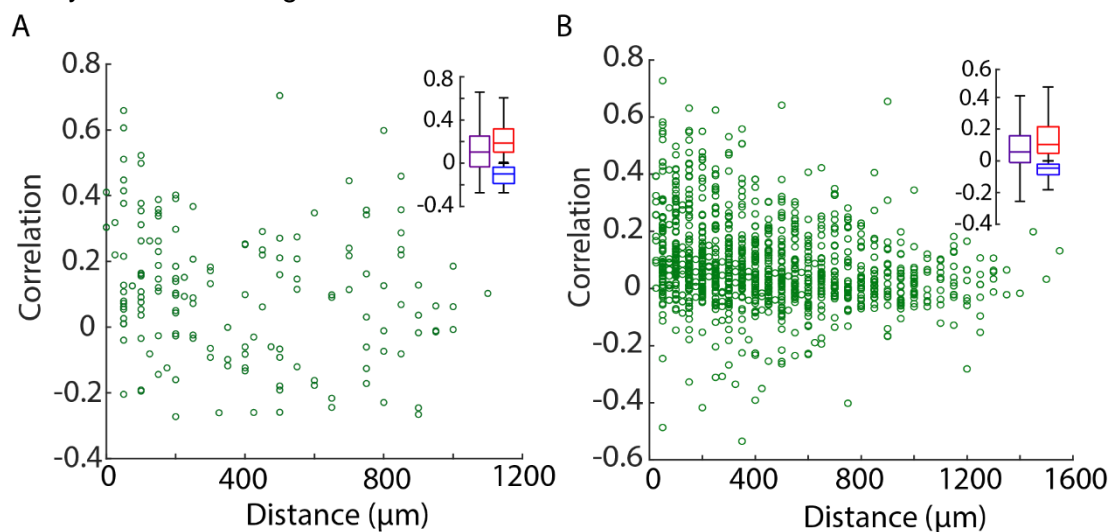


Figure 4.16: Relationship between Distance between IC cells and correlation strength for a single time bin. (A) SUA (B) MUA. Insets, boxplots of overall strengths of correlation

In this figure, IC distance against correlation strength is plotted to look for any distance dependant effects. As there are relatively few single unit pairs, there is no apparent relationship at any stimulus length (absolute values of adjusted R^2 are < 0.0398 for all stimulus lengths). However, looking at MUA, there could be said to be a slight trend

for the highest correlation values being at smallest depths, though this is by no means a strong relationship (absolute values of Adjusted R^2 are < 0.0468 for all stimuli).

Pairs of Narrow Spiking Cells Show Higher Noise Correlations than Pairs of Broad or Broad-to-Narrow Pairs

Previously, it was observed that differences between narrow and broad spiking cell properties, and so pairwise correlations are examined in this context. To focus on cell type differences, local and distal pairs are combined to create 3 groups sorted only by cell type. In Figure 4.17, correlations for the longest stimulus, 1000 ms, are compared. There are three classifications of neuronal pairs in this analysis: BS (both cells of the pair are broad spiking) NS (both cells are narrow spiking) and BS-NS (one cell is broad spiking and the other is narrow).

Looking at “all” correlations, there is a significant effect of cell pair typing, across all stimulus lengths ($p < 2.94e-27$, Kruskal-Wallis). This is the same for positive correlations ($p < 4.99e-23$) and in some stimuli for negative (significant p values < 0.029).

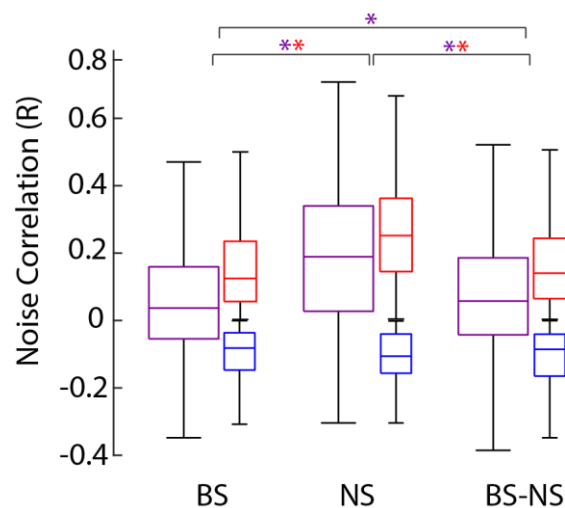


Figure 4.17: Pairwise noise correlation strengths for cortical cell types, 1000ms example figure. Purple – all, Red – positive, Blue – negative. Significance stars indicate $p < 0.029$ Kruskal-Wallis with Bonferroni post hoc comparison

After applying post hoc comparisons to all stimulus lengths, not only the example 1000ms, pairs of narrow spiking cells showed significantly higher correlations than pairs of broad spiking ($p < 1.07e-27$, Bonferroni after Kruskal-Wallis), or pairs of broad-narrow ($p < 0.840e-21$). Broad spiking pairs showed significantly lower correlations than broad-narrow pairs also ($p < 7.57e-3$). It can thus be said that pairs

of narrow spiking cells have higher correlations than broad spiking, or broad-narrow pairs.

Positive correlations show the same trend, with narrow spiking pairs being significantly stronger at all stimulus lengths than broad spiking pairs ($p < 2.11e-23$) and broad-narrow pairs ($p < 1.29e-16$). Broad spiking pairs had significantly smaller correlations than broad-narrow pairs, except at 1000ms ($p < 6.55e-2$).

There is rarely a difference for negative after multiple comparisons. Between broad and narrow pair groups, there are 5 stimuli where narrow is stronger i.e. more negative ($p < 0.04$), whereas all other comparisons have a single stimulus where there is a significant difference ($p > 0.0588$).

In summary, it can be said that in general, for all and for positive correlations, pairs of narrow spiking cells have significantly higher correlations than equivalent broad spiking pairs. Considering that narrow spiking cells have a higher Fano factor, but narrow pairs have higher correlations, it can be said that cell responses are variable across trials but the narrow spiking cells are varying as a population (or as pairs).

4.2.10 Signal Correlations

Pairwise signal correlations were also briefly examined. This will not be an extensive analysis, as there are only 10 stimuli. Signal correlations (Figure 4.18) are plotted in the same way as noise correlations previously, to examine their range.

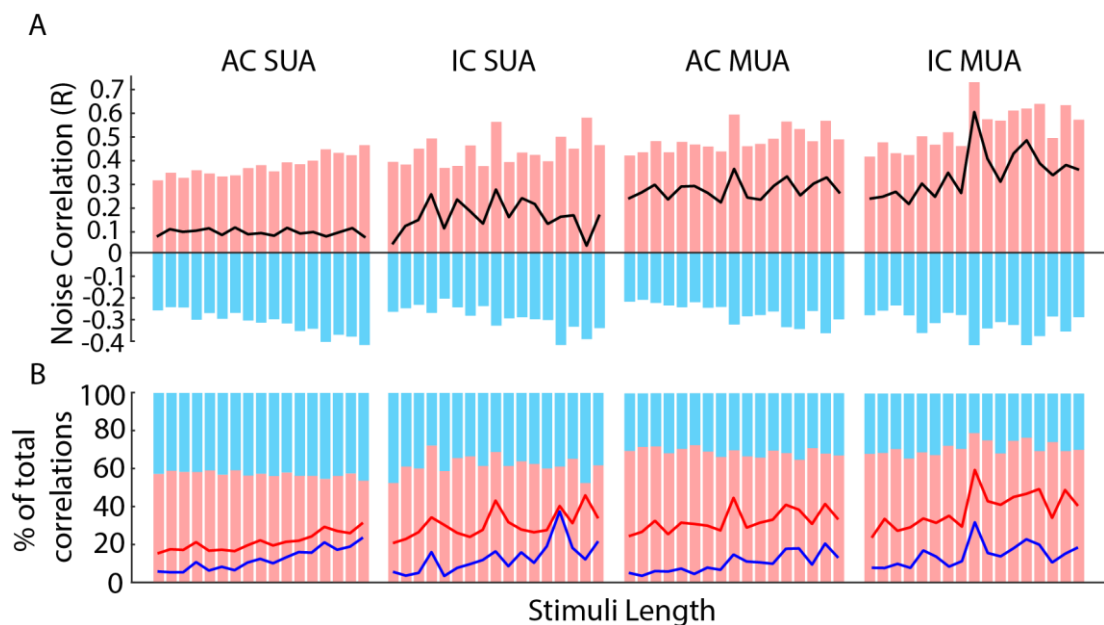


Figure 4.18: Summary of pairwise signal correlations across increasing time windows, for single and multi units in the auditory cortex and inferior colliculus. (A) Mean signal correlations at each stimulus length (25-1000 as previous) – blue = negative, pink = positive. Black line indicates the median. (B) Proportion of each type of signal correlation. Pink/red – positive, Light blue/blue – negative. Lines indicate the proportion of significant correlations at each stimulus length $p < 0.05$. Stimulus lengths not shown, go from 25-1000 ms

General Appearance of Signal Correlations

In Figure 4.18, it is observed that, although there are some strong negative correlations, in most cases the strength of positive correlations is enough to pull the overall correlation more positive than observed with noise. The trace is also more “jagged” across stimuli and doesn’t rise smoothly as with noise correlations. Overall, there are generally slightly more positive correlations when compared to noise correlation (60-70% vs ~60%), although proportions are generally similar. For MUA, there seems to be a particular stimulus length causing a peak in strength and significance of the correlations. The general upwards trend of correlations strength is not as clear here as it is with noise, being almost flat in SUA.

Pairwise Signal Correlations Show Little Dependence on Brain Area

Looking at single units, combining all correlations, only 8 of 17 stimulus lengths have IC correlations significantly higher than AC ($p < 0.0369$, Wilcoxon rank-sum tests). For positive only, this is the same ($p < 0.048$). There are no differences in negative correlation strength (but then these are very small in general, and fewer). There is also no particular pattern in significances/non-significance related to stimulus lengths.

For multi units, 13 of 17 lengths with all correlations show colliculus multi units being higher ($p < 0.0129$). Positive only, again 13 of 17 ($p < 0.0254$), 10 of 17 for negative ($p < 0.0052$).

Multi Unit Pairs have Significantly Higher Correlation Strength in Both the AC and IC

For the cortex, multi units are always significantly higher strength for all correlations ($p < 2.81e-55$, Wilcoxon rank-sum test), positive ($p < 0.0065$), and 12 lengths for negative ($p < 0.0071$). In the colliculus, at all stimulus lengths the overall correlation is higher for multi units ($p < 0.022$), and only 9 of 17 for positive ($p < 0.0256$) and only 2 for negative ($p = 7.35e-5$, $p = 0.0249$).

In summary, it can be said that both single and multi units, colliculus correlations are higher, not quite the same as with noise correlations. Multi units are also the highest signal correlations in both brain areas, again differing from noise correlations.

High Pairwise Signal Correlations May Accompany Poor Classification Performance

As with noise, signal correlations are plotted against performance, in Figure 4.19.

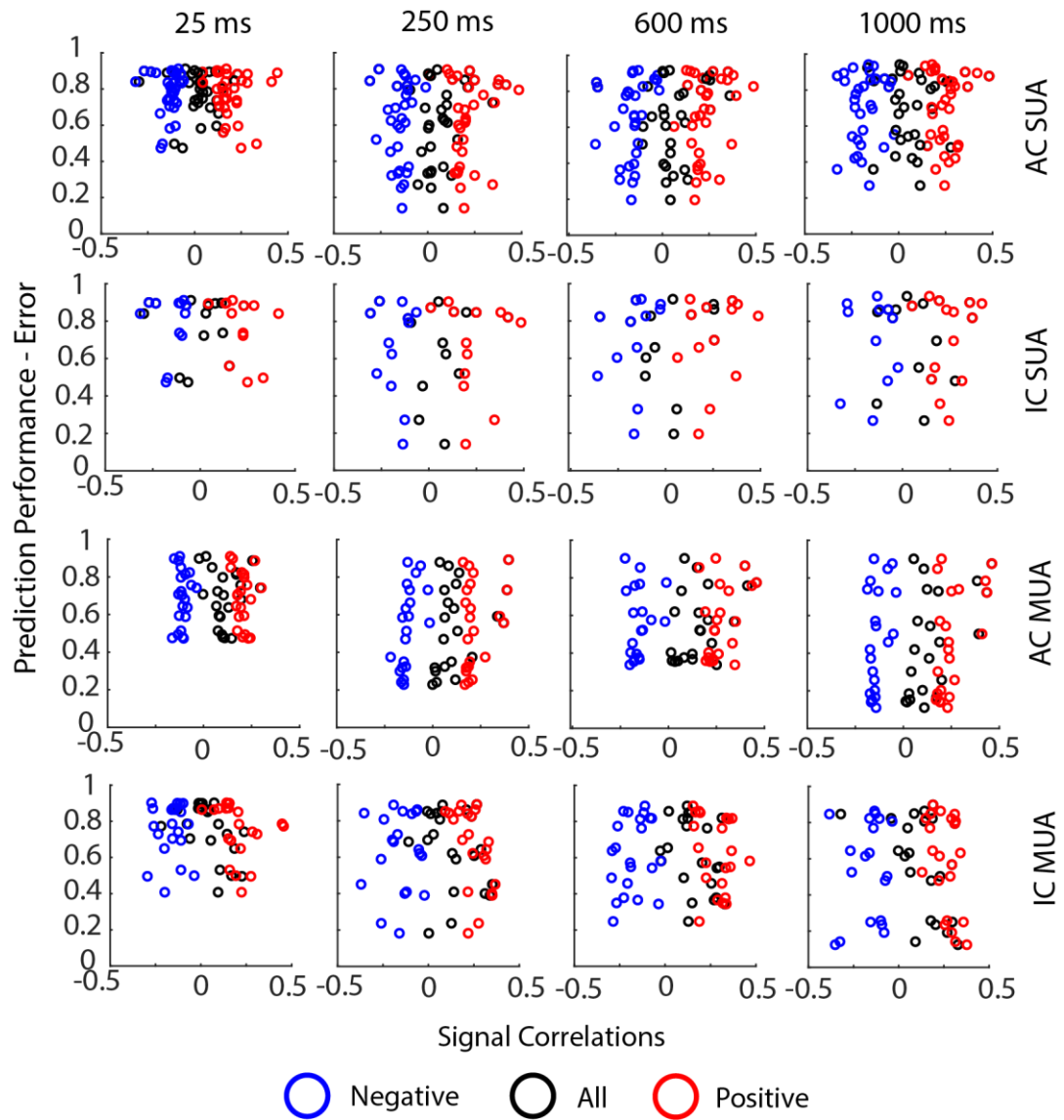


Figure 4.19: Relationship of pairwise signal correlations and prediction error. Rows, top to bottom show different input types, columns are 4 example stimulus lengths. R-squared values are summarised in Table 4.3

Table 4.3: Correlations between pairwise signal correlations and prediction performance. Bold numbers indicate some evidence of a relationship

Condition (mean (STD))	All Correlations	Positive Only	Negative Only
AC SUA	0.035 (0.0850)	-0.001 (0.041)	0.026 (0.108)
IC SUA	-0.057 (0.019)	-0.056 (0.037)	-0.080 (0.051)
AC MUA	0.107 (0.092)	0.051 (0.066)	0.087 (0.113)
IC MUA	0.058 (0.0821)	0.101 (0.010)	-0.005 (0.061)

As the data is skewed, the median of each dataset is taken, to provide a more conservative estimate.

Once again, there is very little evidence of a relationship, except in AC MUA and a few examples. As with noise correlations, it appears that high signal correlations may correlate with low performance. Again, across stimulus lengths, standard deviation is high and generally, R^2 is close to and around zero (Table 4.3), so this relationship is by no means consistent at all.

Effect of Proximity on Pairwise Signal Correlations is Less Apparent than for Noise Correlations

Depth grouping is applied to the cell pairs as described previously. This is plotted in Figure 4.20.

Considering single units, for all correlations, 11 of 17 stimuli showed no evidence between group differences ($p < 0.0216$ for the significant groups, Kruskal-Wallis). For positive correlations, this number was 10 of 17 ($p < 0.0381$). There was no evidence of differences for negatives ($p > 0.124$). Multiple comparisons did not reveal any clear trends or relationships regarding cell positions, for any type of correlation – unlike noise.

For MUA, an effect of cell grouping was observed for the “all” correlations, at all stimulus lengths ($p < 3.64e-24$, Kruskal-Wallis) and positive ($p < 3.37e-7$). This is not seen for negatives (except at two time bins, $p = 0.0103$, $p = 0.0169$, otherwise $p > 0.114$). As with single units, multiple comparisons (Bonferroni) did not reveal the same trend as with noise, with no clear split between local and distal pairs.

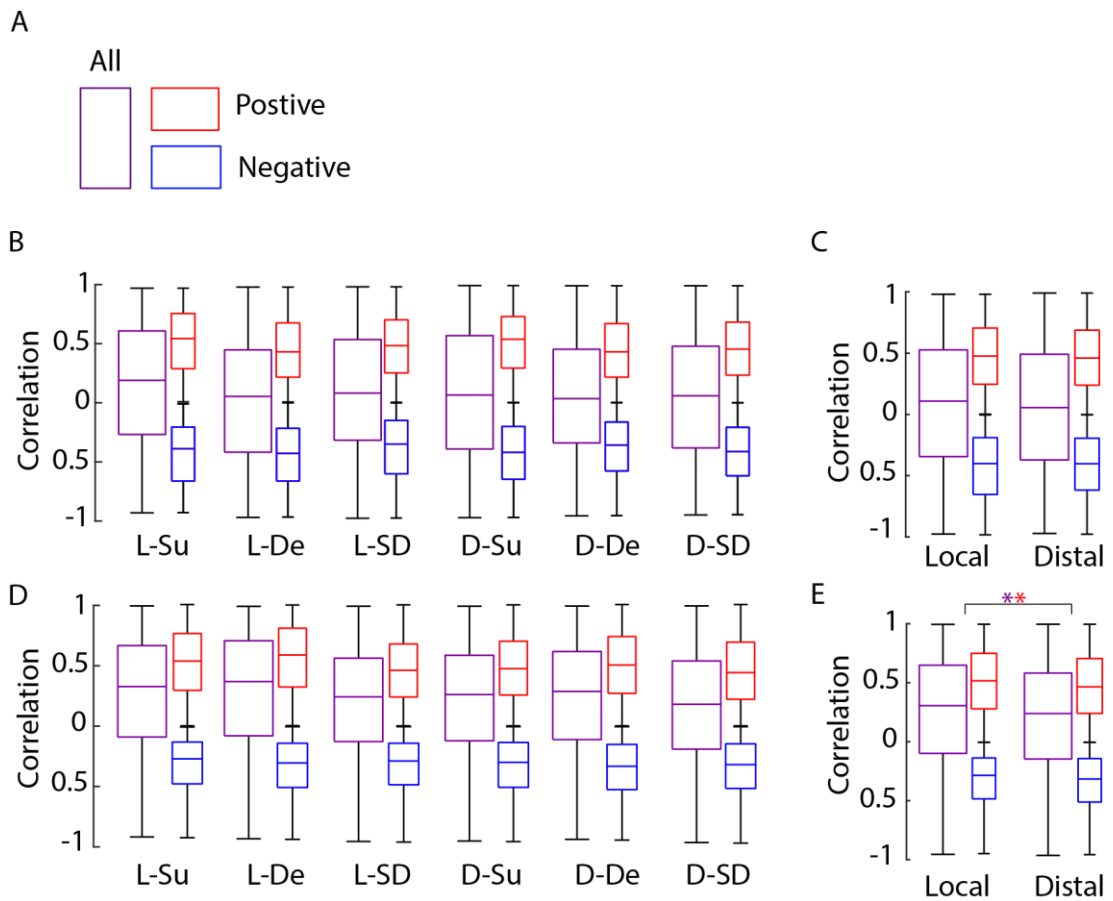


Figure 4.20: Signal correlations with cell pairs grouped by depth and relative distance, for one example stimulus (1000ms). (A) Key. (B) signal correlations for all cell pair groups. Purple – all, red – positive, blue – negative. (C) Local and distal pairs only. (D) as (B), but for multi units, (E) as (D), but for multi units. Significance stars of colours indicate p values at all stimulus length < 0.05 , Wilcoxon rank-sum tests.

However, as with noise correlation, the 6 groups are condensed to compare only local and distal pairs. As expected from the 6 group comparisons, for single units, only 2 of 17 stimuli showed a significant effect for All correlations ($p = 0.0014$, $p = 0.02$, Wilcoxon rank-sum test), with 4 for positive correlations ($p < 0.016$). One stimulus showed significance for negative ($p = 0.0103$).

In multi units, there is a significant effect of pair grouping, with distal pairs having an overall lower correlation for all ($p < 1.40e-4$) and positive correlations ($p < 6.35e-4$), at all stimuli lengths. Only two stimuli see a difference in negative ($p = 0.035$ and $p = 0.0068$). Visually though, this is difficult to see in Figure 4.20, as these differences are very small.

In general, compared to pairwise noise correlations, there is less evidence for a clear local-distal pair split, particularly with single units. In multi units, though significance, the differences is relatively very small.

Signal Correlations in the IC are not Related to Distance between Cells in a Pair

As with noise correlations, IC signal correlations using distances between cell pairs is briefly examined (Figure 4.21).

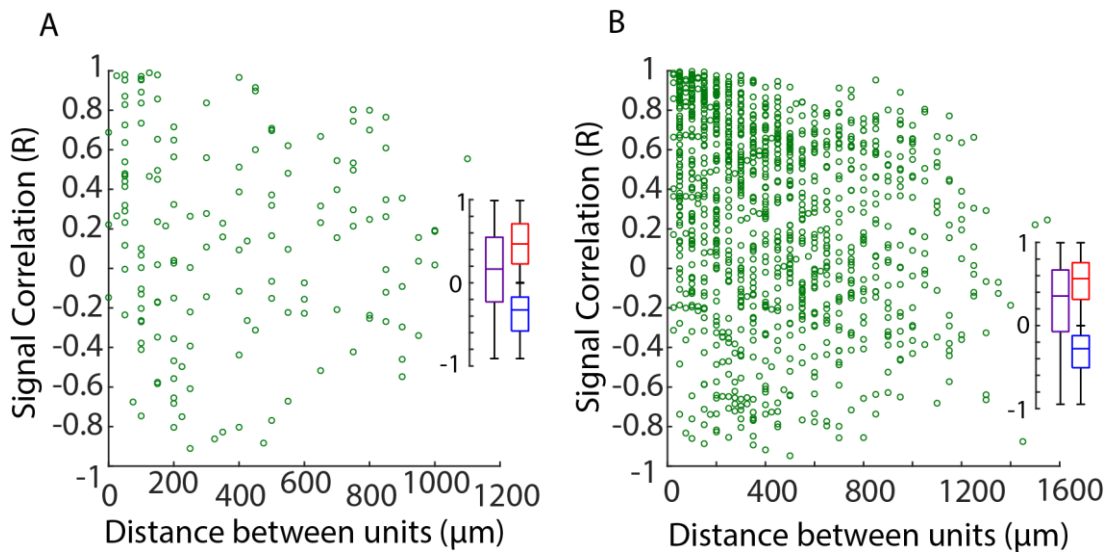


Figure 4.21: Relationship between Distance between IC cells and signal correlation strength for a single stimulus length (1000ms) (A) Distance between single units of a cell pair against the signal correlation of the pair. (B) as (A), but for multi units. Insets left and right – overall strength of IC signal correlations. All – purple, Red – positive, Blue – negative

It is somewhat difficult to distinguish a relationship in this data. There may be an argument to be made for longer distances in fact resulting in correlations closer to zero. But for both single (absolute values of adjusted $R^2 < 0.0501$) and multi units (absolute values of adjusted $R^2 < 0.0805$), there is no quantifiable evidence of a relationship at any stimuli length.

Narrow-Spiking Cell Pairs Show Higher Signal Correlations than other Groupings

As with noise correlations, signal correlations are split into cell type pairings, displayed in Figure 4.22. For the All correlations condition, there is usually a clear effect of cell grouping in all (all but 1 stimuli, p range < 0.0285 , Kruskal-Wallis), positive (11 of 17 stimuli, $p < 0.0443$), but less so for negative (three stimuli, $p = 0.026$, 0.029 and 0.04 , otherwise $p > 0.061$).

For within group differences, looking at all correlations, narrow spiking pairs have significantly stronger correlations than broad spiking, except at a single stimuli length (p value < 0.0235 , $p = 0.0733$). 13 of 17 stimuli lengths show narrow spiking pairs having stronger correlations than broad-narrow pairs ($p < 0.0026$). Broad spiking pairs show no differences to broad-narrow pairs ($p > 0.083$).

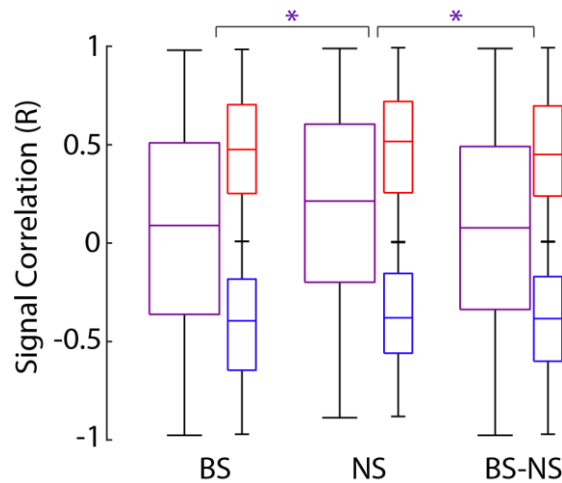


Figure 4.22: Signal correlations in type specific cell pairs, for example 1000ms stimulus length. Significance stars indicate $p < 0.028$ in the vast majority of stim lengths for that set of correlations (see text, Bonferroni after Kruskal-Wallis)

For positive correlations, narrow pairs have significantly stronger correlations than broad spiking in 10 of 17 stimuli ($p < 0.0499$). 12 of 17 stimulus lengths show narrow spiking to be higher than broad-narrow ($p < 0.0441$). There are no differences between broad and broad-narrow groups ($p > 0.0927$).

For negatives, the only differences are in three stimulus lengths for narrow pairs and broad-narrow ($p = 0.0387$, $p = 0.0249$, $p = 0.0489$), and between narrow and broad groups for one stimulus ($p = 0.029$), otherwise, $p > 0.075$.

In general, while not as clear as in noise correlation, there is some evidence for a difference between strength of correlation between broad and narrow spiking cell pairs, with narrow spiking being higher.

4.3 Discussion and Conclusions

4.3.1 Summary of Results

The results described in this chapter have to some degree both met the aims of the chapter and opened interesting avenues for discussion and future work. Classification was generally possible using simple rate codes in both brain areas – with some caveats to be discussed. The number of predictors used was an influencing factor on the classification performance. Though there were no statistical differences in overall performance between the colliculus and cortex, it is notable that when combining the data and examining trends in the data (e.g. x-intercepts with predictor axis), the colliculus seems capable of achieving these performances with a significantly fewer number of input variables. This spoke to a fundamental difference in the spiking activity of AC and IC neurons. The hypothesis of stimulus length having an effect was confirmed to some degree, but with no clear trend observed which was unexpected given previous literature.

The frequency range covered by a dataset was found unlikely to be causing the differences between cortex and colliculus. Comparing measures of trial-trial variability, it was found that the inferior colliculus population had significantly lower values, which is a viable explanation for the results seen, matching the hypothesis put together from previous chapters. Conclusions regarding noise and signal correlations were somewhat weaker than from other analysis, but high values were indicative of very poorly performing datasets. Correlations (of both types) between cell pairs on a single shank were slightly stronger than pairs spread across several probe shanks. Narrow spiking cell pairs displayed stronger correlations than broad spiking ones.

4.3.2 Comparisons to Previous Literature

In the paper on which the classification protocol was based on, there was limited success using only spike rate, with most results being just above chance level (Kayser et al., 2012). This was the case in some of the datasets, but better results were observed in many cases. This is most likely due to this paper looking at neurons individually – in this thesis, all available neurons were included into a single calculation, which should increase the amount of information available. However, it also opens results up to the influence of particularly noisy units. It was also expected that an effect of stimulus length be seen, at least in the cortex, given that the literature (including the study above) in both auditory and visual systems suggests that certain timescales of coding (e.g. delta, theta) are most important (Lakatos et al., 2008,

Kayser et al., 2015). There was a slight trend towards this, but it was not backed up by statistics, not was the trend as clear as seen in Chapter 3. At this time, it is not entirely sure what is causing this discrepancy – it may be a lack of data, high variability of data or our dependence on stimulus-locked time bins, rather than locking to LFP phase, as was done in Kayser 2012.

As previously alluded to, this study is somewhat unique in the number of different groups it is analysing and comparing at the same time (SUA, MUA, AC, IC). In particular, there is to our knowledge no literature comparing AC and IC on exactly the same stimuli.

That trial-trial variability is higher in the presented auditory cortex data is in keeping with current theories of cortical activity modulation (Marguet and Harris, 2011, Sakata, 2016). There are no studies directly comparing AC and IC under the same conditions – however, it is reasonable to assume that the IC will be less affected by global brain state in this way. This is seen in literature already, with frequency tuning of awake neurons matching those in the anaesthetised state (Portfors and Felix, 2005, Alkhatib et al., 2006). This also builds on and supports the trend seen in Chapter 3 for IC Fano factors to be smaller.

It is difficult to make conclusions as to what the noise and signal correlations mean in this case – there was no strong relationship between correlation and performance, except that very high correlations led to poor performance, which is logical given how classification analysis works. Work on relative positions of cells in a pairing did not show particularly strong effects, with differences only observed between local and distal shank pairings. Given that the relative distances between pairs in the cortex were not directly calculated, it cannot be said for sure that correlations decrease with distance as the literature suggests (Smith and Kohn, 2008), though this relationship is observed weakly in the inferior colliculus. Within the current scope of the results it is not believed that the presented data can support any particular argument as to the role of correlations (Panzeri et al., 1999, Fiser et al., 2010, Moreno-Bote et al., 2014). The trend observed for pairs of narrow spiking cells to have higher correlations than pyramidal cells pairs is something seen in previous literature in the prefrontal cortex of the monkey, which is promising (Constantinidis and Goldman-Rakic, 2002).

4.3.3 Limitations and Considerations

Much of the same limitations from Chapter 3 are carried over – namely, the lack of IC single units. This unfortunately meant that direct comparison between simultaneously recorded AC and IC data was difficult, without introducing biases associated with low unit numbers. For this reason, options for paired statistics were limited, and it was required to combine data from multiple datasets. This means the differences observed are less robust, and should be interpreted carefully. Fano factors of greater than 1 were often seen – but as data is being directly comparing, this is acceptable. Again, incorporation brain state information was not possible – this would have been highly informative.

As was brought to light by positive and negative controls, the methodology in picking segments was fairly simplistic. Segments were picked randomly to avoid biasing results, but this also resulted in some segments being taken from “quiet” periods and thus were indistinguishable from spontaneous activity. In the future, it may be beneficial to pose a more direct/specific question to the data, and manually select segments (for example, based on sound envelope powers, amplitude or relative position within the 10 second stimulus). This increases the kinds of questions that can be asked. Phase information may also be incorporated, as has been previously done.

It is also a consideration that the AC may be able to perform maximally but with fewer predictors – a form of saturation that is biasing AC results. This would result in shifting of the intercepts and bringing best fit lines closer to those of the IC. Ideally, there would be a comparable number of predictors for both areas, a systematic analysis would be performed by slowly increasing the number of predictors for the classification. The main reason this style of analysis was not attempted (aside from low numbers of IC units) was the complexity of choosing which predictors to include. If every possible combination was computed in increasing numbers to avoid bias, the analysis would simply take too long. Adding in predictors based on some system (i.e. in decreasing order of spike rate) would require a clearer question. In short, in order to do the analysis justice and search over several datasets, more time/computer processing power than was available would be required.

While saturation is possible, there are a few things that suggest it is not the case – or least is not a major influence. Firstly, the gap between IC and AC intercepts is large – the AC would need to saturate very early for this to be bridged. Secondly, no datasets reach exceptional performances, suggesting there is still potential for better

performance (with more predictors) in all types of data. Secondly, after moving forward with the assumption, potential features of the data that would viably cause the observed difference were found. It cannot be said definitively without systematic analysis, but signs would point to this being a real and significant effect.

The individual contributions of each cell type have also not been examined. As seen in Chapter 3, different cell types (i.e. pyramidal vs narrow-spiking interneurons) may be contributing in different ways. Though not essential, the study would benefit from analysing dimensionality reduction outputs and finding out which cells contributed what. This would allow for even more in-depth analysis of the functional mechanisms at play.

The independence of the variables was also examined for interaction effects or other interesting variables to look at. If such effects are strongly visible in the data, it would restrict the strength of conclusions being made. Apart from the relationship with the number of predictors and frequency range, performance versus spike rate, and spike rate versus number of predictors were both examined. There is no convincing evidence of a relationship between firing rates over the natural sound period and overall performance, suggesting the impetus is on the spiking behaviour at finer timescales, and not that a raw increase in spikes automatically equals better performance. There is a small evidence for a relationship in IC, but not for all stimulus lengths, and it is not strong. A strong relationship for number of predictors vs median spike rate was then seen in IC single units and AC multi units. IC single units somewhat makes sense, as again, in datasets with small numbers of predictors, any increase is just more likely to add to the range. It is unclear why a trend exists for AC MUA. As such, the conclusions of this Chapter would benefit from having additional, higher quality data.

4.3.4 Functional Implications

As a higher cortical area, the AC (particularly A1) is responsible for high level processing and interpretation of sound stimuli. It has a complex layered structure, with constant communications to and from other cortical areas (including other auditory areas) that put the sound into context, connect it to memory, and cause behavioural changes. All of these factors influence spike rates outside of the raw spectrotemporal components of a stimulus, increasing trial-trial variability compared to sub-cortical sensory areas. The results presented here thus support the general function of the AC as the highest level of auditory processing, responsible for ongoing interpretation

and contextualisation of sound stimuli within the organism's multimodal environment – as opposed to a simple auditory information relay.

Sparse coding strategies are emerging as the dominant (but not sole) strategy in the auditory cortex and the cortex in general (Hromadka et al., 2008), where specific stimuli are represented efficiently by the activity of a few neurons. Thus, an additional interpretation of the AC's higher variability is that most neurons are not involved in coding every one of the 10 stimuli or are not particularly active. A given neuron may have a highly distinct response for 1 or 2 stimuli, but reverts to low activity (or a brief, transient response) for the less preferable stimuli. As the variability across all the stimuli was essentially averaged during this analysis, this may account for the higher and (more variable) variability. In particularly poorly performing datasets, it may be that the silicon probe has not sampled enough sparse neuron populations to distinctly represent all the stimuli. Sparse coding lends itself well to the efficient representation of a huge variety of information, fitting the auditory cortex's function as the final, perceptual stage of sound processing (as opposed to simply conveying the spectrotemporal appearance of sound). The results presented here thus support the AC's use of a sparse coding strategy for natural sounds.

That narrow spiking cells showed slightly stronger noise (and to an extent, signal) correlations during natural sound than equivalent broad spiking pairs has interesting implications, alongside supporting the existing knowledge that inhibition is important for shaping tuning curves. The Fano factor of narrow spiking cells was also observed here to be higher than broad spiking counterparts. If these results can be solidified and confirmed further, they suggest that this cell type is influenced by global changes as a whole population. Their particular function is performed as a population rather than as individual cells. These implications match those discussed in Chapter 3.

IC cells are observed to have a more reliable spike rate response to repeated trials of the same stimulus, when compared to the auditory cortex in similar situations. In its role as a hub, it is logical that the IC have robust and reliable encoding patterns, to ensure that the details of the sound is passed on effectively and accurately. The results, when compared alongside the auditory cortex, continue to support the functional role of the IC as a hub for integration of raw sound information, rather than for higher perception purposes. That the spike rate code can usually distinguish stimuli even with very few units further speaks to coding robustness and reliability.

The results from Chapter 4 regarding trial-trial variability and the relative success of a spike rate code, alongside knowledge of the ICs' role as an auditory information integration hub, point to a dense coding being more favoured. With sound stimuli being represented by variations in the spike rate of each isofrequency layer, the system would benefit from incorporating redundancy to better deal with noise or missing information at this crucial stage in the auditory pathway. Literature on the subject is currently somewhat patchy, with evidence for both strategies available as discussed below.

Sparse coding models of the IC have proved successful in the representation of human speech (Zhang et al., 2019, Carlson et al., 2012), and a 2012 study in cats made a strong case for the importance of a sparse strategy in the ICC (Chen et al., 2012a). In mice too, a heterogeneity in ICC neuronal responses was observed to be important for efficient coding of vocalisation (Holmstrom et al., 2010).

However, there is also evidence supporting a mechanistic switch from dense to sparse coding, reducing redundancy as the information ascends to the auditory cortex (Chechik et al., 2006). Work in the midbrain of the electric fish indicates (at least in this species), both methods exist very much in parallel (Vonderschen and Chacron, 2011, Sproule et al., 2015).

More research is clearly required in this area for further clarification on the role, interactivity and relative importance of each coding strategy. For the success of auditory implants, a propensity for a dense model (with a degree of spatial localisation) may be most desirable, given that many cells around the site will be stimulated – though this may become less of a hurdle with advanced optogenetic techniques and technologies.

4.3.5 Future Work

Now that the baseline results have been obtained, the future of the research lies in posing further questions relevant to auditory neuroscience and implants.

Firstly, the complexity of the mathematical modelling should be increased. The choice of algorithms and the operating parameters can be optimised to the (often non-linear) spiking of neurons by using non-linear or partially non-linear solving methods (such as Support Vector Machines). It may also be beneficial to apply different kinds of models such as regression, to look specifically at the coding of a certain variable of the sound (sound envelope amplitude, phase, delta power etc). This kind of analysis

is a powerful tool for asking more specific questions about various aspects of the sound are encoded that are not possible with the current data.

Neuronal data is highly multi-dimensional, and future work should try to incorporate this further. Additional dimensions may include phase information (as in Kayser 2012) or additional time binning. Depending on the questions being asked, it may also be beneficial to create bespoke “populations” of different cell types and cell type proportions in order to see the relative influences of each type and reveal how population act together. Given the functional implications discussed, investigating the degree of coding sparseness in both the AC (where it is well established as a primary mechanism) and the IC, may prove interesting, providing more insight into how the representations of sounds change through each stage in the auditory pathway. More applicable dimensionality reduction may also provide benefits, such as NMF to identify functional populations. The potential of this technique is explored in Chapter 5.

Analysis utilising the simultaneous aspect of the data would be novel, and highly informative for systems neuroscience and auditory implants. One potential study could be predicting AC population activity from the activity of IC neurons, then comparing this predicted activity with that already recorded. The relative success of this, and the methods used to do it, would have implications for the brain’s methods of information transfer through the auditory system – what is the best way to “package” the IC activity to get the most naturalistic AC response? This is excellent information to provide for the development of future auditory implants.

Randomly picking stimuli from 10 seconds of natural sound has provided baseline results. By preselecting segments of the sound to be stimuli, based on variables of interest such as amplitude, frequency power and slope/shape of the sound envelope, functional neuronal populations may be revealed. By applying classification analysis to more varieties of auditory stimuli (vocalisations, puretones, background noise etc), stimulus specific coding mechanisms and dynamic population activity can be investigated further.

With the link between brain state and trial-trial variability in mind, investigating global brain state and its subsequent effect on classification success would be very informative. Levels of pair-wise correlations during spontaneous activity in the evoked and resting state and illuminate any changes in neuronal relationships between

conditions. A more in-depth look into the effect of the relative positions of cells in a pair may better reveal depth or other spatial-based effects.

Chapter 5 Non-Negative Matrix Factorisation for Characterisation of Neuronal Populations During Natural Sound

In this chapter, preliminary results from non-negative matrix factorisation are presented. Analysis was performed on auditory cortex and inferior colliculus data taken during presentation of natural sounds. Section 5.1 provides an introduction to the aims, relevant literature and hypotheses for the analysis. Section 5.2 presents the main qualitative results for spatial modules in both brain areas. In Section 5.3 the outputs of spatiotemporal decomposition are examined, with a single example dataset used to try and determine if cortical state can be derived from module strength. Splitting trials into putative states, linear classification is performed as in Chapter 4 and look for any effects. This is repeated for inferior colliculus data, but with minimal success. Finally, in Section 5.4 the discussion reflects on the potentials of the technique for furthering knowledge of functional neuronal populations, and the limitations of the study. Future research directions are then proposed.

5.1 Introduction

5.1.1 Aims of the Chapter

Neuroscience research has begun a shift from single unit analysis to the consideration of neurons as functional populations. As detailed in the literature review, the advent of silicon probe and advanced imaging technologies has made the simultaneous recording of multitudes of neurons a reality. Analysis of neurons on the level of populations has thus become a popular and highly informative approach in recent years, with new analysis techniques emerging to manipulate the data in useful ways. To conclude the thesis' analysis of cortex and colliculus responses during natural sound, dimensionality reduction is employed in an effort to identify populations and their activity during natural sound. The aims of this exploratory chapter are to:

- Successfully decompose cortical and colliculus data into spatial and spatiotemporal modules of activity (putative populations), using Non-Negative Matrix Factorisation (NMF)
- Make observations about the components (neurons) of modules and how modules change relative to each other, during successive trials of a natural sound stimulus
- Identify qualitative differences between the AC and IC and hypothesis as to their origin
- Determine if the strength of particular NMF modules is in some way indicative of brain state transitions
- Highlight the suitability of NMF for investigating populations of auditory neurons

5.1.2 Relation to Previous Literature

By treating the auditory (and other sensory) systems as populations instead of as individual neurons, over recent years, researchers have gained insight into the multi-layered mechanisms underlying sound encoding, and identified new intricacies in previously mapped systems. For example, with 2-photon calcium imaging, it was confirmed that local neuron populations in the primary auditory cortex are often heterogenous in terms of their frequency tuning, despite a larger global gradient – but despite these differences, neurons in these population exhibited shared fluctuations/noise correlations, indicating their cooperation on some level (Rothschild et al., 2010). An extensive study using Neuropixels probes in multiple brain areas and two-photon calcium imaging grouped neurons into rough populations based on spatial

distance, then quantified their multi-dimensionality using peer-prediction (Stringer et al., 2019). In peer-prediction analysis, the activity of a given neuron is predicted by using the activity of other simultaneously recorded neurons (Harris et al., 2003). By repeating this for different neurons, a detailed picture of which, and how, neurons are working together as population is derived, including putative population numbers and how they alter between spontaneous and various types of evoked activity (Stringer et al., 2019). Currently, inferior colliculus neurons have not been subject to these sorts of analysis, not being a higher brain area, though in a general sense, isofrequency layers in the ICC tend to be treated as “populations”.

As became apparent in the literature review, increasingly simultaneous recordings are often struck with the “curse of dimensionality”. Datasets are becoming huge in both storage size and in number of dimensions, as recording from hundreds of neurons simultaneously from multiple brain areas becomes possible, during various stimuli and attentional states. Dimensionality reduction is thus becoming an important tool, both from a computational timing standpoint, and in capturing the activities and functions of underlying populations. At the present time there are several dimensionality reduction techniques available, which will be applicable to different varieties of data. For further explanations, the author refers the reader to the 2014 Cunningham and Yu review: “Dimensionality reduction for large-scale neural recordings” (Cunningham and Yu, 2014).

Some common dimensionality reduction techniques include (but are not limited to) Principal Component Analysis (PCA), Factor Analysis (FA), and Non-Negative Matrix Factorisation (NMF). The use of PCA to identify and characterise cell populations in ensembles is well established (Chapin and Nicolelis, 1999, Peyrache et al., 2010). However, it may not differentiate well between the variance caused by stimuli, and the variance caused by noise or excitability fluctuations – thus, extensive pre-processing may be required to minimise their influence. In addition, depending on the implementation, it may produce components with negative weightings, and in the context of neuronal spiking, this is difficult to interpret (Cunningham and Yu, 2014). In the present thesis (Chapter 4), success using PCA for classification analysis was limited – potentially due to noisy or low-quality data skewing results. Factor Analysis is a technique somewhat similar to PCA, but can remove variance specific to single neurons (to which PCA is sensitive) while preserving shared “population” variance (Cunningham and Yu, 2014) – so may be more applicable to the study of neuronal

populations. In any case, both techniques are limited in that they tend to only use spike rate (losing the fine spike patterns) or use trial averaged data to circumvent issues with noise.

Non-Negative Matrix Factorisation is becoming increasingly popular as a versatile way to examine population activity. Materials and Methods has previously outlined the data pre-processing requirements and how to interpret the output data. Essentially, this method decomposes neuronal activity into *modules* which describe the data in space and time. It is easily interpretable in terms of neuronal populations – depending on how data is input, it will assign cells to separate modules (read here “populations”), with the second matrix detailing how the cell’s strength changes over time or during each trial. It thus theoretically gives us detailed information regarding dynamic population activity

Due to the non-negative requirement for input and output, it is directly relatable to spike rate, and so is perhaps more easily interpreted than other methods. More specific details on the technique can be found in Lee 1999 (Lee and Seung, 1999).

A common usage in neuroscience up to this point is the transformation of simultaneous neural calcium imaging data to identify populations (Pnevmatikakis et al., 2016). Additionally, the technique has been used to identify important neural spiking patterns in the context of improving BMI (Kim et al., 2005). The technique has also been used extensively outwith neuroscience for processing of images, text, music, etc.

NMF is, in theory, an excellent technique to examine the intricacies of auditory coding at a spiking timescale. A 2016 study on retinal cells used the technique to look at millisecond timescales, finding that stimulus information was encoded in the first spike latencies which was not visible from spike rates alone (Onken et al., 2016). A further study by some of the same authors in 2017 used NMF to identify the subunits composing visual receptive fields in the salamander retina, during white noise stimulation (Liu et al., 2017). Furthermore, a very recent publication derived NMF modules from brainstem neuronal populations. Module activation strengths were found to reflect state dependant activity in distinct populations, and could also predict sleep state transitions (Tsunematsu et al., 2020).

In this chapter, NMF is used in an exploratory sense, as to the best of our knowledge, it has not been used to look at auditory cortex and inferior colliculus activity during

natural sound stimuli – or indeed neuronal auditory signals in general. Given the differences between the AC and IC in cell metrics (e.g. firing rate) and trial-trial variability that have been presented, and the different cell types and anatomical structure area it is hypothesised that some between-area differences to be visible at on a very basic level – such as in the number of modules and in the appearance trial-trial. It is also expected that activity will be modulated strongly by the sound – and given frequency tuning of cells, perhaps modules/populations will be strongest at certain points of the sound. Given recent and past literature, it is theoretically possible to observe these fluctuations in the cortex by examining module strengths. Any technique which can offer additional insight into the auditory system is beneficial both for the goals of this project (in supporting the development of the next generation of midbrain implants) and for the field of neuroscience in general.

5.1.3 Hypotheses

Due to the exploratory nature of this analysis, hypotheses are quite generalised and mainly aim to confirm the potential of the technique for population-based analysis. This technique of dimensionality reduction has shown promise in recent years in characterising large amounts of neuronal data into (functionally) distinct cell populations (including any state dependencies), and so interesting results are expected here, especially in the auditory cortex. In addition, previous thesis chapters have demonstrated quantitative differences between the auditory cortex and inferior colliculus (including trial-trial variability), and presented qualitative observations about neuronal preference for sound (such as the example MUA traces in the beginning of Chapter 3), both of which are theoretically visible or extractable from NMF data. As such, the following general hypotheses can be made:

- The preferences shown by neuronal populations (i.e. our modules derived from NMF) for specific features of the sound will be clearly visible in a simple representation of module activity over time
- Cortex and colliculus modules will visibly differ – for example in trial-trial variability
 - Evidence for state transitions may be evident in cortical data

5.1.4 Main Findings

- High dimensional input can be represented by a handful of modules at most
- Artefacts are generally confined to one module, meaning they are easily identified and removed from any further analysis

- Different modules appear to be important for different parts of the stimulus – with the activity of different modules appear to “slot together” to form continuous activity
- In the inferior colliculus, modules would appear to be tonotopic in nature, with the principal cells in each module being arranged in a depth gradient
- There is some preliminary evidence of state transitions in a single examined dataset, telegraphed by shifts in strength in a particular module and accompanied by changes in the delta ratio of LFP

5.2 Qualitative Analysis of Spatiotemporal Modules

5.2.1 Spatial Module Examples and Initial Thoughts

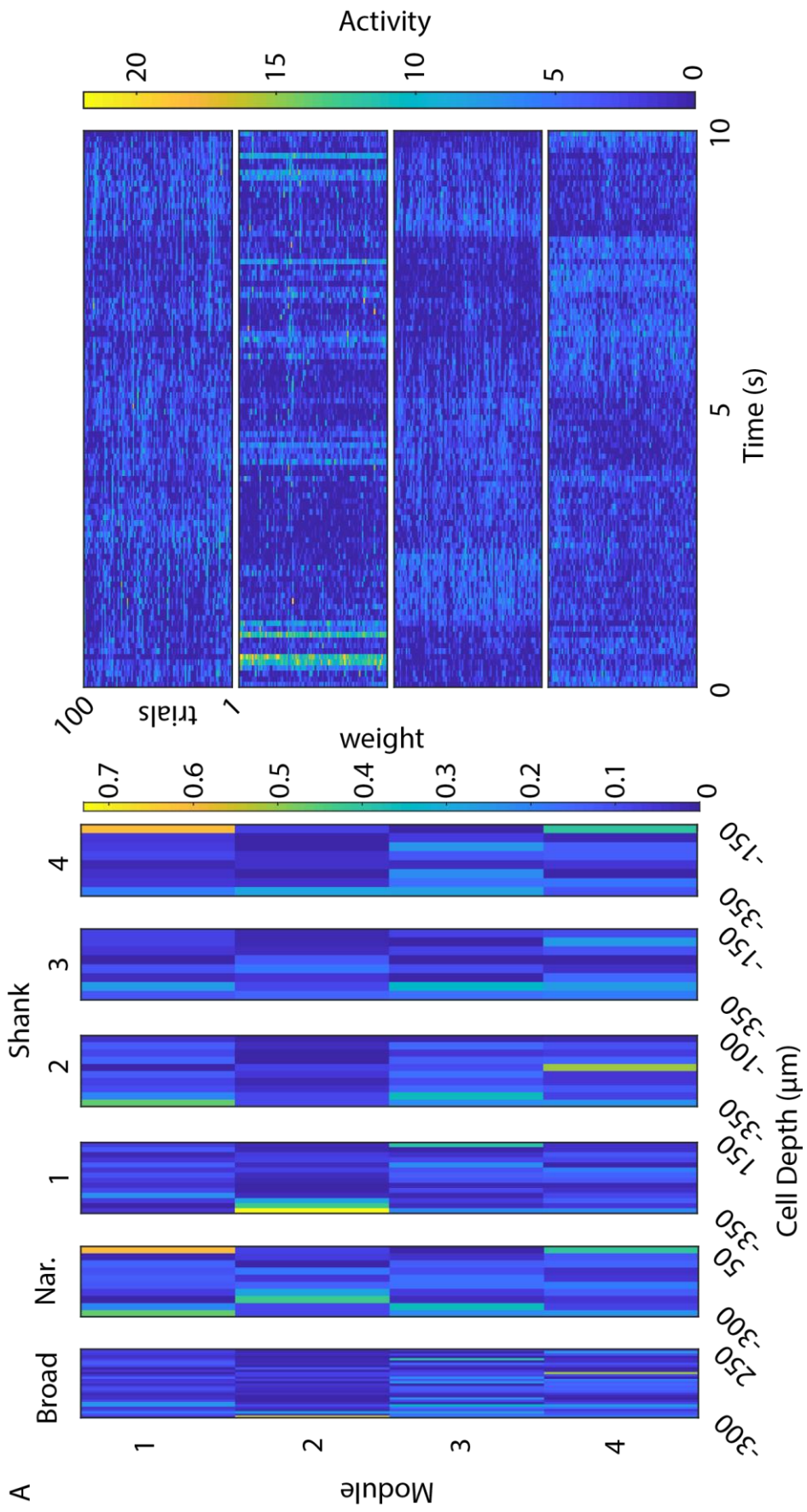
In Figure 5.1 and 5.2 on the following pages, some exemplary examples of spatial modules are shown. The spatial modules derived from NMF can be thought of as neuronal populations, with each cell having a different level of importance to the overall activity of said population, compared to the other cells. This relative importance can be observed in the left-most images in Figure 5.1 and 5.2, where the contributing cells are also sorted by CSD-derived depth. The module/population’s changes in activity over individual time points can then be observed in the right-most images of Figure 5.1 and 5.2 – trials have been visually stacked on top of each other to create a stimuli length by trial matrix of neuronal activity. .

The plots are typical, good quality examples of some of the features observed in this analysis. What is commonly seen is that each module is fairly consistent in each trial (though sometimes a slow increase in power was observed across the trials, perhaps after an animal movement). The auditory cortex also appears to have more modules overall, especially MUA. This makes sense given the data - IC has less cells to work with. It could not be said at this time that this is a purely biological phenomenon.

Each module displays a slightly different pattern, and seems to be responding to different parts of the sound – as one decreases in power, another is taking its place. This split is generally within a few samples (i.e. not a slow change over time), with some transitions sharper than others.

Cells were also split up by shank, depth and type. For the auditory cortex, spatial/depth patterns are not easily observed. In general, it may be said that that each module tends to be dominated by *either* a narrow or a broad spiking cell, but this is simply a by-eye observation.

In the IC, there is evidence of some depth dependency. In the example shown in Figure 5.1, the first module is the shallower cells, while the second then transitions into the other cells. This is a common pattern among other sets, and is likely explained by the tonotopic gradient of the IC depth – each module represents a population of cells coding a small range of frequencies. We are less likely to observe this in the AC, as there will be fewer frequencies represented - with the 4 probe shanks, we are essentially only sampling four locations in the AC's tonotopic gradient.



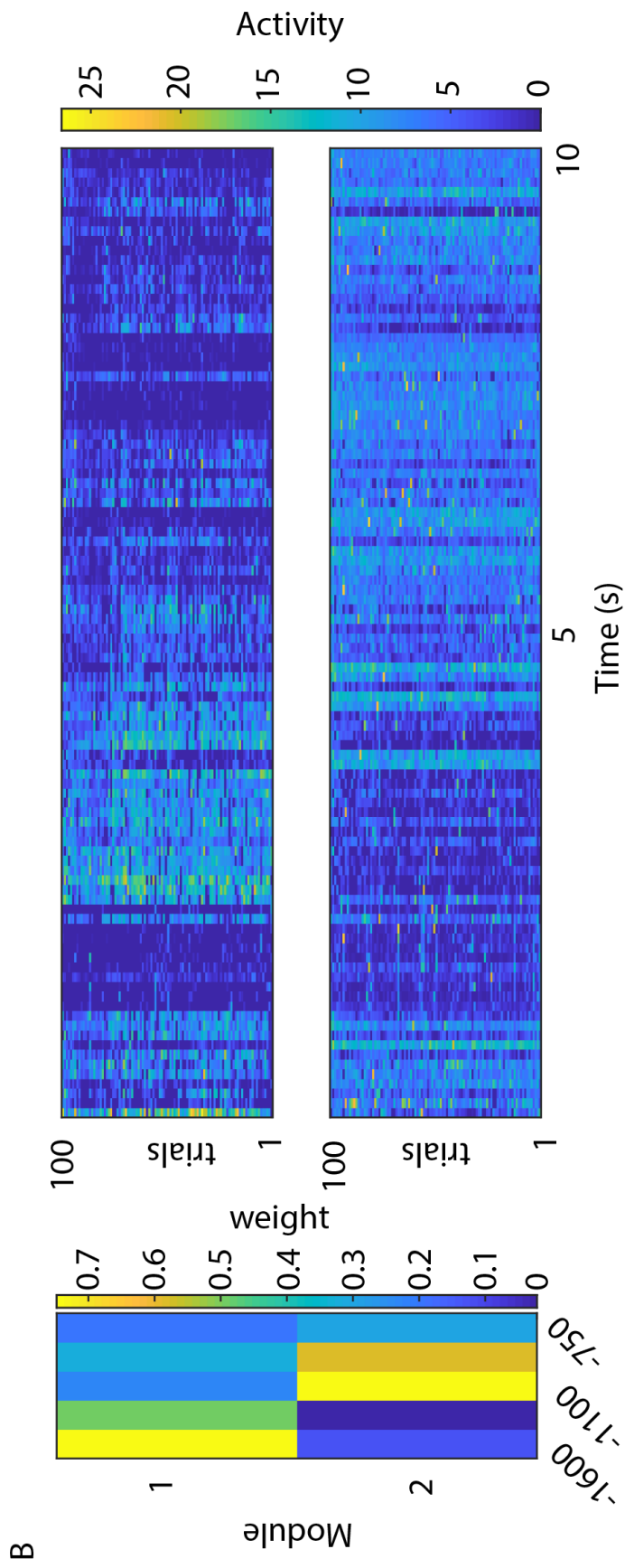
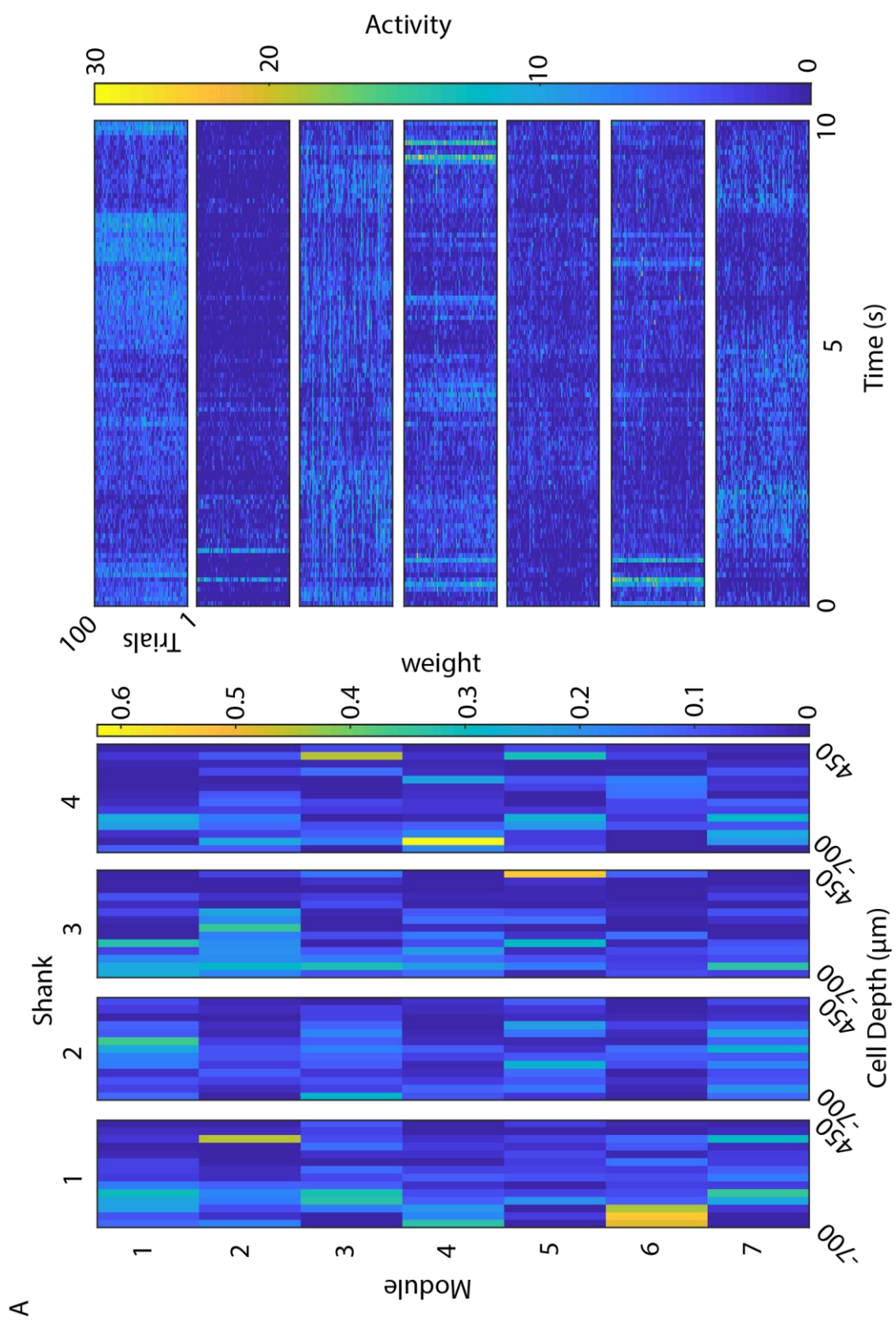


Figure 5.1: Example matrix decompositions for auditory cortex and inferior colliculus single unit populations. (A) Previous page. Cortex example, 4 modules. Far left, cells sorted into broad(left) and narrow(right) cell typings then sorted by depth (this scale is not linear, only ranges are shown for clarity). Left, cells sorted into AC shanks 1-4 and further sorted by depth. Right – for each module, shows the module's activity over the 10 second of sound stimuli (x axis) and across all trials (y axis). (B) Inferior colliculus example, 2 modules. Left, cells sorted by depth. Right, as above, but for colliculus data.



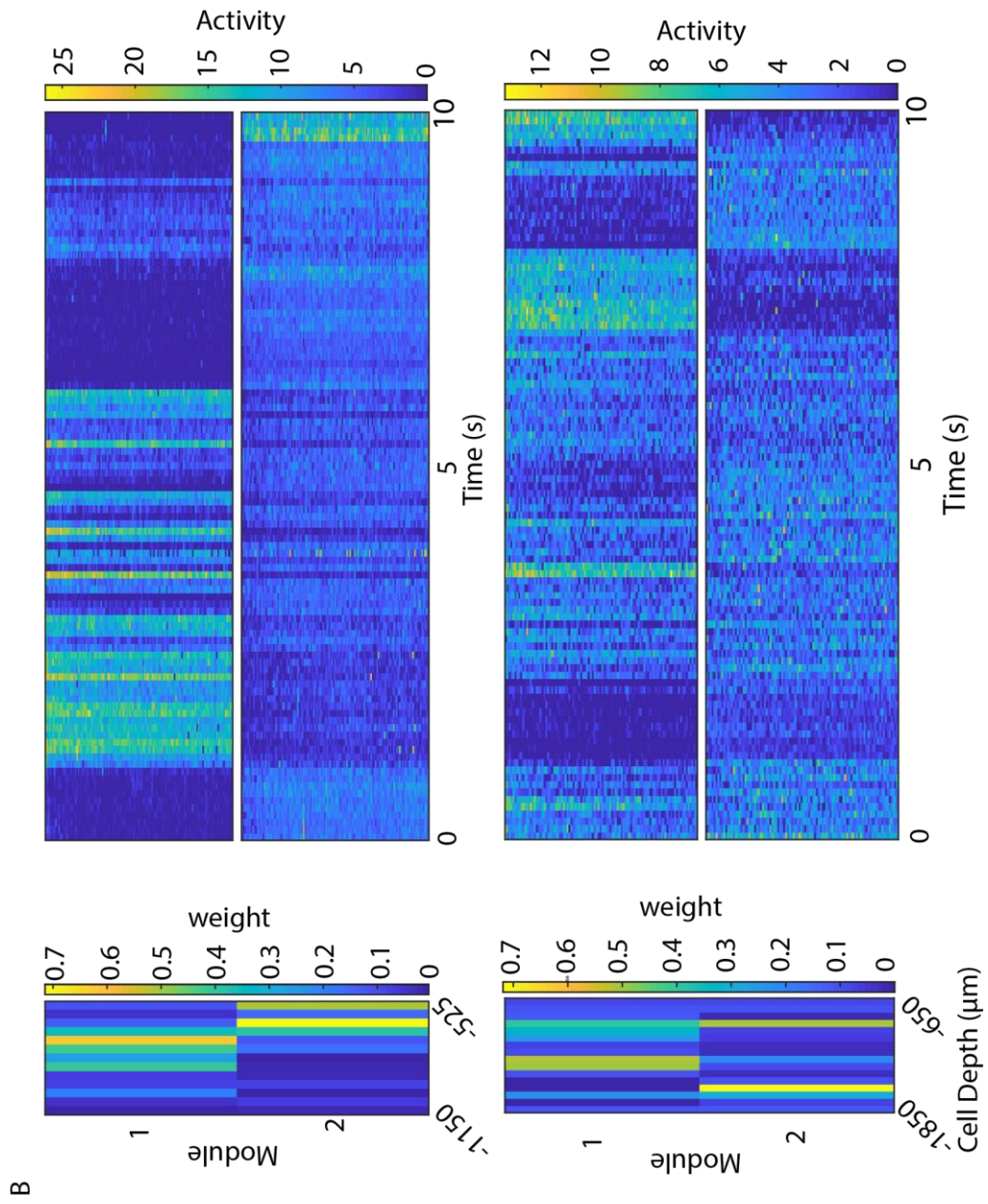


Figure 5.2: Example matrix decompositions for auditory cortex and inferior colliculus multi unit populations. (A) Previous page. Cortex example, 7 modules. Far left, cells sorted into broad(left) and narrow(right) cell typings then sorted by depth. Left, cells sorted into shanks 1-4 and further sorted by depth. Right — for each module, shows the module's activity over the 10 second of sound stimuli (x axis) and across all trials (y axis). (B) Colliculus examples, each two modules. Left, cells sorted by depth. Right, as above, but for colliculus data.

In terms of the number of modules (Figure 5.3), datasets with most units (i.e. AC MUA) tended to have more modules. In general, the number of modules rose roughly linearly with the exception of IC single units and particularly for multi units (AC SUA/IC SUA/AC MUA/IC MUA $R^2 = 0.143/0.038/0.318/0.263$)

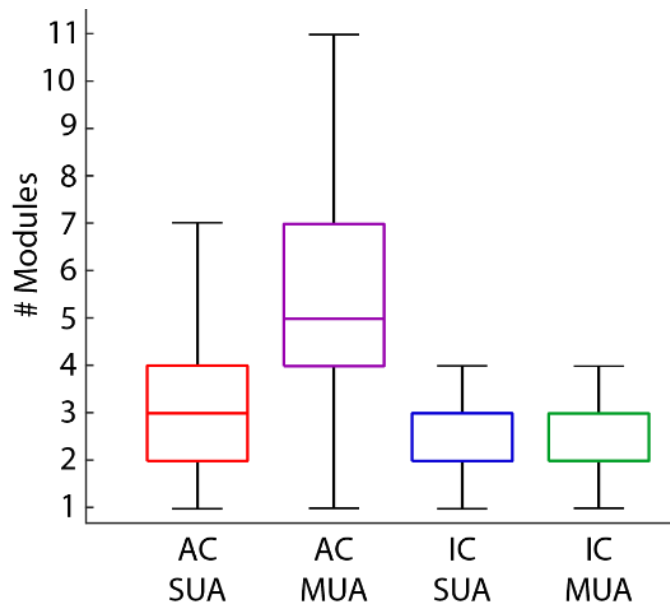


Figure 5.3: Number of resulting modules from spatial decomposition

5.3 Identification of State Through Spatiotemporal Modules

5.3.1 Initial Evidence for Brain State Differences

Spatiotemporal analysis was also run. With this analysis, how the strength of a module changes each trial (not bin by bin) can be derived. As touched upon in the introduction, it is thought that this analysis will reveal potential changes in state, as the activation of a modules changes across trials. Ideally, a bimodality in module strength (with some interim values) would be observed. From the range of datasets, a potential candidate set is selected.

To search for evidence of state transitions, module strength over trial is plotted, then modules are sorted by strength (Figure 5.4A). The delta ratio is also calculated (see Materials and Methods), this is sorted by the same indexing obtained for module strength (Figure 5.4B).

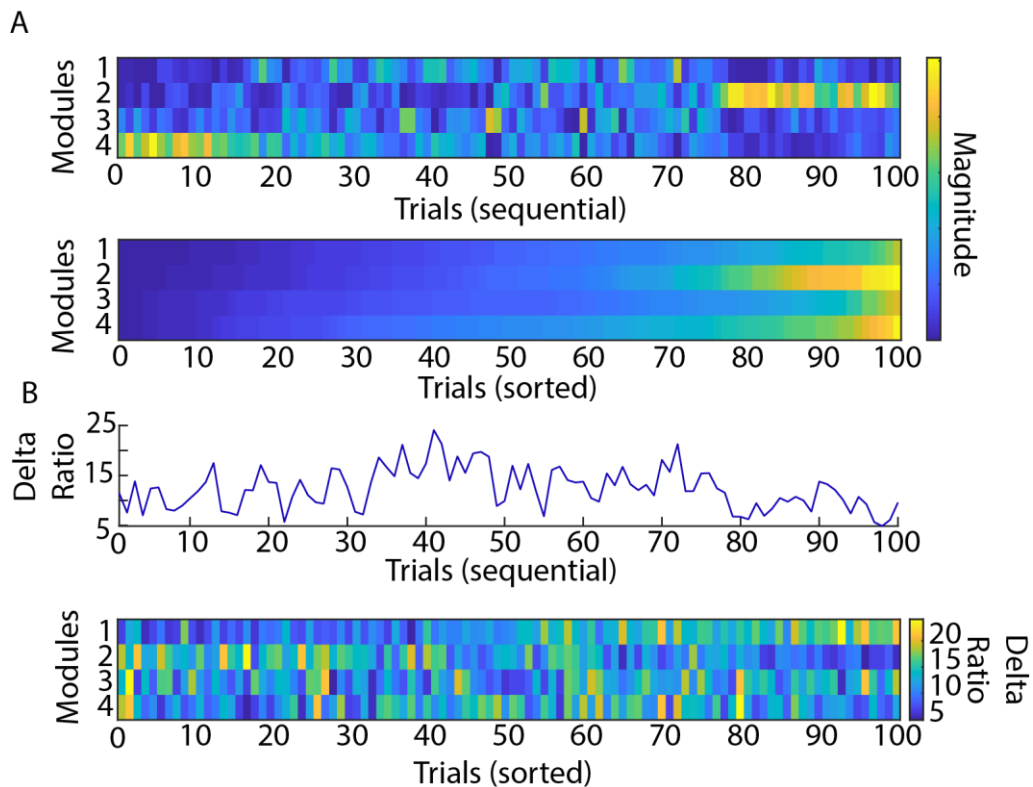


Figure 5.4: Identification of changes in cortical state from spatial module strength in the auditory cortex (A) Top: module strength in each sequential trial, for each module. Bottom: above plot but sorted by module strength. (B) Top – delta ratio calculated using deep LFP channel. Bottom, delta ratio sorted to same indexes as in (A), bottom.

The focus is on module 2 (Figure 5.4A, top, unsorted modules). There are clearly “strong” and “weak” trials, and the delta ratio would also indicate this. When sorting delta ratio (Figure 5.4B, bottom, 2nd row), though it is not a perfect split, it appears that delta ratio for the “weaker” trials is stronger, fading out in the “stronger” half. Speculatively, it could be said that these are indicative of synchronised (high delta power, lower module strength) and desynchronised (lower delta power, higher module strength) trials.

5.3.2 Classification Analysis using Two States

Classifying Natural Sound Trials into States

Module strength was then used as a basis for sorting trials into state 1 (high delta ratio, low module strength, putative synchronised), and state 2 (low delta ratio, high module strength, putative desynchronised). The bottom 40 trials are taken as state 1, top 40 as state 2, and the middle 20 as a transition zone (not to be used). Note, these thresholds were not set in a quantitative way, but were merely done by eye, with some small confirmation of differences.

In separating in this way, clear strength differences are observed, with a generally even middle set. State 1 trials also have a significantly increased delta ratio. Thus, there would seem to be some evidence for NNMF revealing states.

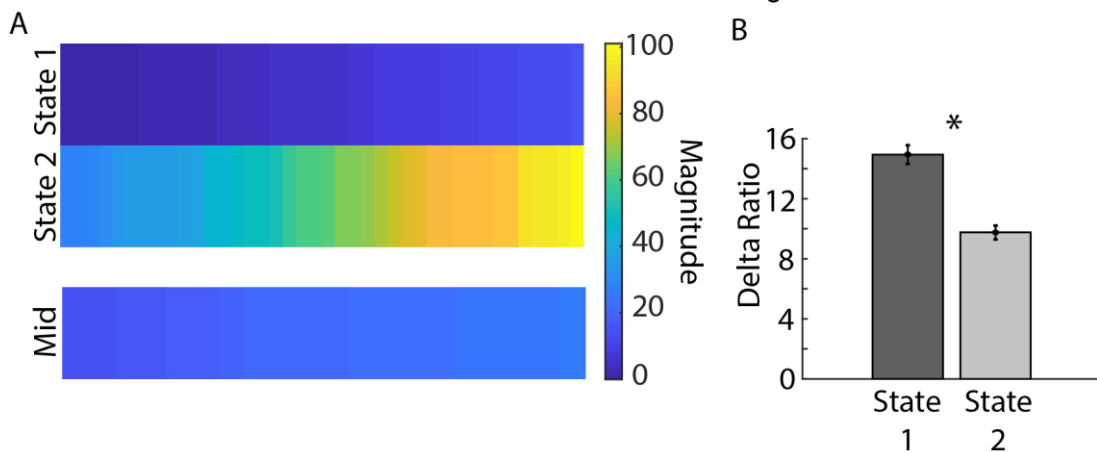


Figure 5.5: Classification of natural sound trials into putative synchronised and desynchronised states. (A) Power of State 1 (first 40), State 2 (last 40) and middle (middle 20) trials. (B) Mean delta power in state 1 and state 2 trials. Error bars indicate SEM. Values are significantly different (p value $2.7462e-9$, t test)

Putative Desynchronised Trials Give Better Classification Performance

As state is known to affect sound coding, each set of 40 trials is used for classification analysis, to look for differences in prediction error. The desynchronised state is expected to perform better given a lowered trial-trial variability. Three different stimulus lengths are examined (down from 17 in Chapter 4).

In each of the three stimulus lengths examined, the set of “desynchronised/State 2” trials (right box plots, Figure 5.6) provided significantly better classification performance than “synchronised/State 1” ($p < 1.978e-131$, Wilcoxon rank-sum test). This is in keeping with expectations.

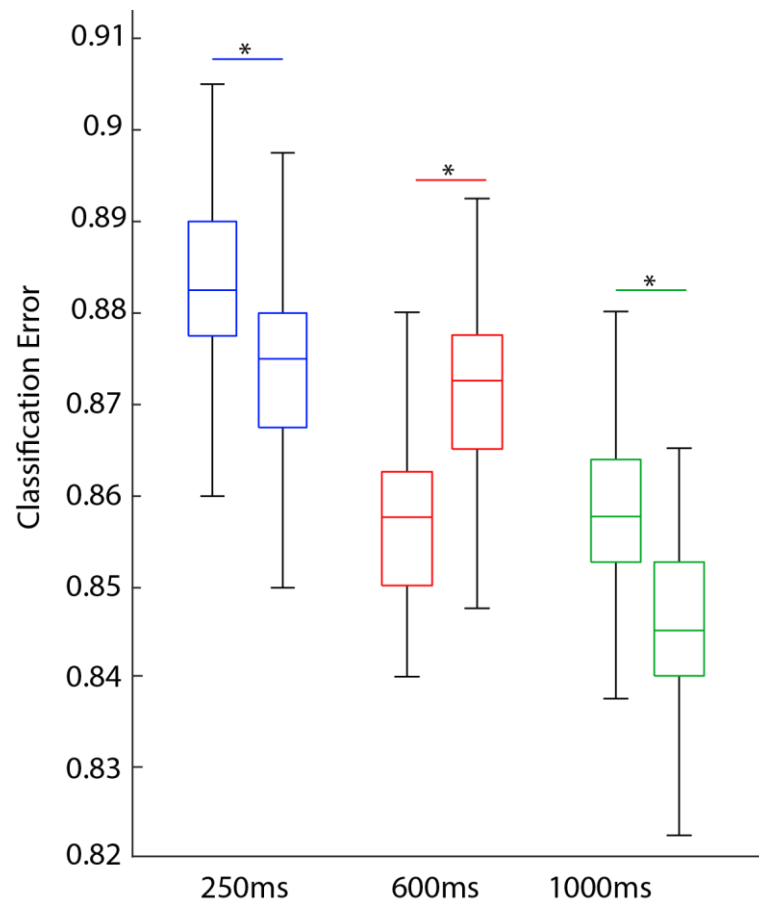


Figure 5.6: Classification error for states 1 and 2 in auditory cortex (three stimuli lengths). Each colour represents a different stimuli length, with the left-hand boxplot as state 1, and right hand as state 2 results. Significances are between states, for each stimuli length. *p* values for 250/600/1000ms: 1.9781e-131/ 1.1872e-307/ 4.6745e-278, Wilcoxon rank-sum test.

5.3.3 Effect of Fano Factor and Spikes Per Bin on Classification

Having previously observed potential influence of Fano factor on the classification outcome, and potential effects of spike rate, these are examined during the trials of each state, where slightly unexpected results are seen. These are displayed in Figure 5.7 on the following page.

Taking the median of the Fano factor across all 10 stimuli, no significant differences in the Fano factor for lengths 250 and 600 are seen, unlike 1000. Overall, there is a trend for state 2 to have a higher (and more variable) Fano factor across trials. Splitting this into each of the 10 stimuli, some (i.e. 2-6) stimuli show the state 2 having a higher Fano factor. This is in conflict with what was observed in Chapter 4, where the comparable classification with fewer predictors was attributed to the lower Fano factor. Potential reasons for the discrepancy will be touched on in the discussion. Splitting by cell strength/module contributed was also attempted in a very basic

manner, and saw similar results. There are no significant differences in spikes per bin between states, for any stimulus.

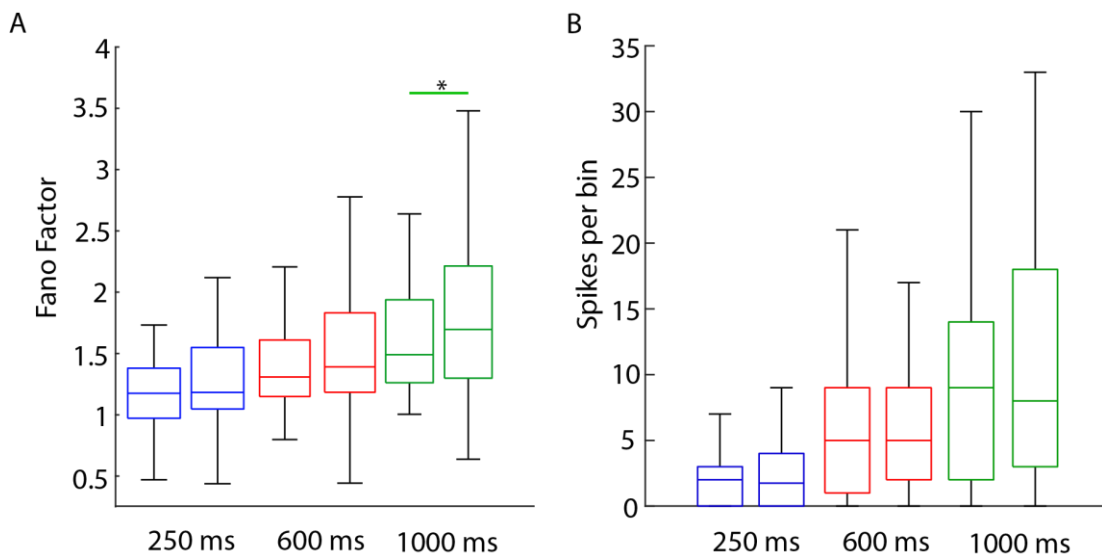


Figure 5.7: Fano factor and spikes per bin in each state (three stimuli lengths). (A) Fano factor. Significant differences seen only in 1000 ms. p values 250/600/1000 – 0.2861/0.1290/0.0102, Wilcoxon rank-sum test (B) Spikes per bin (across all 10 stimuli) for each stimuli length and between states. No significant differences (p values 0.9778/0.8661/0.8165, Wilcoxon rank-sum test).

5.3.4 Noise and Signal Correlations and their Effect on Classification

Another potential contribution to performance is now examined – noise and signal correlations.

Looking at correlations, the median pairwise noise correlations of the population (all and positive only) in state 2, the better performing state, was significantly lower for most conditions ($p < 0.0143$, Wilcoxon rank-sum test). It is slightly more complex for signal correlations, which were significantly different when not splitting into positive and negative ($p < 0.0016$), but this difference was less obvious after a split into positive and negative. Overall, noise correlations in state 2 are significantly smaller than state 1.

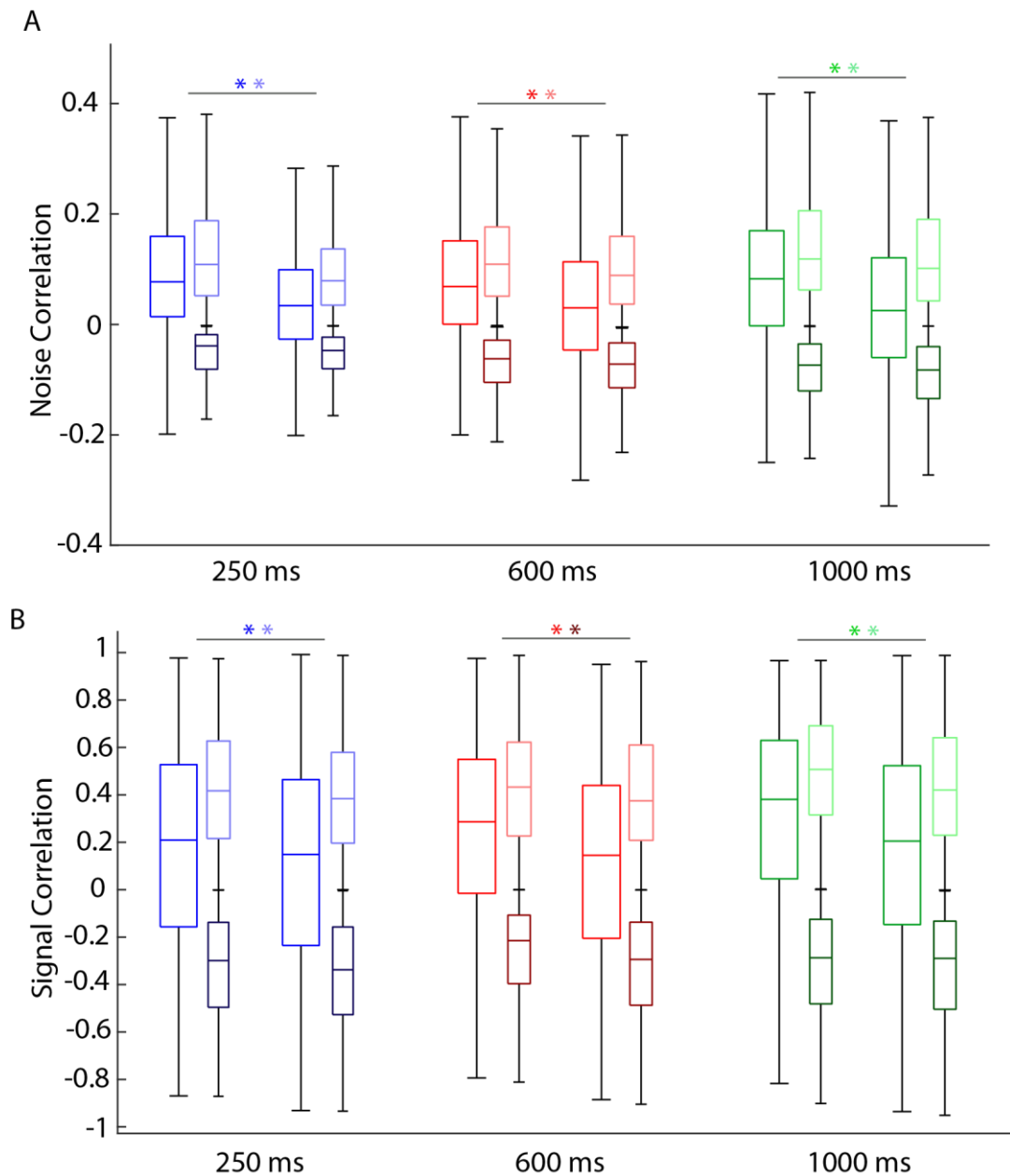


Figure 5.8: Pairwise noise and signal correlations in each state (three stimuli lengths). Mid colour boxplot – all correlations combined. Pale plots – positive correlations only, dark plots – negative correlations. (A) Noise correlations. Significant differences seen in all correlation condition, for all stimuli lengths (p values: $2.081e-23/4.8085e-14/2.39e-16$, Wilcoxon rank-sum test). Significant differences also seen in positive correlations, p values $2.6475e-11/0.0143/0.0012$. Negative correlations were not significant, p values $0.1601/0.0738/0.1469$. (B) Signal correlations, these were significantly different between states for the “all” condition – p values $0.0016/4.755e-11/3.1458e-14$, and significant for 2 of 3 for positions (p values $0.0347/0.0874/2.2167e-6$). They were significant for 1 of 3 for negatives, p values $0.2117/0.0008/0.9577$, Wilcoxon rank-sum test

5.3.5 Inferior Colliculus – Determining State from Module Strength

As the recordings are simultaneous, it may be that splitting the IC activity in the same trials as cortex will produce different and interesting results. Multi unit activity is used as this contained more units than the corresponding single unit data. We have previously sorted trials of auditory cortex activity from low to high strength – in this analysis, IC activity trials are arranged in this same order (i.e. based on AC activity strength, not IC). Using the indexes of the previously sorted the auditory cortex trials,

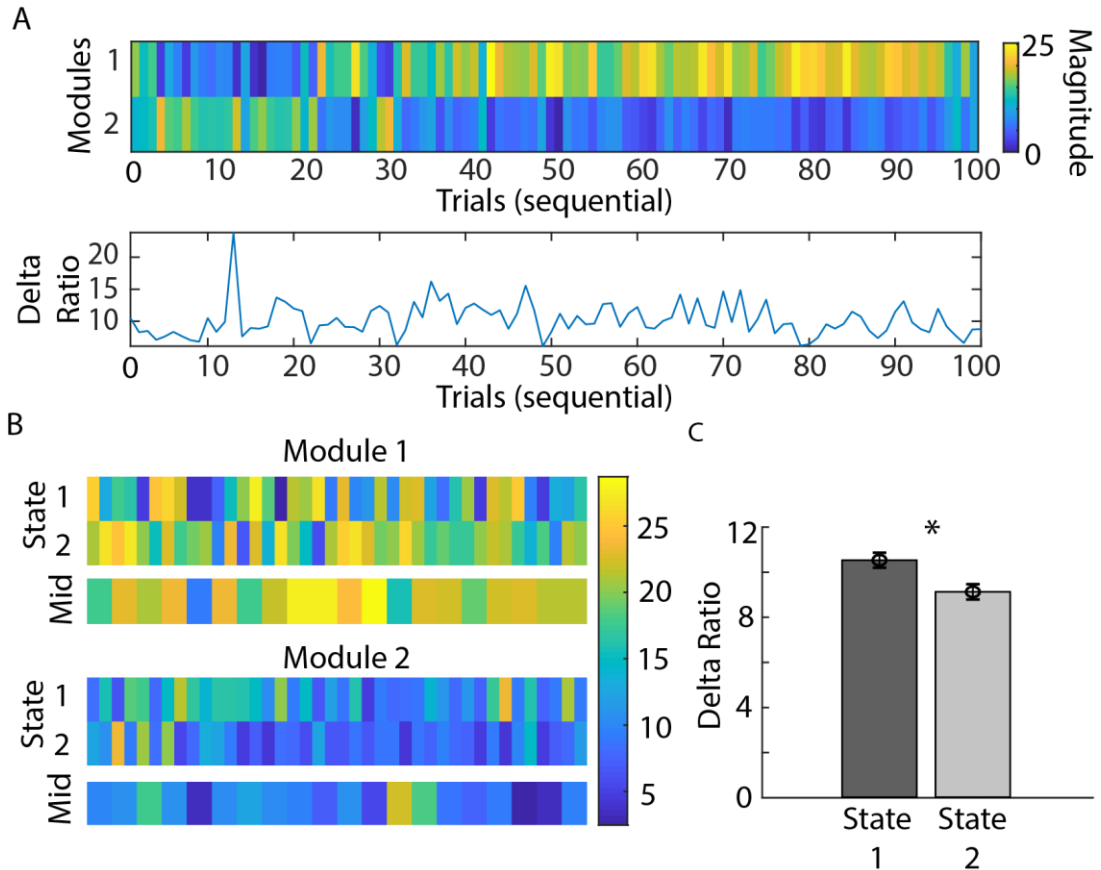


Figure 5.9: Classification of inferior colliculus natural sound trials into putative synchronised and desynchronised states, using auditory cortex results (A) Top, Module strength over consecutive trials. Bottom, delta ratio calculated with middle channel. (B) Module 1 (top) and module 2 (bottom) trial strength sorted using same order as in auditory cortex analysis. (C) Delta ratio in state 1 and state 2, as sorted by auditory cortex trials. Data presented as mean \pm SEM, $p = 0.0041$, t -test.

the module strength of both IC modules is rearranged, and the delta ratio calculated at a middle channel (16). These are displayed in Figure 5.9.

The visual results here are less obviously bimodal than the auditory cortex. In Figure 5.9B, trial strength of each module is sorted according to auditory cortex strength, and unlike in the cortex, there is no split into predominantly high or low strength. A difference in in the delta ratio is still observed, where state 2 has a significantly smaller

average ratio than state 1, though the difference itself is small. Despite the unclear differences, the same classification analysis using these trial subsets was performed.

IC Classification with State Splits Reveals Unexpected Results

The results from the IC analysis are less clear. There are very few cells (5) and performance is near or exceeding chance level error. In Figure 5.10, it is seen that for 2 of 3 stimulus lengths, there is still a smaller error for state 2, but this is reversed for the mid length stimulus (600 ms). Overall, the differences are very small (0.855 vs 0.845), and so the argument of state 2 performing better is weaker, particularly as the 600 ms length shows the opposite relationship.

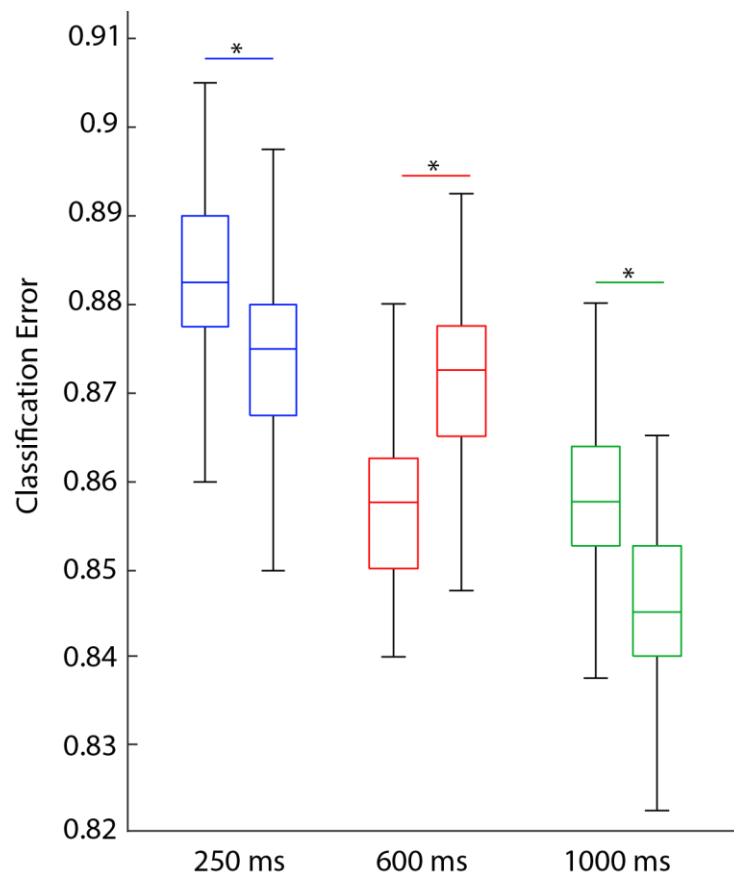


Figure 5.10: Classification error for states 1 and 2 in inferior colliculus (3 time bins). 250 and 1000 ms have state 2 with significantly smaller classification errors (p values, $5.302e-21$, $6.3073e-36$). 600 ms has a higher error (p value $3.0655e-41$, Wilcoxon rank-sum test).

Fano Factor and Spikes per Bin Change Little Between States

There are no significant differences in Fano factor or spikes per bin between states ($p > 0.3125$, Figure 5.11). It should be noted that there is a low number of cells in this dataset, making comparisons more difficult. As before, correlations are also examined.

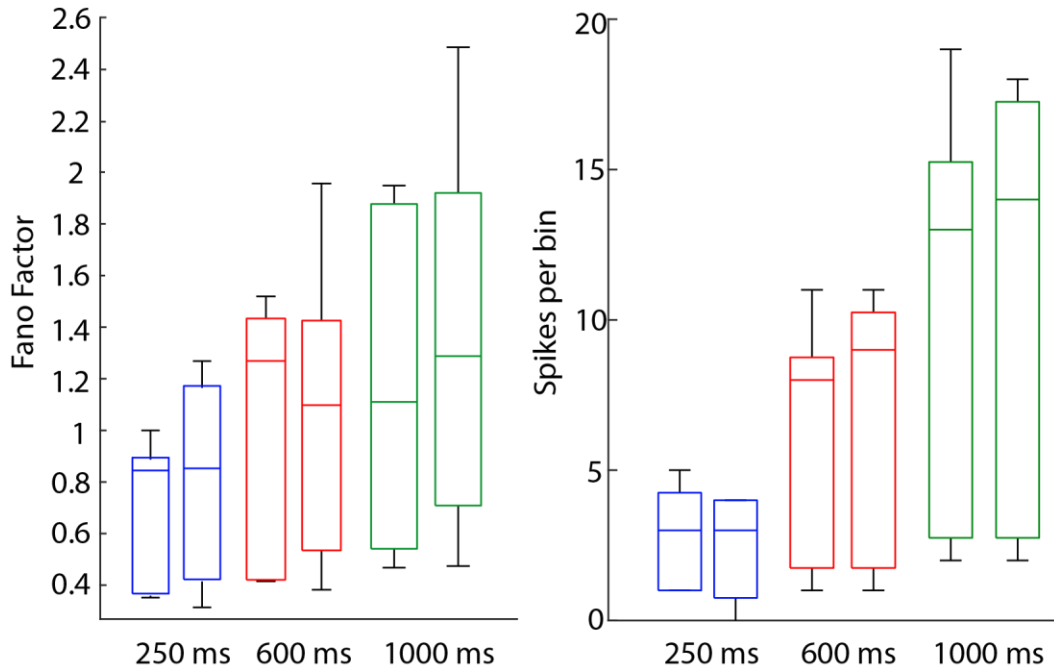
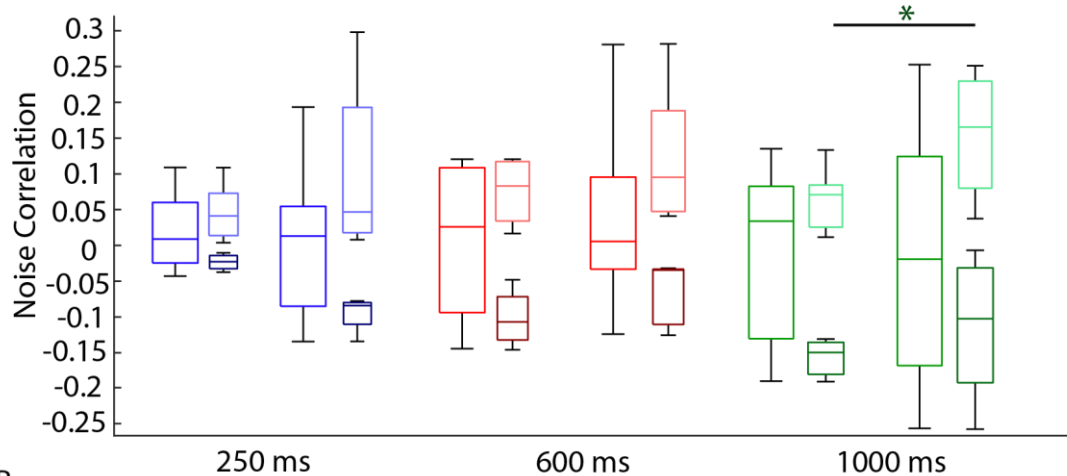


Figure 5.11: Fano factor and spikes per bin in each (three stimuli lengths) (MUA units, $n=5$) (A) Fano factor. There are no significant differences between state 1 and state 2 for any stimuli length ($p = 0.3125/1/0.3125$, rank sum test). (B) Spikes per bin. There is no significant difference between state 1 and state 2 for any stimuli length ($p = 0.7348/0.8389/0.9033$, Wilcoxon rank-sum test).

There is Limited Evidence for Differences in Pairwise Noise Correlation Between State 1 and State 2 for the IC

Except in one isolated instance ($p = 0.0285$), there are no significant differences in correlations ($p > 0.1143$), unlike what was observed in the auditory cortex. Given this and the low cell numbers, it thus cannot be concluded at this time that global brain state is affecting the inferior colliculus populations, especially as the initial classification differences were not consistent.

A



B

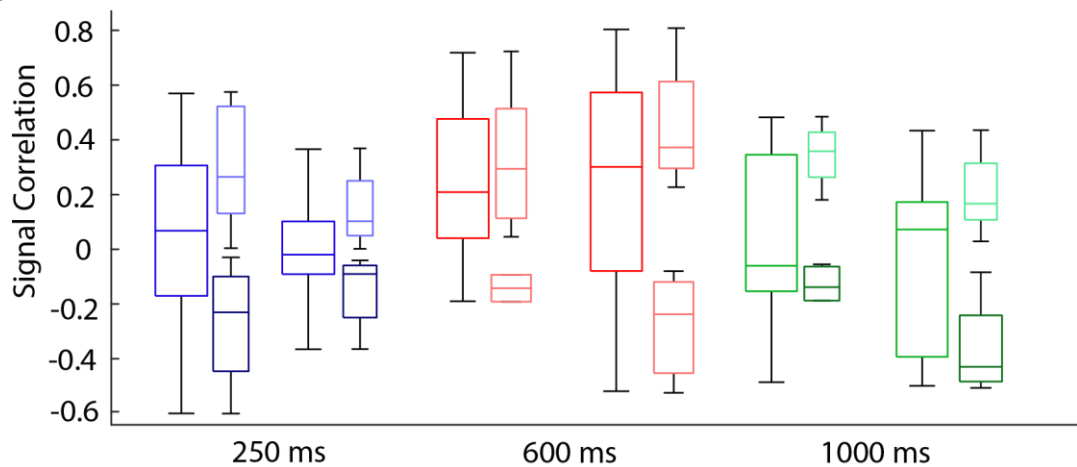


Figure 5.12: Pairwise noise and signal correlations in IC multi units (three stimuli lengths: blue, red, green), between states. State 1, left, single longer boxplot with smaller light and dark coloured boxplots. State 2, as 1, but right hand group. Middle shade – all correlations. Light shade – positive only. Dark shade – negative only. (A) Noise correlations. There are no significant differences between states, except for 250ms in negatives (p values: All – 0.7337/0.7913/0.6776, Pos – 0.6991/0.5368/0.1636, Neg – 0.0285/0.2857/0.9048, Wilcoxon rank-sum test). (B) Signal correlations. There are no significant differences between states at any stimuli length (p values: All – 0.4727/0.7913/0.7913, Pos – 0.2468/0.2810/0.1143, Neg – 0.7302/0.8/0.2571, Wilcoxon rank-sum test).

5.4 Discussion

5.4.1 Brief Summary of Results

As expected from looking at multi unit activity and other related variables of neuronal activity (in previous chapters), and from what is known of the functionality of dimensionality reduction techniques in this area, the observations in spatial decomposition were expected – multi-dimensional activity was reduced down to a handful of smaller populations. These populations appeared to be responsible for different aspects of the sound and worked in harmony, in keeping with the exploratory hypothesis.

Although it was not fully quantified, IC modules were often sorted by depth (i.e. module one cells were shallow, module two cells were in the middle of the shank and so on). In this largely exploratory analysis, there was no obvious trend or pattern of cells within cortical modules – as cells within a single cortical columns are generally tuned in a similar way, observing the same depth dependency seen in the IC was not possible. There was little else qualitatively distinguish between brain areas, despite the hypothesis.

Something also seen is that noise (a single trial with all the activity, unmodulated across 10 seconds, or single overactive cells), tends to be isolated to a single, easily identifiable module that could then be removed.

State transitions were only examined in a single data set. In one of 4 spatiotemporal modules, a clear difference in module strength and associated delta ratio was observed, which was taken as being the synchronised and unsynchronised states. Use trials from each “state”, it was found that the synchronised state performed better in classification analysis, but that noise correlations were unexpectedly higher. Similar analysis in the inferior colliculus saw very limited evidence.

5.4.2 Comparisons to Previous Literature and Results

As mentioned in results, when decomposing into spatial modules, a “shifting” of activity between modules is seen. This is similar to what was observed qualitatively in multi unit activity in Chapter 3, where different neurons responded to different sections of the sound. Seeing IC modules arranged in a tonotopic gradient is also in keeping with what is known of IC tonotopy, each group of cells is responsible for a band of frequency. To our knowledge, this is the first time in which both spatial and spatiotemporal modules have been derived from auditory evoked data using NMF.

Though the work here is largely exploratory, the insight dimensionality reduction can and has provided into the dynamics, function and components of neuronal populations is exciting – and it is hoped the work presented here will be an excellent stepping-stone to posing more pointed questions.

While the work is novel, it was largely exploratory and is yet to provide new knowledge of auditory coding to compare to recent literature on the subject. In this instance, comparisons are thus made to previous literature utilising the NMF technique, in order to highlight the potentials of the technique as a whole. The most relevant literature of comparison (currently) is the 2017 paper by Lui et al, in the retina. Though they based inputs on Spike Triggered Averages (rather than spike rates alone, as was done here), and performed more in-depth analysis, in principle, the spatial decomposition may have identified sub-populations in a larger neuronal population that were responsible for different aspects of the sound, with limited initial constraints or assumptions. Both the current study and Lui et al's study highlight the suitability of NMF for analysing this kind of data.

In the literature review (and also in Chapter 4) trial-trial variability was linked to better decoding performance when using a single spike rate code. In the cortex, there will be less variation between trials when in a desynchronised state: therefore, if this is indeed the case, in applying classification analysis it is expected desynchronised state to perform better. While this was the case, unexpectedly, there were no significant differences in Fano factor between states – and in fact, it appeared as if state 2 had a tendency to be more variable. This does not match either the previous results of this thesis, or the literature, considering state 2 to be desynchronised.

Noise correlations were, however, significantly lower in the “desynchronised state”, which better matched previous results. It is possible that a portion of the cells in this particular dataset are variable across trials, but are similarly variable across all stimuli and are not necessarily contributing to sound coding. By not aiding in the differentiation of stimuli, these neurons contribute less to the classification accuracy (they are background noise).

Overall, these results suggest the capacity of NMF to catch variations in attentional state, something which has only been observed very recently (Tsunematsu et al., 2020) and may prove useful for population analysis. Not unexpectedly, evidence of different states in IC modules was not at all clear, with classification success very low overall.

5.4.3 Limitations and Considerations

The main limitation of this results chapter is its exploratory nature, meaning the extent to which data was analysed is limited. Specific questions relating to auditory population activity were not posed in this instance, but instead (as the analysis has never been done in these brain areas), the analysis aimed to provide a general picture of potential outputs. In this regard, it was reasonably successful, though it was unfortunate that there was no time to take the analysis further.

As with previous chapters, there was a continuing lack of IC units, which may have skewed IC decompositions to low module numbers – without larger datasets, it cannot be said if this is due to the biology or a simple lack of data.

Analysis of state transitions was very brief (a single dataset) and relied on delta ratio recorded from the probe itself as EEG screw data was not clean. Ideally, this analysis would be performed with pupil recordings to get an accurate assessment of state. Classification analysis was performed with fairly few (20) trials in each condition – more would be desirable to increase robustness of observations. Certainly, as the Fano factor results were contradictory to previous work on linear classification, it would be desirable to confirm or deny the observed relationship in other datasets.

5.4.4 Functional Implications

At this exploratory stage, it is difficult to link the results shown here to new implications for functionality of the auditory system – other than general statements regarding the behaviour of populations. To do this, more specific questions should be posed, and the components of each module examined fully. In any case, the analysis has revealed the presence of multiple, seemingly functionally distinct populations of cells with the brain areas, paving the way for further research into their exact function, components, and dynamics.

Though only shown in one dataset, the apparent ability of NMF to at least partially identify different attentional states has implications for the field of auditory research – it may be a new tool to effectively link state and population activity. That trial-trial variability was not lower, despite previous literature and previous results, either speaks to a dataset specific effect or to an interesting avenue of discussion by itself. More analysis (for example, further restricting the focus to the cells most active in the state dependent module) is required before a statement can be made on precisely what is going on in these cell populations.

5.4.5 Future Work

The future analysis to be performed with this technique is potentially endless. Firstly, the component units of each module should be examined at length, to identify trends/patterns in cell type, firing rate, tuning properties, cortical layer, etc. This will provide a wealth of information as to how cells interact with each other, and for what purpose. The work presented on brain states should be expanded upon – it may be that the effect of global brain state is variable between populations.

Another avenue would be to alter the time bin used to bin the data. 100 ms was used here, but given the importance of timescale on sound coding, a systematic analysis and comparison different time bins (similar to Chapter 4) is likely to reveal interesting and dynamic patterns in module activity, which may in turn be linked back to their underlying function.

With putative populations derived from natural sound evoked activity, the details of modules created during different types and lengths of sound stimuli should also be examined. This would serve to identify if population constituents and characteristics are carried over between stimuli - and if not entirely, how and why do they change?

NMF modules are also very suitable as input variables to mathematical models of encoding and decoding – their use would expand upon the results of Chapter 4 and the associated literature. The simultaneous aspect of the recording could be well utilised to explore dynamic functional connections between the IC and AC in various contexts, perhaps employing further prediction analysis to predict AC populations from IC ones, as was proposed in Chapter 4.

Chapter 6 Optogenetics for Auditory Implants

Chapter 6 is the first and only optogenetics results chapter, presenting the work done using the Chronos opsin and μ LED probes. The main results section of this Chapter is split into two distinct sections for different sides of the optogenetic research – 6.2 and 6.3. In Section 6.1, the Aims of this Chapter are stated, and motivations are explained by reintroducing the issue of poorly performing auditory midbrain implants, and the recent move towards optogenetics as part of the solution. Goals and hypotheses are then presented, including an explanatory figure as to how the two results sections cohere. Section 6.2 primarily deals with the optimisation of Chronos expression in the mouse inferior colliculus, and subsequent validation of an optical response *in vivo*. Section 6.3 introduces the work done with the μ LED technology, including GUI and protocol design, *in vivo* experimentation, and issues arising from subsequent analysis of the data. Finally, Section 6.4 presents a discussion of both experiments and how they are relevant to the field of optogenetic auditory implants. Extensive space is devoted to discussing the issues identified through μ LED pilot experiments, with future improvements to the technology and recording procedures suggested.

6.1 Introduction

6.1.1 Aims of the Chapter

Since the discovery of the Chronos opsin in 2014, it is theoretically possible to stimulate neurons with the frequency required for speech processing algorithms. As such, the auditory and optogenetic research communities have begun to consider the application of optogenetics in the auditory system as replacement for electrical stimulation in brain and cochlea neuroprosthetics. Alongside fast opsin kinetics, there is an additional need for high spatial resolution light delivery devices, with μ LEDs emerging as a prominent tool.

In this final chapter, the overarching goal is to prove the feasibility of combining Chronos and μ LEDs as the basis for auditory midbrain implant. However, this was a lofty goal, and only the initial questions were able to be addressed. As such, the realistic aims in this Chapter are to:

- Optimise of Chronos expression through targeted viral injections in the mouse ICC
- Confirm optical responses from excitation of Chronos opsin, using a surface optic fibre
- Design an experimental pipeline for the use of a μ LED probe (including communication software and providing relevant outputs for analysis)
- Perform a pilot study with μ LEDs
- Address identified shortcomings in μ LED experiments

6.1.2 Relation to Previous Literature

Channelrhodopsin-2 (ChR2), while ubiquitous in the field of optogenetics, does not have sufficiently fast recovery times to be considered for auditory applications – implants require control of stimulation to at least 300 Hz, whereas ChR2 can only reliably time-lock to pulses up to ~50 Hz. Recent work in the cochlear nucleus and inferior colliculus has shown Chronos may be able to provide this high frequency temporal fidelity, displaying time-locking to 250-300 Hz light pulses (Guo et al., 2015). Additionally, by stimulating the cochlea and recording through the ICs tonotopic gradient, optogenetic stimulation has been shown to achieve better spatial/spectral resolution than electrical stimulation, and be comparable to auditory stimulation itself (Dieter et al., 2019).

Though much of the focus has shifted to the use of red light, predominantly in the context of cochlear implants (Hight et al., 2015, Mager et al., 2018b), to date, Chronos has not been expressed in the inferior colliculus for the purposes of testing frequency resolution – the motivation for this part of the project.

Histological evidence from past literature indicates limited dorsal-ventral spread of opsin expression using existing protocols (Guo et al., 2015), and so the first task in this chapter was to establish a viral injection protocol that gave sufficient and accurate coverage of the ICC, specifically assessing the medial-lateral, dorsal – ventral and anterior-posterior expression range, as well as any optogenetic activation that was possible from the surface. Though there now exists transgenic, cre-dependant Chronos transgenic mice, this is a very recent publication (Daigle et al., 2018) and so in this project, viral injections continue to be used. Any results from optimisation of these injections may be useful for future, similar viral injection of new opsins.

The other consideration when examining optogenetics as an option for auditory implants is the device used to apply light. The history and state-of-the-art in optogenetic devices and combination optoelectrodes is covered extensively in the literature review. To work as an auditory implant, any device would have to match the configuration of electrical devices as much as possible, immediately discounting bulky and low channel count optical fibre based devices these are still being used in basic research to test opsins and establish basic feasibility of the optogenetic stimulation.

μ LEDs are emerging as the dominant technology for auditory neuroprosthetic applications (currently focused on the cochlea) (Klein et al., 2018, Reddy et al., 2019). As such, potential issues in the creation and implementation of optoelectrodes should be addressed. When combining recording electrodes and light stimulation, recording artefacts are almost unavoidable, and so efforts are ongoing to minimise these through clever device design (Kim et al., 2019). This is explored more in the discussion.

For the auditory midbrain implant, while material flexibility would be desired in a final product to minimise tissue damage, the need for this property is less pressing than for the cochlear implant, which must be bent and curved through the spiral shape of the cochlea. Thus in this project, channel count and resolution are prioritised, utilising the silicon μ LED devices developed recently at Strathclyde University (Scharf et al., 2016). The control and communication system for the presented probe, while suited for the 1 shank device and pilot *in vivo* experiments, is not suitable for the most recent

6 shank version. In the previous software, each LED must be set manually, and data size of protocols was limited due to where instructions were stored (Scharf, 2016). Thus, there is a need for more flexible communication software for creating long, complex protocols.

In the presented experiments, optical fibres are used to test for optical activation of Chronos, and a consideration must be that the intensity of light from optical fibres also decreases quickly in tissue in accordance of established equations (Stanford University, 2018)

6.1.3 Aims and Hypotheses

This chapter presents preliminary work regarding the combinational use of Chronos opsin, and μ LED devices, as hypothetical AMIs. The initial goals of the project summarised in diagram below:

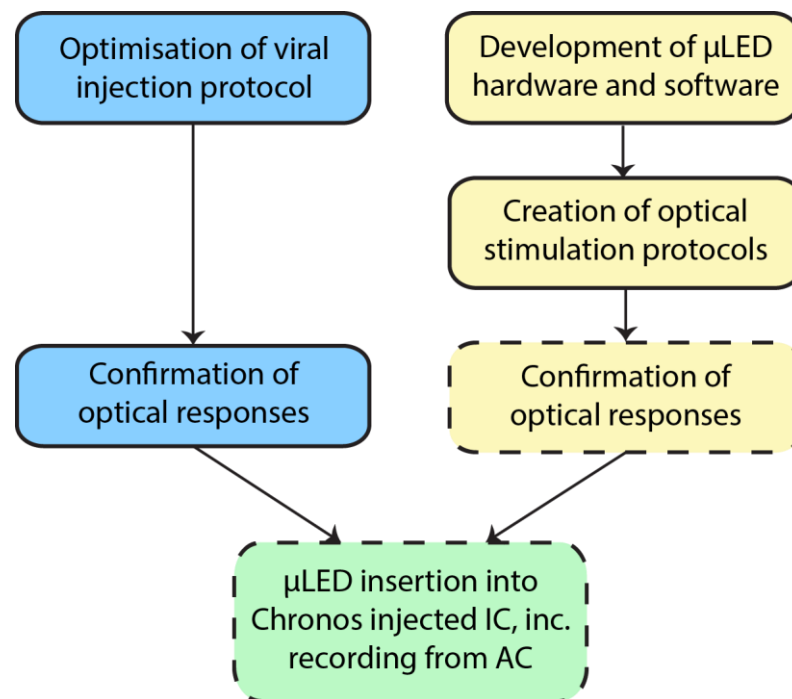


Figure 6.1: Goals of the proposed optogenetic experiments. Blue indicates the virus optimisation experiments, while yellow boxes focus on μ LEDs, with the combination occurring for the green box. Boxes with solid outlined were achieved, dotted outlined were not completed at the present time

As much of the chapter was in the end more technical (optimisation, software design etc), and did not incorporate the Chronos/ μ LED combinatorial experiments previously envisioned creation of true scientific hypotheses posed a challenge. As an alternative, the expectations about how the pilot experiments and experimental optimisation

would progress (given previous literature and existing work within the lab) are presented:

- A single injection of Chronos is expected to not be sufficient for full coverage of the ICC depth given limited medial-lateral spread observed in the histology of previous literature – thus, two injections are likely required
- Chronos should be activatable using optical fibres, and the elicited activity recordable. However, it is likely that the full depth of the ICC will not be able to be activated with a surface optical fibre, particularly the useable intensity may be limited by artefacts. Exactly what depth will be determined by surface intensity and tissue dispersion calculation
- Software/hardware for the *in vivo* implementation of μ LEDs should be integratable into current electrophysiology equipment and analysis pipelines, potentially with significant optimisations required
- The μ LED probe will elicit optically evoked responses, but artefacts may be present

6.1.4 Main Findings

- A pilot study of 8 animals found two injections of 0.4 μ L of rAAV8-syn-Chronos-GFP are most effective at covering the ICC depth
- In chronic preparations, neuronal responses can be elicited using optic fibres and Chronos injected animals – however, this was a rare occurrence due to experimental issues
- Stimulation depth in the ICC roughly matches the predicted values
- μ LED experimental pipelines can be designed and communicated to the probe using a newly designed system in common electrophysiological software, and hardware combined into existing electrophysiology set up
- Stimulation-induced artefacts were incredibly large, and meant that data from a pilot study was not able to be analysed
- Artefacts were dependant on the intensity of stimulation, and may be mostly explained by electromagnetic interference

Though a true proof of concept could not be established (due to hold ups in technology and reasons described above, see discussion), the necessary preliminary stages have been completed to lead into more extensive experiments.

6.2 Expressing the Chronos Virus in the Mouse Inferior Colliculus

6.2.1 Pilot experiment

Summary of Expression

In order to optimise viral injection, 8 mice were used in a pilot study to investigate virus spread in 4 different injection conditions (see Materials and Methods). Coordinates were chosen based on existing literature (Guo et al., 2015), and through logical coverage of the full depth.

Except in one case, viral expression was confirmed (7/8), and was evident in cell bodies (Figure 6.2B). Figure 6.2A, shows an example animal for each of the 4 conditions, plus a summary figure of expression and evidence of localisation to cell bodies. Note that only 10x images are shown for the first condition.

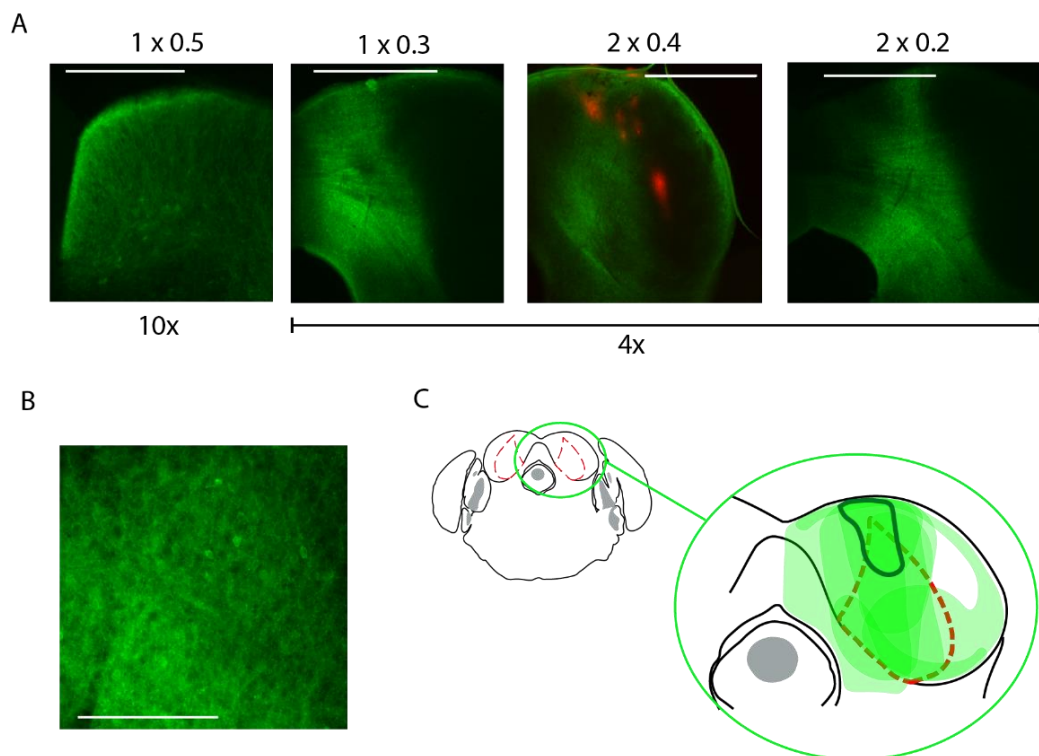


Figure 6.2: Optimisation of Chronos expression in the mouse inferior colliculus central nucleus. (A). Example histology images from each of the 4 injection conditions. The first image is 10x (don't have 4x), while others are 4x, scale bar: 250 μ m (10x), 1 mm (4x). Green – GFP. Red – Dil. (B) 20x image of viral spread, showing cell localisation. (C) Summary of viral expression patterns of all 7 successful pilot animals. Dark green outline indicates the strongest overlap area.

Table 6.1 Summary of initial 8 animals used in optimisation of Chronos expression. Condition 1: 1x0.5 μ L, Condition 2: 1x0.3 μ L, Condition 3: 2x0.4 μ L, Condition 4: 2x0.2 μ L. Leak: indicates if some level of injected liquid leakage out of the injection site was observed during the surgery. Express.: Indicates expression (or not) of GFP, particularly in cell bodies. Widest profile: the anterior-posterior location of the largest area of GFP expression. Full depth: did expression covered the full depth of the ICC. Med-lat: how well was expression centred on the ICC middle? Optical: Was an optical response observed?

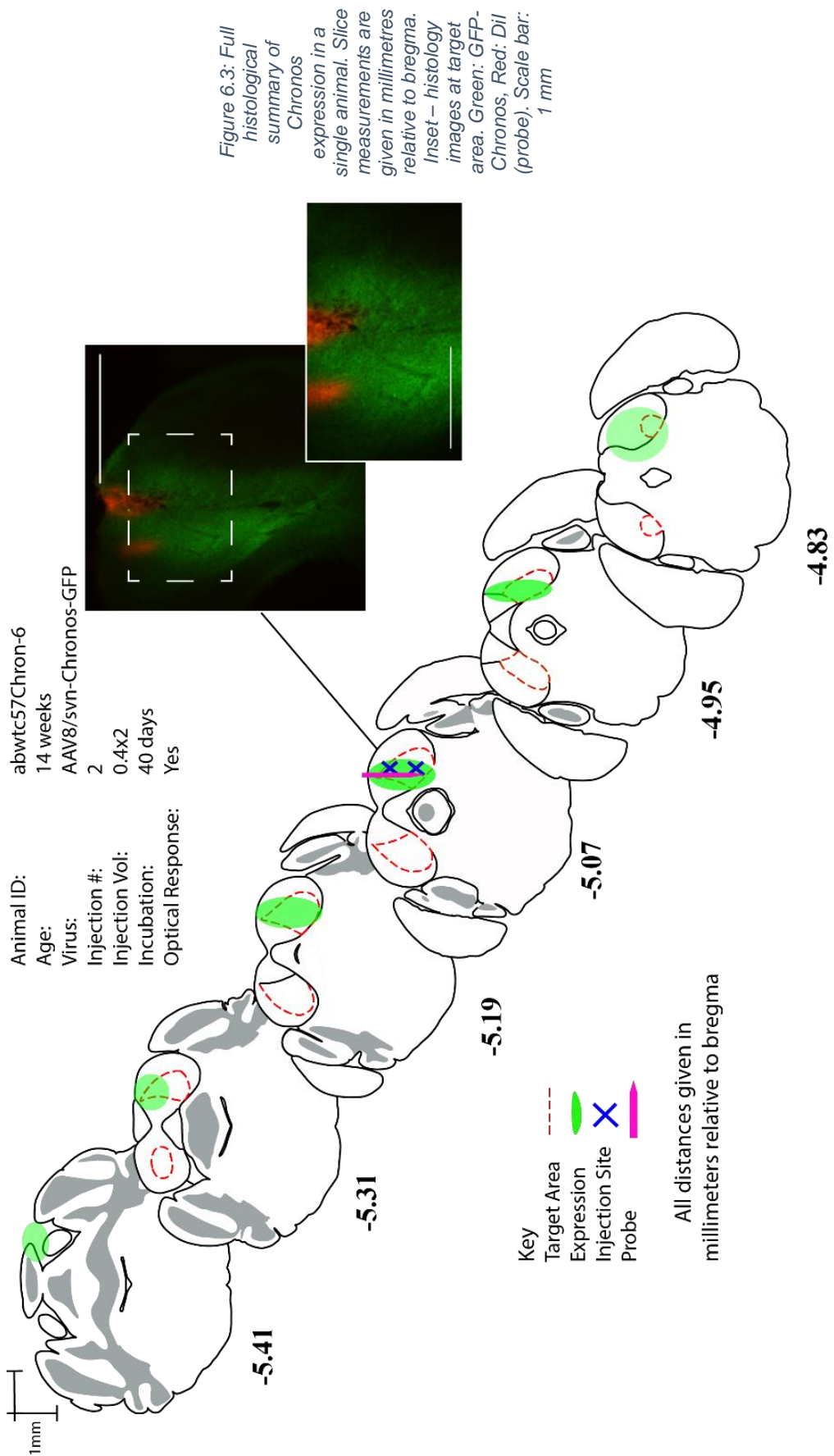
Animal	Condition	Leak	Express.	Widest Profile	Full depth	Med-Lat	Optical?
1	1	Yes	Yes	5.07	No, 800	Ok	No
2	1	Yes	Yes	Can't tell	No, 700	Ok	No
3	2	Some	Yes	4.95	Yes, 1800	Medial	No
4	2	Some	No	N/A	N/A	N/A	No
5	3	No	Yes	5.07	No, 1100	Ok	No
6	3	Some	Yes	5.19	Yes, 1800	Ok	Yes
7	4	Yes	Yes	5.07	Yes, 1600	Ok	N/A
8	4	Some	Yes	4.95	Yes, 1900	Medial	No

What is obvious from the images is that patterns of expression were variable, across conditions and across anterior-posterior gradient. The “best profile” of expression was never more than 0.1mm anterior/posterior from the target coordinate of -5.1 mm – in this regard, the anterior-posterior coordinates were confirmed as valid. However, while anterior-posterior coordinates were correct, medial-lateral was not accurate in all cases, with GFP appearing more medial. Viral leakage was a common issue, resulting in the strong expression at the surface as seen in Figure 6.2A, condition 1.

It was observed that smaller volume injections generally (Figure 6.2A, condition 4) resulted in narrower expression patterns. Ideally, if viral injection, probe and optical fibre were all on target, this would be workable, but more realistically, it is desirable to have as large a volume as possible, ensuring a good medial-lateral spread to maximise chances of finding an optical response.

From Table 6.1 and Figure 6.2, it is apparent that conditions 3 and 4 (2 injections) were more likely to result in expression over the full depth of the IC as desired. To fully investigate the entire IC with optical fibres on the surface and μ LED probes later, it is preferable to cover as much as the structure as possible, and so a 2 injection protocol was selected. To ensure adequate medial/lateral coverage, and to mitigate the effects of leakage, the higher injection volume was chosen (condition 3). Condition 3 was also the only one to result in optical evoked responses – a full histological summary of this is given in Figure 6.3.

Optical stimulation was observed this example animal, but this will be covered alongside the chronic recordings. Optical responses could not be obtained in the remaining animals due to a number of reasons, generally expression being too deep for the optic fibre to reach, or expression being off target (usually medial).



6.2.2 Chronic Optical Recordings and Further Viral Expression

Brief Summary

After selected the most optimal viral injection protocol, a further 9 animals were injected, adding headcaps during the initial surgery. Awake optical recordings were then attempted. Unfortunately, due to a number of variables, this was not entirely successful. From acute and chronic experiments, a total of 4 animals displayed an optical response – with analysable data obtained in only one case due to a combination of technological, software and animal issues (see later discussion). The following text will explore the issues observed with the experiment, and then present some optically evoked data using a dataset obtained from animal 6 in the acute experiments.

Histology Reveals Spatial Mismatch in Probe Location and Viral Expression

Figure 6.4 shows a selection of typical histological images, to illustrate the potential reasons for no optical responses.

From the summary Figure 6.4A (with comparisons to Figure 6.2C), it can be observed that, compared to the pilot study, viral expression patterns were more consistent, and tended to cover the full depth. However, despite using the higher volume, there was occasionally an unexpected lack of medial-lateral coverage (Figure 6.4B ii & iii). Surface expression also was sometimes not present (Bi). These discrepancies are most likely attributable to issues encountered during the injection of the virus (leaking etc). Because of these narrow patterns, the probe often missed the viral expression (Figure 6.4B i). On instances when it appears to overlap (Figure 6.4B iii & iv), it is highly possible that the optical fibre had moved and was not properly illuminating the surface.

Another potential factor limiting optical responses was the level of blood/tissue on the brain surface. As the skull had sometimes only partially healed, the area was often softer and/or less consistent in thickness around the target area. Attempting to create a craniotomy window in these situations increased the inherent risk of sinus bleeding in the IC area.

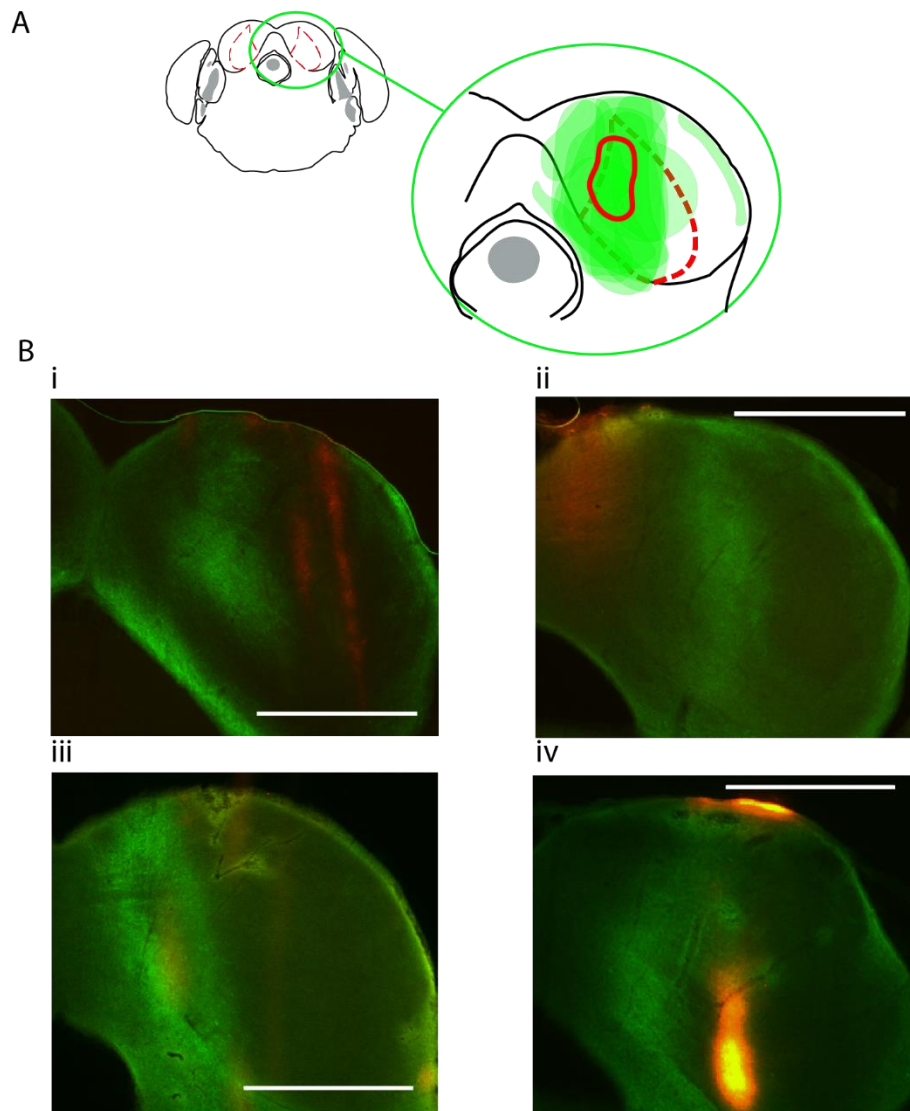


Figure 6.4: Viral expression in chronic recording experiments. (A) Summary figure of expression patterns at 5.07 mm from bregma (the target area). Expression patterns are overlapped. (B) Example viral expression patterns for 4 of 9 animals, illustrating common issues. Green: GFP/Chronos. Red: Dil (probe insertion). Scale bars all 1 mm

In the majority of cases however, probe mispositioning was deemed responsible for not observing an optical response. The next most common issue was the probe and fibre being on target, but then having a lack of expression on the surface or a narrow expression pattern. Issues with accurate/successful probe insertion may be attributed to the difficulty of the experiment (see discussion).

Opsin Activation Decreases with Increasing Tissue Depth

Optical responses were rarely present (4 animals total from 16 tested for optical responses), for a variety of reasons (see Discussion). The recordings taken have not been analysed further than the LED steps, to assess the strength of the optical response with depth. In addition, the last batch of 3 animals, while all displaying an

optical evoked response, have lower quality/less data due to a combination of software, hardware and animal issues. Thus, the data displayed will be a successful acute experiment. Chronos is quoted to respond to intensities as low as 0.05 mW/mm^2 (Klapoetke et al., 2014). The profile of intensity dissipation through tissue is calculated using an online tool – the Optogenetics Resource Centre (Stanford University, 2018). From here, an estimate of how deep responses will be observed can be made (Figure 6.5A). In reality, estimations are likely to be slightly off, due to, for example, blood on the brain surface and the optic fibre being slightly misaligned. From the intensity graph and the knowledge of minimum Chronos activation intensity (0.05 mW/mm^2), it is estimated that activation would be visible down to 1.05 mm ($1050 \mu\text{m}$). Alongside this information, the (background subtracted) MUA activity is plotted, as detailed in Materials and Methods, on each channel and for each stimulation intensity. Only 100ms stimulation was analysed for this figure, and only voltages equal to or less than 1V were utilised (maximum intensity at $1 \text{ V} = 11.65 \text{ mW/mm}^2$). Voltages higher than this resulted in large artefacts in the recording that were problematic to deal with.

With paired stats, baseline values (directly before the light stimulation) are compared with the MUA in the centre (middle 50ms) of the trace, so as to avoid any light evoked artefacts influencing values (Figure 6.5B). MUA values in each channel with intensity are shown in Figure 6.5A. For the highest intensity used (11.65 mW/mm^2) there is a significant difference between baseline and “evoked” activity for the first 24 channels (p range $5.2804\text{e-}14$ at channel 1, up to 0.0177 at channel 24, Wilcoxon sign-rank test). Significance decreases with depth increase). For other intensities, the number of significantly different channels gradually decreases (for example at the middle intensity, effect is significant up to channel 11). In general, the deeper the channel, the less evoked activity is seen, and the less intense the light is, the less deep it reaches overall.

Referring back to the theoretical activation graph which was calculated based on an intensity of 11.65 mW/mm^2 at the surface (Figure 6.5C), Chronos activation is expected up to $1050 \mu\text{m}$ of tissue. It is seen up to channel 24, corresponding to a depth of $1250 \mu\text{m}$, so interestingly a deeper activation than was anticipated. The discrepancy is not large at $200 \mu\text{m}$, and due to the nature of the experimental setup, it’s likely that there may be a slight error in the calibration, or the fibre has shifted during the experiment.

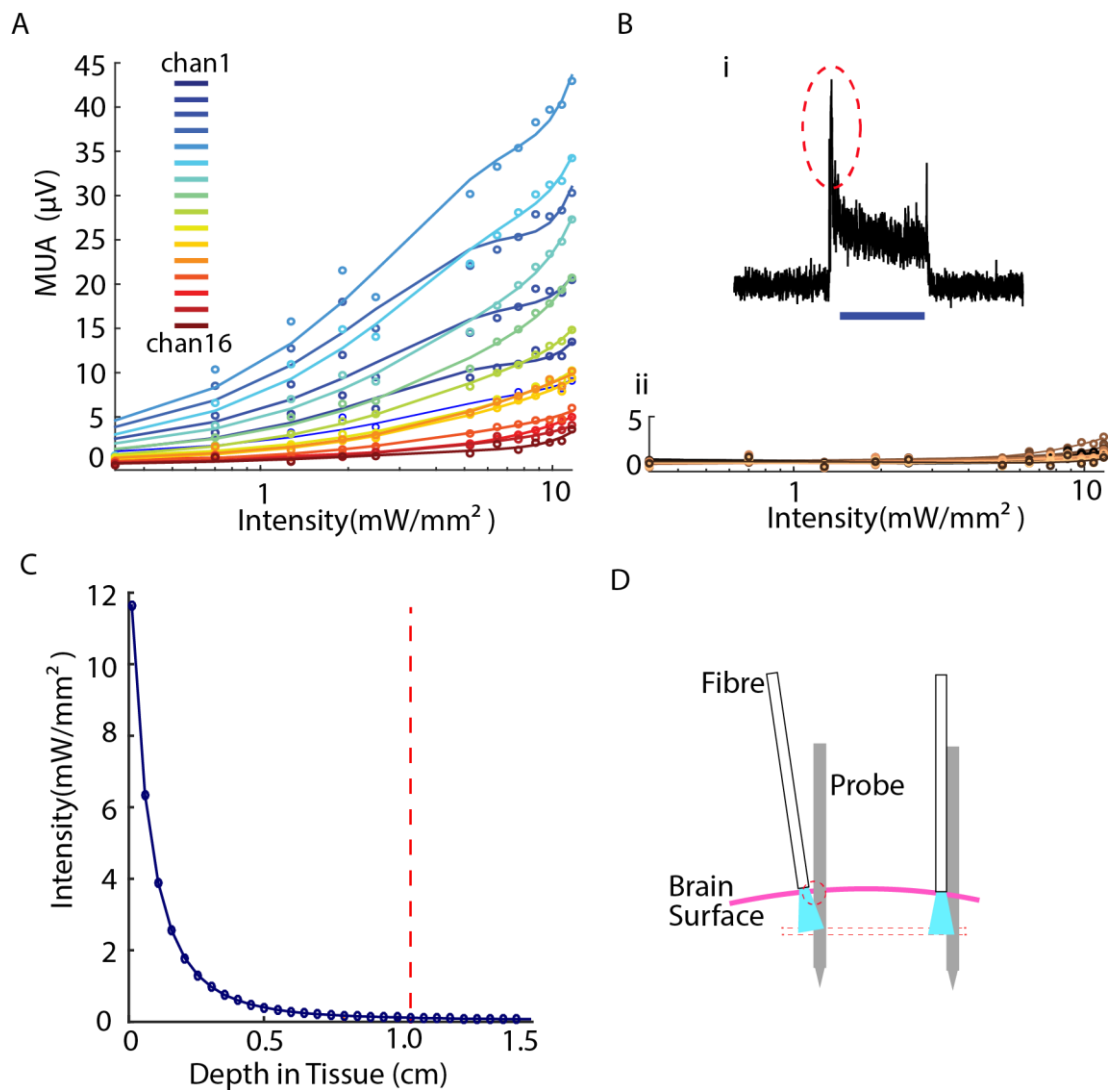


Figure 6.5: Optical activation using Chronos and optic fibre at 0-1 V (A) Average MUA of top 16 channels of 32 channel linear probe, at intensities from 0 to 11.65 mW/mm². Lines are best fit polynomials, order 3. All channels are significant different from baseline $p < 0.01$ (B) ii - As (A), but for bottom 16 channels. Inset (i) shows a typical trace and initial artefact spike. Middle 50 ms was extracted (C) Estimated depth of penetration using highest light intensity in this experiment (11.65 mW/mm²) calculated using Optogenetics Resource Centre (Stanford University, 2018). Red vertical line denotes 1.05cm, after which intensity is not high enough to activate Chronos. (D) Schematic potentially explaining deeper channels activating more than surface channels

Despite the overall dependency on depth, a sequential decrease in MUA through decreasing channels is not observed (i.e., channel 1 does not show the strongest MUA, Figure 6.5C). This discrepancy may be explained if the optic fibre it is not pointing directly down, as illustrated in Figure 6.5D. Stronger light in the centre of the beam may hit lower channels, explaining the highest MUA being at channels a few 100µm below the surface. This non-linearity could also be due to some degree of surface damage (during craniotomy), or other tissue heterogeneities which would impact neuronal activity.

6.3 μ LED Experiments

6.3.1 Introduction

As has been previously discussed in both Chapter 1, and the beginning of this Chapter 6, the μ LED was selected as the most promising device for a hypothetical optical auditory midbrain implant. As a brief summary of the motivations, μ LED devices contain tiny μ LEDs for excellent spatial resolution; can bring the light source directly beside brain tissue; are highly scalable in terms of channel count; can generate sufficient brightness for all opsins, and have a high potential for wireless operation.

Following on from Chronos optimisation, this section was to be done in parallel, and then after establishing both protocols, the sections combined together in a proof of concept experiment. The initial plans for this section were to optimise the experimental setup using a previous iteration of the μ LED probe (the 6 shank, 96 channel), in a mouse expressing ChR2 in PV cells, to both confirm and briefly explore the probe's ability to evoke neuronal responses, optimise the experimental protocol, and have sample data to work with and develop a processing pipeline. The μ LED probe would be inserted alongside a recording electrode to try and examine optically evoked responses.

Unfortunately, due to a variety of issues that will be explored, while an experiment was performed, optical responses from the LEDs could not be confirmed, nor was it possible to use the new iteration of the probe in a Chronos injected mouse. Much of this section will focus on the reasons for the issue, and how they might be mitigated in the future.

6.3.2 Probe Schematic

The appearance of the μ LED probe can be seen in Figure 6.6. Much of the characterisation has been described in the literature review. The probe used in this experiment was the 6-shank version, that had not yet been validated *in vivo*.

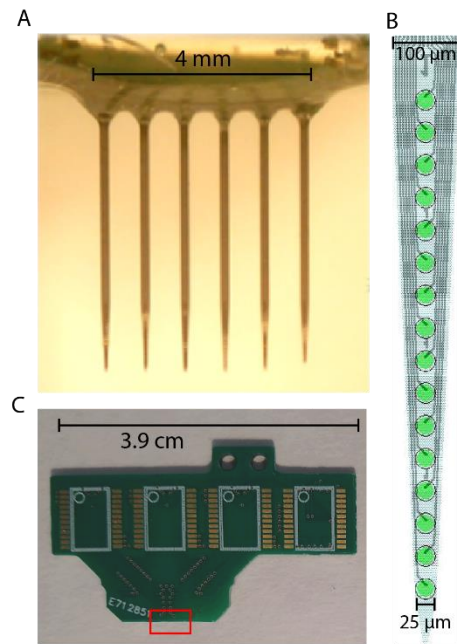


Figure 6.6: Schematic of 96 channel μ LED probe. (A). 6 shank probe, unilluminated. (B) Wire schematic of a single shank, showing wires and LEDs (green). (C) PCB of 96 channel probe, minus probe (red square)

6.3.3 Hardware and Software Optimisation

The user should be able to easily and flexibly communicate instructions to the μ LED probe, and be able to design and run protocols designed to fit the majority of experimental questions. Previously, instructions for a protocol were loaded all at once onto the Arduino board, which had limited storage space. Thus, a communication system was designed by Mr Ruaridh Winstanley (Institute of Photonics, University of Strathclyde), whereby instructions were instead sent, via MATLAB, on an LED by LED basis to the probe. In this endeavour, the researcher provided extensive design input, troubleshooting, and MATLAB code input. The schematic Figure 6.7 shows the basic principles of operation – note that some complexity of connections has been removed. The main purpose of this system is to ensure:

- LEDs are activated in the desired order (i.e. pseudo random, or as the experiment requires)
- LEDs are activated for the desired length of time
- LEDs are supplied with the appropriate current in order to operate correctly and at the desired brightness
- Appropriate meta data is generated to allow post-processing

- The system is easy to use for a typical electrophysiologist

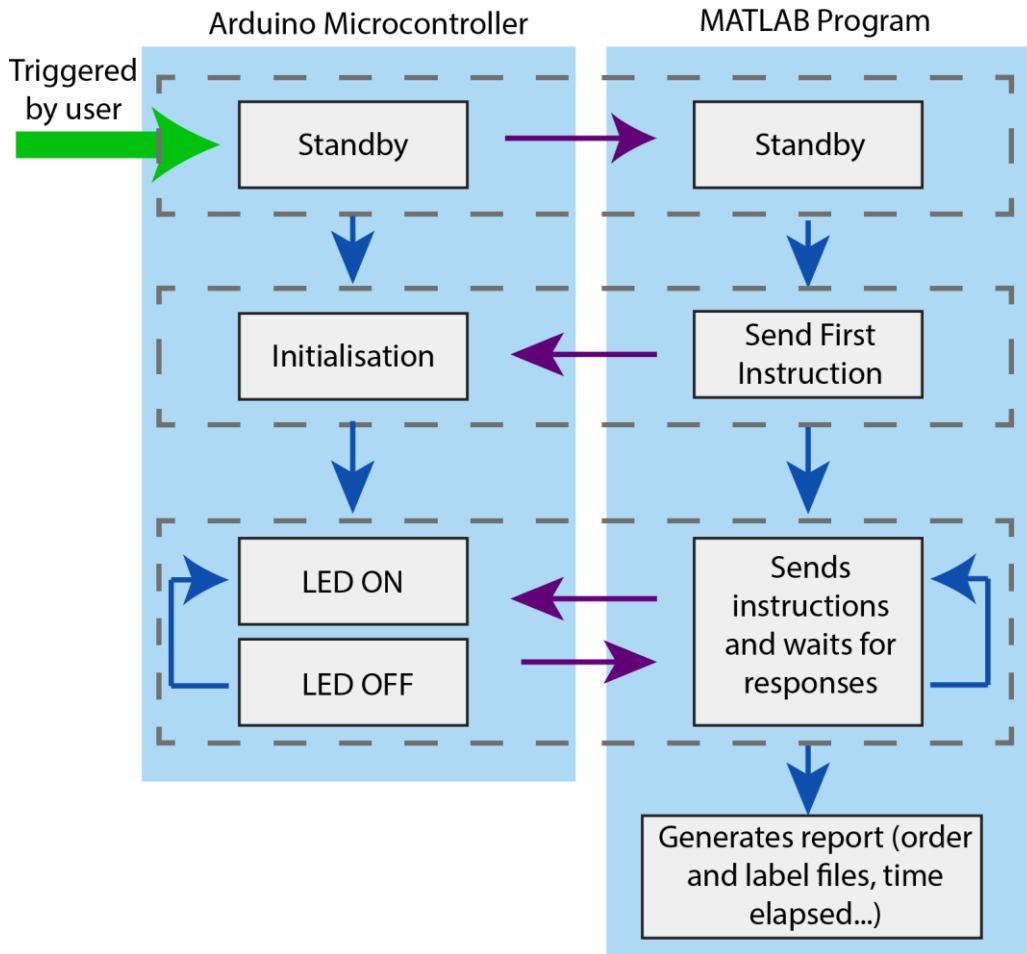


Figure 6.7: Schematic of control software for μ LED probe. Blue arrows indicate steps within a program, purple indicates communication between two programs. Pale blue rectangles mark separate programs, and dotted grey lines show joint program stages.

The general pipeline of operation is as follows. Via a MATLAB GUI, the user designs a protocol for LED illumination, or can load in a pre-created one. Within the GUI, the user can set LEDs to be illuminated, the pattern (i.e. sequentially, pseudorandom), the number of repetitions (and whether or not each should be randomised), intensity, and the on/off times. Generally, only one value of a variable can be examined in one run (for example, if the user wished to examine 3 different intensities, they would have to generate three different protocols, to then be run sequentially). It is possible to generate more complex protocols, but this cannot not be done via the GUI – the user would have to code within MATLAB.

Another, separate program to interpret commands from the MATLAB program is pre-loaded onto the microcontroller. The user then activates the system and the microcontroller (via either MATLAB or LabVIEW depending on which is most

relevant). After initialisation stages, the MATLAB script sends instructions to the microcontroller to activate and deactivate the first LEDs. When the protocol is complete or terminated early by the user, the MATLAB script generates a report of the pattern of LED activations (i.e. order and label files generated from normal auditory protocols), plus the total protocol time. This can then be used in reconstructing the pattern of stimulation and assigning chunks of neural data to the correct stimulation periods. The researcher aided with the design of the μ LED control software (with Mr Winstanley doing the majority of the actual coding due to his extensive knowledge of the LED probe electronics), and then helped with optimisation and implementation in *in vivo* experimental setups.

The main MATLAB script had an additional purpose - calculating the necessary current to activate each LED at the desired intensity. This information was contained in mapping arrays generated by Mr Winstanley. Due to manufacturing discrepancies and failure over time, not every LED was a) able to be operated at all and b) able to be operated in the same range. The mapping told the program which current was necessary to activate each individual LED at the desired intensity, and also if an intensity was impossible for particular LEDs.

LED activation patterns can be made pseudorandom. This means that in “random” activation, LEDs directly adjacent to each other cannot be activated directly after each other. While this might be useful depending on the question, to truly test the basic effects of the device at this stage, interaction effects should be avoided as far as possible by activating an area further away.

The system was designed to be as easy as possible to use. The GUI was intuitive, and a number of template or genetic protocols were created to either run as tests or modify within the GUI. The initial trigger is very simple to modify – an additional MATLAB script was the most effective way (given the GUI), but a very simple LabVIEW VI was also created for implementation into a larger Vis, if desired.

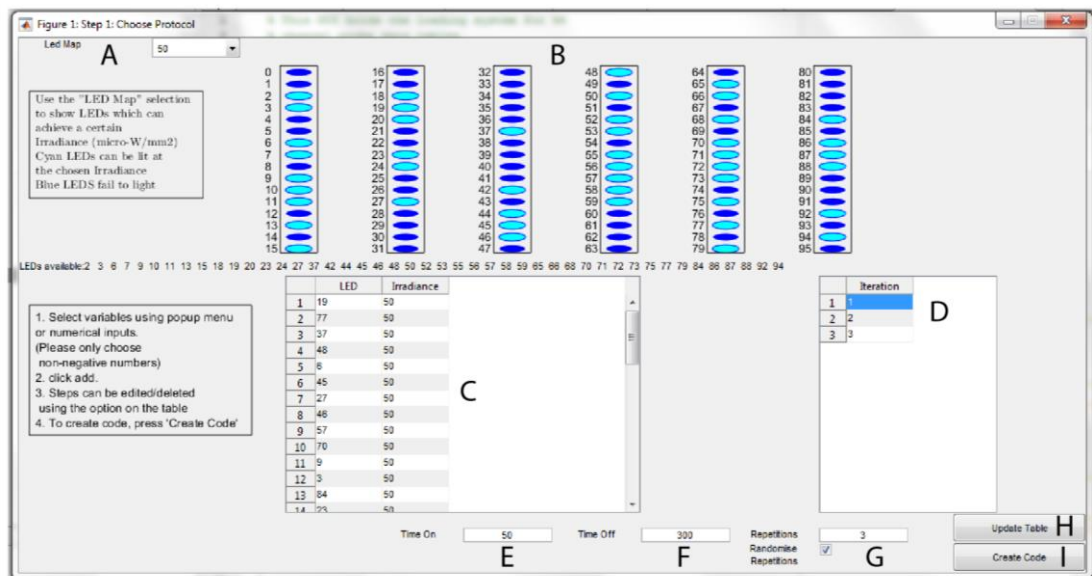


Figure 6.8: Screenshot of protocol creation GUI. (A) LED Map – for choosing which intensity to run the protocol at. The available LEDs will change. (B) Map of available (light blue) and unavailable (dark blue) LEDs at the intensity chosen in (A). (C) Generated order of LEDs to be stimulation. Created by “updating table” with (H). (D) display of how many iterations/repetitions of the protocol will be run. Repetition 1 is selected, this is the order we see displayed in (C), but it can be changed to view others. (E) On time for LED pulse. (F) Off time for LED pulse (G) Set number of repetitions (in this case, 3), and indicate if each repetition should have a new pseudorandom order. (H) Updates the table in (C) with any new settings/repetition numbers. (I) Generates a data table with the information needed to run the protocol – this is then read in by the main MATLAB program which executes the protocol.

The control system was then integrated into the existing recording setup, and some test experiments run before probe insertion. Throughout the optimisation process, issues with using the LEDs were discovered. Some of these were fixed or mitigated before the final experiments, but some still remain to be worked on for future iterations.

- Not all the μ LEDs were working – and those that did often had a limit on their operational frequency. This added an extra layer of complexity when designing protocols, as not all LEDs could generate all intensities. Information within the GUI, plus current mapping arrays in the main MATLAB program, ensured the correct LEDs were activated with the appropriate currents
- GUI was somewhat limiting in the variety that could be examined within a single protocol
- μ LED PCB was incredibly wide compared to other probe, requiring extensive reorganisation of the recording rig to accommodate
- There was only a single probe

6.3.4 Further Optimisation and Success of μ LED Pilot Experiment

Experimental Optimisation

After creating the μ LED communication system, the project aimed to test the probe *in vivo*. Before this could be done, the existing electrophysiology recording setup had to be optimised (this is separate from the main μ LED hardware, and the issue is mainly logistical). This illuminated some practical problems with the existing recording setup (rather than specifically with the software). Examples of these problems are shown in Table 6.2, alongside their solutions (if any).

Table 6.2: Optimisation of μ LED experimental equipment – Problems and Solutions

Problem	Solution
Normal head-fixation in way of probe PCB	Headfix animal with earbars, not head post
Probe PCB is not long, cannot reach brain surface	Lower probe holder rails, raise animal platform
Microscope is blocked by probe manipulators	Worked within very small field of vision, blurry
Lateral accuracy of normal manipulator not sufficient for experiment	Used motorised manipulator instead – bulkier, needed new attachment
Probe is very wide (4mm)	Large craniotomy made

Summary of In Vivo Experiment

The experimental protocol is listed in Materials and Methods, and was performed with a single urethane anesthetised animal. In short, the experiment aimed to successfully insert the 6 shank μ LED probe into the cortex of an anesthetized, ChR2 mouse, while simultaneously recording any optically evoked activity with a 4 shank silicon probe (4x16, linear). Predesigned protocols intended to test the effect of μ LED stimulation at each site, various intensities, and various pulse widths, were then to be run.

In terms of software, the experiment was successful – protocols were run successfully, LEDs were lit inside the brain, and the animal remained anesthetised for the duration of the experiment. It was noted that the PCB heated up considerably – this information was passed onto collaborators. Unfortunately, there were considerable optical artefacts that have prevented the analysis of the recorded data.

Histological Confirmation of Probe Insertions

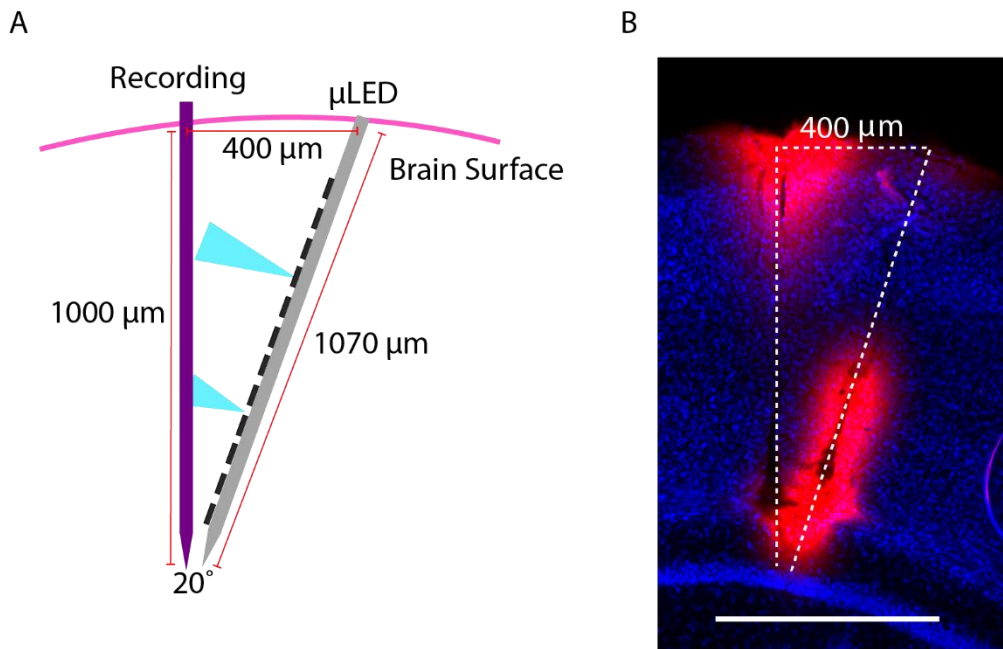


Figure 6.9: Placement of μ LED and recording probes in the mouse cortex. A) Schematic of proposed insertion patterns, with dimensions. Blue cones indicate hypothetical paths of μ LED illumination B) Histological examination of brain tissue after μ LED experiment. Scale bar = 50 μ m/0.5 cm. Red – Dil (both probes painted). Blue – DAPI staining. White lines trace probe insertions, horizontal distance at surface was measured as 400 μ m

It was confirmed histologically (Figure 6.9B) that both the μ LED probe and the recording probe were inserted at the desired depth and angle (Figure 6.9A) along the mouse cortex, allowing optically evoked activity to be recorded if present.

Issues Precluding Data Analysis

Unfortunately, despite a successful probe insertion, there were several issues in analysing the data. The first issue was the overall quality of the recording probe – the probe used was not new, and so spikes were not clear and well defined. An increase in high frequency noise during stimulation periods was observed also, exacerbating this issue. Anecdotally, insertion of the μ LED probe actually resulted in a loss of all spikes, suggesting pressure within the tissue that damped the spiking response. Post hoc, efforts were made to improve signal quality through a variety of filters and averaging techniques, such as Common Average Referencing (where signals are averaged across all channels and this average then subtracted from all channels, essentially removing background activity common to all channels). This did not increase data quality. Additionally, as spike sorting was generally unsuccessful, spike detection thresholds were shifted both up and down, in an attempt to isolate more spikes, but again this did not improve results.

The most pressing issue was the large ON/OFF artefacts observed – appearing as large, almost instantaneous jumps voltage as LEDs were switched on and off. Because both the probes and the PCBs/wires of each probe were close together, illumination and switching off of the LEDs resulted in particularly large artefacts in the recording. On most occasions, particularly at high intensity operation, these saturated the input amplifier, the effect of which can be seen visually in Figure 6.10.

Saturation in this way is a major issue, as it results in the destruction of any underlying neural activity – the neural signals can never be recovered with filtering or other techniques as it was never recorded. Example traces directly from Neuroscope are shown in Figure 6.10, to illustrate the extent of the issue.

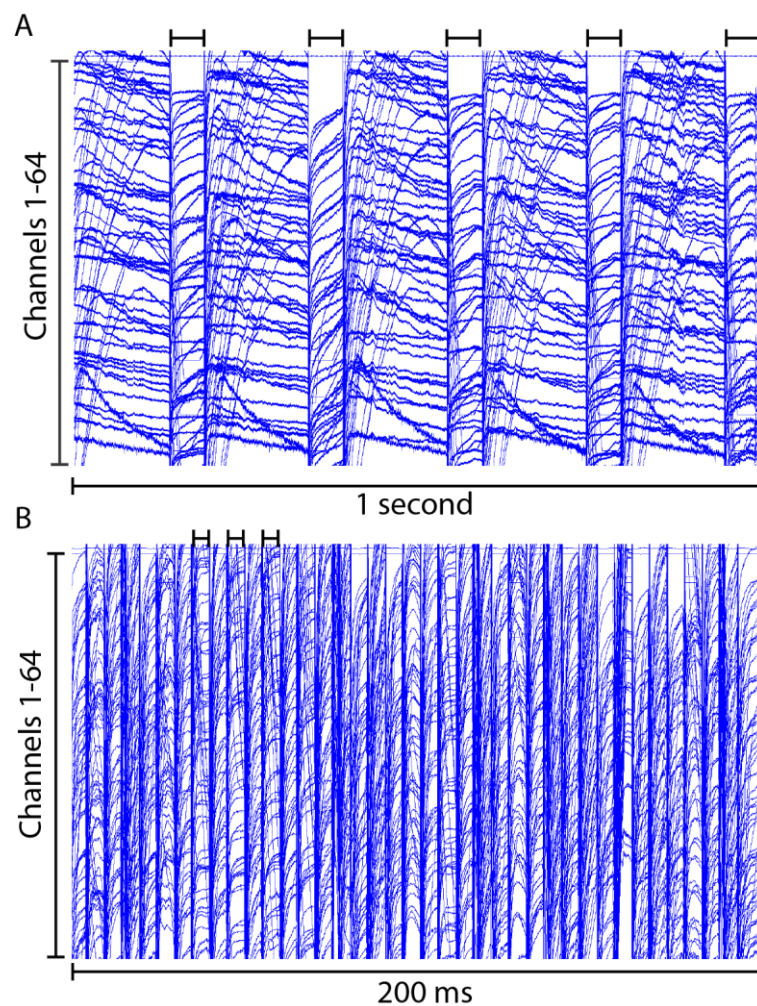


Figure 6.10: Neurotrace screenshots of recording trace during light stimulation. (A) 1 second of recording during 100ms light stimuli. (B) 200 ms of recording during 5ms checkerboard stimulation.

6.3.5 Signal Saturation and Characterisation of Artefacts

Given the pilot nature of this experiment, it was deemed beneficial to examine the artefacts within the data, and identify points of improvement for future protocols, or for the design new probes (potentially incorporating electrodes). The percentage of stimulus repetitions that experienced a degree of input saturation, at three selected currents, is plotted in Figure 6.11.

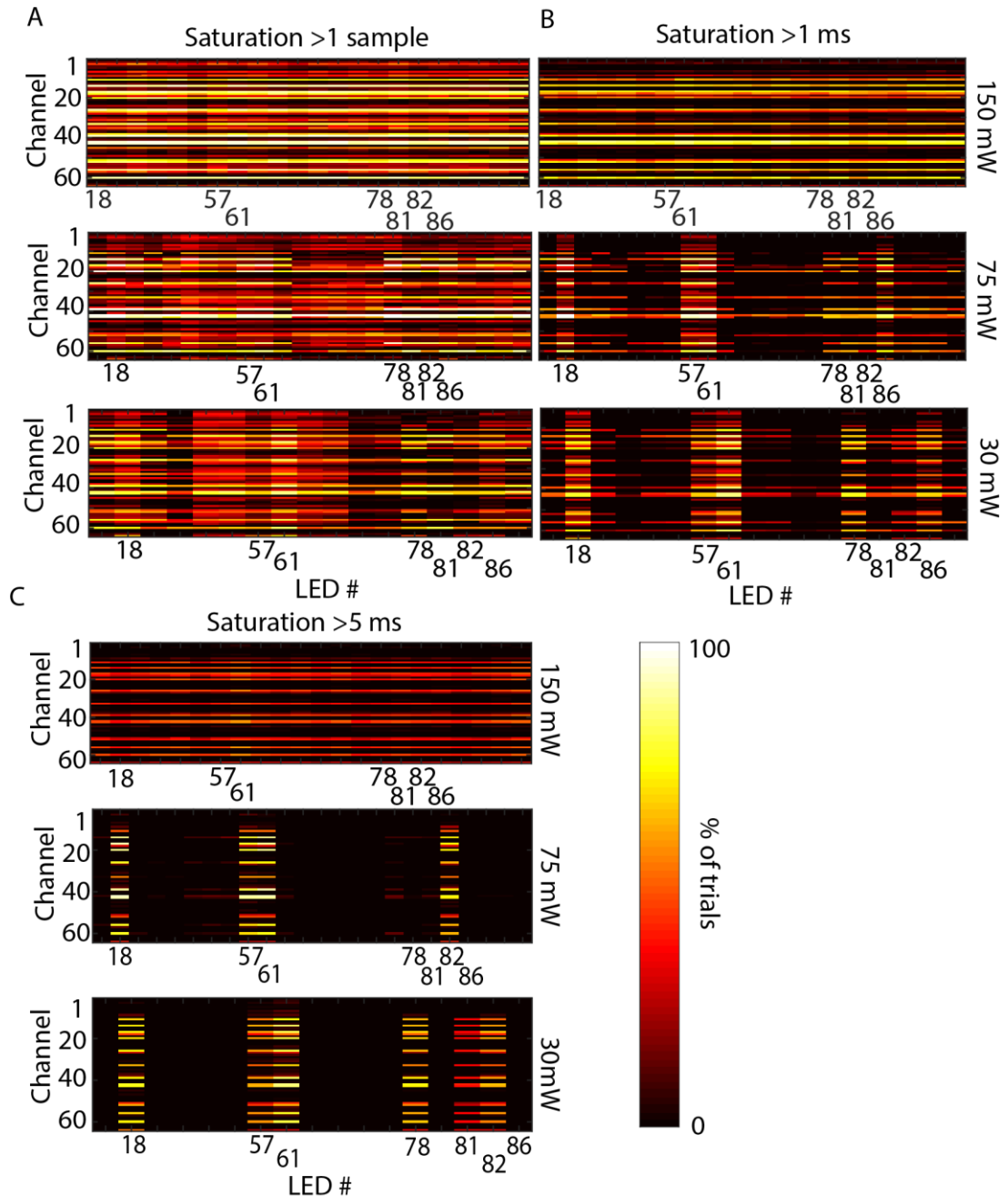


Figure 6.11: Positive saturation of amplifier and recordings during LED stimulation. (A) % of trials where saturation was observed for more than 1 sample. Only problematic LEDs are labelled, for clarity. (B) % of trials where saturation exceeded 1 ms (20 samples). (C) % of trials where saturation lasted longer than 5 ms (100 samples).

Various severities of saturation are also displayed, based on their duration (more than 1 sample, more than 1 ms (20 samples) and more than 5 ms (100 samples)).

From these summaries the situation appears complex. Artefact strength is at least partially influenced by channel, particularly at high intensities, with some channels displaying saturation of more than 1 sample in 100% of trials. At lower intensities and higher degrees of saturation, artefact strength seems less channel specific, and more linked to particular problematic LEDs. This effect is particularly clear in Figure 6.11C (5ms, 30mW). It appears that some LEDs (and then certain channels) are particularly susceptible to causing artefacts.

Next, instances of negative saturation are plotted, where the input to the amplifier exceeded -5 V (Figure 6.12). This data is laid out in a similar manner to Figure 6.11.

There is overall a higher incidence of negative saturation, and interestingly, it seems to increase as the intensity decreases. The exact reason for this is not known, though it may be due to a variation in the influence of various artefact-causing factors as intensity decreased – this will be discussed later. Also, the LEDs identified as problematic for positive saturation are not the same as for negative, and in fact, the positively saturated LED numbers show especially weak negative saturation, lending some support to the idea of opposing electromagnetic or photoelectric forces in the creation of artefacts.

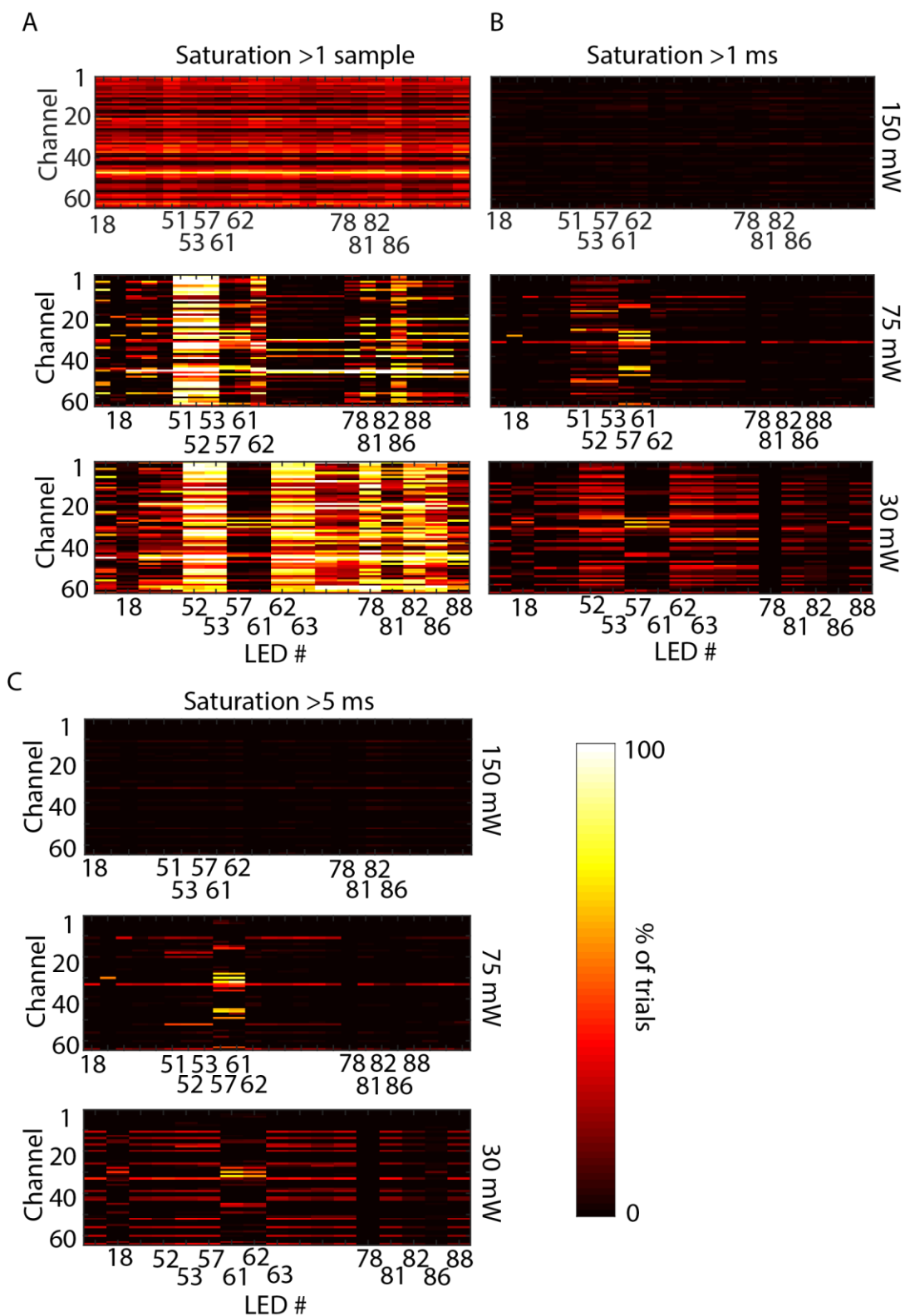


Figure 6.12: Negative saturation of amplifier and recording during LED stimulation. A) % of trials where saturation was observed for more than 1 sample. Only problematic LEDs are labelled, for clarity. B) % of trials where saturation was for more than 1 ms (20 samples). C) % of trials where saturation lasted longer than 5 ms (100 samples).

6.4 Discussion

6.4.1 Brief Summary of Results

Overall, the work presented in this optogenetics was somewhat limited, but several initial hypotheses and expectations were confirmed. A new viral injection protocol was developed and optimised, optical activation of Chronos confirmed (to some degree), and a control system for μ LEDs developed (though the resulting experiment was not particularly successful due to large saturation artefacts within the data).

6.4.2 Comparison with Previous Literature

Previous literature used a single injection of Chronos into the inferior colliculus (Guo et al., 2015), which was sufficient for a focus on temporal experiments but not for a systematic investigation of frequency resolution through the depth of the ICC, such as was envisioned as an expansion to the work presented here. Thus, the protocol was altered to optimise expression of Chronos in the area, using two injections of similar volume to previous literature (and on the same medial-lateral coordinates). This was reasonably successful, and the depth of activation achievable roughly matched that predicted by brain tissue properties and surface irradiance (Stanford University, 2018). Due to the limitations in this new protocol and general lack of success with most optical activation experiments, there are no activation results that can be directly compared to the literature at this time.

For μ LEDs, this work was the first instance of the 6 shank version of the μ LED probe described in 2016 (Scharf et al., 2016) being used *in vivo*. The single shank probe presented in 2016 was controlled with a GUI developed using Visual Basic and C programming (Scharf, 2016), which was limited in the size of protocols and the time required to program multiple LEDs manually. The system developed for the 6 shank probe improved upon the previous software by incorporating bi-directional communication with the Arduino board so that instructions could be sent on an LED by LED basis, thus bypassing the protocol size issue. Additionally, protocols using all the LEDs could be created with ease, the program provided an ongoing log while running, and output order and label files were generated for data pre-processing.

This previous paper does not appear to have experienced the same high levels of artefacts as described in this Chapter. Their presence was acknowledged, but a solution of taking only the middle of the stimulation period (as described in Section 6.2) seems to have eliminated the issue. Though following a similar probe layout in

the brain, the μ LED experiment in this Chapter used a different device (6 shanks vs 1) and a different recording probe (4 shanks vs a single shank 32 channel probe), and so it may be simply that the conditions were more conducive for strong artefacts (the mechanisms behind them will be explored in Limitations and Considerations). Also, the device had been previously used in characterisation tests (saline), and as a result, many μ LEDs had broken and the probe coating had degraded – this may have reduced the electrical shielding available and further increased artefacts.

6.4.3 Limitations and Considerations

Chronos Viral Injections

The presented work has many limitations but acknowledging them and presenting solutions will help to shape future experiments. Due to the combination of the difficulty in lining up the optical fibre with the recording probe, and hitting the infected part of the brain, confirm optical responses were not confirmed in most of our recordings. There have also been reports that Chronos does not traffic well to the cell membrane, which has prompted the development of optimised proteins and could partially explain the limited results (Keppeler et al., 2018).

The last 3 recordings, while optical activation was observed by eye, did not have sufficient data for further analysis, due to some issues with the animal becoming distressed and restless, and technical issues with data saving. The successful recording also contained large artefacts at high intensities, limiting the data that could be used to optic fibre intensities of 11.56 mW/mm². While this intensity is more than sufficient for most opsins, a full analysis of the exact properties of Chronos cannot be done at this time. Using optrodes and/or developing a better skull marking system (tattoo pens, for example) may help line up light stimulation, recording electrodes, and opsin expressing cells in future experiments.

μ LED Hardware Limitations

Experiments with the μ LED allowed the identification of limitations in the current approach and device – which is in itself helpful for future experiments. The PCB was not of useful dimensions for the existing experimental setup, being very wide, and its use required reshuffling of the recording setup and of the head fixation methods. Resigning the PCB to have a similar form factor to conventional probes would aid its adoption in both this and other labs. It was also noted that many of the μ LEDs had failed, or could not be activated at all currents. In general, about 20 of the 96 LEDs were available during experiments. This is obviously a major limitation in a full *in vivo*

characterisation of the device – systematic activation and analysis of the resulting output was not possible. It also meant direct comparisons at all intensities was not completely possible for all LEDs. The lack of LEDs is generally agreed to be the result of coating degradation through successive saline characterisation tests, but the device's overall instability is a major avenue for improvement in the future.

Amplifier Saturation in μ LED Experiments

Perhaps the biggest limitation in these experiments was the large recording artefacts, which prevented any analysis of optically evoked responses. As this is clearly an issue going forward, the likely origin of these artefacts will now be explored, and solutions offered for how to fix them in future experiments and devices.

Initially, recording while stimulating may seem to be a purely research priority – for the hypothetical auditory implant, is this functionality necessary? At present it is unlikely, but its benefits in research into this particular topic are huge – for one example, the spread of optical stimulation could be assessed directly. Also, in other medical uses of brain stimulation (Deep Brain Stimulation for Parkinson's, for example, or indeed directly in seizure monitoring and feedback systems), being able to record neuronal activity is more immediately useful (or is in fact required). Therefore, this issue will be covered here.

The saturation observed could be both positive and negative. During positive saturation, the number of channels and LEDs affected, and to what degree, is affected by the intensity of the illumination, with the effect being stronger for higher intensities. Strangely, the opposite appears to be true for negative saturation – it is possible that reduction of intensity allows another influence to come into play. At the current time, there is no simple explanation for this observation – more work should be done on the exact origin of the artefacts.

It is also observed that not all channels are as strongly affected (though with high intensities, most are to some degree). This is potentially due to the lower quality of the probe at the time of use, with some channels thus having very high impedances and so being affected by the signal differently. It may also be due to the relative positioning of wires. Another feature of the data is that illumination of certain LEDs induces stronger artefacts. Again, this may be due to the relative positioning of the LEDs, or perhaps a manufacturing issue. It did not appear to be the case that problematic LEDs were those closest to the recording probe, so the issue again may lie in the initial manufacturing, or in previous saline tests. The fact that the problematic

LEDs are not necessarily shared between positive and negative saturation suggests artefacts are the result of different influences that take hold/interact in different situations.

Causes of artefacts in stimulation/recording dual systems are well explored, meaning that in the future, mitigation measures can and should be better implemented. The artefacts are caused by interactions between sets of wires – in this case, the stimulation wires on the μ LED PCB and the recording wires on the silicon probe. Thus, simply illuminating the brain with no recording equipment would not have adverse effects, and this may be sufficient for optogenetic implants. However, these devices are still firmly in the research stage, meaning that electrophysiological recordings will generally be desired for validation, either by a separate probe or integrated onto the stimulation device. If the two sets of wires are in close proximity inside or outside the brain, the interaction effects must be considered. The explanation below will relate back to the current experiment – however, the issues raised are also highly applicable in the design of dual recording/stimulation devices with closely packed wires. Note, this will not explain definitively why artefacts are particularly bad at specific LEDs, but it may be assumed that this is due to variations in the reactions described below. As to why positive and negative saturations show different trends in intensity, it may be that as one effect reduces, the other is allowed to increase – but again, it cannot be definitively explained at this time.

Interaction of the photons with probe materials themselves can be causes of artefacts, with the *photoelectrochemical effect* resulting from electrode emission from metal electrons after being hit with high energy photons. Another similar effect is the *photovoltaic effect*, where the material properties of the probe substrate are altered by photon illumination. Their mitigation involves alteration of probe materials (such as using transparent electrodes (Park et al., 2016)) which can be difficult to implement. It is also generally more of a concern in optoelectrodes than in the current experimental setup, and thus somewhat outside the scope of this discussion.

Electromagnetic interference is the most likely cause of the majority of the artefacts seen. Electrical and magnetic interactions (coupling) between the stimulation PCB and wires (the “aggressor”) and the recording PCB and wires (the “victim”) essentially result in the generation of large voltages and currents in the victim wires, which are seen as high, saturating voltage artefacts. Exactly how these are generated is again

somewhat outside the scope of this project, but there are simple ways to reduce their influence. The following two equations are important here:

$$I = C \frac{dV}{dt} \quad (6.1)$$

$$V = L \frac{dI}{dt} \quad (6.2)$$

Where I and V will be the current and voltage generated in the victim wiring, C - Capacitance, dV/dt - change in voltage over time, L - mutual induction, and dI/dt – change in current over time

One of the easiest ways I and V can be reduced is by altering the dV/dt and dI/dt terms. “d” denotes a change in the associated value – so dV/dt is essentially describing how fast the voltage is changing. The issue in the current set up is that the voltage sent to the μ LED device is increasing and decreasing rapidly, therefore there is a large dV term and a small dt term, making the resultant term large. Similar effects happen for current. Thus, by utilising “pulse shaping” techniques and adding a ramp, the resultant current (and thus voltage) can be reduced considerably (see Figure 6.13). This also explains the upward trend observed in positive saturation as intensity (i.e. current, dI) increases (though as mentioned previously, there is no simple explanation for the opposite trend in negative saturation).

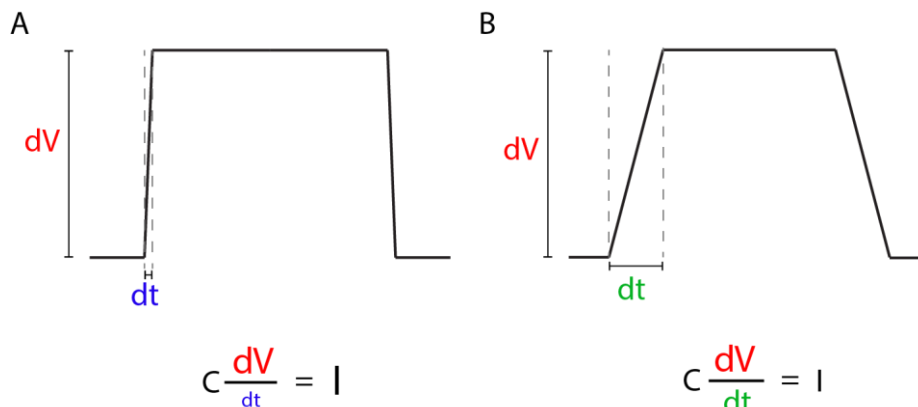


Figure 6.13: Effect of pulse shaping on generated current. (A) A large current is generated as the LED is powered, due to a small rise from zero to peak voltage (dt). (B) By increasing the rise time to the maximum voltage, a smaller current is generated when the LED is turned on

Another way of mitigating these is changing the C and L terms. These are both related to the materials and separation distance between the aggressor and victim wires. Thus, by reducing the distance through various means, or by adding shielding materials between the PCBs, these terms can be reduced to in turn reduce the overall

currents and voltages. Materials such as doped metals (Kampasi et al., 2018) and polymers (e.g. PEDOT) (Guo et al., 2019) are typically incorporated as shielding.

6.4.4 Implications for Future Optogenetic Experiments and Auditory Research

Many of the experimental limitations and issues that arose have been explored in the preceding text, including how they might shape future experiments and device design. At this point, it is not possible to make any novel conclusions about the Chronos/ μ LED approach to improve frequency resolution, as was previously planned.

With the injection procedure optimised in the mouse ICC, future auditory experiments will progress faster, if and when new technologies are obtained. As previously mentioned, future experiments should include updated skull-marking so that probes are inserted into the correct area.

μ LED PCBs may need to be redesigned in order to fit into existing electrophysiology setups. Using the new control system, a range of intensities and pulse widths could be explored. GUIs were designed to help users design their own protocols – and MATLAB is a widely available program. There are also lots of options as to the actual control/triggering of the device too, as the situation demands – thus, it should be reasonably simple to design and run any future protocols.

6.4.5 Future Work

Improvements to Injection Procedures

Any future work involving the Chronos opsin should include additional measures to correctly identify the injected area, for probe insertion. Using μ LED probes over optical fibres should be prioritised (or potentially the use of combined optrodes if further validation is desired), as this will eliminate some of the experimental difficulties that resulted in the optical fibre and probe not being aligned.

Improvements to Current Experimental Pipelines

In the current recording, there is very little that can be done to remove the artefacts. Pulse shaping and optimisation of the recording rig in future experiments should be considered, in an attempt to mitigate artefacts.

Using lower intensities overall may also help – 150 mW/mm² is very unlikely to be required in a typical optogenetic experiment. Removal of problematic LEDs from

rotation may be an option in future devices, but as it stands, there are already very few LEDs.

Future Experiments and Devices

High priority should be placed on creating stable μ LED devices with sufficient shielding to mitigate artefacts to the point where they can be satisfactorily removed. PCBs should be designed around the environment of use and resemble currently existing neural probes as far as possible.

The ideal future of this work would be in the combination of Chronos with μ LED stimulation in the presentation of a viable, hypothetical optogenetic AMI. Future experiments should revolve around characterising the potential spatial, temporal and activation resolution (i.e. effect of intensities) of the approach, so as to illustrate its viability as an implant. Preliminary experiments should involve stimulation of the IC through auditory and optical stimulation, with recording in the IC and/or simultaneously in the AC, in order to compare the “natural” and the light-evoked responses. Ideally, a μ LED illumination would activate the same spatial area of neurons as a pure tone stimulus.

To investigate the functionality of the device’s spatial resolution, a frequency discrimination task is envisioned. After training the animal to perform a behaviour if two successive tones are different in pitch, a two “tone” stimulus can be elicited by illuminating pairs of LEDs one after the other. By incrementally decreasing the distance between illuminated pairs and monitoring the animal’s response, the maximum spatial/spectral resolution of the device can be identified - at what inter-LED distance can the animal no longer distinguish different tones? This experiment would be an excellent way to provide the viability of an optogenetic based auditory midbrain implant.

Chapter 7 General Discussion

7.1 Brief Summary of Key Results and Relation to Hypotheses

The initial aims of the thesis were to compare and contrast the auditory cortex and inferior colliculus, in terms of their general properties and natural sound coding mechanisms. They were expected to differ due to their positions in the auditory pathway, and it was also expected that the timescales on which coding takes place would be especially important, given perceptual mechanisms such as entrainment that make use of underlying brain rhythms of particular frequencies. Results from here would theoretically have a positive effect on the future development of auditory midbrain implants, by expanding knowledge of the ICs mechanisms and helping design accurate stimulation methods. They would also be generally informative for auditory and systems neuroscience. Additionally, the project aimed to prove that an optogenetic approach (using Chronos and μ LEDs) was viable for solving the issue of low spatial resolution in auditory neuroprosthetics, and to make the first steps in creating a hypothetical implant.

The aim of Chapter 3 was to begin comparisons on a low level, contrasting basic properties during the brain's response to natural sound. Differences were confirmed between AC and IC cell populations as expected (cell types, spike rate etc). Both Chapter 3 and to a greater extent Chapter 4 also identified the IC's lower trial-trial variability in spike rate in comparison to the AC, fitting previous literature and the hypothesis given its subcortical position.

The apparent differences in ITC and entrainment strength (and frequency range) observed between the AC and IC, while difficult to interpret as discussed in Chapter 3, nevertheless point to functional and mechanistic differences in each area. Results in the AC were expected, but observation of strong ITC in the IC was not hypothesised. Similarly, observation of entrainment to frequencies up to ~20 Hz was expected in the AC, but seeing entrainment of the IC up to 200 Hz was not.

When splitting AC cells into individual populations, there was a preference for putative narrow spiking interneurons to entrain to either natural sound only, or both natural and spontaneous – but rarely selectively entrain to spontaneous activity alone.

Chapter 4 aimed to look more in-depth at differences in neuronal coding mechanisms for natural sounds, identifying inter-area differences once again and proposing mechanisms behind them. It was found that in both areas, a spike rate code allowed

classification of natural sound stimuli to a reasonable extent. Where they appeared to differ was in the IC neurons' capacity to reach comparable performance levels as the AC with fewer cells, a likely reason/mechanism for this being the lower trial-trial variability of IC cells. This observation matched literature and the Chapter 3 driven hypothesis. Frequency range, while important to overall classification success, did not explain between-area differences, while strong signal and noise pairwise correlations tended to indicate exceptionally low performing datasets. Using different stimulus lengths did not reveal a significant trend, or a tendency for theta/delta lengths to be best classified, in opposition to previous literature both in humans and other mammals which suggests coding on these timescales is important for the accuracy processing of natural sounds (Kayser et al., 2015, Peelle et al., 2013, Kayser et al., 2012, Osman et al., 2018).

Chapter 5 was a largely exploratory chapter, utilising non-negative matrix factorisation to reduce population activity into modules of activity in space and time. Qualitative differences between AC and IC were not as readily apparent as hypothesised, though each IC module appeared to cover a successive part of the tonotopic range. In a novel application, module strength was used to identify state differences (in a single dataset), a split hypothesised as being possible. Separating trials into putative synchronous and desynchronous states then lead to differences in classification success, with the desynchronous (and presumably less variable) state giving better results. Unlike in Chapter 4 however, there was a weak trend for the neural data to be more variable trial-trial in this state, conflicting with the Chapter 4 results which saw the higher performance linked with lower trial-trial variability. A trend for lower noise correlations may better explain the observed results. There was very limited success in applying similar analysis to the IC.

Chapter 6 was the most technical chapter, aiming to explore the viability of the optogenetic approach. A new, 2 injection protocol for full depth expression in the mouse ICC was developed from previous literature, and optical responses confirmed to a limited degree and depth. μ LEDs were, as expected, able to be integrated into the existing electrophysiological equipment, though this required additional communication software and experimental rig optimisation. Even after this, experiments had limited success due to large optoelectrical artefacts, and were unable to confirm the hypothesis of increased spatial/spectral resolution. Despite this, these experiments were highly informative for the future of the work.

7.2 Implications and Relevance of the Project

7.2.1 Systems Neuroscience and Auditory Coding

As discussed in previous chapters, current evidence points to sparse coding strategies being predominant in the auditory cortex of natural sound – by representing sound using small, specific groups of neurons, coding is efficient in energy, but not in the space required to represent the full spectrum of sounds (Hromadka et al., 2008, Dodds and DeWeese, 2019, Terashima and Hosoya, 2009, Zhang et al., 2019). The alternative, a dense strategy, codes stimuli based on variations in the combined activity of a larger number of neurons, and is more robust to noise. The results presented in this thesis support the evidence of a sparse code, particularly Chapter 4. With the AC having comparative classification performance to an area with fewer input variables, this suggests that, for the natural sound stimuli applied, we were not sampling all the specific neurons required to decode the sound accurately. The intermittent loss of neuronal signals (e.g. through animal movement) is also likely to more strongly affect a sparse system, which is inherently less robust than other coding strategies.

The literature review identified the auditory cortex as being the site of sound interpretation and contextualisation, as well as having a multitude of descending connections to sub-cortical auditory nuclei including the MGB, IC, SOC and CN (Feliciano et al., 1995, Budinger et al., 2000, Bajo et al., 2007). These connections are strongly suggested to have a role in contextual modulation of incoming sounds; the higher trial-trial variability observed in this thesis is supportive of this aspect of cortical functionality, as well as the influence of global brain state. While on first listen, aspects of the natural sound stimuli may alert the animal, this is likely to subside over time, plus, the animal may get drowsy (or indeed, fall asleep) during the stimuli repetitions, all of which would affect auditory cortex activity over time and thus its trial-trial variability. Future experiments in which brain state is recorded alongside spiking will likely shed further light on the functionality of the cortex during natural sounds.

Inhibition can shape the frequency response areas of a given tuned neuron (Wu et al., 2008), and the observation that (putative) inhibitory neurons of the cortex are more variable trial-trial during natural sound than excitatory neurons means their activity is likely dynamic, potentially related to ongoing environmental context or global brain

state – without state information and (to give an example) recording of activity from a freely moving, exploring animal.

Results in the inferior colliculus, particularly when compared directly to the auditory cortex, speak to their being different mechanisms (or balancing of mechanisms) for coding natural sounds. Evidence in the IC tends to point towards a sparse coding strategy, but dense and sparse coding may also exist in parallel (Carlson et al., 2012, Chen et al., 2012a, Sproule et al., 2015, Zhang et al., 2019). An existing theory is that the IC is the site of a coding strategy switch from dense (predominant in the brainstem nuclei) to sparse, favoured in higher processing centres (Chechik et al., 2006). This is supported by the results from this thesis, with the IC performing comparably to the AC but with few inputs, speaking to a more robust mechanism (especially if we assume the IC recording was similarly affected by animal movement). Certainly, more work is required in this area, particularly in differences between central, dorsal and lateral nuclei. Additionally, as the IC is a physically smaller area, it may make sense for sparse strategies to be supported by dense ones, so that the entire spectrum of sound can be accounted for.

Though the non-lemniscal parts of the IC are apparently modulated by brain state (Chen and Song, 2019), as of yet there is no evidence for a similar effect in the ICC, a feature supported by the (relative to the AC) lower trial-trial variability in these neurons. The IC, relative to the AC, maintains a reliable spike rate when encoding successive trials of a stimulus. If this is true, may mean that the ICC is acting to convey exact sound details – integrating multi-sensory information and other higher level perception is more likely the job of the auditory cortex and/or thalamus. However, as this result was only relative to the AC, we cannot make definitive statements on the modulation of the ICC – further data incorporating ongoing brain state is required. Additionally, the ICC receives connections from lower nuclei which are known to be modulated by the AC, and so it seems unlikely the area is entirely unaffected. What cannot be said at this time is if the observed robustness is maintained on the level of the exact spiking pattern – something which would be an excellent avenue for future research. , speaking to its subcortical position and role as a hub and an accurate conveyer of exact sound details.

As previously mentioned, any optogenetic-based auditory implants will be unable (at least at the beginning) to activate single neurons with excellent temporal resolution – as such, at least a partial reliance on dense coding in addition to low trial-trial

variability of spike rate is promising for the success of midbrain implants. Implants in the auditory cortex are unlikely to be as successful as to replicate AC activity in a natural manner, it would require extensive coverage of the area to accommodate sparse strategies and a feedback mechanism to recording global brain state and modulate accordingly.

Entrainment results from the cortex roughly matched those seen in literature in that it occurs at frequencies <30Hz, albeit with a lower strength (Kayser et al., 2015, Peelle et al., 2013, Szymanski et al., 2011), supporting entrainment as a mechanism by which the auditory cortex enhances perception of the temporal envelope of natural sounds.

Cell populations are not homogenous – analysing the activity and interactivity of different cell types in a population is important to gain a deeper understanding the brain. This thesis found evidence to further support differing roles of AC cell types during sensory stimuli. That putative inhibitory neurons are also more likely to entrain during natural sound than spontaneous activity suggests that during evoked activity, these neurons change their activity patterns and may take on different roles within the population. Exactly what dictates this modulation is not yet known – brain state is a strong potential candidate as the animal is likely attentive to the sound, but the question is open for more specific answers. These cell types are conserved across other cortical areas, and so observations in the auditory system may be applicable to other sensory modalities.

The apparently high strength of ITC and entrainment in the inferior colliculus central nucleus, though difficult to interpret at face value, nevertheless points to differences in how neuronal populations are structured and recruited in the IC vs the AC. From this and from entrainment analysis, there is clearly rhythmicity to the ICs responses to some degree, if the analysis performed is interpreting spikes to be aligned with LFP phases. What this means precisely will be related to where this rhythmicity is generated – possibilities include other auditory areas, the IC itself, or as a side effect/artefact due to strong synchronous firing of IC layers, but it is difficult to tell without larger IC datasets, further analysis of the simultaneous AC data, or by repeating the experiments and taking simultaneous recordings from other auditory areas (such as the MGB or cochlea nucleus) alongside the IC and AC.. However, if entrainment is truly being observed up to these high frequencies, this has interesting

implications with regards to a new level of function of the ICC, and how it, as a subcortical structure, is connected within the auditory pathway.

The simultaneous nature of the recordings could provide direct links between two connected brain areas and gave additional weight to comparisons. Such experiments are highly likely to be the future of electrophysiology in neuroscience – with individual areas often well characterised, the focus is shifting to the functional interactions between brain areas. Due to the recent advent of high density Neuropixel probes, simultaneous recordings from many brain areas is becoming the common approach.

NMF was applied successfully to auditory evoked spiking activity in two brain areas, something which to our knowledge has not yet been reported, and supports the use of the technique on similar data. It is likely to become highly relevant in future years, given the shift in neuroscience towards investigating neurons as populations. Inter-area differences were not readily apparent, but the data did support the decomposition of overall activity into distinct, functionally relevant populations. Though highly preliminary, the brief research into cortical state being potentially derived from one module (of several) has implications regarding population activity. Are certain populations more affected by state transitions? Why, and what kinds of cells are involved? What is their function in auditory (or other sensory) processing? How are other populations behaving and interacting?

7.2.2 Optogenetics for Auditory Implants

The focus of future auditory implants is very much on optogenetics. Though many obstacles still exist at the current time, the field has seen several promising breakthroughs in the past 5 years. That being said, the existing literature on optogenetics in the ICC (for the purposes of auditory midbrain implants) is reasonably sparse, and so this thesis is able to add more observations to the discussion. A viral injection protocol for depth coverage is developed, which may be used by future researchers investigating frequency resolution (should they choose not to use transgenic animals). It would also be a starting point for introduction of new, improved opsins that do not have transgenic animals.

In the course of μ LED system design and experiments, many issues and considerations were brought to light, that will be invaluable to future research on the

topic. Feedback on devices was given directly to probe designers, and software was developed with significant input from the researcher, a typical end user. As a result, there now exists protocol design and communication software for the μ LED, which is easy to use and should aid planning and implementing *in vivo* experiments. GUIs and MATLAB code for controlling the LEDs will be made available in any publications resulting from the device. The project has highlighted the importance of designing devices with the end user and their existing experimental rigs in mind, to make a product commercially viable.

7.3 Current Limitations and Potential Improvements

7.3.1 Inconsistent IC Recordings Led to Limitations in Analysis and Interpretation

Perhaps the most major limiting factor of this research was the overall low quality of inferior colliculus recording, in particular the lack of clean single units. In turn, this resulted in a low number of good simultaneous datasets. This meant, in a lot of cases, more in-depth analysis could not be performed, or that existing analysis was difficult to interpret fully.

The main reasons for this have been explored in Chapter 3, but in brief, it has been attributed to headcap instability over the IC, and inability of recording and spike sorting methods to clearly distinguish single units. At the time, small additions were made to the headcap to improve stability, but it may be that the procedure should be modified to a greater degree (perhaps moving the headpost fixation point backwards, or redesigning the anchor screw layout further to truly maximise security). It may also be possible to refine habituation protocols to reduce overall movement, for example, by increasing the length of habituation period and the overall number of sessions, or by designing a more comfortable and secure enclosure for the mouse (partially moulded to the body shape for example, instead of a simple tube). Improvements here should translate immediately to better quality recordings, but IC data pre-processing should also be revisited. Though modification of spike sorting thresholds was attempted (with no noticeable improvements), other approaches may be required, such as additional filtering or modification of more complex variables within the spike sorting script. At this point, it may be worth consulting other labs working with similar data, to consolidate experiences and processing approaches. Though tetrodes continue to offer excellent isolation of single units and are often used to map responses in the ICC (Seshagiri and Delgutte, 2007, Chen et al., 2012b, Dorkoski et al., 2020), their

use here would limit the number of neurons able to be recorded simultaneously without extensive damage to the area, and restrict the proportions of the tonotopic gradient we would have simultaneous access to .

The lack of single units in the IC meant that conclusions involving comparisons between AC and IC cells ultimately carry less weight, unless the differences were very significant. Unexpected results were difficult to attribute to any one cause – the effect of low sample sized was always a potential variable. Instead, all AC and all IC cells were typically combined together, rather than being able to make comparisons between individual datasets (i.e. paired statistics). This reduced the weight of some results and conclusions, and often made interpretation difficult.

Some comparisons were simply not possible with the recorded data – for example, comparing populations of equal number in classification analysis. Attempted in the present state, low IC cells would be a very confounding variable outside of what was being examined. It also meant that analysis directly utilising the simultaneous aspect of the data was left mostly unexplored.

7.3.2 Lack of State Information

As explored in the literature review, the question of global brain state and its effect on auditory coding throughout the auditory pathway is still to be explored in detail. Brain state was not the original focus, and so the implementation of pupil monitoring was afforded limited focus. Due to this (plus some general technical issues) a reliable method of determining brain state was available for only a select few recordings. Unfortunately, this means that with the current data, few conclusions can be made regarding its influence and function. Issues with EEG screw recordings (disconnection in chronic preparations) meant that cortical LFP was not a reliable method of determining brain state either. Though the lack of this data did not ultimately prevent conclusions related to the aims of the project, its inclusion would have been highly interesting for systems neuroscience in general. Future work should be sure to afford more focus to brain state measurements.

7.3.3 Technical Difficulties in Optogenetic Experiments

Some of the technical difficulties encountered in optogenetic experiments have been extensively explored in Chapter 6. For Chronos experiments, these centred predominantly around lining up recording, stimulation and Chronos infected cells. While optical evoked responses were confirmed, the lack of success limited the level

of analysis that could be applied – future experiments will probably require additional validation and a systematic assessment of responses. Optimisations including use of optrodes, and better marking of the injection site, have been suggested as options for improvement. Additionally, there now exists an optimised Chronos opsin for improved membrane trafficking, after issues relating to this surfaces with the original Chronos (Keppeler et al., 2018).

The μ LED probe, in its current form, was not suitable for the experiment in which it was used. A lack of shielding, close proximity of stimulation and recording PCBs, and no real pulse shaping meant artefacts saturated the input amplifier and made data analysis impossible. Thus, this thesis is limited in how it can address the original aims of the optogenetic experiments – to assess potential frequency resolution of μ LED devices. The next iteration of μ LED probe has taken the current difficulties and limitations into account, and promises to offer a more viable approach to these experiments.

7.3.4 General Limitations

One of the overarching limitations of the project is its relatively preliminary nature in terms of the analysis performed. It has, however, provided a stable analytical and experimental base for future work. As will be discussed, the future of the research (at least in the context of auditory implants) lies in the asking of more specific questions related to the operation of said implants.

As with most scientific endeavours, additional datasets would help to strengthen the conclusions made in this thesis. Given more time, this would be achievable. Though it would have added considerable experimental and analytical complexity, and was not strictly relevant to the question at hand, having auditory thalamic recordings (simultaneously alongside IC and AC) would have allowed us to examine the full transition between AC and IC coding strategies, and given a fuller picture of natural sound coding overall.

The final two results chapters were largely exploratory, mainly as a result of time constraints and technical issues outwith the researcher's control. While beneficial for the future, the level of functional implications to be made from this work are thus far limited.

The analysis was completed in the mouse only, which must be taken into consideration when interpreting results. Though the principles of natural sound coding

are conserved somewhat between mammalian species – for example, entrainment has been observed in many species including humans (Kayser et al., 2015, Yague et al., 2017, Peelle and Davis, 2012), the results presented here should be confirmed in other species as far as possible.

To some degree, many of the thresholds used for data inclusion or classification were subjective. Narrow spiking/broad spiking thresholds were determined by visualisation of the data and consultation of the literature, but with the current experimental setup, it is impossible to tell exactly which cells are which. Additionally, thresholds for evoked activity may be subjective, and may have potentially missed activity that was truly evoked, but difficult to pick up due to noise or time binning. Histological analysis was also fairly lenient in dataset inclusion, and so it is possible that some cells may be on the boundary of, or just outside, the target area.

7.4 Future of the Work

7.4.1 Systems Neuroscience and Stimulation Design

With simultaneous, chronic, high density recordings from multiple brain areas becoming the norm, the future of the work should lie in investigating population dynamics and long-term functional connectivity/communication between brain areas. Analysis should also be focused on features of the coding that are related to auditory implants, such as timings, spatial relationships within functional neuronal populations, and transformation of the neural code through the pathway.

Analysis specifically incorporating the simultaneous aspect of the recordings would be an excellent place to start. Not only will this provide insight into the auditory pathway, research into functional connectivity and transformation of sensory input will be highly applicable to other sensory systems. With the inclusion of simultaneously recorded auditory thalamic recordings, additional insight may be gained. Determining how populations of neurons interact and how data representation changes between them would be an excellent use of this data and be highly applicable to auditory implants. It may begin by expanding the modelling approaches presented in Chapter 4 to have AC responses predicted from an IC spiking patterns. Understanding the parameters which determine accurate conveyance of auditory information will be highly informative for stimulation strategy and device design. By applying the analysis to other stimuli, altering time-binning methods and creating multi-dimensional, non-linear mathematical models, a fuller and more applicable picture of auditory coding can be uncovered.

That lower trial-trial variability was consistently seen in the IC when compared to the AC is a good starting point for additional research into the phenomenon - to what extent is this coding reliability maintained? For example, does the robustness and reliability extend to the exact spike timing patterns? Some work has been done to examine temporal jitter of the ICC during speech and speech in noise (finding it to be low and then higher, respectively) (White-Schwoch et al., 2017). With simultaneous recording of multiple neurons, temporal and spatial robustness across trials can be further assessed in both single neuron and population responses. The relative importance of precise spike timing in accurate conveyance of information will again support implant design.

With more global measurements becoming the norm, monitoring the influence of brain state throughout the brain is more important than ever in order to stay relevant in the systems neuroscience field. Future work should aim to incorporate this information and gauge its relative influences and function within sound coding through the various stages of the auditory pathway.

Chapter 5 gave a first, qualitative view on the spatiotemporal breakdown of auditory neuron populations during natural stimuli, with NMF proving to be a viable tool for population-based research. Systematically altering input variables here would allow assessment of the technique's spatial and temporal limitations, and determine exactly to what extent population activity can be viewed with this method. Relevant questions can then be posed.

7.4.2 Viability of the Optogenetic Midbrain Implant

The other avenue for future work would be proving the viability of a μ LED approach, specifically for high spatial resolution stimulation. A preliminary experiment might involve comparing the responses to auditory pure tone stimuli to those generated by spatially constrained optogenetic activations within the tonotopic gradient (aiming to generate a perception of pure tone without auditory stimulation) With simultaneous recording in the IC and AC, plus illumination of single μ LEDs, these optically evoked "puretones" can be compared with auditory puretones, in terms of properties like latency, adaptation, waveform, number of active units etc, giving a general picture of how neurons across the brain might respond to such stimulation. With this established, the next aim would be to prove the hypothetical frequency resolution of our devices through behavioural tasks, as previously discussed. A far-reaching aim may be to attempt the stimulation that will induce the perception of complex sounds

(such as vocalisations), proving more definitively the potentials of the optogenetic system.

The research should also seek to keep up to date with technological advancements and incorporate them as they become available. Judging by the direction the literature is taking, and by the most pressing needs for optogenetic neuroprosthetics, these are likely to include dual recording/stimulation devices, more flexible materials, and wireless solutions. Results from these should be compared with original results and examined for evidence of any trade-offs (in data quality, stimulation flexibility etc). The results of the two-shank auditory midbrain implant clinical trial (due to be completed in 2021) will also be crucial in determining the direction of research.

7.5 Final Thoughts

The initial motivations for this thesis were scientifically sound, and highly relevant within the rapidly expanding field of optogenetic auditory neuroprosthetics. Though limitations with data quality and technological hold-ups have prevented full and robust answers to the questions proposed, the thesis has nevertheless presented an extensive review of the relevant topics and the application of a wide variety of relevant analytical techniques. The results from these were intriguing and applicable to both systems neuroscience and auditory prosthetics. This thesis thus provides an excellent starting point for devising new analytical and experimental approaches to eventually answer the fields' outstanding questions.

References

- ADRIAN, E. D. 1926. The impulses produced by sensory nerve endings: Part I. *J Physiol*, 61, 49-72.
- AITKIN, L., TRAN, L. & SYKA, J. 1994. The responses of neurons in subdivisions of the inferior colliculus of cats to tonal, noise and vocal stimuli. *Exp Brain Res*, 98, 53-64.
- AITKIN, L. M., DICKHAUS, H., SCHULT, W. & ZIMMERMANN, M. 1978. External nucleus of inferior colliculus: auditory and spinal somatosensory afferents and their interactions. *J Neurophysiol*, 41, 837-47.
- AITKIN, L. M., KENYON, C. E. & PHILPOTT, P. 1981. The representation of the auditory and somatosensory systems in the external nucleus of the cat inferior colliculus. *J Comp Neurol*, 196, 25-40.
- AITKIN, L. M., PETTIGREW, J. D., CALFORD, M. B., PHILLIPS, S. C. & WISE, L. Z. 1985. Representation of stimulus azimuth by low-frequency neurons in inferior colliculus of the cat. *J Neurophysiol*, 53, 43-59.
- AITKIN, L. M., WEBSTER, W. R., VEALE, J. L. & CROSBY, D. C. 1975. Inferior colliculus. I. Comparison of response properties of neurons in central, pericentral, and external nuclei of adult cat. *J Neurophysiol*, 38, 1196-1207.
- ALEXANDROU, A. M., SAARINEN, T., KUJALA, J. & SALMELIN, R. 2018. Cortical entrainment: what we can learn from studying naturalistic speech perception. *Language, Cognition and Neuroscience*. DOI: 10.1080/23273798.2018.1518534
- ALJADEFF, J., LANSDELL, B. J., FAIRHALL, A. L. & KLEINFELD, D. 2016. Analysis of Neuronal Spike Trains, Deconstructed. *Neuron*, 91, 221-59.
- ALKHATIB, A., BIEBEL, U. & SMOLDERS, J. 2006. Inhibitory and Excitatory Response Areas of Neurons in the Central Nucleus of the Inferior Colliculus in Unanesthetized Chinchillas. *Experimental brain research*, 174, 124-43
- ALLEN, W. E., CHEN, M. Z., PICHAMOORTHY, N., TIEN, R. H., PACHITARIU, M., LUO, L. & DEISSEROTH, K. 2019. Thirst regulates motivated behavior through modulation of brainwide neural population dynamics. *Science*, 364, 1-9.
- ALLERGAN. 2015. *Phase I/IIa, Open-Label, Dose-Escalation Study of Safety and Tolerability of Intravitreal RST-001 in Patients With Advanced Retinitis Pigmentosa (RP) - NCT02556736* [Online]. [Accessed January 2020].
- ANDERSEN, R., ROTH, G., AITKIN, L. & MERZENICH, M. 1980. The Efferent Projections of the Central Nucleus and the Pericentral Nucleus of the Inferior Colliculus in the Cat. *The Journal of comparative neurology*, 194, 649-662
- ANDERSON, L., MALMIERCA, M., WALLACE, M. & PALMER, A. 2006. Evidence for a Direct, Short Latency Projection From the Dorsal Cochlear Nucleus to the Auditory Thalamus in the Guinea Pig. *The European journal of neuroscience*, 24, 491-498.
- ANDONI, S. & POLLAK, G. D. 2011. Selectivity for spectral motion as a neural computation for encoding natural communication signals in bat inferior colliculus. *J Neurosci*, 31, 16529-40.
- ARMSTRONG-JAMES, M. & MILLAR, J. 1979. Carbon fibre microelectrodes. *J Neurosci Methods*, 1, 279-287.
- ARORA, K. 2012. Cochlear Implant Stimulation Rates and Speech Perception. In: RAMAKRISHNAN, S. (ed.) *Modern Speech Recognition Approaches with Case Studies*. IntechOpen. Available at: <https://www.intechopen.com/books/modern-speech-recognition-approaches-with-case-studies/cochlear-implant-stimulation-rates-and-speech-perception>

- ASERINSKY, E. & KLEITMAN, N. 1953. Regularly occurring periods of eye motility, and concomitant phenomena, during sleep. *Science*, 118, 273-274.
- ASHMORE, J. 2008. Cochlear Outer Hair Cell Motility. *Physiological reviews*, 88, 173-210
- ATENCIO, C. A. & SCHREINER, C. E. 2008. Spectrotemporal processing differences between auditory cortical fast-spiking and regular-spiking neurons. *J Neurosci*, 28, 3897-910.
- BAI, Q. & WISE, K. D. 2001. Single-unit neural recording with active microelectrode arrays. *IEEE Trans Biomed Eng*, 48, 911-920.
- BAIR, W., ZOHARY, E. & NEWSOME, W. T. 2001. Correlated firing in macaque visual area MT: time scales and relationship to behavior. *J Neurosci*, 21, 1676-1697.
- BAJO, V., NODAL, F., MOORE, D. & KING, A. 2010. The Descending Corticocollicular Pathway Mediates Learning-Induced Auditory Plasticity. *Nature neuroscience*, 13, 253-60.
- BAJO, V. M., NODAL, F. R., BIZLEY, J. K., MOORE, D. R. & KING, A. J. 2007. The ferret auditory cortex: descending projections to the inferior colliculus. *Cereb Cortex*, 17, 475-91.
- BALDWIN, H. A., FRENK, S. & LETTVIN, J. Y. 1965. Glass-Coated Tungsten Microelectrodes. *Science*, 148, 1462-1464.
- BANSAL, M. 2013a. Conductive Hearing Loss and Ostosclerosis. *Diseases of the Ear, Nose and Throat*. 1st ed. New Dehli, India: Japee Brothers Medical Publishers.
- BANSAL, M. 2013b. Sensioneural Hearing Loss. *Diseases of the Ear, Nose and Throat*. New Dehli, India: Japee Brothers Medical Publishers.
- BAR-YOSEF, O., ROTMAN, Y. & NELKEN, I. 2002. Responses of neurons in cat primary auditory cortex to bird chirps: effects of temporal and spectral context. *J Neurosci*, 22, 8619-8632.
- BARLOW, H. B. 1972. Single units and sensation: a neuron doctrine for perceptual psychology? *Perception*, 1, 371-394.
- BARNSTEDT, O., KEATING, P., WEISSENBERGER, Y., KING, A. & DAHMEN, J. 2015. Functional Microarchitecture of the Mouse Dorsal Inferior Colliculus Revealed Through In Vivo Two-Photon Calcium Imaging. *The Journal of neuroscience : the official journal of the Society for Neuroscience*, 35, 10927-39
- BASTA, D. & VATER, M. 2003. Membrane-based gating mechanism for auditory information in the mouse inferior colliculus. *Brain Res*, 968, 171-178.
- BEEBE, N., YOUNG, J., MELLOTT, J. & SCHOFIELD, B. 2016. Extracellular Molecular Markers and Soma Size of Inhibitory Neurons: Evidence for Four Subtypes of GABAergic Cells in the Inferior Colliculus. *The Journal of neuroscience : the official journal of the Society for Neuroscience*, 36, 3988-3999
- BEHR, R., COLLETTI, V., MATTHIES, C., MORITA, A., NAKATOMI, H., DOMINIQUE, L., DARROUZET, V., BRILL, S., SHEHATA-DIELER, W., LORENS, A. & SKARZYNSKI, H. 2014. New outcomes with auditory brainstem implants in NF2 patients. *Otol Neurotol*, 35, 1844-1851.
- BERNDT, A. & DEISSEROTH, K. 2015. Expanding the optogenetics toolkit: A naturally occurring channel for inhibitory optogenetics is discovered. *Science*, 349, 590-1.
- BERNDT, A., LEE, S. Y., RAMAKRISHNAN, C. & DEISSEROTH, K. 2014. Structure-guided transformation of channelrhodopsin into a light-activated chloride channel. *Science*, 344, 420-424.
- BERREBI, A. S. & MUGNAINI, E. 1991. Distribution and targets of the cartwheel cell axon in the dorsal cochlear nucleus of the guinea pig. *Anatomy and Embryology*, 183, 427-454.
- BINNS, K. E., GRANT, S., WITHINGTON, D. J. & KEATING, M. J. 1992. A topographic representation of auditory space in the external nucleus of the inferior colliculus of the guinea-pig. *Brain Res*, 589, 231-242.

- BIZLEY, J. K., NODAL, F. R., NELKEN, I. & KING, A. J. 2005. Functional organization of ferret auditory cortex. *Cereb Cortex*, 15, 1637-1653.
- BLANCHE, T. J., SPACEK, M. A., HETKE, J. F. & SWINDALE, N. V. 2005. Polytrodes: high-density silicon electrode arrays for large-scale multiunit recording. *J Neurophysiol*, 93, 2987-3000.
- BODENHAMER, R. D. & POLLAK, G. D. 1981. Time and Frequency domain processing in the inferior colliculus of echolocating bats. *Hear Res*, 5, 317-335.
- BOUCETTA, S., CISSE, Y., MAINVILLE, L., MORALES, M. & JONES, B. E. 2014. Discharge profiles across the sleep-waking cycle of identified cholinergic, GABAergic, and glutamatergic neurons in the pontomesencephalic tegmentum of the rat. *J Neurosci*, 34, 4708-27.
- BOYDEN, E. S., ZHANG, F., BAMBERG, E., NAGEL, G. & DEISSEROTH, K. 2005. Millisecond-timescale, genetically targeted optical control of neural activity. *Nat Neurosci*, 8, 1263-8.
- BRAND, A., BEHREND, O., MARQUARDT, T., MCALPINE, D. & GROTHE, B. 2002. Precise Inhibition Is Essential for Microsecond Interaural Time Difference Coding. *Nature*, 417, 543-7
- BRAWER, J. R., MOREST, D. K., KANE & EILEEN, C. 1974. The neuronal architecture of the cochlear nucleus of the cat. *The Journal of Comparative Neurology*, 155, 251-299.
- BRUNSO-BECHTOLD, J. K., THOMPSON, G. C. & MASTERTON, R. B. 1981. HRP study of the organization of auditory afferents ascending to central nucleus of inferior colliculus in cat. *J Comp Neurol*, 197, 705-722.
- BUDINGER, E., HEIL, P. & SCHEICH, H. 2000. Functional Organization of Auditory Cortex in the Mongolian Gerbil (*Meriones Unguiculatus*). IV. Connections With Anatomically Characterized Subcortical Structures. *The European journal of neuroscience*, 12, 2425-2451
- CALFORD, M. B. & AITKIN, L. M. 1983. Ascending projections to the medial geniculate body of the cat: evidence for multiple, parallel auditory pathways through thalamus. *J Neurosci*, 3, 2365-2380.
- CAMPBELL, P. K., JONES, K. E., HUBER, R. J., HORCH, K. W. & NORMANN, R. A. 1991. A silicon-based, three-dimensional neural interface: manufacturing processes for an intracortical electrode array. *IEEE Trans Biomed Eng*, 38, 758-768.
- CANOLTY, R. T., EDWARDS, E., DALAL, S. S., SOLTANI, M., NAGARAJAN, S. S., KIRSCH, H. E., BERGER, M. S., BARBARO, N. M. & KNIGHT, R. T. 2006. High gamma power is phase-locked to theta oscillations in human neocortex. *Science*, 313, 1626-1628.
- CANT, N. B. & BENSON, C. G. 2006. Organization of the inferior colliculus of the gerbil (*Meriones unguiculatus*): differences in distribution of projections from the cochlear nuclei and the superior olivary complex. *J Comp Neurol*, 495, 511-28.
- CANT, N. B. & MOREST, D. K. 1979. The bushy cells in the anteroventral cochlear nucleus of the cat. A study with the electron microscope. *Neuroscience*, 4, 1925-45.
- CARLSON, N. L., MING, V. L. & DEWEESE, M. R. 2012. Sparse Codes for Speech Predict Spectrotemporal Receptive Fields in the Inferior Colliculus. *PLoS Comput Biol*, 8, e1002594.
- CASTRO-ALAMANCOS, M. A. 2004. Absence of rapid sensory adaptation in neocortex during information processing states. *Neuron*, 41, 455-464.
- CHAPIN, J. K. & NICOLELIS, M. A. 1999. Principal component analysis of neuronal ensemble activity reveals multidimensional somatosensory representations. *J Neurosci Methods*, 94, 121-140.
- CHECHIK, G., ANDERSON, M. J., BAR-YOSEF, O., YOUNG, E. D., TISHBY, N. & NELKEN, I. 2006. Reduction of information redundancy in the ascending auditory pathway. *Neuron*, 51, 359-368.

- CHEN, C., CHENG, M., ITO, T. & SONG, S. 2018. Neuronal Organization in the Inferior Colliculus Revisited With Cell-Type-Dependent Monosynaptic Tracing. *The Journal of neuroscience : the official journal of the Society for Neuroscience*, 38, 3318-3332
- CHEN, C., READ, H. L. & ESCABI, M. A. 2012a. Precise feature based time scales and frequency decorrelation lead to a sparse auditory code. *J Neurosci*, 32, 8454-8468.
- CHEN, C., RODRIGUEZ, F. C., READ, H. L. & ESCABÍ, M. A. 2012b. Spectrotemporal sound preferences of neighboring inferior colliculus neurons: implications for local circuitry and processing. *Front Neural Circuits*, 6, 1-16
- CHEN, C. & SONG, S. 2019. Differential cell-type dependent brain state modulations of sensory representations in the non-lemniscal mouse inferior colliculus. *Commun Biol*, 2, 356.
- CHEN, T. W., WARDILL, T. J., SUN, Y., PULVER, S. R., RENNINGER, S. L., BAOHAN, A., SCHREITER, E. R., KERR, R. A., ORGER, M. B., JAYARAMAN, V., LOOGER, L. L., SVOBODA, K. & KIM, D. S. 2013. Ultrasensitive fluorescent proteins for imaging neuronal activity. *Nature*, 499, 295-300.
- CHEUNG, S. W., BEDENBAUGH, P. H., NAGARAJAN, S. S. & SCHREINER, C. E. 2001. Functional organization of squirrel monkey primary auditory cortex: responses to pure tones. *J Neurophysiol*, 85, 1732-49.
- CHOI, C. T. & HSU, C. H. 2009. Conditions for generating virtual channels in cochlear prosthesis systems. *Ann Biomed Eng*, 37, 614-24.
- CHOW, B. Y., HAN, X., DOBRY, A. S., QIAN, X., CHUONG, A. S., LI, M., HENNINGER, M. A., BELFORT, G. M., LIN, Y., MONAHAN, P. E. & BOYDEN, E. S. 2010. High-performance genetically targetable optical neural silencing by light-driven proton pumps. *Nature*, 463, 98-102.
- CLERICI, W. & COLEMAN, J. 1990. Anatomy of the Rat Medial Geniculate Body: I. Cytoarchitecture, Myeloarchitecture, and Neocortical Connectivity. *The Journal of comparative neurology*, 297, 14-31
- CLERICI, W., MCDONALD, A., THOMPSON, R. & COLEMAN, J. 1990. Anatomy of the Rat Medial Geniculate Body: II. Dendritic Morphology. *The Journal of comparative neurology*, 297, 32-54
- COHEN, D. 1968. Magnetoencephalography: evidence of magnetic fields produced by alpha-rhythm currents. *Science*, 161, 784-786.
- COHEN, D. 1972. Magnetoencephalography: detection of the brain's electrical activity with a superconducting magnetometer. *Science*, 175, 664-6.
- COHEN, M. R. & KOHN, A. 2011. Measuring and interpreting neuronal correlations. *Nat Neurosci*, 14, 811-819.
- COLLETTI, L., SHANNON, R. V. & COLLETTI, V. 2014. The development of auditory perception in children after auditory brainstem implantation. *Audiology and Neurotology*, 19, 386-394.
- COLLETTI, V., SHANNON, R., CARNER, M., VERONESE, S. & COLLETTI, L. 2009. Outcomes in nontumor adults fitted with the auditory brainstem implant: 10 years' experience. *Otol Neurotol*, 30, 614-618.
- CONNORS, B. W. & GUTNICK, M. J. 1990. Intrinsic firing patterns of diverse neocortical neurons. *Trends Neurosci*, 13, 99-104.
- CONSTANTINIDIS, C. & GOLDMAN-RAKIC, P. S. 2002. Correlated discharges among putative pyramidal neurons and interneurons in the primate prefrontal cortex. *J Neurophysiol*, 88, 3487-3497.
- CORTEXLAB. 2019. *The Cortical Processing Laboratory at UCL (GitHub)* [Online]. University College London. Available: <https://github.com/cortex-lab>.

- COUCHMAN, K., GROTHE, B. & FELMY, F. 2010. Medial Superior Olivary Neurons Receive Surprisingly Few Excitatory and Inhibitory Inputs With Balanced Strength and Short-Term Dynamics. *The Journal of neuroscience : the official journal of the Society for Neuroscience*, 30, 17111-21
- COVEY, E. & CASSEDAY, J. H. 1991. The monaural nuclei of the lateral lemniscus in an echolocating bat: parallel pathways for analyzing temporal features of sound. *J Neurosci*, 11, 3456-3470.
- CRABTREE, J. 1998. Organization in the Auditory Sector of the Cat's Thalamic Reticular Nucleus. *The Journal of comparative neurology*, 390, 167-182
- CSICSVARI, J., HENZE, D. A., JAMIESON, B., HARRIS, K. D., SIROTA, A., BARTHO, P., WISE, K. D. & BUZSAKI, G. 2003. Massively parallel recording of unit and local field potentials with silicon-based electrodes. *J Neurophysiol*, 90, 1314-1323.
- CUNNINGHAM, J. P. & YU, B. M. 2014. Dimensionality reduction for large-scale neural recordings. *Nat Neurosci*, 17, 1500-1509.
- CURTO, C., SAKATA, S., MARGUET, S., ITSKOV, V. & HARRIS, K. D. 2009. A simple model of cortical dynamics explains variability and state dependence of sensory responses in urethane-anesthetized auditory cortex. *J Neurosci*, 29, 10600-12.
- DAIGLE, T. L., MADISEN, L., HAGE, T. A., VALLEY, M. T., KNOBLICH, U., LARSEN, R. S., TAKENO, M. M., HUANG, L., GU, H., LARSEN, R., MILLS, M., BOSMA-MOODY, A., SIVERTS, L. A., WALKER, M., GRAYBUCK, L. T., YAO, Z., FONG, O., NGUYEN, T. N., GARREN, E., LENZ, G. H., CHAVARHA, M., PENDERGRAFT, J., HARRINGTON, J., HIROKAWA, K. E., HARRIS, J. A., NICOVICH, P. R., MCGRAW, M. J., OLLERENSHAW, D. R., SMITH, K. A., BAKER, C. A., TING, J. T., SUNKIN, S. M., LECOQ, J., LIN, M. Z., BOYDEN, E. S., MURPHY, G. J., DA COSTA, N. M., WATERS, J., LI, L., TASIC, B. & ZENG, H. 2018. A Suite of Transgenic Driver and Reporter Mouse Lines with Enhanced Brain-Cell-Type Targeting and Functionality. *Cell*, 174, 465-480.e22.
- DAL MASCHIO, M., DONOVAN, J. C., HELMBRECHT, T. O. & BAIER, H. 2017. Linking Neurons to Network Function and Behavior by Two-Photon Holographic Optogenetics and Volumetric Imaging. *Neuron*, 94, 774-789.e5.
- DALLOS, P. & HARRIS, D. 1978. Properties of Auditory Nerve Responses in Absence of Outer Hair Cells. *Journal of neurophysiology*, 41, 365-83
- DATTA, S. & SIWEK, D. F. 1997. Excitation of the brain stem pedunculopontine tegmentum cholinergic cells induces wakefulness and REM sleep. *J Neurophysiol*, 77, 2975-88.
- DAVIS, H., DAVIS, P. A., LOOMIS, A. L., HARVEY, E. N. & HOBART, G. 1937. Changes in Human Brain Potentials During the Onset of Sleep. *Science*, 86, 448-50.
- DE LA MOTHE, L., BLUMELL, S., KAJIKAWA, Y. & HACKETT, T. 2006. Thalamic Connections of the Auditory Cortex in Marmoset Monkeys: Core and Medial Belt Regions. *The Journal of comparative neurology*, 496, 72-96
- DE LA ROCHA, J., DOIRON, B., SHEA-BROWN, E., JOSIC, K. & REYES, A. 2007. Correlation between neural spike trains increases with firing rate. *Nature*, 448, 802-6.
- DEFELIPE, J. & FARIÑAS, I. 1992. The Pyramidal Neuron of the Cerebral Cortex: Morphological and Chemical Characteristics of the Synaptic Inputs. *Progress in neurobiology*, 39, 563-607
- DEISSEROTH, K. 2011. Optogenetics. *Nature methods*, 8, 26-29.
- DEISSEROTH, K. 2015. Optogenetics: 10 years of microbial opsins in neuroscience. *Nature neuroscience*, 18, 1213-1225.
- DELORME, A. & MAKEIG, S. 2004. EEGLAB: an open source toolbox for analysis of single-trial EEG dynamics including independent component analysis. *J Neurosci Methods*, 134, 9-21.

- DI LIBERTO, G. M., O'SULLIVAN, J. A. & LALOR, E. C. 2015. Low-Frequency Cortical Entrainment to Speech Reflects Phoneme-Level Processing. *Curr Biol*, 25, 2457-65.
- DIETER, A., DUQUE-AFONSO, C. J., RANKOVIC, V., JESCHKE, M. & MOSER, T. 2019. Near physiological spectral selectivity of cochlear optogenetics. *Nat Commun*, 10, 1962.
- DING, N., CHATTERJEE, M. & SIMON, J. Z. 2014. Robust cortical entrainment to the speech envelope relies on the spectro-temporal fine structure. *Neuroimage*, 88, 41-6.
- DODDS, E. M. & DEWEESE, M. R. 2019. On the Sparse Structure of Natural Sounds and Natural Images: Similarities, Differences, and Implications for Neural Coding. *Front Comput Neurosci*, 13, 39
- DOELLING, K. B., ARNAL, L. H., GHITZA, O. & POEPEL, D. 2014. Acoustic landmarks drive delta-theta oscillations to enable speech comprehension by facilitating perceptual parsing. *Neuroimage*, 85, 761-768.
- DONG, S., HAMPSON, R. E., ROBINSON, B. S., MARMARELIS, V. Z., DEADWYLER, S. A. & BERGER, T. W. 2016. Decoding memory features from hippocampal spiking activities using sparse classification models. *Conf Proc IEEE Eng Med Biol Soc*, 2016, 1620-1623.
- DORKOSKI, R., HANCOCK, K., WHALEY, G., WOHL, T., STROUD, N. & DAY, M. 2020. Stimulus-frequency-dependent Dominance of Sound Localization Cues Across the Cochleotopic Map of the Inferior Colliculus. *Journal of neurophysiology*, 123, 1791-1807
- DRUGA, R. & SYKA, J. 1984. Projections from auditory cortex to superior colliculus in the rat. *Neuroscience Letters*, 45, 247-252
- ECKER, A. S., BERENS, P., COTTON, R. J., SUBRAMANIAN, M., DENFIELD, G. H., CADWELL, C. R., SMIRNAKIS, S. M., BETHGE, M. & TOLIAS, A. S. 2014. State dependence of noise correlations in macaque primary visual cortex. *Neuron*, 82, 235-248.
- EDELIN, J. M. 2003. The thalamo-cortical auditory receptive fields: regulation by the states of vigilance, learning and the neuromodulatory systems. *Exp Brain Res*, 153, 554-72.
- EDELIN, J. M., DUTRIEUX, G., MANUNTA, Y. & HENNEVIN, E. 2001. Diversity of receptive field changes in auditory cortex during natural sleep. *Eur J Neurosci*, 14, 1865-1880.
- EDGERTON, B. J., HOUSE, W. F. & HITSELBERGER, W. 1982. Hearing by cochlear nucleus stimulation in humans. *Ann Otol Rhinol Laryngol Suppl*, 91, 117-124.
- EGGERMONT, J. J. 1998. Azimuth coding in primary auditory cortex of the cat. II. Relative latency and interspike interval representation. *J Neurophysiol*, 80, 2151-2161.
- EGGERMONT, J. J. 2011. Context dependence of spectro-temporal receptive fields with implications for neural coding. *Hear Res*, 271, 123-132.
- EGOROVA, M., EHRET, G., VARTANIAN, I. & ESSER, K.-H. 2001. Frequency response areas of neurons in the mouse inferior colliculus. I. Threshold and tuning characteristics. *Experimental brain research*, 140, 145-161.
- EHRET, G., EGOROVA, M., HAGE, S. R. & MULLER, B. A. 2003. Spatial map of frequency tuning-curve shapes in the mouse inferior colliculus. *Neuroreport*, 14, 1365-9.
- EHRET, G. & SCHREINER, C. E. 2005. Spectral and Intensity Coding in the Auditory Midbrain. In: WINER, J. A. & SCHRIENER, C. E. (eds.) *The Inferior Colliculus*. 1st ed. New York, USA: Springer Science + Business Media, Inc.
- ELLIOTT, T. M. & THEUNISSEN, F. E. 2009. The modulation transfer function for speech intelligibility. *PLoS Comput Biol*, 5, e1000302.
- CALLAWAY, E.M. 2008. Transneuronal Circuit Tracing With Neurotropic Viruses. *Current opinion in neurobiology*, 18, 617-623
- EVANS, D. G. 2015. Neurofibromatosis type 2. *Handb Clin Neurol*, 132, 87-96.
- EVANS, D. G. R. 2009. Neurofibromatosis type 2 (NF2): A clinical and molecular review. *Orphanet J Rare Dis*, 4, 16.

- FANSELOW, E., RICHARDSON, K. & CONNORS, B. 2008. Selective, State-Dependent Activation of Somatostatin-Expressing Inhibitory Interneurons in Mouse Neocortex. *Journal of neurophysiology*, 100, 2640-2652
- FAYE-LUND, H. & OSEN, K. K. 1985. Anatomy of the inferior colliculus in rat. *Anat Embryol (Berl)*, 171, 1-20.
- FEKETE, D. M., ROUILLER, E. M., LIBERMAN, M. C. & RYUGO, D. K. 1984. The central projections of intracellularly labeled auditory nerve fibers in cats - Fekete - 1984 - Journal of Comparative Neurology - Wiley Online Library. *The Journal of Comparative Neurology*, 299, 432-450.
- FELDMAYER, D., LÜBKE, J., SILVER, R. & SAKMANN, B. 2002. Synaptic Connections Between Layer 4 Spiny Neurone-Layer 2/3 Pyramidal Cell Pairs in Juvenile Rat Barrel Cortex: Physiology and Anatomy of Interlaminar Signalling Within a Cortical Column. *The Journal of physiology*, 538, 803-822
- FELICIANO, M., MUGNAINI, E. & SALDANA, E. 1995. Direct projections from the rat primary auditory neocortex to nucleus sagulum, paralemniscal regions, superior olivary complex and cochlear nuclei. *Auditory Neuroscience*, 1, 287-308.
- FENNO, L., YIZHAR, O. & DEISSEROTH, K. 2011. The development and application of optogenetics. *Annual review of neuroscience*, 34, 389-412.
- FERRAGAMO, M. J., HARESIGN, T. & SIMMONS, J. A. 1998. Frequency tuning, latencies, and responses to frequency-modulated sweeps in the inferior colliculus of the echolocating bat, *Eptesicus fuscus*. *J Comp Physiol A*, 182, 65-79.
- FISER, J., ORBAN, G., BERKES, P. & LENGYEL, M. 2010. Statistically optimal perception and learning: From behavior to neural representations. *Trends in Cognitive Sciences*, 14, 119-130.
- FRANK, L. M., BROWN, E. N. & WILSON, M. A. 2001. A comparison of the firing properties of putative excitatory and inhibitory neurons from CA1 and the entorhinal cortex. *J Neurophysiol*, 86, 2029-2040.
- FREEMAN, J. A. & NICHOLSON, C. 1975. Experimental optimization of current source-density technique for anuran cerebellum. *J Neurophysiol*, 38, 369-82.
- FRITZ, J., ELHILALI, M. & SHAMMA, S. 2005. Active listening: task-dependent plasticity of spectrotemporal receptive fields in primary auditory cortex. *Hear Res*, 206, 159-76.
- FU, T. M., HONG, G., VIVEROS, R. D., ZHOU, T. & LIEBER, C. M. 2017. Highly scalable multichannel mesh electronics for stable chronic brain electrophysiology. *Proc Natl Acad Sci U S A*, 114, E10046-e10055.
- FU, Y., TUCCIARONE, J., ESPINOSA, J., SHENG, N., DARCY, D., NICOLL, R., HUANG, Z. & STRYKER, M. 2014. A Cortical Circuit for Gain Control by Behavioral State. *Cell*, 156.
- FUENTEALBA, P. & STERIADE, M. 2005. The reticular nucleus revisited: intrinsic and network properties of a thalamic pacemaker. *Prog Neurobiol*, 75, 125-41.
- GAESE, B. H. & OSTWALD, J. 2001. Anesthesia changes frequency tuning of neurons in the rat primary auditory cortex. *J Neurophysiol*, 86, 1062-6.
- GAO, E. & SUGA, N. 1998. Experience-dependent corticofugal adjustment of midbrain frequency map in bat auditory system. *Proc Natl Acad Sci U S A*, 95, 12663-70.
- GARCIA-LAZARO, J., SHEPARD, K., MIRANDA, J., LIU, R. & LESICA, N. 2015. An Overrepresentation of High Frequencies in the Mouse Inferior Colliculus Supports the Processing of Ultrasonic Vocalizations. *PLoS one*, 10. e0133251
- GEIS, H. & BORST, J. 2013. Large GABAergic Neurons Form a Distinct Subclass Within the Mouse Dorsal Cortex of the Inferior Colliculus With Respect to Intrinsic Properties, Synaptic Inputs, Sound Responses, and Projections. *The Journal of comparative neurology*, 521, 189-202

- GENSIGHT BIOLOGICS. 2018. *Gene Therapy* [Online]. Available: <https://www.gensight-biologics.com/gene-therapy/> [Accessed 2018].
- GIRAUD, A. L. & POEPEL, D. 2012. Cortical oscillations and speech processing: emerging computational principles and operations. *Nat Neurosci*, 15, 511-517.
- GLEESON, P., CANTARELLI, M., MARIN, B., QUINTANA, A., EARNSHAW, M., SADEH, S., PIASINI, E., BIRGIOLAS, J., CANNON, R. C., CAYCO-GAJIC, N. A., CROOK, S., DAVISON, A. P., DURA-BERNAL, S., ECKER, A., HINES, M. L., IDILI, G., LANORE, F., LARSON, S. D., LYTTON, W. W., MAJUMDAR, A., MCDUGAL, R. A., SIVAGNANAM, S., SOLINAS, S., STANISLOVAS, R., VAN ALBADA, S. J., VAN GEIT, W. & SILVER, R. A. 2019. Open Source Brain: A Collaborative Resource for Visualizing, Analyzing, Simulating, and Developing Standardized Models of Neurons and Circuits. *Neuron*, 103, 395-411.e5.
- GLENDENNING, K. K., BAKER, B. N., HUTSON, K. A. & MASTERTON, R. B. 1992. Acoustic chiasm V: inhibition and excitation in the ipsilateral and contralateral projections of LSO. *J Comp Neurol*, 319, 100-122.
- GOFFI-GOMEZ, M. V. S., MAGALHÃES, A. T., NETO, R. B., TSUJI, R. K., GOMES, M. D. Q. T. & BENTO, R. F. 2012. Auditory brainstem implant outcomes and MAP parameters: report of experiences in adults and children. *International journal of pediatric otorhinolaryngology*, 76, 257-264.
- GONZÁLEZ-HERNÁNDEZ, T., MANTOLÁN-SARMIENTO, B., GONZÁLEZ-GONZÁLEZ, B. & PÉREZ-GONZÁLEZ, H. 1996. Sources of GABAergic Input to the Inferior Colliculus of the Rat. *The Journal of comparative neurology*, 372, 309-326
- GRADINARU, V., THOMPSON, K. R. & DEISSEROTH, K. 2008. eNpHR: a Natronomonas halorhodopsin enhanced for optogenetic applications. *Brain Cell Biol*, 36, 129-39.
- GRADINARU, V., ZHANG, F., RAMAKRISHNAN, C., MATTIS, J., PRAKASH, R., DIESTER, I., GOSHEN, I., THOMPSON, K. R. & DEISSEROTH, K. 2010. Molecular and Cellular Approaches for Diversifying and Extending Optogenetics. *Cell*, 141, 154-165.
- GRANA, G. D., HUTSON, K. A., BADEA, A., PAPPA, A., SCOTT, W. & FITZPATRICK, D. C. 2017. The organization of frequency and binaural cues in the gerbil inferior colliculus. *J Comp Neurol*, 525, 2050-2074.
- GROFF, J. A. & LIBERMAN, M. C. 2003. Modulation of cochlear afferent response by the lateral olivocochlear system: activation via electrical stimulation of the inferior colliculus. *J Neurophysiol*, 90, 3178-3200.
- GUNAYDIN, L. A., YIZHAR, O., BERNDT, A., SOHAL, V. S., DEISSEROTH, K. & HEGEMANN, P. 2010. Ultrafast optogenetic control. *Nat Neurosci*, 13, 387-392.
- GUO, W., CHAMBERS, A. R., DARROW, K. N., HANCOCK, K. E., SHINN-CUNNINGHAM, B. G., POLLEY, D. B. 2012. Robustness of Cortical Topography across Fields, Laminae, Anesthetic States, and Neurophysiological Signal Types. *J Neurosci*, 32, 9159-9172
- GUO, W., HIGHT, A. E., CHEN, J. X., KLAPOETKE, N. C., HANCOCK, K. E., SHINN-CUNNINGHAM, B. G., BOYDEN, E. S., LEE, D. J. & POLLEY, D. B. 2015. Hearing the light: neural and perceptual encoding of optogenetic stimulation in the central auditory pathway. *Scientific reports*, 5, 10319-10319.
- GUO, Z., WANG, M., WANG, L., YANG, B., LI, C., JI, B., GE, C., GU, X., WANG, X. & LIU, J. 2019. A Polyimide-based Flexible Optoelectrodes for Low-Noise Neural Recording. *IEEE Electron Device Letters*, 40, 1190-1193.
- HACKETT, T. A. 2011. Information flow in the auditory cortical network. *Hear Res*, 271, 133-146.
- HAGE, S. R. & EHRET, G. 2003. Mapping responses to frequency sweeps and tones in the inferior colliculus of house mice. *Eur J Neurosci*, 18, 2301-2312.

- HAIDER, B., DUQUE, A., HASENSTAUB, A. R. & MCCORMICK, D. A. 2006. Neocortical network activity in vivo is generated through a dynamic balance of excitation and inhibition. *J Neurosci*, 26, 4535-4545.
- HAN, X., CHOW, B. Y., ZHOU, H., KLAPOETKE, N. C., CHUONG, A., RAJIMEHR, R., YANG, A., BARATTA, M. V., WINKLE, J., DESIMONE, R. & BOYDEN, E. S. 2011. A high-light sensitivity optical neural silencer: development and application to optogenetic control of non-human primate cortex. *Front Syst Neurosci*, 5, 18
- HARRIS, K. D., CSICSVARI, J., HIRASE, H., DRAGOI, G. & BUZSAKI, G. 2003. Organization of cell assemblies in the hippocampus. *Nature*, 424, 552-556.
- HARRIS, K. D. & THIELE, A. 2011. Cortical State and Attention. *Nat Rev Neurosci*, 12, 509-23.
- HAVENITH, M. N., YU, S., BIEDERLACK, J., CHEN, N. H., SINGER, W. & NIKOLIC, D. 2011. Synchrony makes neurons fire in sequence, and stimulus properties determine who is ahead. *J Neurosci*, 31, 8570-8584.
- TSAI, H., ZHANG, F., ADAMANTIDIS, A., STUBER G. D., BONCI, A., LECEA L., DEISSEROTH, K.. 2009. Phasic Firing in Dopaminergic Neurons Is Sufficient for Behavioral Conditioning. *Science*. 324, 1080-1084
- HEARING SOLUTIONS. 2020. *Symptoms & Causes of Hearing Loss | Hearing Solutions* [Online]. Professional Hearing Aid Fittings - hearingsolutions.ca. Available: <https://hearingsolutions.ca/hearing-loss-causes/> [Accessed 2020].
- HENRY, K. R. & CHOLE, R. A. 1980. Genotypic differences in behavioral, physiological and anatomical expressions of age-related hearing loss in the laboratory mouse. *Audiology*, 19, 369-383.
- HERBERT, H., ASCHOFF, A. & OSTWALD, J. 1991. Topography of projections from the auditory cortex to the inferior colliculus in the rat. *J Comp Neurol*, 304, 103-22.
- HERNANDEZ, O., PAPAGIAKOUMOU, E., TANESE, D., FIDELIN, K., WYART, C. & EMILIANI, V. 2016. Three-dimensional spatiotemporal focusing of holographic patterns. *Nat Commun*, 7, 11928.
- HERRMANN, B., PARTHASARATHY, A. & BARTLETT, E. L. 2017. Aging affects dual encoding of periodicity and envelope shape in rat inferior colliculus neurons. *Eur J Neurosci*, 45, 299-311.
- HIGHT, A. E., KOZIN, E. D., DARROW, K., LEHMANN, A., BOYDEN, E., BROWN, M. C. & LEE, D. J. 2015. Superior Temporal Resolution of Chronos versus Channelrhodopsin-2 in an Optogenetic Model of the Auditory Brainstem Implant. *Hearing Research*. 322, 235-241
- HODGKIN, A. L. & HUXLEY, A. F. 1952. Propagation of electrical signals along giant nerve fibers. *Proc R Soc Lond B Biol Sci*, 140, 177-183.
- HODGKIN, A. L., HUXLEY, A. F. & KATZ, B. 1952. Measurement of current-voltage relations in the membrane of the giant axon of *Loligo*. *J Physiol*, 116, 424-448.
- HOLMSTROM, L. A., EEUWES, L. B., ROBERTS, P. D. & PORTFORS, C. V. 2010. Efficient encoding of vocalizations in the auditory midbrain. *J Neurosci*, 30, 802-819.
- HOMMA, N. Y., HAPPEL, M. F. K., NODAL, F. R., OHL, F. W., KING, A. J. & BAJO, V. M. 2017. A Role for Auditory Corticothalamic Feedback in the Perception of Complex Sounds. *Journal of Neuroscience*, 37, 6149-6161
- HORIE, M., TSUKANO, H., HISHIDA, R., TAKEBAYASHI, H. & SHIBUKI, K. 2013. Dual Compartments of the Ventral Division of the Medial Geniculate Body Projecting to the Core Region of the Auditory Cortex in C57BL/6 Mice. *Neuroscience research*, 76, 207-12.
- HROMADKA, T., DEWEESE, M. R. & ZADOR, A. M. 2008. Sparse representation of sounds in the unanesthetized auditory cortex. *PLoS Biol*, 6, e16.

- HTTP://CHRONUX.ORG. 2018. *Chronux* [Online]. [Accessed 2018].
- HUANG, C., LARUE, D. & WINER, J. 1999. GABAergic Organization of the Cat Medial Geniculate Body. *The Journal of comparative neurology*, 415, 368-392
- HUANG, C. L. & WINER, J. A. 2000. Auditory thalamocortical projections in the cat: laminar and areal patterns of input. *J Comp Neurol*, 427, 302-331.
- HUBEL, D. H. 1957. Tungsten Microelectrode for Recording from Single Units. *Science*, 125, 549-550.
- HUFFMAN, R. & COVEY, E. 1995. Origin of Ascending Projections to the Nuclei of the Lateral Lemniscus in the Big Brown Bat, *Eptesicus Fuscus*. *The Journal of comparative neurology*, 357, 532-545
- IMAIZUMI, K. & SCHREINER, C. E. 2007. Spatial interaction between spectral integration and frequency gradient in primary auditory cortex. *J Neurophysiol*, 98, 2933-42.
- IMEC. 2020. *Neuropixels 1.0 Probe* [Online]. IMEC. Available: <https://www.neuropixels.org/probe> [Accessed 2020].
- IMIG, T. J. & MOREL, A. 1985. Tonotopic organization in ventral nucleus of medial geniculate body in the cat. *J Neurophysiol*, 53, 309-340.
- INCE, R. A., PANZERI, S. & KAYSER, C. 2013. Neural codes formed by small and temporally precise populations in auditory cortex. *J Neurosci*, 33, 18277-87.
- ISSA, E. B. & WANG, X. 2011. Altered neural responses to sounds in primate primary auditory cortex during slow-wave sleep. *J Neurosci*, 31, 2965-2973.
- ITO, T., BISHOP, D. C. & OLIVER, D. L. 2009. Two Classes of GABAergic Neurons in the Inferior Colliculus. *J Neuroscience*. 29, 13860-9
- ITO, T., BISHOP, D. C. & OLIVER, D. L. 2011. Expression of Glutamate and Inhibitory Amino Acid Vesicular Transporters in the Rodent Auditory Brainstem. *J Comp Neurol*, 519, 316-340.
- ITO, T. & OLIVER, D. L. 2012. The basic circuit of the IC: tectothalamic neurons with different patterns of synaptic organization send different messages to the thalamus. *Front Neural Circuits*, 6, 48
- IWATA, J., LEDOUX, J. E., MEELEY, M. P., ARNERIC, S. & REIS, D. J. 1986. Intrinsic neurons in the amygdaloid field projected to by the medial geniculate body mediate emotional responses conditioned to acoustic stimuli. *Brain Res*, 383, 195-214.
- JACKSON, A. F. & BOLGER, D. J. 2014. The neurophysiological bases of EEG and EEG measurement: a review for the rest of us. *Psychophysiology*, 51, 1061-1071.
- JASPER, H. H. & ANDREWS, H. L. 2010. Human Brain Rhythms: I. Recording Techniques and Preliminary Results. *The Journal of General Psychology*, 14, 98-126.
- JEN, P. H. & ZHANG, J. P. 1999. corticofugal regulation of excitatory and inhibitory frequency tuning curves of bat inferior collicular neurons. *Brain Res*, 841, 184-188.
- JESCHKE, M. & MOSER, T. 2015. Considering optogenetic stimulation for cochlear implants. *Hearing research*, 322, 224-234.
- JONES, E. 2003. Chemically Defined Parallel Pathways in the Monkey Auditory System. *Annals of the New York Academy of Sciences*, 999.
- JORIS, P. X., SCHREINER, C. E. & REES, A. 2004. Neural processing of amplitude-modulated sounds. *Physiol Rev*, 84, 541-77.
- JOUVET, M. 1962. Research on the neural structures and responsible mechanisms in different phases of physiological sleep. *Arch Ital Biol*, 100, 125-206.
- JUN, J. J., STEINMETZ, N. A., SIEGLE, J. H., DENMAN, D. J., BAUZA, M., BARBARITS, B., LEE, A. K., ANASTASSIOU, C. A., ANDREI, A., AYDIN, Ç., BARBIC, M., BLANCHE, T. J., BONIN, V., COUTO, J., DUTTA, B., GRATIY, S. L., GUTNISKY, D. A., HÄUSSER, M., KARSH, B., LEDOCHOWITSCH, P., LOPEZ, C. M., MITELUT, C., MUSA, S., OKUN, M., PACHITARIU, M., PUTZEYS, J., RICH, P. D., ROSSANT, C., SUN, W., SVOBODA, K., CARANDINI, M.,

- HARRIS, K. D., KOCH, C., O'KEEFE, J. & HARRIS, T. D. 2017. Fully Integrated Silicon Probes for High-Density Recording of Neural Activity. *Nature*, 551, 232-6.
- KAAS, J. H. & HACKETT, T. A. 1998. Subdivisions of auditory cortex and levels of processing in primates. *Audiol Neurootol*, 3, 73-85.
- KAAS, J. H. & HACKETT, T. A. 2000. Subdivisions of auditory cortex and processing streams in primates. *Proc Natl Acad Sci U S A*, 97, 11793-9.
- KAMPASI, K., ENGLISH, D. F., SEYMOUR, J., STARK, E., MCKENZIE, S., VOROSLAKOS, M., BUZSAKI, G., WISE, K. D. & YOON, E. 2018. Dual color optogenetic control of neural populations using low-noise, multishank optoelectrodes. *Microsyst Nanoeng*, 4, 10
- KANARI, L., RAMASWAMY, S., SHI, Y., MORAND, S., MEYSTRE, J., PERIN, R., ABDELLAH, M., WANG, Y., HESS, K. & MARKRAM, H. 2019. Objective Morphological Classification of Neocortical Pyramidal Cells. *Cerebral cortex*. 29, 1719–1735.
- KARNANI, M., JACKSON, J., AYZENSHTAT, I., HAMZEHEI SICHANI, A., MANOOCHERI, K., KIM, S. & YUSTE, R. 2016. Opening Holes in the Blanket of Inhibition: Localized Lateral Disinhibition by VIP Interneurons. *The Journal of neuroscience : the official journal of the Society for Neuroscience*, 36, 3471-3480
- KATO, H. K., ASINOF, S. K. & ISAACSON, J. S. 2017. Network-Level Control of Frequency Tuning in Auditory Cortex. *Neuron*, 95, 412-423.e4.
- KAYSER, C., INCE, R. A. A. & PANZERI, S. 2012. Analysis of Slow (Theta) Oscillations as a Potential Temporal Reference Frame for Information Coding in Sensory Cortices. *PLoS Comput Biol*, 8. e1002717
- KAYSER, C., MONTEMURRO, M. A., LOGOTHETIS, N. K. & PANZERI, S. 2009. Spike-phase coding boosts and stabilizes information carried by spatial and temporal spike patterns. *Neuron*, 61, 597-608.
- KAYSER, C., WILSON, C., SAFAAI, H., SAKATA, S. & PANZERI, S. 2015. Rhythmic Auditory Cortex Activity at Multiple Timescales Shapes Stimulus–Response Gain and Background Firing. *J Neurosci*, 35, 7750-7762.
- KELLY, J. B., GLENN, S. L. & BEAVER, C. J. 1991. Sound frequency and binaural response properties of single neurons in rat inferior colliculus. *Hear Res*, 56, 273-80.
- KELLY, J. P. & WONG, D. 1981. Laminar connections of the cat's auditory cortex. *Brain Res*, 212, 1-15.
- KEPPELER, D., MERINO, R. M., LOPEZ DE LA MORENA, D., BALI, B., HUET, A. T., GEHRT, A., WROBEL, C., SUBRAMANIAN, S., DOMBROWSKI, T., WOLF, F., RANKOVIC, V., NEEF, A. & MOSER, T. 2018. Ultrafast optogenetic stimulation of the auditory pathway by targeting-optimized Chronos. *Embo j*, 37. e99649
- KIEFER, J., HOHL, S., STURZEBECHER, E., PFENNIGDORFF, T. & GSTOETTNER, W. 2001. Comparison of speech recognition with different speech coding strategies (SPEAK, CIS, and ACE) and their relationship to telemetric measures of compound action potentials in the nucleus CI 24M cochlear implant system. *Audiology*, 40, 32-42.
- KIM, E., JUAVINETT, A., KYUBWA, E., JACOB, M. & CALLAWAY, E. 2015. Three Types of Cortical Layer 5 Neurons That Differ in Brain-wide Connectivity and Function. *Neuron*, 88, 1253-1267
- KIM, H. N., SHIM, Y. J., CHUNG, M. H. & LEE, Y. H. 2000. Benefit of ACE compared to CIS and SPEAK coding strategies. *Adv Otorhinolaryngol*, 57, 408-11.
- KIM, K., VÖRÖSLAKOS, M., SEYMOUR, J. P., WISE, K. D., BUZSÁKI, G. & YOON, E. 2019. Artifact-free, high-temporal-resolution in vivo opto-electrophysiology with microLED optoelectrodes. *bioRxiv*.
- KIM, S.-P., RAO, Y. N., ERDOGMUS, D., SANCHEZ, J. C., NICOLELIS, M. A. L. & PRINCIPE, J. C. 2005. Determining Patterns in Neural Activity for Reaching Movements Using

Nonnegative Matrix Factorization. *EURASIP Journal on Advances in Signal Processing*. 19

- KIM, S. J., MANYAM, S. C., WARREN, D. J. & NORMANN, R. A. 2006. Electrophysiological mapping of cat primary auditory cortex with multielectrode arrays. *Ann Biomed Eng*, 34, 300-309.
- KIMURA, A., DONISHI, T., OKAMOTO, K. & TAMAI, Y. 2004. Efferent Connections of "Posterodorsal" Auditory Area in the Rat Cortex: Implications for Auditory Spatial Processing. *Neuroscience*, 128, 399-419
- KIMURA, A., DONISHI, T., SAKODA, T., HAZAMA, M. & TAMAI, Y. 2003. Auditory Thalamic Nuclei Projections to the Temporal Cortex in the Rat. *Neuroscience*, 117, 1003-1016
- KLAPOETKE, N. C., MURATA, Y., KIM, S. S., PULVER, S. R., BIRDSEY-BENSON, A., CHO, Y. K., MORIMOTO, T. K., CHUONG, A. S., CARPENTER, E. J., TIAN, Z., WANG, J., XIE, Y., YAN, Z., ZHANG, Y., CHOW, B. Y., SUREK, B., MELKONIAN, M., JAYARAMAN, V., CONSTANTINE-PATON, M., WONG, G. K.-S. & BOYDEN, E. S. 2014. Independent optical excitation of distinct neural populations. *Nature methods*, 11, 338-346.
- KLEIN, E., GOSSLER, C., PAUL, O. & RUTHER, P. 2018. High-Density μ LED-Based Optical Cochlear Implant With Improved Thermomechanical Behavior. *Front Neurosci*, 12, 659
- KLEIN, E., KAKU, Y., PAUL, O. & RUTHER, P. 2019. Flexible μ LED-Based Optogenetic Tool with Integrated μ -Lens Array and Conical Concentrators Providing Light Extraction Improvement Above 80%. *2019 IEEE 32nd International Conference on Micro Electro Mechanical Systems (MEMS)*. Seoul, South Korea: IEEE.
- KLIMESCH, W. 1999. EEG alpha and theta oscillations reflect cognitive and memory performance: a review and analysis. *Brain Res Brain Res Rev*, 29, 169-195.
- KLIMESCH, W., DOPPELMAYR, M., RUSSEGGER, H., PACHINGER, T. & SCHWAIGER, J. 1998. Induced alpha band power changes in the human EEG and attention. *Neurosci Lett*, 244, 73-76.
- KOCH, D. B., DOWNING, M., OSBERGER, M. J. & LITVAK, L. 2007. Using current steering to increase spectral resolution in CII and HiRes 90K users. *Ear Hear*, 28, 38s-41s.
- KOHN, A. & SMITH, M. A. 2005. Stimulus Dependence of Neuronal Correlation in Primary Visual Cortex of the Macaque. *J Neurosci*, 25, 3661-3673.
- KONG, L., XIONG, C., LI, L. & YAN, J. 2014. Frequency-specific Corticofugal Modulation of the Dorsal Cochlear Nucleus in Mice. *Frontiers in systems neuroscience*, 8, 125
- KRISHNA, B. S. & SEMPLE, M. N. 2000. Auditory temporal processing: responses to sinusoidally amplitude-modulated tones in the inferior colliculus. *J Neurophysiol*, 84, 255-73.
- KUBOTA, Y., KARUBE, F., NOMURA, M. & KAWAGUCHI, Y. 2016. The Diversity of Cortical Inhibitory Synapses. *Frontiers in neural circuits*, 10, 27
- LAKATOS, P., KARMOS, G., MEHTA, A. D., ULBERT, I. & SCHROEDER, C. E. 2008. Entrainment of neuronal oscillations as a mechanism of attentional selection. *Science*, 320, 110-113.
- LAKATOS, P., SHAH, A. S., KNUTH, K. H., ULBERT, I., KARMOS, G. & SCHROEDER, C. E. 2005. An oscillatory hierarchy controlling neuronal excitability and stimulus processing in the auditory cortex. *J Neurophysiol*, 94, 1904-1911.
- LANGNER, G. 2004. Topographic representation of periodicity information: the 2nd neural axis of the auditory system. In: SYKA, J. & MM, M. (eds.) *Plasticity of the Central Auditory System and Processing of Complex Acoustic Signals*. New York, USA: Springer-Verlag.

- LANGNER, G., ALBERT, M. & BRIEDE, T. 2002. Temporal and spatial coding of periodicity information in the inferior colliculus of awake chinchilla (*Chinchilla laniger*). *Hear Res*, 168, 110-130.
- LANGNER, G., SCHREINER, C. & MERZENICH, M. M. 1987. Covariation of latency and temporal resolution in the inferior colliculus of the cat. *Hear Res*, 31, 197-201.
- LASZIG, R., KUZMA, J., SEIFERT, V. & LEHNHARDT, E. 1991. The Hannover auditory brainstem implant: a multiple-electrode prosthesis. *Eur Arch Otorhinolaryngol*, 248, 420-421.
- LAUDANSKI, J., EDELINE, J. M. & HUETZ, C. 2012. Differences between Spectro-Temporal Receptive Fields Derived from Artificial and Natural Stimuli in the Auditory Cortex. *PLoS One*, 7, e50539
- LEDoux, J. E., FARB, C. R. & ROMANSKI, L. M. 1991. Overlapping projections to the amygdala and striatum from auditory processing areas of the thalamus and cortex. *Neurosci Lett*, 134, 139-144.
- LEE, C., IMAIZUMI, K., SCHREINER, C. & WINER, J. 2004. Concurrent Tonotopic Processing Streams in Auditory Cortex. *Cerebral cortex*. 14, 441-451
- LEE, C. & WINER, J. 2008a. Connections of Cat Auditory Cortex: I. Thalamocortical System. *The Journal of comparative neurology*, 507, 1879-1900.
- LEE, C. & WINER, J. 2008b. Connections of Cat Auditory Cortex: III. Corticocortical System. *The Journal of comparative neurology*, 507, 1920-1943
- LEE, C. C. 2015. Exploring functions for the non-lemniscal auditory thalamus. *Front Neural Circuits*, 9, 69
- LEE, C. C. & WINER, J. A. 2008c. Connections of Cat Auditory Cortex: II. Commissural System. *J Comp Neurol*, 507, 1901-1919.
- LEE, D. D. & SEUNG, H. S. 1999. Learning the parts of objects by non-negative matrix factorization. *Nature*, 401, 788-791.
- LEE, S., HJERLING-LEFFLER, J., ZAGHA, E., FISHELL, G. & RUDY, B. 2010. The Largest Group of Superficial Neocortical GABAergic Interneurons Expresses Ionotropic Serotonin Receptors. *The Journal of neuroscience : the official journal of the Society for Neuroscience*, 30, 16796-808
- LEE, S., KRUGLIKOV, I., HUANG, Z., FISHELL, G. & RUDY, B. 2013. A Disinhibitory Circuit Mediates Motor Integration in the Somatosensory Cortex. *Nature neuroscience*, 16, 1662-1670
- LENARZ, T., LIM, H. H., REUTER, G., PATRICK, J. F. & LENARZ, M. 2006. The auditory midbrain implant: a new auditory prosthesis for neural deafness-concept and device description. *Otol Neurotol*, 27, 838-43.
- LEONG, V. & GOSWAMI, U. 2014. Assessment of rhythmic entrainment at multiple timescales in dyslexia: evidence for disruption to syllable timing. *Hear Res*, 308, 141-161.
- LI, B., LEE, K., MASMANIDIS, S. C. & LI, M. 2018. A nanofabricated optoelectronic probe for manipulating and recording neural dynamics. *J Neural Eng*, 15, 046008.
- LI, L. Y., JI, X. Y., LIANG, F., LI, Y. T., XIAO, Z., TAO, H. W. & ZHANG, L. I. 2014. A feedforward inhibitory circuit mediates lateral refinement of sensory representation in upper layer 2/3 of mouse primary auditory cortex. *J Neurosci*, 34, 13670-83.
- LI, Y., EVANS, M. S. & FAINGOLD, C. L. 1999. Synaptic response patterns of neurons in the cortex of rat inferior colliculus. *Hear Res*, 137, 15-28.
- LIANG, L., LU, T. & WANG, X. 2002. Neural representations of sinusoidal amplitude and frequency modulations in the primary auditory cortex of awake primates. *J Neurophysiol*, 87, 2237-2261.

- LIM, H., LENARZ, M. & LENARZ, T. 2011. Auditory Midbrain Implants. *In*: ZENG, F.-G., POPPER, A. N. & FAY, R. R. (eds.) *Auditory Prosthesis: New Horizons*. New York: Springer.
- LIM, H. H., LENARZ, M. & LENARZ, T. 2009. Auditory Midbrain Implant: A Review. *Trends Amplif*, 13, 149-180.
- LIM, H. H. & LENARZ, T. 2015. Auditory midbrain implant: research and development towards a second clinical trial. *Hearing research*, 322, 212-223.
- LIM, H. H., LENARZ, T., JOSEPH, G., BATTMER, R. D., SAMII, A., SAMII, M., PATRICK, J. F. & LENARZ, M. 2007. Electrical stimulation of the midbrain for hearing restoration: insight into the functional organization of the human central auditory system. *J Neurosci*, 27, 13541-51.
- LIN, P. A., ASINOF, S. K., EDWARDS, N. J. & ISAACSON, J. S. 2019. Arousal regulates frequency tuning in primary auditory cortex. *Proc Natl Acad Sci U S A*, 116, 25304-25310.
- LING, G. & GERARD, R. W. 1949. The normal membrane potential of frog sartorius fibers. *J Cell Comp Physiol*, 34, 383-396.
- LIU, J. K., SCHREYER, H. M., ONKEN, A., ROZENBLIT, F., KHANI, M. H., KRISHNAMOORTHY, V., PANZERI, S. & GOLLISCH, T. 2017. Inference of neuronal functional circuitry with spike-triggered non-negative matrix factorization. *Nat Commun*, 8, 149.
- LIVINGSTON, G., SOMMERLAD, A., ORGETA, V., COSTAFREDA, S. G., HUNTLEY, J., AMES, D., BALLARD, C., BANERJEE, S., BURNS, A., COHEN-MANSFIELD, J., COOPER, C., FOX, N., GITLIN, L. N., HOWARD, R., KALES, H. C., LARSON, E. B., RITCHIE, K., ROCKWOOD, K., SAMPSON, E. L., SAMUS, Q., SCHNEIDER, L. S., SELBAEK, G., TERI, L. & MUKADAM, N. 2017. Dementia prevention, intervention, and care. *Lancet*, 390, 2673-2734.
- LOFTUS, W., BISHOP, D. & OLIVER, D. 2010. Differential Patterns of Inputs Create Functional Zones in Central Nucleus of Inferior Colliculus. *The Journal of neuroscience : the official journal of the Society for Neuroscience*, 30, 13396-13408
- LOFTUS, W. C. & SUTTER, M. L. 2001. Spectrotemporal organization of excitatory and inhibitory receptive fields of cat posterior auditory field neurons. *J Neurophysiol*, 86, 475-491.
- LOIZOU, P. C. 2006. Speech processing in vocoder-centric cochlear implants. *Adv Otorhinolaryngol*, 64, 109-143.
- LOIZOU, P. C., POROY, O. & DORMAN, M. 2000. The effect of parametric variations of cochlear implant processors on speech understanding. *J Acoust Soc Am*, 108, 790-802.
- LOMBARDO, J. A., MACELLAIO, M. V., LIU, B., PALMER, S. E. & OSBORNE, L. C. 2018. State dependence of stimulus-induced variability tuning in macaque MT. *PLoS Comput Biol*, 14.
- LUMANI, A. & ZHANG, H. 2010. Responses of Neurons in the Rat's Dorsal Cortex of the Inferior Colliculus to Monaural Tone Bursts. *Brain research*, 1351, 115-129
- LUNDIN, K. 2016. Experiences from Cochlear Implantation and Auditory Brainstem Implantation in Adults and Children: Electrophysiological Measurements, Hearing Outcomes and Patient Satisfaction. PhD Thesis. Uppsala Universitet.
- LUO, H. & POEPEL, D. 2007. Phase patterns of neuronal responses reliably discriminate speech in human auditory cortex. *Neuron*, 54, 1001-1010.
- MAFFI, C. L. & AITKIN, L. M. 1987. Differential neural projections to regions of the inferior colliculus of the cat responsive to high frequency sounds. *Hear Res*, 26, 211-9.
- MAGER, T., DE LA MORENA, D. L., SHEVCHENKO, V., SENN, V., WOOD, P. G., LETZKUS, J. J., GORDELIY, V., MOSER, T. & BAMBERG, E. 2018a. Improved Microbial Rhodopsins for Ultrafast Red-Shifted Optogenetics. *Biophysical Journal*, 114, 669a.

- MAGER, T., LOPEZ DE LA MORENA, D., SENN, V., SCHLOTTE, J., A, D. E., FELDBAUER, K., WROBEL, C., JUNG, S., BODENSIEK, K., RANKOVIC, V., BROWNE, L., HUET, A., JUTTNER, J., WOOD, P. G., LETZKUS, J. J., MOSER, T. & BAMBERG, E. 2018b. High frequency neural spiking and auditory signaling by ultrafast red-shifted optogenetics. *Nat Commun*, 9, 1750.
- MAKEIG, S., DEBENER, S., ONTON, J. & DELORME, A. 2004. Mining event-related brain dynamics. *Trends Cogn Sci*, 8, 204-210.
- MALMIERCA, M., HERNÁNDEZ, O. & REES, A. 2005a. Intercollicular Commissural Projections Modulate Neuronal Responses in the Inferior Colliculus. *The European journal of neuroscience*, 21, 2701-2710
- MALMIERCA, M., SAINT MARIE, R., MERCHAN, M. & OLIVER, D. 2005b. Lamina Inputs From Dorsal Cochlear Nucleus and Ventral Cochlear Nucleus to the Central Nucleus of the Inferior Colliculus: Two Patterns of Convergence. *Neuroscience*, 136, 883-94.
- MALMIERCA, M. S., IZQUIERDO, M. A., CRISTAUDO, S., HERNÁNDEZ, O., PÉREZ-GONZÁLEZ, D., COVEY, E. & OLIVER, D. L. 2008. A discontinuous tonotopic organization in the inferior colliculus of the rat. *Journal of Neuroscience*, 28, 4767-4776.
- MALMIERCA, M. S., MERCHÁN, M. A., HENKEL, C. K. & OLIVER, D. L. 2002. Direct Projections from Cochlear Nuclear Complex to Auditory Thalamus in the Rat. *J Neuroscience*. 15, 10891-7
- MARGUET, S. L. & HARRIS, K. D. 2011. State-Dependent Representation of Amplitude-Modulated Noise Stimuli in Rat Auditory Cortex. *J Neurosci*. 31, 6414-20.
- MARKRAM, H., TOLEDO-RODRIGUEZ, M., WANG, Y., GUPTA, A., SILBERBERG, G. & WU, C. 2004. Interneurons of the Neocortical Inhibitory System. *Nature reviews. Neuroscience*, 5, 793-807
- MATSUNO-YAGI, A. & MUKOHATA, Y. 1977. Two possible roles of bacteriorhodopsin; a comparative study of strains of Halobacterium halobium differing in pigmentation. *Biochem Biophys Res Commun*, 78, 237-243.
- MATTHIES, C., BRILL, S., VARALLYAY, C., SOLYMOSI, L., GELBRICH, G., ROOSEN, K., ERNESTUS, R. I., HELMS, J., HAGEN, R., MLYNSKI, R., SHEHATA-DIELER, W. & MULLER, J. 2014. Auditory brainstem implants in neurofibromatosis Type 2: is open speech perception feasible? *J Neurosurg*, 120, 546-58.
- MATTIS, J., TYE, K. M., FERENCZI, E. A., RAMAKRISHNAN, C., O'SHEA, D. J., PRAKASH, R., GUNAYDIN, L. A., HYUN, M., FENNO, L. E., GRADINARU, V., YIZHAR, O. & DEISSEROTH, K. 2011. Principles for applying optogenetic tools derived from direct comparative analysis of microbial opsins. *Nat Methods*, 9, 159-72.
- MAYNARD, E. M., HATSOPOULOS, N. G., OJAKANGAS, C. L., ACUNA, B. D., SANES, J. N., NORMANN, R. A. & DONOGHUE, J. P. 1999. Neuronal interactions improve cortical population coding of movement direction. *J Neurosci*, 19, 8083-93.
- MCALINDEN, N., GU, E., DAWSON, M. D., SAKATA, S. & MATHIESON, K. 2015. Optogenetic activation of neocortical neurons in vivo with a sapphire-based micro-scale LED probe. *Frontiers in neural circuits*, 9, 25
- MCALINDEN, N., MASSOUBRE, D., RICHARDSON, E., GU, E., SAKATA, S., DAWSON, M. D. & MATHIESON, K. 2013. Thermal and optical characterization of micro-LED probes for in vivo optogenetic neural stimulation. *Opt Lett*, 38, 992-4.
- MCCORMICK, D. A., CONNORS, B. W., LIGHTHALL, J. W. & PRINCE, D. A. 1985. Comparative electrophysiology of pyramidal and sparsely spiny stellate neurons of the neocortex. *J Neurophysiol*, 54, 782-806.
- MCCREERY, D. B. 2008. Cochlear nucleus auditory prostheses. *Hear Res*, 242, 64-73.

- MCCREERY, D. B. & OTTO, S. R. 2011. Cochlear Nucleus Auditory Prostheses. In: ZENG, F.-G., POPPER, A. N. & FAY, R. R. (eds.) *Auditory Prostheses: New Horizons*. New York: Springer.
- MCDERMOTT, H. J., MCKAY, C. M. & VANDALI, A. E. 1992. A new portable sound processor for the University of Melbourne/Nucleus Limited multielectrode cochlear implant. *J Acoust Soc Am*, 91, 3367-3371.
- MCNAUGHTON, B. L., O'KEEFE, J. & BARNES, C. A. 1983. The stereotrode: a new technique for simultaneous isolation of several single units in the central nervous system from multiple unit records. *J Neurosci Methods*, 8, 391-397.
- MED-EL. 2017a. *Ensuring a Hearing Future* [Online]. MED-EL. [Accessed 2017]. Available: <https://www.medel.com/ca/electrodes>
- MED-EL. 2017b. *MED-EL Electrode Arrays* [Online]. MED-EL. [Accessed 2017] Available: <http://www.medel.com/uk/maestro-eas-electrodes>
- MEININGER, V., POL, D. & DERER, P. 1986. The inferior colliculus of the mouse. A Nissl and Golgi study. *Neuroscience*, 17, 1159-1179.
- MEITL, M. A., ZHU, Z.-T., KUMAR, V., LEE, K. J., FENG, X., YONGGANG, H., Y., ADESIDA, I., NUZZO, R. G. & ROGERS, J. A. 2005. Transfer printing by kinetic control of adhesion to an elastomeric stamp. *Nature Materials*, 5, 33-38.
- MELLOTT, J., MOTTS, S. & SCHOFIELD, B. 2011. Multiple Origins of Cholinergic Innervation of the Cochlear Nucleus. *Neuroscience*, 180, 138-147
- MELTZER, N. & RYUGO, D. 2006. Projections From Auditory Cortex to Cochlear Nucleus: A Comparative Analysis of Rat and Mouse. *The anatomical record. Part A, Discoveries in molecular, cellular, and evolutionary biology*, 288, 397-408
- MERCHÁN, M., AGUILAR, L., LOPEZ-POVEDA, E. & MALMIERCA, M. 2005. The Inferior Colliculus of the Rat: Quantitative Immunocytochemical Study of GABA and Glycine. *Neuroscience*, 136, 907-925
- MERZENICH, M. M., KNIGHT, P. L. & ROTH, G. L. 1975. Representation of cochlea within primary auditory cortex in the cat. *J Neurophysiol*, 38, 231-49.
- MICKLE, A. D., WON, S. M., NOH, K. N., YOON, J., MEACHAM, K. W., XUE, Y., MCILVRIED, L. A., COPITS, B. A., SAMINENI, V. K., CRAWFORD, K. E., KIM, D. H., SRIVASTAVA, P., KIM, B. H., MIN, S., SHIUAN, Y., YUN, Y., PAYNE, M. A., ZHANG, J., JANG, H., LI, Y., LAI, H. H., HUANG, Y., PARK, S. I., GEREAU, R. W. & ROGERS, J. A. 2019. A Wireless Closed Loop System for Optogenetic Peripheral Neuromodulation. *Nature*, 565, 361-5.
- BLACKROCK MICROSYSTEMS. 2018. *Electrophysiology Electrodes* [Online]. [Accessed 2019]. Available: <https://www.blackrockmicro.com/electrode-main/>
- MIDDLEBROOKS, J. C. 2004. Effects of cochlear-implant pulse rate and inter-channel timing on channel interactions and thresholds. *J Acoust Soc Am*, 116, 452-68.
- MITCHELL, J. F., SUNDBERG, K. A. & REYNOLDS, J. H. 2007. Differential attention-dependent response modulation across cell classes in macaque visual area V4. *Neuron*, 55, 131-41.
- MITCHELL, J. F., SUNDBERG, K. A. & REYNOLDS, J. H. 2009. Spatial attention decorrelates intrinsic activity fluctuations in macaque area V4. *Neuron*, 63, 879-88.
- MITRA, P. & BOKIL, H. 2008. *Observed Brain Dynamics*, New York, USA, Oxford University Press, New York.
- MIYAKAWA, A., GIBBONI, R. & BAO, S. 2013. Repeated exposure to a tone transiently alters spectral tuning bandwidth of neurons in the central nucleus of inferior colliculus in juvenile rats. *Neuroscience*, 230, 114-20.
- MOORE, A. & WEHR, M. 2013. Parvalbumin-expressing Inhibitory Interneurons in Auditory Cortex Are Well-Tuned for Frequency. *The Journal of neuroscience : the official journal of the Society for Neuroscience*, 33, 13713-23

- MOORE, J. K. & MOORE, R. Y. 1971. A comparative study of the superior olivary complex in the primate brain. *Folia Primatol (Basel)*, 16, 35-51.
- MORENO-BOTE, R., BECK, J., KANITSCHIEDER, I., PITKOW, X., LATHAM, P. & POUGET, A. 2014. Information-limiting correlations. *Nat Neurosci*, 17, 1410-1417.
- MOREST, D. 1971. Dendrodendritic Synapses of Cells That Have Axons: The Fine Structure of the Golgi Type II Cell in the Medial Geniculate Body of the Cat. *Zeitschrift fur Anatomie und Entwicklungsgeschichte*, 133, 216-246
- MOREST, D. K. & OLIVER, D. L. 1984. The neuronal architecture of the inferior colliculus in the cat: defining the functional anatomy of the auditory midbrain. *J Comp Neurol*, 222, 209-236.
- MORRISON, J. A., VALDIZON-RODRIGUEZ, R., GOLDREICH, D. & FAURE, P. A. 2018. Tuning for rate and duration of frequency-modulated sweeps in the mammalian inferior colliculus. *J Neurophysiol*, 120, 985-997.
- MOSER, T. 2015. Optogenetic stimulation of the auditory pathway for research and future prosthetics. *Current opinion in neurobiology*, 34, 29-36.
- MOTTS, S. D. & SCHOFIELD, B. R. 2010. Cholinergic and Non-Cholinergic Projections from the Pedunculo-pontine and Laterodorsal Tegmental Nuclei to the Medial Geniculate Body in Guinea Pigs. *Frontiers in Neuroanatomy*, 4, 137
- MULLER-PREUSS, P., FLACHSKAMM, C. & BIESER, A. 1994. Neural encoding of amplitude modulation within the auditory midbrain of squirrel monkeys. *Hear Res*, 80, 197-208.
- NAGEL, G., OLLIG, D., FUHRMANN, M., KATERIYA, S., MUSTI, A. M., BAMBERG, E. & HEGEMANN, P. 2002. Channelrhodopsin-1: a light-gated proton channel in green algae. *Science*, 296, 2395-2398.
- NAGEL, G., SZELLAS, T., HUHN, W., KATERIYA, S., ADEISHVILI, N., BERTHOLD, P., OLLIG, D., HEGEMANN, P. & BAMBERG, E. 2003. Channelrhodopsin-2, a directly light-gated cation-selective membrane channel. *Proc Natl Acad Sci U S A*, 100, 13940-5.
- NAKAMOTO, K. T., JONES, S. J. & PALMER, A. R. 2008. Descending projections from auditory cortex modulate sensitivity in the midbrain to cues for spatial position. *J Neurophysiol*, 99, 2347-56.
- NASH-KILLE, A. & SHARMA, A. 2014. Inter-trial coherence as a marker of cortical phase synchrony in children with sensorineural hearing loss and auditory neuropathy spectrum disorder fitted with hearing aids and cochlear implants. *Clin Neurophysiol*, 125, 1459-70.
- NAYAGAM, D. A., CLAREY, J. C. & PAOLINI, A. G. 2005. Powerful, Onset Inhibition in the Ventral Nucleus of the Lateral Lemniscus. *J Neurophysiol*, 94, 1651-1654
- NEHER, E. & SAKMANN, B. 1976. Single-channel currents recorded from membrane of denervated frog muscle fibres. *Nature*, 260, 799-802.
- NEURONEXUS. 2019. *NeuroNexus 2019 Electrode Array Design Catalogue* [Online]. [Accessed 2019]. Available: http://neuronexus.com/wp-content/uploads/2018/11/2019_NNxCatalog_20181113.pdf
- CAMBRIDGE NEUROTECH. 2019. *Cambridge NeuroTech Product Catalogue October 2019* [Online]. [Accessed 2019]. Available: <https://www.cambridgeneurotech.com/neural-probes>
- NEVISON, B., LASZIG, R., SOLLMANN, W. P., LENARZ, T., STERKERS, O., RAMSDEN, R., FRAYSSE, B., MANRIQUE, M., RASK-ANDERSEN, H., GARCIA-IBANEZ, E., COLLETTI, V. & VON WALLEMBERG, E. 2002. Results from a European clinical investigation of the Nucleus multichannel auditory brainstem implant. *Ear Hear*, 23, 170-83.
- NICHOLSON, C. & FREEMAN, J. A. 1975. Theory of current source-density analysis and determination of conductivity tensor for anuran cerebellum. *J Neurophysiol*, 38, 356-68.

- NIDCD. 2015. *Cochlear Implants* [Online]. NIH. Available: <https://www.ncbi.nlm.nih.gov/pubmed/> [Accessed 2017].
- NIENBORG, H. & CUMMING, B. 2010. Correlations between the activity of sensory neurons and behavior: how much do they tell us about a neuron's causality? *Curr Opin Neurobiol*, 20, 376-81.
- NOACHTAR, S. & REMI, J. 2009. The role of EEG in epilepsy: a critical review. *Epilepsy Behav*, 15, 22-33.
- NODA, T. & TAKAHASHI, H. 2015. Anesthetic effects of isoflurane on the tonotopic map and neuronal population activity in the rat auditory cortex. *Eur J Neurosci*, 42, 2298-311.
- NUNEZ, P. L., SILBERSTEIN, R. B., CADUSCH, P. J., WIJESINGHE, R. S., WESTDORP, A. F. & SRINIVASAN, R. 1994. A theoretical and experimental study of high resolution EEG based on surface Laplacians and cortical imaging. *Electroencephalogr Clin Neurophysiol*, 90, 40-57.
- O'CONNELL, M. N., BARCZAK, A., ROSS, D., MCGINNIS, T., SCHROEDER, C. E. & LAKATOS, P. 2015. Multi-Scale Entrainment of Coupled Neuronal Oscillations in Primary Auditory Cortex. *Front Hum Neurosci*, 9, 655.
- OESTERHELT, D. & STOECKENIUS, W. 1971. Rhodopsin-like protein from the purple membrane of Halobacterium halobium. *Nat New Biol*, 233, 149-152.
- OGAWA, S. & LEE, T. M. 1990. Magnetic resonance imaging of blood vessels at high fields: in vivo and in vitro measurements and image simulation. *Magn Reson Med*, 16, 9-18.
- OGAWA, S., LEE, T. M., NAYAK, A. S. & GLYNN, P. 1990. Oxygenation-sensitive contrast in magnetic resonance image of rodent brain at high magnetic fields. *Magn Reson Med*, 14, 68-78.
- OGAWA, T., RIERA, J., GOTO, T., SUMIYOSHI, A., NONAKA, H., JERBI, K., BERTRAND, O. & KAWASHIMA, R. 2011. Large-scale heterogeneous representation of sound attributes in rat primary auditory cortex: from unit activity to population dynamics. *J Neurosci*, 31, 14639-53.
- OLIVER, D. & SHNEIDERMAN, A. 1989. An EM Study of the Dorsal Nucleus of the Lateral Lemniscus: Inhibitory, Commissural, Synaptic Connections Between Ascending Auditory Pathways. *The Journal of neuroscience : the official journal of the Society for Neuroscience*, 9, 967-982
- OLIVER, D. L. 1987. Projections to the inferior colliculus from the anteroventral cochlear nucleus in the cat: Possible substrates for binaural interaction. *The Journal of Comparative Neurology*, 264, 24-46
- OLIVER, D. L. 2005. Neuronal Organization in the Inferior Colliculus. In: WINER, J. A. & SCHREINER, C. E. (eds.) *The Inferior Colliculus*. 1st ed. USA: Springer Science + Business Media.
- OLIVER, D. L., KUWADA, S., YIN, T. C., HABERLY, L. B. & HENKEL, C. K. 1991. Dendritic and axonal morphology of HRP-injected neurons in the inferior colliculus of the cat. *J Comp Neurol*, 303, 75-100.
- OLIVER, D. L. & MOREST, D. K. 1984. The central nucleus of the inferior colliculus in the cat. *J Comp Neurol*, 222, 237-264.
- OLIVER, D. L., WINER, J. A., BECKIUS, G. E. & SAINT MARIE, R. L. 1994. Morphology of GABAergic neurons in the inferior colliculus of the cat. *J Comp Neurol*, 340, 27-42.
- OLSHAUSEN, B. A. & FIELD, D. J. 2004. Sparse coding of sensory inputs. *Curr Opin Neurobiol*, 14, 481-487.
- OLTHOF, B. M. J., REES, A. & GARTSIDE, S. E. 2019. Multiple Nonauditory Cortical Regions Innervate the Auditory Midbrain. *J Neurosci*, 39, 8916-8928.

- ONKEN, A., LIU, J. K., KARUNASEKARA, P. P., DELIS, I., GOLLISCH, T. & PANZERI, S. 2016. Using Matrix and Tensor Factorizations for the Single-Trial Analysis of Population Spike Trains. *PLoS Comput Biol*, 12, e1005189.
- ONO, M., BISHOP, D. & OLIVER, D. 2017. Identified GABAergic and Glutamatergic Neurons in the Mouse Inferior Colliculus Share Similar Response Properties. *The Journal of neuroscience : the official journal of the Society for Neuroscience*, 37, 8952-8964
- ONO, M. & OLIVER, D. 2014. The Balance of Excitatory and Inhibitory Synaptic Inputs for Coding Sound Location. *The Journal of neuroscience : the official journal of the Society for Neuroscience*, 34, 3779-3792
- ONO, M., YANAGAWA, Y. & KOYANO, K. 2005. GABAergic Neurons in Inferior Colliculus of the GAD67-GFP Knock-In Mouse: Electrophysiological and Morphological Properties. *Neuroscience research*, 51, 475-492
- ORTON, L. & REES, A. 2014. Intercollicular Commissural Connections Refine the Representation of Sound Frequency and Level in the Auditory Midbrain. *eLife*, 3, e03764
- OSMAN, A. F., LEE, C. M., ESCABI, M. A. & READ, H. L. 2018. A Hierarchy of Time Scales for Discriminating and Classifying the Temporal Shape of Sound in Three Auditory Cortical Fields. *J Neurosci*, 38, 6967-6982.
- OTAZU, G. H., TAI, L. H., YANG, Y. & ZADOR, A. M. 2009. Engaging in an auditory task suppresses responses in auditory cortex. *Nat Neurosci*, 12, 646-54.
- OTTO, S. R., SHANNON, R. V., WILKINSON, E. P., HITSELBERGER, W. E., MCCREERY, D. B., MOORE, J. K. & BRACKMANN, D. E. 2008. Audiologic outcomes with the penetrating electrode auditory brainstem implant. *Otol Neurotol*, 29, 1147-1154.
- OYSTER, F. T. 2010. Cross section of the cochlea. Image available: <https://commons.wikimedia.org/wiki/File:Cochlea-crosssection.svg>. Wikipedia.
- PACHITARIU, M., LYAMZIN, D. R., SAHANI, M. & LESICA, N. A. 2015. State-dependent population coding in primary auditory cortex. *J Neurosci*, 35, 2058-2073.
- PACHITARIU, M., STEINMETZ, N., KADIR, S., CARANDINI, M. & D., H. K. 2016. Kilosort: realtime spike-sorting for extracellular electrophysiology with hundreds of channels. *bioRxiv*.
- PACKER, A. M., RUSSELL, L. E., DALGLEISH, H. W. & HAUSSER, M. 2015. Simultaneous all-optical manipulation and recording of neural circuit activity with cellular resolution in vivo. *Nat Methods*, 12, 140-146.
- PANINSKI, L., PILLOW, J. & LEWI, J. 2007. Statistical models for neural encoding, decoding, and optimal stimulus design. *Prog Brain Res*, 165, 493-507.
- PANZERI, S., BRUNEL, N., LOGOTHETIS, N. K. & KAYSER, C. 2010. Sensory neural codes using multiplexed temporal scales. *Trends Neurosci*, 33, 111-120.
- PANZERI, S., MACKE, J. H., GROSS, J. & KAYSER, C. 2015. Neural population coding: combining insights from microscopic and mass signals. *Trends Cogn Sci*, 19, 162-172.
- PANZERI, S., PETERSEN, R. S., SCHULTZ, S. R., LEBEDEV, M. & DIAMOND, M. E. 2001. The role of spike timing in the coding of stimulus location in rat somatosensory cortex. *Neuron*, 29, 769-777.
- PANZERI, S., SCHULTZ, S. R., TREVES, A. & ROLLS, E. T. 1999. Correlations and the encoding of information in the nervous system. *Proc Biol Sci*, 266, 1001-1012.
- PARK, D. W., BRODNICK, S. K., NESS, J. P., ATRY, F., KRUGNER-HIGBY, L., SANDBERG, A., MIKAEL, S., RICHNER, T. J., NOVELLO, J., KIM, H., BAEK, D. H., BONG, J., FRYE, S. T., THONGPANG, S., SWANSON, K. I., LAKE, W., PASHAIE, R., WILLIAMS, J. C. & MA, Z. 2016. Fabrication and utility of a transparent graphene neural electrode array for electrophysiology, in vivo imaging, and optogenetics. *Nat Protoc*, 11, 2201-2222.

- PATEL, C., REDHEAD, C., CERVI, A. & ZHANG, H. 2012. Neural Sensitivity to Novel Sounds in the Rat's Dorsal Cortex of the Inferior Colliculus as Revealed by Evoked Local Field Potentials. *Hearing research*, 286, 41-54
- PAULA-BARBOSA, M. & SOUSA-PINTO, A. 1972. Auditory cortical projections to the cat superior colliculus. *Brain Research*, 50, 47-61.
- PAXINOS, G. & FRANKLIN, K. 2012. *Paxinos and Franklin's the Mouse Brain in Stereotaxic Coordinates - 4th Edition*, Cambridge, MA, USA, Academic Press.
- PE, M. & RJ, S. 2000. Adeno-associated Virus Vectors for Gene Therapy: More Pros Than Cons? *Molecular medicine today*, 6, 433-440
- PEELLE, J. E. & DAVIS, M. H. 2012. Neural Oscillations Carry Speech Rhythm through to Comprehension. *Front Psychol*, 3, 320
- PEELLE, J. E., GROSS, J. & DAVIS, M. H. 2013. Phase-locked responses to speech in human auditory cortex are enhanced during comprehension. *Cereb Cortex*, 23, 1378-87.
- PENA, J. L., PEREZ-PERERA, L., BOUVIER, M. & VELLUTI, R. A. 1999. Sleep and wakefulness modulation of the neuronal firing in the auditory cortex of the guinea pig. *Brain Res*, 816, 463-70.
- PERUZZI, D., SIVARAMAKRISHNAN, S. & OLIVER, D. L. 2000. Identification of cell types in brain slices of the inferior colliculus. *Neuroscience*, 101, 403-416.
- PEYRACHE, A., BENCHENANE, K., KHAMASSI, M., WIENER, S. I. & BATTAGLIA, F. P. 2010. Principal component analysis of ensemble recordings reveals cell assemblies at high temporal resolution. *J Comput Neurosci*, 29, 309-325.
- PHILLIPS, D. P. & IRVINE, D. R. 1981. Responses of single neurons in physiologically defined primary auditory cortex (AI) of the cat: frequency tuning and responses to intensity. *J Neurophysiol*, 45, 48-58.
- PI, H., HANGYA, B., KVITSIANI, D., SANDERS, J., HUANG, Z. & KEPECS, A. 2013. Cortical Interneurons That Specialize in Disinhibitory Control. *Nature*, 503, 521-524
- PICCOLINO, M. 1998. Animal electricity and the birth of electrophysiology: the legacy of Luigi Galvani. *Brain Res Bull*, 46, 381-407.
- PINHEIRO, A. D., WU, M. & JEN, P. H. 1991. Encoding repetition rate and duration in the inferior colliculus of the big brown bat, *Eptesicus fuscus*. *J Comp Physiol A*, 169, 69-85.
- PISANELLO, F., SILEO, L., OLDENBURG, I. A., PISANELLO, M., MARTIRADONNA, L., ASSAD, J. A., SABATINI, B. L. & DE VITTORIO, M. 2014. Multipoint-emitting optical fibers for spatially addressable in vivo optogenetics. *Neuron*, 82, 1245-1254.
- PLANT, K., HOLDEN, L., SKINNER, M., ARCAROLI, J., WHITFORD, L., LAW, M. A. & NEL, E. 2007. Clinical evaluation of higher stimulation rates in the nucleus research platform 8 system. *Ear Hear*, 28, 381-893.
- PNEVMATIKAKIS, E. A., SOUDRY, D., GAO, Y., MACHADO, T. A., MEREL, J., PFAU, D., REARDON, T., MU, Y., LACEFIELD, C., YANG, W., AHRENS, M., BRUNO, R., JESSELL, T. M., PETERKA, D. S., YUSTE, R. & PANINSKI, L. 2016. Simultaneous Denoising, Deconvolution, and Demixing of Calcium Imaging Data. *Neuron*, 89, 285-99.
- POLANCO, M., BAWAB, S. & YOON, H. 2016. Computational Assessment of Neural Probe and Brain Tissue Interface under Transient Motion. *Biosensors (Basel)*, 6, 27
- POON, P. W., SUN, X., KAMADA, T. & JEN, P. H. 1990. Frequency and space representation in the inferior colliculus of the FM bat, *Eptesicus fuscus*. *Exp Brain Res*, 79, 83-91.
- PORTFORS, C. V. & FELIX, R. A. 2005. Spectral integration in the inferior colliculus of the CBA/Cal mouse. *Neuroscience*, 136, 1159-1170.
- PORTFORS, C. V., ROBERTS, P. D. & JONSON, K. 2009. Over-representation of species-specific vocalizations in the awake mouse inferior colliculus. *Neuroscience*, 162, 486-500.

- PSARROS, C. E., PLANT, K. L., LEE, K., DECKER, J. A., WHITFORD, L. A. & COWAN, R. S. 2002. Conversion from the SPEAK to the ACE strategy in children using the nucleus 24 cochlear implant system: speech perception and speech production outcomes. *Ear Hear*, 23, 18s-27s.
- PUJOL, R. 2016. *Auditory Brain* [Online]. Available: <http://www.cochlea.eu/en/auditory-brain:cochea.eu>. [Accessed 2019].
- QI, X. L. & CONSTANTINIDIS, C. 2012. Variability of prefrontal neuronal discharges before and after training in a working memory task. *PLoS One*, 7, e41053.
- RAMACHANDRAN, R., DAVIS, K. A. & MAY, B. J. 1999. Single-unit responses in the inferior colliculus of decerebrate cats. I. Classification based on frequency response maps. *J Neurophysiol*, 82, 152-63.
- READ, H. L., WINER, J. A. & SCHREINER, C. E. 2002. Functional architecture of auditory cortex. *Curr Opin Neurobiol*, 12, 433-40.
- REALE, R. A. & T.J. I. 1983. Auditory cortical field projections to the basal ganglia of the cat. *Neuroscience*, 8, 67-86.
- RECANZONE, G. H., GUARD, D. C. & PHAN, M. L. 2000. Frequency and intensity response properties of single neurons in the auditory cortex of the behaving macaque monkey. *J Neurophysiol*, 83, 2315-31.
- RECANZONE, G. H., SCHREINER, C. E., SUTTER, M. L., BEITEL, R. E. & MERZENICH, M. M. 1999. Functional organization of spectral receptive fields in the primary auditory cortex of the owl monkey. *J Comp Neurol*, 415, 460-81.
- REDDY, J. W., KIMUKIN, I., STEWART, L. T., AHMED, Z., BARTH, A. L., TOWE, E. & CHAMANZAR, M. 2019. High Density, Double-Sided, Flexible Optoelectronic Neural Probes With Embedded muLEDs. *Front Neurosci*, 13, 745.
- REDIES, H., SIEBEN, U. & CREUTZFELDT, O. D. 1989. Functional subdivisions in the auditory cortex of the guinea pig. *J Comp Neurol*, 282, 473-88.
- REES, A. & MOLLER, A. R. 1987. Stimulus properties influencing the responses of inferior colliculus neurons to amplitude-modulated sounds. *Hear Res*, 27, 129-43.
- REETZ, G. & EHRET, G. 1999. Inputs from three brainstem sources to identified neurons of the mouse inferior colliculus slice. *Brain Res*, 816, 527-43.
- REIMER, J., FROUDARAKIS, E., CADWELL, C. R., YATSENKO, D., DENFIELD, G. H. & TOLIAS, A. S. 2014. Pupil fluctuations track fast switching of cortical states during quiet wakefulness. *Neuron*, 84, 355-62.
- REIMER, J., MCGINLEY, M. J., LIU, Y., RODENKIRCH, C., WANG, Q., MCCORMICK, D. A. & TOLIAS, A. S. 2016. Pupil fluctuations track rapid changes in adrenergic and cholinergic activity in cortex. *Nat Commun*, 7, 13289.
- RHODE, W. S. & GREENBERG, S. 1992. Physiology of the Cochlear Nucleus. In: FAY, R.R (eds.) *The Mammalian Auditory Pathway: Neurophysiology*. Springer Handbook of Auditory Research. New York, USA: Springer.
- RIQUELME, R., SALDAÑA, E., OSEN, K., OTTERSEN, O. & MERCHÁN, M. 2001. Colocalization of GABA and Glycine in the Ventral Nucleus of the Lateral Lemniscus in Rat: An in Situ Hybridization and Semiquantitative Immunocytochemical Study. *The Journal of comparative neurology*, 432, 409-424
- RODRIGUES-DAGAEFF, C., SIMM, G., DE RIBAUPIERRE, Y., VILLA, A., DE RIBAUPIERRE, F. & ROUILLER, E. M. 1989. Functional organization of the ventral division of the medial geniculate body of the cat: evidence for a rostro-caudal gradient of response properties and cortical projections. *Hear Res*, 39, 103-125.
- RODRIGUEZ, F. A., READ, H. L. & ESCABI, M. A. 2010. Spectral and temporal modulation tradeoff in the inferior colliculus. *J Neurophysiol*, 103, 887-903.

- ROMAND, R. & EHRET, G. 1990. Development of tonotopy in the inferior colliculus. I. Electrophysiological mapping in house mice. *Brain Res Dev Brain Res*, 54, 221-234.
- RONZITTI, E., CONTI, R., ZAMPINI, V., TANESE, D., FOUST, A. J., KLAPOETKE, N., BOYDEN, E. S., PAPAGIAKOUMOU, E. & EMILIANI, V. 2017. Submillisecond Optogenetic Control of Neuronal Firing with Two-Photon Holographic Photoactivation of Chronos. *J Neurosci*, 37, 10679-10689.
- ROSE, G. J. & CAPRANICA, R. R. 1985. Sensitivity to amplitude modulated sounds in the anuran auditory nervous system. *J Neurophysiol*, 53, 446-465.
- ROSSANT, C., KADIR, S., GOODMAN, D., HUNTER, M. & HARRIS, K. 2017. Phy: Interactive visualization and manual spike sorting of large-scale ephys data. Git Hub: University College London. Available: <https://github.com/cortex-lab/phy>
- ROTH, G. L., AITKIN, L. M., ANDERSEN, R. A. & MERZENICH, M. M. 1978. Some features of the spatial organization of the central nucleus of the inferior colliculus of the cat. *J Comp Neurol*, 182, 661-680.
- ROTHSCHILD, G., NELKEN, I. & MIZRAHI, A. 2010. Functional organization and population dynamics in the mouse primary auditory cortex. *Nat Neurosci*, 13, 353-60.
- ROUILLER, E. M., RODRIGUES-DAGAEFF, C., SIMM, G., DE RIBAUPIERRE, Y., VILLA, A. & DE RIBAUPIERRE, F. 1989. Functional organization of the medial division of the medial geniculate body of the cat: tonotopic organization, spatial distribution of response properties and cortical connections. *Hear Res*, 39, 127-142.
- RUBINSTEIN, J. T. & MILLER, C. A. 1999. How do cochlear prostheses work? *Curr Opin Neurobiol*, 9, 399-404.
- RUDY, B., FISHELL, G., LEE, S. & HJERLING-LEFFLER, J. 2011. Three Groups of Interneurons Account for Nearly 100% of Neocortical GABAergic Neurons. *Developmental neurobiology*, 71, 45-61
- RYAN, A. & DALLOS, P. 1975. Effect of Absence of Cochlear Outer Hair Cells on Behavioural Auditory Threshold. *Nature*, 253, 44-46.
- RYTKONEN, K. M., ZITTING, J. & PORKKA-HEISKANEN, T. 2011. Automated sleep scoring in rats and mice using the naive Bayes classifier. *J Neurosci Methods*, 202, 60-64.
- GONG, S., DOUGHTY, M., HARBAUGH, C. R., CUMMINS, A., HATTEN, M.E., HEINTZ, N., GERFEN, C. R. 2007. Targeting Cre Recombinase to Specific Neuron Populations With Bacterial Artificial Chromosome Constructs. *The Journal of neuroscience : the official journal of the Society for Neuroscience*, 27, 9817-9823
- SAINT MARIE, R. L., SHNEIDERMAN, A. & STANFORTH, D. A. 1997. Patterns of γ -aminobutyric acid and glycine immunoreactivities reflect structural and functional differences of the cat lateral lemniscal nuclei. *The Journal of Comparative Neurology*, 389, 264-726
- SAKAI, K. 2012. Discharge properties of presumed cholinergic and noncholinergic laterodorsal tegmental neurons related to cortical activation in non-anesthetized mice. *Neuroscience*, 224, 172-190.
- SAKATA, S. 2016. State-dependent and cell type-specific temporal processing in auditory thalamocortical circuit. *Scientific reports*, 6, 18873-18873.
- SAKATA, S. & HARRIS, K. D. 2009. Laminar structure of spontaneous and sensory-evoked population activity in auditory cortex. *Neuron*, 64, 404-418.
- SAKATA, S. & HARRIS, K. D. 2012. Laminar-dependent effects of cortical state on auditory cortical spontaneous activity. *Front Neural Circuits*, 6.
- SALDANA, E., FELICIANO, M. & MUGNAINI, E. 1996. Distribution of descending projections from primary auditory neocortex to inferior colliculus mimics the topography of intracollicular projections. *J Comp Neurol*, 371, 15-40.

- SALDANA, E. & MERCHAN, M. A. 2005. Intrinsic and Commissural Connections of the Inferior Colliculus. *In: WINER, J. A. & SCHREINER, C. E. (eds.) The Inferior Colliculus*. New York, USA: Springer.
- SALDAÑA, E. 2015. All the Way From the Cortex: A Review of Auditory Corticosubcollicular Pathways. *Cerebellum*, 14, 584-596
- SALLY, S. L. & KELLY, J. B. 1988. Organization of auditory cortex in the albino rat: sound frequency. *J Neurophysiol*, 59, 1627-1638.
- SAMII, A., LENARZ, M., MAJDANI, O., LIM, H. H., SAMII, M. & LENARZ, T. 2007. Auditory midbrain implant: a combined approach for vestibular schwannoma surgery and device implantation. *Otol Neurotol*, 28, 31-38.
- SAMINENI, V. K., YOON, J., CRAWFORD, K. E., JEONG, Y. R., MCKENZIE, K. C., SHIN, G., XIE, Z., SUNDARAM, S. S., LI, Y., YANG, M. Y., KIM, J., WU, D., XUE, Y., FENG, X., HUANG, Y., MICKLE, A. D., BANKS, A., HA, J. S., GOLDEN, J. P., ROGERS, J. A. & GEREAU, R. W. 2017. Fully implantable, battery-free wireless optoelectronic devices for spinal optogenetics. *Pain*, 158, 2108-2116.
- SANDERSON, M. I. & SIMMONS, J. A. 2000. Neural responses to overlapping FM sounds in the inferior colliculus of echolocating bats. *J Neurophysiol*, 83, 1840-1855.
- SCHARF, R. 2016. *Microfabrication of high-density optoelectronic devices for optogenetic studies of neural tissue*. PhD Thesis, University of Strathclyde.
- SCHARF, R., REICHE, C. F., MCALINDEN, N., CHENG, Y., TATHIREDDY, P., RIETH, L., MATHIESON, K. & BLAIR, S. A compact integrated device for spatially selective optogenetic neural stimulation based on the Utah Optrode Array. SPIE BIOS 2018: Optogenetics and Optical Manipulation 2018: 104820M, 2018 San Francisco, California, United States. SPIE.
- SCHARF, R., TSUNEMATSU, T., MCALINDEN, N., DAWSON, M. D., SAKATA, S. & MATHIESON, K. 2016. Depth-specific optogenetic control in vivo with a scalable, high-density μ LED neural probe. *Scientific Reports*, 6, 28381.
- SCHMITZER-TORBERT, N., JACKSON, J., HENZE, D., HARRIS, K. & REDISH, A. D. 2005. Quantitative measures of cluster quality for use in extracellular recordings. *Neuroscience*, 131, 1-11.
- SCHNEIDMAN, E., PUCHALLA, J. L., SEGEV, R., HARRIS, R. A., BIALEK, W. & BERRY, M. J., 2ND 2011. Synergy from silence in a combinatorial neural code. *J Neurosci*, 31, 15732-41.
- SCHNUPP, J. W., GARCIA-LAZARO, J. A. & LESICA, N. A. 2015. Periodotopy in the gerbil inferior colliculus: local clustering rather than a gradient map. *Front Neural Circuits*, 9, 37.
- SCHOFIELD, B. 2005. Superior Olivary Complex and Lateral Lemniscal Connections of the Auditory Midbrain. *In: WINER, J. & SCHREINER, C. (eds.) The Inferior Colliculus*. New York, USA: Springer.
- SCHOFIELD, B. & CANT, N. 1997. Ventral Nucleus of the Lateral Lemniscus in Guinea Pigs: Cytoarchitecture and Inputs From the Cochlear Nucleus. *The Journal of comparative neurology*, 379, 363-385
- SCHOFIELD, B. & COOMES, D. 2005. Auditory Cortical Projections to the Cochlear Nucleus in Guinea Pigs. *Hearing research*, 199, 89-102
- SCHOFIELD, B., MOTTS, S., MELLOTT, J. & FOSTER, N. 2014. Projections From the Dorsal and Ventral Cochlear Nuclei to the Medial Geniculate Body. *Frontiers in neuroanatomy*, 8, 10
- SCHOOL, H. M. 2016. Auditory Midbrain Implant Study. NCT02984202, NIH U01 DC013030. Available: clinicaltrials.gov.
- SCHREINER, C. E. & CYNADER, M. S. 1984. Basic functional organization of second auditory cortical field (AII) of the cat. *J Neurophysiol*, 51, 1284-1305.

- SCHREINER, C. E., FROEMKE, R. C. & ATENCIO, C. A. 2010. Spectral Processing in the Auditory Cortex. *In: WINER, J. A. & SCHREINER, C. E. (eds.) The Auditory Cortex*. New York, USA: Springer.
- SCHREINER, C. E. & LANGNER, G. 1988. Periodicity coding in the inferior colliculus of the cat. II. Topographical organization. *Journal of neurophysiology*, 60, 1823-1840.
- SCHREINER, C. E. & LANGNER, G. 1997. Laminar fine structure of frequency organization in auditory midbrain. *Nature*, 388, 383-6.
- SCHREINER, C. E., READ, H. L. & SUTTER, M. L. 2000. Modular organization of frequency integration in primary auditory cortex. *Annu Rev Neurosci*, 23, 501-29.
- SCHREINER, C. E. & WINER, J. A. 2007. Auditory cortex mapmaking: principles, projections, and plasticity. *Neuron*, 56, 356-365.
- SCHROEDER, C. E., LAKATOS, P., KAJIKAWA, Y., PARTAN, S. & PUCE, A. 2008. Neuronal oscillations and visual amplification of speech. *Trends Cogn Sci*, 12, 106-113.
- SCHULLER, G. 1979. Coding of small sinusoidal frequency and amplitude modulations in the inferior colliculus of 'CF-FM' bat, *Rhinolophus ferrumequinum*. *Exp Brain Res*, 34, 117-132.
- SCHULTZ, A. E. & KUIKEN, T. A. 2011. Neural interfaces for control of upper limb prostheses: the state of the art and future possibilities. 3, 55-67.
- SCHWARTZ, I. R. 1992. The Superior Olivary Complex and Lateral Lemniscal Nuclei: Neuroanatomy. *In: FAY, R.R., POPPER, A. N. (eds.) The Springer Handbook of Auditory Research*. New York, USA: Springer.
- SCHWARTZ, M. S., OTTO, S. R., SHANNON, R. V., HITSSELBERGER, W. E. & BRACKMANN, D. E. 2008. Auditory brainstem implants. *Neurotherapeutics*, 5, 128-136.
- SENNAROGLU, L. & ZIYAL, I. 2012. Auditory brainstem implantation. *Auris Nasus Larynx*, 39, 439-450.
- SERVIERE, J., WEBSTER, W. R. & CALFORD, M. B. 1984. Isofrequency labelling revealed by a combined [¹⁴C]-2-deoxyglucose, electrophysiological, and horseradish peroxidase study of the inferior colliculus of the cat. *J Comp Neurol*, 228, 463-77.
- SESHAGIRI, C. & DELGUTTE, B. 2007. Response Properties of Neighboring Neurons in the Auditory Midbrain for Pure-Tone Stimulation: A Tetrode Study. *Journal of neurophysiology*, 98. 2058-2073
- SHADLEN, M. N. & NEWSOME, W. T. 1998. The variable discharge of cortical neurons: implications for connectivity, computation, and information coding. *J Neurosci*, 18, 3870-3896.
- SHAHEEN, L. A. & LIBERMAN, M. C. 2018. Cochlear Synaptopathy Changes Sound-Evoked Activity Without Changing Spontaneous Discharge in the Mouse Inferior Colliculus. *Front Syst Neurosci*, 12.
- SHANNON, R. V., CRUZ, R. J. & GALVIN, J. J. 2011. Effect of Stimulation Rate on Cochlear Implant Users' Phoneme, Word and Sentence Recognition in Quiet and in Noise. *Audiol Neurootol*.16, 113-123.
- SHEN, J. X., XU, Z. M. & YAO, Y. D. 1999. Evidence for columnar organization in the auditory cortex of the mouse. *Hear Res*, 137, 174-177.
- SHNEIDERMAN, A., OLIVER, D. L. & HENKEL, C. K. 1988. Connections of the dorsal nucleus of the lateral lemniscus: an inhibitory parallel pathway in the ascending auditory system? *J Comp Neurol*, 276, 188-208.
- SIGWORTH, F. J. & NEHER, E. 1980. Single Na⁺ channel currents observed in cultured rat muscle cells. *Nature*, 287, 447-449.
- SINGH, N. C. & THEUNISSEN, F. E. 2003. Modulation spectra of natural sounds and ethological theories of auditory processing. *J Acoust Soc Am*, 114, 3394-3411.

- SINGHEISER, M., GUTFREUND, Y. & WAGNER, H. 2012. The representation of sound localization cues in the barn owl's inferior colliculus. *Front Neural Circuits*, 6, 45
- SIVAJI, V., GRASSE, D. W., HAYS, S. A., BUCKSOT, J. E., SAINI, R., KILGARD, M. P. & RENNAKER, R. L., 2019. ReStore: A wireless peripheral nerve stimulation system. *J Neurosci Methods*, 320, 26-36.
- SIVARAMAKRISHNAN, S. & OLIVER, D. L. 2001. Distinct K currents result in physiologically distinct cell types in the inferior colliculus of the rat. *J Neurosci*, 21, 2861-2877.
- SKINNER, M. W., HOLDEN, L. K., WHITFORD, L. A., PLANT, K. L., PSARROS, C. & HOLDEN, T. A. 2002. Speech recognition with the nucleus 24 SPEAK, ACE, and CIS speech coding strategies in newly implanted adults. *Ear Hear*, 23, 207-223.
- SMITH, M. A. & KOHN, A. 2008. Spatial and temporal scales of neuronal correlation in primary visual cortex. *J Neurosci*, 28, 12591-603.
- SMITH, P., BARTLETT, E. & KOWALKOWSKI, A. 2006. Unique Combination of Anatomy and Physiology in Cells of the Rat Paralamina Thalamic Nuclei Adjacent to the Medial Geniculate Body. *The Journal of comparative neurology*, 496, 314-334
- SMITH, P., UHLRICH, D., MANNING, K. & BANKS, M. 2012. Thalamocortical Projections to Rat Auditory Cortex From the Ventral and Dorsal Divisions of the Medial Geniculate Nucleus. *The Journal of comparative neurology*, 520, 34-51
- SMITH, P. H. & POPULIN, L. C. 2001. Fundamental differences between the thalamocortical recipient layers of the cat auditory and visual cortices. *J Comp Neurol*, 436, 508-19.
- SPANGLER, K. M., CANT, N. B., HENKEL, C. K., FARLEY, G. R. & WARR, W. B. 1987. Descending projections from the superior olivary complex to the cochlear nucleus of the cat. *J Comp Neurol*, 259, 452-465.
- SPOENDLIN, H. 1969. Innervation Patterns in the Organ of Corti of the Cat. *Acta otolaryngologica*, 67, 239-254
- SPROULE, M. K., METZEN, M. G. & CHACRON, M. J. 2015. Parallel sparse and dense information coding streams in the electrosensory midbrain. *Neurosci Lett*, 607, 1-6.
- STANFORD-UNIVERSITY. 2018. *Optogenetics Resource Center: Brain Tissue Light Transmitter Calculator* [Online]. Stanford University. [Accessed 2018]. Available: <https://web.stanford.edu/group/dlab/cgi-bin/graph/chart.php>
- STEINSCHNEIDER, M., AREZZO, J. & VAUGHAN, H. G., JR. 1980. Phase-locked cortical responses to a human speech sound and low-frequency tones in the monkey. *Brain Res*, 198, 75-84.
- STERIADE, M., AMZICA, F. & CONTRERAS, D. 1996. Synchronization of fast (30-40 Hz) spontaneous cortical rhythms during brain activation. *J Neurosci*, 16, 392-417.
- STERIADE, M., NUNEZ, A. & AMZICA, F. 1993. A novel slow (< 1 Hz) oscillation of neocortical neurons in vivo: depolarizing and hyperpolarizing components. *J Neurosci*, 13, 3252-3265.
- STIEBLER, I. & EHRET, G. 1985. Inferior colliculus of the house mouse. I. A quantitative study of tonotopic organization, frequency representation, and tone-threshold distribution. *J Comp Neurol*, 238, 65-76.
- STRINGER, C., PACHITARIU, M., STEINMETZ, N., REDDY, C. B., CARANDINI, M. & HARRIS, K. D. 2019. Spontaneous behaviors drive multidimensional, brainwide activity. *Science*, 364, 255.
- NATIONAL INSTITUTE OF NEUROLOGICAL DISORDERS AND STROKE. 2019. *Neurofibromatosis Fact Sheet* [Online]. [Accessed 2019]. Available: <https://www.ninds.nih.gov/Disorders/Patient-Caregiver-Education/Fact-Sheets/Neurofibromatosis-Fact-Sheet>
- SUGA, N. & JEN, P. H. 1976. Disproportionate tonotopic representation for processing CF-FM sonar signals in the mustache bat auditory cortex. *Science*, 194, 542-544.

- SUTA, D., KVASNAK, E., POPELAR, J. & SYKA, J. 2003. Representation of species-specific vocalizations in the inferior colliculus of the guinea pig. *J Neurophysiol*, 90, 3794-808.
- SUTTER, M. L. & SCHREINER, C. E. 1991. Physiology and topography of neurons with multipeaked tuning curves in cat primary auditory cortex. *J Neurophysiol*, 65, 1207-1226.
- SYKA, J., POPELAR, J., KVASNAK, E. & ASTL, J. 2000. Response properties of neurons in the central nucleus and external and dorsal cortices of the inferior colliculus in guinea pig. *Exp Brain Res*, 133, 254-266.
- SZABO, V., VENTALON, C., DE SARS, V., BRADLEY, J. & EMILIANI, V. 2014. Spatially selective holographic photoactivation and functional fluorescence imaging in freely behaving mice with a fiberscope. *Neuron*, 84, 1157-1169.
- SZYMANSKI, F. D., RABINOWITZ, N. C., MAGRI, C., PANZERI, S. & SCHNUPP, J. W. 2011. The laminar and temporal structure of stimulus information in the phase of field potentials of auditory cortex. *J Neurosci*, 31, 15787-801.
- TALLON-BAUDRY, C., BERTRAND, O., DELPUECH, C. & PERNIER, J. 1996. Stimulus specificity of phase-locked and non-phase-locked 40 Hz visual responses in human. *J Neurosci*, 16, 4240-4249.
- TASIC, B., MENON, V., NGUYEN, T., KIM, T., JARSKY, T., YAO, Z., LEVI, B., GRAY, L., SORENSEN, S., DOLBEARE, T., BERTAGNOLLI, D., GOLDY, J., SHAPOVALOVA, N., PARRY, S., LEE, C., SMITH, K., BERNARD, A., MADISEN, L., SUNKIN, S., HAWRYLYCZ, M., KOCH, C. & ZENG, H. 2016. Adult Mouse Cortical Cell Taxonomy Revealed by Single Cell Transcriptomics. *Nature neuroscience*, 19, 335-346
- TERASHIMA, H. & HOSOYA, H. 2009. Sparse Codes of Harmonic Natural Sounds and Their Modulatory Interactions. *Network*, 20, 253-267.
- THOMAS, H., TILLEIN, J., HEIL, P. & SCHEICH, H. 1993. Functional organization of auditory cortex in the mongolian gerbil (*Meriones unguiculatus*). I. Electrophysiological mapping of frequency representation and distinction of fields. *Eur J Neurosci*, 5, 882-897.
- TOLLIN, D. 2003. The Lateral Superior Olive: A Functional Role in Sound Source Localization. *Neuroscientist*, 9, 127-143
- TSUNEMATSU, T., PATEL, A. A., ONKEN, A. & SAKATA, S. 2020. State-dependent brainstem ensemble dynamics and their interactions with hippocampus across sleep states. *eLife*. 9, e52244
- URBAN-CIECKO, J. & BARTH, A. 2016. Somatostatin-expressing Neurons in Cortical Networks. *Nature reviews. Neuroscience*, 17, 401-409
- VAN DORT, C. J., ZACHS, D. P., KENNY, J. D., ZHENG, S., GOLDBLUM, R. R., GELWAN, N. A., RAMOS, D. M., NOLAN, M. A., WANG, K., WENG, F. J., LIN, Y., WILSON, M. A. & BROWN, E. N. 2015. Optogenetic activation of cholinergic neurons in the PPT or LDT induces REM sleep. *Proc Natl Acad Sci USA*. 112, 584-589
- VANDALI, A. E., WHITFORD, L. A., PLANT, K. L. & CLARK, G. M. 2000. Speech perception as a function of electrical stimulation rate: using the Nucleus 24 cochlear implant system. *Ear Hear*, 21, 608-24.
- VERSCHOOTEN, E., SHAMMA, S., OXENHAM, A. J., MOORE, B. C. J., JORIS, P. X., HEINZ, M. G. & PLACK, C. J. 2019. The upper frequency limit for the use of phase locking to code temporal fine structure in humans: A compilation of viewpoints. *Hear Res*, 377, 109-121.
- VINJE, W. E. & GALLANT, J. L. 2000. Sparse coding and decorrelation in primary visual cortex during natural vision. *Science*, 287, 1273-1276.

- VON KRIEGSTEIN, K., PATTERSON, R. D. & GRIFFITHS, T. D. 2008. Task-dependent modulation of medial geniculate body is behaviorally relevant for speech recognition. *Curr Biol*, 18, 1855-1859.
- VONDERSCHEIN, K. & CHACRON, M. J. 2011. Sparse and dense coding of natural stimuli by distinct midbrain neuron subpopulations in weakly electric fish. *J Neurophysiol*, 106, 3102-3118.
- WALLACE, M. N. & HE, J. 2010. Intrinsic Connections of the Auditory Cortex. In: WINER, J. A. & SCHRIENER, C.E (eds.) *The Auditory Cortex*. New York, USA: Springer.
- WALLACE, M. N. & PALMER, A. R. 2008. Laminar differences in the response properties of cells in the primary auditory cortex. *Exp Brain Res*, 184, 179-191.
- WANG, J., CASPARY, D. & SALVI, R. J. 2000. GABA-A antagonist causes dramatic expansion of tuning in primary auditory cortex. *Neuroreport*, 11, 1137-1140.
- WANG, X. 2007. Neural coding strategies in auditory cortex. *Hear Res*, 229, 81-93.
- WANG, X., LU, T. & LIANG, L. 2003. Cortical Processing of temporal modulations. *Speech Communication*, 41, 107-121.
- WANG, X., LU, T., SNIDER, R. K. & LIANG, L. 2005. Sustained firing in auditory cortex evoked by preferred stimuli. *Nature*, 435, 341-346.
- WANG, Y., WANG, P. & YU, Y. 2018. Decoding English Alphabet Letters Using EEG Phase Information. *Front Neurosci*, 12, 62
- WARR, W. B. 1992. Organization of Olivocochlear Efferent Systems in Mammals. In: WEBSTER, D.B., FAY, R.R (eds.) *The Mammalian Auditory Pathway: Neuroanatomy. Springer Handbook of Auditory Research*. New York, USA: Springer.
- WASIF, K., MONICA, S., ERIN, P. & WEN, L. 2019. Micro-Reflector Integrated Multichannel μ LED Optogenetic Neurostimulator With Enhanced Intensity. *Frontiers in Mechanical Engineering*, 4, 17
- WEBER, B. P., LAI, W. K., DILLIER, N., VON WALLENGER, E. L., KILLIAN, M. J., PESCH, J., BATTMER, R. D. & LENARZ, T. 2007. Performance and preference for ACE stimulation rates obtained with nucleus RP 8 and freedom system. *Ear Hear*, 28, 46s-48s.
- WEISS, R. S., VOSS, A. & HEMMERT, W. 2016. Optogenetic stimulation of the cochlea—A review of mechanisms, measurements, and first models. *Network: Computation in Neural Systems*, 27, 212-236.
- WENSTRUP, J. & LEROY, S. A. 2001. Spectral integration in the inferior colliculus: role of glycinergic inhibition in response facilitation. *J Neurosci*, 21, 124.
- WHITE-SCHWOCH, T., NICOL, T., WARRIER, C. M., ABRAMS, D. A. & KRAUS, N. 2017. Individual Differences in Human Auditory Processing: Insights From Single-Trial Auditory Midbrain Activity in an Animal Model. *Cereb Cortex*, 27, 5095-5115.
- WILLIAMS, P. E., MECHLER, F., GORDON, J., SHAPLEY, R. & HAWKEN, M. J. 2004. Entrainment to video displays in primary visual cortex of macaque and humans. *J Neurosci*, 24, 8278-8288.
- WILSON, B. S., FINLEY, C. C., LAWSON, D. T., WOLFORD, R. D., EDDINGTON, D. K. & RABINOWITZ, W. M. 1991. Better speech recognition with cochlear implants. *Nature*, 352, 236-238.
- WINER, J., KELLY, J. & LARUE, D. 1999. Neural Architecture of the Rat Medial Geniculate Body. *Hearing research*, 130, 19-41
- WINER, J. A. 1992. The Functional Architecture of the Medial Geniculate Body and Primary Auditory Cortex. In: WEBSTER, D. B., POPPER, A. N. & FAY, R. R. (eds.) *The Mammalian Auditory Pathway: Neuroanatomy*. 1st ed. New York, USA: Springer-Verlag.
- WINER, J. A. 2006. Decoding the auditory corticofugal systems. *Hear Res*, 212, 1-8.

- WINER, J. A., DIEHL, J. J. & LARUE, D. T. 2001. Projections of auditory cortex to the medial geniculate body of the cat. *J Comp Neurol*, 430, 27-55.
- WINER, J. A., LARUE, D. T., DIEHL, J. J. & HEFTI, B. J. 1998. Auditory cortical projections to the cat inferior colliculus. *J Comp Neurol*, 400, 147-74.
- WINER, J. A., MILLER, L. M., LEE, C. C. & SCHREINER, C. E. 2005. Auditory thalamocortical transformation: structure and function. *Trends Neurosci*, 28, 255-63.
- WINER, J. A. & PRIETO, J. J. 2001. Layer V in cat primary auditory cortex (AI): cellular architecture and identification of projection neurons. *J Comp Neurol*, 434, 379-412.
- WINER, J. A. & SCHREINER, C. E. 2005. The Central Auditory System: A Functional Analysis. In: WINER, J. A. & SCHREINER, C. E. (eds.) *The Inferior Colliculus*. New York, USA: Springer Science + Business Media, Inc.
- WONG, K., KOZIN, E. D., KANUMURI, V. V., VACHICOURAS, N., MILLER, J., LACOUR, S., BROWN, M. C. & LEE, D. J. 2019. Auditory Brainstem Implants: Recent Progress and Future Perspectives. *Front Neurosci*, 13, 10
- WOUTERS, J., MCDERMOTT, H. J. & FRANCAERT, T. 2015. Sound Coding in Cochlear Implants: From electrical pulses to hearing. *IEEE Signal Processing Magazine*, 32, 67-80.
- WU, F., STARK, E., IM, M., CHO, I.-J., YOON, E.-S., BUZSÁKI, G., WISE, K. D. & YOON, E. 2013. An implantable neural probe with monolithically integrated dielectric waveguide and recording electrodes for optogenetics applications. *Journal of neural engineering*, 10, 56012-56012.
- WU, F., STARK, E., KU, P.-C., WISE, K. D., BUZSÁKI, G. & YOON, E. 2015. Monolithically integrated μ LEDs on silicon neural probes for high-resolution optogenetic studies in behaving animals. *Neuron*, 88, 1136-1148.
- WU, G. K., ARBUCKLE, R., LIU, B. H., TAO, H. W. & ZHANG, L. I. 2008. Lateral sharpening of cortical frequency tuning by approximately balanced inhibition. *Neuron*, 58, 132-43.
- XIONG, X., LIANG, F., ZINGG, B., JI, X., IBRAHIM, L., TAO, H. & ZHANG, L. 2015. Auditory Cortex Controls Sound-Driven Innate Defense Behaviour Through Corticofugal Projections to Inferior Colliculus. *Nature communications*, 6, 7224.
- XU, X., ROBY, K. & CALLAWAY, E. 2010. Immunochemical Characterization of Inhibitory Mouse Cortical Neurons: Three Chemically Distinct Classes of Inhibitory Cells. *The Journal of comparative neurology*, 518, 389-404
- YAGUE, J. G., TSUNEMATSU, T. & SAKATA, S. 2017. Distinct Temporal Coordination of Spontaneous Population Activity between Basal Forebrain and Auditory Cortex. *Front Neural Circuits*, 11, 64.
- YAN, J., ZHANG, Y. & EHRET, G. 2005. Corticofugal shaping of frequency tuning curves in the central nucleus of the inferior colliculus of mice. *J Neurophysiol*, 93, 71-83.
- YANG, X., ZHOU, T., ZWANG, T. J., HONG, G., ZHAO, Y., VIVEROS, R. D., FU, T. M., GAO, T. & LIEBER, C. M. 2019. Bioinspired neuron-like electronics. *Nat Mater*, 18, 510-517.
- YIN, T. C. & CHAN, J. C. 1990. Interaural time sensitivity in medial superior olive of cat. *J Neurophysiol*, 64, 465-488.
- YIZHAR, O., FENNO, L. E., DAVIDSON, T. J., MOGRI, M. & DEISSEROTH, K. 2011. Optogenetics in neural systems. *Neuron*, 71, 9-34.
- ZENG, F. G. 2002. Temporal pitch in electric hearing. *Hear Res*, 174, 101-106.
- ZHANG, D., LI, L., KELLY, J. & WU, S. 1998. GABAergic Projections From the Lateral Lemniscus to the Inferior Colliculus of the Rat. *Hearing research*, 117, 1-12
- ZHANG, F., GRADINARU, V., ADAMANTIDIS, A. R., DURAND, R., AIRAN, R. D., DE LECEA, L. & DEISSEROTH, K. 2010. Optogenetic interrogation of neural circuits: technology for probing mammalian brain structures. *Nat Protoc*, 5, 439-456.

- ZHANG, F., PRIGGE, M., BEYRIÈRE, F., TSUNODA, S. P., MATTIS, J., YIZHAR, O., HEGEMANN, P. & DEISSEROTH, K. 2008. Red-shifted optogenetic excitation: a tool for fast neural control derived from *Volvox carteri*. *Nat Neurosci*, 11, 631-633.
- ZHANG, Q., HU, X., HONG, B. & ZHANG, B. 2019. A hierarchical sparse coding model predicts acoustic feature encoding in both auditory midbrain and cortex. *PLoS Comput Biol*, 15, e1006766.
- ZHANG, Y. & SUGA, N. 1997. Corticofugal amplification of subcortical responses to single tone stimuli in the mustached bat. *J Neurophysiol*, 78, 3489-3492.
- ZHANG, Y., SUGA, N. & YAN, J. 1997. Corticofugal modulation of frequency processing in bat auditory system. *Nature*, 387, 900-903.
- ZHENG, J., SHEN, W., HE, D., LONG, K., MADISON, L. & DALLOS, P. 2000. Prestin Is the Motor Protein of Cochlear Outer Hair Cells. *Nature*, 405, 149-55
- ZHENG, Y. & ESCABI, M. A. 2013. Proportional spike-timing precision and firing reliability underlie efficient temporal processing of periodicity and envelope shape cues. *J Neurophysiol*, 110, 587-606.
- ZION GOLUMBIC, E. M., DING, N., BICKEL, S., LAKATOS, P., SCHEVON, C. A., MCKHANN, G. M., GOODMAN, R. R., EMERSON, R., MEHTA, A. D., SIMON, J. Z., POEPEL, D. & SCHROEDER, C. E. 2013. Mechanisms underlying selective neuronal tracking of attended speech at a "cocktail party". *Neuron*, 77, 980-991.
- ZUK, N. J., TEOH, E. S. & LALOR, E. C. 2019. EEG-based classification of natural sounds reveals specialized responses to speech and music. *Neuroimage*. 210, 116558